Sreevalsa Kolathayar
Arpita Mondal
Siau Chen Chian   *Editors*

Climate Change and Water Security

Select Proceedings of VCDRR 2021

Springer

Lecture Notes in Civil Engineering

Volume 178

Lecture Notes in Civil Engineering (LNCE) publishes the latest developments in Civil Engineering—quickly, informally and in top quality. Though original research reported in proceedings and post-proceedings represents the core of LNCE, edited volumes of exceptionally high quality and interest may also be considered for publication. Volumes published in LNCE embrace all aspects and subfields of, as well as new challenges in, Civil Engineering. Topics in the series include:

- Construction and Structural Mechanics
- Building Materials
- Concrete, Steel and Timber Structures
- Geotechnical Engineering
- Earthquake Engineering
- Coastal Engineering
- Ocean and Offshore Engineering; Ships and Floating Structures
- Hydraulics, Hydrology and Water Resources Engineering
- Environmental Engineering and Sustainability
- Structural Health and Monitoring
- Surveying and Geographical Information Systems
- Indoor Environments
- Transportation and Traffic
- Risk Analysis
- Safety and Security

To submit a proposal or request further information, please contact the appropriate Springer Editor:

– Pierpaolo Riva at pierpaolo.riva@springer.com (Europe and Americas);
– Swati Meherishi at swati.meherishi@springer.com (Asia - except China, and Australia, New Zealand);
– Wayne Hu at wayne.hu@springer.com (China).

All books in the series now indexed by Scopus and EI Compendex database!

More information about this series at https://link.springer.com/bookseries/15087

Sreevalsa Kolathayar · Arpita Mondal ·
Siau Chen Chian
Editors

Climate Change and Water Security

Select Proceedings of VCDRR 2021

🦅 Springer

Editors
Sreevalsa Kolathayar
Department of Civil Engineering
National Institute of Technology Karnataka
Surathkal, India

Arpita Mondal
Department of Civil Engineering
Indian Institute of Technology Bombay
Mumbai, Maharashtra, India

Siau Chen Chian
Department of Civil and Environmental
Engineering
National University of Singapore
Singapore, Singapore

Contents

Groundwater Conservation Measures and Modeling Techniques

Natural Hazards

About the Editors

Dr. Sreevalsa Kolathayar pursued his M.Tech. from Indian Institute of Technology (IIT) Kanpur, Ph.D. from Indian Institute of Science (IISc) and served as International Research Staff at UPC BarcelonaTech Spain. He is presently Assistant Professor in the Department of Civil Engineering, National Institute of Technology (NIT), Karnataka. Dr. Kolathayar has authored six books and over 75 research articles. He is Associate Editor of two International Journals. His broad research areas are geotechnical earthquake engineering, geosynthetics & geonaturals, and water geotechnics. He is currently the Secretary of the Indian chapter of International Association for Coastal Reservoir Research (IACRR), and Executive Committee Member of Indian Society of Earthquake Technology. In 2017, The New Indian Express honored Dr. Kolathayar with 40 under 40 - South India's Most Inspiring Young Teachers Award. He is the recipient of ISET DK Paul Research Award from Indian Society of Earthquake Technology, IIT Roorkee. He received "IEI Young Engineers Award" by The Institution of Engineers (India), in recognition of his contributions in the field of Civil Engineering. He was recently featured in *Geostrata Magazine* by American Society of Civil Engineers (ASCE). Dr Sreevalsa is the Organizing Chair of the Virtual Conference on Disaster Risk Reduction (VCDRR 2021).

Dr. Arpita Mondal works as an assistant professor in the Department of Civil Engineering at the Indian Institute of Technology (IIT) Bombay. She is also an associate faculty member in the Interdisciplinary Program in Climate Studies at IIT Bombay. Arpita's research focuses on hydroclimatic extremes—how they can be characterized, what causes them and how they are likely to evolve with climate change. She uses a combination of statistical analysis, physical understanding and computer model simulations. Arpita serves as an associate editor of the Springer journal Regional Environmental Change. She received the Early Career Research Award from the Science and Education Research Board (SERB), and the INSPIRE Faculty Award, both funded by the Department of Science and Technology, Government of India. She also received the Asian University Alliance (AUA) Scholars' Award. Arpita completed her Ph.D. at the Indian Institute of Science (IISc), Bangalore, M.Tech at IIT Bombay and Bachelors in Civil Engineering at Jadavpur University, Kolkata. As

a Ph.D. student, Arpita had received the Endeavour Research Fellowship (Government of Australia), Fulbright-Nehru Research Fellowship (USIEF) and the Berkner Travel Grant of the American Geophysical Union (AGU). Arpita scored the first rank in the university in both her bachelors and masters.

Dr. Siau Chen Chian is an associate professor at the Department of Civil and Environmental Engineering, National University of Singapore (NUS). He obtained his Ph.D. and B.Eng.(1st Class with Gold Medal) from Cambridge University and Nanyang Technological University, respectively. Dr. Chian's contribution in earthquake engineering lies in the field of catastrophe modelling, landslides and damage vulnerability of underground structures. He was funded by the UK Engineering and Physical Sciences Research Council (EPSRC) as the geotechnical specialist to carry out reconnaissance missions at the Mw7.6 Padang Earthquake in 2009, Mw9.0 Great East Japan Earthquake in 2011 and Mw7.8 Muisne Earthquake in 2016. Dr. Chian was named Top 10 Innovators Under 35 in Asia by the MIT Technology Review for his novel contribution in catastrophe modelling in 2016. Dr. Chian is a nominated member of the Technical Committee on Earthquake Geotechnical Engineering under the International Society for Soil Mechanics and Geotechnical Engineering (ISSMGE). He is also an Integrated Research on Disaster Risk (IRDR) Young Scientist supported by the International Science Council (ISC) and the United Nations Office for Disaster Risk Reduction (UNDRR).

Climate Change and Water Security—An Introduction

Surendar Natarajan, Arpita Mondal, and Sreevalsa Kolathayar

1 Introduction and Background

There is unequivocal evidence that the earth's climate is changing with an unprecedented rise in temperatures globally that subsequently leads to alterations in the hydrological cycle. The three most prominent signals of climate change, that is, increasing global average temperature, changes in precipitation patterns, and rising sea levels, all have significant implications on global and regional water security [1]. Further, such variations are expected to alter not only mean hydro climatic conditions, but also affect intensities, durations, frequencies, and areal extents of extreme events such as floods and droughts. As a result, water resources availability, acceptable water quality for consumption or environmental sustainability, and disaster risk protection come under direct threat. Agricultural water demands are also expected to go up, further resulting in threats to food security. Finally, energy also plays an important role in this nexus.

Rising global temperatures have been uniquely attributed to man-made emissions of greenhouse gases and aerosols [2]. However, changes in hydrologic variables, particularly at regional [6] or river-basin scales [5], are hard to attribute owing to large natural variability or the inability of climate models to represent such processes at smaller scales. Risk is perceived to be a combination of hazard of a disastrous event, and exposure and vulnerability of communities [7]. The latter component is more significant for developing countries owing to the large populations, poor socio-economic conditions, and frail, inadequate infrastructure. Therefore, disaster risk

S. Natarajan
Sri Sivasubramaniya Nadar (SSN) College of Engineering, Kalavakkam, India

A. Mondal
Indian Institute of Technology Bombay, Powai, Mumbai 400076, India

S. Kolathayar (✉)
National Institute of Technology Karnataka, Surathkal, India
e-mail: sreevalsa@nitk.edu.in

reduction efforts are already under stress in low-income countries, resulting from an imbalance in demands and availability of resources.

This book volume offers technical terms, a collective of research studies trying to understand and improve disaster resilience pertaining to water resources under climate change. Water quantity and quality issues are discussed, along with implications on agriculture or energy sectors. Risk assessment of natural hazards are also presented. While some studies are universal or methodological in nature, the primary focus is on developing countries. Further, environmental stressors may often lead to multi-hazard risk [3] necessitating interdisciplinary approaches to mitigate or adapt to such risk. Most of the studies presented in this book offers cross-disciplinary efforts to this end.

2 Climate Change Impact on Water Resources

2.1 Climate Change

Climate change has become an increasingly pressing issue that needs to be tackled by scientists and researchers around the globe in current years. It is necessary to go for modelling the climate change and its impacts on surface and groundwater as an important tool for decision-making. Still, huge uncertainties are associated with climate change and its impacts on our world as it is extremely difficult to quantify the effects of climate change.

2.2 Agriculture and Irrigation

The extreme climate events and climate variability affecting production and access to water for different social groups in various regions were studied as empirical analysis to assess *climate change and its effects on water scarcity through Participatory Rural Appraisal (PRA) approach* in Chirirbandar Upazila, Dinajpur. The climate change also has an impact on irrigation and agriculture in terms of crop productivity and yield.

The climate change impacts on crop yield at Muzza irrigation district in Lombardy, Italy is studied by *Ahmed and Mohammed* by considering two Representative Concentrations Pathways (RCPs) or scenarios, namely, RCP8.5 and RCP4.5 of the fifth assessment report of Intergovernmental Panel on Climate Change (IPCC).

2.3 Flood Risk Assessment and Techniques

Flood is an unusual high stage of the river. Floods are highly destructive natural disasters which results in massive damages to human and nature. This is due to severe storm of unusual meteorological combination, sometimes combined with melting of accumulated snow on the catchment. This may also be due to shifting of the course of the river, earthquake causing bank erosion, or blocking of river, or beaching of the river flood banks. Floods cannot be prevented but can be controlled by suitable structural and non-structural measures. Some of the chapters in this study discuss about non-structural, flood modelling tools, techniques, and case studies.

2.4 Non-Structural Measures

Milkecha et al. in their chapter discussed about impacts of possible *future climate change* scenarios on the stream in the *Upper Dhidhesa river sub-basin.* The future impacts of climate changes in the Upper Dhidhesa river basin is assessed from the hydrological response of new emission scenarios based on the IPCC fifth assessment report (AR5). The hydrological model Hydrologic Engineering Centre Hydrological Modelling System (*HEC-HMS*) was used for calibration and validation for streamflow simulation in Upper Dhidhesa river-sub-basin.

The *OpenDA software* is used to determine flood risk model parameters and coefficient values. Flood risk assessment at the Douro river estuary characterizes the hydrodynamic behaviour under extreme flood events. The chapter *Flood modelling for an urban Indian catchment: Challenges and way forward* used a one-dimensional flood model (MIKE 11) for estimating the river discharge along with storm water drainage discharge coupled with a *two-dimensional flood model (MIKE 21). Geo-SWMM* is used to assess storm water runoff of Padma bridge link road at southwest part of Dhaka in Bangladesh. The peak runoff for each catchment was determined for 5-year and 10-year return period using the *Geo-SWMM* model.

Mahesh et al. discussed advanced *Physics Informed Neural Network* (PINN) for spatial–temporal flood forecasting based upon Saint Venant's equations. The proposed article *Simulation of the flood of El Maleh River by GIS in the city of Mohammedia-Morocco* aims to explain how the flood occurs and the extent to which it may be affected by the region, as well as developing scenarios for the rise in the water level and the extent of its vulnerability and production of various risks, especially since the region contains industrial facilities for oil refining.

Flood hazard mapping is to reduce the risk of losing lives of people. *Reshma Antony* et al. in their chapter discussed about generating flood hazard mapping using Geographical Information System (GIS) and *Analytical Hierarchy Process* (AHP) for planning infrastructure development, disaster management or mitigation measures, and emergency services.

Machine Learning Techniques (MLT) are the latest techniques used in the field of flood modelling. The classification methods like *logistic regression* and *decision tree* are normally used in flood prediction studies. The chapter feature selection for rainfall prediction and drought assessment using *Bayesian Network technique* (BN) explores the potential of Bayesian Network (BN), which is a class of *Graphical Modelling* (GM), a feature selection technique for examining the association of monthly rainfall and probable meteorological drivers and subsequent drought assessment.

The study on *open-access precipitation networks* and *Machine Learning (ML) algorithms* adopted as tools for flood severity prediction, a case study in Echaz catchment, aims to develop a simple model to predict flood severity. This ML model is based on open-access precipitation data from a Personal Weather Station (PWS) network and water level measurements from a low-cost ultrasonic sensor.

2.5   Structural Measures

Gautam Das et al. in their chapter discussed about the conceptualization, planning, and design of a flood-proof house for Assam, India's flood plain, as a replacement to the normally used building typology in highly flood-prone areas of Assam. *Palomino Carlos* et al. used *Recycled Plastic Fibres as Concrete Retaining Walls for River Defenses.* In their study design, the two alternatives of *cyclopean concrete*, the one with recycled plastic fibres and the other without it, is adopted and compared for technical, economic, and environmental criteria. *Jun Lim Wong* et al. reviewed the relationship between rainfall variations under climate change and its impacts on slope stability.

2.6   Case Studies on Flood Modelling

The chapter *traditional knowledge* to read hydro-meteorological hazards in Teesta floodplain, Bangladesh is an experience, practices and observations provides valuable aid to forecast local hydro-meteorological hazards. However, traditional knowledge is less documented, often neglected by science, and consequently in danger of being lost. *Thankachan* et al. in this chapter discuss a case study about issues of draining surface water in Kothamangalam town, in Ernakulam district of Kerala with emphasis placed on the *design and planning process.*

2.7   Sedimentation

The primary purposes of creating impounding in the rivers with dams in the form of reservoirs is flood control. The loss of reservoir capacity due to deposition of

sediments is major concern in reservoir management. The *sedimentation* in Chulliyar Reservoir in Kerala is considered for a case study. For sedimentation analysis, along with *bathymetric survey,* the entire catchment area is divided into zones with suitable grid size.

The *Particle Image Velocimetry* (*PIV*) experimental approach is used for the flow visualization on coastal problem. The PIV experiment involved the use of laser illumination system, high speed camera, filler particles, and wave-motion generator. The PIV experimental method is discussed in a case study titled *Particle Image Velocimetry Analysis on the Liquid Sediment Model.*

2.8 Extremity in Oceans

In the last few decades, extreme conditions of precipitation and drought have raised concern due to their severity and increasing risks to inhabitants, infrastructures, and other anthropic activities. In recent days, coastal structures overtopping, erosion in stream, and destruction of infrastructures are common along the coasts around the world. There are different methods to analyse extreme conditions like physical, mathematical, and numerical modelling. *Ana Gomes and José Pinho*, in their chapter, used a numerical model on coastal structure at full scale level for simulating the pressures and shear stresses that act on the piers that support the structure, considering different heights of the air gap and assessing the respective CPU simulation times using *CFD modelling.*

3 Drought Analyses and Indices

Droughts are recognized as a natural disaster that is caused by extreme and continuous shortage of precipitation. Total water available on this earth remains constant but its distribution with respect to time at a place is highly variable leading to hydrological extremes of drought (water deficiency) and flood (water surplus in a stream). Among the two extremes of flood and drought, the former is characterized by quick inception, vigorous growth, and evident speed terminating eventually with disastrous impacts. But, drought is a non-event and a creeping phenomenon. Its beginning is subtle and invisible, progress is insidious and deceptively lethargic in spread, and the effect can be devastation. Drought planning, mitigation, and management involve short- and long-term strategies. Drought Impacts are generally non-structural and difficult to quantify. Drought indices quantify a number of tasks, including drought early warning and monitoring by computing severity levels and proclaiming the start and end of drought. Various drought indices were formulated for the forecasting and prediction of spatio–temporal drought characteristics using various *hydro climatological variables*, such as precipitation, evapotranspiration, runoff, soil moisture, etc.

Drought risk mapping is a pre-requisite to identify the severe drought-prone areas. *Landsat satellite* images using ArcGIS is discussed in chapter *drought risk mapping in the North-West region of Bangladesh using Landsat time series satellite images.* The separate spatial maps were generated for each index to identify the most drought-prone districts in Bangladesh. *Rashmi Singh* et al. in their chapter mentioned about quantification of drought condition using drought indices, i.e. a review discussion about *several indices* which can be used for *drought assessment*, *monitoring, and prediction purpose.*

Pallavi Kumari et al. in their chapter adopted *Standardized Precipitation Evapotranspiration Index* (SPEI) as one of the evapotranspiration-based drought indices to understand the drought variability at various time scales along with *Hargreaves model* to calculate *Potential Evapotranspiration* (PET).

Sreedevi and Adarsh studied about spatio–temporal analysis of drought persistence of peninsular India and discuss about drought persistence of the Peninsular India (PI) using a *meteorological drought index*. In this study, they used *Standardized Precipitation Index* (SPI) time series for computing in different aggregation time scales.

4   Water Security

The chief motive of water security is to make sure of water availability at all times. It should ensure enough water to satisfy diverse and sometimes conflicting needs. Water security discusses about good water management, ability to transport, store, provide, regulate, and conserve water. The Global Water Partnership considers water security as the overarching goal of water management [4]. Water security in India has always been one of the major concerns, especially in terms of water quality, availability, and its accessibility as only 40% of the population has access to safe drinking water.

The chapter role of *water governance in ensuring water security*: a case of Indian city discusses about a working definition of water governance, context-specific to the Indian Context. The chapter also critically analyses the *legal and regulatory framework* existing in such a context and provides an empirical foundation for further engagement on a fit-to-purpose implication of such terms and concepts amongst water professionals, academicians, urban planners, and researchers interested in urban water and systems.

India, with merely 4% of the world's freshwater sources and almost one-fifth of the world's population, is facing a water crisis affecting 1 million people every year. The poor urban planning practices and unsustainable use of land and water resources have resulted in frequent urban flooding and threatened many cities with the unavailability of water. The research on *Making Indian Cities Water-sensitive: A Critical Review of Frameworks* critically reviews these toolkits, assessing their scope and replicability in the Indian context. The recommendations from this research include suitable keys taken for Indian cities from the existing *toolkits and framework*.

5 Urbanization and Its Impact on Ground Water Security

The impacts of urbanization on surface water-groundwater security in rapidly urbanizing cities is discussed in chapter *Assessing Groundwater Depletion in Southern India as a function of Urbanization and change in Hydrology*. It discusses about a threat to tank irrigation in Madurai city and an integration of data like rainfall *groundwater*, remote sensing, and *survey* for modelling purpose.

Arif Khan et al. in their chapter developed prediction models on Saskatchewan's water security level by categorizing and assessing the time series parameters of water security using *linear* and *non-linear regression methods*. The seven critical parameters under three significant factors: water consumption, quality, and risk were chosen based on the literature review and available data to quantify the water security and prediction model in Saskatchewan's water security.

The chapter in the water scarcity in the downstream due to factors in the upstream—a case study analyses the sustainability in living conditions in LMRM countries, in concern with the issues in social-economic, and environmental aspects among LMRB countries. In many previous studies, both nationwide and worldwide have indicated negative impacts of hydropower dams on land and water use, especially in *Lower Mekong River Basin* (LMRB).

The study on model prediction for evaluating the raw water quality parameters and its significance in pipe failures of nuclear power plant discusses about prediction and evaluation of raw water quality and the majority of the nuclear system failures could have been minimized by ensuring proper *chemical conditioning* and preventive maintenance.

Rafi et al. assessed drinking water quality of public tube-wells and their spatial distribution in the Rangpur City of Bangladesh and their study aims to assess the water quality of the public tube-wells and find out its suitability as drinking water according to the Bangladesh ECR1997 and WHO guidelines. The *geo-spatial map* generated during study period depicts the distribution of each water quality parameter in Rangpur City. *Farhana Afroz* et al. in their chapter discuss about the water, sanitation, and hygiene condition of the educational institution of Rajshahi known as the educational city of Bangladesh.

The nature's response to river restoration is by limiting the anthropogenic activities as discussed in the chapter analysing the impact of lockdown on the rejuvenation of rivers in Uttar Pradesh, India. During lockdown phases due to restrictions on the upliftment of industrial activities, the rivers restored themselves due to the absence of human anthropogenic activities.

Electro kinetic barrier is the best remediation technology for prevention of saltwater intrusion which allows water and some ion transport but prevents some ions reducing salt intrusion. The methodology adopted for electro kinetic barrier is discussed in the topic prevention of saltwater intrusion: a laboratory-scale study on electro kinetic remediation. The *grey water treatment* by *Biochemical Oxygen Demand* (BOD_5), *Chemical Oxygen Demand* (COD), turbidity, acidity, alkalinity, chloride, phosphorus, and nitrogen were discussed in chapter *integrated onsite grey*

water treatment with constructed wetland for household application. The development in the field of *Nano-technology* for waste water treatment and the solution of water crisis through Nano-technology is presented in chapter *application of Nano-technology in waste water treatment.*

6 Groundwater Conservation Measures and Modelling Techniques

Storm Water Management (SWM) systems involve many challenges including flooding and associated property damage, combined sewer over-flows, and poor water quality in surface waters. Design of storm tech chambers for critical areas by multi-criteria analysis technique is used for identification of water stressed areas as discussed as a case study in chapter *design of storm water management system for the water stressed areas in Palakkad district.*

Mangukiya et al. discussed a case study about efficient and separate storm water drainage network for the Sardar Vallabhbhai National Institute of Technology campus to safely discharge storm water. The *STORMCAD v10.01* is used in design of storm water drainage network and this method can be useful to other educational institutes in India also.

Developing a *Web Application-based Water Budget Calculator (WBC)* in attaining water security in rural Nashik, India is another advanced technique discussed in this book chapter. *Amman Srivatsava* et al. developed a web application-based water budget calculator for attaining water security in rural Nashik in India. The manual calculation of water budget is a challenging one and to overcome this a web application-based WBC is adopted for better water management policies.

7 Natural Hazards

Natural hazards are naturally occurring physical phenomena caused by rapid or slow events. The slow set events can be geophysical, hydrological, climatological, and meteorological. According to United Nations International Strategy for Disaster Reduction (UNISDR), natural hazards may pose a negative impact on the economy, society, and ecology [8].

The chapter in a review of *energy dissipater as a mitigation for dam risk management* reviews energy dissipaters in connection with dam and spillway structure. This study also describes the different types of energy dissipators with different appurtenances used in hydraulic structures for protection work. It includes topics such as energy dissipation of block ramp, hydraulic jump type stilling basin, stepped spillway, and the deflector (flip bucket and ski-jump bucket).

The study *overview of water resources in Kerala and feasibility of coastal reservoirs to ensure water security* presents the current scenario of water resources in the state and proposes alternative ways to ensure water security considering the unique geography of the state.

The next form of natural hazard is *Landslide,* a common geomorphic hazard in most regions of the Western Ghats in India. A number of *environmental*, *geotechnical*, *geological,* and *geomorphological* factors contribute to the occurrence of landslides in this region but rainfall often is the most common and important triggering factor. The case study related to landslide is discussed in chapter location specific rainfall threshold for landslides in select micro-watersheds in Coonoor Taluk, Tamil Nadu, India.

8   Summary

The subsequent chapters in this book discuss relevant topics for assessment of water quantity and quality in a changing environment, disaster risk, their possible future prognosis, as well as adaptation and protection measures. Some of the chapters also pertain to agricultural or energy sectors. Collectively, they cover topics related to hydrology, atmospheric science, remote sensing, energy studies, social sciences, agriculture, as well as environmental science and engineering. Such a collection of state-of-art scientific studies can potentially guide disaster risk resilience, particularly for densely populated highly vulnerable low-income countries of the world.

References

1. Adhikari A, Shah R, Baral S, Khanal R (2011) Terminologies used in climate change. IUCN, Kathmandu, Nepal
2. Bindoff NL, Stott PA, AchutaRao KM, Allen MR, Gillett N, Gutzler D, Hansingo K, Hegerl G, Hu Y, Jain S, Mokhov II, Overland J, Perlwitz J, Sebbari R, Zhang X (2013) Detection and attribution of climate change: from global to regional. In: Climate Change 2013: The Physical Science Basis. Contribution ofWorking Group I to the Fifth Assessment Report of the Intergovernmental Panel on Climate Change. Cambridge University Press, Cambridge, United Kingdom and New York, NY, USA
3. Devendiran DK, Banerjee S,Mondal A (2021) Impact of climate change on multihazard performance river-crossing bridges—Risk, Resilience and Adaptation. J Perform Constructed Facil 35(1), 04020127–1–10
4. GWP Global Water Partnership (2000) (Stockholm: Global Water Partnership) Towards water security: a framework for action
5. Mondal A, Mujumdar PP (2015) On the basin-scale detection and attribution of human-induced climate change in monsoon precipitation and streamflow. Water Resour Res 48:W10520
6. Mondal A, Mujumdar PP (2012) On the detection of human influence in extreme precipitation over India. J Hydrol 529(3):1161–1172
7. SahanaV, Sreekumar P,MondalA,RajsekharD(2020)On the rarity of the 2015 drought in India: a country-wide drought atlas using the multivariate standardized drought index and copula-based

severity-duration-frequency curves. J Hydrol: Reg Stud 31. https://doi.org/10.1016/j.ejrh.2020.100727
8. Shi P (2019) Hazards, disasters, and risks. In: Disaster Risk Science. IHDP/Future Earth-Integrated Risk Governance Project Series. Springer, Singapore. https://doi.org/10.1007/978-981-13-6689-5_1

Climate Change Impact on Water Resources

An Empirical Analysis to Assess Climate Change and Its Effects on Water Scarcity Through Participatory Rural Apprasial (PRA) Approach in Chirirbandar Upazila, Dinajpur

Shabik Zaheer [ID]**, Shabab Ahsan, Md. Mostakim Ahmed, and Abraul Ahmed**

1 Introduction

1.1 Background

Climate change is a big challenge to the water, food security, and welfare of people in the twenty-first century. The impacts of climate change are multi-scale, all-round, multi-level, both positive and negative impacts. Negative climate impacts on water resources are apperceived as having deleterious effects on human health. Insufficient water supplies for drinking, bathing, and farming are not only a current problem but also would increase difficulties for the world's growing population in the future. The Safe Drinking Water Foundation (SDWF 2018) told that 80% of all illnesses in developing countries occurred from unsafe drinking water and the spread of water-borne diseases (Abedin, Collins, Habiba, & Shaw, 2018) [1]. Water resources are affected by climate change because of the water and water quality changes caused by climate factors (mainly includes rainfall and temperature changes) (Nan, Bao-hui, & Chun-kun, 2011) [2]. The most important effect of climate change for water resources is the increase in uncertainty which complicates rational water resources. Because of climate change, surface temperatures were increasing which affected the quantity and quality of water resources which caused water scarcity (Bari, M.N., Roknuzzaman, Islam, & M.T., 2019) [3].

Bangladesh is one of the most astronomically enormous deltas in the world which is highly vulnerably susceptible to natural disasters because of its geographical location. Climate events and climate variability affect production and access to food and water for the different social groups in various regions. As a riverine nation,

S. Zaheer (✉) · S. Ahsan · Md. M. Ahmed · A. Ahmed
Department of Urban & Regional Planning, Rajshahi University of Engineering & Technology (RUET), Rajshahi-6203, Bangladesh

Bangladesh depends on river water for much human consumption like irrigation, transportation, fisheries, etc. Dinajpur district is not different from the conditions and effects of climate change. In Dinajpur, temperature is one of the significant factors of climate which depends on the availability of water. When water loss increases, it increases the temperature through evaporation. It is estimated by the Intergovernmental Panel on Climate Change (IPCC) that the global average surface temperature has risen 0.6 ± 0.2 °C since 1861, and expects an increase of 2 to 4 °C over the next 100 years and that sea levels will rise between 10 and 25 cm since the last nineteenth century (Bari, M.N., Roknuzzaman, Islam, & M.T., 2019) [3]. The more preponderant variability in rainfall could mean more frequent and perpetuated periods of high or low groundwater levels. Overexploitation of groundwater increases the temperature and evaporation and decrease soil moisture.

The component of more preponderant Rajshahi, Dinajpur, Rangpur, and Bogra District of Bangladesh and the Indian territorial Maldah district of West Bengal is geographically identified Barind Tract (Bari, M.N., Roknuzzaman, Islam, & M.T., 2019) [3]. The Dinajpur Barind Tract is in the North-West region of Bangladesh. In the Barind Area, surface water sources are minimal because rainfall is less than the other parts of the country. Chirirbandar Upazila of Dinajpur district is also affected by climate change (Fig. 1).

Chirirbandar Upazila of Dinajpur district has been found as negligible critical areas where annual groundwater level instability varies from 1.5 m to 6.5 m (HASSAN & ISLAM, 2007) [4]. The average maximum temperature from 2005 to 2015 was about 33°C during July and the average minimum temperature was about 12 °C during January (Climate & Weather Averages in Dinajpur, Bangladesh, 2020) [5]. The annual rainfall in Dinajpur is about 1644 mm (Bangladesh Burro Statistics, 2011) [6]. Almost 80% of rain occurs from June to October. High temperature exists in this area during the dry season. Because of Barind, it is located in the flood-free zone. So rainfall is the primary source of groundwater recharging.
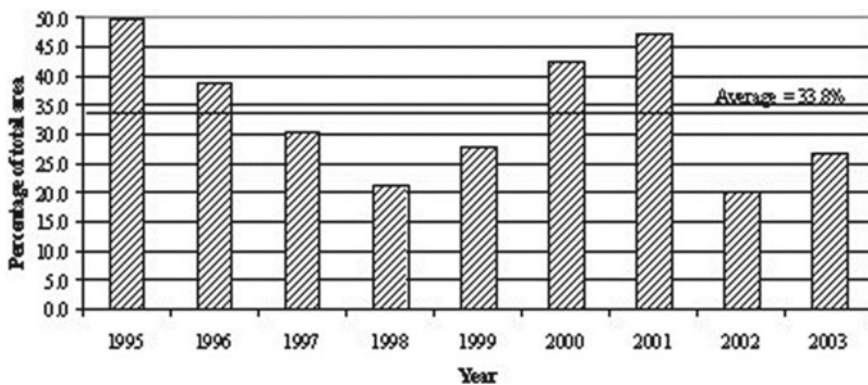
Fig. 1 Percentage of drinking water scarcity during the dry period of different years. *Source* (HASSAN & ISLAM, 2007) [4]

But the lowest amount of precipitation occurs here. Many people of Chirirbandar Upazila are associated with agricultural activities. Because of climate change, the people of Chirirbandar have been suffering badly from the changes in temperature during winter and summer. The primary source of food of Chirirbandar Upazila is their production. But unpredictable weather damage their crops and livestock. As a result, food scarcity and high prices at that time of market make them have only one or two meals in a day; because of high temperature, the moisture of soil is less than is required for the growth of crops. Because of the low level of groundwater, people fail to get deep tube well water. Therefore, many people drink pond water which causes severe illnesses. Groundwater is the primary source of irrigation in Chirirbandar Upazila of Dinajpur. Groundwater is also used for household purposes. Due to decreased ground water level, local livelihood strategies are affected by climate impacts. It also impacts the availability access and use of food through the local food system. This study aims to identify the factors of climate change and the effect of climate change on water scarcity.

2 Methodology

Primary data were collected from field survey and tools of Participatory Rural Appraisal were conducted at Chiribandar upazila, Dinajpur during the period of December 2020. A pre-tested Structured Questionnaire was used to collect the primary data. According to the confidence level of 95 percent and confidence interval of 10 percent, a field survey has been conducted for sample size 78. On the other side, secondary data were collected from various journal papers, articles, newspaper articles, etc. To interact with the people, some PRA (Participatory Rural Appraisal) tools have been selected to reach the depth of the probable outcomes. Through focus group discussion, historical timeline, resource map, mobility map, seasonal calendar, cause and effect diagram, pair wise ranking, etc. Detailed data was found according to our study method. Along with all these measures of PRA tools, the quantitative data analysis with the help of questionnaire survey will provide the statistical data about the targeted objectives of the study.

3 Result and Discussion

3.1 Identification of the Location of the Study Area

Resource map

In the north portion of the map, there are two ponds (Fig. 2). One pond near the mosque has been used for household and fish cultivation purposes. There are also some mixed agricultural lands with crop field, paddy field, wheat, and vegetation fields. Most of

Fig. 2 Resource map of Chirirbandar upazila

the house owners try to adopt the new strategy by growing vegetables behind their houses or on their lawns. There are also some ponds around the houses, some are unable to be used due to bad condition and some are leased by the government. As a result, the villagers have to depend on the Atrai River for drinking water but because of the excessive different usages like bathing and cleaning clothes on the river, it's becoming hard for the villagers to use the river as it's producing many water-borne diseases among the villagers. In the south portion, there is a park named "Abdul Hamid Park." And also there are some potato fields. Besides, there are also three

ponds in the portion, but one of the pond is Government leased and rest of the ponds are unable to be used.

Mobility map

Chirirbandar is an upazila of Dinajpur District in the Division of Rangpur, Bangladesh. Chirirbandar Upazila is divided into 12 union parishads and has a population of 232,409. Almost all the areas of Chirirbandar upazilla have problem of water scarcity. We prepared mobility map through Chirirbandar village people.

Mobility map helps to illustrate people's movement and purpose in the village of Chirirbandar (Fig. 3). From the above mobility map, we can clearly see that in the north, there is a school and some brick kiln. In the north-west part, there is a river named Ichamoti which is used for fishing purpose by local people. On the north south side of Chirirbandar upazila, there is a dam in Atrai river which is used for controlling water flow and sand lifting. There are several ponds but most of them

Fig. 3 Mobility Map of Chiribandar upazila

Table 1 Historical timeline

Time	Important events	Remarks
1914	Establishment of Chirirbandar Thana	
1984	Turned into Upazila	
1971	Archeological heritage	
1991	Irregular rainy season	Establishment of irrigation facility
1994	Drought	Less production in agriculture
2004–2005	Pond became polluted	Less source of pure water
2008	Prolonged dry season	Decreased production rate in agriculture
2017	Shifted toward vegetable cultivation	Need less irrigation

are leased and not repairable. People can only wash their daily cloths and dishes in those ponds. But they can't collect water from those ponds.

Though every household have their own deep tube well, but in the dry season, especially in winter and summer season, the ground water level goes down. So, in some portions, people cannot collect water properly and they have to travel to other households where ground water level doesn't go so far.

Historical timeline

Timeline is an important Participatory Rural Appraisal (PRA) method used to explore the temporal dimensions from historical perspective. It is drawn as a sequential aggregate of past events. The timeline according to local people of Chirirbandar upazila is given in Table 1.

In focus group discussion, some events related to ups and downs of Chirirbandar upazila area have been exposed. Timeline has been used to illustrate diagrammatically the past events which the community remember as being significant.

A focus group of 12 people is formed for timeline. According to them, Chirirbandar thana was established in 1914 and turned into upazila in 1984. After that people began to build massive houses and structures which increased archaeological heritage. Most archaeological heritage is found in 1971 in Chirirbandar upazila. In 1994, a severe drought occurred which decreased the agricultural production and people were starving for a year. From 2004, the use of sanitizer, chemical, poison, plastic increased for agricultural purposes, which polluted the pond and other water resources severely. People shifted towards vegetable cultivation rather than irrigation as they can earn much profit by cultivating different seasonal vegetables and crops like cress, maize, sugarcane, garlic, etc. Though some people earn their livelihood

through fishing in Icahmoti River and Attrai River, but they can hardly lead a happier and healthier life with this limited income.

3.2 Present Condition of the Study Area Due to the Effect of Climate Change

Distance of the water source

The bar chart shows the distance of the water sources like the pump, well, or pond from the villager's house (Fig. 4). It is found from the information that maximum villagers, who are about 26 people from our survey, have to cross more than 1 km to reach their destined water sources. About 21 people have to cross 600 m to 1 km, and about 18 people have to cross 300-600 m to reach the water source. Only, a very small number of people have to cross less than 300 m to reach their destined water source.

Water source type

The above pie chart shows the main water source the villagers use the most (Fig. 5). So, as shown in the chart, the most number of villagers, who are 50%, use well as
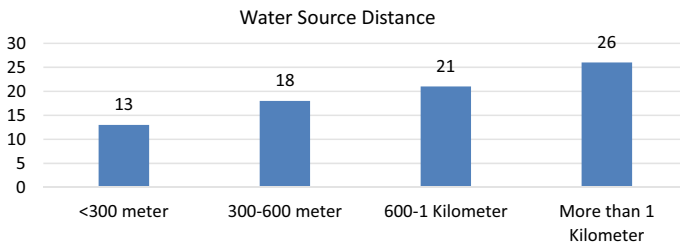
Fig. 4 Distance of water source
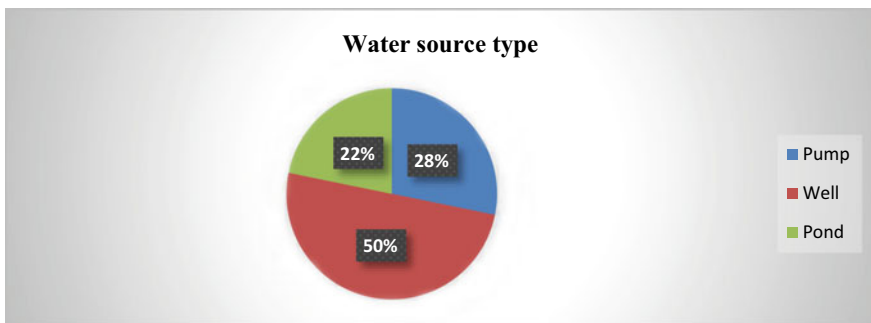
Fig. 5 Water source type

the main water source because they can't afford a pump. About 28% of people use the pump as the main water source. And 22% of people use the pond as the main water source.

Water level

The below bar chart represents the present situation of water ground level according to villagers. As the bar chart shows, according to a maximum number of people, water ground level is increasing day by day. It is becoming hard to get water for the villagers for both drinking and for their agricultural purposes.

Chirirbandar Upazila Agriculture officer says, "The problem is increased by climate change. Drought is constant every year. Due to decreased rainfall irrigation is required even in in the monsoon (Fig. 6). Every year the water level is going down by 0.5 to 0.6 m which is alarming."

Usage of pond

The below pie chart shows the most significant reasons of usage of ponds (Fig. 7). As shown in the chart, maximum number of people use pond water for washing which is about 49%. About 34% people use pond water to cultivate fish and only 17% people use pond water as a source of drinking water. Chirirbandar Upazila
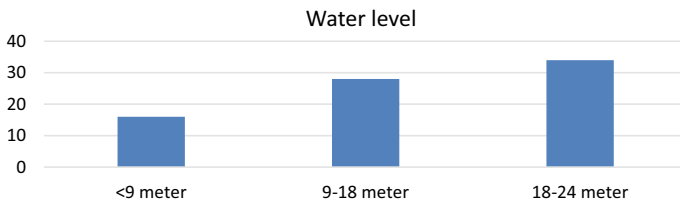
Fig. 6 Water level
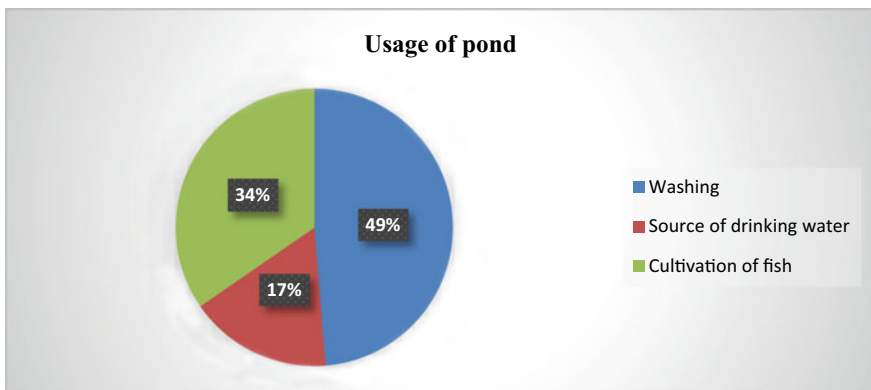
Fig. 7 Usage of pond

Agriculture officer says, "Due to increased use of insecticide and pesticide ponds water are polluting. Also people throwing garbage into ponds which is polluting the ponds. For these reasons fishes are not growing well and people gave up interest for drinking pond water."

3.3 Effects and Causes of Water Scarcity Problem of the Study Area

Cause–effect diagram

With the help of the residents, several causes have been identified that have direct influence behind water crisis during drought (Fig. 8).

The causes of the problem faced by slum people are:

(i) Old ponds are not used because of unrepairable situation and financial problem: There are several ponds in the study area but most of them are unusable because of unrepairable situation. Moreover, most of the people did not want to invest for repairing the pond as they can't get enough profit comparing with the cost.

(ii) High elevation of land: Most of the land in Chirirbandar upazilla is situated on the upland. During dry season, especially winter season, water swipe away to lower land which creates great scarcity of water.

Effects	Problem in Agricultural	Problem in managing livestock	Problem in household activity	Diseases	Huge load shedding occurred for excessive irrigation	Crowd on water pump	Decreased production in agriculture

Problem 1	Water crisis during drought

Causes	Old ponds are not able to use because of unrepairable situation and financial problem	High elevation of land	Reduced rainfall	Prolonged dry season	Decreasing ground water level due to irrigation

Fig. 8 Cause–effect diagram

(iii) Reduced rainfall: Water comes into the atmosphere through evaporation. The air cools down in the study area especially in winter season and it could become oversaturated and the water can come out in the form of precipitation which reduced the rainfall of the study area.

(iv) Prolonged dry season: Chirirbandar upazila experiences a hot, wet, and humid tropical climate. Under the Köppen climate classification, Chirirbandar has a tropical wet and dry climate. The district has a distinct monsoonal season, with an annual average temperature of 25 °C (77 °F) and monthly mean varying between 18 °C (64 °F) in January and 29 °C (84 °F) in August.

(v) Decreasing ground water level due to irrigation: Farmers use pump for irrigation which decreases the ground water level.

Effects of the problem:

The water crisis during drought led to many adverse effects. According to the opinion of the community, the most arising effects are.

(i) Problem in Agriculture: Farmers don't get proper water because of scarcity of water as water level goes down during drought.

(ii) Problem in household activity: People use electricity pump during irrigation that increases their cultivation cost. People cannot get enough water from deep tube well as water level goes down due to more use of pump and they can't maintain their household activity properly.

(iii) Diseases: Waterborne diseases increased in a huge number.

(iv) Huge load shedding occurred for excessive irrigation: Farmers use mostly electrical pump for irrigation that creates much pressure on electricity. As a result, load shedding is a common problem during irrigation time.

(v) Decreased production in agriculture: facilities agricultural production decreasing day by day.

Agricultural crop type

This pie chart represents the crops villagers grow the most (Fig. 9). As shown in the chart, almost half of the percentage grow grains which is 42%. And as the water
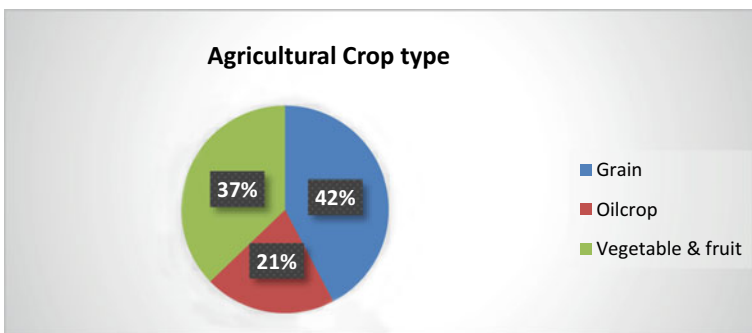
Fig. 9 Agricultural crop type

level is going down, so a lot of people have shifted from growing rice to growing vegetables and fruits. About 37% people grow vegetables and fruits. Rest percentage of people grow oil crop which is about 21%.

Farmer Nazmul says, "Ground water is declined. Paddy is not feasible for livelihood. So, we want to shift into vegetable. But there is no irrigation facility or training program for us. If we can have training then we can shift into other crops and vegetables for better income."

Pair wise ranking

The Chirirbandar upazilla has identified a number of problems. Due to these labyrinths, the scarcity of water is increasing day by day. It's very difficult to solve all the problems at once. But in order to improve the water demand, they need to be addressed. So, it is important to rank these problems in order to solve the labyrinths on priority basis. For these purposes, community was asked to prioritize problem among all problems. By following these, all the problems have been ranked through their priority. Finally, the most critical problems and most wanted solving issues are recognized among the identified problems.

Problems of the community that needs to be solved

Most prioritized problem: Scarcity of pond: Pressure on water resources is increasing in several parts of Chirirbandar upazila. Pollution is becoming one of the main threat to the availability and reuse of water. Increasing use of fertilizers, soil depletion, and poor waste disposal condition are decreasing the water sources and polluting the pond water. Moreover, construction of building and structures filling the pond is one of the main reason of scarcity of pond in Chirirbandar Upazila.

Second prioritized problem: Excessive irrigation: Farmers use pump for irrigation and there is no other way to collect water for irrigation. Excessive use of pump pressurizes the limited water resources and thus leads to scarcity of water in Chirirbandar upazila. Again, most of the soil in Chirirbandar Upazila is Loamy soil which absorb less rain water.

Third prioritized problem: Prolonged dry season: Chirirbandar upazila experiences a hot, wet, and humid tropical climate. Under the Köppen climate classification, Chirirbandar has a tropical wet and dry climate. The longevity of dry season in Chirirbandar upazila is nearly 6 months beginning from winter season. In this time, farmers cultivate Boro rice and they need more water. But for the prolonged dry season and hot weather, the ground water level goes down and thus increases water scarcity in the study area (Table 2).

Seasonal calendar

Code: LP (Land preparation), M (Application of animal manure), PS (Planting seeds), W1 (Digging; 1st weeding), W2 (Weeding), BS (bird scaring), HV (Harvesting), T (Threshing), ST (Storing), SL (Selling), Quantity(x) (Table 3).

Different seasonal issues of the community:

- Use of adjacent water source: Though every household have their own deep tube well, but in dry season especially in winter and summer season, the ground water

Table. 2 Pair wise ranking

Problems	Excessive irrigation (a)	Prolonged dry season (b)	Irregular rainy season and reduced rainfall (c)	Scarcity of pond (d)	Loamy soil which absorb less rain water (e)	High elevation of land (f)	Frequency	Ranking
Excessive irrigation (a)	X	a	a	d	a	a	4	Second
Prolonged dry season (b)	X	X	b	d	b	b	3	Third
Irregular rainy season and reduced rainfall (c)	X	X	X	d	e	c	1	Fifth
Scarcity of pond (d)	X	X	X	X	d	d	5	First
Loamy soil which absorb less rain water (e)	X	X	X	X	X	e	2	Fourth
High elevation of land (f)	X	X	X	X	X	x	0	Sixth

level goes down. So in some portions, people cannot collect water properly and they have to travel to other households where ground water level doesn't go so far.

- River water Quality: The quality of the river water is bad for 5 months throughout the year. The months are April to August. The quality is good for the rest of the months.
- Sanitation status: Overall, the sanitation facility of this area is not good. But during 3 months (June, July, and August) of the monsoon, the situation becomes more miserable.
- Income: Most of the people here are farmers. They earn fairly well all year long. Income increases in November and December because people harvest crops such as Aman and Boro in this period.

Table. 3 Seasonal calendar

Month / Criteria	Vote	Aug	Sep	Oct	Nov	Dec	Jan	Feb	Mar	Apr	May	Jun	July	Aug	Sep
Rice (Aman)	9								LP	LP	M		PS	W1,W2	T,ST	SL
Rice (Aman)	4		LP	LP,	M,	PS	W1,	W2	HV						
Rice (Boro)	8					LP	LP, M	M, PS	PS,	W1, W2	W2	HV (g)	PS	W1,W2	T,ST	SL
Precipitation High / Low	9	↓	↓	↓	↓	↓	↓	↓	↓	↑	↑	↑	↑	↓	↓
Drought (x)	9					xxxx	xxxx	xxxx	xxxxx						
Use of adjacent water source	9	(pump)	(pump)	(pump)	(pump)	River/ Pond	River/ Pond	River/ Pond	River/ Pond	(pump)	(pump)	(pump)	(pump)	(pump)	(pump)
River water quality	9	👍	👍	👍	👍	👍	👍	👍	👍	👎	👎	👎	👎	👍	👍
Sanitation Poor / Very poor	9	●	●	●	●	●	●	●	●	(vp)	(vp)	(vp)	(vp)	●	●
Income Ok / Not ok	9	✓	✓	✓	✓	OK	OK	OK	OK	✓	✓	✓	✓	✓	✓
Wheat										LP	PS	W1,W2	T	ST+SL	ST+SL
Maize	5		LP	LP		PS	PS, W1	W2		HV	T+SL				
Eggplant	4						W1			ST					
Charcoal making	4	Xx	xx	xx	x					x	xx	xx			
Livestock	9	Xx	xx	xx	x			xx	xx	x	xx	xx	xx	x	xx
Fishing in pond	3	X	x	x	x	x	x	x	x	x	xxx	xxx	xxx		
Potato	2		LP	LP			PS	PS, W1	W2		HV	T+SL			

- Shifting towards vegetables: Because of the huge requirement for irrigation in grain crops, farmers nowadays are more interested in vegetable farming. Due to lack of ground water, people need to shift to vegetable production as vegetables need less irrigation.

4 Conclusion

This research implies that PRA is a useful method for assessing groundwater degradation and its impact on the livelihoods of Chirirbandar, overcoming data gaps and better understanding of the views of local stakeholders on the issues, their causes,

and appropriate adaptation strategy. PRA method gave a clear picture about groundwater degradation due to its excessive use and the effect this had on the livelihood of the community (a higher cost of farming, increased poverty, and lack of irrigation source and drinking water source). Nowadays, it has become a crying need to have safe drinking water in the study area of Chirirbandar. Rainwater recharge, excavation, regeneration and protection of ponds, large surface and spring water storage for lean times are possible options that need immediate attention for developing sound multisource water system for Chirirbandar. Also, Modern water management technology such as alternative wetting and drying (AWD), water-saving technology such as hose irrigation, drip irrigation, adaptive climate change technologies such as drought-tolerant crop varieties, etc., need to be introduced to local farmers with proper training and campaign. Training regarding vegetable farming need to be organized. Unfit ponds need to be renovated and unfit wells and pumps need to be replaced immediately to solve water scarcity problem. Community views and suggestions need to be considered and studied in a multidisciplinary manner, including technical, social, and economic factors, by the relevant government institutions to solve this water scarcity issue. In addition, attention needs to be given to examining the wider impacts of the suggested solutions which will help in the policy- and decision-making process and facilitate effective implementations.

References

1. Abedin MA, Collins AE, Habiba U, Shaw R (2019) Climate change, water scarcity, and health adaptation in Southwestern Coastal Bangladesh. Int J Disaster Risk Sci 10(1):28–42. https://doi.org/10.1007/s13753-018-0211-8
2. Yang N, Men BH, Lin CK (2011) Impact analysis of climate change on water resources. Procedia Eng 24:643–648. https://doi.org/10.1016/j.proeng.2011.11.2710
3. Bari NM, Roknuzzaman M, Islam MT, Niamul M (2019) Effect of climate change on water resources in Barind tract of Rajshahi District effect of climate change on water resources in Barind tract of Rajshahi district department of civil engineering. Hajee Mohammad Danesh Science & Technology
4. Hassan T, Islam S (2007) Application of GIS to identify spatial and temporal extent of critical condition for rural drinking water supply during dry season. Int Conf Water Flood Manag 1:413–420
5. Climate & Weather Averages in Dinajpur, Bangladesh. https://www.timeanddate.com/weather/bangladesh/dinajpur/climate?fbclid=IwAR3nF8zmhzKTYM8_gyuQso64U2QicgvZpfPapERdhIc8v1zhiQx6QGHQgV8. (Accessed 15 Jan 2021)
6. Statistics D, District B (2013) Bangladesh Bureau of Statistics (BBS) Statistics and Informatics Division (SID) Ministry of Planning, Government of the People's Republic of Bangladesh. www.bbs.gov.bd. (Accessed 15 Jan 2021)

Scenario-Based Analysis of Climate Change Impacts on Muzza Irrigation District

Ahmed O. Khalid and Mohammed Al-Ajamee

1 Introduction

Agriculture is globally affected by the extent of climate change. Agricultural patterns and yield depend heavily on the variation of average temperatures which in turn influence climate extremes such as droughts and heat waves, as well as rainfall, variations in atmospheric carbon dioxide and ground-level ozone concentrations, and other phenomena. Other environmental factors such as pests and plant-borne diseases are also of concern.

Anthropogenic greenhouse gas (GHG) emissions result directly from population inflation, wasteful lifestyles, energy expenditure, economic boom, land utilization structures, commercial technological advances, and current scope of climate regulations. As far as the previously mentioned factors are concerned, greenhouses gas (GHG) emissions will follow one of four routes in the twenty-first century. These routes are the Representative Concentration Pathways (RCPs), projecting GHG presence in the atmosphere, air pollution, and land utilization. A tight reduction strategy (RCP2.6), two medium options (RCP4.5 and RCP6.0), and one option with excessive GHG emissions are all included in the RCPs (RCP8.5). Nonetheless, scenarios with no further measures to restrict emissions ("baseline scenarios") result in RCP6.0 to RCP8.5 pathways. RCP2.6 is a scenario effort to maintain global warming less than 2 °C [1].

The precipitation and temperature projections were obtained from the work carried out by EURO-CORDEX [2], a software package led by the World Climate Research Program (WRCP) that aims to put in place a globally coordinated body to enhance

A. O. Khalid

Department of Civil and Environmental Engineering, Politecnico di Milano, p.za L. da Vinci 32, 20133 Milan, Italy

e-mail: Ahmedothman.khalid@mail.polimi.it

A. O. Khalid · M. Al-Ajamee (✉)

Water Research Center, Faculty of Engineering, University of Khartoum, Khartoum, Sudan

regional climate change estimates. It is worth mentioning that CORDEX results are being used as a source of data for studies on the implications and adaptation within the timeframe defined in the Intergovernmental Panel on Climate Change (IPCC) fifth Assessment Report (AR5).

Downscaling is used to link between climate model outputs' temperature and precipitation cropped spatially over Muzza irrigation district, and the values of the same variables on a local scale are matched using quintile mapping statistical downscaling method [3, 4].

Finally, the crop yield is estimated by the famous Food and Agriculture Organization (FAO) productivity model, AquaCrop [5].

2 Material and Methods

This work is built using MATLAB [6], allowing easy processing of data and results. Work flow can be seen in three steps: processing the data, downscaling, and productivity estimation.

2.1 Processing Data

Data of EURO-CORDEX are in 5 years blocks distributed as NetCDF files, starting from 1951 to 2005 as historical data, and scenarios are projected from 2006 to 2100. The model domain expands over latitudes (27 N–72 N) and longitudes (22 W–45E). The exact models, the resolution, and all other information of specific block of the data appear in the name (e.g., "pr_EUR-44_NOAA-GFDL-GFDL-ESM2M_rcp85_r1i1p1_SMHI-RCA4_v1_day_20960101-21,001,231.nc").

As mentioned before, RCP8.5 and RCP4.5 were compared, and to roughly look through the climate change, each scenario presenting a snapshot of January 15th has been observed for every 10 years starting from 2010 until 2100, as approximately it represents the coldest day of the year. In the same way, July 15th also may be the warmest day of the year, so it has been also compared over the same years.

The domain which contains the area under consideration lies down from, longitudes (9.3E–9.9E) and latitudes (45.05 N–45.5 N), which is cut in the larger domain available by EURO-CORDEX; this step presents the dynamical downscaling.

2.2 Downscaling

Global Climate Models (GCMs) currently do not provide reliable information on scales below 200 km [7]. Hydrological processes typically occur on finer scales

[8]. In particular, GCMs cannot resolve circulation patterns leading to hydrological extreme events [9].

A combination of dynamical and statistical downscaling is adopted. The project observations of precipitation and temperature for the period between 1/1/1993 till 31/12/2007 were available, as a single value could not represent the wide Muzza district, there are several observations spatially distributed. Space unit is a cell, each cell has different properties (e.g., soil characteristics), the cell considered is number 25.

Downscaling is based on the quantile-quantile (Q-Q) plot between observed time-series and control time series simulated through a climate model over the same time period of the observed series. A Q-Q plot is a probability plot (i.e., a graphical method for comparing two probability distributions) by plotting their quantiles against each other. The Q-Q plot is used as a correction function in order to match the control time series cumulative distribution function (CDF) with the observed CDF. The scenario time series, i.e., the series simulated through the climate model over a future period, is downscaled using the same correction function used to downscale the control time series.

The climate model outputs for both precipitation and temperature between 1/1/2001 and 31/12/2005 are set as the control time series to estimate the correction function that relates them to observations over the same period. Then, correction function is applied to obtain a local estimate of the same variables for every 10 years starting from 2010 until 2100.

2.3 *Productivity Estimation*

AquaCrop is a crop-water productivity model that simulates yield response to water availability, as it describes the relationship between crop yield and water shortage because of inadequate irrigation or rainfall during the agricultural lifecycle.

Yield approximations can provide an insight into worst and best-case scenarios over different years. To estimate the yield, one cell in the project is adopted, the cell data changed are temperature and precipitation, other data are assumed to be the same in the future. Multiple crops are cultivated in the area; planting Maize constantly is adopted to compare climate scenarios.

3 Results and Discussion

First, to understand the nature of RCP8.5 and RCP4.5, Fig. 1 illustrates the trend in average annual temperature at Muzza irrigation district following RCP8.5 and RCP4.5; RCP8.5 predicted a continuous increase in average temperature up to over 15 °C by the end of the century.
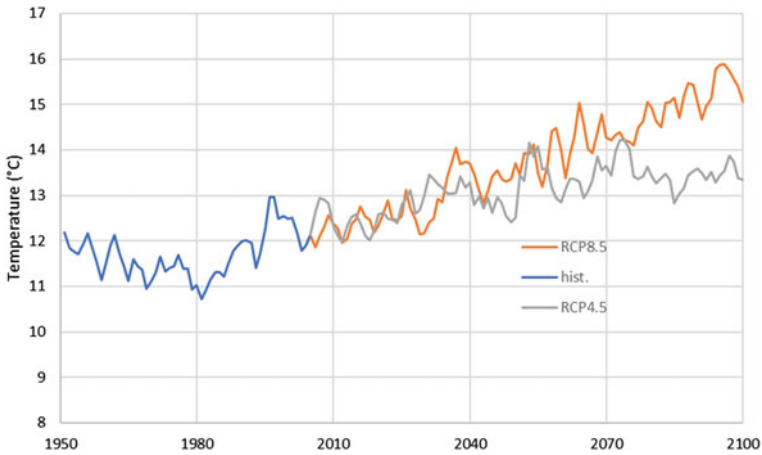
Fig. 1 Annual average temperature from 1951 to 2100 for RCP8.5 and RCP4.5

For RCP 8.5, the precipitation trend shows a reduction until mid-century followed by a period of stabilization in cumulative annual precipitation. When the case for RCP 4.5 shows a drop by half for the last quarter of the century Fig. 2, seasonal variability of rainfall amount is discussed further for specific years with extraordinary crop yield.

The projections of temperature and precipitations are downscaled considering two scenarios (RCP 8.5 and RCP 4.5) for ten non-consecutive years (2010 to 2100
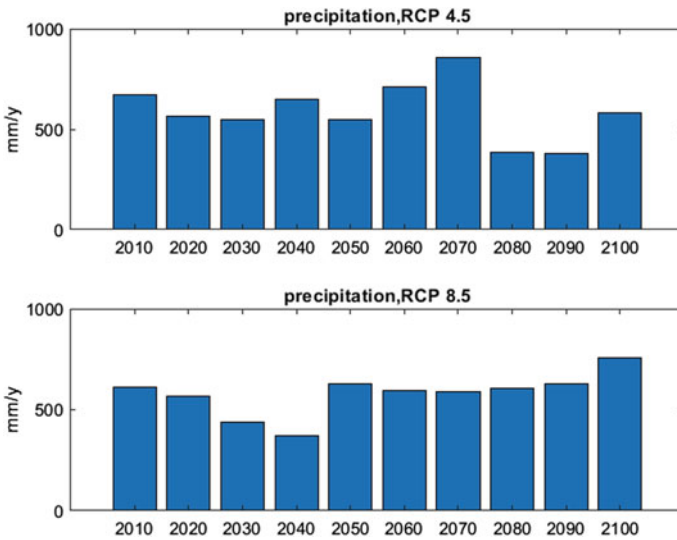
Fig. 2 Cumulative annual precipitation every 10 years from 2010 to 2100 for RCP8.5 and RCP4.5

with ten years interval). As a result, the downscaling process has been repeated 40 times. Each time, the control and observed data are GCM data and locally measured records, respectively—both over five years period from 1/1/2001 to 31/12/2005. The projection series in each process is a five years block that must contain the year of interest. In the following paragraph, a full distribution of downscaling of precipitation output of climate model powered with RCP8.5 to obtain local precipitation for the year 2010 is given.

Projection series includes 2010 extended from 1/1/2006 to 31/12/2010, the first phase, calibration phase to obtain the correction function. The CDF plot Fig. 3, shows how control underestimates the observed and Fig. 4 shows the correction function for the control period, which will increase the values of control data. Downscaling may well represent the amount of precipitation to some extent, but it fails to represent the temporal variability (see Fig. 5).

Concerning temperature, the GCM predictions fluctuate between underestimating and overestimating the observed data. Worth mentioning, the model outputs are slightly higher than observations for records between 0 °C and 8 °C, while for over 8 °C, the observations are three degrees warmer than model predictions (see Fig. 6).

Fig. 3 Cumulative distribution function for observed and control daily precipitation (2001–2005)
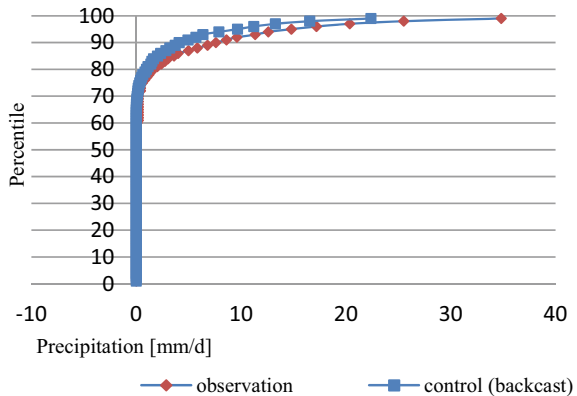
Fig. 4 Q-Q (correction function) of precipitation data, solid line is the reference
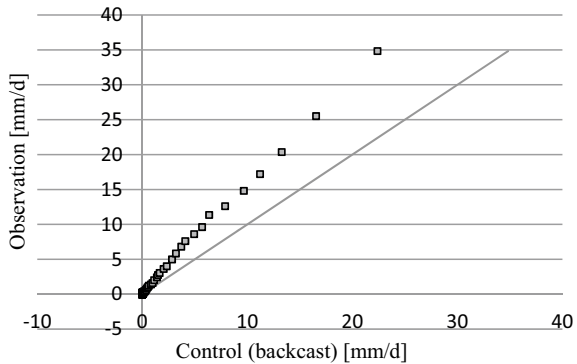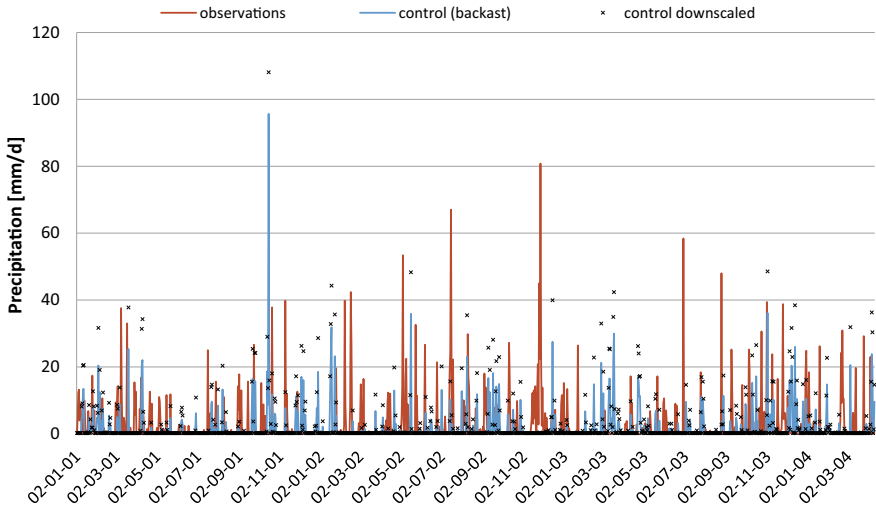
Fig. 5 Observed, GCM, and Downscaled precipitation
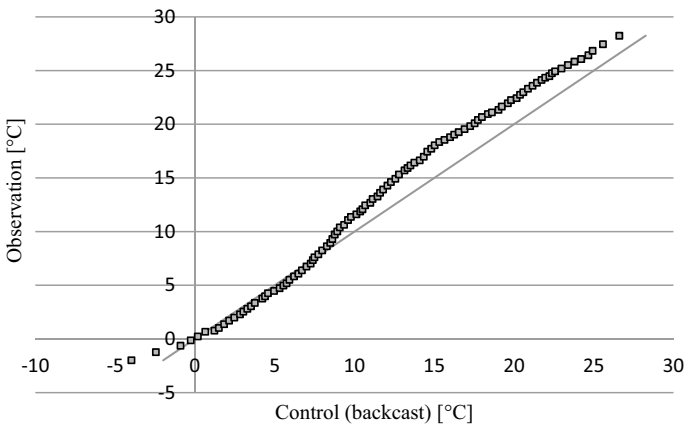
Fig. 6 Q-Q (correction function) of temperature data, solid line is the reference

Eventually, looking into the yield of Maize, Table 1 shows huge variation in results, which can be further investigated by looking into the figures deeply. However, RCP4.5 guarantees a weaker yield generally, with the lowest yield in 2050, on the other hand, RCP8.5 shows better results.

The year of maximum and minimum yield is compared with full projections of temperature and precipitation, the zone of the maize planting cycle is illustrated, it is obvious how precipitation intensity is the key factor in crop yield as shown in Figs. 7, 8, 9, and 10.

Table 1 Yield for every year and scenario with corresponding average temperature and cumulative precipitation

Year	Average Temperature [°C]		Cumulative Precipitation [mm]		Yield	
	RCP4.5	RCP8.5	RCP4.5	RCP8.5	RCP4.5	RCP8.5
2010	12.73	13.11	669.48	610.68	816.57	3502.53
2020	12.75	11.82	566.54	569.15	6482.54	10,571.86
2030	13.34	12.52	548.78	436.77	5360.54	3442.70
2040	12.48	14.23	649.84	374.02	10,961.90	995.19
2050	13.49	13.26	549.84	627.38	793.00	6750.31
2060	13.02	13.16	712.15	594.98	5654.94	17,229.42
2070	12.57	14.46	855.16	590.60	7600.61	1700.11
2080	13.71	14.87	386.84	607.99	862.41	2938.53
2090	13.95	14.95	379.51	626.10	2903.08	1197.68
2100	13.10	14.58	581.75	757.64	817.14	11,560.68
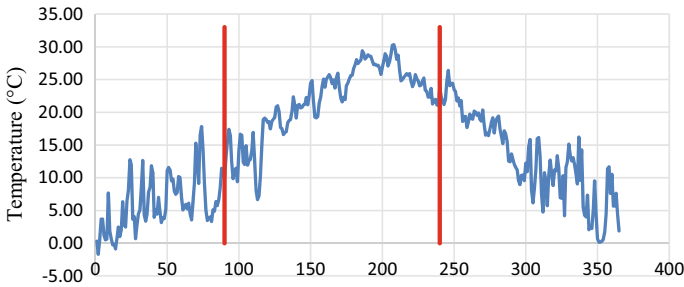
Fig. 7. 2050 daily average temperature, maize planting cycle indicated with red lines (RCP4.5 minimum yield)
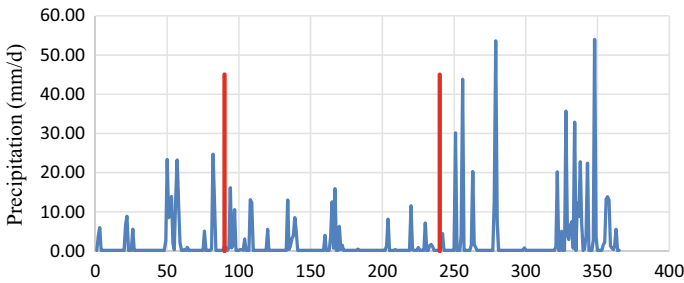
Fig. 8. 2050 daily precipitation, maize planting cycle indicated with red lines (RCP4.5 minimum yield)
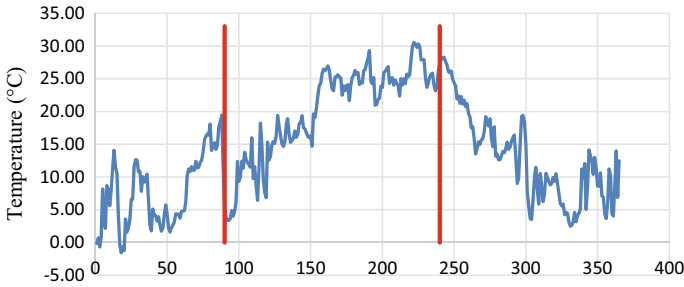
Fig. 9. 2060 daily average temperature, maize planting cycle indicated with red lines (RCP8.5 maximum yield)
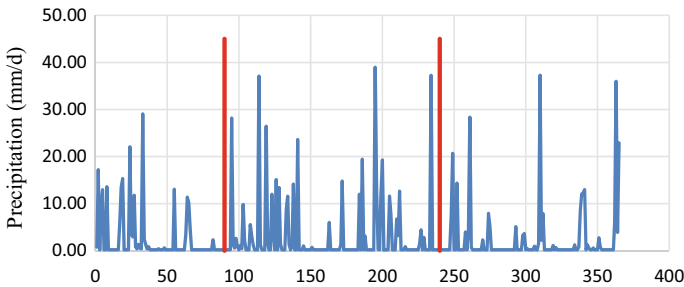
Fig. 10. 2060 daily precipitation, maize planting cycle indicated with red lines (RCP8.5 maximum yield)

4 Conclusions

Climate change impacts crop yield at Muzza irrigation district in Lombardy, Italy considering two scenarios, namely, RCP8.5 and RCP4.5 of the Intergovernmental Panel on Climate Change (IPCC) fifth assessment report. Conclusions obtained from the study are as follows.

(1) Downscaling needs to be developed to minimize the uncertainty it imposes.
(2) Crop yield is more sensitive towards precipitation than thermal variation.
(3) Agricultural productivity depends not only on water availability but also on other factors like land use and the proficiency of agricultural managers, so results must be further adjusted upon mentioned factors. Extended periods of extreme-hot weather accompanied by below-average precipitation can cause moisture stress to maize that would negatively affect yield.

References

1. Pachauri R, Meyer L (2014) Contribution of working groups I, II and III to the fifth assessment report of the intergovernmental panel on climate change. In: Pachauri RK, Meyer LA (eds) Core Writing Team
2. EURO-CORDEX (2021) [Internet]. https://www.euro-cordex.net/
3. Déqué M (2007) Frequency of precipitation and temperature extremes over France in an anthropogenic scenario: model results and statistical correction according to observed values. Glob Planet Change 57(1–2):16–26
4. Boé J, Terray L, Habets F, Martin E (2007) Statistical and dynamical downscaling of the Seine basin climate for hydro-meteorological studies. Int J Climatol A J R Meteorol Soc 27(12):1643–55
5. AquaCrop (2021) Food and agriculture organization of the United Nations [Internet]. http://www.fao.org/aquacrop/en/
6. MATLAB (2021) MathWorks - MATLAB & Simulink [Internet]. https://www.mathworks.com/products/matlab.html
7. Meehl GA, Stocker TF, Collins WD, Friedlingstein P, Gaye AT, Gregory JM et al (2007) Climate change 2007: the physical science basis. In: Contribution of Working Group I to the Fourth Assessment Report of the Intergovernmental Panel on Climate Change. Cambridge University Press, pp 10013–2473
8. Kundzewicz ZW, Mata LJ, Arnell NW, Doll P, Kabat P, Jimenez B, et al (2007) Freshwater resources and their management. In: Parry ML, Canziani OF, Palutikof JP, van der Linden PJ, Hanson CE (eds) pp 173–210
9. Christensen JH, Christensen OB (2003) Severe summertime flooding in Europe. Nature 421(6925):805–806

Flood Risk Assessment at the Douro River Estuary

Willian Weber de Melo, José Pinho, Isabel Iglesias, Ana Bio, Paulo Avilez-Valente, José Vieira, Luísa Bastos, and Fernando Veloso-Gomes

1 Introduction

Understanding the effects of climate change (CC) and forecasting the associated impacts is a global challenge that encompasses different science fields. The increase of greenhouse gases concentration in the atmosphere is hardly modifying the environment, and forecasting its consequences is essential to elaborate and implement proper mitigation measures. Estuaries are among the most threatened ecosystems to CC [1]. The expected increase in the number and intensity of extreme events and the

W. Weber de Melo (✉) · J. Pinho · J. Vieira
Department of Civil Engineering, University of Minho, Campus of Gualtar, 4710-057 Braga,
Portugal
e-mail: id9257@alunos.uminho.pt

J. Pinho
e-mail: jpinho@civil.uminho.pt

J. Vieira
e-mail: jvieira@civil.uminho.pt

I. Iglesias · A. Bio · P. Avilez-Valente · L. Bastos · F. Veloso-Gomes
Interdisciplinary Centre of Marine and Environmental Research (CIIMAR/CIMAR), Terminal de
Cruzeiros Do Porto de Leixões, University of Porto, Av. General Norton de Matos s/n, 4450-208
Matosinhos, Portugal
e-mail: iiglesias@ciimar.up.pt

A. Bio
e-mail: anabio@ciimar.up.pt

P. Avilez-Valente
e-mail: pvalente@fe.up.pt

L. Bastos
e-mail: lcbastos@fc.up.pt

F. Veloso-Gomes
e-mail: vgomes@fe.up.pt

sea-level rise (SLR) jointly with anthropogenic actions can modify estuarine complex dynamics, with potential effects over the fauna and flora, generating economic and social losses [2].

One methodological approach to study estuarine hydrodynamics is based on numerical modelling tools. It consists of solving the estuarine physical governing equations by numerical methods, creating digital models of these complex systems, and collecting field data, such as bathymetry, river flow discharges, water levels, and current velocities, to set up and calibrate the model. The model calibration parameters/coefficients values can be estimated by reducing the differences between simulated and observed data. Different numerical tools can assist in the accomplishment of this objective, lowering the computational and human implementation costs. After the previously mentioned steps, the last one is the definition of scenarios of interest, in which conditions are defined and imposed as model boundary conditions.

The Douro estuary, located in northern Portugal (Fig. 2), was the focus of previous studies. Balsinha et al. [3] studied the textural composition of the Douro sediments and its relation with hydrodynamics, Bordalo et al. [4] evaluated the water quality of the river during 10 years, and Iglesias et al. [5] linked observed hydrodynamic patterns with the distribution of several pollutants and set up two numerical models of the Douro estuary to assess the flood risk and the breakwater effects in the estuary considering river flows from historical floods [6]. This work intends to update the flood risk assessment in the Douro estuary, the impacts of which regarding previous climate scenarios were already studied [7], by considering the effects of different representative concentration pathway (RCP) scenarios, which represents future greenhouse gases concentration in the atmosphere that can be associated to different ESL [8].

The Douro estuary region is densely occupied, and the lower 8 km of the estuary margins are heavily modified by urbanization (cities of Porto and Vila Nova de Gaia with 700,000 inhabitants) [9]. The estuarine region is economically important mainly due to intense touristic activity and Port wine cellars businesses, being important to preserve the navigation conditions [10, 11].

2 Methodology

The methodological approach comprises five main steps. Firstly, forecasted future trends and field data such as bathymetry, river flow discharges, and historical water levels were selected. Secondly, the model was set up with the Delft3D software, which can simulate the possible effects of the CC over the hydrodynamic patterns. The grid was generated and the open boundary conditions were defined, the first one, an ocean

P. Avilez-Valente · F. Veloso-Gomes
Faculty of Engineering, University of Porto, Rua Dr Roberto Frias s/n, 4200-465 Porto, Portugal

L. Bastos
Department of Geosciences Environment and Spatial Planning, Faculty of Sciences, University of Porto, Porto, Portugal

boundary, at the Atlantic ocean boundary and the second one, a fluvial boundary located at the upstream estuarine limit located at Crestuma dam. Thirdly, the model was calibrated with the data assimilator OpenDA software [12], which automatically estimates the model calibration parameters/coefficients values by minimizing the error between observed data and simulated results.

After that, simulation scenarios were defined, considering different extreme sea levels (ESL) and extreme flood discharges (EFD), according to different RCP scenarios. Uncertainty was taken into account by considering different return periods (50, 100, and 1000 years) for the ESL and EFD. Also, these return periods allow estimating extreme events water levels and current velocities for planning and designing of estuarine infrastructures. Lastly, the simulated results are analysed.

2.1 Numerical Model

The Delft3D software was selected to implement a 2DH model of the Douro estuary. This software solves the Reynolds averaged conservation equations of mass and momentum, being able to simulate hydrodynamics with acceptable accuracy [6, 13].

Fluvial discharges were imposed at the upstream open boundary, considering the extreme values derived from historical data. At the downstream (oceanic) open boundary, delimited by the 26 m-depth isobaths, the extreme ocean water levels were also imposed. The model grid was limited by the river banks and the open boundaries. The spatial resolution varies from 22 m at the river mouth to 360 m at the ocean boundary. The time step was 0.5 min to guarantee numerical stability during simulations. The model's bathymetry was obtained from the Hydrographic Institute of the Portuguese Navy (IH, https://www.hidrografico.pt/).

2.2 Climate Change Scenarios

Simulated scenarios considered the future climate change effects in terms of ESL at the coastal zone near the river Douro estuary mouth and river flood peak discharges. Different ESL resulting from different RCP scenarios [8] and EFD with 50, 100, and 1000 years return period was considered, estimated according to a Gumbel law for the upstream open boundary. Scenarios information is summarized in Table 1.

The fluvial boundary was defined as a constant discharge, thevalue of which varied according to the considered EFD. The ESL for each scenario was defined at the open ocean boundary. This value was also used as the estuarine initial water level.

Table 1 Climate change conditions scenarios

Scenario	Return period (years)	EFD (m^3/s)	RCP scenario	ESL elevation at the ocean boundary (m)
S1_50	50	11,235	Historical	2.9
S2_50	50	11,235	RCP 4.5 2050	3.1
S3_50	50	11,235	RCP 4.5 2100	3.4
S4_50	50	11,235	RCP 8.5 2050	3.2
S5_50	50	11,235	RCP 8.5 2100	3.7
S1_100	100	17,634	Historical	3.0
S2_100	100	17,634	RCP 4.5 2050	3.2
S3_100	100	17,634	RCP 4.5 2100	3.5
S4_100	100	17,634	RCP 8.5 2050	3.2
S5_100	100	17,634	RCP 8.5 2100	3.7
S1_1000	1000	24,629	Historical	3.3
S2_1000	1000	24,629	RCP 4.5 2050	3.5
S3_1000	1000	24,629	RCP 4.5 2100	3.7
S4_1000	1000	24,629	RCP 8.5 2050	3.4
S5_1000	1000	24,629	RCP 8.5 2100	4.0

2.3   Automatic Calibration with OpenDA

The calibration procedure consists of adjusting the model's calibration parameters/coefficients values to minimize the error between observed data and simulated results. To reach a successful result, it is needed to run many simulations with different parameters/coefficients values, until the combination that results in an acceptable error is found. This procedure generates large amounts of data that need to be analysed. The use of automatic calibration methods can optimize this task and reduce the time needed to reach an acceptable error.

To automatize the model calibration task, the OpenDA tool was selected. The procedure consists of running the model several times while determining the value of an error cost function (Eq. 1) that calculates the difference between the observed data and model results.

$$J_{(x0)} = \sum_{K=1}^{N} (y^0(k) - H \cdot x(k)) R^{-1} ((y^0(k) - H \cdot x(k)))$$

(1)

where: $\times 0$ is the initial value of the parameter(s) to be determined, x(k) is the parameter(s) value at time k, H is the observatory operator, y^0(k) is the observation value at time k, N is the total number of time steps, and R is the covariance.

For the proper performance of this tool, it is also needed to select observation points in the model, where observed data are available. In this work, the observation

point located at Cais dos Banhos (Fig. 1) was chosen. At this location, the root square mean error (RMS), bias, and standard deviation (STD) were computed. Selected calibration parameters/coefficients were the Manning coefficient and the phase and amplitude of the harmonic tidal constituents M2 and S2.
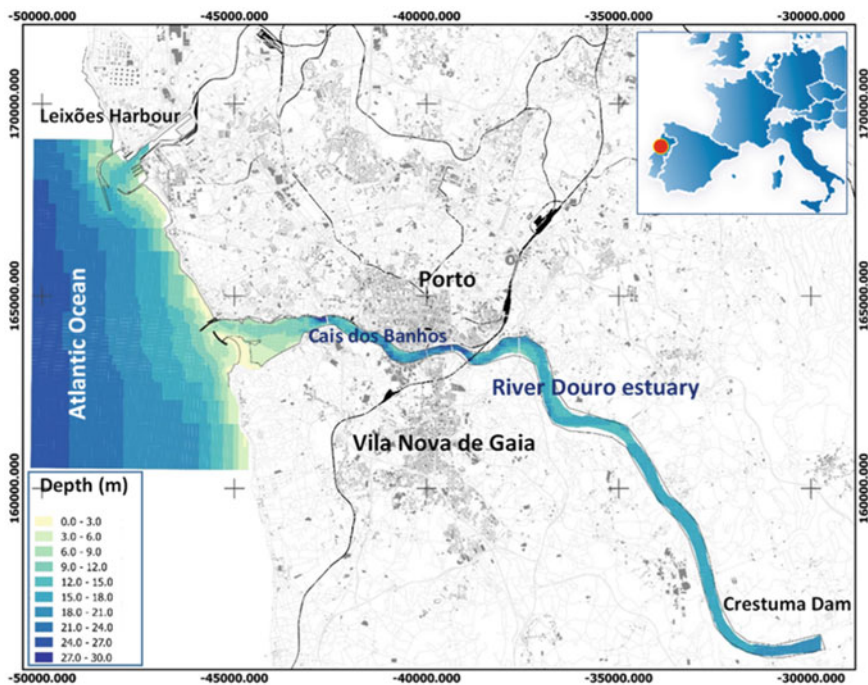
Fig. 1 Douro estuary location
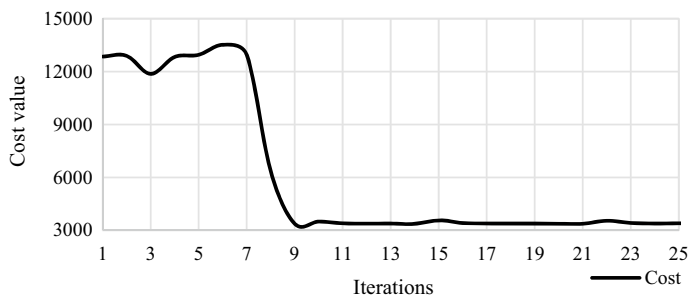
Fig. 2 Cost function values variation during the calibration procedure

Table 2 Statistical analysis of calibration results at Cais dos Banhos observation point

RMS (m)	Bias	STD (m)
0.199	−0.068	0.187

Table 3 Calibrated parameters value

Parameter	Value	Unit
Manning coefficient	3.46E-02	$m^{-1/3}$ s
M2 amplitude	1.075	m
M2 phase	88.787	degrees
S2 amplitude	0.373	m
S2 phase	117.391	degrees

3 Results

3.1 Calibration Results

Figure 2 shows the cost function values during the calibration procedure, which helps to understand how the OpenDA tool works. Firstly, it analyses each calibration parameter individually, using a variation equal to the standard deviation of the parameter set by the user. This first analysis explains the oscillations until the seventh iteration. After that, the algorithms vary all parameters at the same time, until it reaches one of the stop criteria defined by the user. In this work, three different stop criteria were selected: the number of maximum iterations, the maximum absolute difference between the costs of two best parameter estimates, and the maximum relative difference between the costs of two best parameter estimates [12].

Analysing the calibration results for the cost function, the stop criteria could be changed since there was no significant improvement in the cost function after iteration 13. This modification would result in less time to achieve an acceptable result. Besides, the OpenDA also returns a statistical analysis of the results (Table 2). The obtained calibration parameters values are presented in Table 3.

3.2 Extreme Water Levels Results

The water level estuarine profile for each scenario (Fig. 3) shows that there are only slight differences between scenarios associated with the same return period. It can be noted that the main factor that conditioned the water levels inside the estuary is the river discharge, with the sea level affecting mainly scenarios associated with lower river discharges. Indeed, it can be seen that the water level differences between scenarios are smaller for the set corresponding to 1000 years return period (13 cm) and higher for scenarios involving 50 years return period EFD (40 cm).
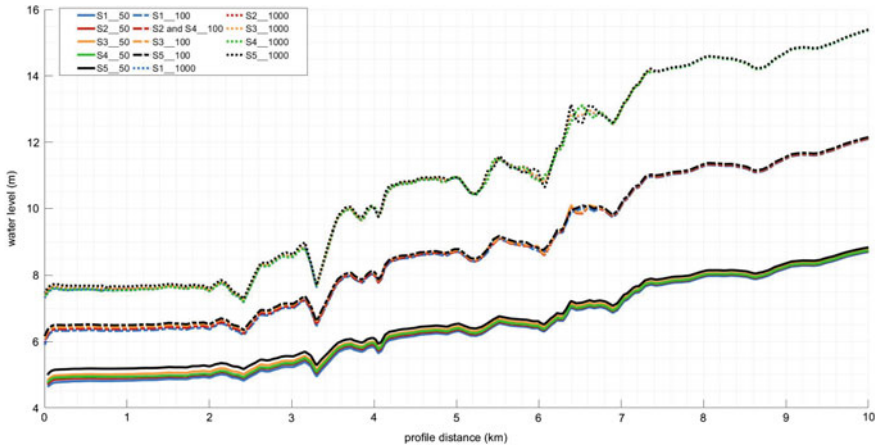
Fig. 3 Water level estuarine profiles results for all the simulated scenarios

A spatial analysis of the simulated water levels (Fig. 4) demonstrated the negative effect of the breakwaters during floods, restricting the river mouth and resulting in an upstream water elevation. The effect of the breakwaters is more evident for EFD scenarios that considered river flow associated with 1000 years return period. However, it was also observed in other scenarios. The results of the scenarios with 100 years return period were not showed because they were intermediaries among the others, being unnecessary for this analysis.

The results demonstrated that the Douro estuary presented river discharge dominance. The narrow main channel of the estuary jointly with the presence of two breakwaters at the estuary mouth created a geometric constrain to the river discharges into the ocean, producing a water elevation along the estuarine region that is much greater than the expected effects associated with the SLR. When the water levels upstream and downstream of the breakwaters are compared, the scenario with the lower water level difference presented a 1 m height difference between these two locations (Fig. 5). For the other scenarios, that value is higher.

3.3 Velocity Results

Velocity results (Figs. 6 and 7) confirm that the discharge is also the main factor that affects the water velocity within the estuary. Scenarios associated with the same return period presented similar current velocities. For scenarios that considered river flow associated with the 50 years return period EFD, the maximum velocity obtained, between the breakwaters, was around 5 m/s, while for the scenarios associated with 1000 years return period, the velocity reached 8 m/s.
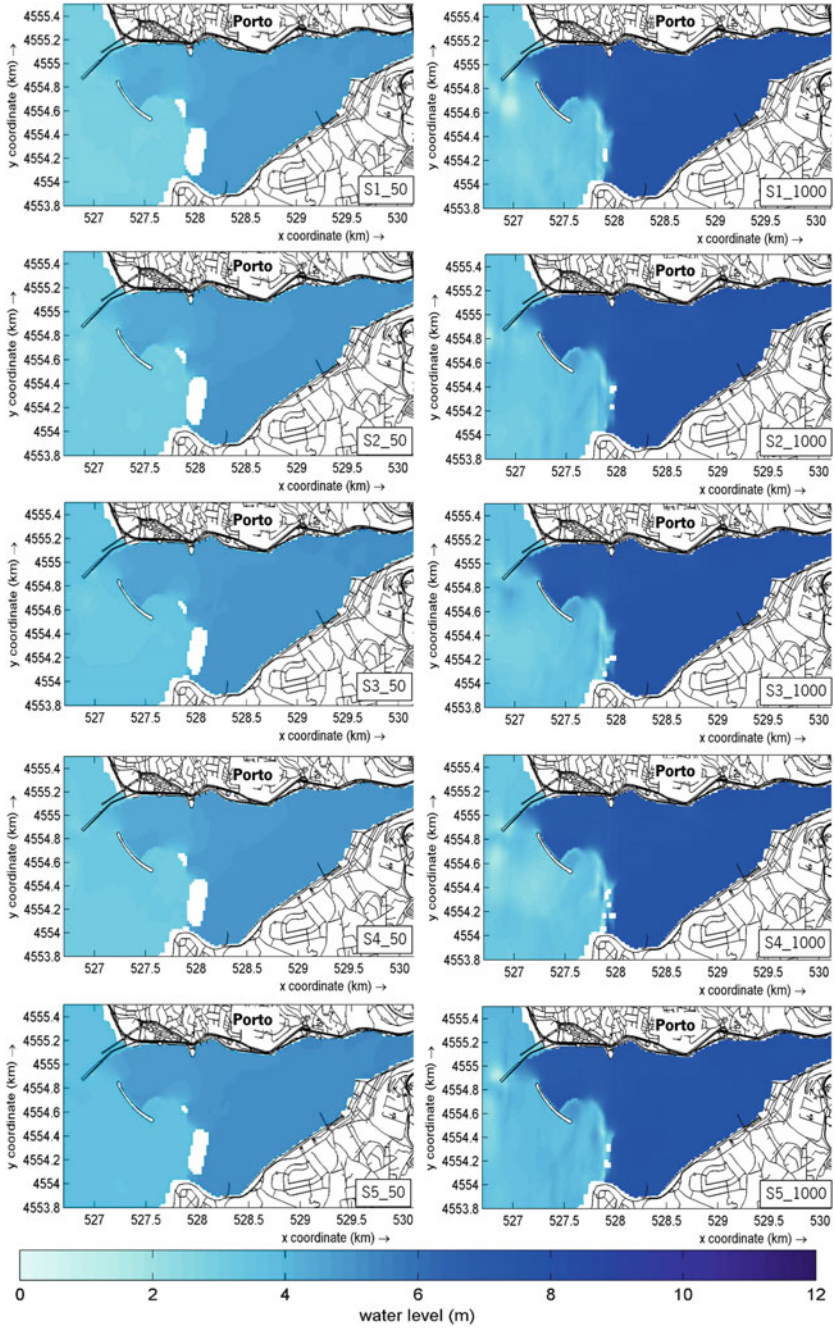
Fig. 4 Simulated water levels for 50 and 1000 years return period scenarios
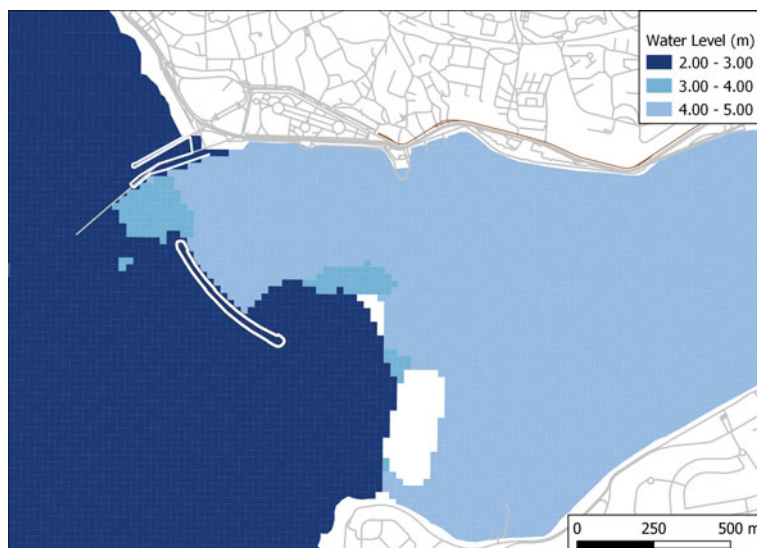
Fig. 5 Water levels around the breakwater

It must be highlighted that these results are not entirely realistic, since the sand spit around the south breakwater will be probably eroded during flood events, which would affect the current velocities near the estuary mouth. Also, the model was calibrated considering the differences between measured and simulated water levels. The velocities were not calibrated, which increase the uncertainties in the velocity results.

4 Conclusions

Delft3D software was applied to simulate and analyse the impact of extreme events in the Douro estuary. The automatic calibration procedure based on the OpenDA tool reduced the time necessary to achieve acceptable errors and helped to minimize these errors by the automatization of the procedure. Considering that this procedure will have a direct effect on the model results reliability, the adoption of automatic methods to avoid systematic errors and to reduce the time spent on this procedure during model implementation is recommended.

Regarding the water level results, it can be observed that the breakwaters can present both positive and negative hydrodynamic impacts. During extreme floods, they can restrict the river mouth and reduce its flow capacity, resulting in higher flood risk within the estuarine area. The obtained results are useful to identify possible flood areas, which can be the focus of future studies. However, it must be highlighted that this problem only would occur during extreme floods. In average conditions,
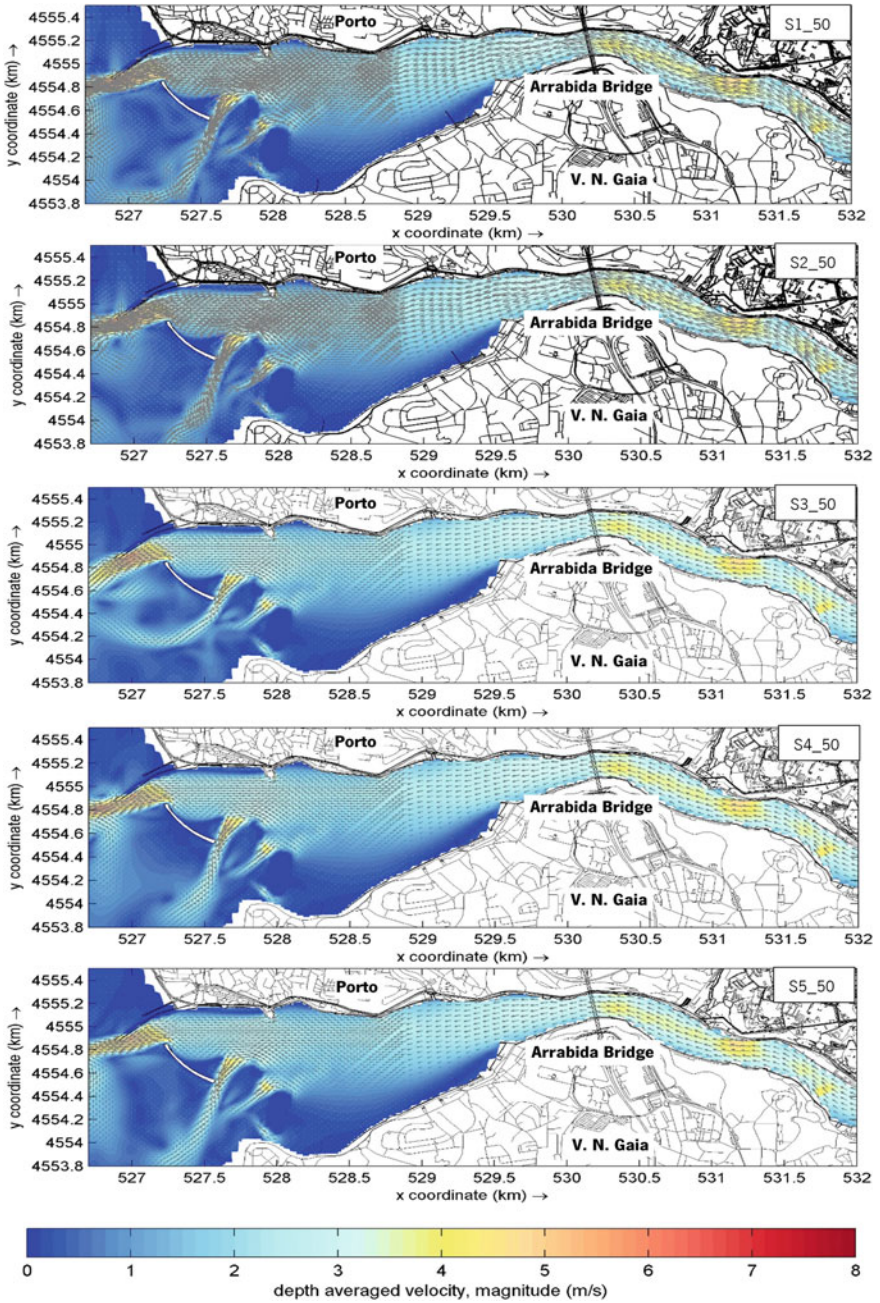
Fig. 6 Velocity results for scenarios associated with 50 years return period
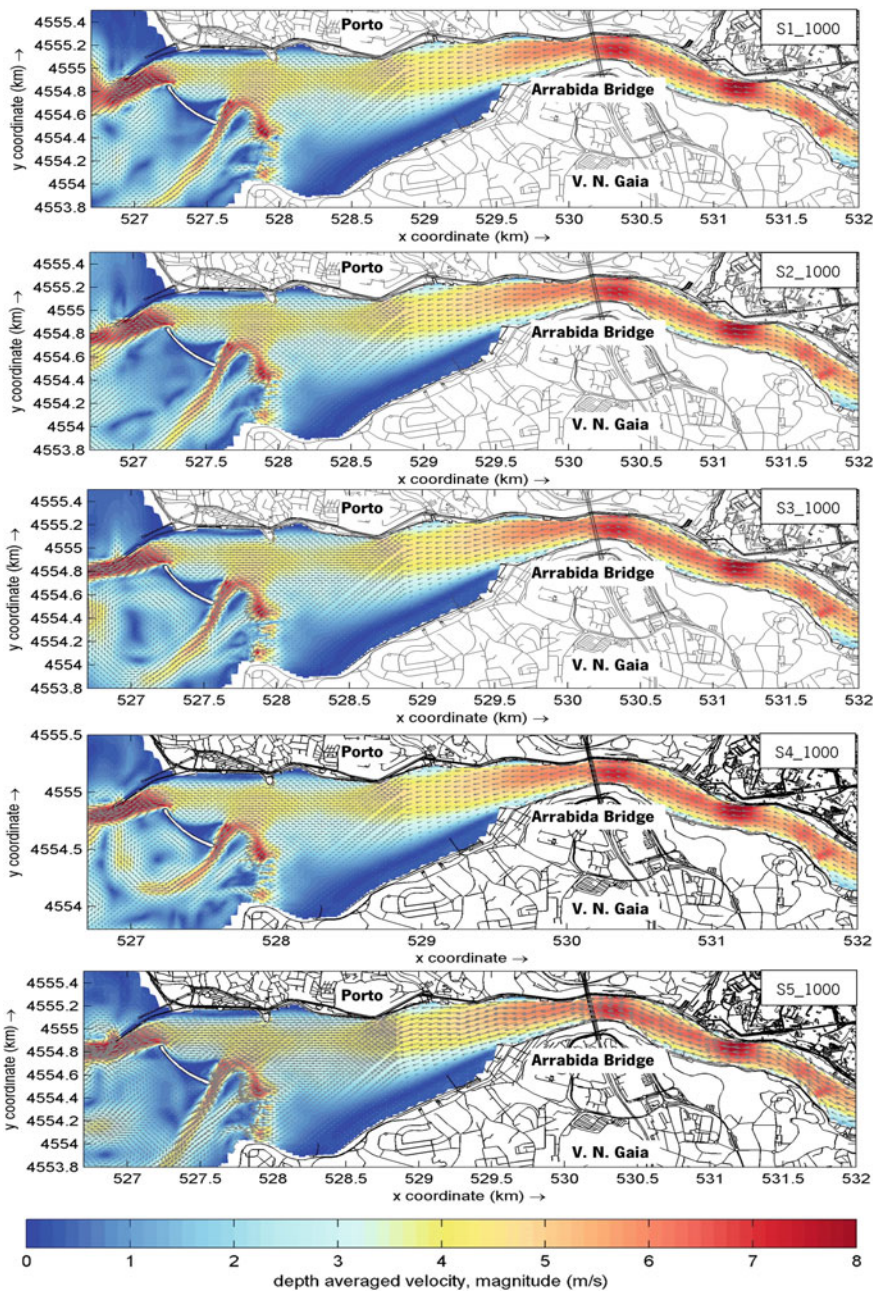
Fig. 7 Velocity results for scenarios associated with 1000 years return period

the breakwaters help to weaken the impacts of storm waves, reducing the wave propagation to the interior of the estuary and protecting the navigation activities.

The velocity results indicated that the sea-level elevation practically does not interfere with its intensity. It is expected that higher sea levels would result in lower flow velocities. However, at the Douro estuary, during flood events, the breakwaters constrain the flow discharges imposing an intense water surface elevation gradient that is much greater than the effects of SLR, which explains why there is not a significant impact on current average velocities. Also, it is necessary to analyse these results with caution, considering the characteristics of the sand spit around the south breakwater that is expected to be eroded during those events.

Lastly, it is concluded that the use of numerical models is extremely important to analyse complex hydrodynamic problems, like the ones that take place within estuaries and coastal areas. This methodology is essential to forecast the impacts of human interventions and extreme events, helping to plan and design mitigating measures considering different scenarios of interest.

References

1. Iglesias I, Avilez-Valente P, Bio A, Bastos L (2019) Modelling the main hydrodynamic patterns in shallow water estuaries: the Minho case study. Water 11(5):1040
2. Hallett CS, Hobday AJ, Tweedley JR, Thompson PA, McMahon K, Valesini FJ (2018) Observed and predicted impacts of climate change on the estuaries of south-western Australia, a Mediterranean climate region. Reg Environ Chang 18(5):1357–1373
3. Balsinha MJ, Santos AI, Oliveira ATC, Alves AMC (2009) Textural composition of sediments from Minho and Douro estuaries (Portugal) and its relation with hydrodynamics. J Coast Res 56:1330–1334
4. Bordalo AA, Teixeira R, Wiebe WJ (2006) A water quality index applied to an international shared river basin: The case of the Douro River. Environ Manage 38(6):910–920
5. Iglesias I et al (2020) Linking contaminant distribution to hydrodynamic patterns in an urban estuary: the Douro estuary test case. Sci Total Environ 707:135792
6. Iglesias I, Venâncio S, Pinho JL, Avilez-Valente P, Vieira JMP (2019) Two models solutions for the Douro estuary: flood risk assessment and breakwater effects. Estuaries Coasts 42(2):348–364
7. Mendes R, Vaz N, Dias JM (2013) Potential impacts of the mean sea level rise on the hydrodynamics of the Douro river estuary. J Coast Res 165:1951–1956
8. Vousdoukas MI, Mentaschi L, Voukouvalas E, Verlaan M, Feyen L (2017) Extreme sea levels on the rise along Europe's coasts. Earth's Futur 5(3):304–323
9. Azevedo IC, Duarte PM, Bordalo AA (Aug. 2006) Pelagic metabolism of the Douro estuary (Portugal)—Factors controlling primary production. Estuar Coast Shelf Sci 69(1–2):133–146

10. Pessoa A (2008) Tourism and regional competitiveness: the case of the Portuguese Douro valley. Rev Port Estud Reg 55–75
11. Rebelo J, Caldas J (2013) The Douro wine region: a cluster approach. J Wine Res 24(1):19–37
12. The OpenDA Association (2016) OpenDA User Documentation. https://www.openda.org/docu/openda_2.4/doc/OpenDA_documentation.pdf. Accessed 16 Jan 2020
13. Siqueira AG, Fiedler MFM, Yassuda EA (2019) Delft3D morphological modeling downstream of Sergio Motta reservoir dam. In: IAEG, AEG Annual Meeting Proceedings, San Francisco, California, vol 4, S. A. and C. K. Eds. Cham: Springer International Publishing 17–24

Flood Modelling for an Urban Indian Catchment: Challenges and Way Forward

Mousumi Ghosh, Subhankar Karmakar, and Subimal Ghosh

1 Introduction

The unprecedented rainfall extremes accompanied by climate change and rapid urbanization have resulted in an increasing number of incessant flooding events across the globe. Floods account for the most catastrophic natural hazards in the Indian subcontinent [10]. The flood-affected areas in the country sum up to around 7.56 million hectares of area (2.32% of the entire area of the country) every year, which includes 3.3 million hectares of croplands (4 per cent of the crop area). As per a Central Water Commission report, around 37 million hectares (nearly 1/8th of India's geographical area) of fertile land are likely to be flooded at one time or another throughout the monsoon months. Urbanization and climate change accompanied by rapid population growth have further worsened the flooding scenario all across the world. The major causes of urban floods are inundation from water logging due to heavy precipitation or tides or maybe due to the combination of both [3]. Some other causes include local drainage problems like inadequate capacity, blockage, river overflows, coastal storm surges and wave actions, flash floods, or a combination of these [18].

M. Ghosh (✉) · S. Karmakar · S. Ghosh
Interdisciplinary Program in Climate Studies, Indian Institute of Technology Bombay, Mumbai 400076, India

S. Karmakar
Environmental Science and Engineering Department, Indian Institute of Technology Bombay, Mumbai 400076, India

S. Karmakar · S. Ghosh
Centre for Urban Science and Engineering, Indian Institute of Technology Bombay, Mumbai 400076, India

S. Ghosh
Department of Civil Engineering, Indian Institute of Technology Bombay, Mumbai 400076, India

This has encouraged the scientific community and governing bodies to come together and develop technologies and frameworks for efficient flood mitigation and management. Flood modelling and mapping for assessment of extent and damage due to floods are being widely implemented by several countries for effective flood management to lessen the possible harmful effects as much as possible [11]. Flood inundation refers to the rising of a body of water from a well-established watercourse and coverage of surrounding areas resulting from heavy precipitation, cyclones, etc. The ability of the flood models to generate time-series inundation information regarding onset, duration, and withdrawal of an extreme event has made them suitable for the reduction of risks [19]. This information helps the authorities in land use planning, identify the appropriate evacuation routes, and provide optimum protection to the population by the establishment of emergency centres. These models when coupled with remote sensing and GIS data provide a better computation of flood assessment [15]. The flood models are primarily classified into three categories; (1) Empirical methods, (2) Simplified conceptual models, and (3) Hydrodynamic models. **Empirical methods** are a classical approach to flood modelling. The flood-related data(observations) of past events are collected, processed, integrated, and analysed to estimate return periods of floods, depth–area–duration curves, and rating curves. These curves are used to derive flood characteristics of future events. These data collected through interviews, surveys, on-ground measurements, and satellite imageries are a reflection of past events. The model results are often used as inputs to other techniques, for example, information of flood extent obtained from remotely sensed data are widely used for monitoring of floods, as well as a reference for calibration and validation of hydrodynamic models [16]. Although these methods are relatively faster and easier to implement than other methods, their non-predictive nature and coarse temporal and spatial resolution have limited their use in the present time. However, due to rapid advances in the field of remote sensing, the accuracy of these methods is improving. **Simplified conceptual models** describe all components of hydrological processes. They follow a grey box model or a parametric approach. These models assess the model parameters from the field data as well as calibrated data through the use of semi-empirical equations. The physical elements of the catchments are represented through the number of interconnected reservoirs. The calibration requires a large number of hydrological and meteorological records. Interpretation becomes difficult as curve fitting is involved in calibration. Therefore, the impact of land use changes cannot be assessed with much confidence [5]. **Hydrodynamic models** are mathematical tools that are directed by laws of physics to describe or replicate the motion of water. Equations are established amongst different hydraulic variables like velocity, pressure, depth, etc., based on conservation of energy, mass, and momentum. They are classically grouped into 1D, 2D, and 3D models on the basis of their on their spatial illustration of flows in floodplains [17]. These models can also be coupled with each other to provide a more realistic scenario of stormwater flows across the river channel and overland areas by considering the influence and linkage between the 1D and 2D flows.

The flood-related information obtained from these hydrodynamic and hydrological models is demonstrated as flood inundation and hazard maps to identify the

potential areas at risk so that necessary measures can be taken for flood management [9]. Flood inundation depth is determined by factors such as magnitude and duration of rainfall, drainage density, size and slope of the watershed, soil and land use, and gradient of water bodies. Flood hazard maps represent various other flood characteristics such as flood extent and inundation depth, the velocity of flow, duration of inundation, and sediment or contamination load. These maps can be utilized by common public and civic bodies to take necessary action to reduce the flood damages. The hydrodynamic flood modelling approach is the most widely implemented technique by governing and research bodies of several countries. These models are highly data-intensive and, therefore, enable the assessment of flood characteristics with greater precision. Therefore, the lack of long-term reliable data poses a major challenge in flood modelling especially for developing and underdeveloped countries. There exist very few studies in the literature which have considered a coupled approach in hydrodynamic flood modelling. The current study attempts to develop a holistic hydrodynamic flood modelling framework using a three-way coupled approach while addressing these challenges. The framework which has been demonstrated over Mithi catchment in Mumbai is generic and hence can be implemented over other geographical locations, especially the ones where data scarcity created hindrance in flood modelling. This article comprises of "Introduction" which elucidates the past literature and objectives of the study. This manuscript comprises of the first section, i.e., Introduction which elucidates the past literature and objectives of the study, the second section describes the study area and its importance in demonstrating the proposed framework followed by the third section which illustrates the development of the proposed framework. The fourth and fifth sections discuss the challenges addressed while developing the proposed framework and its application, respectively. Finally, the "Conclusion" section gives an enclosure to the article by giving insights into the proposed framework and the future prospects in regards to its application.

2 Study Area

The Mithi catchment in Mumbai with an area of around 73 Km^2 is amongst the major flood-prone areas in Mumbai city (Fig. 1). The decline in water carrying capacity of the Mithi river due to encroachment of land along the river banks, destruction of the Mangroves uncontrolled population growth, and outdated drainage network of the city have also contributed to the aggravation of the flooding situation. The river originates from the Vihar lake in the east of the Sanjay Gandhi National Park at an elevation of 246.5 m above sea level and undergoes a rapid change in slope [7] while travelling a distance of 18.4 km to drain into the sea at Mahim creek.

Fig. 1 Location of Mithi catchment in Mumbai city (India)
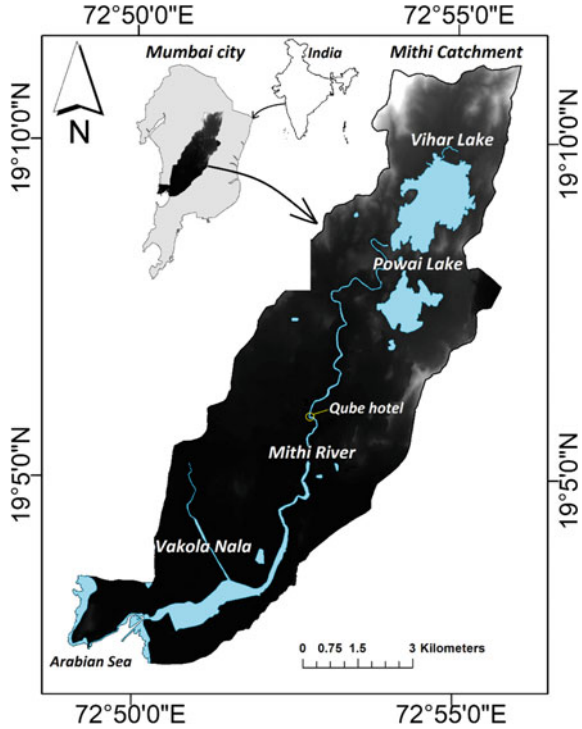
3 Development of Hydrodynamic Flood Modelling Framework

We have developed a flood modelling framework in the current study through a three-way coupled hydrodynamic approach in the MIKE FLOOD interface. It assimilates the MIKE 11 model to represent the flow through river channel with stormwater drainage network with MIKE 21 model to represent the overland flow and has been illustrated in Fig. 2.

MIKE 11

MIKE 11 is an engineering software model which has been developed by the Danish Hydraulic Institute (DHI) to simulate the 1D fully dynamic flows in rivers, irrigation systems, channels, estuaries, and other water bodies [12]. It has various editors like river cross-section editor, river network editor, boundary editor, and hydrodynamic editor. The Hydrodynamic (HD) module forms the primary component of the model amongst these. It solves the Saint–Venant equations by using the implicit finite difference six points Abbott–Ionescu scheme. Various add-on modules for assessment of
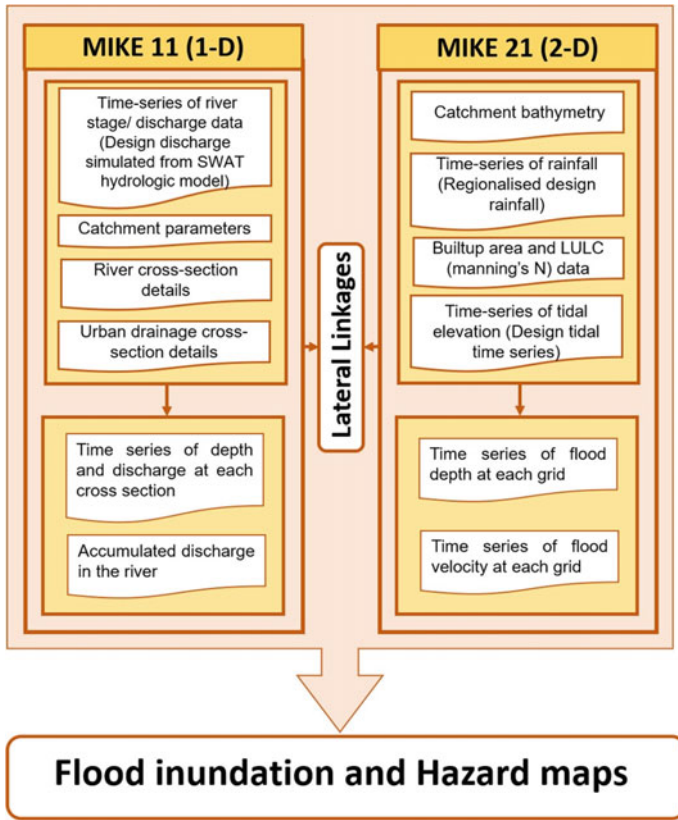
Fig. 2 Development of three-way coupled hydrodynamic flood modelling framework for Mithi catchment

water-quality, Advection–Dispersion (AD), Rainfall-Runoff (RR), Sediment Transport (ST), Flood Forecasting (FF) dam-break, etc., are also available in addition to the other editors in the model.

This model is governed by equations for the conservation of mass and momentum. The continuity and momentum equations are quasi-linear, simultaneous, and hyperbolic type partial differentiation equations of the first order. The implicit finite difference scheme is used to solve these equations numerically. These equations are transformed into a set of finite difference equations in a computational grid. A weir equation is used to compute the lateral inflow/ outflow between the streamflow and floodplain at the river bank.

MIKE 21

MIKE 21 model is a widely used software used for simulation of physical, chemical, and biological processes in marine and coastal regions [6]. It is suitable for areas where flow paths are not well defined, two-dimensional flows and detailed knowledge

of velocity and depth patterns are important. It comprises of three simulation engines, i.e., single grid, multiple grids, and flexible mesh. We have used the MIKE 21 HD FM (Hydrodynamic Modelling Flexible Mesh) model for this current study. The non-linear equations for conservation of mass and momentum which are space and time-dependent are solved in the MIKE 21 HD FM by utilizing an Alternate Direction Implicit (ADI) technique [8].

In the current study, the Mithi catchment's shapefile with the river network obtained from the Municipal Corporation of Greater Mumbai (MCGM) along with a synthetic stormwater drainage network has been utilized for the network editor in the MIKE 11 model. The cross-section editor utilizes the cross-section details at various chainages of the Mithi river and the Vakola Nala provided by the MCGM. The time series of discharge at the start and end of the river serves as an input for the boundary editor. The hydrodynamic editor utilizes the initial depth and discharge of the water. For the MIKE 21 HD 1FM model, the World Digital Elevation Model (DEM) for the Mithi catchment which describes the characteristics of terrain along with building layer data obtained from MCGM is utilized to generate a flexible mesh. The Manning's M of the floodplain is deduced from the Land Use Land Cover (LULC) acquired from National Remote Sensing Centre (NRSC). The tidal time series at the Mahim creek obtained from Indian National Centre for Ocean Information Services (INCOIS) is provided along the coastline where the river meets the sea in the model. Thus, after both the 1D and 2D models are individually set up, the MIKE 11 with the stormwater drainage network is coupled with the MIKE 21 HD FM through lateral links in the MIKE FLOOD interface. Subsequently, the flood simulations are performed for the required extreme precipitation events to derive the inundation and hazard maps.

4 Challenges in the Development of Hydrodynamic Flood Model

A fine resolution Digital Elevation Model (DEM) data, the network and cross-section details of the water bodies in the catchment, and the information about flood influencers such as rainfall, discharge, and tidal elevation are the major requirements in a hydrodynamic flood model. A time series of longer duration for these influencers is primarily required to derive flood inundation and hazard maps for different return periods which facilitate the urban planners, governing bodies, and disaster management bodies for effective flood management and mitigation purpose. To compensate for the unavailability of long-term data, we have adapted alternate robust techniques which can be efficiently applied over other catchments as well. A detailed description of the same has been enumerated in the following subsections.

4.1 Rainfall Data

The long-term rainfall data for Mumbai city was obtainable only for the locations of Santacruz and Colaba until 2005 when a very heavy precipitation event on 26th July 2005 brought the city to a standstill and caused huge losses. This prompted the civic body of Mumbai, the Maharashtra Corporation of Greater Mumbai (MCGM), to establish a dense network of Automatic Weather Stations to establish a data repository for future research. However, since long-term rainfall data is an important requirement for estimation of design rainfall, we have adapted a regionalization-based approach as described by [14] to obtain the rainfall depth for the required return period. The rainfall data of Santacruz IMD for the June, July, August, and September months between the years 1969–2012, which is situated inside the Mithi river catchment, is utilized to derive and represent the design rainfall for the entire area. The Peak-over-Threshold (PoT) or extreme value analysis is used to select an optimum threshold for rainfall depth based on the Generalized Pareto Distribution (GPD) approach.

4.2 Tidal Data

The hourly astronomical tidal data between 1900–2100 and observed minute-wise storm tide data between 2001–2011 are obtained from Indian National Centre for Ocean Information Services (INCOIS), Hyderabad. A tide fitting toolbox is used to determine the tidal constituents from the astronomical tidal data [7]. Thereafter, these components are utilized to generate a synthetic tidal time series for the observed storm tide duration. The difference between the observed and synthetic time series gives the surge component. The astronomical tidal height and surge component for the desired return periods are obtained by fitting into a Generalized Extreme Value (GEV) model and GPD model, respectively. Finally, the 24-h design tidal elevation obtained is provided as a boundary condition along the coastline where the river confluences into the sea to the MIKE 21 HD FM model.

4.3 Discharge Data

River discharge and water level serve as essential inputs and are provided as boundary conditions to the 1D model. Therefore, in absence of its observed data, the hydrological model proves beneficial to simulate the discharge. In the current study, the Soil and Water Assessment Tool, a continuous long-term physically based conceptual model has been used to simulate discharge at the mouth of the river originating from Vihar Lake [1]. This model has had a wide application for modelling watershed hydrology and for prediction of the impact of land management practices on water,

agricultural chemical yields, and sediment in small as well as large complex basins with varying land use land cover conditions and soil type over long periods. In this model, the DEM is used to delineate the watershed, followed by utilizing the land use land cover data and soil and slope data to define the Hydrological Response Units (HRUs) and providing the weather data into the model followed by a model run to subsequently generate discharge at the desired locations. In the current study, discharge time series has been generated corresponding to the observed rainfall time of Santacruz IMD station with the help of the SWAT model. Following this, the POT is performed over the simulated discharge time series to obtain the design discharge for the desired return period.

4.4 Stormwater Drainage Network Data

The details of the river network, urban network, and their cross-sections which are very crucial for a hydrodynamic flood model are many a time difficult to obtain especially for developing and underdeveloped countries. The cost of manually surveying the details is also very high. Therefore, the fine resolution DEM data can be delineated to extract the river network and cross-section details. However, the urban drainage network cannot be delineated from the digital elevation model data. Therefore, to overcome the issue of the unavailability of details of the urban drainage network, several discussions were conducted with the MCGM. For an urban city, usually, the road drainage system is designed during the construction of road networks. The MCGM also confirmed that the stormwater drainage network is located along the major roads of the city. Hence, the drainage network along the roads has been considered in a manner that they join the laterals and confluence into the Mithi river at the 22 different outlets. The locations of these 22 outlets were gathered from the civic governing body. The open drains with 2 m × 2 m dimensions are created in MIKE HYDRO from the considered synthetic drainage network (major road network) and DEM of the study area. The cross-section details at different chainages of the river and Vakola Nala from MCGM are utilized for cross-section editor.

5 Application of the Hydrodynamic Flood Modelling Network

The hydrographs, flood inundation, and hazard maps are finally derived from the developed flood modelling framework. Figure 3 represents the hydrographs at two points of the Mithi river, i.e., at Vihar lake where the Mithi river originates and at a point near Qube hotel in the catchment. The peak discharge observed is higher at the Qube hotel (1173 m³/second) than that of the upstream of the river at Vihar lake (915 m³/second).
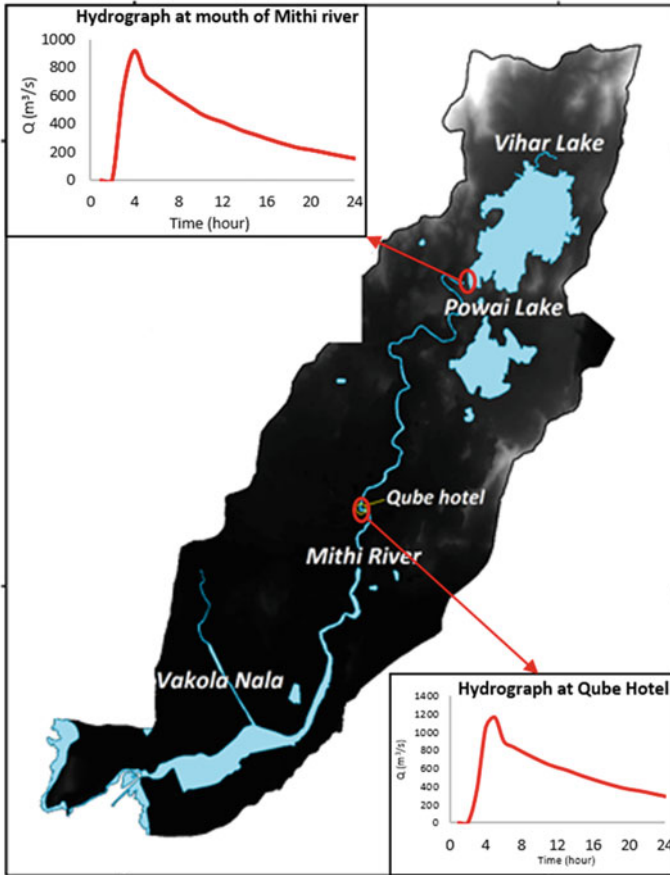
Fig. 3 Hydrograph of 200-year return period event at different points along the Mithi river

The flood inundation maps consider the inundation depth while the flood hazard maps take into account both inundation depth and velocity of flow. In this study, the Australian Flood Hazard Classification is considered to classify flood inundation and hazard into various classes [2] as depicted in the legend of Fig. 4a, b. The inundation is classified into low (I, II), medium (III, IV), and high (V, VI, VII) categories on the basis of depth only, and hazard is quantified into low (I, II), medium (III, IV), and high (V, VI) categories on the basis of both inundation depth and velocity. Figure 4a, b represents the flood inundation and hazard map, respectively, for the 200-year return period of rainfall, tidal data and discharge data. These types of maps can be utilized to categorize the flooded areas into low, medium, and high hazard zones which will help the administrative bodies and planning bodies in various administrative decisions, flood zonation, identify areas where hydraulic structures need to be constructed for flood management.
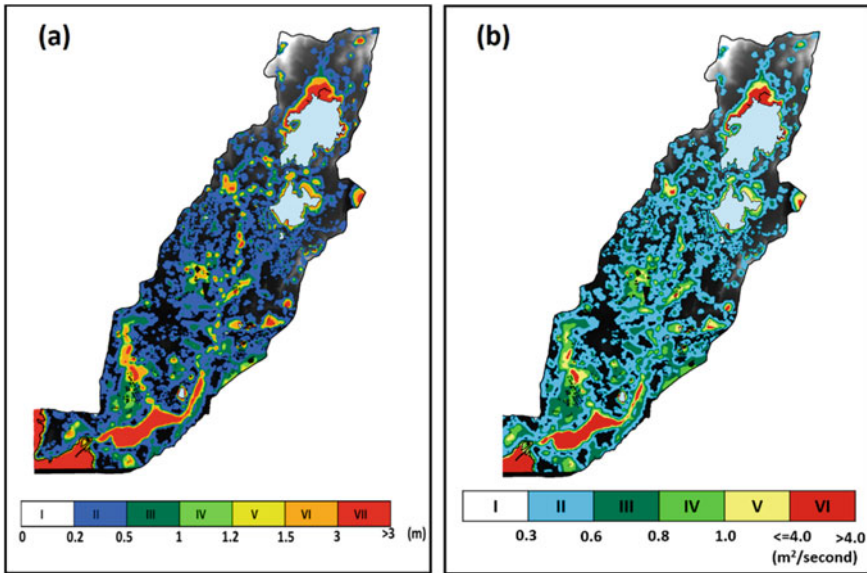
Fig. 4 **a** Flood inundation map; **b** Flood hazard map for 200-year return period

Since no observed inundation maps are available to verify the performance of the flood model, the model was run for an observed heavy rainfall event, i.e., the highest rainfall day of the year 2013. Various reliable newspaper articles were collected to identify the areas which had been inundated in that particular event and have been encircled in Fig. 5. It can be seen that the flood modelling framework can simulate the flooding scenario for the event and identify the inundated areas on the map.

6   Conclusion

The current study illustrates the development of a comprehensive flood modelling framework based on a three-way coupled approach for a data-scarce densely populated urban coastal catchment. The MIKE FLOOD has several features such as compatibility and integration in GIS interface, incorporation of hydraulic structures module, assimilation of flooding, wetting and drying depths, a module for considering steep gradients, parallel GPU computations for faster simulations, and provision for inclusion of tidal influences, which gives the hydrodynamic model an edge over other flood models [4, 11, 13] and has been used in this study studies. The 1D model (MIKE 11) which accounts for the river discharge with the stormwater drainage network is coupled with the 2D model (MIKE 21) which accounts for the overland flow, to develop a three-way coupled hydrodynamic flood modelling framework in the MIKE FLOOD interface. The lack of data of major flood influencers like rainfall,

Fig. 5 Validation of flood hotspots identified from the news reports for the 2013 event with the inundation maps derived from the hydrodynamic flood model
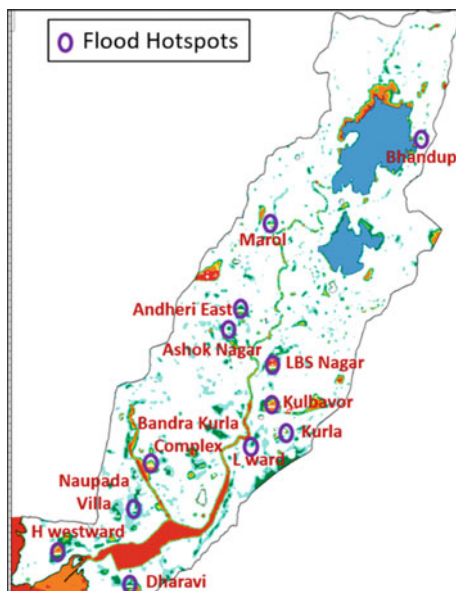
discharge, tidal height as well as details of stormwater drainage network has been addressed by adapting alternate robust methods. The Mithi catchment, an extremely flood-prone area in Mumbai, has been utilized to demonstrate the framework. The flood inundation maps (based on flood depth) and hazard maps (based on depth and flood velocity) have been derived for the study area and were validated for a past flood event by identifying the flooded areas from newspaper articles which testifies the credibility of the framework. The proposed framework is generic and can be applied to other geographical locations. The information obtained from flood maps helps the authorities in land use planning, identify the appropriate evacuation routes, and provide optimum protection to the population by the establishment of emergency centres. Additionally, the flood models can be integrated with rainfall forecasts to obtain flood forecasts. The data inventorization of flood hazard maps, along with vulnerability and risk maps and flood forecasts on a timely basis, can be utilized to create a web-based flood information system and categorize the flood-prone areas into different zones based on the intensity of hazard and can increase awareness amongst public, stakeholders, and authorities about the likelihood of floods and vulnerable areas and enable in informed decision making.

References

1. Arnold JG, Srinivasan R, Muttiah RS, Williams JR (1998) Large area hydrologic modeling and assessment part I: model development. J Am Water Resour Assoc 34:73–89
2. Australian Institute for Disaster Resilience (AIDR) (2017) Guideline 7–3, Supporting document

for implementation of Australian disaster resilience handbook 7 managing the floodplain: a guide to best practice in flood risk management in Australia

3. Chang F-J, Chen P-A, Lu Y-R, Huang E, Chang K-Y (2014) Real-time multi-step-ahead water level forecasting by recurrent neural networks for urban flood control. J Hydrol 517:836–846

4. Chowdhury MR (2000) An assessment of flood forecasting in Bangladesh: The experience of the 1998 flood. Natural Hazards 22:139–163

5. Devi GK, Ganasri BP, Dwarakish GS (2015) A Review on Hydrological Models. In: International Conference on water resources, coastal and ocean engineering (ICWRCOE'15) 4:1001–1007

6. Danish Hydraulic Institute (DHI) (2017) Mike 21Hydrodynamic module, User Guide, MIKE by DHI

7. Ghosh M, Mohanty MP, Kishore P, Karmakar S (2020) Performance evaluation of potential inland flood management options through a three-way linked hydrodynamic modelling framework for a coastal urban watershed. Hydrol Res 52(1):61–77

8. Gustafsson B (1971) An alternating direction implicit method for solving the shallow-water equations. J Comput Phys 7(2):239–254

9. Linham MM, Nicholls RJ (2010) Adaptation: coastal erosion and flooding. ISBN 9788755038554

10. Mishra S, Mazumdar S, Suar D (2010) Place attachment and flood preparedness. J Environ Psychol 30:187–197

11. Mohanty MP, Mudgil S, Karmakar S (2020) Flood management in India: a focused review on the current status and future challenges. Int J Disaster Risk Reduction 101660

12. Mohanty MP, Vittal H, Yadav V, Ghosh S, Rao GS, Karmakar S (2020) A new biva- riate risk classifier for flood management considering hazard and socio-economic dimen- sions. J Environ Manage 255:109733

13. Ngo LLE, Lyngby D-K, Madsen H (2005) Application of MIKE 11 in managing reservoir operation. Advances

14. Paudyal GN (2002) Forecasting and warning of water-related disasters in a complex hydraulic setting the case study of Bangladesh. Hydrol Sci J 47:5–18

15. Sherly MA, Karmakar S, Chan T, Rau C (2015) Design rainfall framework using multivariate parametric nonparametric approach. J Hydrol Eng 21:4015049

16. Sinnakaudan SK, Ab Ghani A, Ahmad MSS, Zakaria NA (2003) Flood risk mapping for Pari River incorporating sediment transport. Environ Model Softw 18:119–130

17. Smith LC (1997) Satellite remote sensing of river inundation area, stage, and discharge: a review. Hydrol Process 11:1427–1439

18. Teng J, Jakeman A, Vaze J, Croke B, Dutta D, Kim S (2017) Flood inundation modelling: a review of methods, recent advances and uncertainty analysis. Environ Model Softw 90:201–216

19. Willems P, Arnbjerg-Nielsen K, Olsson J, Nguyen VTV (2012) 8th International workshop on precipitation in urban areas climate change impact assessment on urban rainfall extremes and urban drainage: methodologies and difficulties

20. Zerger A, Wealands S (2004) Beyond modelling: Linking models with GIS for flood risk management. Nat Hazards 33:191–208

Assessment of Stormwater Runoff of Padma Bridge Link Road at Southwest Part of Dhaka Using Geo-SWMM

Sabrina Rashid Sheonty, Joyti Mabruk, and Sabbir Mostafa Khan

1 Introduction

Drainage congestion is a common phenomenon for urban areas of Bangladesh. The capital Dhaka faces frequent waterlogging just after a short rainfall event. Especially during monsoon many areas of Dhaka go under water because the inadequate drainage cannot carry the huge volume of stormwater. The main reasons behind it are the encroachment of canals or khals and the unplanned and inadequate drainage in the city. Moreover, the impact of climate change can make the situation worse in future. The change in precipitation pattern can generate much more stormwater than expected. Thus, climate factors are creating challenges for sustainable stormwater management for future. Apart from that, the unplanned urbanization is increasing due to the population growth surrounding Dhaka. As a result, unplanned drainage network is being constructed which can impose significant threat to these newly developed areas. Keraniganj is such an urbanized area near Dhaka beside the river Buriganga and Dhaleshwari where several development projects like 'China-proposed housing project', 'Construction of 252 long girder bridge project', and 'Jhilmil Project' are going on [1–3]. Especially the southwest part consisting of Tegharia and Baghair are being developed rapidly.

The Padma Bridge is called the dream project of Bangladesh. Basically, it is a multimodal transportation system of road-rail bridge across the Padma River. Previously there was no directly connected transportation from the southern part of the country with the capital Dhaka. It used to take a long time to cross the ferry to

S. R. Sheonty (✉)
Military Institute of Science and Technology, Dhaka, Bangladesh

J. Mabruk
Murdoch University, Perth, Australia

S. M. Khan
Bangladesh University of Engineering and Technology, Dhaka, Bangladesh

move from south part of the country to Dhaka. This project will connect Louhajang, Munshiganj, Shariatpur, and Madaripur to northern and eastern regions. Moreover, it will provide direct connectivity between the central and southwestern part of the country through a fixed link on the Padma River at Mawa-Janjira points. The project will boost the economic and industrial development of this region which was previously underdeveloped due to the lack of transportation facilities. It is going to increase the GDP of Bangladesh by 1.2%. The Padma Bridge link road from Dhaka to Mawa through Keraniganj is an important part of the Padma Bridge Multipurpose project. Significant development is taking place at of Keraniganj and surrounding areas due to the construction of the Padma bridge. The link road passes through two unions, Tegharia and Baghair, which are two important unions of Keraniganj. Due to the construction of the link road, unplanned constructions are observed around these areas. These unplanned activities can obstruct the storm water to flow and create waterlogging. To overcome the problem of waterlogging in the study area, it is important to make proper analysis in this regard. Thus, in this study area, two separate hydrologic models have been developed in two unions—one in Tegharia and another in Baghair. Both the catchments have been modeled in GeoSWMM, and the peak runoff of this catchment is determined for 5 years and 10 years return period. Finally, the stormwater drainage network is designed using the GeoSWMM model results.

Previously many areas in Bangladesh were modeled in GeoSWMM, and the runoff was estimated from the model simulation. Maliha [4] worked on design of stormwater network on Bogra city. In this study, peak runoff and the maximum flows in the design canals were estimated using the GeoSWMM model. Abdullah [5] applied GeoSWMM model in the Tangail Sadar Upazilla, where there is a lack of planned and adequate drainage network system. The main objectives of the study were to evaluate present drainage circumstances, recognize the future necessities, and design of cross-sectional areas of conduits. Chattogram is a megacity with serious drainage problems. Several studies were observed there using GeoSWMM. Mohammad [6] applied GeoSWMM in the Eastern part of Chattogram City where Islam [7] did the same for Western part of Chattogram City.

2 Study Area

Keraniganj stands on the southwest side of Dhaka City on the bank of the Buriganga and Dhaleshwari rivers. It is located in between $23° 36' 27.924''$ N and $23° 46' 45.628''$ N latitudes and in between $90° 13' 16.089''$ E and $90° 28' 35.531''$ E longitudes. The study area comprises Tegharia and Baghair union and its surroundings of Keraniganj. The different upazillas/thanas of Dhaka along with Keraniganj and different unions of Keraniganj are shown in parts 'a' and 'b' of Fig. 1 accordingly.
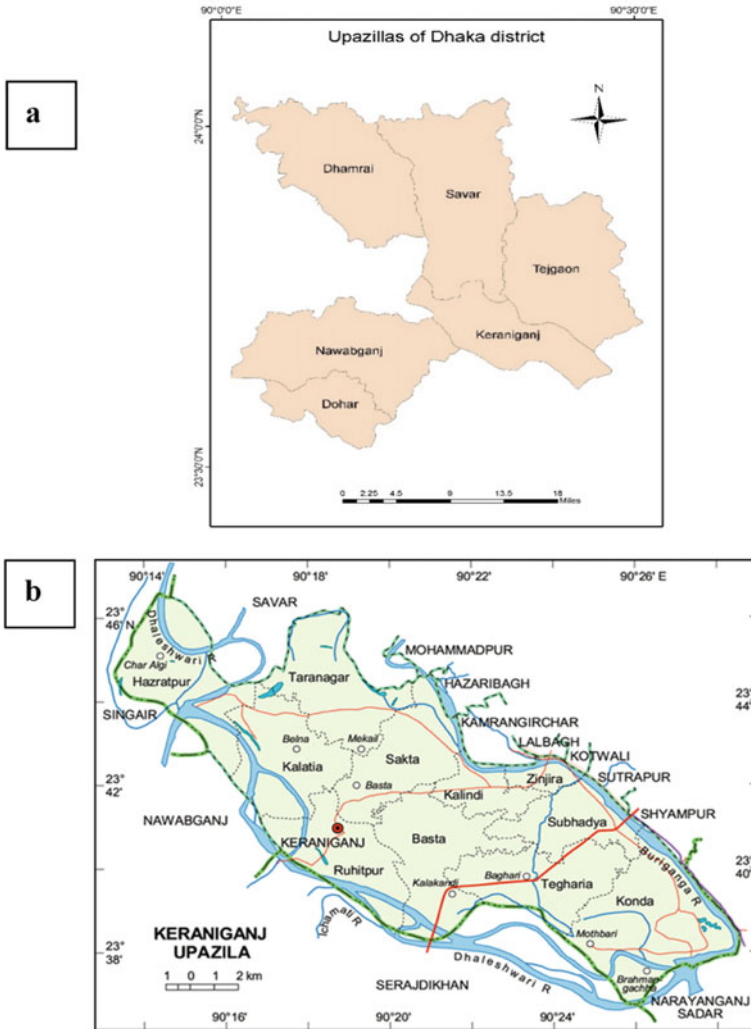
Fig. 1 a Keraniganj Upazilla in Dhaka District (*Source* Author) **b** Unions of Keraniganj (*Source* Banglapedia)

3 Methodology

3.1 Data Collection

Digital Elevation Model (DEM) and rainfall data of the study area were required for this study. The ASTER Global DEM of Bangladesh having resolution of 30 m was collected from USGS Earth Explorer website. After that, the study area was clipped

from it. For this study, the Daily rainfall data at Dhaka station for the time period of (1965–2015) was collected from Bangladesh Meteorological Department (BMD).

3.2 Frequency Analysis

Numerous distributions can be applied on the basis of their ability to fit the plotted data from streams. Log Normal, Log-Pearson Type III (LP3), Extreme Values Type 1 (EV1), or Gumbel Distribution has been widely used for frequency analysis. For Bangladesh EV1 Distribution was found suitable to fit peak flow data in several rivers [8]. Thus, the EV1 or Gumbel Distribution was selected to estimate extreme rainfall during the considered period. Moreover, 2 h 5 and 10 years were selected as return period in this study. It was selected based on some previous studies and guidelines. In Bangladesh, 5 years return period was applied in the Master Plan for Greater Dhaka Protection Project of Bangladesh Flood Action Plan no. 8A (FAP 8A) in 1992 for Khal Improvement and Trunk Drain. In another study of BWDB after flood event of 2004, the design return period was taken as 5 year for internal drainage for upgrading previous studies on combined flood protection embankment and bypass project for Eastern Dhaka. In India, 2–5 years return period for rainfall is taken as common practice for design of drainage system in the residential areas. According to the reference of Rajasthan Urban Infrastructure Development Project, if there is any industrial and commercial area, the design return period is considered as 5–10 years. Apart from that, a study [9] had been done to define a methodology to identify the optimal rainfall return period for the design of urban drainage systems which was applied to a small urban catchment in Palermo (Italy) and the optimal solution was found a design rainfall period of 10 years.

Thus, from maximum annual rainfall data of study area, the frequency analysis was done for 5 years and 10 years return period by Gumbel distribution using Eq. (1)

$$X_T = \bar{x} + K\sigma_{n-1} \tag{1}$$

where

X_T value of the variable x of a hydrologic series with a return period T
$\bar{x}$ mean of the variate
K   frequency factor
σ_{n-1} standard deviation of the sample.

According to JICA reports, percentage of the rainfall with 5 years and 10 years return period is determined for different time steps which is shown in Table 1.

Table 1 Percentage of rainfall for different time steps for 5 and 10 years return periods (according to JICA reports)

Time step (h)	Percentage (%)	5 years return period $X_T =$ 187.3136 mm	10 years return period $X_T =$ 226.1656 mm
0–4	9	16.858224	20.354904
4–8	15	28.09704	33.92484
8–12	44	82.417984	99.512864
12–16	16	29.970176	36.186496
16–20	9	16.858224	20.354904
20–24	7	13.111952	15.831592

3.3 Watershed Delineation and Model Simulation

For delineation watersheds of the two models in Tegharia and Baghair, ASTER DEM file of Bangladesh was used. This raster was clipped according to the study area shapefile for both the models. Existing stream network was digitized with the help of Google earth for the creation of "AGREE DEM". Watershed delineation of both the models of the study area was done using GeoSWMM. The subcatchments of delineated watershed of both the models are shown in Fig. 2.

After the delineation of watershed, the conduits, junctions, and outfalls were generated and widths and slopes of subcatchments were calculated for both the
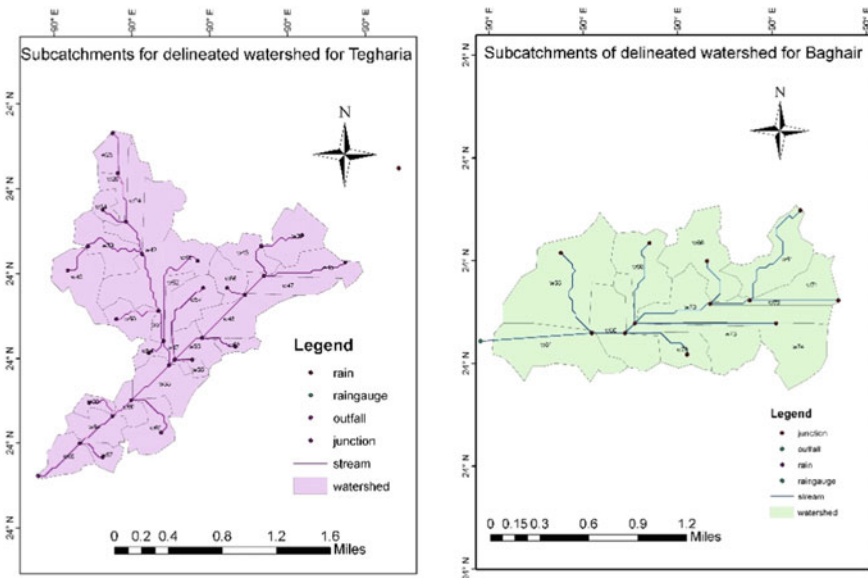
Fig. 2 Subcatchments of delineated watershed of Tegharia and Baghair

models. Finally, the models were simulated for 5 and 10 years return period. Maximum flow, average water depth, maximum flow velocity, volume of water, etc. were obtained from model outputs of 5 and 10 years model simulation.

4 Results and Discussions

4.1 Model Simulated Results

After delineating the watershed using GeoSWMM, the model of Tegharia was divided into 30 subcatchments and Baghair into 12 subcatchments. After the model simulations for 5 and 10 years return period, the runoff values were exported from model output. The runoff values of each subcatchment for both the models are given in Tables 2, 3, 4, 5, 6 and 7. The maximum value of peak runoff for 5 years return period for Tegharia is 1.77 CMS and for Baghair is 1.23 CMS and for 10 years return period the value for Tegharia is 2.25 CMS and for Baghair is 1.56 CMS. The maximum value of total runoff for 5 years return period is around 116.67 mm for Tegharia and 127.97 mm for Baghair and for 10 years return period it is 141.97 mm for Tegharia and 155.87 mm for Baghair. The maximum value of runoff co-efficient for 5 years return period is around 0.62 for Tegharia and 0.68 for Baghair and for 10 years return period it is 0.63 and 0.69.

4.2 Estimation of Area of the Drainage Conduit

The cross-sectional areas of the conduits are estimated by using the continuity equation from the model simulated values. While designing the drainage conduits, non-silting and non-scouring velocity 0.8 m/s was considered as design velocity. The proposed cross sections of the conduits are shown in Tables 8–9.

4.3 Calibration

To evaluate the performance of the model it is important to calibrate and validate both the models. As the study area is rapidly changing due to the development of the Padma bridge, there are limitations of observed up to date data for calibration. Also, relevant MODIS data was not available for calibration. So, following a different methodology, the pseudo calibration was done for both the models. Land use map was collected from CEGIS (Center for Environment and Geographic Information Services) for pseudo calibration. Using the land use map the surface cover of every catchment can be determined and the runoff coefficient can be calculated from it.

Table 2 Subcatchment runoff for 5 years return period for Tegharia

Subcatchment no	Total precipitation (mm)	Total runoff (mm)	Peak runoff (CMS)	Runoff coefficient
W24	187.4	102.1	0.89	0.55
W25	187.4	109.58	0.05	0.59
W28	187.4	76.48	0.11	0.41
W34	187.4	94.8	0.29	0.51
W37	187.4	87.5	0.60	0.47
W39	187.4	80.22	0.78	0.43
W40	187.4	72.93	0.83	0.39
W42	187.4	116.67	1.77	0.62
W43	187.4	87.51	0.56	0.47
W45	187.4	102.83	0.82	0.55
W46	187.4	76.57	0.65	0.41
W47	187.4	113.01	0.45	0.61
W48	187.4	87.51	0.90	0.47
W50	187.4	109.38	0.48	0.59
W51	187.4	94.80	0.21	0.51
W52	187.4	105.74	0.39	0.57
W53	187.4	72.93	0.19	0.39
W54	187.4	105.74	0.23	0.57
W55	187.4	98.45	0.55	0.53
W56	187.4	87.51	0.11	0.47
W57	187.4	96.98	0.64	0.52
W58	187.4	109.38	0.96	0.59
W59	187.4	80.22	0.20	0.43
W60	187.4	76.57	0.31	0.41
W62	187.4	72.92	0.59	0.39
W64	187.4	105.74	0.76	0.57
W67	187.4	109.37	0.20	0.59
W69	187.4	102.09	0.64	0.55
W86	187.4	94.8	0.52	0.51
W87	187.4	91.16	0.12	0.49

The types of land use are divided into the following categories: residential built ups, city business areas, cultivated lands or vegetation, waterbodies, and barren land. According to the Ohio Department of Transportation Hydraulics Manual, Runoff Coefficient for the Rational Method for 3 types of slopy lands are shown in Table 10.

Table 3 Subcatchment runoff for 10 years return period for Tegharia

Subcatchment no	Total precipitation (mm)	Total runoff (mm)	Peak runoff (CMS)	Runoff coefficient
W24	226.2	124.42	1.10	0.55
W25	226.2	133.38	0.07	0.59
W28	226.2	93.03	0.14	0.41
W34	226.2	115.69	0.36	0.51
W37	226.2	106.45	0.77	0.47
W39	226.2	97.73	0.97	0.43
W40	226.2	89.04	1.04	0.39
W42	226.2	141.97	2.25	0.63
W43	226.2	106.59	0.69	0.47
W45	226.2	125.42	1.01	0.55
W46	226.2	93.39	0.81	0.41
W47	226.2	137.48	0.58	0.61
W48	226.2	106.57	1.12	0.47
W50	226.2	133.07	0.61	0.59
W51	226.2	115.83	0.26	0.51
W52	226.2	128.86	0.48	0.57
W53	226.2	88.94	0.24	0.39
W54	226.2	129.07	0.28	0.57
W55	226.2	120.05	0.68	0.53
W56	226.2	105.55	0.14	0.47
W57	226.2	118.02	0.80	0.52
W58	226.2	133.11	1.21	0.59
W59	226.2	97.88	0.25	0.43
W60	226.2	93.38	0.38	0.41
W62	226.2	88.81	0.73	0.39
W64	226.2	128.91	0.94	0.57
W67	226.2	133.05	0.27	0.59
W69	226.2	124.32	0.80	0.55
W86	226.2	115.68	0.65	0.51
W87	226.2	111.38	0.15	0.49

The slope of the study area was found less than 2%, so the area is considered as flat. So, the runoff co-efficient values taken are as follows: for apartments dwelling areas or residential built ups: 0.5; City Business areas: 0.8; Cultivated lands or vegetation: 0.5; Barren land: 0.25; and Waterbodies: 0. Depending on land use, the run-off coefficient of a catchment is obtained by the following equation:

Table 4 Subcatchment runoff for 5 years return period for Baghair

Subcatchment no	Total precipitation (mm)	Total runoff (mm)	Peak runoff (CMS)	Runoff coefficient
W61	187.4	88.89	0.85	0.47
W65	187.4	93.93	1.19	0.50
W66	187.4	61.67	0.72	0.33
W68	187.4	69.29	0.70	0.37
W71	187.4	105.83	0.68	0.58
W72	187.4	127.97	0.20	0.68
W73	187.4	90.64	1.23	0.48
W74	187.4	69.28	0.75	0.37
W75	187.4	110.09	0.96	0.59
W76	187.4	54.81	0.29	0.29
W80	187.4	61.95	0.63	0.33
W81	187.4	69.06	1.00	0.37

Table 5 Subcatchment runoff for 10 years return period for Baghair

Subcatchment no	Total precipitation (mm)	Total runoff (mm)	Peak runoff (CMS)	Runoff coefficient
W61	226.2	108.23	1.06	0.48
W65	226.2	115.83	1.56	0.51
W66	226.2	74.89	0.88	0.33
W68	226.2	84.13	0.85	0.37
W71	226.2	128.52	0.83	0.57
W72	226.2	155.87	0.25	0.69
W73	226.2	110.09	1.50	0.49
W74	226.2	84.12	0.91	0.37
W75	226.2	134.07	1.20	0.59
W76	226.2	66.67	0.36	0.29
W80	226.2	75.22	0.76	0.33
W81	226.2	83.86	1.22	0.37

Runoff coefficient $=$ (% of residential built ups $*\,0.5\,+\,$% of City Business areas $*\,0.8\,+$ % of vegetation $*\,0.5\,+\,$% of barren land $*\,0.25\,+\,$% of waterbodies $*\,0)/100$

Using this equation, the runoff co-efficient of each subcatchment of both Tegharia and Baghair were calculated. After that, these values were compared with the model simulated runoff co-efficient values found from both the model outputs. Thus, the

Table 6 Conduit flow for 5 and 10 years return period for Tegharia

Conduit	Maximum flow (CMS) (5 year)	Maximum flow (CMS) (10 year)	Conduit	Maximum flow (CMS) (5 year)	Maximum flow (CMS) (10 year)
C19	0.05	0.07	C52	0.63	0.80
C24	0.16	0.21	C53	5.33	6.69
C33	0.29	0.36	C54	6.58	8.24
C36	0.59	0.76	C55	0.19	0.24
C38	1.62	2.01	C56	0.23	0.28
C39	1.30	1.62	C57	4.49	5.62
C40	0.84	1.04	C58	0.11	0.14
C42	4.67	5.85	C59	5.33	6.68
C43	1.13	1.43	C60	12.85	16.09
C45	0.84	1.04	C61	0.20	0.25
C46	0.67	0.83	C62	13.71	17.17
C47	2.41	3.04	C64	0.60	0.74
C48	3.78	4.74	C66	14.58	18.24
C49	0.52	0.65	C69	0.20	0.26
C51	0.47	0.61	C71	15.37	19.24

Table 7 Conduit flow for 5 and 10 years return period for Baghair

Conduit	Maximum flow (CMS) (5 year)	Maximum flow (CMS) (10 year)
C63	0.83	1.04
C67	1.71	1.53
C68	0.72	0.88
C70	0.72	0.88
C73	0.70	0.86
C74	1.68	2.08
C75	3.59	4.44
C76	0.77	0.94
C77	6.01	7.42
C78	0.30	0.38
C82	8.95	11.13
C88	6.89	8.50

calibration was completed. In Table 11, a summary of calibration is shown by comparing between the 5 years simulated runoff co-efficient and estimated runoff co-efficient values of both the models.

For both models, almost for all the subcatchments the model simulated and calculated runoff coefficients are close which indicates the model can predict the runoff

Table 8 Cross-sectional area for 5 and 10 years return period for Tegharia

Conduit	Area (m^2) (5 year)	Area (m^2) (10 year)	Conduit	Area (m^2) (5 year)	Area (m^2) (10 year)
C19	0.06	0.09	C52	0.79	1.00
C24	0.20	0.26	C53	6.66	8.36
C33	0.36	0.45	C54	8.23	10.30
C36	0.74	0.95	C55	0.24	0.30
C38	2.03	2.51	C56	0.29	0.35
C39	1.63	2.03	C57	5.61	7.03
C40	1.05	1.30	C58	0.14	0.18
C42	5.84	7.31	C59	6.66	8.35
C43	1.41	1.79	C60	16.06	20.11
C45	1.05	1.30	C61	0.25	0.31
C46	0.84	1.04	C62	17.14	21.46
C47	3.01	3.80	C64	0.75	0.93
C48	4.73	5.93	C66	18.23	22.80
C49	0.65	0.81	C69	0.25	0.33
C51	0.59	0.76	C71	19.21	24.05

Table 9 Cross-sectional area for 5 and 10 years return period for Baghair

Conduit	Area (m^2) (5 year)	Area (m^2) (10 year)	Conduit	Area (m^2) (5 year)	Area (m^2) (10 year)
C63	1.04	1.30	C75	4.49	5.55
C67	2.14	1.91	C76	0.96	1.18
C68	0.90	1.10	C77	7.51	9.28
C70	0.90	1.10	C78	0.38	0.48
C73	0.88	1.08	C82	11.19	13.91
C74	2.10	2.60	C88	8.61	10.63

quite efficiently. Slightly more variation between simulated and calculated runoff coefficient has been observed for subcatchment 57 and 58 at Tegharia and subcatchment 65 and 72 at Baghair. It indicates Tegharia and Baghair models slightly overestimate runoff for w57, w58 and w72 where for w72 the Baghair model estimates slightly lower runoff. But overall, the variation in total runoff is not too significant for both the models.

Table 10 Runoff coefficient for the rational method (Source: ODOT)

Land use	Flat	Rolling	Hilly	Land use	Flat	Rolling	Hilly
Pavement & roofs	0.9	0.9	0.9	Side slopes, turf	0.3	0.3	0.3
Earth shoulders	0.5	0.5	0.5	Median areas, turf	0.25	0.3	0.3
Drives and walks	0.75	0.8	0.85	Cultivated lands, clay and loam	0.5	0.55	0.6
Gravel pavement	0.85	0.85	0.85	Cultivated lands, sand and gravel	0.25	0.3	0.35
City business area	0.8	0.85	0.85	Industrial areas, light	0.5	0.7	0.8
Apartment dwelling areas	0.5	0.6	0.7	Industrial areas, heavy	0.6	0.8	0.9
Light residential	0.35	0.4	0.45	Parks & cemeteries	0.1	0.15	0.25
Normal residential	0.5	0.55	0.6	Playgrounds	0.2	0.25	0.3
Dense residential	0.7	0.75	0.8	Woodlands & forests	0.1	0.15	0.2
Lawns	0.17	0.22	0.35	Meadows & pasture land	0.25	0.3	0.35
Grass shoulders	0.25	0.25	0.25	Unimproved areas	0.1	0.2	0.3
Side slopes, Earth	0.6	0.6	0.6				

5 Conclusion

The Padma Bridge Link road is one of the most important parts of the Padma bridge multipurpose project. Hence, stormwater drainage management of its corresponding area is essential to protect it. Now-a-days, GeoSWMM is considered as an effective tool to estimate the urban stormwater. Thus, in this study, Geo-SWMM was used to develop two models in Tegharia and Baghair. The maximum value of total runoff for 5 years return period is around 116.67 mm for Tegharia and 127.97 mm for Baghair and for 10 years return period it is 141.97 mm for Tegharia and 155.87 mm for Baghair. The maximum value of runoff co-efficient for 5 years return period is around 0.62 for Tegharia and 0.68 for Baghair and for 10 years return period it is 0.63 and 0.69 for Tegharia and Baghair. The findings of the study indicate that Tegharia and Baghair may experience an increase of 21.8% and 21.7% stormwater runoff in future.

Table 11 Summary of calibration

Tegharia			Baghair		
Subcatchment	Model simulated runoff co-efficient	Calculated runoff co-efficient	Subcatchment	Model simulated runoff co-efficient	Calculated runoff co-efficient
W24	0.55	0.54	W61	0.47	0.59
W25	0.59	0.57	W65	0.50	0.55
W28	0.41	0.40	W66	0.33	0.33
W34	0.51	0.52	W68	0.37	0.38
W37	0.47	0.48	W71	0.58	0.55
W39	0.43	0.44	W72	0.68	0.63
W40	0.39	0.44	W73	0.48	0.49
W42	0.62	0.60	W74	0.37	0.36
W43	0.47	0.48	W75	0.59	0.58
W45	0.55	0.55	W76	0.29	0.3
W46	0.41	0.42	W80	0.33	0.32
W47	0.61	0.60	W81	0.37	0.35
W48	0.47	0.49			
W50	0.59	0.57			
W51	0.51	0.52			
W52	0.57	0.59			
W53	0.39	0.38			
W54	0.57	0.56			
W55	0.53	0.52			
W56	0.47	0.48			
W57	0.52	0.49			
W58	0.59	0.56			
W59	0.43	0.44			
W60	0.41	0.40			
W62	0.39	0.40			
W64	0.57	0.58			
W67	0.59	0.59			
W69	0.55	0.56			
W86	0.51	0.50			
W87	0.49	0.48			

References

1. Local Government Engineering Department Homepage, http://oldweb.lged.gov.bd/DistrictProj ectSchemeDetailsView.aspx?DistrictID=24. Accessed 10 Mar 2021
2. The Newage Bangladesh, https://www.newagebd.net/article/88525/china-proposed-housing-projects-at-ashulia-keraniganj-draw-flak. Accessed 10 Mar 2021
3. Public Private Partnership Authority Homepage, https://www.pppo.gov.bd/projects-residential-apartment-building-jhilmil-residential-dhaka.php. Accessed 10 Mar 2021
4. Maliha M (2017) Design of stormwater drainage network with limited data using GeoSWMM: a case study for Bogra city. B.Sc. thesis, Department of Water Resources Engineering, Bangladesh University of Engineering and Technology, Dhaka, Bangladesh
5. Abdullah F (2017) Design of stormwater drainage network with limited data using GeoSWMM: a case study for Tangail Sadar Upazilla. B.Sc. thesis, Department of Water Resources Engineering, Bangladesh University of Engineering and Technology, Dhaka, Bangladesh
6. Mohammad A (2017) Assessment of stormwater runoff from the eastern part of Chittagong city using GeoSWMM. B.Sc. thesis, Department of Water Resources Engineering, Bangladesh University of Engineering and Technology, Dhaka, Bangladesh
7. Islam M (2017) Assessment of stormwater runoff from the western part of Chittagong city using GeoSWMM. B.Sc. thesis, Department of Water Resources Engineering, Bangladesh University of Engineering and Technology, Dhaka, Bangladesh
8. Saleque MG (1991) Flood flows of the Jamuna: a study of magnitudes and frequencies. M. Engineering thesis, Department of Water Resources Engineering, Bangladesh University of Engineering and Technology, Dhaka
9. Fortunatoa A, Oliveria E, Mazzolaa MR (2014) Selection of the optimal design rainfall return period of urban drainage systems. In: 16th conference on water distribution system analysis (WDSA), pp 742–749

Physics Informed Neural Network for Spatial-Temporal Flood Forecasting

Ragini Bal Mahesh, Jorge Leandro, and Qing Lin

1 Introduction

Flood forecasting plays a prominent role today in flood management. There has been a transition in flood mitigation measures from a structural approach to non-structural approaches such as flood forecasting and early warning system; this transition is because no single mitigation or defense measure is entirely adequate [12]. The flood forecasting techniques help in flood management preparedness and early warning systems by providing an extended lead time for the decision-makers [29].

Conventionally, flood forecasting is performed by physically based models or conceptual models [5]. The conceptual hydrological models are usually based on the continuity equation where the dynamic and kinematic wave is applied, while the hydraulic routing is physically based and the fully dynamic Saint Venant Equations is numerically solved [12, 22]. A physically based model provides accurate results but is computationally expensive, scales with domain size, requires large geometry data, and does not meet real-time applications due to the large number of computations performed.

The data-driven model, such as Artificial Neural Network (ANN) for flood forecasting, has been very promising [17]. Artificial Neural Networks are algorithms used to map input and output through a mathematical relation. It is made of a neuron structure organized in layers. Stacking multiple layers of this structure allows determining complex non-linear relationships [10]. Rumelhart et al. [26] were the first to train such a neural network to learn with backpropagation training. LeCun et al. [18] pioneered deep learning where multilayer perceptron stacked with a dense number of hidden layers to form a deep neural network. Thus, such a network that determines complex non-linearities finds its place in a hydrological application. However, the

R. B. Mahesh (✉) · J. Leandro · Q. Lin
Department of Civil, Geo and Environmental Engineering, Technical University of Munich, Munich, Germany
e-mail: ragini.mahesh@tum.de

ANNs are still inferior to the classical method of solving the Saint Venant Equations in terms of accuracy. Therefore, it has always resulted in tradeoff between the model performance and computational efforts while selecting an appropriate model. Several architectures that are available under the ANN structure have been applied to flood forecasting. Lin et al. [19] used ANN to determine the flood inundation maps. Kasiviswanathan et al. [15] applied ANN for flood forecasting, where they compared Wavelet-Based Neural network (WNN) with ANN in terms of the forecast accuracy and precision at various lead-times. Elsafi [7] did an ANN study for flood prediction where ANN was applied at specific locations to determine the prediction using the upstream boundary condition. Kratzert et al. [17] tackle the loss of the input information's sequential order in a neural network using the Recurrent Neural Network (RNN), where Long Short-Term Memory (LSTM) models are state of the art. Another similar test was performed by Sit and Demir [31] for the applicability of neural networks for flood forecasting where the gradient vanishing problem of RNN was addressed, and the Gated Recurrent Unit (GRU) was used as the network architecture. Bhola et al. [3] have used Computer Vision to determine flood inundation forecast. Due to the complex nature of flood forecasting, researchers have always implemented leading and promising architecture.

Research in deep learning has progressed to utilize physics information to either solve PDE or enhance a PDE solver. The latter uses neural networks to boost the PDE solver; such a field is called Geometric Deep Learning. Haehnel et al. [11] used the domain decomposition technique from Computational Fluid Dynamics, where the deep learning models are trained at subdomain levels under the boundary condition constraint to monitor and forecast air pollution. In a CFD-driven machine learning model, Zhao et al. [35] used RANS to model turbulence and a machine learning model to correct the error between the turbulence and direct numerical simulation. Dockhorn [6], through his work, discussed solving PDE such as Navier Stokes Equation using combined loss function and BFGS optimizer. Baymani et al. [2] also utilized ANN to solve the Navier Stokes Equation, where a stream function is used in the error function to drive it to a minimum. Wave propagation with the neural network has been explored with different architecture on image datasets [8, 32]. The most popular research to solve the PDE using a neural network is by Raissi et al. [25]. They introduced PINN that is capable of solving any physical law governing the data. PINNs are deep learning techniques used to solve the Partial Differential Equation (PDE) by approximating a solution to the PDE. The hypothesis for PINNs is to bridge the gap between classical methods and the data-driven neural networks by utilizing available physics information. The Navier Stokes Equation has been encoded in the PINNs in such an application case [24]. PINN implementations further include seismic wave propagation [14] and flood forecasting with image datasets [23]. The PINNs could be an efficient solution to tackle the tradeoff between the performance and the computational efforts. They are very recent advancements; therefore, there is currently every less or no research where the PINNs are constrained with Saint Venant Equations for flood forecasting using numerical data.

This work focuses on PINNs for spatial-temporal scale flood forecasting with priori information of the Saint Venant Equations. It comprises an encoded structure of physics law with the inclusion of PDE loss function, which introduces the priori information into the system of neural network explicitly. Numerical simulations of the Saint Venant Equations are performed to generate synthetic datasets to establish and evaluate the performance PINNs.

2 Methodology

2.1 Artificial Neural Network

Artificial Neural Network (ANN) is a machine learning algorithm inspired by biological neurons. Perceptron [33] is the simplest available ANN architecture. It is a single layer neural network that consists of a single neuron, input parameters, weights, bias, and activation function. The output (y) is computed by multiplying the input parameters (x_n) with weights (w_n) and later added together to form a weighted sum on which an activation function (f) is applied to introduce non-linearity. The output is mathematically expressed by Eq. (1), where w_0 is the bias. The perceptron converges to a solution only if the training data is linearly separable, and a multi-layer perceptron overcomes the limitation of the perceptron by stacking many perceptrons together [9]. It consists of an input layer, one or more hidden layers, and an output layer. Each layer is a collection of vertically stacked neurons. Every neuron in a layer is connected to every neuron in the next layer and, therefore, is fully connected.

$$y = f\left(w_0 + \sum_{i=1}^{n} w_i x_i\right) \tag{1}$$

Rumelhart et al. [26] were the first to apply the backpropagation algorithm to a multilayer neural network. Backpropagation is the backward propagation of error for the training of a feed-forward neural network. At the end of feed-forward propagation, the error between predicted and target output is determined with a loss function. The objective of training with backpropagation is to reduce the loss function to a minimum. It is achieved by gradually adjusting the weights in a backward direction. A chain rule is used to approximate the derivative of the loss function with respect to every weight in the network as given by Eq. (2), where L is the loss function, $w_{i,j}$ are the weights for node (i, j), y_i is the output, and $\sum w_i x_i$ is the weighted sum of input node and weights.

$$\frac{\partial L}{\partial w_{i,j}} = \frac{\partial L}{\partial y_i} \cdot \frac{\partial y_i}{\partial \sum w_i x_i} \cdot \frac{\partial \sum w_i x_i}{\partial w_{i,j}} \tag{2}$$

Backpropagation is extremely efficient as the weights are computed at each layer and reused for calculation at the next layer rather than applying chain rule at every weight individually. The new computed weights are later updated throughout the network. There are various algorithms to perform this backpropagation. The basic algorithm is stochastic gradient descent, where a single training example is used for each iteration and weight updates. The learning process is regulated by the learning rate (L), which remains constant throughout the training. The Adam optimizer [16] is an extension to the stochastic gradient descent where the update for each weight $w_{i,j}$ is performed with Eqs. (3)–(7), where ϵ is the learning rate, g_t is the gradient, v_t is the exponential gradient, s_t is the exponential gradient of the squares of the gradient, and $\beta_1 = 0.9$, $\beta_2 = 0.999$ are hyperparameters with default values.

$$w_{i,j}^{t+1} = w_{i,j}^t - \eta \frac{\partial L^t}{\partial w_{i,j}^t} \tag{3}$$

$$v_t = \beta_1 v_{t-1} - (1 - \beta_1) * g_t \tag{4}$$

$$s_t = \beta_2 s_{t-1} - (1 - \beta_2) * g_t^2 \tag{5}$$

$$\Delta w_t = -\eta \frac{v_t}{\sqrt{s_t + \epsilon}} * g_t \tag{6}$$

$$w_{t+1} = w_t + \Delta w_t \tag{7}$$

In this work, the implemented model is a Keras (2.2.4 version) sequential model that allows for stacking multiple layers in sequential order. A fully connected network is created with one input layer, three hidden layers, and one output layer. The shape of the input is five unless specified and output neurons are two. The model is compiled after defining the structure and the hyperparameter setting. The hyperparameter configuration is based on (i) hyperparameter tunning through grid search of neurons (5, 15, 25), (ii) industry expertise, (iii) published research [19, 28], or (iv) default values of the library. An overview of the parameter and hyperparameter setting for this work is tabulated in Appendix 1. The parameters in the Saint Venant Equations (Eq. (8)), along with boundary discharge, were used as the input information. The flow of information is from five input neurons with data labels as boundary discharge (q, m^3/s), manning's friction coefficient (n), slope (S), time (t, s), and distance (x, m). The vector of these input data is passed through the input layer, hidden layers, and finally to the output layer with two outputs: water depth (h, m) and velocity (v, m/s), creating an encoded structure ANN. Apart from this encoded architecture, a basic architecture is created to evaluate the significance of the encoded structure. This basic architecture has one input neuron, i.e., boundary discharge (q), and two output neurons: h and u.

2.2 Physics Informed Neural Network

Physics Informed Neural Network (PINN) is a deep learning technique for solving PDE. A neural network is built that minimizes the loss function with the priori information encoded. Priori information acts as a regularizing agent by narrowing the true solution space, and also, the encoded structure quickly steers toward the right solution. As a priori information, the PDE is introduced in the neural network by implementing a loss function leveraging the Automatic Differentiation (AD) [1] technique to determine its derivatives. AD works on the principle of augmenting the standard computation with derivative computation. This leads to a numerical computation consisting of operators whose derivatives are known. An overall derivative is determined by combining the operators with the chain rule. The gradients are calculated using the Kgradients from the Keras library.

The total loss function of the PINNs includes regression loss and a PDE loss. The PDE loss is implemented such that the equation reduces to zero when the error is zero. The Saint Venant Equations with source terms given in Eq. (8) [4, 20, 27, 34] is implemented as the PDE loss, where S_0 is the bed slope, S_f is the friction term, and n is the manning's coefficient. The constructed loss function is given by Eqs. (10)–(13), where $\widehat{u_i}$ (m/s) and $\widehat{h_i}$ (m) are outputs.

$$\frac{\partial u_i}{\partial t} + u_i \frac{\partial u_i}{\partial x} + g \frac{\partial h_i}{\partial x} - g S_0 + g S_f = 0 \tag{8}$$

$$S_0 = -S \qquad S_f = \frac{n^2 \widehat{u_i^2}}{\widehat{h_i^{4/3}}} \tag{9}$$

$$\text{Loss} = \text{MSE}_u + \text{MSE}_f + \text{MSE}_{\text{PDE}} \tag{10}$$

$$\text{MSE}_u = \frac{1}{N} \sum_{i=1}^{N} \left| u_i - \widehat{u_i} \right|^2 \tag{11}$$

$$\text{MSE}_f = \frac{1}{N} \sum_{i=1}^{N} \left| h_i - \widehat{h_i} \right|^2 \tag{12}$$

$$\text{MSE}_{\text{PDE}} = \frac{1}{N} \sum_{i=1}^{N} \left| \frac{\partial u_i}{\partial t} + u_i \frac{\partial u_i}{\partial x} + g \frac{\partial h_i}{\partial x} - g S_0 + g S_f \right|^2 \tag{13}$$
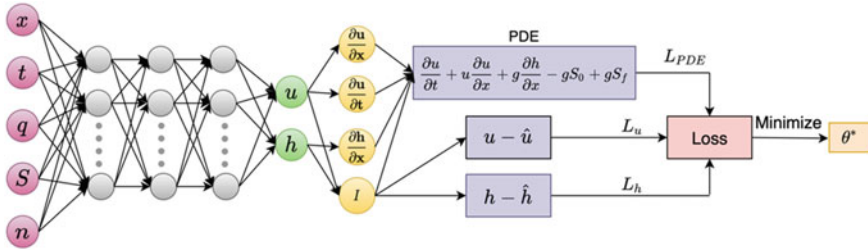
Fig. 1 A schematic representation of physics informed neural networks (PINNs) for solving Saint Venant equations with combined loss function

A schematic representation of the physics informed artificial neural network is given in Fig. 1, which consists of standard neural network and PDE is the partial differential equation. The loss function is evaluated by computing the derivatives through automatic differentiation. The combined loss is minimized to obtain an approximation for the PINN. In this work, in addition to the artificial neural network described in Sect. 2.1, the physics informed artificial neural network was established while keeping the remaining settings and hyperparameters the same.

2.3 Synthetic Dataset

The synthetic dataset used to train, validate, and test the neural networks are generated with FullSWOF-2D (Full Shallow Water Equation for Overland Flows) [4]. Firstly, a study area of 1000 m is set up in FullSWOF-2D with the input boundary condition synthesized from the SCS Hydrograph method [30]. Only 14 Direct Runoff Hydrographs resulting from the best combination of effective rainfall duration (1–6 m) and rainfall depth (1–8 cm) are selected. The selection is made such that the peak discharges (q_p) are between the range of 2–18 m^3/s, and it is spread over low (2–5 m^3/s), medium (6–14 m^3/s), and high (15–18 m^3/s) flow. The data is generated by running the simulations in FullSWOF-2D for 34 flood scenarios designed by creating a combination of the three stream characteristics: slope, friction coefficient, and peak discharge. Only the necessary features as that of the Saint Venant Equations are extracted and split into training, validation, and test dataset at 1 s timestep interval and 500 grid points. The validation and test dataset remains the same for all model except for the dataset with varied slope.

The datasets are designed to meet the requirement of different model analyses. The original training dataset (Appendix 3) has 8 flood scenarios respecting the split rule of ~70% of the entire dataset while the rest ~30% made up validation dataset with 3 flood scenarios. The test dataset is carefully designed with 6 different flood scenarios. In the original training dataset, the 8 flood scenarios are designed by varying 3 slope values (1/100, 1/500, 1/1000) with 3 friction coefficients (0.025, 0.035, 0.045), resulting in 8 combinations (except one scenario with Fr > 1) for

which low, medium, and high peak discharges are assigned. Larger timesteps (3 s, 5 s) in addition to the original 1 s timestep were explored to find a feasible larger timestep for the PINN in order to reduce the training time.

2.4 Model Evaluation

The model's performance is measured through accuracy. The metrics used in this work are Mean Squared Error (MSE), Coefficient of Determination (R^2), and Nash Sutcliffe Efficiency (NSE) [13]. MSE is the squared absolute error between the output and the target values. It is given by Eq. (14), where N is the number of training samples, d_i are the target values, and y_i is the output values. R^2 is used to evaluate the linear correlation between target and output values. It signifies the goodness of fit of the model. It is given by Eq. (15), where $\bar{\bar{d}}$ is the mean of target values and $\bar{\bar{y}}$ is the mean of output values. NSE metric is used for hydrological prediction evaluation; it takes into consideration different catchment dynamics. It is determined using Eq. (16).

$$\text{MSE} = \frac{1}{N} \sum_{i=1}^{N} (d_i - y_i)^2 \tag{14}$$

$$R^2 = \left[\frac{\sum_{i=1}^{N} \left(d_i - \bar{\bar{d}} \right)\left(y_i - \bar{\bar{y}} \right)}{\sqrt{\sum_{i=1}^{N} \left(d_i - \bar{\bar{d}} \right)^2 \sum_{i=1}^{N} \left(y_i - \bar{\bar{y}} \right)^2}} \right]^2 \tag{15}$$

$$\text{NSE} = 1 - \frac{\sum_{i=1}^{N} (d_i - y_i)^2}{\sum_{i=1}^{N} \left(d_i - \bar{\bar{d}} \right)^2} \tag{16}$$

The model architectures in this work consist of two outputs (h, u). For each output, an average metric (MSE, NSE, R^2) is computed by taking the average of 6 flood scenarios in the test dataset. The model's overall performance is evaluated as an average of averaged metric values, i.e., average MSE = 0.5 * (average MSE of u + average MSE of h). Similarly, the average R^2 and average NSE is determined.

Table 1 ANN 1 and ANN 2 model performance on evaluation metrics for test dataset

Model	Avg. MSE	Avg. h MSE	Avg. u MSE	Avg. R^2	Avg. NSE
ANN 1	0.3771	0.4824	0.2719	0.70	0.44
ANN 2	0.0554	0.0785	0.0323	0.98	0.93

3   Results and Discussions

3.1   Artificial Neural Network Model

A basic ANN (ANN 1) architecture and an encoded structure ANN (ANN 2) is implemented under the ANN Framework with hyperparameter settings that were preconfigured (Appendix 1) or obtained through grid search (Appendix 2). The results of both models are shown in Table 1. The average MSE of ANN 1 is high with a value of 0.3371, and the average MSE of h is higher than the average MSE of u. Therefore, this model forecasts velocity better than the water depth. According to Moriasi et al. [21], NSE > 0.50 is considered satisfactory, and with a 0.44 average NSE, ANN 1 is not satisfactory. The reason is attributed to only one input variable to the model; usually more features help provide more information to the network, which the model currently lacks.

   With the encoded structure of ANN 2, the model performs better with an average MSE loss of 0.0554. An increase of 85% in average MSE performance was observed from ANN 1 to ANN 2. A similar increase was seen for average u MSE (88%) and average h MSE (84%). ANN 2 outperforms ANN 1, indicating that the encoded structure of the Saint Venant Equations provides good results. Specifically, the value introduced for q is a boundary condition. A single flood scenario is regulated by the boundary condition, similar to how the PDE is solved under boundary condition has a unique solution. The other input neurons, such as slope and friction coefficient, are constant while x and t are fixed with study channel and simulation time. Therefore, it could be said that the output variables are calculated similarly to that of the solver. However, this may not be true for complex cases such as hydraulic jump and dam break. It further may require the governing equation constraint itself. ANN 2 results serve as a reference point while evaluating the performance of PINNs.

3.2   Physics Informed Neural Network Model

PINN model was implemented to constrain the neural network in the solution search space of the Saint Venant Equations. The ANN 2 was extended to PINN with the implementation of a custom loss function of PDE loss + MSE loss, along with the best parameters from grid search (Appendix 2). The results are shown in Table 2. The average MSE of PINN is 0.0535. PINN has h average MSE lower than u average

Table 2 PINN model performance on evaluation metrics for test dataset

Model	Avg. MSE	Avg. h MSE	Avg. u MSE	Avg. R^2	Avg. NSE
PINN	0.0535	0.0562	0.0509	0.97	0.92

MSE, and the model has very good NSE (0.92) and accuracy ($R^2 = 0.97$). Figure 2 shows good predictions for water height level and velocity for the best performing test flood scenario with the PINN model.

On average MSE, PINNs perform better than ANN 2. The h average MSE is better than u average MSE, contrary to the result in ANN 2. This shift might be attributed to the PDE loss as it contains depth-averaged terms. Since these terms are a part of the loss function, the model is well trained to predict water depths, and this is also an indication of the constraints successfully imposed by the PDE loss. A significant amount of improvement was seen using ANN 2, where the network's encoded input-output structure had considerable influence on improving the results. In comparison, the physics loss function could introduce a minimal improvement (0.2%) over ANN 2. A 28% increase is seen in the case for predictions for h, and a 58% decrease in velocity predictions was observed. The physics constraint works well for predicting h; therefore, PINNs could be potentially used to predict water depths as the main output.
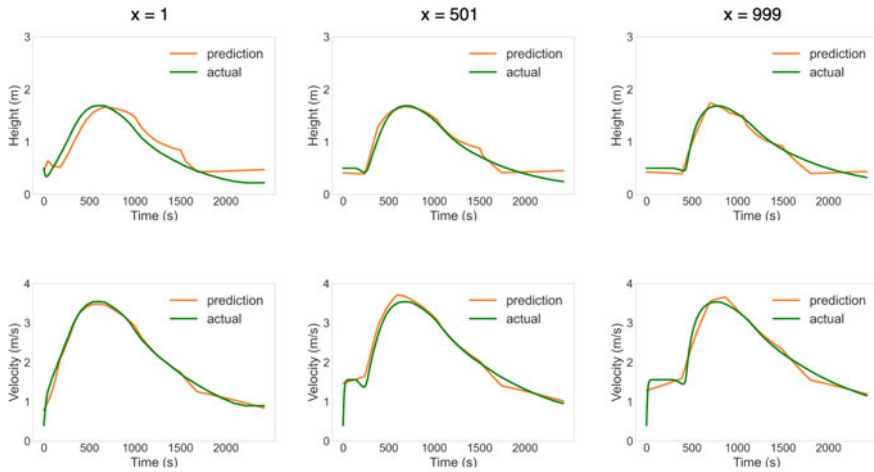
Fig. 2 Comparison of predicted versus actual water height level and velocity for a test flood scenario ($S = 1/1000$, $n = 0.040$, $q_p = 6$ m^3/s) at distance $x = 1$, $x = 501$, and $x = 999$ for PINN

Table 3 Different PINN model performance on evaluation metrics for test dataset

Model	Avg. MSE	Avg. h MSE	Avg. u MSE	Avg. R^2	Avg. NSE
PINN 3s	0.0913	0.1041	0.0784	0.93	0.86
PINN 5s	0.1219	0.1317	0.1122	0.90	0.78

3.3 Timestep Sensitive Analysis

Timestep sensitivity analysis was performed to check the stability of the PINN at larger timesteps. The original training dataset was truncated for every value at 3 s and 5 s interval to develop PINN 3s and PINN 5s models. The model's performance is tabulated in Table 3. PINN 3s model had a 71% decrease, and PINN 5s model had >100% performance decreased compared to PINN. The results validate that the 1 s timestep was ideal for this work. Compared to timesteps in the numerical solvers, the 1 s timestep is still relatively large and contributes to less computational effort in PINNs.

3.4 Model Comparison

The different model results are presented in the above sections, and to be able to compare the models' overall performance, the average MSE of the six test scenarios is considered. The average MSE for each model is represented in the form of box plots. Figure 3a represents the model performance on velocity forecasting, and Fig. 3b represents the model performance on water height forecasting. Overall model performance for different models is shown in Fig. 3c. The model comparison was made to determine the best performing model, including the timestep sensitivity analysis. The best performing model on average MSE metric is PINN, and it can be observed there is performance improvement due to the reduction of error from water height predictions, as shown in Fig. 3b.

4 Conclusion

In this work, Physics Informed Neural Network (PINN) was established to spatially and temporally forecast floods on a 1D channel. It consists of neural network architecture, which is encoded with physics or a priori information, in this case, the Saint Venant Equations in the form of a PDE loss function. The automatic differentiation technique is used to calculate the derivatives for the PDE loss to facilitate the training process.
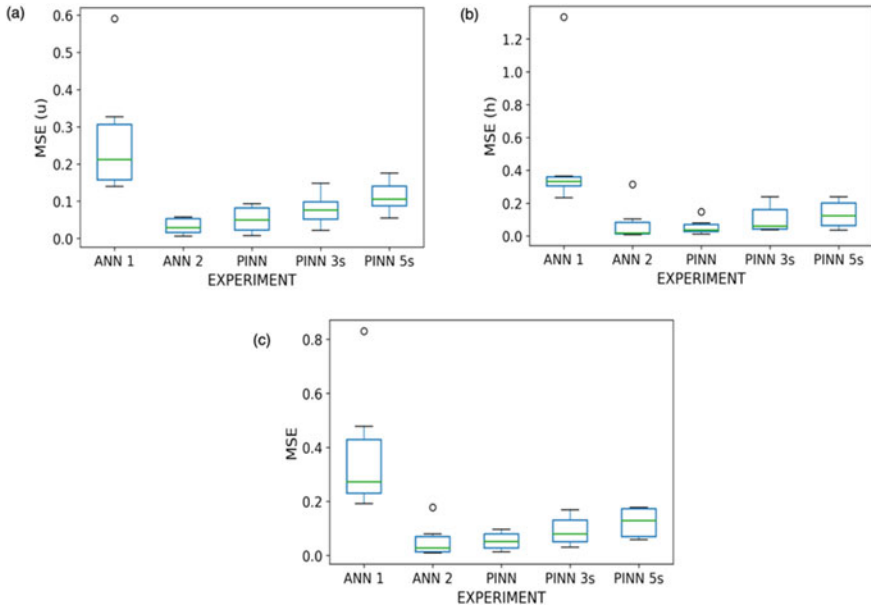
Fig. 3 Box plot for different established models for **a** average u MSE metric, **b** average h MSE metric, and **c** average MSE; average of u + h

Synthetic datasets containing physics information were generated using the SCS Hydrograph Method and FullSWOF-2D to train data driven models. The workflow in this work was modeling from a simple case to a more complex scenario. Foremost, ANN 1 with just q as input was modeled with MSE loss, and later ANN 2 with inputs (q, x, t, S, n) were modeled with outputs h and u. It was observed that ANN 2 has much lower MSE loss than ANN 1, indicating that the neural network learns better with encoded structure, which consisted of the discharge as an input boundary conditions.

The physics constraint was added to the encoded structure through the PINNs modeled using the combined MSE and PDE loss. The performance of PINN was better than the earlier established ANN 2. The majority of performance improvement was introduced by the encoded structure in comparison to the combined loss function. Better performance was seen for water depth forecasting in PINN than ANN 2 due to the depth-averaged terms in the PDE Loss. This confirms that PDE loss was being imposed positively to constrain the solution search space respecting the governing equations.

PINN with 1 s timestep performed better in a timestep analysis while the performance decayed with the increase in timestep (PINN 3s & PINN 5s). However, the 1 s timestep is larger than the timesteps generally used in the numerical solver, which help reduce the computational effort for PINN.

Through this work, it is concluded that flood forecasting can be performed with neural networks constrained with Saint Venant Equations through a physics informed neural network architecture resulting in improved performance.

Appendix

Appendix 1: Hyperparameter Settings

Attribute	Value
Activation function	ReLU
Number of layers	3 [19]
Number of neurons	Gird search; (n1, n2, n3)
Number of epochs	Early stopping
Learning rate	0.0001
Early stopping patience	1
Batch size	128
Optimizer	Adam
Loss function	MSE

Appendix 2: Grid Search Result for Best Number of Neurons in Each Layer for Every Model

Model	Grid (n1, n2, n3)
ANN 1	5, 5, 5
ANN 2	25, 25, 5
PINN	5, 5, 5
PINN 3s	15, 5, 5
PINN 5s	25, 15, 25

Appendix 3: Generated Datasets for Training, Validation and Testing for Different PINN Models with Flood Scenarios in the Legend

(a) Training dataset.

(b) Validation dataset.

(c) Test dataset.
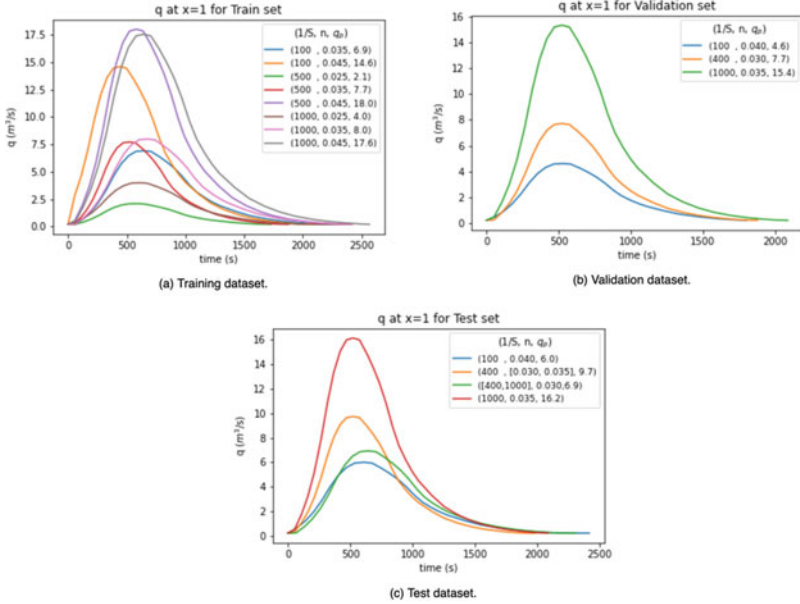
References

1. Baydin AG, Pearlmutter BA, Radul AA, Siskind JM (2017) Automatic differentiation in machine learning: a survey. J Mach Learn Res 18(1):5595–5637
2. Baymani M, Effati S, Niazmand H, Kerayechian A (2015) Artificial neural network method for solving the Navier–Stokes equations. Neural Comput Appl 26(4):765–773
3. Bhola PK, Nair BB, Leandro J, Rao SN, Disse M (2019) Flood inundation forecasts using validation data generated with the assistance of computer vision. J Hydroinf 21(2):240–256
4. Delestre O, Darboux F, James F, Lucas C, Laguerre C, Cordier S (2017) FullSWOF: full shallow-water equations for overland flow. J Open Source Softw 2(20):448. https://doi.org/10.21105/joss.00448
5. Devia GK, Ganasri BP, Dwarakish GS (2015) A review on hydrological models. Aquat Procedia 4:1001–1007
6. Dockhorn, T. (2019) A discussion on solving partial differential equations using neural networks. ArXiv Preprint arXiv:1904.07200
7. Elsafi SH (2014) Artificial neural networks (ANNs) for flood forecasting at Dongola station in the River Nile Sudan. Alex Eng J 53(3):655–662
8. Fotiadis S, Pignatelli E, Valencia ML, Cantwell C, Storkey A, Bharath AA (2020) Comparing recurrent and convolutional neural networks for predicting wave propagation. ArXiv Preprint arXiv:2002.08981

9. Géron A (2019) Hands-on machine learning with Scikit-Learn, Keras, and TensorFlow: concepts, tools, and techniques to build intelligent systems. O'Reilly Media, Sebastopol

10. Goodfellow I, Bengio Y, Courville A, Bengio Y (2016) Deep learning, vol 1. MIT Press, Cambridge

11. Haehnel P, Mareček J, Monteil J, O'Donncha F (2020) Using deep learning to extend the range of air pollution monitoring and forecasting. J Comput Phys 408:109278

12. Jain SK, Mani P, Jain SK, Prakash P, Singh VP, Tullos D, Kumar S, Agarwal SP, Dimri AP (2018) A brief review of flood forecasting techniques and their applications. Int J River Basin Manag 16(3):329–344

13. Kao I-F, Zhou Y, Chang L-C, Chang F-J (2020) Exploring a long short-term memory based encoder-decoder framework for multi-step-ahead flood forecasting. J Hydrol 124631

14. Karimpouli S, Tahmasebi P (2020) Physics informed machine learning: seismic wave equation. Geosci Front 11(6):1993–2001

15. Kasiviswanathan KS, He J, Sudheer KP, Tay J-H (2016) Potential application of wavelet neural network ensemble to forecast streamflow for flood management. J Hydrol 536:161–173

16. Kingma DP, Ba J (2014) Adam: a method for stochastic optimization. ArXiv Preprint arXiv: 1412.6980

17. Kratzert F, Klotz D, Brenner C, Schulz K, Herrnegger M (2018) Rainfall–runoff modelling using long short-term memory (LSTM) networks. Hydrol Earth Syst Sci 22(11):6005–6022

18. LeCun Y, Bengio Y, Hinton G (2015) Deep learning. Nature 521(7553):436–444

19. Lin Q, Leandro J, Wu W, Bhola P, Disse M (2020) Prediction of maximum flood inundation extents with resilient backpropagation neural network: case study of Kulmbach. Front Earth Sci 8:332

20. Martins R, Leandro J, Djordjević S (2018) Wetting and drying numerical treatments for the Roe Riemann scheme. J Hydraul Res 56(2):256–267

21. Moriasi DN, Arnold JG, Van Liew MW, Bingner RL, Harmel RD, Veith TL (2007) Model evaluation guidelines for systematic quantification of accuracy in watershed simulations. Trans ASABE 50(3):885–900

22. Mujumdar PP (2001) Flood wave propagation. Resonance 6(5):66–73

23. Qian K, Mohamed A, Claudel C (2019) Physics informed data driven model for flood prediction: application of deep learning in prediction of urban flood development. ArXiv Preprint arXiv: 1908.10312

24. Raissi M, Karniadakis GE (2018) Hidden physics models: machine learning of nonlinear partial differential equations. J Comput Phys 357:125–141

25. Raissi M, Perdikaris P, Karniadakis GE (2019) Physics-informed neural networks: a deep learning framework for solving forward and inverse problems involving nonlinear partial differential equations. J Comput Phys 378:686–707

26. Rumelhart DE, Hinton GE, Williams RJ (1985) Learning internal representations by error propagation

27. de Saint-Venant AJC (1871) Theorie du mouvement non permanent des eaux, avec application aux crues des rivieres et a l'introduction de marees dans leurs lits. Comptes Rendus Des Seances de l'Academie Des Sciences 36:154–174

28. Scarselli F, Tsoi AC (1998) Universal approximation using feedforward neural networks: a survey of some existing methods, and some new results. Neural Netw 11(1):15–37

29. Sene K (2012) Flash floods: forecasting and warning. Springer Science & Business Media, Berlin

30. Singh PK, Mishra SK, Jain MK (2014) A review of the synthetic unit hydrograph: from the empirical UH to advanced geomorphological methods. Hydrol Sci J 59(2):239–261

31. Sit M, Demir I (2019) Decentralized flood forecasting using deep neural networks. ArXiv Preprint arXiv:1902.02308

32. Sorteberg WE, Garasto S, Cantwell CC, Bharath AA (2019) Approximating the solution of surface wave propagation using deep neural networks. INNS big data and deep learning conference, pp 246–256

33. Stephen I (1990) Perceptron-based learning algorithms. IEEE Trans Neural Netw 50(2):179

34. Zhang R, Zen R, Xing J, Arsa DMS, Saha A, Bressan S (2020) Hydrological process surrogate modelling and simulation with neural networks. In: Pacific-Asia conference on knowledge discovery and data mining, pp 449–461
35. Zhao Y, Akolekar HD, Weatheritt J, Michelassi V, Sandberg RD (2020) RANS turbulence model development using CFD-driven machine learning. J Comput Phys 109413

Simulation of the Flood of El Maleh River by GIS in the City of Mohammedia-Morocco

Abderrahmane Jadouane and Azzeddine Chaouki

1 Introduction

The city of Mohammedia and its surrounding areas knew a group of natural and technological disasters, the most severe of which were recorded in 2002 [1], which killed several people who lived next to the river that penetrates the city, which came with a large load during a very rainy night, which led to this natural disaster that in turn led to a technological disaster where a fire broke out at the nearby oil refinery, causing heavy human and material losses. The floods of the "El Maleh", this River that crosses the city of Mohammedia, are frequent over time. If it was in the past once in ten years, then during the last decade of the last century and the beginning of the current century, it became semi-annual. We can recall the following floods years: 1978, 1995, 1996, 2000, 2001, and 2002 [1]. In the last century, the River overflowed on its margins and water filled deserted turns, depressions and meadows (wet areas), and they had no negative consequences because the lands adjacent to the River were bare from built and human, such as areas where salt plants grow, and left for grazing and migratory birds, but there were implications for the area built in these areas [2]. So the purpose of this study is to know the risk areas to take appropriate precautions, by means of maps they show the risk areas.

2 Study Area

The city of Mohammedia is located on the coast of the Atlantic Ocean, 25 km to the north-east of Casablanca and 65 km south-west of Rabat. The urban perimeter of the city covers an area of 34 km^2, between the mouths of El Maleh River in the

A. Jadouane (✉) · A. Chaouki
CEDoc: Spaces, Societies and Cultures, Faculty of Arts and Humanities, Hassan II, B.P.546, Mohammedia, Morocco
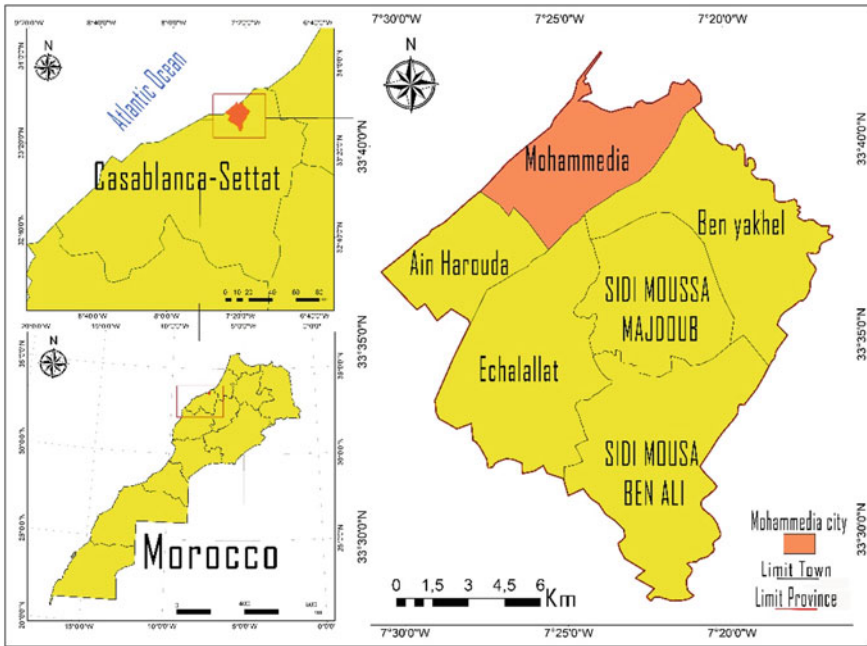
Fig. 1 Location of the city of Mohammedia-Morocco

west and El Nfifikh River to the east, and the motorway axis to the south. The city is bounded to the north by the Atlantic Ocean, to the east and south by the province of *Benslimane,* and to the west by the commune of *Aïn Harrouda* (Fig. 1).

It is located between 7° 22' and 7° 25' west longitude and 33° 41' and 33° 43' north latitude [3].

The topography of the city of Mohammedia consists of two parts:

The Mohammedia plateau and the coastal plain. The area of the city is characterized by a general slope heading from the southeast to the northwest, as elevations are recorded from 56 to 25 m (Fig. 2) at the borders of the Dead Cliff, which forms a barrier between the plateau and the coastal plain [3].

The coastal plain area is characterized by its flatness at a maximum height of 25 m, extending from the Dead Cliff toward the coast line, and this area includes the wet area of El Maleh River, estimated at 1,200 hectares, consisting of salt marshes and the mouth of the Salt River, and includes an important biological diversity of plants and birds [3].

As for the coast line, we can divide it into two parts: a south-western coast extending from cap Mohammedia to the south, consisting mostly of sand and a straight line, in addition to containing humid zone and the mouth of El Maleh River, while the second coast takes a northeastern direction extending from cap Mohammedia toward the mouth of El Nfifikh River. It is characterized by the prominence of rocky heads.
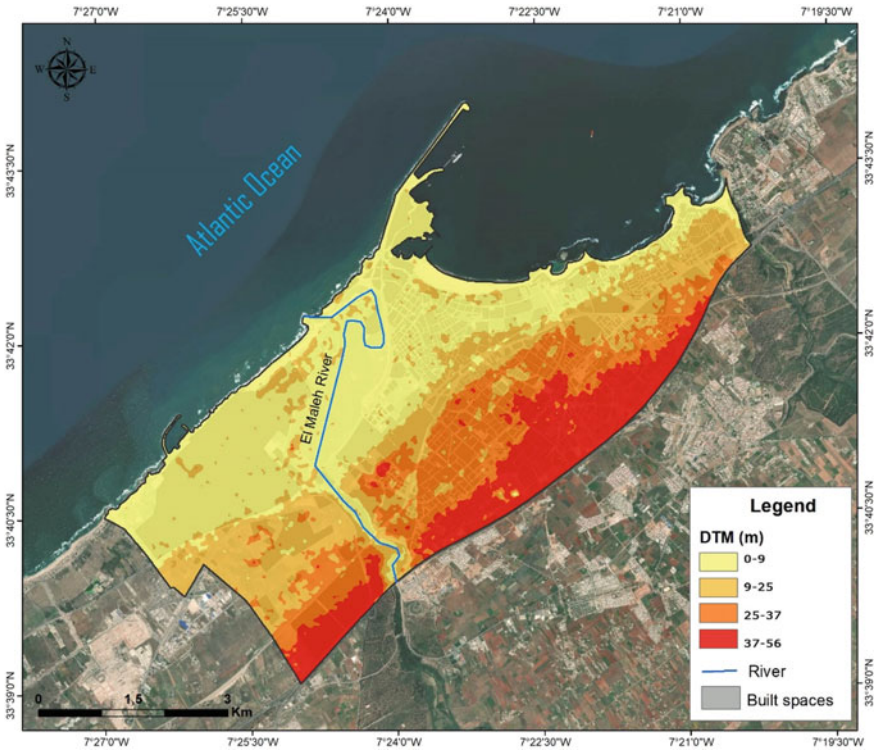
Fig. 2 Digital terrain model of Mohammedia city

El Maleh River is one of the most important coastal rivers. Its length is about 160 km, and its drainage basin area Call 2485 km^2 starts from the central plateau toward the Atlantic coast. It is a constant flowing river, it takes a southeastern, north-west direction, and it is fed by some tributaries on the left bank, especially Hesar River, which flows into El Maleh River through a waterfall [1].

The El Malleh basin covers an area of 2485 km^2, and it drains a hydrographic network with a total length of 1598 km. The basin is built by 5 dams (Fig. 3) [1].

- El Malleh dam 35.0 Mm^3.
- Tamesna Dam: 57.0 Mm^3.
- Hessar Dam: 2.0 Mm^3.
- Zamerine dam: 0.37 Mm^3.
- Aricha dam: 1.8 Mm^3.

The El Maleh Dam controls an area total of 2100 km^2, and it is intended mainly to the city's flood protection from Mohammedia.

The El Malleh basin has 11 flood warning posts (Fig. 3), divided between [1] the following:
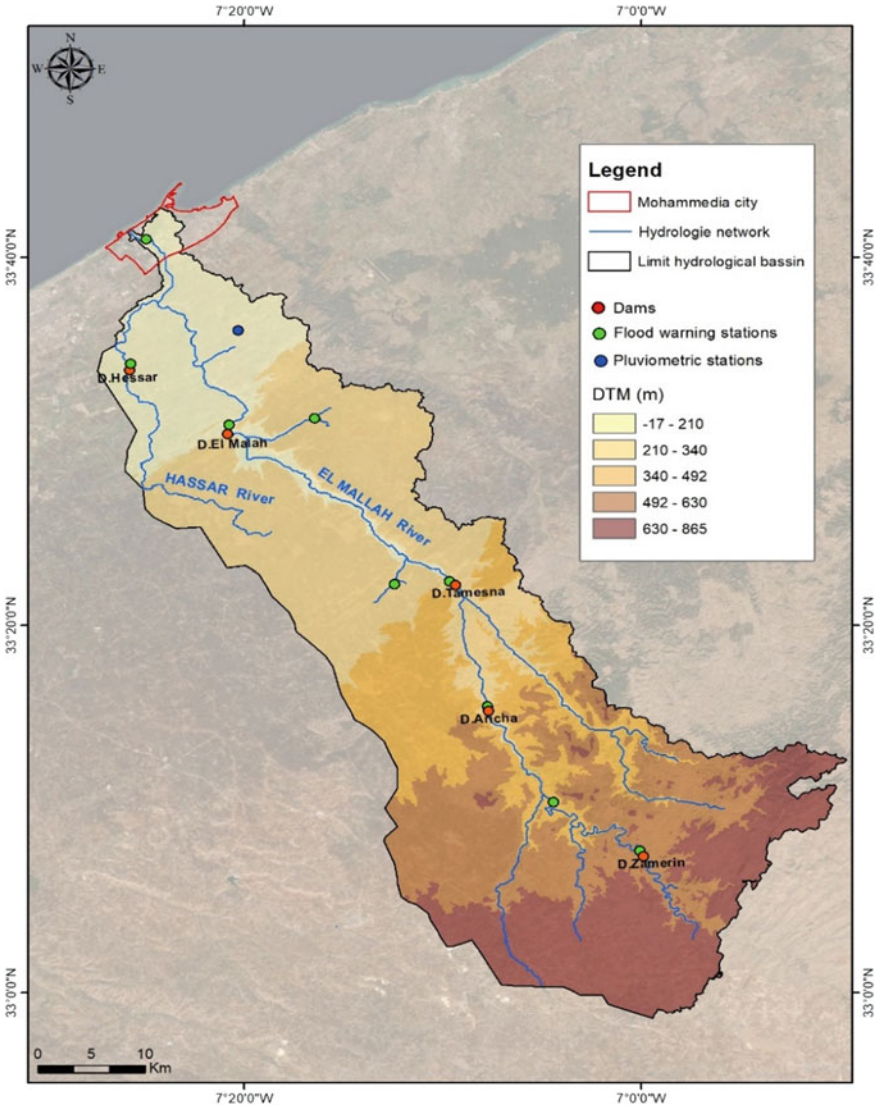
Fig. 3 Location and hydrographic network of El Maleh river watershed

- 5 Dams: Tamesna, Malleh, Zamerine, Hessar, and Aricha.
- 4 hydrological stations: Mellila, Oued laatach, Gara, and Mohammedia.
- 1 new pluviometric station: Fdalate.

By virtue of the location of the city of Mohammedia in the mouth of El Maleh River, we see that collecting water from the basin flows into the dusty area of the city, and with the presence of a decrease in the height in the city, it was a helpful

reason for the occurrence of the flood, which is why most of the constructions built are to cope with the floods in the city.

3   Materials and Methods

This study It was based process (Fig. 4),we first relied on collecting information and data about the area and the target topic, then we dealt with these data by the methodological methods used in analyzing Rivers and flood risk, and we used a software of GIS "ArcGIS 10.4" and "HecRAS 4.0", These software help to understand the sphere of the water network and give two- and three-dimensional analyzes by studying cross-sections, slopes, sediments and temperature…, and also enable us to perform flood simulations [4].

After collecting data and information related to the field of study, its first result was the representation of the city's infrastructure by virtue of it being the one concerned with the matter, especially if it was exposed to the risk of flooding.

The territorial area of the city of Mohammedia city was represented by what it contains of the exploited areas "facilities—housing—industrial neighborhoods—…", and the summary of these data was the result that is in Map (Fig. 5) [5].

Through it, it was found that the areas close to EL Maleh River are largely the industrial neighborhood, in addition to some facilities and residential areas. So we

Data references
- TOPOGRAPHIC MAP
- SATELLITE IMAGE
- DATA FROM PREVIOUS FLOODS
- DEM
- DATA HYDROLOGY
- LOCALISATION BUILD

Analytical processes
- MODEL FLOOD
- PROCESSING ON HEC-RAS
- RAS GEOMETRY
- CALCULATION OF FLOWS
- SIMULATION

Result
- RESULT VERIFICATION
- FLOOD HAZARD MAP
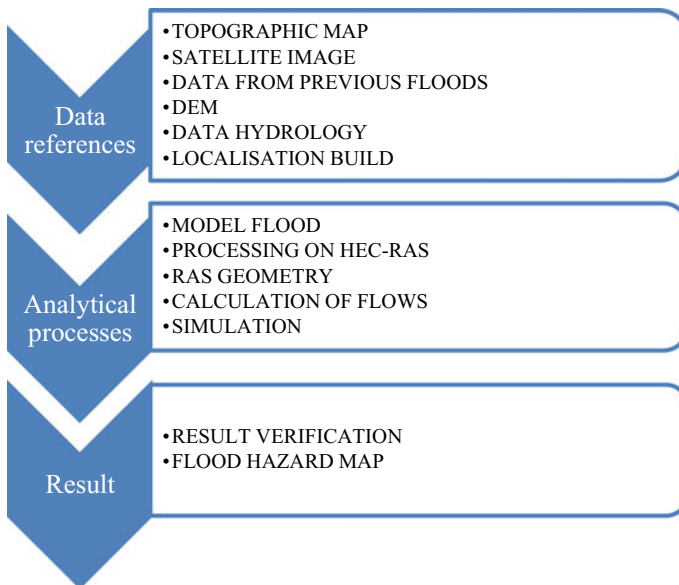
Fig. 4 Process of elaboration of the flood map
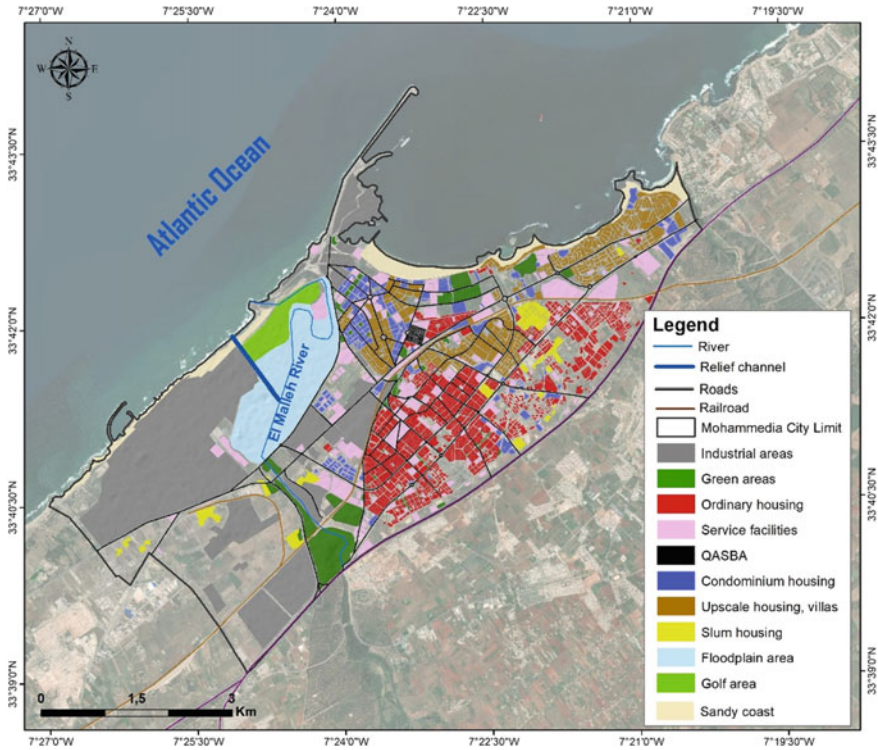
Fig. 5 Map territorial stakes in the city of Mohammedia 2020

conclude that if there is any flooding then these areas are most likely to be exposed to flood risk [6].

After identifying the infrastructure that could form the flood losses, now we know what these potential areas are threatened by flooding through the hydrological analysis of EL Maleh River and also the topographic analysis, all through an Analytical processes by software "ArcGIS 10.4 and HEC GeoRAS 4.0" (Fig. 6) [4], based on the digital elevation model (DEM 12.5 m). This analysis predicts the places that will be inundated by the floods and in which we can know the losses before the disaster strikes to save what can be saved.

So knowing the infrastructure and knowing the flood risk analysis, now we combine these data in one box to know the impact and the result on the ground, so that we will know the places that will be exposed to flooding, and the extent of the height of the water.

We will also get acquainted with a general idea about the loss and its quality by synchronizing the location of the flood on the quality of the exploitation of the field and what it contains of the materials that would cause harm. As for the data and measures that we worked on to obtain the final result, they are the same that occurred 18 years ago "November 2002" in terms of water height, the amount of flow that
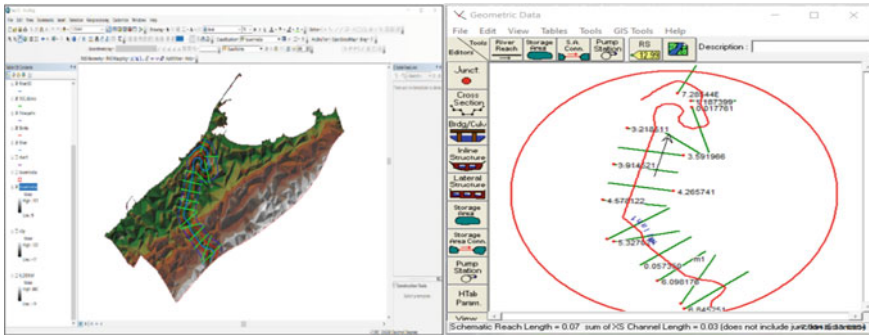
Fig. 6 The triangular irregular network (TIN) and the transverse lines of the mouth of El Maleh River by ArcGIS 10.4 and Hec-RASGeo 4.0

the river brought and the speed. This flood was the most powerful in these last two decades, with the greatest height of the water level reaching 169 mm and in some areas 200 mm [2], and it fell on the basin on this date by 950 m³/s at the dam station. And it flowed from the dam 430 m³/s, which descended strongly from the dam in the direction of the city at around 6 pm [7].

To produce a risk map and determine the degree of risk (R) and to know whether there are material losses, whether homes, industrial neighborhoods, or roads, or there are residents at risk, we worked with the following equation [8], which consists of 2 main elements: vulnerability (V)—hazard (H). Can be written in a form: R = V * H.

To classify the dusty area that will be exposed to flooding and to determine the level of risk in it, it was divided into cells measuring 500 m², and risk index is classified as a reference: Low-Medium-High (Table 1).

And for each cell, an integer value ranging from 0 to 3 was assigned as a hazard index according to flood depth. Equation (1) was used for calculating vulnerability index. Weight factors 5 and 1 used for area covered by house/living place/industrial, respectively.

After this calculation a risk index for each cell is calculated by multiplying hazard and vulnerability indexes.

Table 1 Assigned hazard index (H) for varying flood depth and classification area level of risk

Assigned hazard index (H)		Classification area level of risk	
Flood depth	Hazard index (H)	Risk index	Level of risk
No	0	1 to less than 5	Low
Less than 0.5 m	1	5 to less than 10	Medium
0.5 m to less 1.5 m	2	More than 10	High
1.5 or more	3		

H_{Index} = Hazard index about flood depth, and it is expressed in values (0-1-2-3).

V_{Index} = vulnerability index (ranging from 0 to 3), A_H = area covered by house/living place, A_I = area covered by industrial land, and A_{Cell} = area of one cell. Weight factors 5 and 10 used for area covered by house/living place and industrial land, respectively.

$$V_{Index} = (5 * A_H + 10 * A_{Ind}) / A_{cell} \tag{1}$$

$$R_{Index} = H_{Index} * V_{Index} \tag{2}$$

R_{Index} = risk index (ranging from 0 to 2), H_{Index} = hazard index (ranging from 0 to 3), and V_{Index} = vulnerability index (ranging from 0 to 10).

Finally, these extracted values are converted into a software Arcgis 10.4 to represent them as a Raster, to obtain a risk map with 3 level of risk. (Fig. 7).

Fig. 7 Satellite image of 4 cells

4 Discussion

The city of Mohammedia, especially the area near the River El Maleh, has been exposed in the past 20 years to floods, some of which are expected due to the occurrence of rain, and some of them are not expected, especially those of years 1996, 2002, 2010, and 2014 [9], which exceeded 283 mm [7]. These floods, especially the last ones, had an important impact, as roads were cut off and fires broke out in the remote area and oil refining warehouses, in addition to dispersal of the sewage network. Statistics reported by the Water Basin Agency in the hydrological scheme that 460 m^3 and two million tons of sludge [5].

Depending on the previous cases in which the height of the flood reached its maximum in two meters, this criterion is what we will adopt in renewing the simulation of the flood mass with the data bank to exploit the new dirt field for the year 2020 so that the simulation showed us that in the event of a flood again with the same standards as the previous floods. It occurred in the last 20 years that there are places that will damage the consciousness of the actress in (Fig. 8).
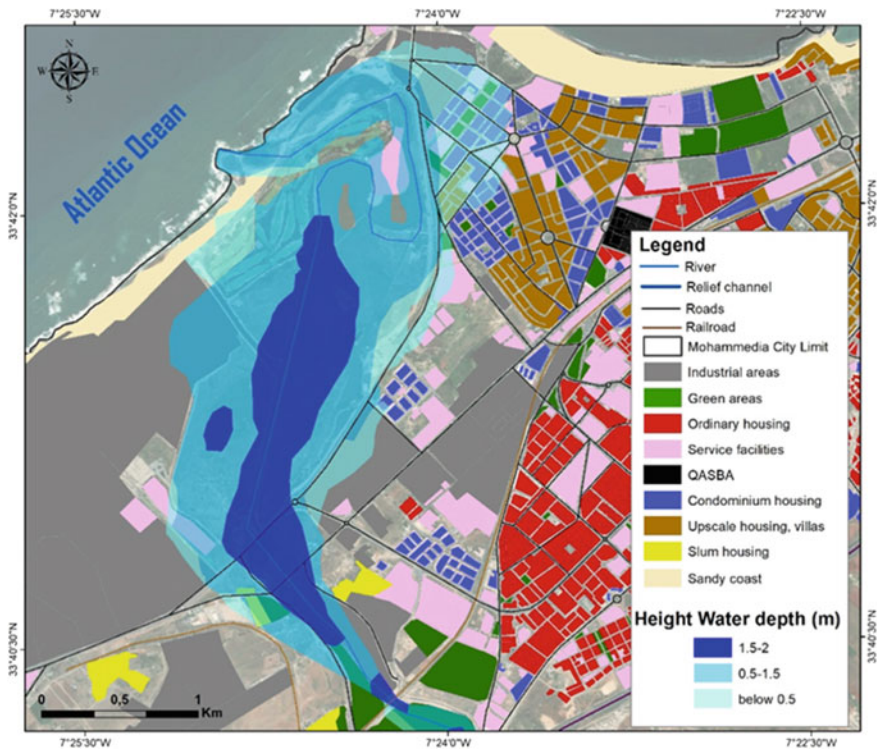
Fig. 8 Flood simulation on the map of land use in year 2020

By analyzing this final result, it becomes evident that there are some areas that are already threatened by flooding. It was discussed that the high water would reach these lands and thus could pose a threat to them. Among these places at risk of flooding, we find:

"*the province Mohammedia city*" – "*the Portuguese bridge*" – "*the main street at the entrance to the city*" – "*the oil refining industrial zone*" "*the southern part of Samir Company*", some neighborhoods whose topographic level is low.

These areas are very important because of their properties that can be of high material value in the event of a danger, but the most important thing is the industrial zone for oil refining so that the risk may be greater in the occurrence of a breakout, a radioactive leak, or an explosion in the event of a contact problem. But we can also say that the danger of flooding occurs in the city of Mohammedia due to strong precipitation, but also due to the weakness of the infrastructure and the fragility of the natural area, so that the site of the city is located in the mouth of the River, which is a humid area with water harvesting characteristics.

What added to the problem is the presence of housing, facilities, and industrial neighborhoods in this region, which is not one of its standards to be built in this region.

However, there were only efforts to prevent and repair what could be repaired, for example, barriers were built along the River at the city's borders in addition to the role played by El Maleh dam that protects the city from the force of water (Fig. 9).

It is noticed from (Fig. 8) that the depth of the water ranges to 2 m, 25% of the flooded area is 0.5 m deep and less, and these areas are located in the periphery, and the most important sensitive areas that were exposed to this flood we find the northern region, where there is the administrative district and some of the population, either 42% of the area covered by 0.5 and 1.5 m, it is a low area beside the river depression, and it is in contact with the industrial district of oil refining on the western and southern sides; while the most depth ranges between 1.5 and 2 m, it represents 33% representing the submerged area and most of it is with a line. The river and the most important areas through which it passes are the main roads that lead to the city.

In addition to understanding the risks that could be caused by this flood and the level of risk according to regions is it low, medium, or high; the values produced

Fig. 9 The main road is near the "Portuguese bridge" and fire in the "Samir" oil refining company in 25 November 2002
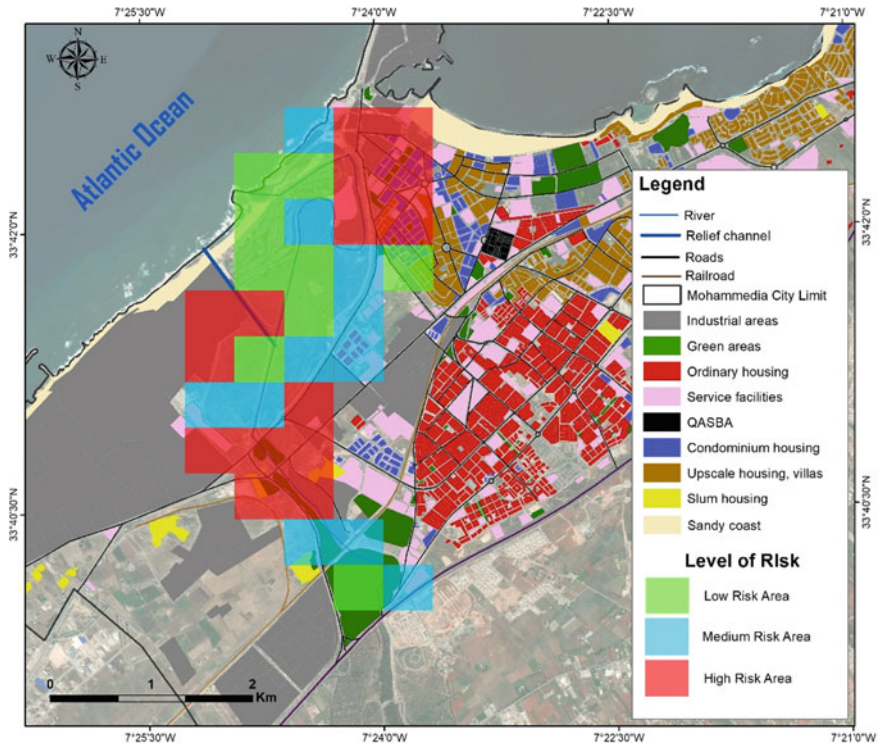
Fig. 10 Level of risk map during the flood

by Eq. (2) that consist of risk and vulnerability were converted, and a risk map was produced (Fig. 10).

The goal of it is forecasting the occurrence of disaster risks and work to identify the necessary interventions to avoid the occurrence of victims and material losses. Because a flood can be destructive, it can be non-destructive depending on what is found in the area in which it is located. The map (Fig. 10) classified its degrees of risk and the possibility of losses and classified it into 3 levels: the green color is a low degree of danger, the most that can happen in this area is slight soil erosion, and surface runoff with a depth of no more than 0.5 m in most cases, especially since these areas are not exploited by residents or construction, and most of them are located on the northwestern side.

As for the medium level of danger represented by the blue color, which is likely to be material damage such as road damage and interruption, and the effect on traffic movement, the emergence of water ponds and the emergence of significant amounts of mud. As for the high degree of danger represented by the red color, material and human damage may occur in these areas, represented by damage to roads, especially since these roads are the main (Fig. 10), and the emergence of water pools negatively affected traffic, and affected residential buildings, especially in the northern region,

and the occurrence of flooding with High water depth, in addition to the occurrence of oil and gas spills and fires, because these areas contain oil refining facilities and underground channels for storing them (Fig. 9).

5 Conclusion

We tried to simulate the flood of November 2002 if it happened today with the new data, and we learned through geographic information systems that it is possible to predict the risks after meeting the information between them. This system classifies the studied area according to the risk, regardless of the type of the latter. The purpose of this system is to prevent the reconstruction of areas where the probability of the risk of occurrence is strong, and to take the necessary preventive measures in areas where the probability of the occurrence of the risk while encouraging reconstruction in areas where the possibility of the occurrence of the risk is not possible.

References

1. ABHBC (2020) Hydraulic basin agency "Bouregreg and Chaouia"
2. Chaabane M-S (2016) The contribution of GIS in the management of natural risks and urban planning case study: management of floods in the region of Mohammedia
3. Commune of Mohammedia (2017) Monographic Mohammedia city
4. Merwade V (2016) School of Civil Engineering, Purdue University Tutorial on using HEC-GeoRAS with ArcGIS 10.x and HECRAS Modeling
5. Jadouane A (2019) EQP Mohammedia: www.equipment-publics-mohammedia.com
6. Lahlaoi H, Rhinane H, Hilali A, Lahssini S, Khalile L (2015) Potential erosion risk calculation using remote sensing and GIS in Oued El Maleh watershed Morocco. J Geogr Inf Syst 7:128–139
7. Saloui A (2008) XIII world water congress 1–4 September 2008 in Montpellier, France
8. Wisner B, Blaikie P, Cannon T, Davis I (2004) At risk, natural hazard, people's vulnerability and disasters, 2nd edn. Routledge; Taylor & Francis Group, London, pp 49–5
9. Chaabane MS, Abouali N, Boumeaza T, Zahouily M (2016) The contribution of GIS in the management of natural risks and urban planning case study: floods in the region of Mohammedia. Int J Eng Res Dev (IJERD) 12(12):57–64
10. Khouakhi.A (2008) Le Système d'Information Géographique (SIG): un outil pour l'évaluation des terres à risque d'inondation côtière liée aux changements climatiques. Cas du littoral de Mohammedia

Flood Hazard Mapping Using Geographical Information System (GIS) and Analytical Hierarchy Process (AHP)

Reshma Antony, K. U. Abdu Rahiman, and Subha Vishnudas

1 Introduction

Flood hazard is defined as a chance of exceeding highly damaging flood conditions in a given area in a given time phase [1]. Even though flood hazards are of natural origin, they are the outcome of the combined interaction between the social, economic, and political environments [2]. A previous study shows that floods affected nearly 2.8 billion people during the time frame 1980–2009 [3].

Flood monitoring using multi-sensor data and hazard management helps to mitigate the damages due to flood, which ultimately reduces the loss of life [4]. The analytical hierarchy process (AHP) was introduced by Saaty in 1980 [5], which is a very powerful tool for decision-making in problems where many criteria are contributing. AHP methodology provides a very good understanding of contributing factors, based on the weights assigned to them [6]. The application of spatial technologies and flood risk mapping in identifying the susceptible areas of an urban catchment was established by Sanat Nalini Sahoo et al. [7] in his work.

The main objective of the present study is to delineate the flood hazard zone in Pudukad city using geographical information system (GIS) and remote sensing techniques and to generate the flood hazard zone map of the study area. The factors considered for the current study are rainfall, slope, elevation, distance to the main channel, soil type, and land use. It helps in emergency planning, reallocation of facilities and infrastructure, and also for the formulation of plans for future expansion.

R. Antony (✉)
Sahrdaya College of Engineering & Technology, Kodakara, Kerala, India
e-mail: reshmaantony@cusat.ac.in

K. U. Abdu Rahiman · S. Vishnudas
School of Engineering, CUSAT, Kalamassery, Kerala, India
e-mail: arku@cusat.ac.in
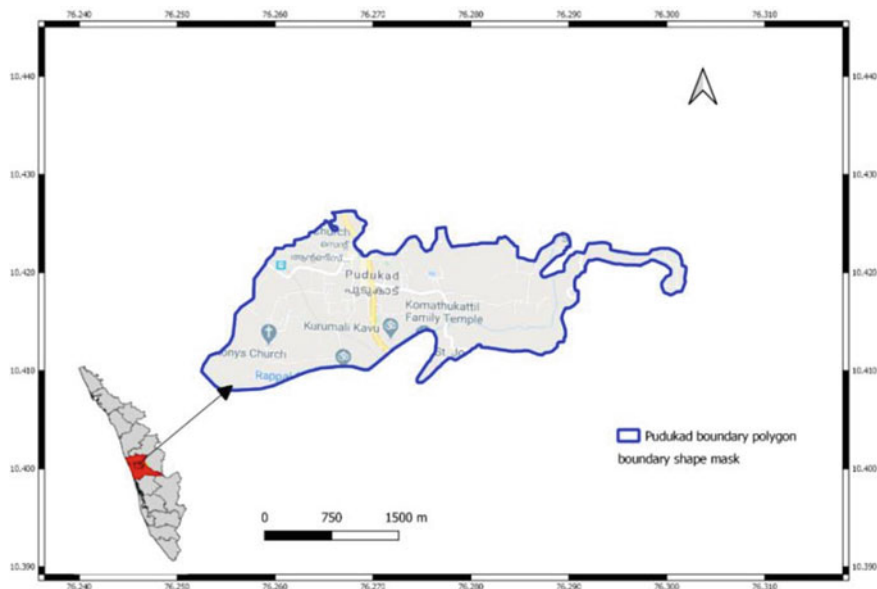
Fig. 1 Study area—Pudukad city (*Courtesy* Google Maps)

2 Study Area

The area taken for the study purpose is Pudukad, which is a small town located between 76.25°–76.34° E longitude and 10.4°–10.43° N latitude as shown in Fig. 1. The city is located in the Thrissur District of Kerala State. The area considered for this study comes around 5.25 km^2. The Kurumali river and its tributaries can be seen in the vicinity of the study area. The area near to Kurumali river got flooded in Kerala Floods 2018.

3 Materials and Methods

3.1 Materials Used

In this study, various thematic layers were created from different sources including Survey of India toposheets of scale 1:50,000, satellite images, and secondary data. Several thematic layers such as slope, soil, rainfall map, distance to the main channel, elevation, and land use are prepared in Quantum GIS, an open-source GIS software. Cartosat 1 Digital Elevation Model (DEM) Geotiff image of 1 arc sec or 30 m spatial resolution was obtained from 'Bhuvan'—Indian Geo-Platform of ISRO. 23 years monthly rainfall data was collected from IMD Pune to calculate the annual average

rainfall. Soil map prepared by the National Bureau of Soil Survey and Landuse Planning,

Regional Centre Bangalore in cooperation with the Department of Agriculture, Kerala, was used in this study. Land use/Land cover Geotiff image of Kerala was obtained from 'Bhuvan'.

3.2 Methodology

Preparation of Maps. For the current study, six thematic layers were prepared in QGIS software, reclassified, and assigned weightage for each class [8]. The higher value of weightage is given for the class which contributes seriously toward flooding.

Preparation of Weighted Slope Map. Terrain slope is a vital geomorphological parameter in assessing flood hazards. The chance of flooding is highly susceptible to topographical changes [9]. Lower the slope gradient, the higher is the chance of flooding and flood events [10]. DEM was reprojected to EPSG:32,643—WGS 84/UTM zone 43 N in QGIS 3.1 platform and using *Slope* tool, slope map was generated. The slope of the study area ranges between 0 and 27°, which was categorized under five equal intervals. The slope map was then reclassified (Fig. 2) by assigning weight- ages ranging from 1 to 5 (Table 1) by *Reclassify* option under Raster Analysis tools in the processing toolbox.

Preparation of Weighted Elevation map. The chance for the occurrence of flood decreases as the elevation increases [11]. Xie et al. [12], in their study stated that the
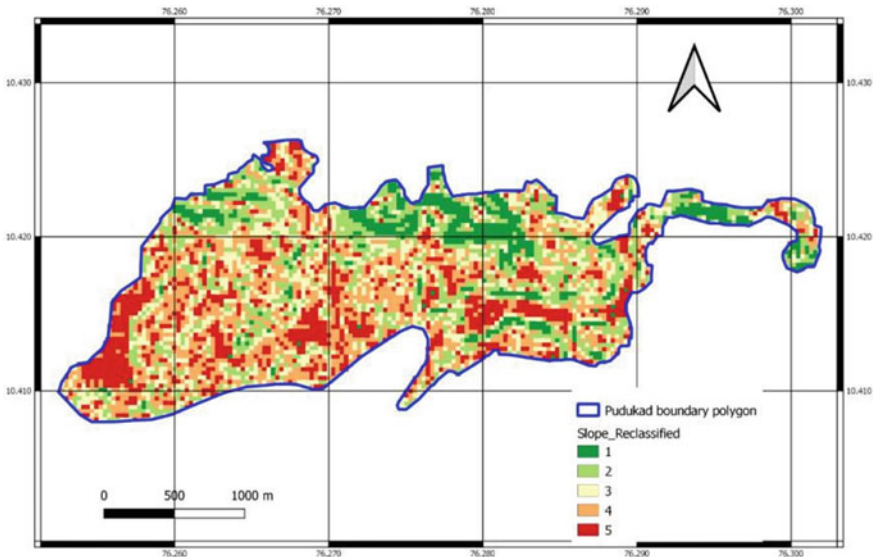
Fig. 2 Weighted slope map

Table 1 Weightages given for reclassifying slope map

Slope	Weightage
0–2	5
2–4	4
4–6	3
6–10	2
10–27	1

lower the terrain absolute height and the less the degree of terrain changes, the more is the flood vulnerability. The weights assigned for reclassifying the elevation map (Fig. 3) are shown in Table 2.

Preparation of Weighted Soil Map. Permeable soil keeps away flooding by facilitating high infiltration. Here the weights are assigned in the range 1–5, where higher weightage for poorly drained clay and least weightage for well-drained soil. Skyler
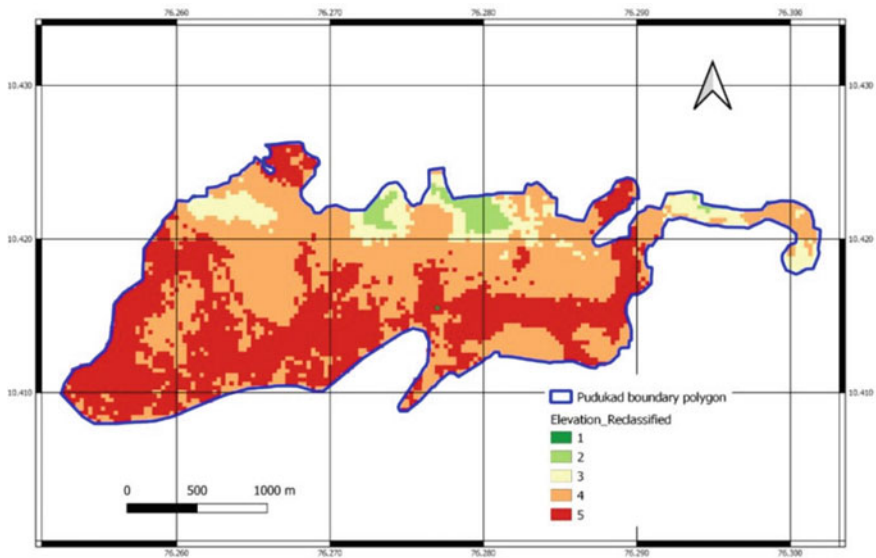
Fig. 3 Weighted elevation map

Table 2 Weights given for reclassifying elevation map

Elevation (m)	Weightage
−103 to −90	5
−90 to −70	4
−70 to −50	3
−50 to −25	2
−25 to 0	1

E. Sampson [13], in his study, shows that there is a direct correlation between soil permeability and flooded zone. Soil map prepared by the National Bureau of Soil Survey and Landuse Planning, Regional Centre Bangalore in cooperation with the Department of Agriculture, Kerala, was used in this study. When the map was clipped to the study area, mainly two types of soil are seen such as, well-drained gravelly clayey soil, for which a weightage of 2 is assigned and poorly drained soil for which a weightage of 5 is given. The soil map was reclassified (Fig. 4) by assigning weights as shown in Table 3.

Preparation of Weighted Rainfall Map. Assessment of extreme precipitation events in relation to intensity, duration, and influence of climate variability is substantial to deal with the flood-related issues [14]. Rainfall data for 23 years of 2 rain gauge stations Chalakudy and Irinjalakuda, which are very near to the study area, were collected from the Indian Meteorological Department (IMD), Pune. The annual average rainfall was calculated for both stations. The rainfall distribution map was prepared using the inverse distance weighted interpolation method (IDW) in QGIS and weights assigned while reclassifying the map (Fig. 5), is given in Table 4.
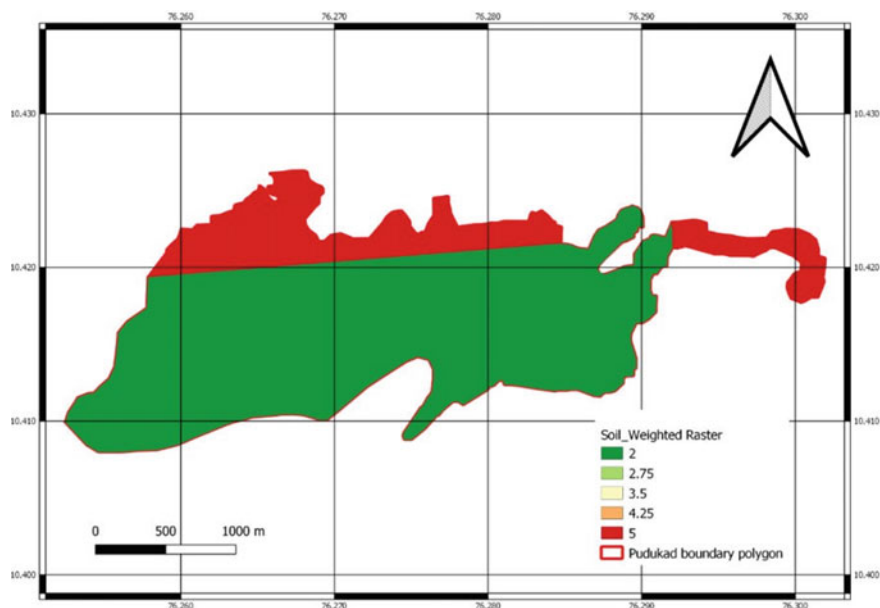
Fig. 4 Weighted soil map

Table 3 Weights given for reclassifying soil map

Soil type	Weightage
Well-drained gravelly clayey soil	2
Poorly drained clay	5
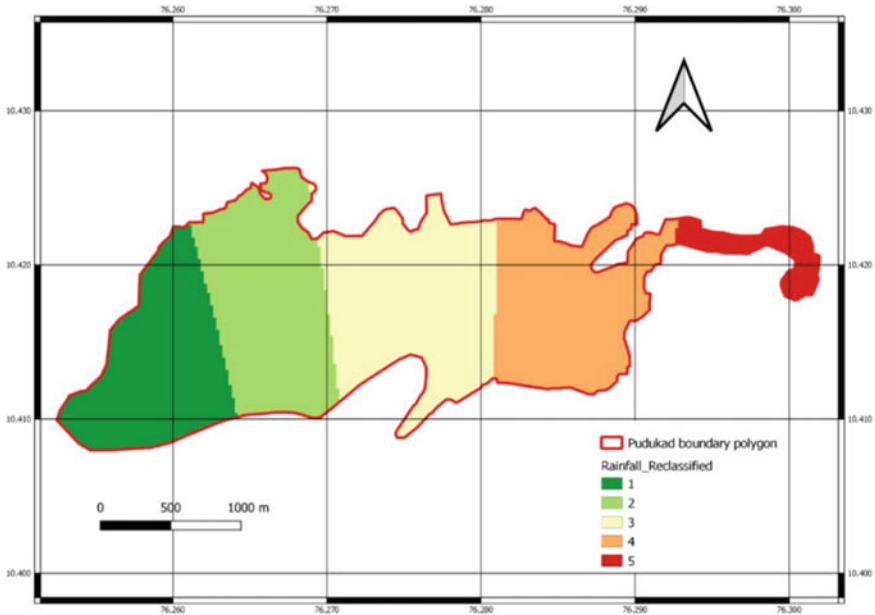
Fig. 5 Weighted rainfall map

Table 4 Weight given for reclassifying rainfall map

Annual average rainfall (mm)	Weightage
2650–2690	1
2690–2710	2
2710–2740	3
2740–2770	4
2770–2800	5

Preparation of Landuse Map. A change in land use pattern, especially urbanization, can cause an increase in peak discharge for greater return periods and ultimately enlarges the flood inundated area [15, 16]. A good vegetation cover helps to mitigate flood through the detention of rainfall by interception and infiltration and also reduces runoff by enhancing evaporation and evapotranspiration [17]. Landuse landcover map obtained from 'Bhuvan' was clipped to the study area and reclassified (Fig. 6) by providing weights (Table 5).

Preparation of Map Showing Distance to the Main Channel. The areas located very near to the main channel will get flooded soon. This factor will help for planning development activities in the future and for implementing flood mitigation measures in areas at high risk [18]. The river network was digitized from SoI Toposheet 58B/7. Three buffers were created in the QGIS platform for the current study; 100 m, 200 m, and greater than 200 m, and the reclassified map (Fig. 7) is obtained by assigning
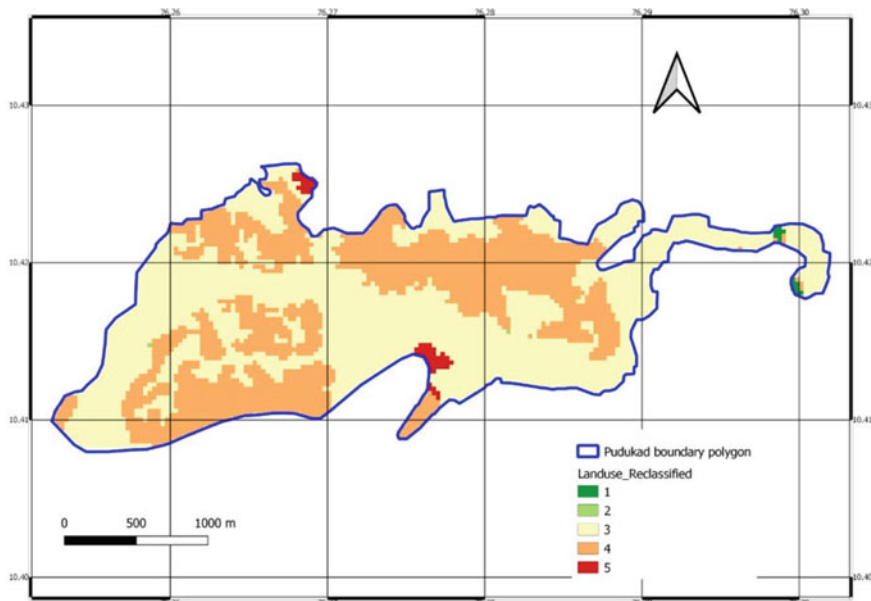
Fig. 6 Weighted land use map

Table 5 Weights given for reclassifying land use map

Land Use	Weightage
Water body	5
Agricultural land	4
Built up urban	3
Built up mining	2
Barren land	1

weights (Table 6), ranging between 1 and 5. As the study area chosen is very small in size and there may be a chance of flooding from nearby tributaries, here a weightage 2 is assigned for distance >200 m.

Multi-Criteria Analysis Using AHP Technique. The analytic hierarchy process (AHP) is a multi-criteria decision-making tool which makes use of pairwise comparison method to arrive at a scale of preferences among a set of choices [19]. In AHP, pairwise comparisons are entered in a square matrix of size n × n (where n is the number of criteria or factors under consideration), also called a criteria comparison matrix. The aij element of this matrix is 1/aji or the reciprocal of the aji element. Here aij represents the relative importance of ith criteria over jth criteria [20]. The scale used to indicate the judgmental preference of one factor over the other is given in Table 7.

Random Index value or otherwise called as average consistency indices for various values of 'n' has been established by [5], which is given in Table 8. Here the consis-
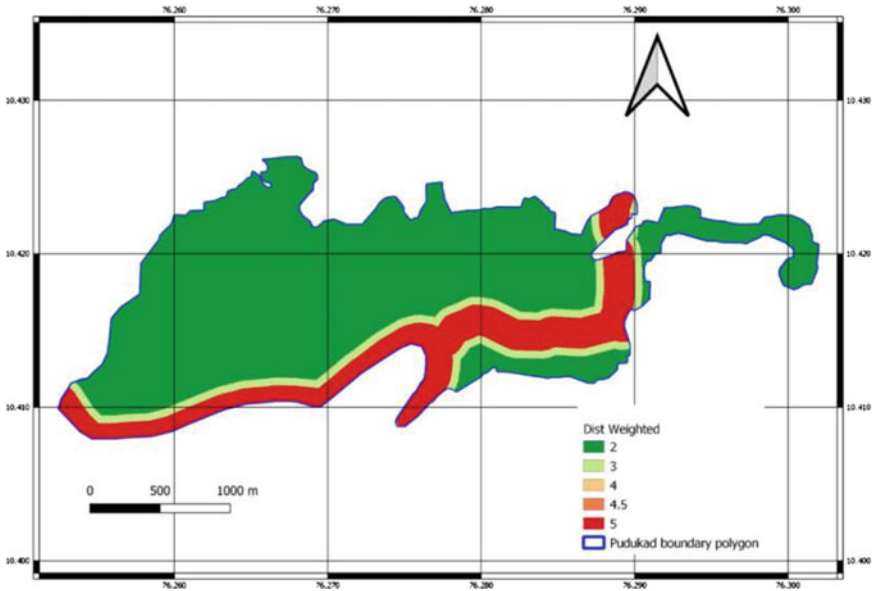
Fig. 7 Weighted map showing distance to the main channel

Table 6 Weightages given for reclassifying the map showing distance to the main channel

Distance to the main channel	Weightage
Up to 100 m	5
100–200 m	3
>200 m	2

Table 7 Scale of relative importance (*Source* Saaty [5])

Intensity of Relative Importance	Definition	Explanation
1	Equal Importance	Two activities contribute equally to the objective
3	Moderate importance of one over another	Experience and judgment slightly favor one activity over another
5	Essential or strong importance	Experience and judgment strongly favor one activity over another
7	Demonstrated importance	An activity is strongly favored and its dominance is demonstrated in practice
9	Absolute importance	The highest possible order of affirmation
2, 4, 6, 8	Intermediate values between the two adjacent judgments	When compromise is needed

Table 8 Random index values (*Source* Saaty [5])

n	2	3	4	5	6	7	8
Random index (RI)	0.00	0.58	0.90	1.12	1.24	1.32	1.41

Table 9 Criteria comparison matrix C

	Rainfall	Elevation	Slope	Soil	Distance to main channel	Land use
Rainfall	1	2	3	4	5	6
Elevation	0.5	1	2	3	4	5
Slope	0.333	0.5	1	2	3	4
Soil	0.25	0.333	0.5	1	2	3
Distance to main channel	0.2	0.25	0.333	0.5	1	2
Landuse	0.167	0.2	0.25	0.333	0.5	1

tency of the criteria comparison matrix, which is shown in Table 9, has to be checked, by using the parameter 'Consistency Ratio', which is given by Eq. 1. As per the study conducted by [5], the Consistency Ratio <0.1 is tolerable, but, if it exceeds this limit, a revision in judgments is needed.

$$CR = CI/RI, \tag{1}$$

where CI = consistency index and RI = Random Index

$$CI = (\lambda max - n)/(n - 1) \tag{2}$$

The Weightage (W) is the row average of the normalized criteria matrix for each factor which is shown in Table 10.

Here the Consistency Index (CI) is obtained (Eq. 2) as 0.016764 and RI = 1.24 (Table 8) for n = 6 and maximum eigenvalue, λ max = 6.0838 as per Saaty [5].

The Consistency Ratio (CR) is obtained (Eq. 1) as 0.01352 < 0.1, therefore it is consistent. And we can apply these weights for each factor, in performing Weighted Overlay Analysis.

In the current study, each factor was given a rank based on its expected significance into the cause of flooding [8]. Ranks assigned for each factor are given in Table 11. Flood hazard index (FHI) is used to assess the chance of flooding in the study area and it is calculated using the equation given below.

$$FHI = Rainfall \times 0.379 + Elevation \times 0.249 + Slope \times 0.160 + Soil \times 0.102$$
$$+ Distance\ to\ main\ channel \times 0.065 + Land\ Use \times 0.043 \tag{3}$$

Table 10 Normalized criteria matrix

Factors	Rainfall	Elevation	Slope	Soil	Distance to main channel	Land use	W (weightage)
Rainfall	0.408	0.466	0.424	0.369	0.323	0.286	0.379
Elevation	0.204	0.233	0.282	0.277	0.258	0.238	0.249
Slope	0.136	0.116	0.141	0.185	0.194	0.190	0.160
Soil	0.102	0.077	0.071	0.092	0.129	0.143	0.102
Distance to main channel	0.082	0.058	0.047	0.046	0.065	0.095	0.065
Landuse	0.068	0.046	0.035	0.031	0.032	0.048	0.043
Sum of column	1	1	1	1	1	1	1

Table 11 Ranks given for various factors

Factors	Rank
Rainfall	6
Elevation	5
Slope	4
Soil	3
Distance to main channel	2
Land use	1

The final flood hazard zone map of the study area is shown in Fig. 8. The hazard zones are categorized into five classes, based on the flood hazard index values, which are shown in Table 12.

4 Conclusion

In this study, the flood hazard zone map of Pudukad city was prepared using weighted overlay technique in GIS and analytical hierarchy process. Remote sensing data together with geospatial technology plays a vital role in mapping flood hazard zones. The flood hazard map obtained helps in future infrastructure planning and land developmental activities. Better results can be obtained by executing land use classification in GIS using the latest Landsat image, instead of using land use map of previous years. More accurate results can be obtained by considering additional factors contributing to floods.
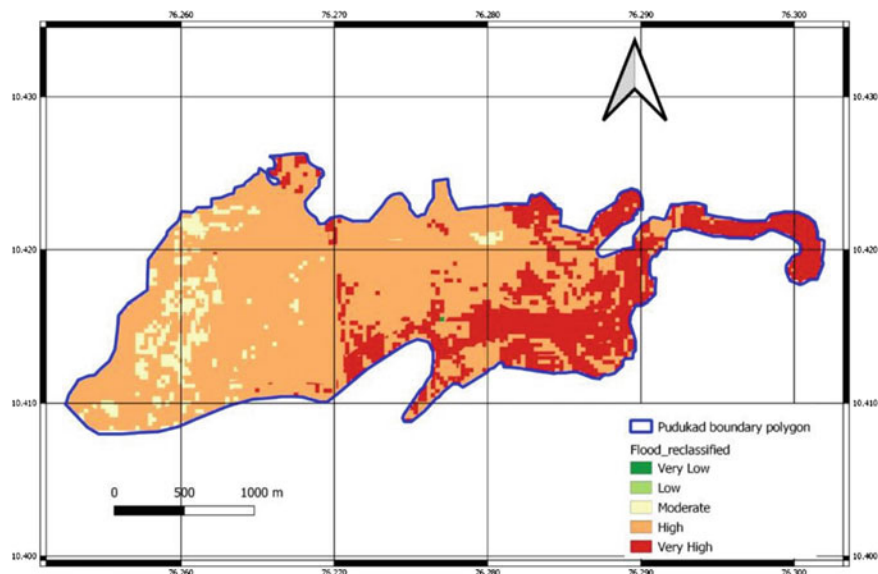
Fig. 8 Flood hazard zone map

Table 12 Flood hazard zones classification based on index value	FHI	Hazard zones
	−23 to −9	Very low
	−9 to 1	Low
	1–2.5	Moderate
	2.5–3.5	High
	3.5–4.503	Very high

References

1. Begum S et al (2007) Flood risk mapping at local scale: concepts and challenges. In: Flood risk management in Europe: innovation in policy and practice, Chap 13. Springer, Berlin, pp 231–252
2. Parker DJ (2000) Introduction to floods and flood management, floods, vol 1. Routledge; Taylor and Francis Group, London, pp 3–39
3. Doocy S et al (2013) The human impact of floods: a historical review of events 1980- 2009 and systematic literature review. PLOS Curr Disasters
4. Prasad AK et al. (2006) Potentiality of multi-sensor satellite data in mapping flood hazard. J Indian Soc Remote Sens 34(3)
5. Saaty TL (1980) The analytic hierarchy process. McGraw Hill, New York
6. Danumah JH et al (2016) Flood risk assessment and mapping in Abidjan district using multi-criteria analysis (AHP) model and geoinformation techniques. Geoenvironmental Disasters 3(10)

7. Sahoo SN et al (2017) Development of flood inundation maps and quantification of flood risk in an urban catchment of Brahmaputra river. ASCE-ASME J Risk Uncertain Eng Syst Part A: Civ Eng 3(1)

8. Elkhrachy I (2015) Flash flood hazard mapping using satellite images and GIS tools: a case study of Najran city, Kingdom of Saudi Arabia (KSA). Egypt J Remote Sens Space Sci 18:261–278

9. Zope PE (2015) Impacts of urbanization on flooding of a coastal urban catchment: a case study of Mumbai city India. Nat Hazards 75:887–908

10. Masoudian M (2009) The topographical Impact on effectiveness of flood protection measures. Kassel University Press, Kassel

11. Teegavarapu RSV (2012) Floods in a changing climate: extreme precipitation. Cambridge University Press, New York

12. Olanrewaju R et al (2017) Analysis of rainfall pattern and flood incidences in Warri Metropolis, Nigeris. Geogr Environ Sustain 10(4):83–97

13. Iqbal MS et al (2018) Impact of climate change on flood frequency and intensity in the Kabul river basin. Geosciences 8:114

14. Goudie AS (2004) Encyclopedia of geomorphology, vol 1&2. Taylor and Francis Group; Routledge, London

15. Ameur F (2016) Floods in Jeddah, Saudi Arabia: unusual phenomenon and huge losses. What prognoses. In: FLOOD risk 2016 - 3rd European conference on flood risk management

16. Zope PE et al (2016) Impacts of land use–land cover change and urbanization on flooding: a case study of Oshiwara river basin in Mumbai India. CATENA 145:142–154

17. Ajibade LT et al (2010) Morphometric analysis of Ogunpa and Ogbere drainage basins, Ibadan, Nigeria

18. Islam MM, Sado K (2002) Development priority map for flood countermeasures by remote sensing data with geographic information system. J Hydrol Eng (ASCE) 7(5):346–355

19. Saaty TL (1984) The analytic hierarchy process: decision making in complex environments. In: Avenhaus R, Huber RK (eds) Quantitative assessment in arms control. Springer, Boston

20. Saaty RW (1987) The analytic hierarchy process—what it is and how it is used. Math Model 9(3–5). Pergamon Journals Ltd. Great Britain

Feature Selection for Rainfall Prediction and Drought Assessment Using Bayesian Network Technique

Prabal Das and Kironmala Chanda

1 Introduction

Droughts are hydrological extreme events that are characterized by very low values of rainfall, and therefore feature in the tail of statistical distributions. Moreover, several researchers around the globe have pointed out that, in the current context of climate change, drought frequency and severity are going to increase in the future [23, 27]. Therefore, the assessment of drought is of utmost importance because they have the potential to impact society in terms of human life, as well as the environment, economy, infrastructure, and agriculture. Assessment of drought events can be challenging due to the complex interaction of the causal variables. Also, being unique events, the sample size is usually small which leads to considerable uncertainty in the assessment of droughts [29]. Drought occurs in nearly all climatic zone, including both high and low rainfall regions [3]. Unlike most of the countries, India also has a long history of drought that has impacted the country's economy and society vastly. Since India is predominantly an agricultural country, drought possesses some serious challenges like food and water scarcity [26]. Drought is basically a rainfall-driven hydrological extreme and so a better prediction and forecasting of rainfall will help to mitigate these unforeseen drought scenarios.

Modeling and prediction of rainfall is always a challenging task for hydrologists and water resource researchers. The major challenges arising in rainfall prediction are because of the nature of data. First of all, any hydrological time series is a space-time data and modeling the same both in space and time is quite challenging. Rainfall, just like any other spatiotemporal data, follows the "first law of geography", i.e., data that is similar in space and time appears to be more comparable than data far away [4]. Furthermore, it is not always possible to find the required amount of reliable data needed for modeling any hydrological time series. The three main

P. Das (✉) · K. Chanda
Department of Civil Engineering, Indian Institute of Technology (Indian School of Mines), Dhanbad, India

features of any hydrological time series are amount, intensity, and duration. These values vary in a great extent both spatially and temporally and as a result consists of nonlinearities (non-stationarity) in the data set. An additional difficulty in this regard is the extraction of useful and interesting details or trends from this enormous volume of data. This is often attempted through statistical techniques. In fact, most of the early studies on rainfall prediction focussed on using various statistical approaches, where in a statistical analysis of data set for a given system under specified conditions is performed. These statistical analyses are employed in two ways, namely linear and multiple regressions to provide a relationship between variables [14]. These include Auto-Regressive (AR), Moving Average (MA), Auto Regressive Moving Average (ARMA), Auto-Regressive Integrated Moving Average (ARIMA) [7, 15]. However, with the advent of Artificial Intelligence (AI) in the past decade, Machine Learning (ML) has opened a new path for research in the field of hydrology. These approaches, often termed as black-box models, comprehend the pattern of the time series and develop a connection between inputs and outputs without taking into account the physical nature of the process.

Since any component of the hydrological cycle is heavily linked to several causal variables, the dimensionality of the problem is always an essential issue in hydro-climatic studies. Typically, not all the available data is equally helpful for efficient modeling; some might be redundant. Also, using all the variables or features for modeling will unnecessarily make the model complex and will increase the chance of overfitting. That is why, it is of utmost necessity, to develop a more pruned and better selection of input features in any hydrological studies by implementing feature selection techniques.

Feature selection techniques have been widely used in the modeling of high-dimensional hydrological studies. Any hydrological study has inherent randomness due to its complex process and variability over space and time. Therefore, in order to accurately predict the performance of such process, it is important to include the effects of input uncertainties in the model system and to measure the spread of uncertainties in the system response. Although in a theoretical sense it is more appealing to have a greater number of features for the prediction of a particular hydrological or meteorological variable, but in reality, it is not always the case. Rodriguez-Galiano et al. [24] states that there can be several explanations for choosing a variable subset. Irrelevant features can lead to overfitting of training data thus compromising model accuracy. With a smaller number of input features, the model is less complex and learns faster. Also, understanding which variables are important will provide insight into the essence of the problem of prediction at hand [12]. Das and Chanda [5] have reviewed some of the important feature selection approaches used in hydrological studies and their respective limitations.

The main issue with most of the feature selection techniques is that they use the performance of the model learned in the selection process and thereafter select the important features, due to which, the computational burden is increased [1]. In this regard, Bayesian Networks (BN), which is a special class of Probabilistic Graphical Model (PGM) offers a model-free feature selection process, i.e., the number of features selected is independent of the accuracy of the model. The basic idea for BN

is to consider only those relations that are conditionally dependent given a set of other features. It represents a joint probability distribution between a set of random variables from which the conditional probability can be determined [28]. Details about the methodology and working principle of the same have been discussed in Sect. 4.

In the present study, an attempt has been made to develop a feature subset of monthly rainfall from a pool of several meteorological variables using the Bayesian Network (BN) technique. The feature subset formed from BN is used as inputs to Artificial Neural Network (ANN) model, which is used to predict the monthly rainfall. Furthermore, the predicted rainfall is used to assess the drought events in terms of wet, intermediate, and dry scenarios.

2 Study Area

Vidarbha is the northeastern region of the state of Maharashtra. The region of Vidarbha can be broadly classified into western and eastern sections that fall under the division of Amravati and Nagpur. This includes 11 districts with an area of approximately 97,950 km^2 between latitude 19.05°–21.25° N and longitude 75.59°–79.11° E. The Nagpur region is famous for its oranges and cotton. It is designated as one of the homogeneous rainfall subdivisions in the country (36 in total) by the India Meteorological Department (IMD). Vidarbha is located in the northern half of the Deccan Plateau. The region can be classified as semi-arid which receives rainfall mainly from the southwest monsoon. The rainfall varies from 700 mm in the west to 1300 mm in the east spatially. In summer, the temperature varies from a high of 47 °C to a minimum of 12 °C in winter [20]. The economy of the region is predominantly agricultural. Vidarbha has witnessed some of the worst droughts in recent years because of which Vidarbha records most number of farmer's suicide cases in India [10]. Figure 1 shows the location map of the study area.

3 Data

In the present study, the possible drivers of monthly rainfall in the study area are selected based on available past scientific literature [5, 9, 13]. Monthly mean data sets of the following hydro-meteorological variables—air temperature, soil moisture, relative humidity, geo-potential height at 250 mb and 850 mb pressure levels, total precipitation water, zonal wind, meridional wind, omega at 250 mb and 850 mb pressure level, each up to a lead time of 6 months, are used in this analysis. The soil moisture data is collected from the Climate Prediction Centre (CPC) Soil Moisture data provided by the NOAA/OAR/ESRL PSL, Boulder, Colorado, USA, from their website at https://psl.noaa.gov/. All the other meteorological drivers are obtained from the National Centre for Environmental Prediction—Department of
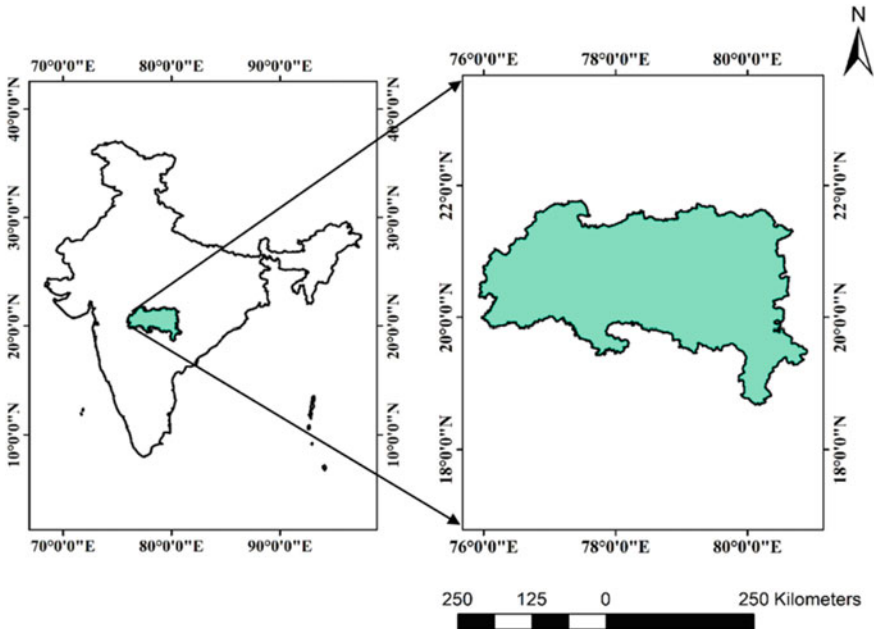
Fig. 1 Location map of the study area, Vidarbha

Energy Atmospheric Model Inter Comparison Project II (NCEP–DOE AMIP-II) (also known as the Reanalysis 2 data set). The monthly rainfall data for the Vidarbha region is obtained from the homogeneous rainfall data developed by the Indian Institute of Tropical Metrology (IITM), Pune. A more detailed information about the homogeneous rainfall data can be found at ftp://www.tropmet.res.in/pub/data/rain/Readme.pdf. The data obtained from NCEP and CPC are gridded data and therefore those grid points falling within the study area are spatially averaged to convert it into a time-series data. The spatial resolution of all the meteorological drivers, excluding soil moisture, is 2.5° lat × 2.5° long, and that of soil moisture is 0.5° lat × 0.5° long. A total of 36 years (1980–2016) of data has been considered in the present study.

4 Methodology

4.1 Bayesian Networks

Bayesian Network (BN) is a class of Probabilistic Graphical Modelling (PGM). PGM is a graphical representation of the distribution of a joint probability from which marginal and conditional probabilities can be derived [28]. These are elegant structures that combine the concept of probability and graph theory to represent complex

real-world phenomena. The cornerstone of graphical modeling is to establish a conditional independence structure between a set of random variables. There are namely two important elements in a graph structure—edges (arcs) and nodes (vertices). Nodes (vertices) denote the random variables whereas edges (arcs) represent the association between them. Based on whether the edges are directed or undirected, a graph can be classified as directed graph and undirected graph, respectively.

The essence of the Bayesian network representation is a directed graph or more specifically a Directed Acyclic Graph (DAG). As the name suggests, a Directed Acyclic Graph represents a directed graph with no directed cycles. In simpler words, when an edge is directed from a node v, there is no way that by following a constantly directed sequences of edges, it will eventually loop back to v again. BN uses the concept of Bayes theorem of probability to form the network and thus establishing the conditional independence structure or joint probability distribution between the random variables. Each random variable in the network has a related distribution of conditional probabilities or as commonly known as Conditional Probability Distribution (CPD) [17]. Let G represent a BN graph structure over a set of random variables $X_1, X_2, \ldots, X_n$, then the CPD of any random variable X_i is denoted by

$$CPD(X_i) = P(X_i|Pa(X_i))$$ (1)

and the joint probability distribution can be specified by

$$P(X_1, X_2, \ldots, X_n) = \prod_{i=1}^{n} P(X_i|Pa(X_i))$$ (2)

where $Pa(X_i)$ represents the parents of the variables of X_i in the BN structure. A node is said to be the parent node of another if there exists a directed edge from the former to the later and a node is known as a child node if there exists a directed edge from the later to the former.

The learning of the BN structure is known as structural learning. Several heuristic algorithms have been used in scientific literature for learning the structure of BN. They are broadly categorized as score-based algorithms and constraint-based algorithms. Apart from this two, a hybrid algorithm that encompasses the advantage of both score-based and constraint-based algorithms also exists. For more detailed reading, the authors refer to the work of Nagarajan et al. [19]. In the present study, the most commonly used score-based algorithm Hill-Climb (HC) has been considered to develop the BN structure. In the case of HC, a random graph structure is initially formed with a corresponding score. Then in each step, the structure modifies, either by changing the direction of edges or by removal or addition of edges and correspondingly the score gets modified. Lastly, the structure with the least score is designated as the BN [11]. In the present study, the score function used is the Bayesian Information Criteria (BIC). The "bnlearn" package [25] in R version 4.0.2 is used to develop the network structure.

Once the DAG is formed and the network connections are established, the variables selected from the network are further used as inputs to make a prediction model, in order to access the effectiveness of BN as a feature selection technique. For developing the prediction model, the machine learning technique, Artificial Neural Network (ANN) has been implemented.

4.2 Artificial Neural Networks

Neural networks are attributed to the way the human brain functions. It is one of the most common supervised machine learning techniques that has been used in the scientific literature for the prediction and forecasting of hydrological time series [5, 6, 16]. Neural networks have the intrinsic capabilities of modeling complex, nonlinear time-series data, without considering the physics of the problem at hand. That is why they are often termed as black-box models. A basic neural network structure follows a three-layered architecture. There is a set of inputs, a processor (hidden layer consisting of neurons), and a set of outputs. These layers are connected to each other through fixed weights or variable weights. A transformation function (activation function) is then applied to the output layer to learn arbitrary nonlinear complex transformations. It limits the permissible range of output signal to some finite value [8]. In the present study, the commonly used logistic or sigmoid function was used as the activation function and the back-propagation algorithm was implemented. The number of hidden neurons in the hidden layer was varied from 1 to 10 and the network with the least error was selected as the optimal network. The optimal ANN architecture found in this study was 8—4—1,, i.e., a network with 1 input layer consisting of 8 inputs, 1 hidden layer with 4 hidden neurons, and a single output (monthly rainfall). This is discussed further in the following Sect. 5. All the ANN models are developed using the "neuralnet" package of R Version 4.0.2.

4.3 Pre-processing Raw Data and Post-processing Predicted Rainfall

All the datasets are initially normalized between 0 and 1 before using as inputs to both BN and ANN. However, the interpretation and performance evaluation of the results was done by back-transforming the data to its original scale. For calibration of the model, a total of 25 years of data from 1980 to 2004 (about 70%) has been considered and the remaining 12 years of data from 2005 to 2016 (about 30%) has been considered for validation of the models.

The model-predicted monthly rainfall is further used for accessing the drought condition within the study area. Standard Precipitation Anomaly Index (SPAI) [2] was used as the drought index and each month was categorized as dry/intermediate/wet

months. In order to calculate the SPAI, firstly, the rainfall anomalies are simply fitted to an empirical distribution and the reduced variates, ranging from 0 to 1, are obtained. Next, these reduced variates are converted to standard normal variates which are the required SPAI. The calculation of SPAI was also carried out in R Version 4.0.2. Any SPAI values below -0.99 and above 0.99 was designated as dry and wet scenario respectively, whereas any values ranging between -0.99 and 0.99 was designated as intermediate. The SPAI is a generalized version of the Standard Precipitation Index (SPI), which is suitable for both monsoon-dominated and other climatic regimes [2].

5 Results and Discussion

For developing BN-based feature selection method, a total of 12 possible probable predictors were identified as mentioned earlier. Each of these possible predictors consists of (t-1) to (t-6) months of preceding time series (lead months), which makes the total count of probable predictors to 72. The DAG formed from the Hill-Climb (HC) algorithm within BN is presented in Fig. 2. The description and abbreviations used are presented in Table 1.

In Fig. 2, the last digit after the abbreviation refers to the number of lead months. The acronym of probable predictors was followed in accordance with Das and Chanda
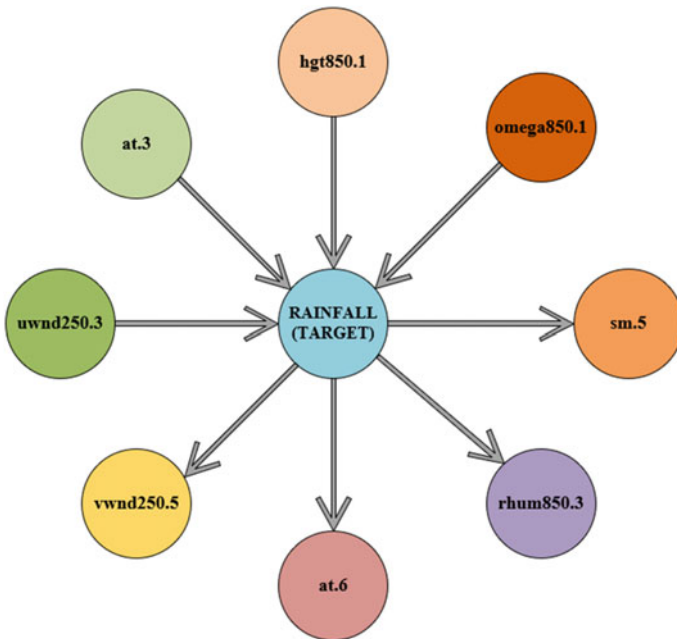
Fig. 2 DAG formed through HC algorithm

Table 1 Description and abbreviations of several hydro-meteorological variables used

Abbreviation of probable predictors	Description
at	Air temperature at surface (K)
tpw	Total precipitable water (kg/m^2)
rhum850	850 mb relative humidity (%)
hgt250	250 mb geo-potential height (m)
hgt850	850 mb geo-potential height (m)
uwnd250	250 mb zonal wind (m/s)
uwnd850	850 mb zonal wind (m/s)
vwnd250	250 mb meridional wind (m/s)
vwnd850	850 mb meridional wind (m/s)
omega250	250 mb omega (Pascal/s)
omega850	850 mb omega (Pascal/s)
sm	Soil moisture (mm)

[5]. The figure shows that only eight predictors are retained from a pool of 72 probable predictors. This means given the eight predictors, only eight predictors (hgt850.1, omega850.1, at.3, uwnd250.3, vwnd250.5, at.6, rhum850.3, sm.5) can predict the monthly rainfall within the study area. Among these eight variables, four variables are parent nodes of target (hgt850.1, omega850.1, at.3, uwnd250.3), whereas the other four variables are child nodes (vwnd250.5, at.6, rhum850.3, sm.5). Basically, the variables having no directed edges with the target variables are considered redundant and are hence removed from the dataset, thus forming a more pruned dataset (feature subset). It is to be noted that, the variables that are retained in the structure, mostly represent 1-, 3-, and 5-months antecedent information. This shows that the variables that are retained are conditionally dependent on the target variable (in this case monthly rainfall) or the variables that are left out are conditional independent on the target variable.

After developing the feature subset of all the probable predictors, the features retained from the BN structure are further used to develop the prediction model in order to evaluate the utility of BN in feature selection. A basic three-layered ANN model was developed to predict monthly rainfall using the eight variables as input retained from the DAG of BN. The structure of ANN followed in the study was 8—4—1 as mentioned earlier. Also, the prediction feature present within the "bnlearn" package was also used for prediction and the performance of both the hybrid and the standalone models (BN-ANN and BN) was evaluated using suitable statistical indices. Coefficient of determination (R^2), Normalized Root Mean Square Error (NRMSE), Nash–Sutcliff efficiency (NSE) [21] and Modified Index of agreement (MD) [30] are used as the performance measures.

The scatter plots of both models for the calibration and validation are presented in Fig. 3. The monsoon season, i.e., June-July-August-September (JJAS) and the rest
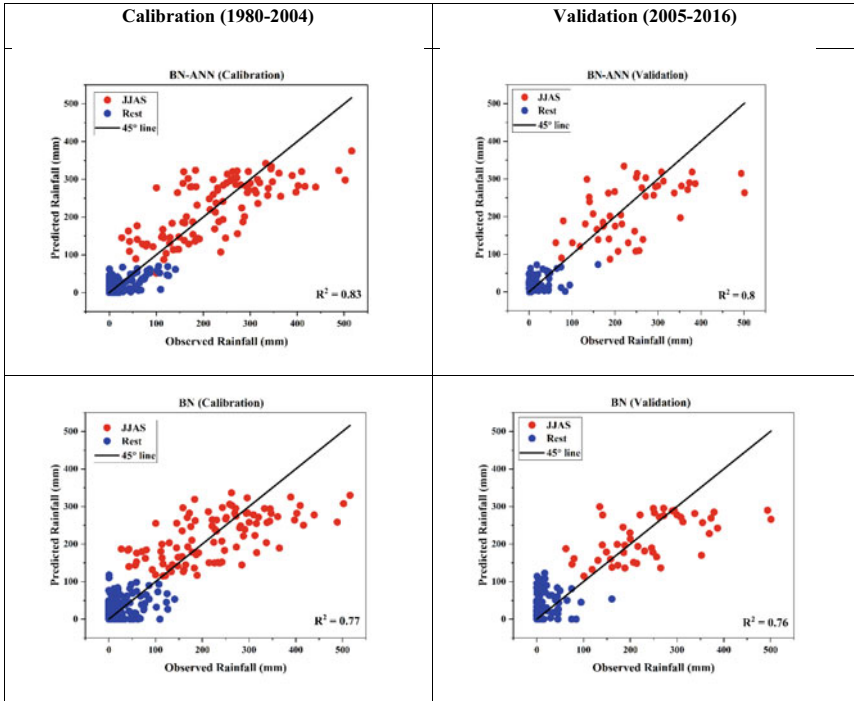
Fig. 3 Scatter plots of calibration and validation for both the models (BN-ANN and BN)

of the year is shown separately, so that a clearer scenario about the model performance in the monsoon and non-monsoon season can be depicted. The scatter plots are color-coded as Red (JJAS) and Blue (Rest). From the plots, it is very clear that the hybrid BN-ANN outperformed the standalone BN model in both the periods and also predicted rainfall much better for the non-monsoon season. For both models, the monsoon season is captured better than the non-monsoon season. The performance of the hybrid BN-ANN is much better than its counterpart in terms of all the performance metrics. Table 2 shows the performance metrics of both the models in the calibration and validation phase. Since Vidarbha is generally a drought-prone region, the maximum rainfall in both the calibration and validation period is not more than 550 mm during the period of study.

Table 2 Performance measures of both the models in the calibration and validation phase

	Calibration (1980–2004)				Validation (2005–2016)			
	R^2	NRMSE	NSE	MD	R^2	NRMSE	NSE	MD
BN-ANN	0.83	0.4	0.83	0.83	0.8	0.45	0.8	0.81
BN	0.77	0.47	0.77	0.79	0.76	0.5	0.74	0.75

Since Vidarbha is a drought-prone region, in order to analyze the drought scenarios in the region, the predicted monthly rainfall from the models is further used to classify the dry, intermediate, and wet scenarios. SPAI has been used as the drought quantification index. Contingency tables were used to access the degree of association between the SPAI derived from observed and predicted rainfall. A coefficient known as contingency coefficient (C) was calculated from the contingency tables [22]. The chi-square statistic (Q), with 4 degrees of freedom (since there are three categories), was also presented along with the p-values associated with it [18]. The upper limit of C cannot be greater than 1 and is given by

$$C_{max} = \sqrt{\frac{(x-1)}{x}} \tag{3}$$

where $x = \min(i, j)$ and i, j represent the number of categories in observed and predicted scenarios. In the present study, both the values of i and j is 3 and hence the value of C_{max} is 0.817. The ratio of C/C_{max} is also used as a degree of association. Tables 3 and 4 presents the contingency tables for the calibration and validation period for BN-ANN and BN models, respectively.

From the contingency tables also, it is very apparent that the hybrid BN-ANN model outperformed the standalone BN model. As expected, the degree of association was found to be better in the calibration phase than in the validation phase. All in all, it can be established that the hybrid BN-ANN model showed better performance both in terms of prediction of monthly rainfall and hence the drought scenarios as well.

Table 3 Contingency table for calibration and validation phase of BN-ANN

Predicted category	Calibration			Validation		
	Observed category			Observed category		
	Dry	Intermediate	Wet	Dry	Intermediate	Wet
Dry	25	19	3	9	8	5
Intermediate	17	160	25	5	75	17
Wet	5	23	21	8	13	2
	C = 0.476			C = 0.404		
	$C/C_{max} = 0.582$			$C/C_{max} = 0.494$		
	Q = 87.56			Q = 27.71		
	p value = < 0.0001			p value = < 0.0001		

Table 4 Contingency table for calibration and validation phase of BN

Predicted category	Calibration			Validation		
	Observed category			Observed category		
	Dry	Intermediate	Wet	Dry	Intermediate	Wet
Dry	24	20	3	10	11	1
Intermediate	11	154	38	6	69	22
Wet	12	28	8	5	18	1
	$C = 0.420$			$C = 0.4$		
	$C/C_{max} = 0.514$			$C/C_{max} = 0.489$		
	$Q = 64.03$			$Q = 27.167$		
	p value $= < 0.0001$			p value $= < 0.0001$		

6 Conclusion

The present study deals with extracting a feature subset from a pool of 72 meteoro-logical variables or probable predictors for the prediction of monthly rainfall in the drought-prone region of Vidarbha, India. Bayesian Network (BN) which is a class of Probabilistic Graphical Model (PGM), has been implemented as a feature selection technique. The popularly used score-based heuristic algorithm, Hill-Climb (HC), was used to form the Directed Acyclic Graph (DAG) structure, which establishes the conditional dependence structure between the probable predictors. The variables that are connected by a directed arc with the target variable constitute the feature subset for monthly rainfall.

The variables selected as feature subset was used as the inputs to the Artificial Neural Network (ANN) model for predicting the monthly rainfall. The standalone BN model was also used as a prediction model and the results from both the models (BN-ANN and BN) were compared using suitable performance measures. The results indicated that the hybrid BN-ANN model outperformed the standalone BN model in terms of all the performance measures (R^2, NRMSE, NSE, and MD). The results from the prediction models are further used to categorize each month as wet, intermediate, and dry months to evaluate the drought scenario in the study area in terms of the Standard Precipitation Anomaly Index (SPAI). The results from the drought analysis also showed that the BN-ANN model performs much better than the BN model in terms of all the degrees of association.

References

1. Bolón-Canedo V, Sánchez-Maroño N, Alonso-Betanzos A (2015) Feature selection for high-dimensional data. Springer International Publishing, Berlin. https://doi.org/10.1007/978-3-319-21858-8_3

2. Chanda K, Maity R (2015) Meteorological drought quantification with standardized precipitation anomaly index for the regions with strongly seasonal and periodic precipitation. J Hydrol Eng 20:1–8. https://doi.org/10.1061/(ASCE)HE.1943-5584.0001236

3. Chen L, Singh VP, Guo S, Mishra AK, Guo J (2013) Drought analysis using copulas 18:797–808. https://doi.org/10.1061/(ASCE)HE.1943-5584.0000697

4. Das M, Ghosh SK (2020) Introduction BT - enhanced Bayesian network models for spatial time series prediction: recent research trend in data-driven predictive analytics. In: Das M, Ghosh SK (eds). Springer International Publishing, Cham, pp 1–9. https://doi.org/10.1007/978-3-030-27749-9_1

5. Das P, Chanda K (2020) Bayesian network based modeling of regional rainfall from multiple local meteorological drivers. J Hydrol 591:125563. https://doi.org/10.1016/j.jhydrol.2020.125563

6. Das P, Naganna SR, Deka PC, Pushparaj J (2020) Hybrid wavelet packet machine learning approaches for drought modeling. Environ Earth Sci 79:1–18. https://doi.org/10.1007/s12665-020-08971-y

7. Dawood M, Rahman AU, Ullah S, Mahmood S, Rahman G, Azam K (2020) Spatio-statistical analysis of rainfall fluctuation, anomaly and trend in the Hindu Kush region using ARIMA approach. Nat Hazards 101:449–464. https://doi.org/10.1007/s11069-020-03881-5

8. Deka PC (2019) A primer on machine learning applications in civil engineering. CRC Press, Boca Raton

9. Di Y, Ding W, Mu Y, Small DL, Islam S, Chang NB (2015) Developing machine learning tools for long-lead heavy precipitation prediction with multi-sensor data. In: ICNSC 2015 - 2015 IEEE 12th international conference on networking, Sensing and Control, pp 63–68. https://doi.org/10.1109/ICNSC.2015.7116011

10. Dongre AR, Deshmukh PR (2012) Farmers' suicides in the Vidarbha region of Maharashtra, India: a qualitative exploration of their causes. J Inj Violence Res 4:2–6. https://doi.org/10.5249/jivr.v4i1.68

11. Dutta R, Maity R (2020) Temporal networks-based approach for nonstationary hydroclimatic modeling and its demonstration with streamflow prediction. Water Resour Res 56:e2020WR027086. https://doi.org/10.1029/2020WR027086

12. Hruschka ER, Hruschka ER, Ebecken NFF (2014) Feature selection by Bayesian networks. Lecture notes in computer science (including subseries lecture notes in artificial intelligence and lecture notes in bioinformatics), vol 3060, pp 370–379. https://doi.org/10.1007/978-3-540-24840-8_26

13. Huang Q, Mao J, Liu Y (2012) An improved grid search algorithm of SVR parameters optimization. In: International conference on communication technology proceedings (ICCT), pp 1022–1026. https://doi.org/10.1109/ICCT.2012.6511415

14. Jajarmizadeh M, Harun S, Salarpour M (2012) A review on theoretical consideration and types of models in hydrology. J Environ Sci Technol. https://doi.org/10.3923/jest.2012.249.261

15. Karmakar P, Muley AA, Kulkarni G, Bhalchandra PU (2019) Assessment of rainfall pattern using ARIMA technique of Pachmarhi region, Madhya Pradesh, India. Communications in computer and information science. Springer, Singapore. https://doi.org/10.1007/978-981-13-9187-3_42

16. Khan MYA, Tian F, Hasan F, Chakrapani GJ (2019) Artificial neural network simulation for prediction of suspended sediment concentration in the river Ramganga, Ganges basin India. Int J Sediment Res 34:95–107. https://doi.org/10.1016/j.ijsrc.2018.09.001

17. Koller D, Friedman N, Getoor L, Taskar B (2007) Graphical models in a nutshell. In: Introduction to statistical relational learning, vol 43

18. Maity R, Ramadas M, Govindaraju RS (2013) Identification of hydrologic drought triggers from hydroclimatic predictor variables. Water Resour Res 49:4476–4492. https://doi.org/10.1002/wrcr.20346
19. Nagarajan R, Scutari M, Lèbre S (2013) Bayesian networks in R. https://doi.org/10.1007/978-1-4614-6446-4
20. Nair SC, Mirajkar AB (2020) Spatio–temporal rainfall trend anomalies in Vidarbha region using historic and predicted data: a case study. Model Earth Syst Environ. https://doi.org/10.1007/s40808-020-00928-1
21. Nash JE, Sutcliffe JV (1970) River flow forecasting through conceptual models part I — A discussion of principles. J Hydrol 10:282–290. https://doi.org/10.1016/0022-1694(70)90255-6
22. Pearson K (1904) On the theory of contingency and its relation to association and normal correlation; On the general theory of skew correlation and non-linear regression. Cambridge University Press, Cambridge
23. Pour SH, Wahab AKA, Shahid S (2020) Physical-empirical models for prediction of seasonal rainfall extremes of Peninsular Malaysia. Atmos Res 233:104720. https://doi.org/10.1016/j.atmosres.2019.104720
24. Rodriguez-Galiano VF, Luque-Espinar JA, Chica-Olmo M, Mendes MP (2018) Feature selection approaches for predictive modelling of groundwater nitrate pollution: an evaluation of filters, embedded and wrapper methods. Sci Total Environ 624:661–672. https://doi.org/10.1016/j.scitotenv.2017.12.152
25. Scutari M (2010) Learning Bayesian networks with the bnlearn R Package. J Stat Softw 35:1–22. https://doi.org/10.18637/jss.v035.i03
26. Shah D, Mishra V (2020) Drought onset and termination in India. J Geophys Res Atmos 125:e2020JD032871. https://doi.org/10.1029/2020JD032871
27. Shin JY, Ajmal M, Yoo J, Kim TW (2016) A Bayesian network-based probabilistic framework for drought forecasting and outlook. Adv Meteorol 2016:8–13. https://doi.org/10.1155/2016/9472605s
28. Sucar LE (2015) Probabilistic graphical models. Springer, London. https://doi.org/10.1007/978-1-4471-6699-3
29. Tabari H (2019) Statistical analysis and stochastic modelling of hydrological extremes. Water (Switzerland) 11:1–11. https://doi.org/10.3390/w11091861
30. Willmott CJ, Ackleson SG, Davis RE, Feddema JJ, Klink KM, Legates DR, O'Donnell J, Rowe CM (1985) Statistics for the evaluation and comparison of models. J Geophys Res Ocean 90:8995–9005. https://doi.org/10.1029/JC090iC05p08995

Open-Access Precipitation Networks and Machine Learning Algorithms as Tools for Flood Severity Prediction

Luis O. K. M. Imagiire, Benedikt Mester, Stefan Haun, and Jochen Seidel

1 Introduction

As widely reported, floods are among the most frequent, deadly, and costly natural disasters [1–4], affecting on average 520 million people globally per year [5]. A recent estimate of economic losses results in 104 billion dollars [2] and is likely to increase as a consequence of changes in socioeconomic aspects, land use, and climate [3, 6, 7].

Among other types of flooding, flash floods constitute significant hazards in urban areas. Flash floods are short-term, temporally, and spatially concentrated floods that result from convective precipitation and usually have a high damage potential [8]. Such events are generally not predictable in time, which makes it difficult to take appropriate measures [4]. Especially in catchments with steep topography, these events can be further amplified, leading to a rapid concentration of runoff [7, 9]. In addition, factors such as a high degree of surface sealing due to urbanization, artificial drainage systems, or unsustainable land use can amplify runoff [10]. Thus, flash floods pose a major threat to settlements in exposed areas. The intensification of the hydrological cycle due to global warming [11] is expected to increase the occurrence of heavy convective precipitation which may lead to a possible increase in floods as well [1, 12].

Small settlements in areas prone to flash floods are especially vulnerable to the associated impacts, as they usually have limited resources to cope with flood impacts and to implement preventive measures. As an example, in May 2016, an extreme flash flood event triggered a landslide causing severe damage and economic losses in the range of 104 million Euros to the small municipality of Braunsbach and

L. O. K. M. Imagiire (✉) · S. Haun · J. Seidel
Institute for Modelling Hydraulic and Environmental Systems (IWS), University of Stuttgart, 70569 Stuttgart, Germany

B. Mester
Potsdam Institute for Climate Impact Research (PIK), 14412 Potsdam, Germany

nearby villages in the federal state of Baden-Württemberg, Germany [13, 14]. In this context, early warning systems are one of the most important non-structural measures to reduce the impacts of flash floods by allowing more time for local authorities to implement flood protection measures before the exceedance of critical water levels [4, 5, 15]. The reliability of warning systems for medium to large river basins has considerably increased in the past two decades, resulting in longer response times and a reduction of flood impacts [4]. However, flash floods in small basins remain difficult to predict due to their localized and rapid character, resulting in a limited warning time [16].

Regarding flash floods, the most important requirement of a warning system is early identification of critical threshold values which are likely to be exceeded, rather than the accurate prediction of the magnitude, duration, and timing of the flood peak [17].

The objective of this paper is the development of a simple early warning model based on the relationship between maximum rainfall intensities and water level response to predict flood severity. The small catchment of the River Echaz, located in the southwest of Germany, serves as a case study for the proposed model.

2   Study Area and Data Acquisition

The River Echaz is a small tributary (23 km long) to the River Neckar, which in turn is a major tributary to the River Rhine. The Echaz has a small catchment, located in the center of the federal state of Baden Württemberg, southwest of Germany (Fig. 1). Some aspects of the catchment enhance the potential for flash flood occurrence, specifically: (i) the small drainage area (135 km^2); (ii) the steep topography, with elevations ranging from 270 to 900 m.a.s.l; and (iii) the degree of urbanization and the land use, as 20% can be considered as an urban area with a high degree of impermeabilization (in 2010).

Precipitation data is obtained from a network of currently 31 personal weather stations using tipping bucket gauges. This data is available through an open-access online platform (https://weathermap.netatmo.com/). Although the amount of PWS contributes to a high density of one rain gauge every 4.2 km^2, the spatial distribution is not homogenous, as the PWS are concentrated to the settlements in the downstream part of the catchment. Despite the potential to increase spatial coverage and resolution in urban catchments, these PWS are prone to different types of errors, as they are not professionally operated [18]. To confirm the reliability of the available PWS, the recorded data of three precipitation events was compared with measurements from eight professional weighing rain gauges operated by the city of Reutlingen. Similar average values were observed for the whole catchment for both networks. An important finding from the individual assessment of the PWS is the high spatial variability of precipitation events for both networks (e.g., differences in maximum rainfall intensity up to more than 10 mm/hour for small distances of only 2 km).
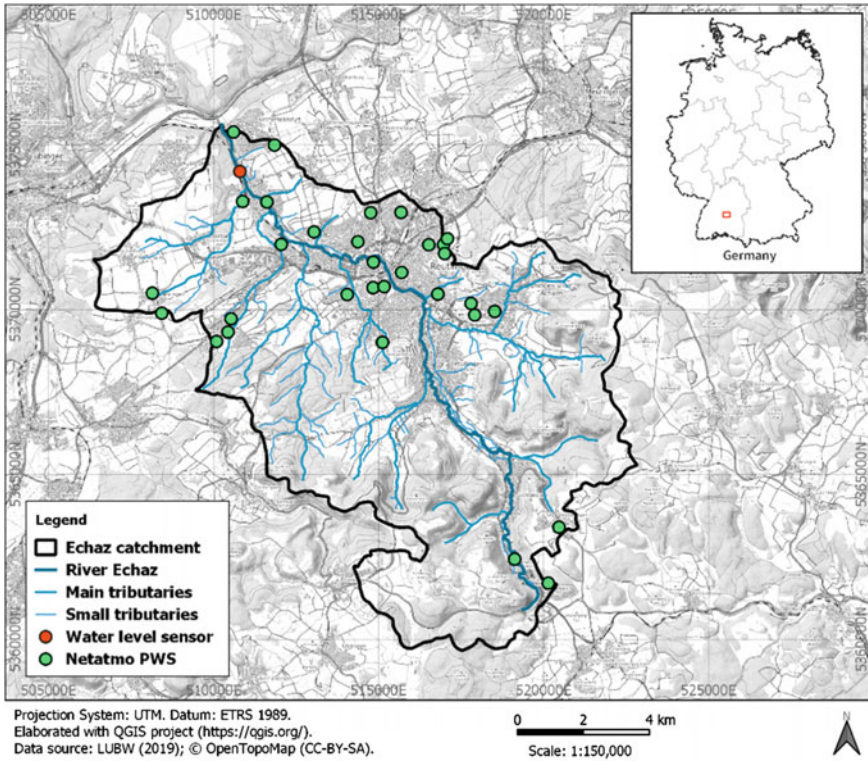
Fig. 1 Location of water level sensors and personal weather stations (PWS) in the Echaz catchment

In addition, a network of 21 low-cost ultrasonic water level sensors was recently implemented (2020) by the municipality of Reutlingen, distributed over the whole catchment. One sensor which was considered for the initial setup of the model is located at the mouth of the Echaz, close to an operational hydrological gauging station (Wannweil) from the Landesanstalt für Umwelt Baden-Württemberg (LUBW). This setup allowed for the comparison of the measurements between both sources during three precipitation events in 2020. A high correlation was observed, not only validating the ultrasonic device as a low-cost alternative but also enabling the estimation of past data for the location by linear regression.

Measurement recordings from the water level gauge station, along with information on the reported flood events from online newspapers, point out that the flash flood events in the Echaz catchment were associated with summer convective precipitation. As 80% of the discharges with a return period greater than 2 years occurred between June and August, including all major flood events since 2002. Therefore, a selection of the events considering heavy precipitation and all the flood discharges with return periods longer than 2 years were selected to derive the thresholds for the model.

3 Methodology

For this study, soil moisture, one of the input parameters for similar approaches such as flash flood guidance [19, 20], was not considered, as at higher rates the antecedent soil moisture conditions on the process of transition from precipitation to runoff can be neglected [21]. The reason is that during these conditions the production of runoff can be significantly faster than ground infiltration [22], especially in steep mountain areas due to low storage capacity [23]. Therefore, the warning levels of the proposed model essentially rely on maximum rainfall intensity thresholds for different accumulation periods of rainfall from 5 to 60 min associated with the exceedance of critical water levels at the outlet of the drainage basin.

This study considers two distinct periods for analysis: (i) Recent events—comprising ten of the most significant precipitation events that occurred during the summer season 2020. This period comprises water level data from the low-cost ultrasonic sensor at the outlet of the drainage basin as well as precipitation data from the PWS network. Two of these precipitation events led to floods with a return period of 2 years (HQ2); (ii) Past events—comprising 14 of the most significant precipitation events between 2016 and 2019 (during summer seasons). This period considers water level data estimated by linear regression from the Wannweil gauging station and precipitation data from the PWS network. Since only minor events occurred in 2020, this additional data was used to account for higher flood discharges with return periods of 5 (HQ5), 10 (HQ10), and 20 years (HQ20).

3.1 Input Data

The model in this study is based on the direct relationship between the water level increase at the outlet of the drainage basin and the rainfall intensity [24]. As a preliminary analysis of the data, the maximum rainfall intensity is evaluated as the most representative parameter for the water level variations. Hence, the maximum rainfall intensity was used as a trigger for the proposed flood warning model.

The PWS transmit the precipitation as sum parameters of 5 min intervals. A non-weighted average for the whole catchment, including all online PWS, was considered for each 5 min interval. To represent the precipitation events, the maximum rainfall depths (mm) accumulated in 5, 10, 15, 30, and 60 min were considered. An initial assessment showed that most of the events occurred with peaks concentrated in a period up to 60 min. An exemplary flood event (June 24, 2016) is displayed in Fig. 2. Therefore, for the Echaz catchment, the maximum rainfall accumulated in 60 min usually refers to the total amount of rainfall or at least to most of the rainfall depth accumulated during the precipitation event.

Although the water level rise is quantitative, this study aims to predict the severity of flooding according to the exceedance of critical water levels associated with different flood discharge references. For this purpose, a binary classification (i.e.,
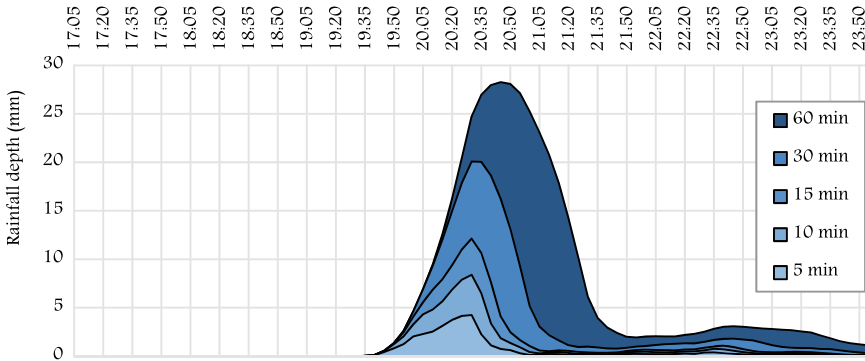
Fig. 2 Rainfall depths accumulated in different periods for the event on June 24, 2016

Table 1 Examples of model input data with respect to precipitation and water level

Event	Maximum rainfall intensity (mm/period)					Water level (cm)		Flood return period
	5 min	10 min	15 min	30 min	60 min	Prior	Peak	
24/06/2016	4.2	8.4	12.1	20.1	28.3	33	168	HQ20
15/08/2017	3.5	6.5	9.0	16.5	21.1	31	120	HQ5
11/06/2018	4.1	7.7	10.8	18.7	28.4	24	144	HQ10
22/06/2019	2.1	3.9	5.7	10.0	14.4	26	116	HQ5
02/07/2020	2.6	4.3	6.0	9.0	12.9	22	109	HQ2

exceedance of the reference discharge or not) of the peak water level at the catchment's outlet was considered. Also, the water level prior to the precipitation event is an important parameter, as the amount of discharge, necessary to exceed the defined critical water level, directly depends on it. Table 1 presents examples of the input data for a selected event for each year.

For a total of 24 events, 2 machine learning techniques (Logistic Regression and Decision Trees) were applied to determine maximum rainfall intensity thresholds for the exceedance of the critical water levels. Hence, the flood severity is determined by the exceedance of the water levels and the corresponding flood discharges with return periods of HQ2, HQ5, and HQ10. Due to high uncertainties, a threshold for HQ20 is not considered, as there was only one event during the study period that exceeded this flood discharge.

3.2 Logistic Regression

The logistic regression method is a useful tool to assign probabilities to the occurrence of a certain event such as a flash flood (Y) based on the relationship between the chosen independent variables (X) observed in the input (training) data. The method uses the logistic function (S-curved line) (Eq. 1) to display the probability range of 0 (non-exceedance) to 1 (exceedance), whereas the range for the independent variable (X) is unlimited [25]. The coefficients, obtained with maximum likelihood estimation, refer to the y-intercept (a) and slope (b) for the linear relationship between the log (odds of Y) and the independent variable (X). Figure 3 illustrates an example of the application of the method for an HQ2 exceedance.

$$\Pr(Y = 1|X) = p(X) = \frac{e^{a+bX}}{1 + e^{a+bX}} = \frac{e^{\log(odds)}}{1 + e^{\log(odds)}} \tag{1}$$

From the figure, it can be seen that there is an overlapping interval for the independent variable (from 1.4–3.1) in which both outcomes (e.g., exceedance/non-exceedance of HQ2) may occur. The fitted line provides a probability for the response (Y = 1) for the given X value. Variables with high correlation yield steeper curves (smaller overlapping zones) that result in better classification of the outcome. The uncertainty is higher around the value for X corresponding to a probability of 50% (approximately 2.4 in this case). The further away from this point the more certain is the prediction of the outcome. For the case of floods, the choice of a threshold closer to the upper boundary of the overlapping zone is useful to avoid false alarms, however, it increases the chance for the occurrence of missed warnings.

If there is a complete separation of the outcomes, a clear threshold exists and the assigning of the probabilities is not necessary. In this case, other methods (e.g., Decision Tree) are more appropriate.
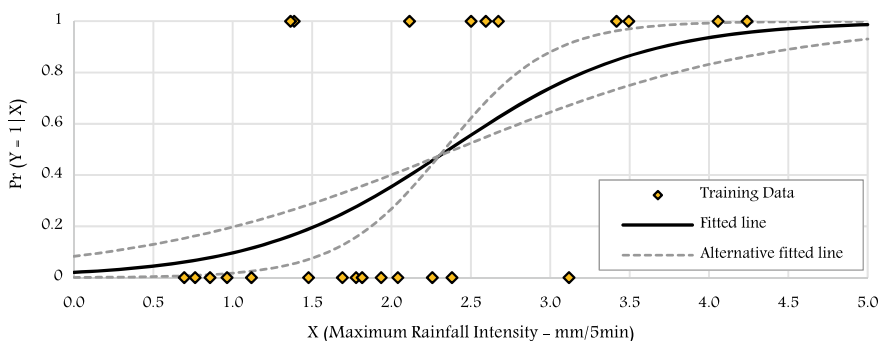
Fig. 3 Example of the logistic regression application to determine the probability of an HQ2 exceedance

3.3 Decision Tree

As a classification method, the decision tree is used to predict in which categorical response (binary or classes) the outcome will result, given the node where the independent variable value of interest is located [26]. Figure 4 presents an example of the resulting decision tree for a 20 events sample, considering the maximum rainfall intensity (mm/60 min) and prior water level as variables.

The training data (i.e., one or more independent variables together with the corresponding outcome) is given as input. Initially, all data belongs to the same root node (i.e., the whole training data interval). Next, the use of splitting rules creates branches to divide the data into two nodes (leaves). The splitting rules are associated with the purity of the resulting nodes (i.e., the predominance of a certain class/outcome). Among other options, the Gini Index, which represents the total variance across the classes, is a common indicator for purity. The closer to 0 the purer the node is. The algorithm continues to create branches and new nodes until predefined criteria are met (e.g., minimum split sample size, maximum tree depth, minimum impurity decrease, among others).

For this example, values below 4.25 mm/60 min result in non-exceedance of the critical water level (i.e., no flood) and values above 6.25 mm/60 min result in potential exceedance (i.e., flood). Also, these values constitute the lower and upper boundary of the overlapping zone, in which the maximum rainfall intensity alone is not sufficient to predict the outcome. In this case, the decision tree creates a new branch using the prior water level to classify the outcome for the four remaining
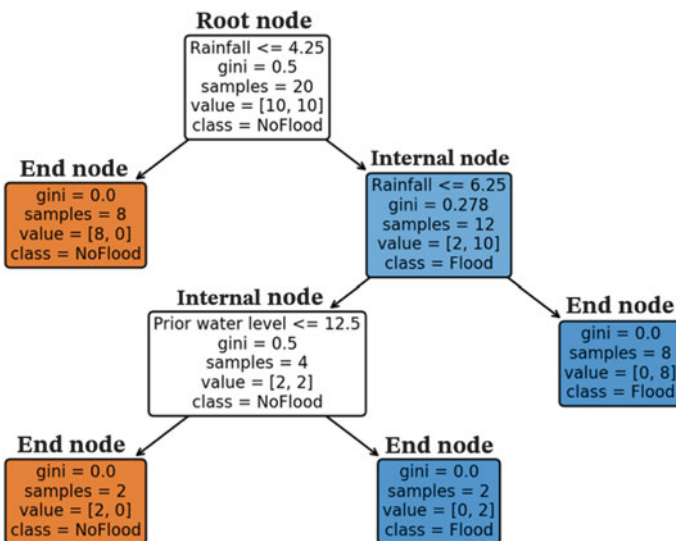
Fig. 4 Example of the decision tree application

samples in the overlapping zone. As a result, this decision tree yields nodes with complete purity (i.e., only one class per node).

3.4 Proposed Model for the Echaz Catchment

The proposed model considers the Decision Tree to obtain maximum rainfall thresholds and the Logistic Regression to obtain the associated probability of exceedance. To avoid false alarms, the criteria for branching in the Decision Tree consider purity in the exceedance node, i.e., setting the threshold larger than the upper boundary of the overlapping zone. As the uncertainty is higher for the shorter accumulation periods (i.e., wider overlapping zones), the second branch, which includes the prior water level, is only considered for the 60 min rainfall accumulation period, which has the smallest overlapping zone (i.e., better correlation with the outcome). The Logistic Regression allows the identification of the corresponding probability of exceedance associated with the found thresholds. All detected thresholds are taken into account simultaneously and compared with live data from the PWS network. If any of them is reached, the model triggers an alarm (i.e., notification) for the corresponding critical water level, also indicating which flood severity needs to be expected.

The main characteristics for the model are: lumped (non-weighted average for areal precipitation); classification (categorical response for each flood discharge return period); data-driven (relationship between the rainfall and the water level, without physical interpretation of the rainfall-runoff process); threshold-based (a simplified version of the flash flood guidance method with machine learning approaches to obtain the thresholds); multivariate (maximum rainfall intensities and prior water level as inputs); early warning model (monitors live data and provides alert to increase the response time for preventive actions against the impacts of flash floods).

The steps for the model implementation are: (i) data acquisition (precipitation average values and water level measurements); (ii) data filtering (check for inconsistency, gaps, and outliers); (iii) event selection (most representative events for the period including high rainfall intensities and the critical water level reference of interest); (iv) determining thresholds and associated probabilities (Decision Tree to obtain thresholds and Logistic Regression to obtain the corresponding probability of exceedance); (v) dealing with overlapping zones (if necessary, additional branch to the tree for the variable with the best correlation to reduce uncertainty); (vi) setting up a live monitoring (monitor live rainfall data to issue flood severity warnings); (vii) updating when new data are available (every new season, evaluate the performance, incorporate new data and check if thresholds updates are necessary).

4 Results and Discussion

The results of the application of the Decision Tree and Logistic Regression methods to the training data composed of 24 selected events (2016–2020) comprising the maximum rainfall thresholds and the associated probabilities are presented in Table 2. Ten of the selected events exceed an HQ2 discharge, four events exceed HQ5 discharge and two events exceed HQ10 discharge. Hence, the small amount of data for this case study restricts the use of Logistic Regression to obtain probabilities for the thresholds associated with the exceedance of higher flood discharges, as there is a complete or almost complete separation of the outcomes. For the same reason, the uncertainty regarding the accuracy of the obtained thresholds is higher for the more severe floods. Therefore, the application of the Logistic Regression method, and estimation of the probabilities of exceedance (p), is only performed for HQ2 exceedance.

The evaluation of the performance of the model is conducted for the training data, as attempts to reserve part of the dataset for test and cross-validation techniques, showed that important information is removed and the model gets less representative for the relationship between the variables, as it relies on a small amount of data.

The results of the application of the obtained thresholds for HQ2 exceedance to the training data are represented in the following confusion matrix (Fig. 5) and by the associated measures: (i) specificity—1.00 (100% effective in avoiding false alarms); (ii) sensitivity—0.80 (80% effective in predicting the observed HQ2 exceedance); (iii) precision—1.00 (100% of the predicted HQ2 exceedance are correct); and (iv) accuracy—0.92 (92% of the overall predictions are correct).

Severe floods are rare events. Since the data comprise five years of measurements the number of considered events is small for this short period. As result, the risk of overfitting and lower performance measures on test and validation data exists,

Table 2 Resulting maximum rainfall thresholds and associated probabilities of exceedance derived by the decision tree and logistic regression method, respectively

Max. rainfall intensity	HQ2	p (HQ2)	HQ5	HQ10
mm/5 min	3.3	0.82	3.5	3.8
mm/10 min	5.9	0.82	6.4	7.1
mm/15 min	7.2	0.72	8.4	9.9
mm/30 min	9.8	0.75	14.5	17.6
mm/60 min	11.3	0.70	17.8	24.7

Fig. 5 Confusion matrix for HQ2 exceedance

		Observed	
		Yes	No
Predicted	Yes	8	0
	No	2	14

resulting in expected uncertainties for the first upcoming seasons. However, more events and subsequently more data will be available due to the implemented monitoring, enabling (cross) validation. The overall performance is anticipated to steadily increase as exceedance thresholds are updated as well.

Two events exceeding HQ2 could not be identified by these thresholds, as the outcomes also depend on the prior water level (i.e., within the overlapping zone). However, this is solved by implementing a second branch for the 60 min accumulation period. Regarding the performance of the thresholds for HQ5 exceedance, one of the four events is not correctly predicted as it also depended on the prior water level. For the HQ10 exceedance, the two events are correctly predicted by the found thresholds.

As severe floods are associated with high rainfall intensities, the thresholds for shorter accumulation periods (e.g., five or ten minutes) are more easily exceeded (i.e., the rainfall values are larger than the upper boundary of the overlapping zone). Thus, as the model relies on multiple thresholds (one for each of the accumulation periods), the exceedance of critical water levels during such severe events is identified earlier by shorter accumulation periods. On the other hand, smaller floods are only identified by the thresholds for longer accumulation periods and/or by the secondary threshold for prior water level.

The time between the alarm triggering and the exceedance of the associated critical water level, also called lead time, is computed for the events of 2016–2020. On average, the model provides a lead time of 81 min for the HQ2 exceedance, 100 min for HQ5 exceedance, and 105 min for HQ10 exceedance at the water level sensor near the mouth of the Echaz.

5 Conclusions

In this study, a simple flood warning model to predict flood severity at the mouth of the River Echaz catchment is presented. The model architecture includes open-access precipitation data from PWS and water level measurements from a low-cost ultrasonic sensor at the outlet of the drainage basin. These data sources are identified to be suitable and reliable for flood warnings purposes, given the results of the comparison with established and professionally operated public stations. The development of the model is guided by simplicity and interpretability, with a threshold-based approach to provide alerts associated with the exceedance of critical water levels indicative of the flood severity (i.e., flood discharges with return periods of 2, 5, and 10 years). In addition, maximum rainfall depths accumulated over 5, 10, 15, 30, and 60 min are used to characterize the precipitation events and to derive multiple thresholds for the model. The Decision Tree classification machine learning method is used as it has advantages in the interpretability (straightforward visual representation) and allows the use of secondary variables (e.g., prior water level) providing better predictions for overlapping uncertainty zones. Another feature is the branching criterion which considers purity in the exceedance nodes to avoid false alarms. The application of the Logistic Regression method allows the assignment of probabilities of

exceedance to the found thresholds. Currently however, it is restricted to flood events up to HQ2 exceedance due to limited data availability. With the developed method (multiple triggers), the model is able to identify the severe floods earlier and with more reliability. Good performance is observed for the training data, as a severity for most of the observed flash flood events (2016–2020) is correctly predicted by the model. Nevertheless, there is a risk of overfitting and lower performance for the first upcoming events, as the model relies on a small amount of data. Hence, the model needs to be evaluated with the acquisition of new data during upcoming seasons. As the incorporation of additional data will lead to more accurate updated thresholds, the model performance and prediction capacity are likely to enhance. Further improvements could be achieved through better determination of areal precipitation and the development of real-time algorithms to remove PWS with outliers or inconsistent measurements. The model provides an average lead time of 81 min for the HQ2 exceedance, 100 min for HQ5 exceedance, and 105 min for HQ10 exceedance. The reduced complexity and high interpretability of the model allow for short training times of staff and fast decision-making processes. With the upcoming inclusion of the other water level sensors, flood severity can be predicted at most sections along the course of the Echaz. To conclude, this study contributes with an easy to interpret and low-cost solution to increase the response time for local authorities to take preventive actions in the Echaz catchment.

References

1. World Health Organization (2013) Floods in the WHO European region: health effects and their prevention. WHO Regional Office for Europe, Copenhagen
2. Blöschl G, Hall J et al (2017) Changing climate shifts timing of European floods. Science 357(6351):588–590
3. Blöschl G, Hall J et al (2019) Changing climate both increases and decreases European river floods. Nature 573:108–111
4. Perera D, Seidou O et al (2019) Flood early warning systems: a review of benefits, challenges and prospects. UNU-INWEH, Hamilton
5. World Meteorological Organization (2013) Flood forecasting and early warning. In: Integrated flood management tool series no. 19
6. Vorogushyn S, Merz B (2013) Flood trends along the Rhine: the role of river training. Hydrol Earth Syst Sci 17:3871–3884
7. Kundzewicz ZW (2013) Floods: lessons about early warning systems. In: Emerging lessons from ecosystems. European Environment Agency
8. Şen Z (2018) Flood modeling, prediction, and mitigation. Springer, Cham
9. Borga M, Anagnostou EN et al (2011) Flash flood forecasting, warning and risk management: the HYDRATE project. Environ Sci Policy 14(7):834–844
10. Edwards PJ, Williard KW, Schoonover JE (2015) Fundamentals of watershed hydrology. J Contemp Water Res Educ 154:3–20
11. IPCC (2013) Climate change 2013: the physical science basis. In: Stocker TF, Qin D et al (eds) Contribution of working group I to the fifth assessment report of the intergovern-mental panel on climate change. Cambridge University Press, Cambridge
12. Blöschl G, Gaál L et al (2015) Increasing river floods: fiction or reality? WIREs Water 2:329–344

13. Ozturk U, Wendi D et al (2018) Rare flash floods and debris flows in southern Germany. Sci Total Environ 626:941–952
14. Lucía A, Schwientek M et al (2018) Planform changes and large wood dynamics in two torrents during a severe flash flood in Braunsbach, Germany 2016. Sci Total Environ 640–641:315–326
15. Homagk P (1996) Hochwasserwarnsystem am Beispiel Baden-Württemberg. Geowissenschaften 14:539–546. Ernst & Sons GmbH, Berlin
16. Versini PA, Berenguer M et al (2014) An operational flood warning system for poorly gauged basins: demonstration in the Guadalhorce basin (Spain). Nat Hazards 71:1355–1378
17. World Meteorological Organization (1981) Flash flood forecasting. In: Operational hydrology report no. 18
18. Bárdossy A, Seidel J, Hachem AE (2020) The use of personal weather station observation for improving precipitation estimation and interpolation. Preprint Hydrol Earth Syst Sci
19. Norbiato D, Borga M et al (2008) Flash flood warning based on rainfall thresholds and soil moisture conditions: an assessment for gauged and ungauged basins. J Hydrol 362(3):274–290
20. Georgakakos K (2006) Analytical results for operational flash flood guidance. J Hydrol 317(1):81–103
21. Hermann GR, Schumacher RS (2018) Flash flood verification: pondering precipitation proxies. J Hydrometeorol 19(11):1753–1776
22. University Corporation for Atmospheric Research (2011) Flash flood early warning system reference guide 2010. UCAR
23. Wehren B, Weingartner R et al (2010) General characteristics of alpine waters. In: Bundi U (ed) The handbook of environmental chemistry, vol 6. Springer, Heidelberg, pp 17–58
24. Davis RS (2001) Flash flood forecast and detection methods. In: Doswell CA (ed) Severe convective storms. Meteorological monographs no.50, pp 481–525
25. James G, Witten D et al (2013) Classification. In: An introduction to statistical learning. Springer texts in statistics, vol 103. Springer, New York
26. James G, Witten D et al (2013) Tree-based methods. In: An introduction to statistical learning. Springer texts in statistics, vol 103. Springer, New York

Flood-Proof House: An Alternative Approach to Conventional Housing Typology

Gautam Das, Mousom Mrinmoy Kashyap, Niranjan Konwer, and Atanu Kumar Dutta

1 Introduction

Assam, one of the most populous states in North East India, consists broadly of two river basins: the Brahmaputra and the Barak. The flood-prone area of the state is 31500sq km as assessed by Rashtriya Barh Ayog [1], which is about 39.58 percent of the total land area of Assam (Fig. 1).

According to a statistical report released by NDTV India [3], about 12 lakhs of people have been affected by flood and 60 were dead in the year 2017 (Fig. 2).

This work attempts to address the problem of flood-related housing. The work proposes a Flood-proof house, which will serve the basic needs of housing during flood, while serving the normal purpose during the dry season. One of the main objectives in design is to make the house affordable to the weaker section of the society while fulfilling the serviceability condition. Construction material considered here is FRP, steel, timber and bamboo leading to low-cost housing. An anchorage system is proposed to ensure the safety of the structure during the flood. The house is to be tested against possible high water-current and wind during the flood and possible earthquakes while aground.

2 Planning of the Super-Structure

Planning of the super-structure needs knowledge of the geological, geographical, and environmental condition of the area, where the structure is to be constructed. Planning is to be done with an aim of making the structure green by harnessing natural advantages such as light and air. Good orientation can increase the energy efficiency of the house, making it more comfortable to live in and cheaper to run.

G. Das · M. M. Kashyap · N. Konwer · A. K. Dutta (✉)
Jorhat Engineering College, Jorhat, Assam, India
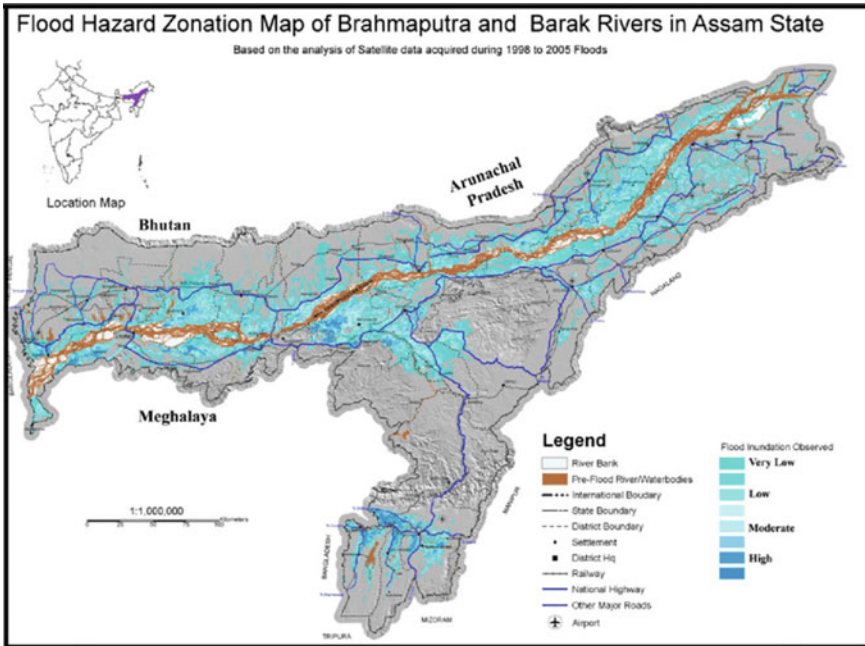
Fig.1 Flood Hazard areas of Assam in the year of 2017 [2]

Fig. 2 Showing flood plain of River Brahmaputra

The proper orientation of the structure is achieved using the Wind Rose diagram and Sun Diagram. The Wind Rose diagram of Jorhat, as shown in Fig. 3, is used to find the direction in which the wind intensity is maximum. This, in conjunction with the Sun Diagram as shown in Fig. 4, is used to plan the house.
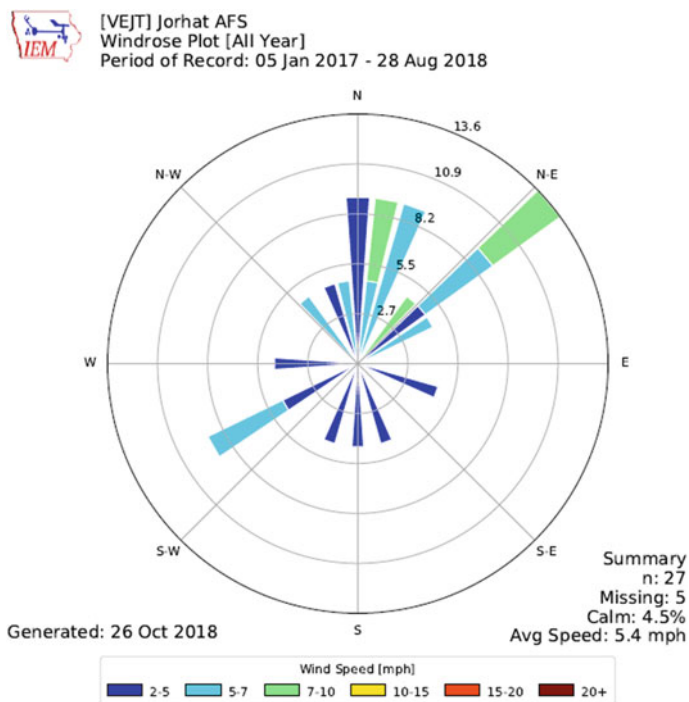
Fig. 3 Wind Rose diagram of Jorhat Airport from January 5, 2017 to August 28, 2018 [4]

The plan of the house is proposed within an area of 150 sq. m. Isometric view (Fig. 5) Plan (Fig. 6) and beam-column layout (Fig. 7) of the house are presented here.

3 Design of Floatable Base

The depth of the floatable base is to be calculated using the principle of buoyancy. The floating base is made using FRP which constitutes of 5 mm PVC foam, sandwiched between fiberglass isophthalic marine grade resin with UV self-pigmented gelcoat (polyester pigment). FRP sheet is used to cover the floating base. The perforated sheet plate in the lower base of the floating base connects the I-section columns (ISLB 100) with the base. The columns are welded to the steel base. The base plate is strengthened by grids using 2 mm steel plates.

FRP sheets are used to envelop the steel framework. These form a trapezoid of height 1 m, bottom base area 10 × 7 sq. m, and top base area 15 × 10 sq. m. Vinyl flooring sheets are used as floor-covering to increase the floor friction and thermal insulation.
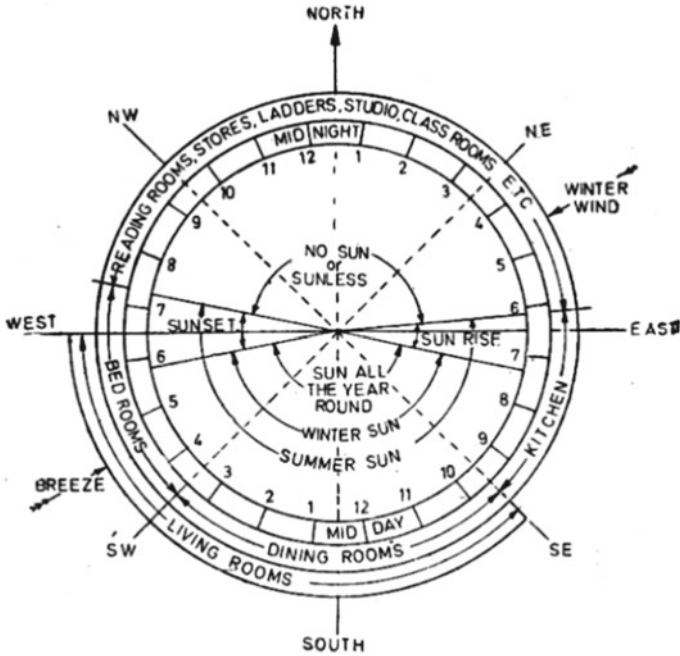
Fig. 4 Aspect and Sun diagram [5]
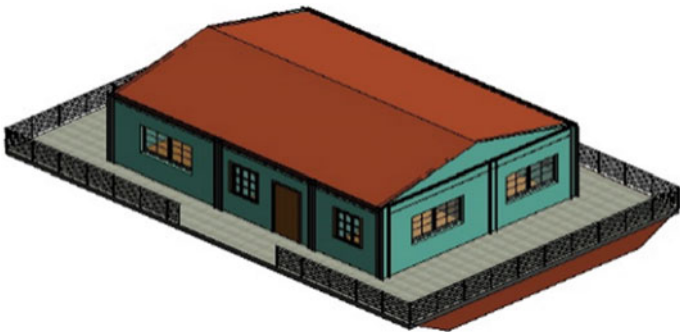
Fig. 5 Isometric of the house facing SW direction

3.1 Check for Buoyancy

A detailed check is done with reference to Fig. 8.

Total load of the structure is found as 11570.95 kg.

Assuming x to be the depth of submerging of the base, using equilibrium condition

$$\Rightarrow W - F_B = 0 \tag{1}$$
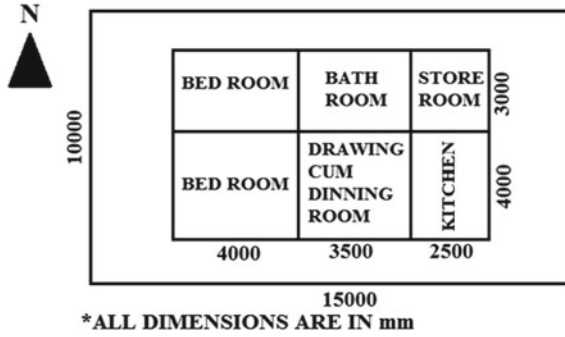
Fig.6 Plan of the house
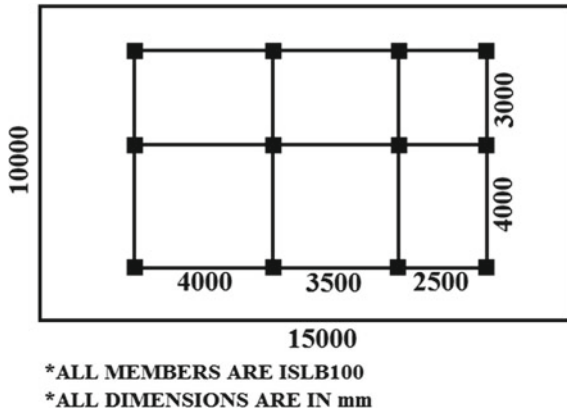
Fig. 7 Column and beam details
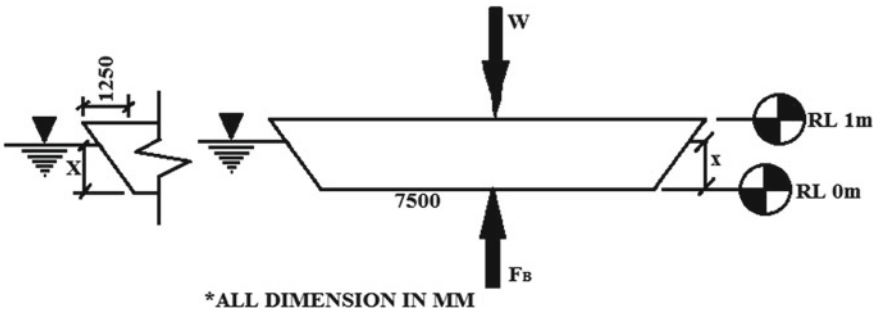
Fig. 8 Free body diagram of the base

Table 1 Details of stress in the steel frame

Solution information	Minimum	Maximum	Average
Equivalent stress	0.89 MPa	124.8 MPa	4.76 MPa
Total deformation	0 mm	14.06 mm	2 mm
Elastic strain	9.15×10^{-7}	6.24×10^{-4}	3.82×10^{-5}

$$orx = 0.097m < 1m, Henceok$$

The base is modeled in Ansys 19.1® and analyzed against floatation stress. The resultant stresses in the steel plates are shown in Table 1.

Maximum Stress developed is 124.81 MPa, which is less than f_y (250 MPa).

Due to the limitation in nodes in the student version of Ansys 19.1®, a smaller model is modeled in Ansys 19.1® (Figs. 9, 10, and 11).
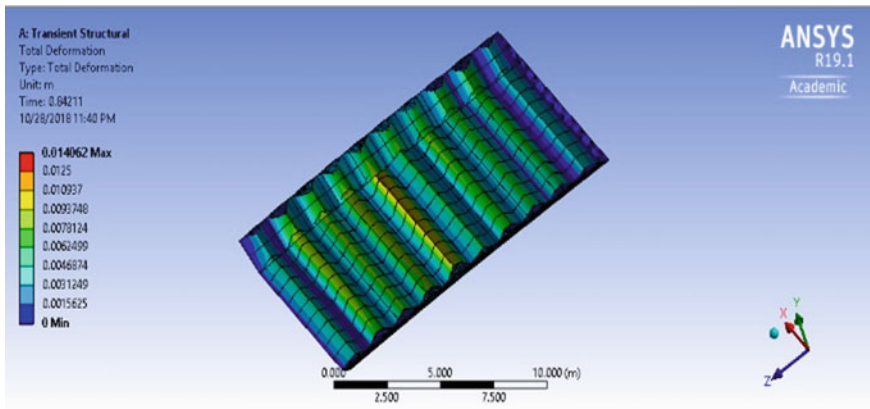
Fig. 9 Image of results in Ansys 19.1®

Fig. 10 Plan of scaled-down house
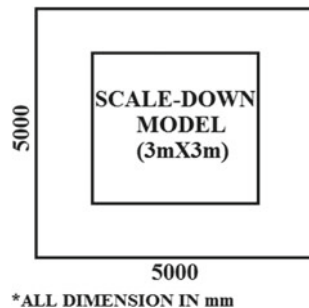
Fig. 11 Elevation of the
scaled-down house
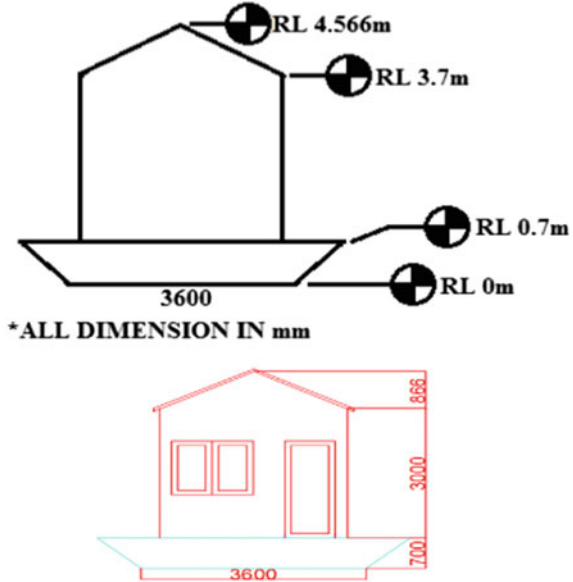
4   Mass Calculation of the Smaller Model

4.1   *Mass of the Steel Framework*

(i)   4 nos. of ISMB 200 = 447.6 kg.
(ii)   4 nos. ISMB 150 = 180 kg.
(iii)   5 nos. thick steel plate $5 \times 5 \text{ m}^2 = 1000$ kg.
(iv)   5-mm-thick steel plate $3.6 \times 5 \text{m}^2 = 720$ kg.
(v)   Trapezoidal plate 5 pieces = 600 kg.
(vi)   Rectangular plate 2 pieces = 396 kg.
(vii)   Rectangular section 4 pieces = 560 kg.
            Total = 3907.6 kg.

4.2   *Mass of Steel Truss*

Roof truss is of 50 mm nominal bore steel tube in the. As per IS: 1239 (Part-I)- 2004, the mass of the tube is 5.03 kg/m.

Mass of the single truss provided in the roof

$$= 8.83 \times 5.03$$

$$= 44.4149 \text{kg}.$$

Total mass of all the trusses $= 44.415 \times 3$

$$= 133.245 \text{kg}.$$

Now the total mass of the truss system $= (6 \times 3 \times 5.03) + 133.245$

$$= 223.785 \text{kg}.$$

4.3 Total Mass of the Structure

Total mass of the whole structure (W) $= 3679.8 + 223.785$

$$= 3903.585 \text{kg}.$$

5 Seismic Check

As per IS: 1893-(Part-I)-2002 clause 6.4.2 the Design Horizontal Seismic Coefficient (A_h) is calculated as

$$A_h = \frac{ZIS_a}{2Rg} = \frac{0.36 \times 1}{2 \times 5} \times 2.5 = 0.09.$$

5.1 Calculation of Design Seismic Base Shear

As per IS: 1893-(Part-I)-2002 clause 7.5.3, the Design Seismic Base Shear (V_B) is calculated as

$$Q_i = V_B = 0.09 \times 3903.585 = 351.322 \text{kg}.$$

Assume Q_i is acted on the C.G. of the roof truss, which provides a maximum moment for the lateral load. The height of the structure to the base from the C.G. of the roof truss is

$$\bar{h} = 0.7 + 3 + \frac{1}{3} \times 0.866 = 3.989\text{m}.$$

Now, moment due to lateral load is calculated as

$$M_i = Q_i\bar{h} = 351.322 \times 3.989 = 1383.86\text{kgm}.$$

5.2 *Check for Overturning*

The structure just rests on ground, without any foundation. Hence this needs to be checked against overturning during an earthquake.

The eccentricity of the structure due to earthquake moment (M_i) is calculated as

$$e = \frac{M_i}{W} = 354.51\text{mm}.$$

Permissible limit of eccentricity is given as $= \frac{1}{6} = e_{max}$.
Since the base length of the structure is (l) $= 5\,\text{m} = 5000\,\text{mm}$.
Now,

$$e_{max} = \frac{5000}{6} = 833.33\text{mm}.$$

Since $e < e_{max}$, hence ok.
The structure is safe against overturning.

6 Calculation of Wind Load

The calculation for designing wind speed as per IS 875: Part 3,
Design wind speed, $V_z = k_1 k_2 k_3 V_b$
As per the wind map of India, V_b=50 m/s for the North Eastern region (Assam).
For design life, $N = 50$ years and risk level, $P_N = 0.63$, height of building $=$ 3.5 m, the value of k_1, k_2 and k_3 are
$k_1 = 1$, $k_2 = 1$, $k_3 = 1$ (considering the plain area).
Now,

$$V_z = 1 \times 1 \times 50$$
$$= 50\text{m/s}.$$

Design wind pressure

$$P_z = 0.6 \times 50^2 = 1.5 \text{kPa}.$$

7 Calculation of Metacentric Height

With reference to Fig. 12,

$$I_{yy} = 30.323 \text{ m}^4$$

$$V = 12.8 \text{ m}^3$$

$$\frac{I}{V} = 2.369 \text{ m}$$

$$y_b = \frac{(4.4 + 2 \times 3.6)}{4.4 + 3.6} \times \frac{.4}{3} = 0.193.$$

$$GM = \frac{I}{V} - (2.2 - 0.193) = 0.362 \text{ m}.$$

Fig. 12 Calculation of Metacentric height of the model
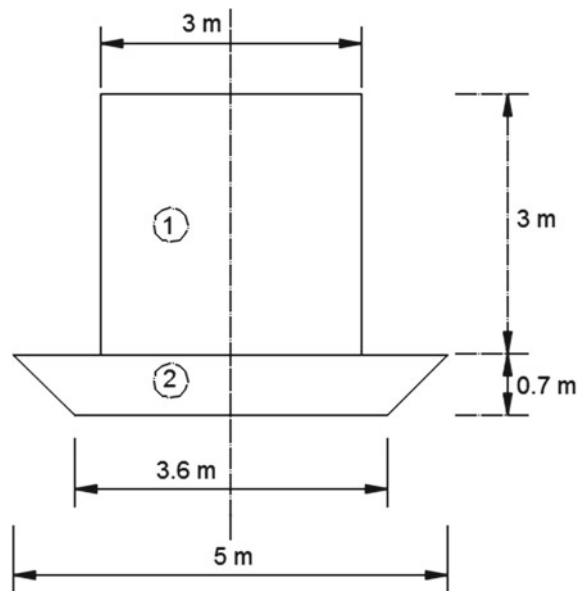
Table 2 Test results

Parameters	Maximum	Minimum	Average	
Total deformation (m)	2.69×10^{-2}	0	1.17×10^{-2}	
Equivalent elastic strain	7.84×10^{-4}	3.76×10^{-8}	1.02×10^{-4}	
Equivalent stress (MPa)	1.31×10^{2}	0.24×10^{-2}	1.56	
Directional deformation (m)	-4.59×10^{-3}	-2.06×10^{-2}	-7.31×10^{-3}	

Table 3 Bed soil parameters of the proposed site [6]

Sample Location	Bulk Unit Weight, γ(gm/cc)	Unit Cohesion, c_u (N/cm^2)	Angle of internal friction, ϕ_u
Barguriagaon	1.79	2.60	27°
Butalikhowa	1.87	2.20	36°
Golaghat	1.54	1.05	30°
Dachmuagaon	1.53	2.00	28°
Average	1.68	1.96	30.25°

8 Analysis Results

The output from **Ansys 19.1®** is summarised in Table 2.

9 Design of Tension Pile and Anchorage Cables

9.1 Soil Properties

Soil properties used for the design of the pile are shown in Table 3.

9.2 Calculation Pressure Due to River Current

Assuming velocity of the river current (v) $= \frac{4m}{sec}$,
    For peak velocity $v_p = 2.5 \times v = 2.5 \times = \frac{10m}{sec}$,

$$p = \rho v_p^2 = 100 kPa.$$
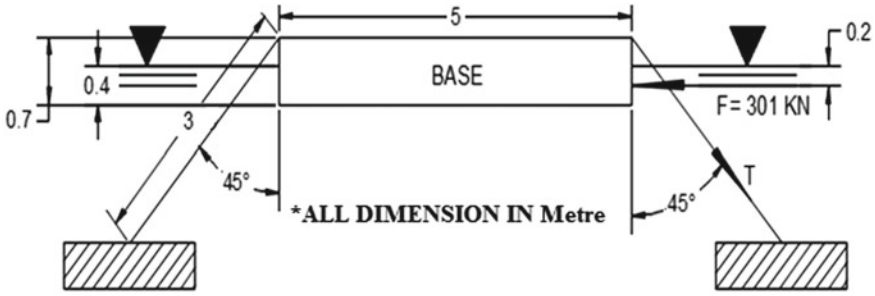
Fig. 13 Anchorage cables connected to the pile cap

9.3 Design of the Anchorage Cable

The projected area of the base $= 3.01 \text{m}^2$

The total force on the base of the structure $= 301 \text{kN}$.

20 mm diameter cables on the upstream side are provided as anchorage.

Downstream side cables are provided for preventing the overturning of the structure due to river current (Fig. 13).

Provided 12 mm diameter cables in the downstream side as anchorage.

9.4 Design of Anchorage Pile

Maximum tension in the cable as per the analysis result is $Q = 425.678 \text{kN}$

Now factored uplift force on the pile $Q_u = 1.5 \times Q = 1.5 \times 425.678 = 638.517 \text{kN}$

For c-Ø soil, the ultimate bearing capacity of bored and cast-in-situ piles is calculated as;

Ultimate skin friction,

$$Q_s = A_s[k\sigma_v \tan\delta + \alpha c_u].$$

For Tension piles, $Q_P = 0$.

Since the piles are made of concrete and $\emptyset = 30.25°$.

$\delta = 22.69°$, $k = 1.179$.

From the graph given by Tomlinson [7], α is calculated from L_f/B ratio and c_u and presented in Table 4 and the number of piles required is shown in Fig. 14.

10 Mooring and Anchorage of the Base

Figure 15 shows the positions of piles P_1, $-P_9$ and anchorage points $A_1 - A_{10}$

Table 4 No. of piles required for different length of the piles

Diameter of the pile (D) in m	Length of the pile (L_f) in m	Ultimate load carrying capacity of the pile in kN (Q_u)	No. of piles required
0.5	4	206.194	4
0.5	5	283.654	3
0.5	6	371.479	2
0.5	7	469.669	2
0.5	8	578.223	2
0.5	9	697.143	1
0.5	9.5	760.489	1
0.5	10	826.426	1
0.5	10.5	894.955	1
0.5	11	966.075	1
0.5	11.5	1039.786	1
0.5	12	1116.088	1

Fig. 14 Variation of total ultimate load-carrying capacity with the length of the piles
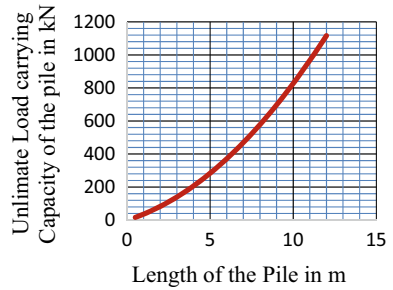
11 Conclusion

This work designed a floating house for flood plans of Assam. If implemented on a mass scale, this typology could result in a safe and affordable house for floodplains. The use of other cost-effective material and technology can be further explored for reducing the cost and for finding the solution to the long-standing problem of Assam.

Fig. 15 Mooring arrangement of the house
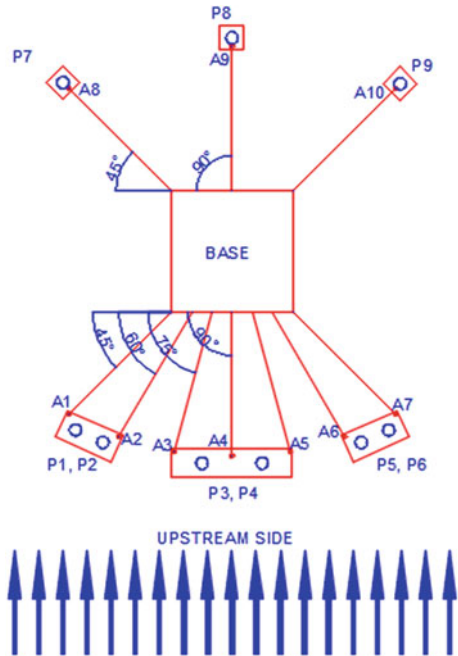
References

1. Government of Assam webpage. http://assam.gov.in/web/department-of-water-resource/flood-and-erosion-problem. Accessed 12 Mar 2021
2. ResearchGate webpage. https://www.researchgate.net/figure/Observed-flood-inundation-map-in-Assam-State-of-India-based-on-satellite-data-analysis_fig1_259871331. Accessed 14 Mar 2021
3. NDTV India Homepage. www.ndtv.com/india-news/12-lakh-affected-in-assam-floods-number-of-deaths-nears-60-1725250. Accessed 14 Mar 2021
4. Iowa State University Homepage. https://mesonet.agron.iastate.edu/sites/windrose.phtml. Accessed 14 Mar 2021
5. Arora and Bindra (1997) A text book of Building Construction (Planning Techniques and Methods of Construction), 4th edn. Dhanpat Rai Publications, New Delhi, India
6. Kotoky P, Dutta M, Goswami R, Borah CG (2011) Geotechnical properties of the bank sediments along the Dhansiri River channel. Assam J Geol Soc India 78(2):175–183
7. Saran S (2018) Analysis and design of substructure-limit state design, 2nd edn. Oxford & IBH, New Delhi, India

A Review of Impacts of Climate Change on Slope Stability

Jun Lim Wong, Min Lee Lee [ID], Fang Yenn Teo [ID], and Kian Wah Liew [ID]

1 Introduction

In recent years, climate change has attracted the interest of many researchers around the world. Global warming is one of the phenomena associated with climate change. The assessment of the impact of climate change on the environment is essential for policy makers to make the best decisions for preserving our natural environment. Climate change is unequivocal but few have studied the impact that climate change has on the stability of the slope. Engineered and natural slopes are threatened by climate variability as it leads to changes in the occurrence of extreme events, which is one of the primary causes of geo-hydrological hazards such as landslides. Therefore, it is extremely important to evaluate the impact of climate change on slopes to help decision-makers and engineers in mitigating the damages that could be incurred from the hazards.

A landslide can be defined as the movement of debris, rock, or earth down a slope, caused by gravity. Both engineered and natural slopes are affected by this mass-wasting process. Landslides include various types of movements such as falling, sliding, spreading, flowing, or toppling. In fact, a combination of these movements can be found in many landslides either simultaneously or during their lifetime. Landslides can occur anywhere and play a major role in the evolution of the landscape.

The stability of a slope can be affected by various phenomena such as temperature, earthquake, rainfall, anthropogenic causes, etc. These phenomena are affected by climate change, particularly temperature and precipitation. However, there are still very limited studies on quantifying the impact that climate change has on slope stability. This paper aims to provide a detailed review of the impacts of climate change on slope stability through currently available literature. Firstly, the potential

J. L. Wong · M. L. Lee (✉) · F. Y. Teo · K. W. Liew
Faculty of Science and Engineering, University of Nottingham Malaysia, 43500 Selangor, Malaysia
e-mail: minlee.lee@nottingham.edu.my

© The Author(s), under exclusive license to Springer Nature Singapore Pte Ltd. 2022
S. Kolathayar et al. (eds.), *Climate Change and Water Security*, Lecture Notes in Civil Engineering 178, https://doi.org/10.1007/978-981-16-5501-2_13

factors that may affect the phenomenon of climate change are reviewed, followed by quantifying the impacts of climate change on rainfall and temperature which constitute two important factors in inducing slope instability. Subsequently, various prediction models for temporal rainfall and temperature variations are reviewed. Lastly, the impacts of rainfall infiltration and temperature variation amidst the climate change phenomenon on the stability of slope are evaluated.

2   Factors Affecting Climate Change

Maracchi and Baldi (2006) found a rise of approximately 1 °C in the mean global air temperature since 1860. They concluded that the twentieth century is the warmest in the last 10 centuries, with the warmest decade of the century identified as the 1990s. During the period of 1990–2100, a rise of 1.5–6.0 °C in the air temperature was estimated [1]. Global Climate Models have projected an air temperature increase of 1.5 °C in the next century but this prediction is plagued by the uncertainties which are internal to the models.

Historical climate change was found to be caused by natural factors, such as the variations in the orbital parameters of the earth (Milankovitch Theory), or due to the natural alterations in the composition of the atmosphere, conductive to either cooling or warming of the atmosphere (Maracchi and Baldi 2006). Warming of the atmosphere can be caused by greenhouse gases whilst the release of natural aerosols due to volcanic activities can have long-term warming or short-term cooling effects. However, it is very challenging to predict the impacts that these natural factors have. The complexity of the climatic system, which is different from other natural systems result in large uncertainties because tiny changes can have significant effects due to the complex feedback mechanisms and non-linear variability of the climatic system. For instance, it is clear that aerosols and greenhouse gases will cause climate change but the quantification of the effects they have on the climate is difficult.

Ding et al. [30] carried out a study in China on the causes of regional climate change using climate models with the consideration of various forcings. They suggested that the warming of the past 50 years could be caused by the increase of atmospheric concentration of greenhouse gases, while temperature change of the first half of the twentieth century could be caused by solar activity, volcanic eruptions, and sea surface temperature change. Their review suggested that a significant decline in sunshine duration and solar radiation at the surface in eastern China had been attributed to the increased emission of pollutants. Anthropogenic climate change will likely lead to a weaker winter monsoon and a stronger summer monsoon in eastern Asia according to their studies. Ding et al. [30] assessed the causes of climate change considering both radiative and anthropogenic forcings. Radiative forcing can be described as the difference between the sunlight that is absorbed by the earth and the energy that is radiated back to space. On the other hand, anthropogenic forcing can be described as the consequences of human activities. Major methods of detection for attributing reasons for climate change are multiple climate

models and numerical-statistic methods based on observed data [11, 55]. Results show that almost all the models with the various human emission scenarios simulate the warming trend in China for the twentieth century to a reasonable degree, especially the obvious warming trend over the past 50 years. This suggests that anthropogenic forcings play a huge part in climate change. This conclusion agrees with that of [46]. A different study by Zhou and Yu (2006) which includes all radiative forcings by 19 global climate system models, two of which are from China, attempted to simulate the annual mean temperature anomaly changes in China for the twentieth century. The radiative forcings considered included changes in solar radiation, volcanic activity, greenhouse gases, sulfate aerosols, black carbon, ozone, land use/vegetation changes, and others [12, 13]. The correlation coefficient obtained from this study was better than when only human emissions were used, which implied that solar and volcanic activity, as well as the interactions between air and sea, could play a part in the temperature change in China during the first half of twentieth century. Based on the findings from [120, 123], it can be summarized that the observed and simulated evidence of climate change in China of the twentieth century have been attributed to anthropogenic activity.

Baum et al. [119] provided an assessment of the evidence of anthropogenic causes on climate change. A decline in temperature was found in the global temperature record between 1940 and 1975 despite the fact that there was a rise in greenhouse gas concentrations. Nonetheless, it is undeniable that the general increase in temperature is primarily caused by greenhouse gases. The effect of sulfur emissions on global temperature was highlighted in the study by Baum et al. [9]. Sulfate aerosols produced by sulfur emissions can have a cooling effect on the surface of the earth since it reflects additional solar radiation back into space. It was found that thin clouds have a warming effect while thick clouds tend to cool the surface of the earth by reflecting solar radiation back to space (Grenci and Nese 2006). Global warming increases the rates of evaporation resulting in more thin and thick clouds. Hence, clouds add to the uncertainty in the projection of temperature changes. Previous studies have presented evidence to prove that the climate is changing and anthropogenic causes play a huge part in climate change. These fundamental findings cannot be disproved even though there is large uncertainty about climate change.

Matteis [14] provided an overview of the anthropogenic causes of climate change. It is widely agreed among climate scientists that human activity is the primary driving force of global warming. The statement from the Intergovernmental Panel on Climate Change (IPCC) stating that "human influence has been the dominant cause of the observed warming since the mid-twentieth century" supports this consensus among scientists [21, 22]. The results from Matteis's [14] study showed that the negative impacts that the growing luxurious lifestyle and demographic pressure have on greenhouse forcings are far more significant in comparison with the effort to reduce greenhouse forcings through technological progress. As a matter of fact, it was found in the research on the driving forces of climate change that models that only consider the natural causes of climate change were not able to simulate the historical global warming while models that include human activities that produce greenhouse gases

are able to better simulate the historical warming. Hence, it can be concluded that human activity is one of the primary driving forces of climate change.

The causes of global and regional changes of climate were investigated by Loginov 10. The highest positive temperature anomalies were observed during periods of low aerosol pollution: 1883–1902, 1933–1942, and 1993–2012. On the other hand, the results showed that the largest negative temperature anomalies coincide with the middle of the period of the largest aerosol pollution: 1973–1982. During the period between 1983 and 2002, the highest positive temperature anomalies in January–February corresponded with a significant increase in the concentration of greenhouse gases. The warmest 5 year-long summer periods were also found to coincide with a period of low aerosol pollution. In recent years, extremely warm 5 year-long summer and winter epochs were found to correspond to the radiation effects of greenhouse gases and aerosols.

Stern and Kaufmann (2013) examined the anthropogenic and natural causes of climate change and found that both natural and anthropogenic factors play a part in temperature change which led to changes in the concentration of greenhouse gases. It was evident that greenhouse gases and volcanic activity had significant effects on temperature change while black carbon was found to have no effect on temperature change. The impact of anthropogenic sulfate aerosols was over-estimated, and changes in solar irradiance did not have a significant effect on temperature change (Boucher and Pham 2002). The results reported in this study also showed that properly specified tests of Ganger causality validate the consensus that human activity is partially responsible for the observed rise in global temperature and that this rise in temperature also has an effect on the global carbon cycle. Table 1 summarizes the factors affecting climate change as reported by numerous researchers in different parts of the world.

Table 1 Summary of factors affecting climate change

Factors	Study Area	Reference
Natural factors such as variations in orbital parameters of the earth, natural alterations in the composition of atmosphere, and release of aerosols due to volcanic activities	Europe	Maracchi and Baldi (2006)
Anthropogenic factors such as greenhouse gases	Europe	Maracchi and Baldi (2006)
Anthropogenic factors such as greenhouse gases	China	Ding et al. [30]
Natural factors including solar activity, volcanic eruptions, and sea surface temperature change	China	Ding et al. [30]
Greenhouse gases and sulfur emissions	Global	Baum et al. (2011)
Human activity and natural factors	Global	Matteis (2019)
Aerosol pollution and greenhouse gases	Global	V. F. Loginov (2014)
Greenhouse gases, volcanic activity, black carbon, sulfate aerosols and changes in solar irradiance	Global	Stern and Kaufmann (2013)

3 Impacts of Climate Change on Rainfall and Temperature

Loo et al. (2015) investigated the effect of climate change on seasonal monsoon in Asia and its impacts on the variability of monsoon rainfall in Southeast Asia. A decreasing trend of temperature was observed during the period of 1945–1973 (Brohan et al. 2006). Since then, the temperature has been increasing as a result of climate change. The chances of rainfall are reduced when there is a rise in temperature because rainfall occurs when the temperature is low. An increase in temperature results in lower rainfall frequency but increased rainfall intensity. A rise in temperature was predicted in the late twenty-first and twenty-second centuries by Schewe and Levermann [22]. Ashfaq et al. [6] suggested that this caused the delay of the monsoon onset in the future. Increases in the intensity of rainfall were observed in Malaysia and other Southeast Asian countries, which is a key factor in the occurrence of landslides and flooding events [12].

Changes to precipitation and temperature of Alberta for historical and future periods were examined by Jiang et al. (2015). Climate data of Alberta was used to examine historical trends as well as the magnitude of these trends through the Mann–Kendall test and Sen's slope. The effects that climate change may potentially have on the temperature and precipitation of Alberta were evaluated using General Circulation Models (GCMs). It was found from the results that Alberta became warmer and drier during the period of 1900–2011, particularly the southern and central Alberta. General Circulation Models projected a change from –25 to 36% in the seasonal precipitation of Alberta as well as an increase in temperature between 2020 and 2080. The peak of the increase, which is 6.8 °C was found in December, January, and February. Increased precipitations in January, February, March, April, May, and December were projected by the GCMs. The projection results indicated a constant increase in temperature for all seasons. These projections agreed to the historical trends of temperature and precipitation.

Sharma and Goyal [93] examined the changes in temperature, precipitation, and climate extremes in the Teesta River basin in Eastern Himalayas between 1951 and 2100. Their study adopted four General Circulation Models (GCMs) and two Representative Concentration Pathways (RCP4.5 and RCP8.5). Projected and observed climates both showed substantial changes in temperature, precipitation, and climate extreme patterns. Their results indicated increases in both temperature and precipitation. F1, F2, and F3 were used to represent three periods of the projected period: F1 (2011–2040), F2 (2041–2070), and F3 (2070–2100). There was an increase of 225 mm, 283 mm, and 385 mm in the mean annual precipitation (MAP) of F1, F2, and F3, respectively, under the RCP4.5 scenario. On the other hand, the MAP of F1, F2, and F3 increased by 160 mm, 418 mm, and 751 mm, respectively, under the RCP8.5 scenario. It was also found that the mean daily maximum temperature increased by 0.46 °C, 0.90 °C, 1.13 °C for F1, F2, and F3, respectively, under RCP4.5. An increase of 0.54 °C, 1.18 °C, and 1.92 °C was found in the mean daily maximum temperature for F1, F2, and F3, respectively, under RCP8.5. It is likely that there will be increased precipitation in both non-monsoon and monsoon seasons. Nonetheless,

a lot of uncertainties surround these projections. The results in this study is similar to the results of existing studies in and around the same study area.

Rana et al. (2014) used Distribution-based Scaling of Global Climate Model projections to examine the effect of climate change on rainfall in Mumbai. The rainfall statistics for three different periods were used in this study: near (2010–2040), intermediate (2041–2070), and distant future (2071–2099). An increased total accumulated annual rainfall was found in the results. An average increase of 140 mm was found for the near future projections. Meanwhile, projections for the intermediate future showed an increase of 300 mm. Lastly, an increase of 420 mm was projected for the distant future period. Numerous studies revealed that the global warming caused by greenhouse gases will likely increase the intensity of monsoon rainfall across a large region including South Asia ([58]; May, 2002, 2004, 2011; [75]). A small average increase of approximately 5% compared to 1990 in the summer precipitation of 2090 was projected in the study of IPCC (2007) using the ensemble mean of General Circulation Model projections. Nonetheless, it should be noted that this small change in the average is a result of the largely negative and positive changes in each projection. Rana et al. (2014) concluded their study by recommending the use of multiple projections because a single projection is not enough to inform an efficient adaptation strategies.

Abdulla [6] attempted to project the precipitation and temperature in Jordan under twenty-first-century climate change. The future and business as usual (BAU) climate scenarios were simulated using maximum temperature, minimum temperature, mean temperature, and precipitation time series at selected eight climatic stations. Trend analysis of the precipitation time series from the majority of the stations revealed decreasing trends since the 1960s. Increasing trends were observed for temperature with the increase in minimum temperature more than that of the maximum temperature. An increase in temperature from about + 2.5 °C to + 5 °C by the end of the century was found from the recent projections of global climate changes following a rise in the concentrations of greenhouse gases. Existing studies of climate change in Jordan revealed that the rate of increase in minimum temperature was almost double compared to the rate of increase in maximum temperature. Results showed that changes in precipitation and the rate of warming varied across different regions on earth. General Circulation Model is adopted with a statistical downscaling model to project future rainfall and temperature for eight locations in Jordan between 2015 and 2099. The projections showed a reduction of approximately 10% to 37% in the annual precipitation.

Ibrahim et al. [47] used 5 regional climate models to simulate the changes in rainfall attributed to climate change in Burkina Faso. The projection of the change in annual rainfall was associated with large uncertainties, which is similar to other climate models. Nonetheless, certain features of the effect of climate change on rainfall were found to be robust in this study. The projections showed a decline of 3% in the number of low rainfall events (0.1–5 mm per day) and an average increase of 15% in the number of strong rainfall events (more than 50 mm per day). All projections indicated a one-week delay of the rainy season onset on average and it was widely agreed that the dry spells would lengthen by approximately 20%.

Gunawardhana et al. [6] attempted to quantify the changes in frequency and intensity of hourly extreme rainfall under climate change in Oman. The annual maximum hourly rainfall in Salalah, Oman for two future periods: 2040–2059 and 2080–2099 were projected using the temporal disaggregation and spatial downscaling technique. The projections indicated a decline of about 20% in the number of wet days while the annual total rainfall was expected to increase by about 44% and 17% in the periods of 2040–2059 and 2080–2099, respectively. The extreme rainfall distribution was likely to be affected by these changes, resulting in more intense and frequent extreme events in the future. In addition, the rainfall regime was expected to intensify more towards the end of the twenty-first century. Table 2 summarizes the quantitative changes in rainfall and temperature from the foregoing reported studies.

4 Prediction of Rainfall and Temperature Patterns

There are various phenomena that can affect the stability of slopes and trigger landslide events. These phenomena include a change in temperature, earthquake, snow melt, volcanic activity, precipitation, and other human activities. Climate change has consequences on these phenomena, particularly temperature and precipitation. Hence, the development of accurate and effective methods to project future temperature and rainfall scenarios under climate change is crucial. In general, there are two types of forecast models: data-driven models and physical models. Historical data combined with statistical and computational intelligence methods are employed in data-driven models for prediction, while physical models simulate the physical process according to the physical laws. Results from comparative studies suggest that data-driven models are capable of producing better predictions when compared to physical models [22].

There are various types of data-driven forecast models, the most commonly used models are multiple linear regression (MLR), clusterwise linear regression (CLR), support vector machines for regression (SVMreg), artificial neural networks (ANNs), and principal component analysis (PCA). Artificial Neural Networks (ANNs) are the most popular model employed for rainfall projection. They are powerful and flexible data modeling tools that can capture and represent complex relationships of the data being modeled. In recent years, researchers have begun to investigate the potential of Artificial Neural Networks (ANNs) as a tool for the simulation of the behavior of systems that are governed by nonlinear multivariate, generally unknown, interconnections within a noisy, less-controllable physical environment. A significant growth in the interest of this computational mechanism has occurred since Rumelhart et al. [13] developed a mathematically rigorous theoretical framework for neural networks. The use of ANNs in the engineering and science field has increased significantly ever since a mathematically rigorous theoretical framework for neural networks was developed by Rumelhart et al. (1986).

Khalili et al. [13] predicted the daily rainfall of Mashad's synoptic station in Iran using Artificial Neural Networks (ANNs). The study adopted ANNs because the

Table 2 Summary of quantitative changes in rainfall and temperature

No	Authors	Changes in rainfall	Changes in Temperature	Location of study
1	Vincent et al. [22]	–	Temperature increase in spring and winter ranging from 2 °C to 5 °C for minimum temperature and 1.5 °C to 4.5 °C for maximum temperature	Southern Canada
2	Jiang et al. (2015)	An increase of 20% in precipitation between 2011 and 2100	Temperature is increased by 4.4 °C between 2011 and 2100 based on projections	Alberta, Canada
3	Sharma and Goyal [93]	Maximum 1-day precipitation increase by 1.11 mm, 9.53 mm and 17.37 mm for 2010–2040, 2041–2070, and 2071–2100, respectively	Maximum and minimum daily temperatures are projected to increase by 0.54 °C and 1.18 °C (2011–2040), 1.92 °C and 0.5 °C (2041–2070) and 1.2 °C and 2 °C (2071–2100) respectively	Himalayan Region, India
4	Singh and Goyal (2016)	–	All projections indicated an increase in temperature ranging from 1.5–2.0 °C in Sikkim Himalayas	Sikkim, India
5	Abdulla (2020)	A reduction in annual precipitation ranging from 10 to 37%	An increase in temperature by 2.5 to 5 °C by the end of century	Jordan
6	Ibrahim et al. [47]	A decline of 3% in the number of low rainfall events and an increase of 15% in the number of strong rainfall events	Dry spells were expected to lengthen by 20%	Burkina Faso

(continued)

Table 2 (continued)

No	Authors	Changes in rainfall	Changes in Temperature	Location of study
7	Gunawardhana (2018)	A decline of about 20% in the number of wet days. Annual total rainfall was expected to increase by about 44% and 17% in the periods of 2040–2059 and 2080–2099, respectively	–	Oman

neural networks are capable of extracting system features intelligently, even when there is limited information about the system dynamics. The model was implemented using a three-layer feed-forward perceptron network with a back propagation algorithm. The mean absolute error, correlation coefficient, and root mean square error obtained from the performance statistical analysis for the proposed models showed that the approach used to forecast daily rainfall in this study was effective. Abbot and Marohasy (2014) adopted the Artificial Neural Networks (ANNs) model to forecast rainfall in Queensland, Australia. Three measures of forecast accuracy were used to compare the projections produced by ANNs and the forecasts obtained from the Predictive Ocean Atmosphere Model for Australia (POAMMA). POAMMA is a General Circulation Model (GCM) adopted currently to predict the seasonal rainfall in Australia. The comparison showed that ANNs outperformed the POAMMA by having lower Mean Absolute Error (MAE), Correlation Coefficients as well as Root Mean Square Errors (RMSE). It was found that ANN was a more skilled forecast compared to climatology given that the input selection for ANN was optimized.

Support Vector Machines (SVM) is a data-driven model based upon statistical learning theory (Vapnik 1998). Original data is mapped into a high-dimensional feature space with a nonlinear mapping function followed by the construction of an optimal hyperplane [87, 88]. Lin et al. [89] used the SVM to obtain a forecasting model for hourly rainfall in Taiwan. Input optimization step integrating multi-objective genetic algorithm (MOGA) was used with the SVM to determine the optimal input combination. This was followed by obtaining the spatial characteristics of the rainfall process by using the rainfall projection from the stations. It can be concluded from the results that the forecasting performance was significantly improved and the negative effects of increased forecast lead time were reduced through the use of this forecast model.

The Multiple Linear Regression (MLR) method is rarely used to project future rainfall. MLR is the extension of a simple linear regression model which predicts dependent variables by using at least two independent variables through the least-squares method. El-Shafie et al. [13] adopted Artificial Neural Network (ANN) model and Multiple Linear Regression (MLR) model in their study for rainfall prediction. The results produced by these two models were evaluated using statistical parameters

such as MAE (Mean Absolute Error), BIAS, CC (Correlation Coefficient), and RMSE (Root Mean Square Error). It was concluded that the ANN model produced better results in comparison with the MLR model. This was attributed to the inability of the MLR model to produce accurate predictions for a variable involving highly nonlinear physics due to the linear nature of the MLR model estimators. Dutta and Tahbilder (2014) implemented the MLR model for rainfall forecasting in their study. The results of their study indicated a 63% accuracy in the rainfall forecasts produced by the MLR model.

The Clusterwise Linear Regression (CLR) approach involves two types of techniques: regression and cluster analysis. The number of clusters as well as the regression coefficients for each cluster are estimated in the CLR method. Various algorithms have been developed in an attempt to solve the CLR problem. These algorithms are based on optimization technique [5, 13], data mining technique [76], and statistical technique [77, 80]. Bagirov et al. [19] adopted the CLR method for forecasting monthly rainfall in Victoria, Australia. Rainfall data from eight different weather stations between 1889 and 2014 was used along with five input meteorological variables for the prediction. Four measures of forecast accuracy were used in the comparison of the predicted and observed rainfall in order to evaluate the performance of the CLR approach. These measures of forecast accuracy include the mean absolute scaled error, the coefficient of efficiency, the mean absolute error, and the root mean squared error. The model used in this study was also compared with other methods such as the artificial neural networks, CLR using maximum likelihood framework by the expectation–maximization algorithm, support vector machines, and multiple linear regression. The comparison revealed that the CLR approach adopted in this study performed better than the other methods.

Poorani and Brindha [80] employed the Principal Component Analysis (PCA) approach in their study to predict rainfall in India. It was found from their results that the PCA has an edge over ANN in the analysis of climatic time series, especially in terms of the interpretability of the extracted signals. The proposed PCA method was recommended when there was vital inter-correlation between the predictors. The PCA model was capable of avoiding the inter-correlation and support to reduce the degrees of liberty by controlling the number of predictors.

Zainudin et al. [5] evaluated and compared the performances of several different data mining techniques for rainfall prediction in their paper. The techniques that were evaluated in their paper were Decision Tree, Neural Network, Random Forest, Support Vector Machine, and Naïve Bayes. The dataset between January 2010 and April 2014 used by these techniques for rainfall forecasting was obtained from the Malaysia Meteorological Department and Malaysia Drainage and Irrigation Department. The dataset consisted of several variables such as rainfall, relative humidity, temperature, river flow, and water level. Results of the study showed that Random Forest and Decision Tree were the best performing models due to their ability to forecast a higher portion of data with higher F-measure while trained on little data. It was also concluded that Neural Network can be an effective technique but a large amount of training data is required for Neural Network to predict little testing data.

Gupta and Ghose [73] carried out a comparative analysis of different rainfall prediction methods such as Neural Network, K-nearest Neighbor, Naïve Bayes, and Regression Tree (CART). Experimental results showed an accuracy of 82.1% for the predictions produced by Neural Networks, 80.7% for K-nearest Neighbor, 80.3% for Regression Tree (CART), and 78.9% for Naïve Bayes. It was concluded that Neural Networks produce the most accurate predictions among all the models. It was also found that Neural Networks produced the best predictions with 10 neurons in the hidden layer. Neural Networks can also manage continuous and noisy values better compared to Regression Trees. However, it can be tough and time consuming to decide the number of neurons and train the network repeatedly. On the other hand, it is easier to understand and implement Decision Trees and Naïve Bayes but it is costly and time consuming to prune the tree, which requires intensive calculations.

5 Impacts of Changing Rainfall Patterns on Slope Stability

There are various factors that can destabilize a slope, such as land and surface erosion, tensile cracking, seismicity, soil softening and fissuring, and soil desiccation. Nonetheless, landslides are usually attributed to dynamic processes, particularly significant long-term and seasonal changes in rainfall patterns. Landslide rates may be accelerated by the destabilizing factors mentioned earlier under extreme climatic conditions. Changes in rainfall patterns can have serious consequences on the near-surface groundwater field as well as soil moisture and strength. Deep-seated landslides are described as slope failures associated with the movement of the underlying bedrock and surficial mantle. These landslides can be impeded by the groundwater field directly [22]. Deep-seated landslides are usually sensitive to the extreme conditions of the hydraulic cycle. Hence, prolonged droughts can put a halt to deep-seated landslides through the increase of groundwater extraction which disrupts groundwater recharge [1]. On the other hand, shallow landslides are described as translational slope failures which are several meters thick, consisting of poorly consolidated soil mantle and underlying bedrock [1]. Climatic factors which include antecedent rainfall, extreme rainfall events, and rapid snowmelt have immense impacts on the magnitude and frequency of shallow landslides [1, 22]. These landslides are described by two different failure mechanisms, namely localized failures and diffused failures [5]. Under diffuse failure mechanisms, the soil is partially or fully undrained and has very weak structures. As pore water pressure rises, the effective stress approaches zero. On the contrary, the soil is drained under a localized failure mechanism which is associated with transient localized pore-water pressures due to specific geological settings and hydraulic boundary conditions [22].

Numerous studies have examined the relationship between landslides and rainfall variations but very little is known about the impacts of climate change on slope stability. Although certain relationships between climate change and slope stability have been ascertained, plenty of works are still needed to determine the magnitude and sign of this correlation. After reviewing literature on the relationship between

climate change and slope stability, it was found that existing studies only covered a small part of the world. Investigations are still needed for many countries, particularly South America, Africa, and Asia. Landslides are expected to occur more often attributed to the increased intensity and frequency of extreme rainfall events under global warming. It was stated in the IPCC special report that there is medium confidence that changes in temperature will affect bed rock stability and there is high confidence that variations in heavy rainfall will influence landslides in certain regions (Seneviratne et al[22]. According to Coe and Godt [22], the existing studies on the prediction of rainfall-induced landslides are associated with large uncertainty because it is very difficult to forecast short-term extreme storms. On the contrary, fewer uncertainties were found in existing studies that used annual or seasonal rainfall and air temperature to predict landslide activities. This is attributed to the fact that annual or seasonal rainfall and air temperature can be predicted more accurately.

Statistically adjusted high-resolution regional climate models were employed by Sangelantoni et al. (2018) to predict the variations of landslides frequency in the eastern Esino river basin, Central Italy. Their results of the comparison between historical and future periods show a general increase in the landslide-triggering rainfall events. An overall increase in landslide occurrence over the twenty-first century was projected. The findings from Sangelantoni et al. (2018) showed good agreements with the findings reported by numerous researchers, i.e. Jakob and Lambert [6], Melchiorre and Frattini [22], and Turkington et al. (2016).

Infiltration of rainwater into hillslope changes its water content, pore pressure as well as groundwater table. This affects the stability of slopes as it changes the total unit weight, effective stress, suction stress, and matric suction throughout the hillslope. Wayllace et al. (2019) presented a study of the hydrological behavior and its effect on slope stability of a seasonally active landslide on an embankment on Interstate-70 west of the Eisenhower Tunnel. Results obtained through numerical modeling showed that the difference between the minimum and peak water table levels in the site may vary by more than 100% depending on the seasonal hydrological conditions. During summer, the pore water pressures near the failure surface were positive, and changed to negative during winter. As a result, suction stresses, as well as the factor of safety, changed throughout the year. The extended Bishop's method of slices for variably saturated soil was performed and it was found that the factor of safety ranged from 1.02 to 1.05 during winter, early spring, and fall but dropped to 0.989 during the beginning of summer, indicating a possible failure.

Robinson et al. [19] attempted to quantify the influence of extreme precipitation events on slope stability. Climate models were used with a non-stationary approach to simulate the upper bound of future rainfall extremes. The coupled model intercomparison project phase 5 (CMIP5) was employed to predict future rainfall. The future and historical rainfall extremes of an area around Seattle were collected, followed by the integration of the rainfall patterns into a series of fully coupled 2D stress—unsaturated flow finite element simulations. Soil strength and soil suction were reduced significantly under intense rainfall as it accelerated the pore-water saturation of unsaturated soils. It was found from the results of this study that the pore pressures of earth retaining structures as well as engineered slopes may be escalated significantly

under increased rainfall intensity. As a result, slopes may be destabilized or active earth pressures behind the wall of retaining structures may be increased. The mean of future rainfall extremes did not have a significant impact on the stability of slopes according to the model employed in this study. Nonetheless, results from the model suggested that if the 95th percentile of the predicted rainfall extremes were taken into account, existing maintenance guidelines and infrastructure design should be reevaluated. It is vital that the aforementioned rainfall extremes are considered in order to make sure that the additional load due to increased rainfall intensity can be safely supported by our structures.

Ran et al. [21] examined the mechanisms of rainfall-induced shallow landslides through numerical modeling. An infinite slope stability model was integrated with Hydrology Model (InHM) to assess slope stability and simulate the hydrologic response. Various failure mechanisms with different characteristics were examined under a variety of rainfall scenarios. A novel mechanism of shallow landslides was reported from the results. This mechanism can be described as a significant vertical change in saturated hydrologic conductivity which causes the accumulation of infiltrated water, resulting in the increase in pore pressures in the unsaturated soil layer, and consequently causing landslides. Furthermore, results showed that rainfall characteristics have an immense impact on the failure types and characteristics. A relationship between rainfall depths and the failure types was discovered because the novel mechanism of shallow landslides occurred at small total rainfall depths. Additionally, it was found that rainfall patterns significantly influenced the failure time as landslides occurred earliest during intense rainfall under every mechanism.

Iverson [21] investigated the effect of rainfall infiltration on landslides. The responses of landslides to rainfall involved transient processes with varying intrinsic timescales. Results from a new model of these transient processes related slope failure and landslide motion to groundwater pressure head which was affected by rainfall. Advanced rainfall can lead to a sudden pressure head growth and slope failure, particularly for shallow soils with high diffusivities. In these situations, normalized time proceeded quickly after rainfall started and the pressure head response function R increased rapidly. On the contrary, slow landslides involved thick soil with a low hydraulic diffusivity. Unlike landslides that occur abruptly, normalized time proceeded slowly for slow landslides and the increase in pressure head function over a long period of time was nearly negligible even under constant heavy rainfall. In such cases, prolonged acceleration preceded any catastrophic movement and landslide occurred gradually.

6 Development of Desiccated Soil Cracks under Seasonal Climate

Climate change can directly influence the frequency and duration of extreme weather events. One of the most significant climate change phenomena is global warming,

which leads to an increased rate of evaporation and surface drying. Consequently, the duration and intensity of droughts may be increased. Additionally, an increase of approximately 7% in the water-holding capacity of air was found per 1 °C increase in temperature (Trenberth, 2011). As a result, the frequency of extreme rainfall events is increased. Changes in the locations of rainfall events were also found, which leads to wet areas becoming wetter and dry areas becoming drier. These changes in extreme rainfall events and droughts can have significant influences on the development of desiccated soil cracks. Therefore, it is crucial that the present study review the development of desiccated soil cracks under seasonal climate conditions (wet-dry cycles).

Stirling et al. [19] developed a pseudo-discrete continuum finite-difference model to examine the effect of soil properties such as hydraulic conductivity, soil–water retention, and elastic modulus on the desiccation process and consequent crack initiation as well as propagation pattern. The study also investigated the impact that projected higher drying rates and seasonal drying-wetting cycles have on the development of crack patterns to better understand progressive deterioration. It was found that as hydraulic gradient developed throughout the soil profile, tensile stress was generated by drying induced negative pore pressures. Consequently, cracking initiated as the tensile stress generated exceeded the tensile strength of the soil. The propagation of existing cracks occurred as the balance between material strength and stiffness increased under ongoing drying, and the development of elevated suctions and associated tensile stress resulted in strain localization. Their results also showed that desiccated crust that formed under prolonged drying usually has a depth of less than 10 mm and can be distinguished by its extremely low relative permeability and highly negative pore pressures. This characteristic helped to hydraulically isolate the wetter layer immediately beneath, slow down drying, and hence prevent infiltration. The increased run-off was expected during high rainfall intensity summer as a result. The crust formation modeled showed that by-pass flow to depth could be accelerated and the critical suction that were crucial for the stability of most geotechnical structures may dissipate as cracked in situ soil traps run-off. It was also found that drying rate affected both the timing of the initiation and propagation of significant cracking as well as the final cracking extent before crust formation. A greater degree of surface disintegration and more primary cracks were found in higher drying rate scenarios. Hence, the projected rise in temperature was expected to accelerate the deterioration process of desiccation cracking.

Zhang et al. [19] conducted a series of analyses to further understand the evolutionary characteristics of shallow slope stability caused by rainwater infiltration considering desiccation crack extension states. Cracks in shallow slopes influenced slope stability by increasing the soil infiltration capacity. It was found that increased soil infiltration capacity due to cracking combined with elevated rainfall intensity caused a slope to become unstable in the case of unsaturated infiltration. Water migration was influenced by the degree of soil cracking which further influenced the evolution of slope stability under ponding infiltration conditions. Slope water saturation state during rainfall infiltration was affected by rainfall conditions and crack development state which will influence the evolution characteristics of the factor of

safety at different depths as a result. Rainwater infiltrated through tension fractures, erosional slits, and desiccation cracks in the soil. Erosional slits developed due to rainwater erosion, as it cut the soil and led to the formation of slits inside the slope. These slits acted as a channel for rainwater infiltration, resulting in an uneven distribution of rainwater in soil. The degree of soil cracking for desiccation crack varied with soil type and its water content. It was observed from the results of physical experiments that the void ratio was reduced as water-tension generated a "compaction effect" on the soil. Crack initiation occurred in the soil when the tension exceeded soil bearing capacity. Once the desiccation cracks have developed, they will further propagate due to environmental factors such as evaporation and rainfall. Additionally, it was found that slope stability for unsaturated infiltration approached critical values at various depths as the soil infiltration capacity increased under more extensive crack development. In conclusion, the factor of safety for slope stability approached unity quicker as extensive cracks developed in the soil.

Huang et al. [21] used Pores and Crack image Analysis System (PCAS), a crack imaging processing software to study the development of surface cracks in expansive soils with different compaction degrees under wet-dry cycles. Expansive soils with different crack development degrees were also tested for their shear strength. Results showed that the degree of crack development increased progressively as the wet-dry cycle times increased, before approaching a steady state. The degree of cracking decreased as the compaction degree increased. It was also found that as the compaction degree increased, the cohesion of the specimen increased under the same amount of wet-dry cycles. Additionally, crack block parameters and crack network parameters were also found to be increasing as wet-dry cycles increase. The first wet-dry cycle typically has more effect on the cracking. Thus, soil cover should be provided as soon as possible during the filling of expansive soil embankment slope to reduce the effect that water content change has on the cracking of expansive soil. A good linear relationship between the cohesive force of expansive soil and the crack rate as well as fractal dimension was also discovered. The measured crack parameters can be used to determine the shear strength parameters of soil.

7 Conclusions

Based on the reviews of previous studies pertaining to the topic of climate change and slope stability, it was found that large uncertainties are still associated with the studies on climate change, particularly in quantifying the effects of climate change and predicting future climate variations. Results from a number of studies have shown that rainfall patterns are likely to change under climate change. Various techniques have been used to project future rainfall. These techniques can be classified into two categories: data-driven and physical models. Data-driven models include Artificial Neural Network (ANN), Support Vector Machines for regression (SVMreg), Clusterwise Linear Regression (CLR), Multiple Linear Regression (MLR), and Principal Component Analysis (PCA) while physical models include Global Circulation

Models (GCMs). Artificial Neural Network (ANN) has been widely used for rainfall prediction in existing studies with proven reliabilities.

Several studies reported that the frequency, intensity, and duration of extreme rainfall events are undergoing changing patterns in the twenty-first century amidst climate change. Studies have also found that climate change has led to an increase in temperature which will directly influence extreme weather events such as storms and droughts. Extreme weather events have been identified as one of the major triggering factors to landslides. However, there are still very limited studies reported explicitly on the impacts of climate change on slope stability, particularly in the tropical regions which receive intense monsoon rainfalls. Changes in extreme weather events under climate change have also resulted in the development of desiccated cracks in the soil. Studies have shown prolonged drying and intensified rainfall across various regions in which these phenomena would greatly affect the extent of cracks development in soil under repetitive wet-dry cycles. In conclusion, there is a pressing need to carry out an extensive study to quantify the changes in rainfall pattern under climate change, investigate how the extreme weather events affect the development of desiccated and rainfall infiltration characteristics in soil, and hence the stability of the soil slope.

References

1. Abbot, J. and Marohasy, J. (2014) 'Input selection and optimisation for monthly rainfall forecasting in queensland, australia, using artificial neural networks', Atmospheric Research. Elsevier B.V., 138, pp. 166–178. https://doi.org/10.1016/j.atmosres.2013.11.002.

2. Abdulla, F. (2020) '21st Century Climate Change Projections of Precipitation and Temperature in Jordan', Procedia Manufacturing. Elsevier B.V., 44(2019), pp. 197–204. https://doi.org/10.1016/j.promfg.2020.02.222.

3. Aftab S et al (2018) Rainfall prediction using data mining techniques: A systematic literature review. Int J Adv Comput Sci Appl 9(5):143–150. https://doi.org/10.14569/IJACSA.2018.090518

4. Ahmadi A et al (2014) Assessment of climate change impacts on rainfall using large scale climate variables and downscaling models-a case study. J Earth Syst Sci 123(7):1603–1618. https://doi.org/10.1007/s12040-014-0497-x

5. Alvioli M et al (2018) 'Implications of climate change on landslide hazard in Central Italy', Science of the Total Environment. The Authors 630:1528–1543. https://doi.org/10.1016/j.scitotenv.2018.02.315

6. Antonio S.Cafino, Rafael Cano, Carmen Sordo, J. M. G. (2009) 'Bayesian Networks for Probabilistic Weather Forecast', 700, pp. 1–5.

7. Asare-Nuamah, P. and Botchway, E. (2019) Understanding climate variability and change: analysis of temperature and rainfall across agroecological zones in Ghana, Heliyon. Elsevier, 5(10), p. e02654. https://doi.org/10.1016/j.heliyon.2019.e02654

8. Ashfaq M et al (2009) Suppression of south Asian summer monsoon precipitation in the 21st century. Geophys Res Lett 36(1):1–5. https://doi.org/10.1029/2008GL036500

9. Bagirov, A. M., Mahmood, A. and Barton, A. (2017) 'Prediction of monthly rainfall in Victoria, Australia: Clusterwise linear regression approach', Atmospheric Research. Elsevier B.V., 188, pp. 20–29. doi: https://doi.org/10.1016/j.atmosres.2017.01.003.

10. Bagirov, A. M., Ugon, J. and Mirzayeva, H. (2013) 'Nonsmooth nonconvex optimization approach to clusterwise linear regression problems', European Journal of Operational Research. Elsevier B.V., 229(1), pp. 132–142. doi: https://doi.org/10.1016/j.ejor.2013.02.059.

11. Baum SD, Haqq-Misra JD, Karmosky C (2012) Climate Change: Evidence of Human Causes and Arguments for Emissions Reduction. Sci Eng Ethics 18(2):393–410. https://doi.org/10.1007/s11948-011-9270-6

12. Billa L, Mansor S, Mahmud AR (2004) Spatial information technology in flood early warning systems: An overview of theory, application and latest developments in Malaysia. Disaster Prevention and Management: An International Journal 13(5):356–363. https://doi.org/10.1108/09653560410568471

13. Boucher O, Pham M (2002) History of sulfate aerosol radiative forcings. Geophys Res Lett 29(9):22–23. https://doi.org/10.1029/2001GL014048

14. Brohan P et al (2006) Uncertainty estimates in regional and global observed temperature changes: A new data set from 1850. Journal of Geophysical Research Atmospheres 111(12):1–21. https://doi.org/10.1029/2005JD006548

15. Buma J, Dehn M (1998) A method for predicting the impact of climate change on slope stability. Environ Geol 35(2–3):190–196. https://doi.org/10.1007/s002540050305

16. Cascini L et al (2010) Modeling of rainfall-induced shallow landslides of the flow-type. Journal of Geotechnical and Geoenvironmental Engineering 136(1):85–98. https://doi.org/10.1061/(ASCE)GT.1943-5606.0000182

17. Cascini L et al (2013) Modelling the post-failure stage of rainfall-induced landslides of the flow type. Can Geotech J 50(9):924–934. https://doi.org/10.1139/cgj-2012-0375

18. Chapman S et al (2017) 'The impact of urbanization and climate change on urban temperatures: a systematic review', Landscape Ecology. Springer, Netherlands 32(10):1921–1935. https://doi.org/10.1007/s10980-017-0561-4

19. Chaudhari, M. S. and Choudhari, N. K. (2017) 'Study of Various Rainfall Estimation & Prediction Techniques Using Data Mining', (7), pp. 137–139.

20. Chiu, Y. Y., Chen, H. E. and Yeh, K. C. (2019) 'Investigation of the influence of rainfall runoff on shallow landslides in unsaturated soil using a mathematical model', Water (Switzerland), 11(6). doi: https://doi.org/10.3390/w11061178.

21. Cifrodelli M et al (2015) The Influence of Climate Change on Heavy Rainfalls in Central Italy. Procedia Earth and Planetary Science 15:694–701. https://doi.org/10.1016/j.proeps.2015.08.097

22. Coe JA, Godt JW (2012) Review of approaches for assessing the impact of climate change on landslide hazards', Landslides and Engineered Slopes: Protecting Society through Improved Understanding - Proceedings of the 11th International and 2nd North American Symposium on Landslides and Engineered Slopes, 2012, (December 2017), pp. 371–377

23. Collobert R, Bengio S (2001) SVMTorch: Support Vector Machines for large-scale regression problems. J Mach Learn Res 1(2):143–160. https://doi.org/10.1162/15324430152733142

24. Cook, J. et al. (2016) 'Consensus on consensus: A synthesis of consensus estimates on human-caused global warming', Environmental Research Letters, 11(4). doi: https://doi.org/10.1088/1748-9326/11/4/048002.

25. Cramer S et al (2017) 'An extensive evaluation of seven machine learning methods for rainfall prediction in weather derivatives', Expert Systems with Applications. Elsevier Ltd 85:169–181. https://doi.org/10.1016/j.eswa.2017.05.029

26. Dash Y, Mishra SK, Panigrahi BK (2018) Rainfall prediction for the Kerala state of India using artificial intelligence approaches. Computers and Electrical Engineering. Elsevier 70(May):66–73. https://doi.org/10.1016/j.compeleceng.2018.06.004

27. DeSarbo WS, Cron WL (1988) A maximum likelihood methodology for clusterwise linear regression. J Classif 5(2):249–282. https://doi.org/10.1007/BF01897167

28. Dehn M et al (2000) Impact of climate change on slope stability using expanded downscaling. Eng Geol 55(3):193–204. https://doi.org/10.1016/S0013-7952(99)00123-4

29. Diel J, Vogel HJ, Schlüter S (2018) (2019) 'Impact of wetting and drying cycles on soil structure dynamics.' Geoderma 345:63–71. https://doi.org/10.1016/j.geoderma.2019.03.018

30. Ding Y et al (2007) Detection, causes and projection of climate change over China: An overview of recent progress. Adv Atmos Sci 24(6):954–971. https://doi.org/10.1007/s00376-007-0954-4

31. Diodato N, Bellocchi G (2018) Using historical precipitation patterns to forecast daily extremes of rainfall for the coming decades in naples (Italy). Geosciences (Switzerland) 8(8):1–11. https://doi.org/10.3390/geosciences8080293

32. Dixon, N. (no date) '(https://dspace.lboro.ac.uk/) by the author and is made available under the following Creative Commons Licence conditions . For the full text of this licence , please go to : Climate change and slope stability in the UK : Challenges and approaches'.

33. Dutta, P. S. and Tahbilder, H. (2014) 'Prediction of Rainfall Using Datamining Technique Over Assam', 5(2), pp. 85–90.

34. El-Shafie AH et al (2011) Artificial neural network technique for rainfall forecasting applied to Alexandria, Egypt. International Journal of Physical Sciences 6(6):1306–1316. https://doi.org/10.5897/IJPS11.143

35. Fustos I et al (2020) 'Rainfall-Induced Landslides forecast using local precipitation and global climate indexes', Natural Hazards. Springer, Netherlands 102(1):115–131. https://doi.org/10.1007/s11069-020-03913-0

36. Gaffney, S. and Smyth, P. (1999) '[doi 10.1145%2F312129.312198] Gaffney, Scott; Smyth, Padhraic -- [ACM Press the fifth ACM SIGKDD international conference - San Diego, California, United States (1999.08.15–1999.08.18)] Procee.pdf', pp. 63–72.

37. García-Escudero, L. A. et al. (2010) 'Robust clusterwise linear regression through trimming', Computational Statistics and Data Analysis. Elsevier B.V., 54(12), pp. 3057–3069. doi: https://doi.org/10.1016/j.csda.2009.07.002.

38. Gariano SL, Guzzetti F (2016) 'Landslides in a changing climate', Earth-Science Reviews. The Authors 162:227–252. https://doi.org/10.1016/j.earscirev.2016.08.011

39. Grenci, L. M. and Nese, J. M. (2006) A World of Weather: Fundamentals of Meteorology. Available at https://he.kendallhunt.com/product/world-weather-fundamentals-meteorology

40. Gunawardhana LN, Al-Rawas GA, Al-Hadhrami G (2018) 'Quantification of the changes in intensity and frequency of hourly extreme rainfall attributed climate change in Oman', Natural Hazards. Springer, Netherlands 92(3):1649–1664. https://doi.org/10.1007/s11069-018-3271-6

41. Huang JB et al (2012) 'Debates on the causes of global warming', Advances in Climate Change Research. Elsevier Masson SAS 3(1):38–44. https://doi.org/10.3724/sp.j.1248.2012.00038

42. Huang Z et al (2019) 'Surface Crack Development Rules and Shear Strength of Compacted Expansive Soil Due to Dry-Wet Cycles', Geotechnical and Geological Engineering. Springer International Publishing 37(4):2647–2657. https://doi.org/10.1007/s10706-018-00784-y

43. Huang C-C, Tsai C, Chen Y-H (2002) (2002) 'Base Stability of Circular Excavations in Soft Clay.' Journal of Geotechnical and Geoenvironmental Engineering 0241:836–848. https://doi.org/10.1061/(ASCE)1090-0241(2002)128

44. Huggel, C. et al. (2013) 'Physical impacts of climate change on landslide occurrence and related adaptation', Landslides, pp. 121–133. doi: https://doi.org/10.1017/cbo9780511740367.012.

45. Hung NQ et al (2009) An artificial neural network model for rainfall forecasting in Bangkok, Thailand. Hydrol Earth Syst Sci 13(8):1413–1425. https://doi.org/10.5194/hess-13-1413-2009

46. IPCC (2001) Climate Change 2001: The Scientific Basis (Online). http://www.ipcc.ch/ (Accessed: 20 June 2020)

47. Ibrahim B et al (2014) Changes in rainfall regime over Burkina Faso under the climate change conditions simulated by 5 regional climate models. Clim Dyn 42(5–6):1363–1381. https://doi.org/10.1007/s00382-013-1837-2

48. Inversion, O. (1998) 'Algorithmica On a Kernel-Based Method for Pattern Recognition ', New York, pp. 211–231.
49. Iverson RM (2000) Landslide triggering by rain infiltration. Water Resour Res 36(7):1897–1910. https://doi.org/10.1029/2000WR900090
50. Jakob, M. and Lambert, S. (2009) 'Climate change effects on landslides along the southwest coast of British Columbia', Geomorphology. Elsevier B.V., 107(3–4), pp. 275–284. doi: https://doi.org/10.1016/j.geomorph.2008.12.009.
51. Jiang R et al (2017) Historical and potential changes of precipitation and temperature of Alberta subjected to climate change impact: 1900–2100. Theoret Appl Climatol 127(3–4):725–739. https://doi.org/10.1007/s00704-015-1664-y
52. Joseph J, T K, R. (2013) Rainfall Prediction using Data Mining Techniques. International Journal of Computer Applications 83(8):11–15. https://doi.org/10.5120/14467-2750
53. K. Poorani, K. Brindha (2013) 'Data Mining Based on Principal Component Analysis for Rainfall Forecasting in India', International Journal of Advanced Research in Computer Science and Software Engineering, 3(9).
54. KIN C. LUK, J. E. B. A. A. S. (2001) '1-s2.0-S0895717700002727-main.pdf', 33.
55. Kashiwao T et al (2017) 'A neural network-based local rainfall prediction system using meteorological data on the Internet: A case study using data from the Japan Meteorological Agency', Applied Soft Computing Journal. Elsevier B.V., 56, pp. 317–330. https://doi.org/10.1016/j.asoc.2017.03.015
56. Khalili, N. et al. (2011) '"Daily Rainfall Forecasting for Mashhad Synoptic Station using Artificial Neural Networks"', 2011 International Conference on Environmental and Computer Science, 19(May 2014), pp. 118–123.
57. Khandelwal N, Davey R (2012) Climatic Assessment Of Rajasthan ' s Region For Drought With Concern Of Data Mining Techniques. International Journal of Engineering Research and Application 2(5):1695–1697
58. Lal M, Meehl GA, Arblaster JM (2000) Simulation of Indian summer monsoon rainfall and its intraseasonal variability in the NCAR climate system model. Reg Environ Change 1(3–4):163–179. https://doi.org/10.1007/s101130000017
59. Lee, J. et al. (2018) 'Application of artificial neural networks to rainfall forecasting in the Geum River Basin, Korea', Water (Switzerland), 10(10). doi: https://doi.org/10.3390/w10101448.
60. Lee, L. M., Gofar, N. and Rahardjo, H. (2009) 'A simple model for preliminary evaluation of rainfall-induced slope instability', Engineering Geology. Elsevier B.V., 108(3–4), pp. 272–285. doi: https://doi.org/10.1016/j.enggeo.2009.06.011.
61. Li JH, Zhang LM (2011) Study of desiccation crack initiation and development at ground surface. Eng Geol 123(4):347–358. https://doi.org/10.1016/j.enggeo.2011.09.015
62. Lima CHR, Kwon HH, Kim YT (2018) A local-regional scaling-invariant Bayesian GEV model for estimating rainfall IDF curves in a future climate. Journal of Hydrology. Elsevier 566(September):73–88. https://doi.org/10.1016/j.jhydrol.2018.08.075
63. Lima, C. H. R., Kwon, H. H. and Kim, J. Y. (2016) 'A Bayesian beta distribution model for estimating rainfall IDF curves in a changing climate', Journal of Hydrology. Elsevier B.V., 540, pp. 744–756. doi: https://doi.org/10.1016/j.jhydrol.2016.06.062.
64. Lin, G. F. and Jhong, B. C. (2015) 'A real-time forecasting model for the spatial distribution of typhoon rainfall', Journal of Hydrology. Elsevier B.V., 521, pp. 302–313. doi: https://doi.org/10.1016/j.jhydrol.2014.12.009.
65. Lin, G. F., Jhong, B. C. and Chang, C. C. (2013) 'Development of an effective data-driven model for hourly typhoon rainfall forecasting', Journal of Hydrology. Elsevier B.V., 495, pp. 52–63. doi: https://doi.org/10.1016/j.jhydrol.2013.04.050.
66. Loginov VF (2014) Global and regional changes of climate: Causes, consequences and adaptation of the economic activities. Geogr Nat Resour 35(1):7–17. https://doi.org/10.1134/S1875372814010028
67. Loo YY, Billa L, Singh A (2015) Effect of climate change on seasonal monsoon in Asia and its impact on the variability of monsoon rainfall in Southeast Asia. Geoscience Frontiers. Elsevier Ltd 6(6):817–823. https://doi.org/10.1016/j.gsf.2014.02.009

68. Lu N et al (2012) Analysis of rainfall-induced slope instability using a field of local factor of safety. Water Resour Res 48(9):1–14. https://doi.org/10.1029/2012WR011830

69. Luo, Y., Y. Ding, Z. Zhao, X. Gao, Y. Xu, and Z. Xie. (2005) 'Projection of the future anthropogenic climate change in China'. Assessment of Climate and Environment Changes in China (1): Climate and Environment Changes in China and their Projection, Qin et al. Eds., China Science Press, p507–555. (in Chinese)

70. Maracchi G, Baldi M (2006) Climate change: Causes and medium range perspectives. Vet Res Commun 30(SUPPL. 1):69–74. https://doi.org/10.1007/s11259-006-0015-y

71. Matteis A (2019) 'Decomposing the anthropogenic causes of climate change', Environment, Development and Sustainability. Springer, Netherlands 21(1):165–179. https://doi.org/10.1007/s10668-017-0028-4

72. May W (2004) Simulation of the variability and extremes of daily rainfall during the Indian summer monsoon for present and future times in a global time-slice experiment. Clim Dyn 22(2–3):183–204. https://doi.org/10.1007/s00382-003-0373-x

73. May W (2011) The sensitivity of the Indian summer monsoon to a global warming of 2°C with respect to pre-industrial times. Clim Dyn 37(9–10):1843–1868. https://doi.org/10.1007/s00382-010-0942-8

74. May, W. (2002) 'Simulated changes of the Indian summer monsoon under enhanced greenhouse gas conditions in a global time-slice experiment', Geophysical Research Letters, 29(7), pp. 22–1–22–4. doi: https://doi.org/10.1029/2001GL013808.

75. Meehl GA, Arblaster JM (2003) Mechanisms for projected future changes in south Asian monsoon precipitation. Clim Dyn 21(7–8):659–675. https://doi.org/10.1007/s00382-003-0343-3

76. Melchiorre C, Frattini P (2012) Modelling probability of rainfall-induced shallow landslides in a changing climate, Otta, Central Norway. Clim Change 113(2):413–436. https://doi.org/10.1007/s10584-011-0325-0

77. Mirhosseini, G., Srivastava, P. and Stefanova, L. (2013) 'The impact of climate change on rainfall Intensity-Duration-Frequency (IDF) curves in Alabama', Regional Environmental Change, 13(SUPPL.1), pp. 25–33. doi: https://doi.org/10.1007/s10113-012-0375-5.

78. Mislan et al. (2015) 'Rainfall Monthly Prediction Based on Artificial Neural Network: A Case Study in Tenggarong Station, East Kalimantan - Indonesia', Procedia Computer Science. Elsevier Masson SAS, 59(Iccsci), pp. 142–151. doi: https://doi.org/10.1016/j.procs.2015.07.528.

79. Nayak DR, Mahapatra, Amitav\Mishra, P. (2013) A Survey on Rainfall Prediction using Artificial Neural Network. International Journal of Computer Applications 72(16):32–40. https://doi.org/10.5120/12580-9217

80. Poorani K, Brindha K (2013) Data Mining Based on Principal Component Analysis for Rainfall Forecasting in India. International Journal of Advanced Research in Computer Sciences and Software Engineering 3(9):1254–1256

81. Rajeevan M et al (2007) New statistical models for long-range forecasting of southwest monsoon rainfall over India. Clim Dyn 28(7–8):813–828. https://doi.org/10.1007/s00382-006-0197-6

82. Ran Q et al (2018) A modelling study of rainfall-induced shallow landslide mechanisms under different rainfall characteristics. Journal of Hydrology. Elsevier 563(May):790–801. https://doi.org/10.1016/j.jhydrol.2018.06.040

83. Ran, Q. et al. (2018b) 'A modelling study of rainfall-induced shallow landslide mechanisms under different rainfall characteristics', Journal of Hydrology. Elsevier B.V., 563, pp. 790–801. doi: https://doi.org/10.1016/j.jhydrol.2018.06.040.

84. Rana, A. et al. (2014a) 'Impact of climate change on rainfall over Mumbai using Distribution-based Scaling of Global Climate Model projections', Journal of Hydrology: Regional Studies. Elsevier B.V., 1, pp. 107–128. doi: https://doi.org/10.1016/j.ejrh.2014.06.005.

85. Rana, A. et al. (2014b) 'Impact of climate change on rainfall over Mumbai using Distribution-based Scaling of Global Climate Model projections', Journal of Hydrology: Regional Studies. Elsevier B.V., 1(August), pp. 107–128. doi: https://doi.org/10.1016/j.ejrh.2014.06.005.

86. Robinson JD, Vahedifard F, Aghakouchak A (2017) Rainfall-triggered slope instabilities under a changing climate: Comparative study using historical and projected precipitation extremes. Can Geotech J 54(1):117–127. https://doi.org/10.1139/cgj-2015-0602

87. Rumelhart, D. E., Hinton, G. E. and Williams, R. J. (1986) 'Learning internal representations by error propagation. In: Rumelhart D E, McClelland J L et al. (eds.) Parallel Distributed Processing: Explorations in the Microstructure of Cognition.', MIT Press, Cambridge, MA, 1(V), pp. 318–362. Available at: https://apps.dtic.mil/docs/citations/ADA164453.

88. Rupa Kumar, K. et al. (2006) 'High-resolution climate change scenarios for India for the 21st century', Current Science, 90(3), pp. 334–345

89. Salimi, M. and Al-Ghamdi, S. G. (2020) 'Climate change impacts on critical urban infrastructure and urban resiliency strategies for the Middle East', Sustainable Cities and Society. Elsevier, 54(November 2019), p. 101948. doi: https://doi.org/10.1016/j.scs.2019.101948

90. Sangelantoni, L., Gioia, E. and Marincioni, F. (2018) Impact of climate change on landslides frequency: the Esino river basin case study (Central Italy), Natural Hazards. Springer Netherlands. https://doi.org/10.1007/s11069-018-3328-6.

91. Schewe, J. and Levermann, A. (2012) 'A statistically predictive model for future monsoon failure in India', Environmental Research Letters, 7(4). https://doi.org/10.1088/1748-9326/7/4/044023.

92. Shan W et al (2015) The impact of climate change on landslides in southeastern of high-latitude permafrost regions of China. Front Earth Sci 3(February):1–11. https://doi.org/10.3389/feart.2015.00007

93. Sharma, A. and Goyal, M. K. (2020) 'Assessment of the changes in precipitation and temperature in Teesta River basin in Indian Himalayan Region under climate change', Atmospheric Research. Elsevier, 231(August 2019), p. 104670. doi: https://doi.org/10.1016/j.atmosres.2019.104670

94. Shrivastava G et al (2012) Application of Artificial Neural Networks in Weather Forecasting: A Comprehensive Literature Review. International Journal of Computer Applications 51(18):17–29. https://doi.org/10.5120/8142-1867

95. Sidle, R.C. (2007) 'Using weather and climate information for landslide prevention and mitigation', Climate and land degradation, p285–307.

96. Singhrattna N et al (2005) Seasonal forecasting of Thailand summer monsoon rainfall. Int J Climatol 25(5):649–664. https://doi.org/10.1002/joc.1144

97. Snapshot, C. S. (2016) 'TEACR Engineering Assessment', (September), pp. 1–77.

98. Sohn KT et al (2005) Statistical prediction of heavy rain in South Korea. Adv Atmos Sci 22(5):703–710. https://doi.org/10.1007/BF02918713

99. Solomon, M. (2013) 'The structure of scientific revolutions (Thomas S. Kuhn, 1970, 2nd ed. Chicago, London: University of Chicago Press Ltd. 210 pages)', Philosophical Papers and Review, 4(4), pp. 41–48. doi: https://doi.org/10.5897/ppr2013.0102.

100. Späth H (1979) Algorithm 39 Clusterwise linear regression. Computing 22(4):367–373. https://doi.org/10.1007/BF02265317

101. Stern DI, Kaufmann RK (2014) Anthropogenic and natural causes of climate change. Clim Change 122(1–2):257–269. https://doi.org/10.1007/s10584-013-1007-x

102. Stirling RA, Glendinning S, Davie CT (2017) Modelling the deterioration of the near surface caused by drying induced cracking. Applied Clay Science. Elsevier 146(June):176–185. https://doi.org/10.1016/j.clay.2017.06.003

103. Stocker, T., Qin, D., Plattner, G. K., Tignor, M. Allen, S. K., Boschung, J., Nauels, A., Xia, Y., Bex, V. and Midgley, P. M. (2014) Climate Change 2013: The physical science basis (Online). Available at: http://www.ipcc.ch/

104. Tang, C. S. et al. (2011) 'Desiccation and cracking behaviour of clay layer from slurry state under wetting-drying cycles', Geoderma. Elsevier B.V., 166(1), pp. 111–118. doi: https://doi.org/10.1016/j.geoderma.2011.07.018.

105. Trafalis TB et al (2002) Data mining techniques for improved WSR-88D rainfall estimation. Comput Ind Eng 43(4):775–786. https://doi.org/10.1016/S0360-8352(02)00139-0

106. Turkington T et al (2016) Assessing debris flow activity in a changing climate. Climatic Change. Climatic Change 137(1–2):293–305. https://doi.org/10.1007/s10584-016-1657-6

107. Vamsidhar E et al (2010) Prediction of rainfall using backpropagation neural network model. International Journal on Computer Science and Engineering 2(4):1119–1121

108. Vapnik, V. (1998) Statistical Learning Theory. Available at: https://www.wiley.com/en-my/Statistical+Learning+Theory-p-9780471030034 (Accessed: 22 June 2020)

109. Vathsala H, Koolagudi SG (2015) 'Closed Item-Set Mining for Prediction of Indian Summer Monsoon Rainfall A Data Mining Model with Land and Ocean Variables as Predictors', Procedia Computer Science. Elsevier Masson SAS 54:271–280. https://doi.org/10.1016/j.procs.2015.06.032

110. Vathsala H, Koolagudi SG (2016) (2017) 'Prediction model for peninsular Indian summer monsoon rainfall using data mining and statistical approaches.' Computers and Geosciences. Elsevier 98:55–63. https://doi.org/10.1016/j.cageo.2016.10.003

111. Vaughan, P. R., Kovacevic, N. and Ridley, A. M. (2002) 'The influence of climate and climate change on the stability of embankment dam slopes.', Reservoirs in a Changing World, pp. 353–366. doi: https://doi.org/10.1680/riacw.31395.0028.

112. Vijayavenkataraman S, Iniyan S, Goic R (2012) 'A review of climate change, mitigation and adaptation', Renewable and Sustainable Energy Reviews. Elsevier Ltd 16(1):878–897. https://doi.org/10.1016/j.rser.2011.09.009

113. Vishal, S. and Sudesh, C. (2016) 'Monsoon Rain Fall Prediction of Haryana 2016 on the Basis of Historical Data', pp. 608–612.

114. Wang X, Shi G (2001) Numerical investigation on the climate effects of anthropogenic sulfate aerosols. Plateau Meteorology 20(3):258–263 (in Chinese)

115. Wayllace, A. et al. (2019) 'Hydrological behavior of an infiltration-induced landslide in Colorado, USA', Geofluids, 2019. doi: https://doi.org/10.1155/2019/1659303

116. Wei SC et al (2018) Potential impact of climate change and extreme events on slope land hazard - A case study of Xindian watershed in Taiwan. Nat Hazard 18(12):3283–3296. https://doi.org/10.5194/nhess-18-3283-2018

117. Xiang, Y. et al. (2018) 'A SVR–ANN combined model based on ensemble EMD for rainfall prediction', Applied Soft Computing Journal. Elsevier B.V., 73, pp. 874–883. doi: https://doi.org/10.1016/j.asoc.2018.09.018.

118. Yang Y et al (2007) A data mining approach for heavy rainfall forecasting based on satellite image sequence analysis. Comput Geosci 33(1):20–30. https://doi.org/10.1016/j.cageo.2006.05.010

119. Zaw, W. and Naing, T. (2008) 'Empirical Statistical Modeling of Rainfall Prediction over Myanmar', World Acad Sci Eng Technol, 2(10), pp. 565–568. Available at: http://citeseerx.ist.psu.edu/viewdoc/download?doi=10.1.1.193.4595&rep=rep1&type=pdf.

120. Zhang, J., Zhu, D. and Zhang, S. (2020) 'Shallow slope stability evolution during rainwater infiltration considering soil cracking state', Computers and Geotechnics. Elsevier, 117(July 2018), p. 103285. doi: https://doi.org/10.1016/j.compgeo.2019.103285

121. Zhao Z, Ding Y, Luo Y, Wang S (2005) Recent studies on attributions of climate change in China. Acta Meteor Sin 19:389–400

122. Zhao Z, S, Wang, Y. Xu, G. Ren, Y. Luo, and X. Gao. (2005) Attribution of the 20th century climate warming in China. Climatic and Environmental Research 10(4):808–817 (in Chinese)

123. Zhou T, Yu R (2006) 20th century surface air temperature over China and the globe simulated by coupled climate models. J Climate 19(22):5843–5858

124. Zhou T, Zhao Z (2006) Attribution of the climate warming in China for the 20th century. Adv Clim Chang Res 2(1):28–31 (in Chinese)

Traditional Knowledge to Read Hydro-Meteorological Hazards in Teesta Floodplain, Bangladesh

Md. Sanaul Haque Mondal

1 Introduction

Traditional knowledge (TK) on disaster is used by the hazard-prone communities as warning signs and to respond to disasters for their survival [1]. These warning signs are understood locally by people and provided a lead time for their preparation [2]. Currently, due to the excessive introduction of modern scientific knowledge, traditional knowledge is at risk to become extinct.

Traditional knowledge can be well understood by the observation and interpretation of ecological indicators, including the behavior of certain animals, fruit production of certain plants, yield of crops, temperature of a season, color of the sky, intensity and direction of winds, and the surrounding environment [3]. People living in the riverine floodplain have an intimate relation with the river and its biophysical environment. By reading river behavior and surrounding environment over a long period of time, local inhabitants perceived their risks and developed several strategies to predict and way to avoid hydro-meteorological disasters.

Studies on the disaster predictions using TK were carried out in recent years and documented numerous ecological symbols for disaster warnings [4, 5]. Efforts were also made to identify TK such as animal behaviors, weather status, and meteorological signs [6] and combined that knowledge with modern technology to forecast hydro-climatological disasters [7].

Literature on disaster-related TK is often limited in Bangladesh. Some notable studies looked at the local wisdom on disaster management practiced by the island *Char* (*Char* is a piece of land which is surrounded by the waters of a stream) communities [8], local peoples' knowledge on the flow characteristics and erosion processes

Md. S. H. Mondal (✉)
Tokyo Institute of Technology, Tokyo, Japan
e-mail: shmondal@ewubd.edu

East West University, Dhaka, Bangladesh

[9], traditional means forecasting used by the indigenous communities [10], and women awareness on local knowledge [11].

The draft version of the National Plan for Disaster Management (2016–2020) of Bangladesh has acknowledged the use of TK and practices in disaster risk assessment and implementation of development policies and programs [12]. However, the integration process at the local level is not visible. Existing disaster-related literature on TK is mostly confined to indigenous, ethnic, or isolated island communities. There is a scanty of documents regarding the TK for the people who are living in the riverine floodplain. Therefore, this research intends to document TK on hydro-meteorological hazards for the riverine areas. The objectives of this research are to document TK related to hydro-meteorological hazards developed and practiced by the riverine communities of the Teesta floodplain in Bangladesh.

2 Methods and Materials

2.1 Study Area

Data for this study were collected from the Teesta floodplain in Bangladesh, located in the northern region of the country. Dharla River, Dudhkumar River, and Teesta River cut through the active Teesta floodplain. Three villages from the three administrative districts were selected, e.g., Pacchim-Chhatnai village from Nilphamari district, Moulovipara village from Kurigram district, and Ujan-Bochagari village from Gaibandha district. These three villages are located near the riverbank and were selected based on the familiarity of the researcher. This study was confined to the riverine communities of the Teesta floodplain.

2.2 Study Design and Data Collection

This study employed a qualitative study design to collect primary data using the semi-structured Focus Group Discussion (FGD) technique. The field survey was conducted in June 2018. A preliminary survey was conducted in each village before the main survey. This approach helped a lot to understand the local culture and build a rapport with the community gatekeepers beforehand. A total of three FGDs, one from each village, were conducted to collect the data. The respondents were selected purposively using a snowball sampling technique from the studied communities. The discussions were held in an open space for a comfortable environment. The discussions were more flexible and respondents were given more room to engage in the process to share their knowledge and stories without any misleading or a bias response. The discussions were informal, even some of the male respondents who participated, their upper bodies were bare. This approach allowed the authors not

Table 1 Demographic information of the respondents. *Source* Field Survey 2018

Variables	FGD locations			Informal interviews	Total (N = 37)
	Pacchim-Chhatnai	Moulovipara	Ujan-Bochagari		
Age group (years)					
30–49	5	5			10
50–69	3	4	9	6	22
70–90		3	2		5
Occupations					
Agriculture	7	12	11	6	36
Business	1				1
Education					
No formal education	3	7	6	2	18
Primary	1	4	5	4	14
Secondary or more	4	1			5

to disturb the samples with exogenous factors. Participation in the discussion was voluntary without any restrictions to join and leave the meeting.

The average age of the FGD respondents was 56 years and half of them had no formal education (Table 1). The majority of the respondents (around 97%) depend on agriculture (Table 1). All the respondents have been living in Teesta floodplain since their birth. Hydro-meteorological disasters are embedded in people's culture since they live with disasters from generation to generation.

2.3 Data Analysis and Scope of This Study

The focus group discussions were conducted in Bengali and were recorded using a voice recorder. Besides, the important indicators were jotted down in a notebook which helped to summarize the points quickly upon completion of the discussions. The recorded discussions were transcribed in Bengali at first and then translated to English with cautions to maintain the originality of the emotions, expressions, and feelings of the respondents. The data were categorized into different themes and sub-themes. Each quote on TK was grouped into sub-themes. The results from this study were presented under five themes, viz. (i) knowledge on faunal behavior, (ii) knowledge on floral behavior, (iii) knowledge on river behavior, (iv) knowledge on celestial bodies, and (v) knowledge on meteorological phenomena.

The scope of this research was to document the local knowledge that the riverine people have, and a physical experiment to check the validity and reliability of the collected knowledge was far beyond its scope. Therefore, no attempt was made

to test the validity and reliability of the collected knowledge. However, for the cross-validation of the collected data, six informal interviews were also conducted (two in each of the study areas) who did not participate in FGDs. The respondents were selected through a convenient sampling technique. It was felt that three FGDs and subsequent six informal interviews were appropriate to draw a meaningful conclusion.

The respondents were informed about the purpose and disclosure (e.g., confidentiality of the personal information, willingness to share information, duration of the discussion, and recording of voice) of the study, before the interview. During the FGD session, the digital voice recorder was used after getting permission from the respondents. Since the discussions were conducted in Bengali the respondents were also informed that the discussions will be translated into English.

3   Results and Discussions

People who reside in the riverine areas have their long-standing experience with river behavior, wind direction, cloud formation, the occurrence of rain in a particular season, and so on. Local people have developed their own ways and means to forecast reasonably the behavior of the river and local climate. This section has described the results of this study under five broad themes:

3.1   Knowledge of Faunal Behavior

A. Behaviors of mammals: The behavior of mammals such as cattle, dog, and fox was reported by the respondents to forecast rain, flood, and riverbank erosion (Table 2). The eating behavior of cattle, for instance, become restless to eat grasses is associated with the onset of storms with heavy rains. The unusual barking of dogs along the river corridor was reported by the respondents as an indicator of bank erosion.

Table 2   Behaviors of mammals to predict hydro-meteorological hazard. *Source* FGD, 2018

Indicator	Indicator description	Indicates
Cattle	Restless to eat grasses in the rainy season	Onset of a storm with rain
	Wails unexpectedly when tethered in a field or in the shed	Probability of flood
Fox	Migrates another place	
Dog	Barks continuously in the rainy season	
	Wails along the river corridors	Possibility of riverbank erosion

Table 3 Behaviors of fishes to predict hydro-meteorological hazard. *Source* FGD, 2018

Indicator	Indicator description	Indicates
Dwarf goonch	Swarms near the riverbank	Possibility of riverbank erosion in that particular area
Moth catfish	Moth catfish swarms near the river corridor	

Table 4 Behaviors of birds to predict hydro-meteorological hazard. *Source* FGD, 2018

Indicator	Indicator description	Indicates
White-breasted water hen	Concentrated along the riverbank and sounds like '*Doub-Doub*'[1]	Possibility of riverbank erosion in that particular area
Lapwing	Walks along the bank of the river	
Little egret	Gather at a roost in a standing crop field	Farmers expect flood in that year
	Fly when the cloud turns into dark color	Onset of the storm with rain
Common iora	Calls out like '*Fo-Tik-Jol*'	Probability of rain soon
Chicken	Dries feathers in the sun during the rainy season	
	Takes shelter on the rooftop	

The exceptional wail of cattle and dogs in the rainy season or foxes migrate to a safer place provided the respondents with the signs of a flood. If these indicators are observed, respondents could expect immediate floods in their locality. Respondents further elaborated that foxes always stay in a peaceful region and will leave an area where there is a possibility of food shortage.

B. Behaviors of fish: The behavior of certain fishes was used by the respondents as local indicators for the prediction of riverbank erosion (Table 3). For example, the presence of dwarf goonch (*Bagarius*, local name: *Baghair*) or moth catfish (*Erethistes pusillus*, local name: *Kutakanti/ Kaiakata* fish) near the riverbank signifies the probability of bank erosion in that particular area. People dismantle/ dislocate their homes soon when they find the abundance of dwarf goonch or moth catfish near the river corridor. Dwarf goonch or moth catfish are voracious and weathered the lower part of the river as a result that part becomes loose and erodes. After several weeks or months, the whole area will become erode (displaced from the mainland) and will go underwater. As one of the respondents informed:

> I was living nearby the Teesta Riverbank. Before I lost my house due to riverbank erosion, I saw an abundance of *Kaiakata* fishes in the river. As a result, plenty of *Kaiakata* fishes were netted by the fishermen surrounding the riverbank. (Ujan-Bochagari, 70 years)

C. Behaviors of birds: The respondents identified the behavior of white-breasted waterhen, lapwing, little egret, common iora, and chicken to predict hazards (Table

4). The concentration of white-breasted waterhen (*Amaurornis phoenicurus*, local name: *Dahuk*) and lapwings (*Vanellus duvaucelii*, local name: *Hot-ti–ti*) near the river corridor provides warnings to the respondents on riverbank erosion in that area. The respondents further elaborated on the reason behind their beliefs. Worms and insects are living inside the earth especially in a sandy floodplain and come out from the ground if there is a likelihood of erosion or already eroding because of moisture content. Since lapwings love to eat those worms and insects they gather along the riverbank where there is a possibility of bank erosion. Similarly, white-breasted waterhens forage by walking along the riverbank and feed on larvae, mollusks, insects, seeds. Respondents were so confident to follow and practice these indicators. As one of the respondents explained:

> I lost my house due to riverbank erosion. Around 20 years later, the submerged area emerged as a Char land. Many of us who lost houses due to riverbank erosion moved to that emerged land. One day we found Dahuk in our locality and after several weeks the Char land was again eroded and submerged. (Ujan-Bochagari, 65 years)

The unusual behavior of little egrets (local name: *Sada-Bok*) such as sudden return in their nest in the daytime when the cloud turns into dark color indicates that a storm will hit that locality within five to ten minutes. As one respondent informed that "we take safe shelter as we see egrets fly when the sky becomes dark. (Pacchim-Chhatnai, 61 years)".

Unique calls out like *'fo-tik-jol'* by common iora (*Aegithina tiphia*, local name: *Fotik Jol*), unusual behavior of chicken such as dry feather in the sun or takes shelter on the rooftop was reported by the respondents as the indicators of immediate rain.

D. Behaviors of amphibians, worms, and insects: The behavior of amphibians, worms, and insects was also used to predict hazards (Table 5). During the FGD, the respondents explained that the call out of toads and frogs during the rainy season is a sign of upcoming rain. Respondents termed this as "wail of frog" (Bengali term: *Banger-kanna*). Respondents also believe that Almighty accepts their (frog/toad) prayers and gives water to them. Likewise, call out of monitor lizards and frogs together are associated with drought. Respondents further explained that these two calls of frogs and toads in two different seasons are varied in sounds. Calls out for the drought are harsher than the earlier.

The migration of ants in a higher ground or random fly of dragonflies, grasshoppers, and termites (before rainfall) are associated with immediate rains. The behavior of some insects such as earthworms or dung-beetles come out from the ground, black ants string people, excessive flies bunch up on cattle or bites people, were also reported as the sign of probability of rains. Respondents also informed that the appearance of grasshoppers and dragonflies after rain is an indication of no further rains. Similarly, there is a little chance of rain if fewer or no earthworms in the surface soil or dragonflies fly in summer. The behavior of cricket insects (local name: *Jhi-jhi poka*) is a reliable source for the respondents to monitor the temperature changes.

---

[1] Doub is a Bengali word which means submerge or sink.

Table 5 Behaviors of amphibians, worms, and insects to predict hydro-meteorological hazard. *Source* FGD, 2018

Indicator	Indicator description	Indicates
Toads, frogs	Call out exceptionally when a cloud appears in the sky or makes noise during the rainy season	Probability of rain
Monitor lizards, frogs	Call out together	Probability of drought in that year
Earthworms	Come out from the ground	Likelihood of rains or river floods
	Fewer or no earthworms even after digging the soil deeper than the surface	Lesser chance of rain
Ants	Climb trees in a row with their (red and black color) eggs and food stuffs	Probability of rain
	Black ants fly in a swarm and string when they contact with human during summer	
Grasshoppers/ locusts	Come out from the ground in a sunny day and fly randomly	Sudden changes in weather and rain will come soon
	Fly randomly in flocks in the sky after rains	No further rains and sun appears soon
Flies	Excessive flies bunch up in a mass on cattle	Probability of torrential rains in that year
	Bites human being	Probability of rain soon
Termites	Come out from the ground and fly abruptly	
Dung-beetles	Excessive dung-beetles	
Dragonflies	Fly in a swarm in rainy season	
	Fly after rains	No further rains
	Fly in summer season	Lesser chance of rains
Cricket insects	Make exceptional loud chirping sound monotonously in the month of *Choitra* (mid-March to mid-April)	Extreme heat in the summer season

3.2 Knowledge of Plants Behavior

The FGD respondents identified the yield of certain crops such as tamarind and summer crops as the indicators of a flood, extreme temperature, and even bank erosion (Table 6). The respondents informed that a bumper yield of tamarind is associated with the possibility of a flood. Similarly, bumper production of crops

Table 6 Plants behavior to predict hydro-meteorological hazard. *Source* FGD, 2018

Indicator	Indicator description	Indicates
Tamarind	Bumper yield of tamarind	Possibility of catastrophic flood
Summer fruits	Excessive yield of summer fruits	Probability of storm, hails or torrential rainfall in that year
	Summer fruits ripe before their normal life-cycle phase	Extreme hot in summer season
Excessive yield of crops	Bumper production of crops in a land located alongside the riverbank	Land will be engulfed by the river soon

in a land alongside the riverbank is an indicator for riverbank erosion. One of the respondents shared his experience as:

> I had a piece of land in *Char* and I used to cultivate maize in that land. On average, this land yields 20-25 mounds[2] of maize in each season and the highest yield was 30 mounds. Surprisingly, that land produced 60 mounds of maize in one season. Just after this bumper production of maize from that land, it was engulfed by the Teesta. I was unable to cultivate the land in the following season. (Pacchim-Chhatnai, 59 years)

Crop production largely depends on the level of moisture content in the soil. Lands alongside the river that yield bumper crops have an underground flow of the river which is due to the down-cut in the riverbed. Thus, standing crops can absorb the required amount of moisture from the soil and can result in a bumper crop. This indicates that the upper portion of the land detaches from the riverbed and land subsidence occurs later on.

3.3   Knowledge of River Behavior

Knowledge of river behaviors such as observing river watercolor, the smell of river water, river roaring, and the presence of water hyacinth in running water was used for hazards prediction (Table 7). The respondents informed that they can forecast river flood or riverbank erosion by looking at the color of the river water. One respondent from Ujan-Bochagari stated: "look at the watercolor of the Teesta River. The turbidity of the river water is increasing. This means somewhere in the upstream of the river is eroding (FGD, 55 years)". This is because erosion is a natural process in a floodplain that destroys riverbanks and washes away soils, trees, and others. Some of these materials are dissolved with water and some of them remain as suspended or bed load. As the riverbank erodes and mixes with the river water, the water becomes muddy or turbid.

---

[2] One mound equals 40 kg.

Table 7 Knowledge on river behavior to predict hydro-meteorological hazard. *Source* FGD, 2018

Indicator	Indicator description	Indicates
River water color	Color of the river water looks transparent in the first few days of the rainy season	River water is increasing and river floods will hit soon
	Transparent color of running water	No bank erosion in the upstream
	The appearance of turbid water in the river	Riverbank erosion in the upstream
Smell of river water	The running water of the river generates bad smell	
Roaring of river	Increased level of river roaring during flood	Flood water is going to recede
Floating water hyacinth	Water hyacinths in the running water of the river	Flood already hits in the upstream

The findings showed that if the running water of the river looks muddy and reddish in color and generates a bad smell, which indicates riverbank erosion. Respondents further elaborated that this odor is generated from the dissolved minerals and weathered materials. The bad smell of river water thus indicates river erosion.

The roaring of the river was reported by the respondents as an indicator of receding floodwater. A large area is flooded in a severe flood. Floodwater spreads in the low-lying areas and the river does not roar. During the water recedes, the river roars as the floodwater route through the main channel which generates powerful water currents and waves. In addition, the presence of water hyacinths in the running water provides information to the respondents on floods in the upstream region.

3.4 Knowledge of Celestial Bodies

The unique behavior of celestial bodies such as the sun, moon, and stars to predict hydro-meteorological hazards were reported by the respondents (Table 8). The bathed red color of the sun before the sunset indicates rainfall on the following day.

The respondents informed that if a ring of light (respondents termed it as 'decoration of moon') encircles the moon in the rainy season, this signifies rain or flood will visit soon. Respondents explained this indicator using a proverb in their locality: "decoration of moon and stars inside the ring of the moon; Indicates for torrential rain (translated)".

The tilt of the moon to the south is an indicator of dense fog with rains during winter. The respondents also informed that dense fog with rains is harmful to the winter crops (Robi crops), result in temporary food scarcity in their areas. People also observe stars for rain or a rainless day on the next day.

Table 8 Celestial bodies to predict hydro-meteorological hazard. *Source* FGD, 2018

Indicator	Indicator description	Indicates
Sun	Color of the sun turns into 'bathed in red' before sunset	Rainfall on the following day
Moon	A 'ring of light' encircle the moon in the rainy season	Probability of rain
	If a star appears within this ring	Flood is approaching
	If the color of the ring appears as red during the full-moon	Probability of rainless days, but there will be clouds
	Tilts to the south during winter	Possibility of dense fog with rains in that winter
Stars	Star-filled sky at night and cloudy in the daytime during the summer season	Possibility of heavy rains in the rainy season
	Star-filled sky at night	More sunshine, less cloud, and fewer chances of rainfall on the following day
	Big star appears (locally known as *Bhutuatara*) in the eastern sky at mid-night	Indication of clear sky

3.5 Knowledge of Meteorological Phenomena

The results showed that meteorological factors such as wind, rainbow, cloud, and fog were important indicators to forecast hydro-meteorological hazards (Table 9). The respondents informed that they could guess the climatic conditions for the upcoming season by observing the weather variability of the current season. For example, winter will be cooler if there is low rainfall in the rainy season.

Weather change largely depends on the wind direction. The wind direction is used by the riparian to predict rainfall and storm. For instance, wind flows from the northwest direction during the summer indicate nor'wester will hit soon. This is because in the pre-monsoon season (March to May) when warm and moist air blowing from the southeast and relatively dry and cold air (jet stream) blowing from northwesterly and westerly direction coincides, they form a violent storm, nor'wester.

The respondents informed that the appearance of the rainbow is a good indicator of rainfall. Respondents shared a proverb: "Rainbow in the eastern sky indicates for coming flood; rainbow in the western sky indicates for dry(translated)". In general, rainbows appear on the opposite side of the sun—they are found in the east in the evening and west in the morning. This means a rainbow in the morning indicates that the observer is looking at the west where showering weather is occurring and a rainbow in the evening indicates the observer is looking at the east. In the rainy season, the surface wind blows from the southerly or southwesterly direction.

The amount of water vapor and dust particles in the atmosphere determine which color we will see in the sky and provide information on weather conditions. The local people draw on observation of color, shape, and movement of clouds to forecast

Table 9 Meteorological phenomena to predict hydro-meteorological hazard. *Source* FGD, 2018

Indicator	Indicator description	Indicates
Weather variability	Mild winter and cloudy summer with less heat	Following rainy season will receive intense rains
	Less rainfall in the rainy season	Following winter will be cooler than usual
Wind direction	Blows from west during rainy season	Indicates for torrential rains
	Blows from north–south direction in autumn (mid-September to mid-October)	
	Blows from north-west direction during summer (mid-April to mid-June)	Nor'wester (local term: *Kal-Baishakhi*) with thunders and hails
	Westerly wind during spring (mid-February to mid-April)	Heatwave in summer and cold wave in winter (mid-December to mid-February)
	Easterly wind during late autumn to the beginning of winter (mid-November to mid-January)	Fair weather in winter
Rainbow	Appears in western sky during rainy season	Possibility of cloud in the sky only but no rainfall, more sunshine with further probability of dryness of that year
	Appears in eastern sky during rainy season and the color looks like dim-red with insertion of white	Probability of rainfall triggers flood and storm with rainfall in everyday throughout the rainy season
Cloud	Shape of cloud resembles a tree before the sunset	Gusty wind at night
	Dark cloud forms in the northern sky	Rains in upstream (India)
	Color of the cloud (north-west direction) becomes reddish or blackish	Hailstorm when it is reddish in color, and storm if it turns into black
Fog	Foggy weather in summer evening	Rainfall in the next day morning

hydro-meteorological hazards. For example, focus group respondents from Pacchim-Chhatnai informed that a dark cloud formation in the northern sky is an indication of rainfall in upstream (India). Rainwater runs through the Teesta River and reaches their locality (Pacchim-Chhatnai) within two to three days and can cause river flood.

Respondents also informed that reddish or black color cloud in the northwest side is harmful to people and standing crops. Soon after the cloud formation, heavy thunder or hailstorm occur according to the appearance (color) of the cloud. Either cloud or wind from the northwest direction is harmful to the studied communities. Respondents from the Pacchim-Chhatnai gave an example from a recent nor'wester

(June 2018) that hit in their locality. Dimla sub-district was badly affected (especially the standing crops were completely damaged) by that nor'wester. Therefore, cloud color is a good indicator of good and bad weather outcomes.

Similarly, foggy weather in the summer evening is considered an indicator of rainfall in the following morning. The fog-like clouds carry excessive water vapor. If the air cools further and saturated, later on, it comes down as rain.

4 Conclusion

This study investigated traditional knowledge on hydro-meteorological warning signs practiced by the riverine communities of Teesta floodplain in Bangladesh using a qualitative research design. This study revealed that riverine people rely on various natural indicators for hazard prediction. Such knowledge helps riverine people for preparedness and responses to avoid/minimize losses from disasters. Respondents believe that their gained knowledge helps them to forecast rainfall, flood, storm, and even bank erosion more accurately than the warning issued by the meteorological station. As an example, respondents from the Pacchim-Chhatnai village informed that if there is a forecast from the Rangpur meteorological station stating that "there will be extreme rainfall tomorrow in the Rangpur region, and the forecast may be wrong for our locality, as the sun will come out with clear skies". The respondents were also asked whether there is any value of their TK in the age of information technology. They informed us that there is no valuation of their knowledge.

The science behind the TK to forecast disaster can be explored through rigorous studies. For example, there is no scientific method to forecast riverbank erosion. TK to predict bank erosion can be a potential research area for the researchers to generate new knowledge to forecast bank erosion. An attempt should be made to integrate these TK into the broader disaster risk reduction (DRR) framework especially prediction, prevention, preparedness, and rehabilitation. Successful integration of traditional knowledge and scientific knowledge will yield productive and meaningful DRR at the local level.

Floodplains are very rich in biological diversity. However, the respondents informed that many plants and animals have already gone extinct from their locality. Therefore, in many cases, local people face it difficult to predict disasters accurately. Some of the documented knowledge may yield invalid outcomes. Indicators of the documented knowledge were not validated either by questionnaire survey or by practical experiments. Therefore, findings from this study are difficult to interpret other than the studied context. There were biases on sampling techniques and tools of data collection which may lead to either over-representation or under-representation of documented knowledge. This study does not claim that TK is self-sufficient for long-term forecasting instead they are good enough for short-range forecasting that can provide a lead-time to the communities for better emergency management.

References

1. McAdoo BG, Moore A, Baumwoll J (2009) Indigenous knowledge and the near field population response during the 2007 Solomon Islands tsunami. Nat Hazards 48:73–82
2. Howell P (2003) Indigenous early warning indicators of cyclones: potential application in coastal Bangladesh, Benfield Greig Hazard Research Centre, London
3. Chisadza B, Tumbare MJ, Nyabeze WR, Nhapi I (2015) Linkages between local knowledge drought forecasting indicators and scientific drought forecasting parameters in the Limpopo River Basin in Southern Africa. Int. J. Disaster Risk Reduct. 12:226–233
4. Codjoe SNA, Owusu G, Burkett V (2014) Perception, experience, and indigenous knowledge of climate change and variability: the case of Accra, a sub-Saharan African city. Reg Environ Chang 14:369–383
5. Hiwasaki L, Luna E, Shaw R (2014) Process for integrating local and indigenous knowledge with science for hydro-meteorological disaster risk reduction and climate change adaptation in coastal and small island communities. Int. J. disaster risk Reduct. 10:15–27
6. Bordoloi, R.; Muzaddadi, A.U. Indigenous technical knowledge associated with disaster management and fisheries related activities in the highest flood affected district (Dhemaji) of Assam, India. **2015**.
7. Roncoli C, Ingram K, Kirshen P (2002) Reading the rains: local knowledge and rainfall forecasting in Burkina Faso. Soc. & Natural Resour. 15:409–427
8. Mondal, M.S.H. Disaster Management through Indigenous Wisdom: Voice from the People of Erendabari Char. *J. South Asian Disaster Stud.* **2012**, 27.
9. Uddin, M.N.; Rahman, M.M. Traditional Ecological Knowledge on Flow and Erosion processes in the Braided Jamuna river in Bangladesh: Part-II. **2013**.
10. Irfanullah, H.M.; Motaleb, M.A. Reading nature's mind: disaster management by indigenous peoples of Bangladesh. **2011**.
11. Kanak Pervez, A.K.M.; Gao, Q.; Uddin, M.E. Rural women's awareness on indigenous technical knowledge: Case of northern Bangladesh. *Anthropol.* **2015**, *21*, 415–426.
12. Ministry of Disaster Management and Relief (MoDMR) National Plan for Disaster Management-2016–2020: Building Resilience for Sustainable Human Development 2017.

Assessment of Sedimentation in the Reservoir—A Case Study

M. N. Sandeep, Nisha Antony, C. E. Suhurban Beegam, S. S. Suja, and B. Sindhu

1 Introduction

Kerala is a state considered to be rich in water resources and 44 rivers are flowing through the state. The state has given utmost importance to the proper utilization of its water resources. Dams have been constructed across the major rivers in Kerala to create reservoirs to meet different needs such as hydroelectricity generation, water for drinking purposes, irrigation, etc. Reservoirs also play a significant role in flood management. Recent floods in Kerala have highlighted the significant role of reservoirs in flood management [1].

Deposition of sediments and loss of reservoir capacity is the main concern in reservoir management. The primary purpose of the reservoir of storage of water is adversely affected by reservoir sedimentation. Based on the sedimentation studies for 43 reservoirs in India, it was reported that the sedimentation rate varies between 30 and 2785 m^3 km^2 /year [2]. Many of the reservoirs in India are having a reduction in capacity at a rate of 0.5–1.5% annually. Monitoring of reservoir capacity and dredging operations are required for the sustainable management of a reservoir. As the sediment-laden stream flows into the relatively quiescent pool, the coarser particles are more rapidly deposited, while the finer particles are transported farther into the reservoir depending on the velocity and dynamics of the water. Sedimentation in a reservoir is influenced by several factors including characteristics of the catchment and river hydrology. Also, the factors include the size and shape of the reservoir and reservoir operation cycle [3]. Soil erosion and sediment yield from the catchment is a major factor affecting sedimentation [4]. Sediment yield is affected by a multitude of factors such as rainfall, soil properties, surface topography, and drainage properties as well as anthropogenic practices of land management.

Many studies were conducted on reservoir sedimentation. Cyan et al. [5] developed a reservoir model using HECHMS and HEC-ResSim models, combined with

M. N. Sandeep (✉) · N. Antony · C. E. Suhurban Beegam · S. S. Suja · B. Sindhu
Kerala Engineering Research Institute, Peechi, Kerala, India

satellite remote sensing data of the Kakki reservoir in southern Kerala to study flood and reservoir management. In another study, the assessment of reservoir sedimentation using Remote Sensing and GIS for Kabani reservoir in Karnataka was done [6]. Goel et al. [7] studied the use of remote sensing data along with a geographic information system to determine the sediment deposition pattern in Bargi Reservoir, Madhya Pradesh.

In this paper, a case study of sedimentation analysis conducted for the Chulliyar reservoir in Kerala is presented. The objectives of the study are to determine the loss of storage capacity of the reservoir due to sedimentation and to assess the percentage composition of sediments based on particle size. The bathymetric survey is conducted to determine the storage capacity of the reservoir. Soil samples from the reservoir are collected for soil testing to classify the sediments deposited based on the grain size and to determine the percentage fraction of each component in the deposition. The percentage composition of sediments helps in assessing the useable part of the soil excavated during desilting after proper processing, for construction purposes.

1.1 Chulliyar Dam

Chulliyar dam is situated 40km away from District Headquarters, Palakkad. The reservoir is located at $10^0 35'$N Latitude and $76^0 50'$E Longitude. The Chulliyar dam is constructed across the Chulliyar River at about 2km upstream of its confluence with Meenkara River. Figure 1 shows the top view of the dam and reservoir. This

Fig. 1 Chulliyar reservoir

dam with a canal system was completed in 1964 and was commissioned in 1966. The catchment area of the river at the dam site is 29.78 km^2. The water spread area of the reservoir is 1.65 km^2. The maximum storage capacity of Chulliyar Reservoir is 13.733 Mm^3

2 Methodology

The sedimentation study involves a bathymetric survey, sample extraction, and soil testing. The sedimentation division of Kerala Engineering Research Institute (KERI), Peechi, has been conducting sedimentation studies in many reservoirs in Kerala. The sample extraction and transportation were conducted by Hydraulics Division, KERI. The sample collection was done by NCESS (National Centre for Earth Science Studies). To assess the composition of sediments samples are extracted and qualitative analysis of sediments samples was done by Soil Mechanics and Foundation Division, KERI [8–10].

3 Bathymetric Survey

The bathymetric study of the reservoir was conducted by the sedimentation division, KERI using Integrated Bathymetric System and Sub-bottom Profiler in 2009. From the study, it was found that that the maximum storage capacity of Chulliyar Reservoir reduced from 13.733Mm^3 to 13.225 Mm^3 for a period of 45 years. There was a loss of capacity in 0.508 Mm^3 (0.08% /year) and the rate of sedimentation is 0.01Mm^3 /year at the full reservoir level. Based on the bathymetric study conducted in 2017, at a level of 147.37m, it was found that the reservoir capacity reduced from the original capacity of 4.589 Mm^3 to 3.449 Mm^3 . The total capacity reduction was 1.14 Mm^3 (0.47% per year) for a period of 53 years and the rate of sedimentation was 0.022 Mm^3 /year at 147.37m. It can be found that sedimentation and capacity reduction is increasing for the past 9 year period [8, 9].

4 Sample Collection

The sample collection was done by NCESS (National Centre for Earth Science Studies) using the gravity corer method for underwater sample extraction and other suitable ground sampling methods for portions where the water level has recessed. The sample extraction and transportation were conducted by Hydraulics Division.The water spread area of the reservoir was divided into zones of size 200m x 200m and each zone was to be divided into grids of size 50m x 50m and samples were extracted from the center of each grid. Sample collection was done in two

Fig. 2 Grid Locations for Sample Collection at Chulliyar Reservoir

modes, namely underwater sampling using gravity corer and on land with the help of a hydraulic excavator. Figure 2 shows the grid locations for sample collections at Chulliyar reservoir. A total of 680 core samples were collected from the Chulliyar reservoir. As per the soil report, the average depth of core samples is calculated as 0.87 m from field studies. Figure 3 shows the sample collection using gravity corer.

5   Soil Testing

To assess the composition of sediments, samples are extracted, qualitative analysis of sediments samples was done by Soil Mechanics and Foundation Division, KERI. Sediments samples were tested for the determination of components and classification of the sediments. Both undisturbed sediments samples and disturbed sediments samples were collected. Undisturbed sediment samples delivered in PVC pipes were mainly from underwater and disturbed samples from dry bed level soil. On visual observation, most of the undisturbed samples were clayey soil and in sticky nature and lead grey/dark blue-grey colour, which is indicative of clayey soil. Most of the disturbed sediments samples were C-φ soil and nearly 10 samples were conformed to sand.

Fig. 3 Sample Collection using Gravity Corer

Cores were divided into 50 cm length or parts thereof; considered as one sample. Representative samples were taken for testing from each sample according to the texture of the soil. Samples were tested in accordance with the IS codes. The result is expressed as the percentage of particles present in each sample. In the analysis, a proportionate percentage of particles is determined and no constant factors are considered in the analysis [11, 12].

Based on the investigation average core depth is obtained as 0.87m. In the analysis of test results to determine the percentage of particles, proportionate averaging with respect to the depth of core has been made. For each core, the total sample is taken as 100% with respect to core depth and the proportionate fraction of each particle present in the total sediments had been arrived at. Finally, the proportionate percentage of particles is arrived at by dividing the sum of the total of the percentage of each component multiplied by each core depth with the sum of the depth of all cores. [10]

6 Results and Discussion

Grain size analysis of collected soil samples is carried to identify different particle sizes in the sediments. During desilting, a large quantity of soil will be excavated from the reservoir and after proper processing, some percentage of sediments can be used for construction purposes as fine aggregates. From grain size analysis [2], it was

Table 1 Percentage of soil components

Soil components	Size in mm	Percentage with respect to depth (% P)
Pebbles	> 80	0
Gravel	80–4.75	1.2031
Coarse sand	4.75–2.00	1.8850
Medium sand	2.00–0.425	13.6907
Fine Sand	0.425–0.075	40.5300
Clay & Residues	< 0.075	42.6912

noted that pebble size (>80mm) grains were absent in the sediments. Gravels (80–4.75 mm) constitute 1.203 % of sediments. Coarse sand present (4.75mm – 2mm) is 1.885% and medium sand (2–0.425 mm) present in the sediments is 13.691%. Fine sands (0.425 mm–0.075 mm) contribute more percentage of sediments, which come to 40.53 % and the remaining portion is contributed by clay and residues (<0.075 mm), which is 42.691%. The total percentage of sand particles in sediments is 56.106%. The calculated soil test result (Grain size analysis) is appended in Table 1.

This field study was conducted before the 2018 heavy rainfall and floods in Kerala, which have influenced the catchment characteristics and sediment transport in the area. Further studies are to be conducted to investigate the features of the catchment and land management influencing reservoir sedimentation. Also, the studies are to be conducted to verify the effectiveness of different methods for mitigation of reservoir sedimentation. Also, the studies can be conducted to develop a sediment transport model for the river.

7 Conclusions

The present study is a part of a project conducted to investigate the sedimentation and reservoir capacity reduction in the Chulliyar reservoir. The study also identifies the percentage constituents of sediments deposited which can be used for construction purposes after processing.

Based on the sedimentation surveys, it was found that the original storage capacity of Chulliyar Reservoir is reduced due to sediment deposition. There is a loss of storage capacity by 0.08 % per year at the full reservoir level for a period of 45 years. The loss of storage capacity increased to 0.46% per year at a level of 147.37m for a period of 53 years, which indicates an increase in sedimentation. The rate of sedimentation increased from 0.01Mm^3 /year to 0.02 Mm^3 /year.

As per the analysis, even though it was observed that 56.106% of sediments deposited in the reservoir constituted sand, of which medium sand (2mm-0.425mm size) is only 13.69%, which can be used for construction purposes. The sediments consist of clay and other finer particles constituting more than 42%.

References

1. Mishra, Vimal, Saran Aaadhar, Harsh Shah, Rahul Kumar, Dushmanta Ranjan Pattanaik, and Amar Deep Tiwari. "The Kerala flood of 2018: combined impact of extreme rainfall and reservoir storage." Hydrology and Earth System Sciences Discussions, 1–13, (2018)
2. Shangle AK (1991) Reservoir sedimentation status in India. Jalvigyan Sameeksha 5:63–70
3. Imanshoar, Farhad, Afshin Jahangirzadeh, Hossein Basser, Shatirah Akib, Babak Kamali, Mohammad Reza M. Tabatabaei, and Masoud Kakouei. "Reservoir sedimentation based on uncertainty analysis." In Abstract and Applied Analysis, vol. 2014. Hindawi, (2014)
4. Dutta, S. "Soil erosion, sediment yield and sedimentation of reservoir: a review." Modeling Earth Systems and Environment 2, no. 3, 123. (2016):
5. Ryan, Ciarán, Mark A. Trigg, and S. Adarsh. "An investigation into the impact of reservoir management Kerala floods 2018: A case study of the Kakki reservoir." IOP Conference Series: Earth and Environmental Science. Vol. 491. No. 1. IOP Publishing, 2020.
6. Avinash, G., and P. N. Chandramouli. "Assessment of Reservoir Sedimentation using RS and GIS techniques-A case study of Kabini Reservoir, Karnataka, India." (2018).
7. Goel, M. K., Sharad K. Jain, and P. K. Agarwal. "Assessment of sediment deposition rate in Bargi Reservoir using digital image processing." Hydrological sciences journal 47(S1), pp.S81-S92.(2002)
8. Annual Report, Kerala Engineering research Institute, Peechi, (2007).
9. Annual Report, Kerala Engineering research Institute, Peechi, (2017).
10. Annual Report, Kerala Engineering research Institute, Peechi, (2018).
11. IS -2720 (Part - IV. "Methods of Test For Soils -Part 4 Grain Size Analysis." 1985.
12. IS -1498, "Classification and Identification of Soils for General Engineering Purposes" 1970.

Particle Image Velocimetry Analysis on the Liquid-Sediment Model

M. H. Zawawi, F. C. Ng, M. A. Abas, A. Azman, and N. H. Hassan

1 Introduction

Particle image velocimetry (PIV) is a non-intrusive optical method used for analysis of the fluid flow visualization. In this method, seeding particles are mixed together with the working fluid where the working fluid must be clear or transparent. The laser in pulses are directed to the fluid and it will illuminate the particles that flows with the fluid. At the same time, high–speed camera captures the movement of the particles. The consecutive images between the two light pulses will be used to track the movement of the particles, which represents the fluid flow through simple relation:

$$V = \frac{\Delta x}{\Delta t},\tag{1}$$

where Δx is the particles displacement, measured using the two consecutive images and Δt is the time interval between the two consecutive images. These images are related with each other which is pixel–by–pixel in order to track down the particle's displacement. Subsequently, the flow velocity and dynamic behavior of the investigated system could be determined [1–3].

M. H. Zawawi (✉) · N. H. Hassan
Department of Civil Enginering, Universiti Tenaga Nasional, 43000 Kajang, Malaysia
e-mail: MHafiz@uniten.edu.my

F. C. Ng · M. A. Abas · A. Azman
School of Mechanical Engineering, Universiti Sains Malaysia, 14300 Nibong Tebal, Penang, Malaysia

2 Experimental Setup and Procedures

The particle image velocimetry (PIV) experiment on the liquid-sediment costal involved various materials and apparatus as detailed in Table 1. The schematic diagram on the PIV experiment was depicted in Fig. 1 while the actual experimental setup was shown in Fig. 2.

The procedure of the experiment is as follow. First, the trapezoid-shaped sediment was constructed in one side of the aquarium using the sand. Afterwards, the tank was filled with water at a level of 11 cm height and then mixed with the seeding particles. The water was moved with the wave maker to generate wave flow pattern and the wave maker was controlled by motor controller to get the desired waveform. The laser from the PIV setup is activated to illuminate the particles flowing in the fluid. At the same time, a high–speed camera captured the flow of the fluid. The laser model used in this experiment is the NANO L135–15 PIV with a pulse duration of 70 ns. The camera model is the Dantec HiSense MKII C8484–52–05CP Hamamatsu Digital Camera C8484–05CP with a frame rate of 12.2 frame per second (fps) at full resolution. This laser and camera are connected to the software provided by Dantec called DynamicStudio. In the DynamicStudio, the time interval between images, Δt is set at 163 ms. Moreover, there are 130 frames of which 260 images are captured for each image acquisition process. These images were then imported to PIVlab, a MATLAB tool for analysing the PIV data.
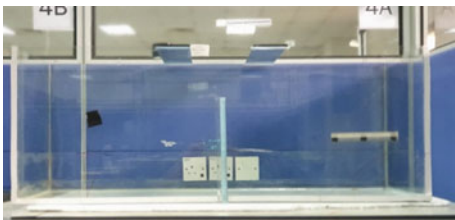
PIVlab is a time–resolved particle image velocimetry (PIV) software that can calculate the velocity distribution within the particle image pairs. Figure 3 depicted the sequences involved in the image processing and data analysis using PIVlab software.

Firstly, the images captured in the PIV experiment were imported into the PIVlab software. Next, the quality of two consecutive images were enhanced so that the filler particles can be clearly seen and identified. The masking procedure was conducted to define the region of interest by excluding the unwanted area. After finishing the pre-processing stage, the images were prepared for analysed, through the image calibration and vector calibration process. Image calibration is a process of selecting a reference distance and setting up the time step, for accurately determine the flow velocities. Meanwhile, the vector calibration is a process of choosing the velocity limits. Lastly, the flow velocity was plotted and a distribution contour for the flow behaviour was generated.

3 Results and Discussion

Figure 4 depicted the PIV experimental findings on the velocity contours of the water flow near the sediment model, for the time of 3 s. The variation of water flow with the interactions of sand sediment due to erosion was depicted, together with the flow velocity.

Table 1 Materials and apparatus involved in the PIV experimental setup

Materials and apparatus	Function/Description
Polyamid seeding particles	The diameter of polyamide is $50 \mu m$ and it serves as tracing particles to allow the motion tracking of water
High-speed camera	Camera model: Dantec HiSense MKII C8484–52–05CP Hamamatsu Digital Camera C8484–05CP with a frame rate of 12.2 frame per second (fps) at full resolution
Computer	The computer is used to open a software provided by Dantec called DynamicStudio to control the laser and camera
Aquarium	The aquarium with size of 1206 mm length, 454 mm width and 463 mm height are used in the experiment

Table 1 (continued)

Materials and apparatus	Function/Description
Motor speed controller	The motor speed controller is used to control the speed of motor to the desired speed
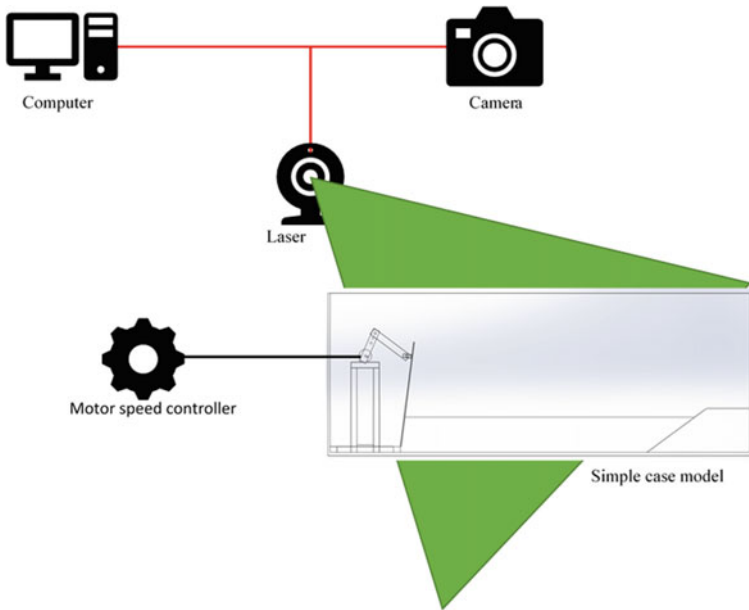
Fig. 1 Schematic diagram of the flow system of the PIV experiment

4 Conclusion

The particle image velocimetry (PIV) experimental setup and procedures to study the coastal problem by using the simple liquid-sediment problem were presented. It had demonstrated that the capability of PIV analyses in the present problem, yielding the transient evolution of flow profile and velocity contours. Therefore, it is expected that this PIV experiment could provide viable solution for the future validation work on the corresponding numerical simulation findings.
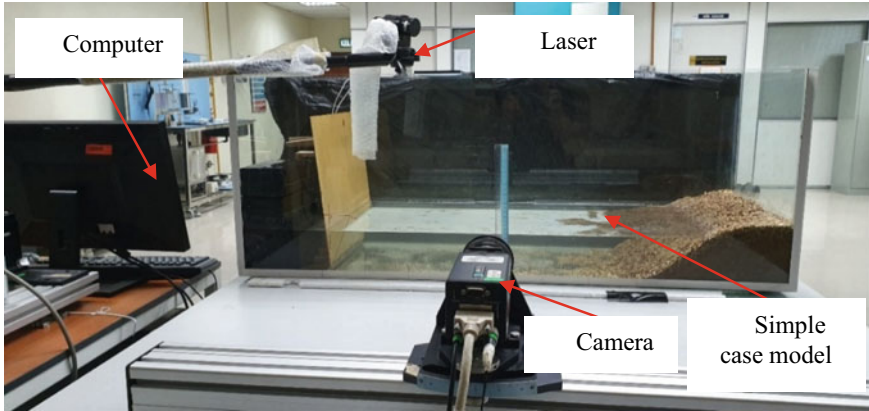
Fig. 2 Actual PIV experimental setup
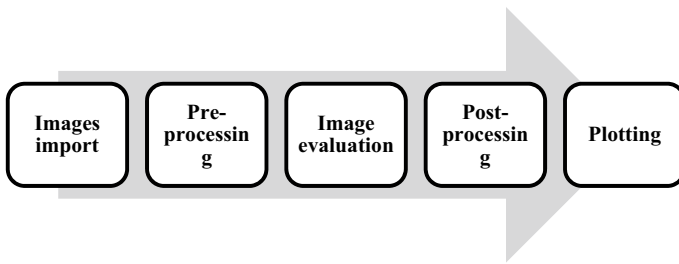
Fig. 3 Process flow in PIVlab stage for image processing and results analysis
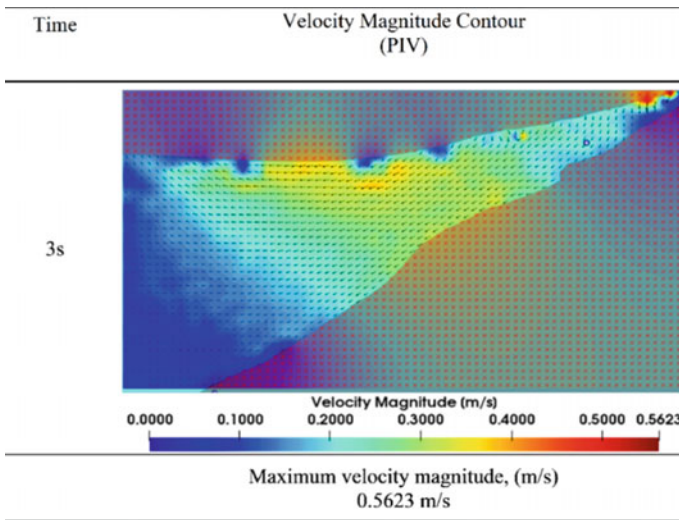
Fig. 4 Velocity contours of water flow at different times of 3 s and 6 s

References

1. Abas MA, Jamil R, Rozainy MR, Zainol MA, Adlan MN, Keong CW (2017). PIV study of aeration efficient of stepped spillway system. IOP Conference Series: Materials Science and Engineering, 209(1)
2. Azman A, Zawawi MH, Hassan NH, Abas A, Razak NA, Mazlan AZA (2018) Effect of Step Height on The Aeration Efficiency of Cascade Aerator System Using Particle Image Velocimetry. MATEC Web of Conferences 04005(August):1–6
3. Azman A, Ng FC, Zawawi MH, Abas A, MAZ, M. R. R., (2020) Effect of Barrier Height on the Design of Stepped Spillway Using Smoothed Particle Hydrodynamics and Particle Image Velocimetry. KSCE J Civ Eng 24(2):451–470
4. Grant I (1997) Particle image velocimetry: A review. Proc Inst Mech Eng C J Mech Eng Sci 211(1):55–76
5. Jain N, Ottino JM, Lueptow RM (2002) An experimental study of the flowing granular layer in a rotating tumbler. Phys Fluids 14(2):572–582
6. Lueptow RM, Akonur A, Shinbrot T (2000) PIV for granular flows. Exp Fluids 28(2):183–186
7. Muste, M., Fujita, I, Hauet, A (2008) Large-scale particle image velocimetry for measurements in riverine environments. Water Resources Research, 44(4)
8. Ng FC, Abas A, Abdullah MZ (2018) Effect of solder bump shapes on underfill flow in flip-chip encapsulation using analytical, numerical and PIV experimental approaches. Microelectron Reliab 81:41–63
9. Peltier Y, Dewals B, Archambeau P, Pirotton M, Erpicum S (2017) Pressure and velocity on an ogee spillway crest operating at high head ratio: Experimental measurements and validation. J Hydro-Environ Res 19:128–136
10. Raffel M, Willert CE, Scarano F, Kähler CJ, Wereley ST, Kompenhans J (2018) Particle Image Velocimetry (Third Edit)
11. Xie X, Le Men C, Dietrich N, Schmitz P, Fillaudeau L (2018) Local hydrodynamic investigation by PIV and CFD within a Dynamic filtration unit under laminar flow. Sep Purif Technol 198:38–51

Wave Loads Assessment on Coastal Structures at Inundation Risk Using CFD Modelling

Ana Gomes and **José Pinho**

1 Introduction

Coastal regions are of great importance to human life and its development assumes great strategic importance in environmental, economic, social, cultural, and recreational terms. In addition to locating the main cities of the world, they are currently among the areas with the highest population densities and most projections indicate that migration to coastal megacities will continue to increase [1, 2]. It is predictable that they will be increasingly affected by extreme phenomena and by natural ocean-coast dynamics. The sudden impact of wave storms on structures located in coastal areas is an increasingly common occurrence in many situations, and will be aggravated, especially, under climate change scenarios, causing serious damage to coastal structures [3–5]. Therefore, it is extremely important to anticipate impacts of these events, to contribute to their mitigation and adopt efficient measures for the conservation of relevant infrastructures located at these areas.

There are many instances where this field of study finds applications but the action of steep sea waves (both breaking and non-breaking) on coastal structures had probably been studied more often than any other [6–10]. The estimation of wave-induced loads on structures has been the subject of many theoretical [11–13], experimental [14–16], and numerical studies, to prevent failures on structures.

In recent years, progress has been made in the subject of computational fluid dynamics (CFD) and has been widely used to investigate, among others, the wave impacts in the built environment. Elevated coastal structures were studied using CFD tools. Xiao and Huang [17] estimated the impact of a solitary wave over a coastal

A. Gomes (✉) · J. Pinho
Department of Civil Engineering, CTAC, University of Minho, Campus of Gualtar, 4710-057 Braga, Portugal
e-mail: carolina_gomes@live.com

J. Pinho
e-mail: jpinho@civil.uminho.pt

structure, assessing the variation of wave forces and overturning torque, based on temporal data and other work [18] proposed a performance-based design approach using fragility functions. The wave interaction with submerged permeable structures and the interaction between regular waves and perforated-wall caisson breakwaters were studied by other authors [19] and [20]. The hydraulic performance of a submerged breakwater was also studied in terms of the wave reflection, transmission, and dissipation coefficients by [21] and [22] using the Flow-3D® [23].

This commercial CFD code, Flow-3D® [23] has been used in this field as it has high capacity to simulate fluid dynamics problems, including the possibility to simulate different types of waves in complex geometry domains, which include three dimensional solid objects. It is based on the Reynolds'averaged Navier Stokes equations (RANS). It has been used for simulating, for example, the intricate flow field details around a submarine pipeline [24] and around bridge piers [25]. Jin and Meng [26] applied the software to analyze wave-structure interaction and calculated wave loads on coastal highway bridges and [27] on rock mound breakwaters with a tetrapods armor layer. Carratelli et al. [28] examine the development of the pressure wave produced by the impact on a vertical wall as it propagates and interacts with the fluid boundaries, as well as the subsequent build-up of high-pressure gradients of high fluid velocities. The results provide new insight about the connection between phenomena with different timescales.

This work presents results of the application of Flow-3D® to study a problem of fluid–structure interaction, and the objective is to estimate the hydrodynamic loads on an elevated coastal structure for a given wave condition in three different heights of the air gap between the water and the structure base levels. The CPU simulation times were also analyzed to assess the suitability of this software to be used in a forecast early warning context.

2 Methodology

2.1 Flow Model

The Computational Fluid Dynamics (CFD) software Flow-3D® [23] has demonstrated high capability to simulate complex fluid dynamics problems, including the possibility to simulate different types of waves in complex geometry domains, including three dimensional solid objects. As mentioned, before it solves the Reynolds' averaged Navier Stokes equations (RANS) using the volume of fluid (VOF) method, considering different alternatives for turbulence closure models. The VOF method enables modeling of the free surface and liquid/solid interactions. It has been widely validated over the past years particularly for problems related with wave loads assessment [29, 30]. Thus, it was applied to analyze the wave load and coastal structure interaction and evaluated to be used for extreme events forecast purposes.

2.2 Model Geometry

Park et al. [31] built a physical model to understand the relationship between an elevated coastal structure's air gap and the resulting horizontal and vertical forces generated by a range of wave conditions. The study was based on a set of experiments involving a 1:10 length scale physical model and the wave characteristics based on an idealization of Hurricane Ike's impact on the Bolivar Peninsula, Texas.

A Large Wave Flume (LWF) equipped with a piston-type wave maker was used together with sensor devices based on load cells and pressure gages to measure wave heights, pressures, and loads for regular, irregular, and transient waves. Physical model setup is presented in Fig. 1. The bathymetry was made of concrete and the structure was constructed of steel with dimensions $1.02\,\text{m} \times 1.02\,\text{m} \times 0.61\,\text{m}$ (Length x Width x Thickness). The structure was mounted on a frame that could be raised or lowered to increase or decrease the air gap, a, between the base of the structure and the elevation of the stillwater.
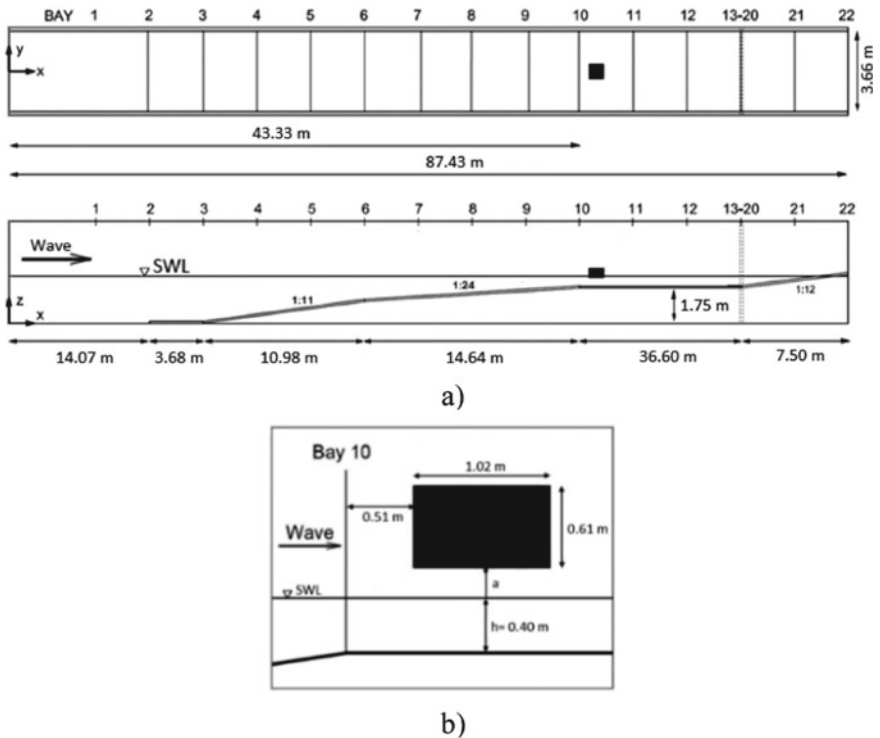
Fig. 1 Physical model setup: **a** large wave flume: profile (top) and plan (bottom) view **b** side view of specimen-frame system elevated at air gap a above the stillwater level (adapted from [31])

3 Numerical Model

3.1 Laboratory Physical Model

The three-dimensional geometry of the physical model (structure and bathymetry) was edited in a CAD tool and exported into a stereo lithographic format (STL) to be used in Flow-3D® (Fig. 2).

Different simulations were defined, at an initial phase, using different grid resolutions to achieve an adequate solution in terms of capturing the relevant flow details with acceptable computational CPU (central process unit) times. The final total number of cells used to discretize the domain was 180,918 of 0.20 m in size. Only one block was adopted.

Three physical processes were considered: gravity, turbulence model based on the well-known two-equation k-model, that has shown to provide reasonable approximations to many types of flows [32] and a generalized moving object (GMO) model to quantify the resulting forces and torques exerted by the fluid on the structure.

At the left open boundary, irregular incident wave conditions were imposed. The experimental wave condition was characterized by a significant wave height, $H_{1/3} = 0.29$ m and peak period, $T_p = 4.10$ s [31]. At the right boundary, a wall limit was adopted. In all other open boundaries, symmetry conditions were defined. As initial conditions, a fluid region was considered along the simulated channel with average elevation, d = 2.15 m. The fluid used in the simulations was water at 20° with null salinity ($\rho = 1000$ kg/m^3). In addition, as the bathymetry in the experimental model is formed by concrete, a roughness of 0.01 m [33] was considered.

3.2 Full-Scale Model

A full-scale model (10 times larger than the experimental model) was also considered for similar conditions to the scaled physical model ones, to compute the loads resulting from the interaction between fluid and the piers that support the structure, considering also different heights of the air gap. A set of piers with a diameter
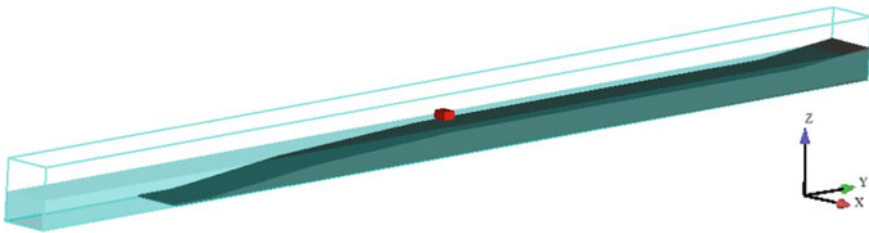
Fig. 2 Numerical model geometry
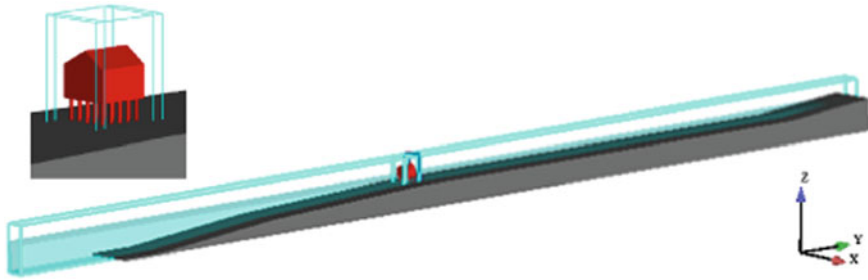
Fig. 3 Numerical model geometry and grid used to discretize the model domain

of 0.6 m was considered. Here too, several initial simulations were defined using different grid resolutions. It is important to minimize the total number of cells, but at the same time it is necessary to consider a sufficiently high spatial resolution to be able to simulate all the relevant flow patterns and all the details of the geometry with acceptable computational CPU times. Five blocks with different cell sizes were adopted throughout the domain (Fig. 3).

The total number of cells used to discretize the domain was 2,553,076 for a channel width of 13 m. The first block presented 845,460 cells of 0.6 m in size, the second block presented 15,180 cells of 0.4 m in size, the third block, which comprises the elevated coastal structure, presented 713,700 cells of 0.2 m in size, the fourth block presented 15,180 cells of 0.4 m in size and the fifth and final block presented 963,556 cells of 0.6 m in size.

The adopted wave type at the boundary was a stokes wave defined according to [34], characterized by the significant wave height, $H_{1/3} = 2.9$ m, $T_p = 12.9$ s, and d $= 21.5$ m. Three scenarios for the stillwater level were adopted: $-1-00$ m, 0.00 m, and 1.00 m in relation to the base of the coastal structure.

4 Results and Discussion

The calibration and validation of the model was performed supported by the results of horizontal and vertical wave forces on the elevated coastal structure obtained from the experimental results. This was achieved by modelling the elevated coastal structure as GMO. Figure 4 shows a detailed comparison of experimental results of horizontal and vertical forces and numerical results for the three air gaps a $= -0.10$ m, a $= 0.00$ m, and a $= 0.10$ m.

As can be observed, numerical results have a good approximation, compared to the experimental results. Comparing the maximum values of the horizontal and vertical forces, the average relative difference considering the three scenarios is 14.35% and 25.4%, respectively is 14.35% and 25.4%, respectively. This proves the excellent performance of the computational model in the simulation of this complex fluid–structure interaction problem.
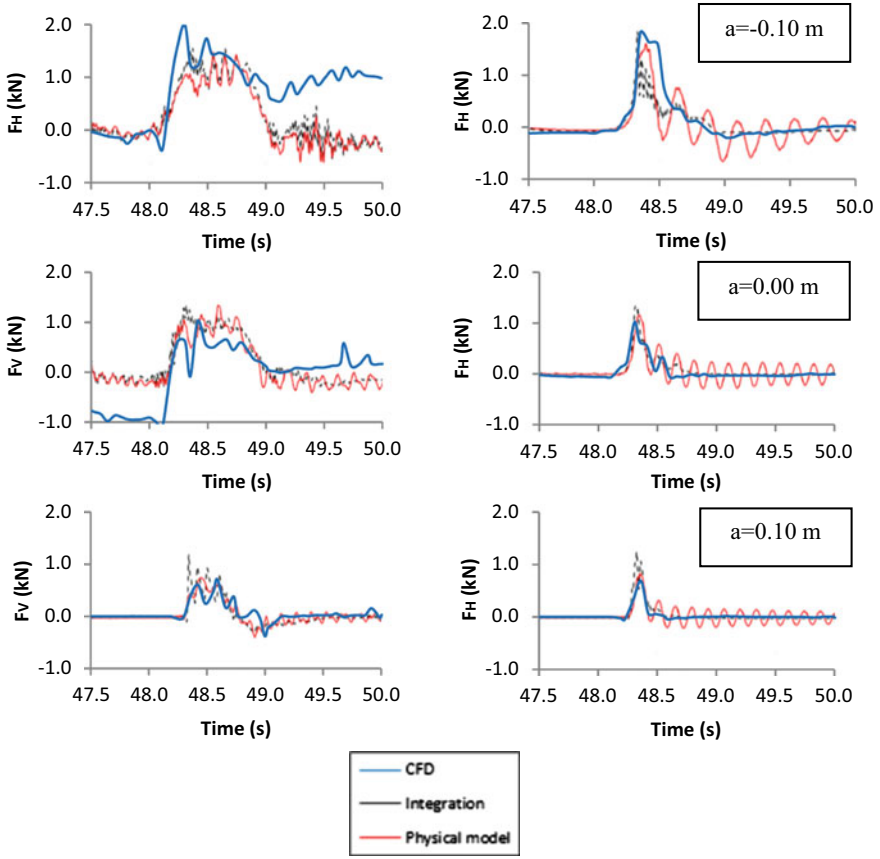
Fig. 4 Detailed time series of pressure integration (black dotted line) and load cell measurements (red solid line) obtained by [31] and model simulations (blue solid line) of horizontal (right) and vertical (left) forces for different air gaps: –0.10 m (top), 0.00 m (middle), and 0.10 m (bottom)

To assess the potential of the software to simulate a full-scale problem and the associated CPU times a similar problem was simulated. Figures 5 and 6 represent, respectively, the pressures and shear stresses that act on the piers that support the structure for different heights of the air gap. Two points located on the central pillar upstream of the channel were analyzed in detail considering different heights h = 0.00 m (red point), and h = 3.00 m (green point) (see heights in Fig. 1b).

From results presented in Fig. 5 (left) it can be seen that in addition to the pressure increasing with the depth, the pressure also increases as the air gap height decreased, for the same average elevation (d = 2.15 m). Consequently, the structure is more exposed to the dynamic actions of the waves. This is also confirmed when we analyze in detail the pressures acting over one of the piers of the structure, at the defined probes (Fig. 5 right side). The maximum pressure in probe 1 and 2 are, respectively, 17,622 Pa and 145,199 Pa for a = -–1.00 m and 149,470 Pa and 122,906 Pa for a
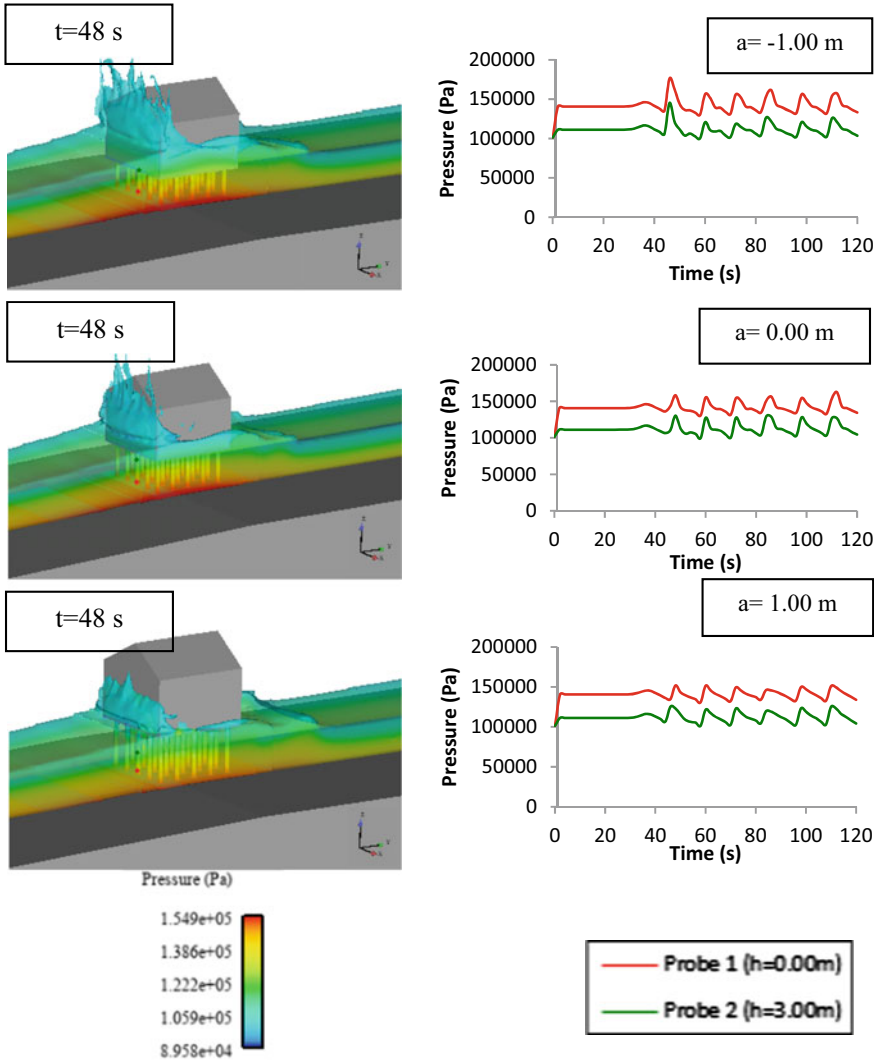
Fig. 5 Pressure results at the instant when the first wave hits the structure (left) and variation of the pressure over the simulation time (right) for different air gaps: –1.00 m (top), 0.00 m (middle), and 1.00 m (bottom)

= 1.00 m, which corresponds to a decrease of about 15% when the height of the air gap is 1.00 m.

Analyzing Fig. 6 on the left side, we see that when the structure is below the average water level (a = −1.00 m), the shear stress is maximum at the bottom of the channel (red point), unlike what happens when the air box is 0.00 m or 1.00 m, that
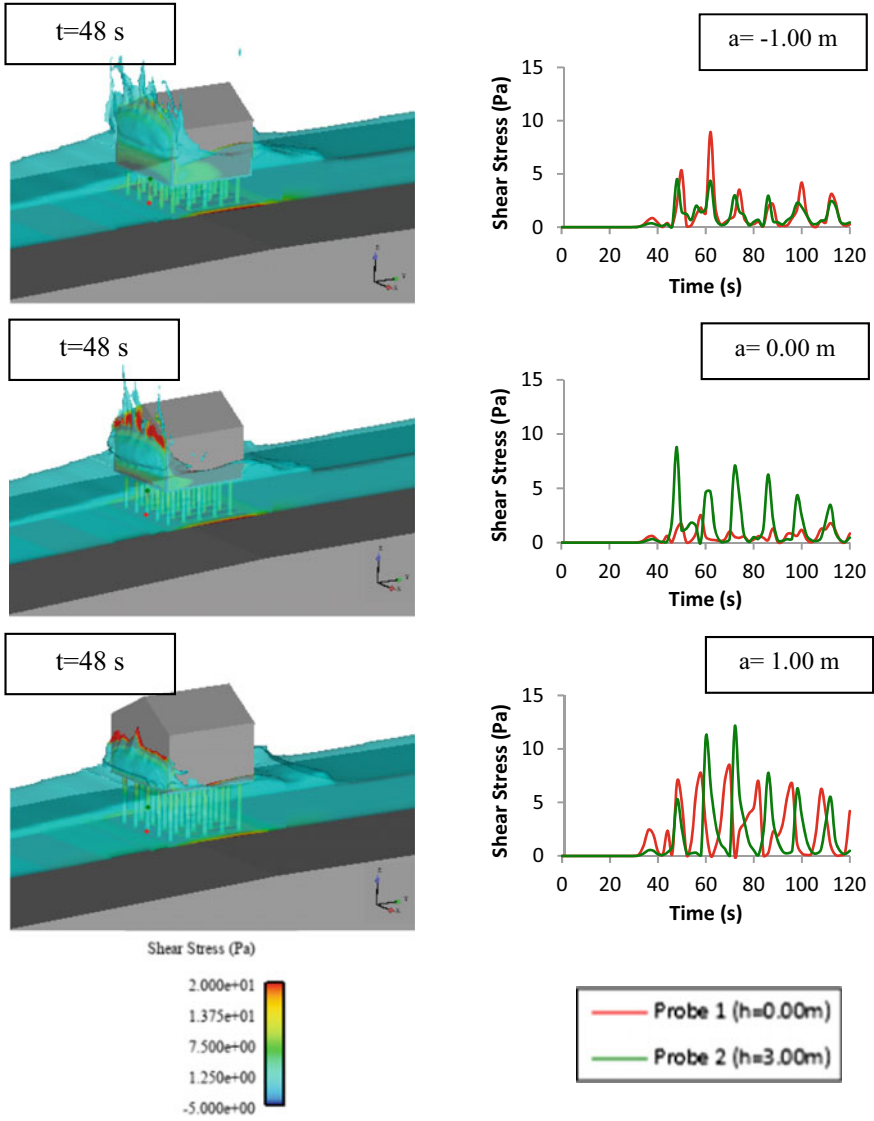
Fig. 6 Shear stress results at the instant when the first wave hits the structure (left) and variation of the shear stress over the simulation time (right) for different air gaps: −1.00 m (top), 0.00 m (middle), and 1.00 m (bottom)
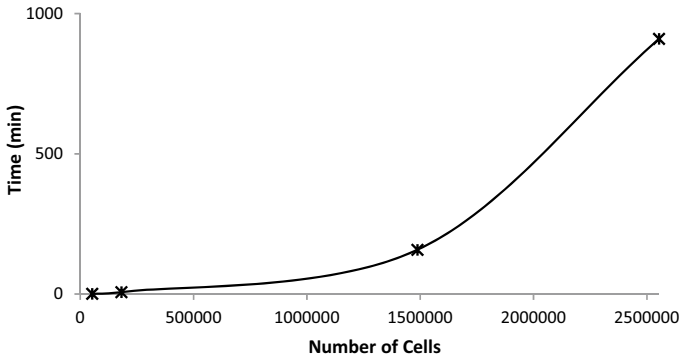
Fig. 7 CPU simulation times

the shear stress is maximum at the intersection area of the piers with the structure (green point).

In addition, the maximum shear stress on the structure's piers was obtained when the structure was positioned at 0.00 m in relation to the water level (Fig. 6 right side).

Finally, the results of the simulation CPU times versus number of cells are shown in Fig. 7.

The simulation time depend on the size and number of the cubic cells. The more discretized the domain the longer the simulation CPU time. Simulations were run in a CPU-4 Intel Core™ i7-6700 k @ 4.0 GHz workstation.

CPU times presented in Fig. 7 correspond to the simulations performed for the calibration of the numerical model, to simulate 60 s of hydrodynamic waves with different domains. It took an average of 7 min to simulate a domain with a cells number of 180,918 of 0.20 m in size (domain used to validate the model). For the same wave conditions, we can see that to simulate a domain approximately 8 times larger (number of cells 1,487,548 with 0.10 m in size) it would take on average 158 min. Regarding the full-scale model, 120 s of hydrodynamic waves were simulated. The simulation time, on average, lasted 910 min, that is, approximately 15 h.

5 Conclusions

Coastal structures are subject to hydrodynamic loads normally estimated through physical models. However, this methodology is subject to high costs and time-consuming procedures.

The adopted methodology for the quantification of the pressure loads on an elevated coastal structure, considering it as a GMO in Flow-3D® proved to be efficient, as evidenced by the obtained results when compared with experimental ones.

This work showed the potential of the Flow-3D® software for wave loads assessment on coastal structures at inundation risk. Obtaining wave loads through CFD tools is an important evolution not only in the assessment of the risks associated with this type of structures, especially during extreme events, but also in the structural analysis of future projects. With these results it is possible to couple these pressures and shear stresses as external actions in the numerical model to conduct the structural analysis in a relatively quick and economical way, and with a high degree of reliability. Through the obtained results it is concluded that the pressures can be reduced when the structure is elevated but it does not mean that the shear stresses are the lowest.

The accuracy of the results and the simulation time depend on the size and number of the cubic cells. It is important to minimize the total number of cells, but at the same time it is necessary to consider a sufficiently high spatial resolution to be able to simulate all the relevant flow patterns and all the details of the geometry. Thus, prior knowledge based on CPU simulation times becomes essential. Based on these results it is possible to predict simulation times for long/very long duration events, when a storm is expected to approach, for example. It is extremely important to have a compromise between the number of cells and the simulation time.

The CFD modelling tools, associated with the increase in computational capacity, allow to analyze the interaction between fluids and structures in a forecasting context. However, the CPU times for common workstations is still very long to be used in an operational forecasting platform. High performance computational resources should be used in this case, or a scaled numerical model approach followed, if wave loads have to be forecasted in real time.

References

1. Neumann B, Vafeidis AT, Zimmermann J, Nicholls RJ (2015) Future coastal population growth and exposure to sea-level rise and coastal flooding-a global assessment. PloS one, n. 10(3), p. X-X
2. Jones B, O'Neill BC (2016) Spatially explicit global population scenarios consistent with the Shared Socioeconomic Pathways. Environmental Research Letters, N. 11(8):1–10
3. Talbot J (2005) Repairing Florida's Escambia Bay Bridge. Associated Construction Publications, available online at http://www.acppubs.com/article/CA511040
4. Kennedy A, Rogers S, Sallenger A, Gravois U, Zachry B, Dosa M, Zarama F (2011a) Building destruction from wave and surge on the bolivar peninsula during hurricane Ike. J. Waterw. Port, Coast. Ocean Eng. 137 (3), 132–141
5. Tomiczek T, Kennedy A, Rogers S (2014) Collapse limit state fragilities of woodframed residences from storm surge and waves during hurricane Ike. J. Waterw. Port, Coast. Ocean Eng. 140 (1), 43–55

6. Dentale F, Donnarumma G, Pugliese Carratelli E (2014a) Simulation of flow within armour blocks in a breakwater. J Coast Res 30(3):528–536
7. Peregrine DH (2003) Water wave impact on walls. Annu Rev Fluid Mech 35:23–43
8. Cuomo G, Piscopia R, Allsop W (2011) Evaluation of wave impact loads on caisson breakwaters based on joint probability of impact maxima and rise times. Coast Eng 58(1):9–27
9. Faltinsen OM, Landrini M, Greco M (2004) Slamming in marine applications. J Eng Math 48(3–4):187–217
10. Peregrine DH. et al (2005) Violent water wave impact on a wall. In: Proceedings of 14th Aha Huliko Winter Workshop, Honolulu, Hawaii
11. Cuomo G, Tirindelli M, Allsop W (2007) Wave in deck loads on exposed jetties. Coast Eng 54(9):657–679
12. Azadbakht M, Yim SC (2015) Simulation and estimation of tsunami loads on bridge superstructures. J Waterw Port Coast Ocean Eng 141(2):20
13. Wiebe DM, Park H, Cox DT (2014) Application of the Goda pressure formulae for horizontal wave loads on elevated structures. KSCE J. Civ. Eng
14. Hayatdavoodi M, Seiffert B, Ertekin RC (2015) Experiments and calculations of cnoidal wave loads on a flat plate in shallow-water. J. Ocean Eng. Mar. Energy 1(1):77–99
15. Wei Z, Dalrymple RA (2016) Numerical study on mitigating tsunami force on bridges by an SPH model. J. Ocean. Eng. Mar. Energy 2(365):365–380
16. Bradner, C., Schumacher, T., Cox, D., Higgins, C.: Experimental Setup for a largescale bridge superstructure model subjected to waves. J. Waterw. Port, Coast. Ocean Eng. 137 (1), 3–11 (2011)
17. Xiao H, Huang W (2008) Numerical modeling of wave runup and forces on an idealized beachfront house. Ocean Eng 35(1):106–116
18. Do T, van de Lindt JW, Cox D (2016) Performance-based design methodology for inundated elevated coastal structures subjected to wave load. Eng Struct 117:250–262
19. Lara JL, Garcia N, Losada IJ (2006) RANS modeling applied to random wave interaction with submerged permeable structures. Coastal Eng 53(5–6):395–417
20. Meringolo DD, Aristodemo F, Veltri P (2015) SPH numerical modeling of wave–perforated breakwater interaction. Coast Eng 101:48–68
21. Al-Banaa K, Liu PLF (2007) Numerical study on the hydraulic performance of submerged porous breakwater under solitary wave attack. J Coast Res 50:201–205
22. Gomes, A., Pinho, J.L.S., Valente, T., Antunes do Carmo, J.S., V. Hegde, A.: Performance Assessment of a Semi-Circular Breakwater through CFD Modelling. J. Mar. Sci. Eng. 2020, 8, 226 (2020).
23. Flow Sciences Inc. Flow-3D User Manual, release 9.4, Santa Fe, NM, USA (2009).
24. Smith, H., Foster., D.L.: Modeling of flow around a cylinder over a scoured bed. J. Waterw., Port, Coastal, Ocean Eng.131(1),14–24 (2005).
25. Richardson JE, Panchang VG (1998) Three-dimensional simulation of scour-inducing flow at bridge piers. J Hydraul Eng 124(5):530–540
26. Jin J, Meng B (2011) Computation of wave loads on the superstructures of coastal highway bridges. Ocean Eng 38(17–18):2185–2200
27. Dentale F, Donnarumma G, Pugliese Carratelli E (2014b) Numerical wave interaction with tetrapods breakwater. Int. J. Nav. Arch. Ocean 6:13
28. Carratelli EP, Viccione G, Bovolin V (2016) Free surface flow impact on a vertical wall: a numerical assessment. Theor. Comput. Fluid Mech. 30(5):403–414
29. Cavallaro, L., Dentale, F., Donnarumma, G., Foti, E., Musumeci, R.E., Pugliese Carratelli, E.: Rubble mound breakwater overtopping: estimation of the reliability of a 3D numerical simulation, In: ICCE 2012, Interntional Conference on Coastal Engineering, Santander, Spain (2012).
30. Vanneste, D., Suzuki, T., Altomare, C.: Comparison of numerical models for wave over-toping and impact on storm return walls. In: ICCE 2014, International Conference on Coastal Engineering, Seoul, Korea (2014).

31. Park H, Tomiczek T, Cox DT, van de Lindt JW, Lomonaco P (2017) Experimental modeling of horizontal and vertical wave forces on an elevated coastal structure. Coast Eng 128:58–74
32. Isfahani AHG, Brethour JM (2009) On the Implementation of Two-Equation Turbulence Models in FLOW-3D; FSI-09-TN86; Flow Science: Santa Fe. NM, USA
33. Novais-Barbosa J (1985) Mecânica dos Fluidos e Hidráulica Geral Vol 1 e II Porto Editora, Porto
34. Le Méhauté B (1976) An Introduction to Hydrodynamics and Water Waves. Springer, Berlin/Heidelberg, Germany

Drought Analyses and Indices

Drought Risk Mapping in the North-West Region of Bangladesh Using Landsat Time Series Satellite Images

Sabrina Rashid Sheonty and Jannatul Nayeem

1   Introduction

Drought is a common hydrometeorological phenomenon [1]. It is regarded as a regional phenomenon whose characteristics vary from one climate region to another [2]. Meteorologically drought can be classified into three different types. They are permanent drought, seasonal drought, and contingent drought. Permanent drought is observed mainly in the arid climate zones where seasonal drought and contingent drought are more common around different parts of the world. Seasonal drought occurs because of the irregularities in rainy and dry seasons and contingent drought is caused by the irregularities in rainfall pattern and intensity. In Bangladesh, seasonal drought and contingent drought are most prominent which are observed mainly in pre-monsoon and post-monsoon periods.

Bangladesh is a disaster-prone country due to its topographic and socioeconomic factors. Various kinds of natural hazards such as floods, cyclones, earthquakes, droughts are quite common here. Though drought is one of the most common natural disasters in Bangladesh, it is the least understood natural hazard in Bangladesh due to its complex and unpredictable nature. It is quite difficult to predict the severity as well as the starting and ending of a drought. Moreover, the effects of drought may build up slowly over a substantial period of time and can last for a prolonged duration which makes it tough to understand the severity and duration of drought [3, 4]. Thus, time-to-time monitoring is necessary in order to be updated with the drought condition and make preparedness for the situation. Drought has become a common phenomenon in some parts of Bangladesh in the past few decades especially in the North-West region of Bangladesh. According to the National Water Management Plan (NWMP), occurrences of drought are considered a major water deficiency related issue in this region. Between 1960 and 1991, about 19 droughts have occurred in Bangladesh [4]. As an agricultural country, the impacts of droughts are detrimental to the economy

S. R. Sheonty (✉) · J. Nayeem
Military Institute of Science and Technology, Dhaka, Bangladesh

of Bangladesh. It can impose a significant threat on the food and water security of the country. Failure to be acquainted with the up-to-date information about the trend, duration, extent, and intensity of droughts can bring losses of crops, economy, and environment as well as add human sufferings. Moreover, climate change impacts can increase the severity of droughts in the future. In order to combat such a prominent threat, the risk assessment of droughts in this region has no alternative.

Remote sensing techniques have been used in different parts of the world to detect drought in recent times. In a study, drought assessment was done within the Flint Hills of Kansas and Oklahoma, United States, after analyzing MODerate resolution Imaging Spectroradiometer (MODIS), Normalized Difference Vegetation Index (NDVI), and Normalized Difference Water Index (NDWI) data from 2001 to 2005 [5]. In a recent study, the drought of the southern coastal region in Bangladesh was detected using Landsat time series satellite images [6]. Some efforts were also observed in the north-west region of Bangladesh to identify drought risk areas based on NDVI by using surface reflectance with 250 m resolution from MODIS satellite data [7]. But the main drawbacks of this study are the usage of low-resolution data (250 m), which is not good enough to capture the drought severity at the local level and assessment of drought-prone areas using only one index. Thus, this study attempts to use 30 m Landsat 7 and Landsat 8 satellite images to identify four drought indices NDVI, VCI, NDWI, and MNDWI to identify the extent of drought in the study area. Moreover, the temporal variation of drought in the north-west region of Bangladesh is also shown in this study from 2000 to 2020 with an interval of 5 years.

2   Study Area

This study area was chosen as the north-west region of Bangladesh, which is the most drought-prone area of Bangladesh. The study area covers two important divisions Rajshahi and Rangpur including 16 districts in total with an area of about 32,000 km^2. This area is located between 26°21 and 24° North latitudes and 88°17 and 89°41 East longitudes. The average seasonal rainfall of this area is about 1000 mm during the five monsoon months (June–October) which is lower than any other part of the country. The study area is shown in (Fig. 1).

3   Methodology

3.1   Data Collection

Landsat 8 and Landsat 7 satellite images were collected from the Earth Explorer database of USGS for this study [8]. Landsat 8 is the most recently launched Landsat satellite that was launched on February 11, 2013. Hence, Landsat 8 images are
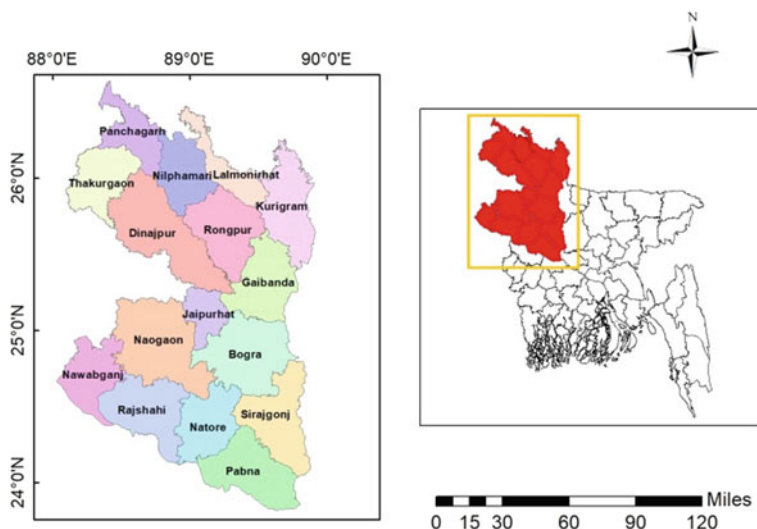
Fig. 1 Study area

Table 1 Details of Satellite images used for the study

Name of Satellite	Path/Row	Spatial Resolution (m)
Landsat 7 ETM + and Landsat 8 OLI and TIRS	138/042	30
	138/043	30
	139/042	30
	139/043	30

available only after 2013. Thus, for analysis of NDVI from 2000 to 2013, Landsat 7 images and from 2014 to 2020, Landsat 8 images of 30 m resolution were used. The scanlines from the images of Landsat 7 were removed using the Landsat Toolbox in ArcGIS. For each year, four scenes of Landsat imagery covering the complete north-west area of Bangladesh were used in this study. Images were primarily collected for the months of October to February to capture the intensity of drought at the dry season. Information about Landsat Images used in this study is given in Table 1.

3.2 Selection of Drought Indices

Different indices can be used to estimate the extent of drought. There are some meteorological drought indices (such as Standardized Precipitation Index (SPI)) which contain information only about rainfall or soil moisture but they do not contain much spatial information where satellite derived drought indices can provide drought related spatial information quite precisely if derived from high-resolution

Table 2 Drought indices

Indices	Remarks
NDVI	This value can vary from −1 to + 1. Usually, healthy vegetation has positive and water bodies have negative values
NDWI	Water bodies usually have positive values and vegetation and soil usually have zero or negative values
MNDWI	The values lie between −1 to + 1. Higher value indicates high vegetation water content
VCI	It is expressed in percentage. Lower values indicate severe cases of drought

satellite data. Moreover, meteorological or climate-based indices depend on data collection methods of different stations. Also, they can be affected by sparsely distributed weather stations in some areas. In this context, satellite-based drought indices are preferable to assess the drought condition. Thus, four satellite derived indices: Normalized Difference Vegetation Index (NDVI), Normalized Difference Water Index (NDWI), Modified Normalized Difference Water Index (MNDWI) and Vegetation Condition Index (VCI) are selected for this study to assess the drought condition of North-West region of Bangladesh. These indices are calculated using Eq. (1), (2), (3), (4).

$$NDVI = \frac{NIR - RED}{NIR + RED} \tag{1}$$

$$NDWI = \frac{NIR - SWIR}{NIR + SWIR} \tag{2}$$

$$MNDWI = \frac{GREEN - SWIR}{GREEN + SWIR} \tag{3}$$

$$VCI = \frac{NDVI - NDVI_{min}}{NDVI_{max} - NDVI_{min}} \tag{4}$$

The values of these indices indicate different vegetation and drought condition. They are mentioned in Table 2

3.3 Generation of Drought Risk Map

At first, the satellite images need to be georeferenced for any analysis in ArcGIS. As the Landsat satellite images obtained from USGS were already georeferenced and projected in WGS84 UTM zone-46 datum thus, no further georeferencing was required in this case. For each year, four scenes of Landsat images were projected and the indices were calculated for each year. Different tools of ArcGIS such as "Raster Calculator", "Extraction by mask", "Spatial analyst tool", etc., were used for this

analysis. The indices were calculated using different Landsat bands. For NDVI of 2001 to 2013, Landsat 7 Band 3 Visible and Band 4 Near-Infrared spectral band and NDVI of 2014 to 2020, Landsat 8 Band 4 Red and Band 5 Near-Infrared spectral band were used for this purpose. For the calculation of NDWI from 2000 to 2013, Landsat 7 Band 4 Near-Infrared Spectral Band and Band 5 Short-Wave Infrared Band and for NDWI from 2014 to 2020 Landsat 8 Band 5 Near-Infrared Spectral Band and Band 6 Short-Wave Infrared Band were used. In the case of MNDWI calculation, Landsat 7 Band 2 Green and Band 5 Short-Wave Infrared Band were used for the years 2000 to 2014. Similarly, for the years 2014 to 2020, Landsat 8 Band 3 Green and Band 5 Short-Wave Infrared Band were used. Drought risk maps of these four indices are shown in (Fig. 2).

4 Results and Discussions

One of the prime objectives of this study is to identify the change in drought conditions in the past two decades. Thus, NDVI, NDWI, MNDWI, and VCI maps are generated from 2000–2020 with an interval of 5 years using Landsat 7 and 8 images. In order to capture the change between 2000 and 2020, the maps of different indices from 2000 to 2020 are shown in (Fig. 3).

From the drought risk maps of different indices, it was noticed that six districts of the central, northern, and southwestern parts of the study area: Thakurgaon, Panchagarh, Dinajpur, Nilphamari, Gaibandha, and Nator are most prone to drought. The area covering low, moderate, and high drought risks are listed in Tables 3, 4, 5 and 6 with the help of NDVI, NDWI, MNDWI, and VCI for the north-west zone of Bangladesh from 2000 to 2020. There was some variation observed in the percentage of areas for these indices in different years. This phenomenon was also observed in past studies. In a study on drought analysis of the coastal region of Bangladesh, the authors described this as a result of the difference in accuracy level of different indices where they showed NDVI and VCI give more accurate results than the other indices [6].

Apart from that, the results show similar temporal changes over the past two decades. It was noticed that in the first half of the decade the drought severity was more than the second half. In the first 5 years of the time period, the overall drought condition was quite severe especially the worst drought condition was seen in the year 2005 where in 2015 an overall low drought condition was observed in comparison to the other years.

NDVI Map of NW region of Bangladesh in 2020

i. NDVI

NDWI Map of NW region of Bangladesh in 2020

ii. NDWI

MNDWI Map of NW region of Bangladesh in 2020

iii. MNDWI

VCI Map of NW Region of Bangladesh in 2020

iv. VCI
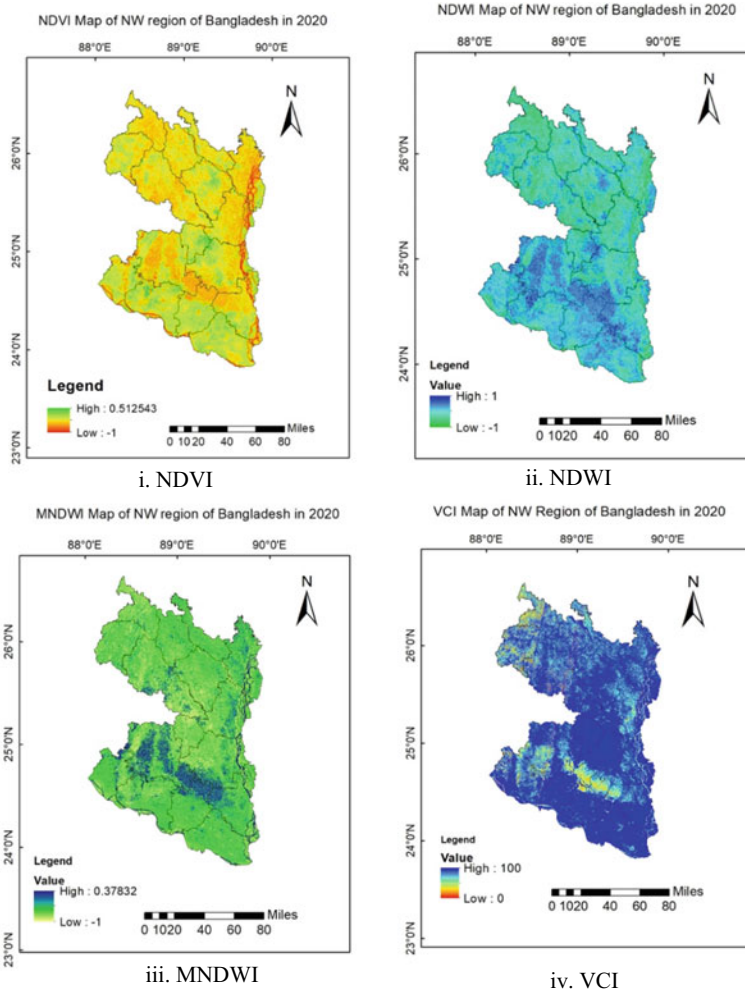
Fig. 2 Drought risk maps of various indices

5 Conclusion

Drought is one of the most common natural disasters of Bangladesh and accurate identification of drought-prone areas is a first step to build resilience against it. In this study, remote sensing and GIS application have been used to detect the spatio-temporal change in drought condition of the north-west region which is the most drought-prone area of Bangladesh. Four satellite-derived drought indices were estimated from Landsat 7 and 8 satellite images for identifying drought risk in the study area for the past two decades. The study reveals that six districts of the central,

Index	2000	2005	2010	2015	2020
NDVI					
NDWI					
MNDWI					
VCI					

Legend

High Drought	
Moderate Drought	
Low or No Drought	
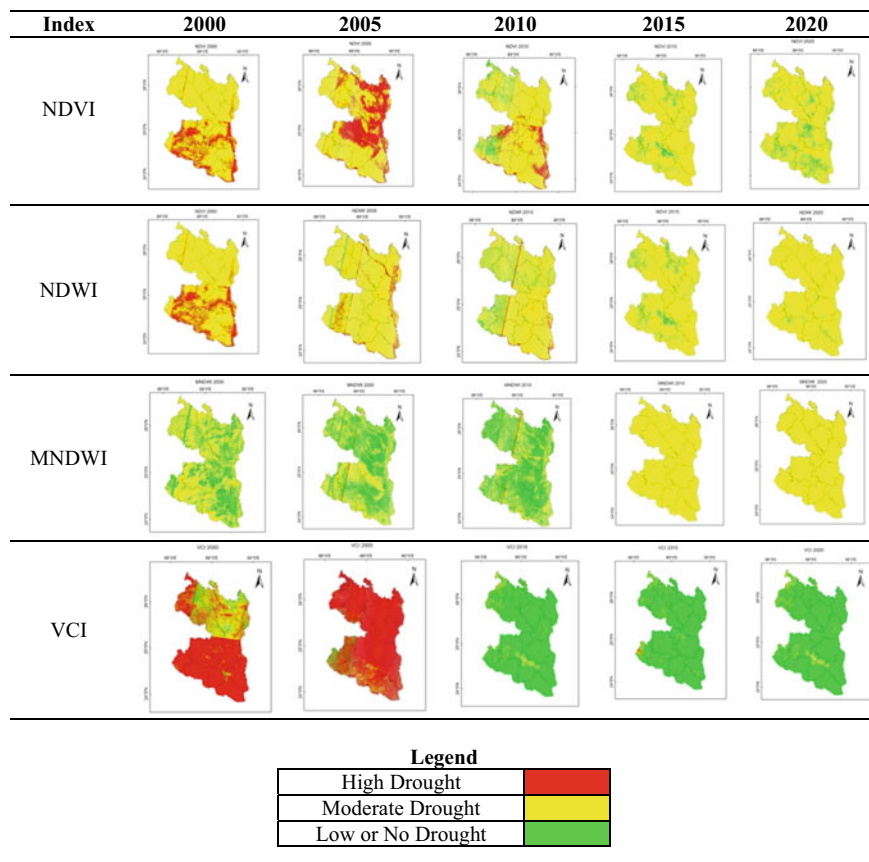
Fig. 3 Drought risk maps from 2000–2020

Table 3 Amount of area in different NDVI ranges over the past two decades

Classification	NDVI value	Area at 2000 (%)	Area at 2005 (%)	Area at 2010 (%)	Area at 2015 (%)	Area at 2020 (%)
High	-1 to -0.3	15.68	33.28	9.19	0	0.003
Moderate	-0.3 to 0.3	84.29	66.11	84.74	95.11	92.21
Low	0.3 to 1	0.03	0.61	6.07	4.89	7.79

northern, and southwestern parts of the study area-Thakurgaon, Panchagarh, Dinajpur, Nilphamari, Gaibandha, and Nator are most susceptible to drought. Apart from that, the temporal analysis indicates the first half of the decade experienced drought severity more than the second half. It was also found that the most severe drought was experienced in 2005 and the lowest drought severity was observed in 2015.

Table 4 Amount of area in different NDWI ranges over the past two decades

Classification	NDWI value	Area at 2000 (%)	Area at 2005 (%)	Area at 2010 (%)	Area at 2015 (%)	Area at 2020 (%)
High	−1 to −0.3	3.45	6.97	3.72	0.002	0.004
Moderate	−0.3 to 0.3	94.36	90.74	87.7	99.96	99.17
Low	0.3 to 1	2.20	2.29	8.58	0.034	0.83

Table 5 Amount of area in different MNDWI ranges over the past two decades

Classification	MNDWI value	Area at 2000 (%)	Area at 2005 (%)	Area at 2010 (%)	Area at 2015 (%)	Area at 2020 (%)
High	−1 to −0.3	0.02	1.90	2.27	0.003	0.003
Moderate	−0.3 to 0.3	71.55	54.99	42.44	99.95	99.96
Low	0.3 to 1	28.43	43.11	55.29	0.044	0.037

Table 6 Amount of area in different VCI ranges over the past two decades

Classification	VCI value	Area at 2000 (%)	Area at 2005 (%)	Area at 2010 (%)	Area at 2015 (%)	Area at 2020 (%)
High	0–33	64.88	88.32	2.69	1.03	1.07
Moderate	33–67	28.64	8.22	16.53	9.37	11.70
Low	67–100	6.48	3.46	80.78	89.60	87.23

References

1. Hayes, M.J., Svoboda, M.D., Wardlow, B.D., Anderson, M.C., Kogan, F.: Drought monitoring. In: Wardlow, B.D., Anderson, M.C., Verdin, J.P. (Eds.), Remote Sensing of Drought: Innovative Monitoring Approaches. CRC Press, New York (2012)
2. Iglesias, A., Garrote, L., Cancelliere, A., Cubillo, F. and Wilhite, A. D.: Coping with Drought Risk in Agriculture and Water Supply Systems, Drought Management and Policy Development in the Mediterranean. Advances in Natural and Technological Hazards Research, 2009th edn, Springer, Heidelberg (2009)
3. Narasimhan, B., Srinivasan, R.: Development and evaluation of soil moisture deficit index and evapotranspiration deficit index for agricultural drought monitoring (2005) Agric For Meteorol 133(1):69–88
4. Smith K (2000) Environmental Hazards: Assessing Risk and Reducing Disaster, 3rd edn. Routledge, Taylor and Francis Group, London and New York
5. Mirza, M.Q., Paul, S.: Prakritik Durgojob O Bangladesh Paribesh (Natural Disaster and Environment in Bangladesh), Centre for Environmental Studies and Research, Dhaka (1992).
6. Gu Y, Brown JF, Verdin JP, Wardlow B (2007) A five-year analysis of MODIS NDVI and NDWI for grassland drought assessment over the central Great Plains of the United States. Geophys Res Lett 34(6):L06407

7. Ahmed, A., Esha, E.J., Shahriar, A. S. M. S., Alam, I.: Drought Monitoring in the Coastal Belt of Bangladesh Using Landsat Time Series Satellite Images. In: Pradhan B. (eds) GCEC 2017. GCEC 2017. Lecture Notes in Civil Engineering, vol 9, pp 941–956. Springer, Singapore (2019).
8. Murad, H.: Agricultural and meteorological drought assessment using remote sensing and GIS in North - West region of Bangladesh. In: BUET Central library, Dhaka (2010). BUET central Library homepage, http://lib.buet.ac.bd:8080/xmlui/handle/123456789/4155, last accessed 2020/12/21.
9. USGS EarthExplorer homepage, https://earthexplorer.usgs.gov/. last accessed 2020/12/21

Quantification of Drought Condition Using Drought Indices: A Review

Rashmi Singh, Madhuri Kumari, Sonal Bindal, and Ila Gupta

1 Introduction

Droughts are a natural part of the climate and can occur in any climate regime, including deserts and rainforests, all over the world. On a year-to-year basis, draughts are one of the most expensive natural hazards; their effects are severe and pervasive, impacting many economic sectors and individuals at any one time. Usually, the hazard footprints of droughts are greater than those for other threats, typically limited to floodplains, coastal areas, storm tracks, or fault zones. The slow onset of droughts gives time to track changes in precipitation, temperature, and the overall condition of surface water and groundwater sources in an area.

Preparedness and preparation to deal with the adverse effects of a drought occurrence depend on the degree, severity, and length of the knowledge. This information can be collected by drought monitoring and forecasting, which is typically achieved using drought indices that provide decision-makers with quantitative information on the characteristics of drought. Several indices have been proposed for drought characterization such as Deciles [1], Crop Moisture Index [2], Palmer Drought Severity Index [3], Standardized Precipitation Index [4], Soil Moisture Deficit Index [5], Reconnaissance Drought Index [4].

Based on the applicability in the region and the input data availability, drought indices are selected for the purpose. Ease of use along with authenticity and extendibility (application across long time span) are also considered while selecting

R. Singh · M. Kumari (✉)
Department of Civil Engineering, Amity University Uttar Pradesh, Noida, Uttar Pradesh, India
e-mail: mkumari@amity.edu

S. Bindal
National Institute of Disaster Management, Ministry of Home Affairs, Govt. of India, New Delhi, India

I. Gupta
Amity School of Architecture and Planning, Amity University, Gurugram, India

231

the suitable set of indexes. Depeng et al. [6] performed agricultural and meteorological drought assessments in Northeast China using the remote sensing data and historical observations. For assessing meteorological drought, they used Standardized Precipitation Index (SPI) and Standardized Precipitation Evapo-Transpiration Index (SPEI) at 1-, 3-, and 6-month time scales. Alijianian et al. [7] and Vidhya et al. [8] also employed SPI at time series 1-, 3-, and 6-month for monitoring meteorological drought while Rong et al. [3], Kaiwei et al. [9] used SPEI at 1-, 3-, and 6-month time scales for assessment.

Depeng et al. [6] also conducted an agricultural drought assessment and used Combined Deficit Index (CDI) using 3 months rainfall deficit and NDVI monthly deficit. The CDI was later validated using crop yield data, LST, and evapotranspiration data. Figure 2 shows the flowchart of the entire process.

A new approach was adopted by Alijianian et al. [7] for obtaining long-term satellite-derived high-resolution precipitation data for Iran. These are termed as Satellite rainfall estimates (SREs) datasets, which provide long-term data, at least 30 years, mandatory for drought analysis. Alijianian et al. [7] used PERSIANN-CDR and MSWEP as SREs for obtaining precipitation data and used it for computation of SPI and compared the result with that obtained from gauged station data. It was found that, for shorter time series, i.e., for SPI-1 and SPI-3, SREs yield a greater number of drought incidences compared to gauged rainfall data. Although, for a longer time duration, i.e., SPI-6 and SPI-12, the results were concurrent (for SREs and gauged data). Also, among the two SREs used, MSWEP was more effective than the PERSIANN-CDR. Both SREs successfully captured the historic drought incidences well.

Sahana et al. [10] carried out the first ever country-wide drought assessment for India, with over 30 meteorological divisions. For this, Multivariate Structured Drought Index (MSDI) was used to evaluate the drought conditions caused by simultaneous precipitation and soil moisture shortages. It was done to study the spatial and historical extent of the 2015 drought. Copula-based distribution was used to obtain (Severity-Duration-Frequency) SDF curve, which was then used to prepare the drought map for the country.

Although SPI [4] is widely used as a meteorological drought index and is being recommended by WMO (2009) as the main index for meteorological drought assessment, it has been used in many studies for comparing with the agricultural drought index. Dutta et al. [11] used SPI along with the rainfall anomaly index and crop yield index for checking the results of the Vegetation Condition Index (derived from NDVI) for agricultural drought. This showed good connectivity between the results and gave a clear picture of drought occurrences in the state of Rajasthan for the year 2002. A similar approach was adopted by Vidhya Lakshmi et al. [8] in which, NDVI and NDWI are used to study the agricultural drought in the Namakkal district of Tamil Nadu, and SPI is then used to consider the years in which the region has been susceptible to drought. Thus, this gives a better check for agricultural drought occurrences too.

A new index was used by Soares et al. [12] for agricultural drought monitoring. It used usual SPI-1, -3, -12 as meteorological index while for agricultural drought,

Soil Moisture Agricultural Drought Index (SMADI) [13, 14] was used which uses soil moisture data, surface temperature and vegetation data derived using Remote Sensing products. SMADI has proved to be very efficient for monitoring drought, as it uses multiple indicators which make the assessment more efficient covering all the possible indicators.

2 Types of Drought

In the natural climate cycle, drought is a prolonged dry period that can occur anywhere in the world. Drought is a normal feature of climate and its recurrence is inevitable (Mishra and Desai 2005). It is a gradual on-set phenomenon caused by a lack of precipitation. In general, long-term deficiency in moisture, whether in the form of precipitation, soil moisture deficiency, or surface water and groundwater drying, is termed as drought. The susceptibility to drought is enhanced by compounding factors, such as poverty and inadequate land use. There can be many consequences on the health of the population when drought causes water and food shortages, which can increase morbidity and result in death [15].

So far, several definitions have been suggested for drought, but each is viewed from a particular point of view. Since all aspects of life and multiple parts of society, particularly the natural environment, are directly or indirectly affected by drought, understanding this definition will enable practitioners and policy-makers to effectively manage different parts of the economy.

Based on the cause of the occurrence, drought is classified into three broad categories: Meteorological drought, Hydrological drought, and Agricultural drought. Figure 1 shows the drought propagation leading to different drought types.

2.1 Meteorological Drought

This form of drought is defined when the rainfall is less than the long-term normal of that area. This deficit in precipitation, reaching a certain level, is defined as meteorological drought. According to the Indian Meteorological Department (IMD), when the rainfall in an area is less than 25% of the long-term average value, it is said to be under a meteorological drought situation. When the deficiency is 26–50%, it is termed as moderate drought, and when the shortfall is above 50% it is a severe drought.
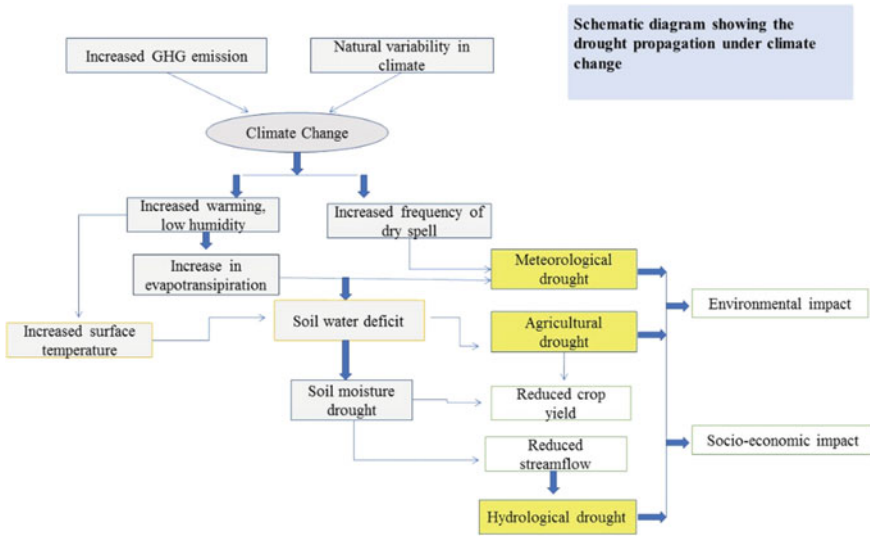
Fig. 1 Drought Propagation under climate change leading to different types of drought

2.2 Hydrological Drought

Hydrological drought is a consequence of meteorological drought prevailing in an area. It is defined as deficiency in the surface water (river, lake, pond, etc.) and sub-surface water (groundwater) leading to water shortage in an area. Climate variations serve as the primary factor for assessing the magnitude of the physical and natural basis of this drought. In addition, human activities such as changes in land use, land erosion, and building of dams have effects on the characteristics of the basin as well as the frequency and severity of hydrological drought.

2.3 Agricultural Drought

Meteorological and hydrological droughts typically cause agricultural droughts and occur when soil moisture and rainfall are insufficient during the crop growing season, causing severe crop stress, and wilting. In India, agricultural drought is announced when the rainfall deficit of more than 50% prevails for 4 consecutive weeks, or a weekly rain of less than equal to 5 cm in Kharif season or else for 6 weeks in a row during the rest of the year.

3 Drought Monitoring Using Indicators

The magnitude and duration of the drought are represented by an index according to the indicators of the drought in question. An index unifies various meteorological and hydrological parameters into a single numerical value or formula, including precipitation, temperature, evapotranspiration, runoff, and other water supply indicators, and presents a brief picture of decision-making. Many drought indices have been developed and used by meteorologists and climatologists around the world over the years. Those ranged from basic indices such as the percentage of normal rainfall and percentiles of precipitation to more nuanced indices such as that of Palmer Drought Severity Index. The authorities or public and private committees take steps to determine and respond to drought using these indices.

3.1 Selection of Drought Indices

There is no single index or measure that can account for and be generalized to all forms of droughts and climate regimes affected by droughts. The drought index should or must meet certain criteria to serve best for the purpose [16]. Some of these criteria are mentioned below:

- To activate effective communication and coordination of drought response or mitigation measures, the indicators/indices must allow for timely identification of drought.
- To assess drought emergence and termination, the indicators/indices must be climate, space, and time sensitive.
- The data source needed for the index must have a long record set available that can provide a clear historical and statistical reference to planners and decision-makers.
- The ease with which, the indices can be implemented.
- The index must be applicable to the drought in question.
- It is important to set up an index to track all aspects of hydrological or climatic cycles and not just droughts.

Based on these criteria, indices are selected to yield the best possible result. Either single index or multiple indices can be selected for drought monitoring.

3.2 Methods for Drought Monitoring

Methods used for drought monitoring are mainly classified into five groups as shown in Fig. 2.
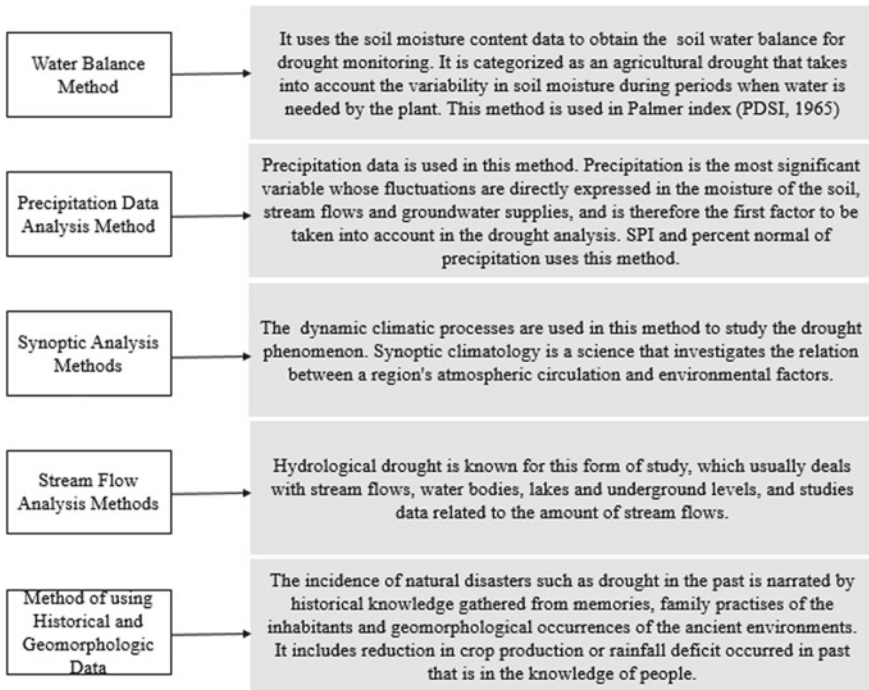
Fig. 2 Methods for drought monitoring

3.3 Drought Indices

3.3.1 Decile

This index was developed by Gibbs and Maher in 1967. Decile index is a basic mathematical approach and uses only one indicator, i.e., precipitation for the calculation. Due to its easy computation and requiring less data, the Deciles index was selected as a meteorological index for drought monitoring by the Australian Drought Watch System (Australian Bureau of Meteorology). Long-term precipitation record of a region is used to obtain the precipitation rank by dividing it into 10% parts [1, 17]. The first decile consists of the values of the lowest 10% precipitation while the fifth one is the median. This index can indicate drought as well as wet conditions. Table 1 shows the classes in which deciles are grouped [18]:

Advantage. A single indicator used (hence simple)—Used for both, wetter than normal and drier than a normal condition—Flexible timescale.

Limitation. Long period record is required—The impact of other meteorological factors like temperature is not considered for drought.

Table 1 Decile group for drought classification

Decile class	Percentage	Category
1–2	Lowest 20%	Much below normal
3–4	Next lowest 20%	Below normal
5–6	Mid 20%	Near to normal
7–8	Next highest 20%	Above the normal
9–10	Highest 20%	Much above the normal

3.3.2 Standardized Precipitation Index: SPI

Since shortfall in precipitation has different effect on various water resources like soil moisture, surface water, and groundwater. American scientists, T.B. McKee, N.J. Doesken [19], and J. Kleist, considered this and developed SPI in 1993 [15]. SPI is a much simpler index to use and it has one input parameter, i.e., precipitation, which makes its computation easy. The use of SPI has been proved to be equally effective for the analysis of dry as well as wet cycles globally. More than 70 countries are using SPI for monitoring drought [15]. In 2009, the World Meteorological Organization (WMO) recommended the SPI as the key index of meteorological drought [20, 21].

The precipitation record needed to compute SPI must be of at least 30 years. SPI as an index provides the benefit of working even with missing data, although the obtained result will vary from the actual one. Since SPI was designed keeping in mind, the impact of rainfall deficit (or drought) on different water resources, the multiple timescales for which SPI is calculated give an idea of the impact on various resources. For SPI-1, -3, -6, soil moisture conditions react to precipitation anomalies while the response of surface water and groundwater is seen for SPI-12 and above. Table 2 shows the SPI values given by McKee and others in 1993. *Advantage.* Simple computation—Flexible timescale—Provides drought early warning (DEW)—access to drought severity—accepts data with missing values—consistent spatially.

Limitation. Impact of other factors like temperature and soil moisture is not considered on drought—Evapotranspiration/potential evapotranspiration (ET/PET) cannot be calculated—Values change based on preliminary data.

Table 2 SPI classification

SPI	Category
$\geq +2.0$	Extremely wet
1.5–1.99	Very wet
1.0–1.49	Moderately wet
-0.99 to $+0.99$	Near to normal
-1.0 to -1.49	Moderate drought
-1.5 to -1.99	Severe drought
≤ -2.0	Extreme drought

3.3.3   Standardized Precipitation Evapotranspiration Index: SPEI

A relatively new index was developed by Vicente-Serrano et al. [22] to meet the limitations of SPI. It is very simple to compute the SPEI and it is based on the original method for calculating the SPI, the only difference being the use of temperature along with precipitation for SPEI calculation. The requirement of multiple indicators makes it somewhat complex, although, computation complexity is minimal. Missing data are not entertained which makes a difference from SPI [22]. Code/program required for the computation is readily accessible.

The SPEI measures the difference between precipitation and PET. This illustrates a basic climate water balance that is measured to obtain the SPEI at various time scales. It is represented by values which contain a scale for dry as well as wet condition. The same as SPI, it can be calculated over multiple time scales from 1 to 48 months or more. It is actively used in Peru and Switzerland.

Advantage. Usage of temperature data along with precipitation—Applicability of output in all climatic regions.

Limitation. Missing data are not entertained—Being a monthly indicator, drought conditions that grow rapidly cannot be easily detected.

3.3.4   Palmer Drought Severity Index: PDSI

PDSI is the very first detailed drought index developed by Palmer in 1965 and an efficient instrument for long-term drought determination. It is a meteorological drought index. Using monthly temperature and precipitation data, it is calculated along with information on the ability of the soil to retain water [16]. This index is calculated effectively on monthly basis (distinctly 9); however, it does not account for the short duration drought, usually of weekly scale. It can capture the fundamental impact of global warming on drought through changes in potential evapotranspiration, as it uses temperature data and a physical water balance model (soil moisture's demand and supply model) [23]. Table 3 shows different index categories given by Palmer.

Advantage. Effectively determines long-term drought—Provides historical aspect of prevailing condition (spatio-temporally)—Provides drought early warning (DEW)—Access to drought severity.

Limitation. Lacks functionality with multi-timescale—Cannot be calculated over wider range of climate—Arbitrary selection of values used for drought quantification has little scientific meaning and is region specific—snowpack, frozen ground is not included, and all the precipitation is considered as rain, therefore, it is ineffective in regions where snow occur—widely used in the United States, but has minimal acceptance in other countries—Natural time taken between rainfall and runoff is not considered—Runoff is not considered until the soil layer is saturated, therefore, runoff remains underestimated [24].

Table 3 PDSI-based drought category

PDSI value	Category
≤−4.0	Extreme drought
−3 to −3.99	Severe drought
−2 to −2.99	Moderate drought
−1 to −1.99	Mild drought
−0.5 to −0.99	Incipient drought
−0.49 to +0.49	Near normal
0.5–0.99	Incipient wet spell
1–1.99	Slightly wet
2–2.99	Moderately wet
3–3.99	Very wet
≥4.0	Extremely wet

3.3.5 Self-Calibrated Palmer Drought Severity Index: SC-PDSI

The major drawback of PDSI was its spatial inconsistency, which made it difficult for its application in various locations. To circumvent this limitation, self-calibrated PDSI was introduced in 2004 by Wells, N., S. Goddard, and M.J. Hayes. The sc-PDSI calibrates the behavior of the index automatically at any place by substituting dynamically determined values for empirical constants in the index computation [25]. This make is consistent for different locations. For each station and changes based on the location's climate regime, the self-calibrating nature of sc-PDSI is created. It has scales that are wet and dry [26]. It can be used for all the 3 types of drought: meteorological, hydrological, and agricultural.

Advantage. Spatially consistent and comparable—flexible timescale.

Limitation. It shares the same limitation as PDSI, i.e., snowpack, frozen ground is not included in computation—Natural time taken between rainfall and runoff is not considered.

4 Conclusion

Detrimental effects of drought have long been observed in all regions, a condition arising from both climate change and human activity, and humanity's inability to cope with this crisis has been seen so far. In recent years, the arid and semi-arid regions have experienced several drought and below average records of precipitation, resulting in irreversible harm, particularly in the agricultural sector. It is now, a need of the hour to bring a check to this accelerating drought years. Drought monitoring, using modern indices to forecast the beginning and end of the drought season, severity, and other

characteristics, is, therefore, considered important in order to establish the necessary pre-occurrence drought management steps.

References

1. Gibbs WJ, Maher JV (1967) Rainfall deciles as drought indicators. Bureau Meteorol Bull 48. Commonwealth of Australia, Melbourne, Australia
2. Palmer WC (1965) Meteorological drought. Research Paper No. 45. US Weather Bureau, Washington, DC
3. Zhang R, Chen Z-Y, Xu L-J, Ou C-Q (2019) Meteorological drought forecasting based on a statistical model with machine learning techniques in Shaanxi province, China. Sci Total Environ 665:338–346, ISSN 0048-9697. https://doi.org/10.1016/j.scitotenv.2019.01.431
4. McKee TB, Doesken NJ, Kleist J (1993) The relationship of drought frequency and duration to time scales. In: Proceedings of the 8th conference on applied climatology, Anaheim, CA. Boston, MA, American Meteorological Society
5. Narasimhan B, Srinivasan R (2005) Development and evaluation of Soil Moisture Deficit Index (SMDI) and Evapotranspiration Deficit Index (ETDI) for agricultural drought monitoring. Agric For Meteorol 133(1):69–88. https://doi.org/10.1016/j.agrformet.2005.07.012
6. Zuo D, Cai S, Xu Z, Peng D, Kan G, Sun W, Pang B, Yang H (2019) Assessment of meteo-rological and agricultural droughts using in-situ observations and remote sensing data. Agric Water Manage 222:125–138, ISSN 0378-3774. https://doi.org/10.1016/j.agwat.2019.05.046
7. Alijanian M, Rakhshandehroo GR, Mishra A, Dehghani M (2019) Evaluation of remotely sensed precipitation estimates using PERSIANN-CDR and MSWEP for spatio-temporal drought assessment over Iran. J Hydrol 579(124189), ISSN 0022-1694
8. Vidhya Lakshmi S, Ramalakshmi M, Krishnappa Rakshith R, Christobel MJ, Kumar PP, Priyad-harshini B, Kumar PR (2020) An integration of geospatial technology and standard precipitation index (SPI) for drought vulnerability assessment for a part of Namakkal district, South India. Mater Today Proc 33(1):1206–1211, ISSN 2214-7853. https://doi.org/10.1016/j.matpr.2020.08.157
9. Li K, Tong Z, Liu X, Zhang J, Tong S (2020) Quantitative assessment and driving force analysis of vegetation drought risk to climate change: methodology and application in Northeast China. Agric Forest Meteorol 282–283 (107865), ISSN 0168-1923. https://doi.org/10.1016/j.agrformet.2019.107865
10. Sahana V, Sreekumar P, Mondal A, Rajsekhar D (2020) On the rarity of the 2015 drought in India: a country-wide drought atlas using the multivariate standardized drought index and copula-based severity-duration-frequency curves. J Hydrol Region Stud 31(100727), ISSN 2214-5818. https://doi.org/10.1016/j.ejrh.2020.100727
11. Dutta D, Kundu A, Patel NR, Saha SK, Siddiqui AR (2015) Assessment of agricultural drought in Rajasthan (India) using remote sensing derived Vegetation Condition Index (VCI) and Stan-dardized Precipitation Index (SPI). Egyp J Rem Sens Space Sci 18(1):53–63, ISSN 1110-9823. https://doi.org/10.1016/j.ejrs.2015.03.006
12. Souza AGSS, Neto AR, de Souza LL (2021) Soil moisture-based index for agricultural drought assessment: SMADI application in Pernambuco State-Brazil. Rem Sens Environ 252(112124), ISSN 0034-4257. https://doi.org/10.1016/j.rse.2020.112124
13. Sánchez N, Gonzalez-Zamora A, Martinez-Fernández J, Piles M, Pablos M (2018) Inte-grated remote sensing approach to global agricultural drought monitoring. Agric For Meteorol 259:141–153. https://doi.org/10.1016/j.agrformet.2018.04.022
14. Sánchez N, Gonzalez-Zamora A, Piles M, Martinez-Fernández J (2016) A new soil moisture agricultural drought index (SMADI) integrating MODIS and SMOS products: a case of study over the Iberian Peninsula. Remote Sens 8:25. https://doi.org/10.3390/rs8040287

15. World Meteorological Organization (2012) Standardized precipitation index user guide (M. Svoboda, M. Hayes and D. Wood). (WMO-No. 1090), Geneva

16. Wu H, Hayes MJ, Wilhite DA, Svoboda MD (2005) The Effect of the Length of Record on the Standardized Precipitation Index Calculation. Int J Climatol 25(4):505–520. https://doi.org/10.1002/joc.1142

17. Haieda N, Foufou A, Chaab S, Azlaoui M, Khadri S, Benzahia K, Benzahi I (2017) Drought assessment and monitoring using meteorological indices in a semi-arid region. Energy Proc 119:518–529

18. Eslamian S, Ostad-Ali-Askari K, Singh V, Dalezios N, Woldeyohannes Y, Matouq M (2017) A review of drought indices. Int J Constr Res Civ Eng 3:48–66. https://doi.org/10.20431/2454-8693.0304005

19. Doesken NJ, Garen D (1991) Drought monitoring in the Western United States using a surface water supply index. In: Seventh conference on applied climatology, Salt Lake City, UT. American Meteorological Society, pp 266–269. https://doi.org/10.1175/1520-0442(2004)017<2335ASPDSI>2.0.CO;2

20. Hayes M, Svoboda M, Wall N, Widhalm M (2011) The Lincoln declaration on drought indices: universal meteorological drought index recommended. Bull Am Meteor Soc 92(4):485–488. https://doi.org/10.1175/2010BAMS3103.1

21. Mlenga DH, Jordaan AJ (2019) Monitoring droughts in Eswatini: a spatiotemporal variability analysis using the Standard Precipitation Index. Jamba (Potchefstroom, South Africa) 11(1):712. https://doi.org/10.4102/jamba.v11i1.712

22. Vicente-Serrano SM, Beguería S, López-Moreno JI (2010) A multiscalar drought index sensitive to global warming: the standardized precipitation evapotranspiration index. J Clim 23(7):1696–1718

23. Dai A, National Center for Atmospheric Research Staff (eds) (2019) The climate data guide: palmer drought severity index (PDSI). National Center for Atmospheric Research. https://climatedataguide.ucar.edu/climate-data/palmer-drought-severity-index-pdsi

24. Alley WM (1984) The Palmer Drought Severity Index: limitations and assumptions. J Appl Meteorol 23(7):1100–1109. https://doi.org/10.1175/1520-0450(1984)023%3c1100:TPDSIL%3e2.0.CO;2

25. Hayes MJ, Svoboda MD, Wilhite DA, Vanyarkho OV (1999) Monitoring the 1996 drought using the standardized precipitation index. Bull Am Meteor Soc 80(3):429–438

26. Wells N, Goddard S, Hayes MJ (2004) A self-calibrating Palmer Drought Severity Index. J Clim 17:2335–2351

Assessment of Meteorological Drought Using Standardized Precipitation Evapotranspiration Index—Hyderabad Case Study

Pallavi Kumari, Sharath Chandra Vannam, Rehana Shaik, and M. Inayathulla

1 Introduction

Drought, a natural disaster, occurs in all types of climate. Temperature, wind, relative humidity, rainfall intensity and rainfall duration play a significant part in the phenomenon of droughts. It affects natural sources of water and also can reduce the water supply, quality of water, crop yield, as well as the economy and social activities. Drought is an extreme event that affects natural resources, environment and society for a long time. Usually, drought occurs gradually; but it can be more terrible than floods. Meteorological, hydrological and agricultural are its broad types as described in Fig. [1]. Out of these, meteorological drought, defined as an abnormal shortage of precipitation, is the main cause of all other types of droughts. Drought index measures the levels of drought by acquiring data into a single numerical value from one or more hydrological variables. Several drought indices are found to assess the change in climatic variables. Those are Palmer Drought Severity Index, Crop Moisture Index, Standardized Precipitation Index (SPI), Standardized Precipitation Evapotranspiration Index (SPEI) and Reconnaissance Drought Index (RDI) [1]. Based on the drought studies, almost all drought indices use precipitation as the sole variable or with the other hydrological elements, as per the type of demand, which is indicated by WMO [2]. There have been many attempts over the last few decades to develop a new drought index on the basis of a climatological precipitation study [1, 3, 4]. Vicente-Serrano et al. [5] proposed a new evapotranspiration-based index which is Standardized Precipitation Evapotranspiration Index (SPEI) based on the calculation of Potential Evapotranspiration.

The study used SPEI as one of the evapotranspiration-based drought indices to understand the drought variability. SPEI is capable of depicting the multi-secular

P. Kumari (✉) · M. Inayathulla
Department of Civil Engineering, UVCE, Bangalore University, Bangalore, India

S. C. Vannam · R. Shaik
International Institute of Information Technology, Hyderabad, India
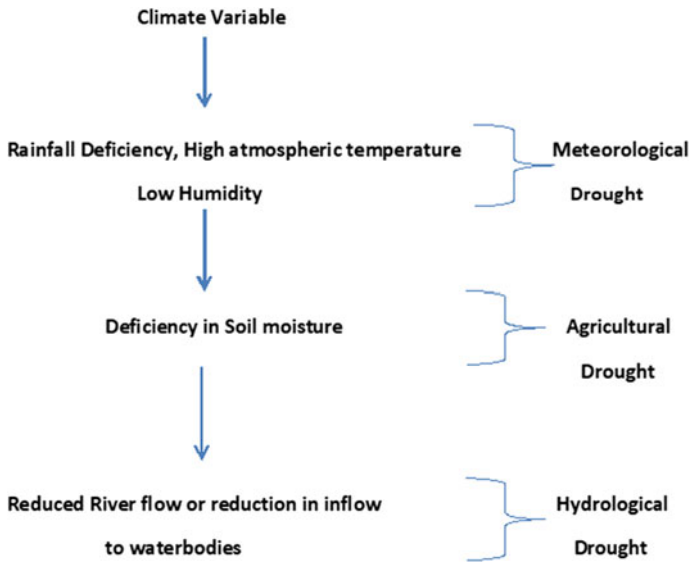
Fig. 1 Various forms of drought and its sequence

nature of hydrological, meteorological and agricultural droughts which consists of computation at multi time scales based on the distribution of precipitation and potential evapotranspiration differences [5]. SPEI has been recommended to quantify in the cumulated climate water balance (D), incorporating PET [6]. The SPEI index can also be used to study the wet and dry periods including Evapotranspiration along with precipitation. In the present study, SPEI is used to understand the dry and wet years over an urban semi-arid region, Hyderabad, capital and the biggest city of the southern Indian state of Telangana. The details of the study area are provided in the following section. The data and methodology, the results and discussions, and the findings of this work are presented in the subsequent sections. All the figures of this article are generated by the use of MATLAB and ArcGIS.

2 Material and Methodology

2.1 Study Area and Data Products

Hyderabad, the capital of Telangana state also known as the City of Pearls, defined in the region 17°33′50″N and 78°46′10″E, covering 625 km^2 land area, is observed in the present study (Fig. 2). The population of Hyderabad is 68.1 lakhs making it the fourth most populous city in India and suffering from huge water-shortage issues. Hyderabad has a wet and dry climate bounding on a hot semi-arid climate. The
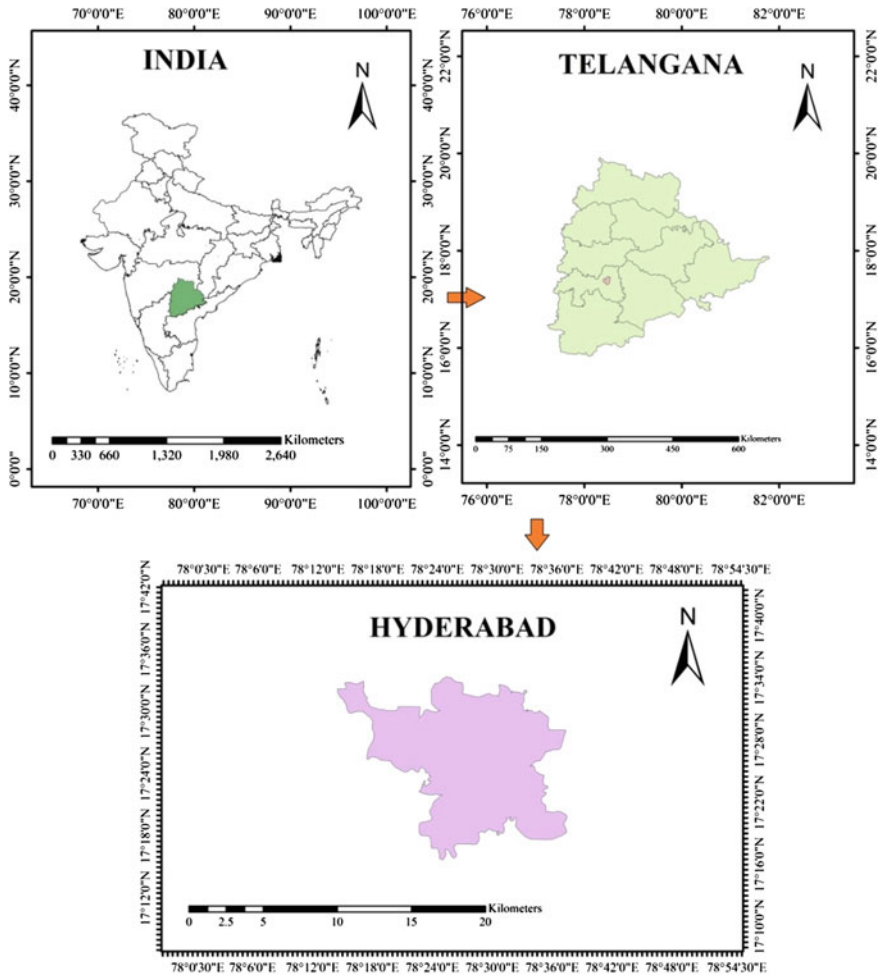
Fig. 2 Location of Hyderabad, Telangana, India

Southwest Monsoon is responsible for 75 percent of the rain in Hyderabad. Annually, the region receives an average of 810 mm of rain. During the month of September, the area receives maximum rain. This study made efforts to understand the wet and dry years of the urban semi-arid region of Hyderabad city for the years 1965–2015. The present study used rainfall and temperature data for the year 1965–2015 collected from India Meteorological Department.

2.2 *Methodology*

Estimation of potential evapotranspiration (PET)

In this study, SPEI is formulated by log-logistic distribution, using three parameters (scale, shape and origin) [5, 7]. The climate water balance (D) and the drought index SPEI are estimated as follows:

$$D = [P - PET] \tag{1}$$

P and PET are the monthly rainfall and potential evapotranspiration in mm, respectively.

According to Stagge et al. [6], the Hargreaves method can give better results if minimum data is available. Thus, this study chose the Hargreaves method to formulate potential evapotranspiration (PET). This method considers the temperature and location of the study area to compute PET. The Hargreaves [8] equation of PET (mm/day) is mentioned as

$$\text{Potential Evapotranspiration (PET)} = 0.0023 * \sqrt{T \max - T \min}$$
$$* (T_{mean} + 17.80) * R_a \tag{2}$$

Here, T_{max}, T_{min} and T_{mean} are the maximum, minimum and mean monthly temperature, sequentially. Ra is the extra-terrestrial radiation which is calculated based on the latitude of the area and sunshine hours in the year.

The present study used 12-month time scales in the calculation of D_i^n value.

$$D_i^n = P_i^n - PET_i^n \tag{3}$$

Here, P_i^n and PET_i^n are the cumulated rainfall and potential evapotranspiration value.

Formulation of Drought Index, SPEI

The SPEI values can be calculated using the values of F(x), as follows:

$$\text{SPEI} = W - \frac{C0 + C1W + C2W2}{1 + d1W + d2W2 + d3W3} \tag{4}$$

Here, W = square root of $-(2\ln(p))$ for p less than or equal to 0.50;

P is probability of D = 1 − F(x). If p is greater than 0.5, then P is replaced by 1-P and the sign of SPEI is reversed.

C_0, C_1 and C_2 and d_1, d_2 and d_3 are constants [9].

F(x) is the Cumulative Distribution Function (CDF) which is calculated based on probability distribution.

Table 1 Standard ranges and classification of SPEI values [11]

Classification	SPEI Value	Classification	SPEI Value
Extreme dry	−2.0 or less	Moderate wet	1.0–1.5
Severe dry	−1.50 to −1.99	Severe wet	1.51–1.99
Moderate dry	−1.0 to −1.49	Extreme wet	2.0 or above

$$F(x) = \left[1 + \left(\frac{x - y}{\alpha} \right)^{-\beta} \right]^{-1} \tag{5}$$

where α, β and γ are the parameters

$$\alpha = \frac{(wo - 2w1)\beta}{\gamma(1 + \frac{1}{\beta})\Upsilon(1 - 1/\beta)} \tag{6}$$

$$\beta = \frac{2w1 - wo}{6w1 - wo - 6w2} \tag{7}$$

$$\gamma = w_o - \alpha\gamma(1 + 1/\beta)\gamma(1 - 1/\beta) \tag{8}$$

Weighted moments w_0, w_1 and w_2 are estimated using the equation by Sheng and Hashino [10], as follows:

$$Wr = \frac{1}{n}\binom{n-1}{r}^{-1} \sum_{j=1}^{n-r}\binom{n-j}{r} Xj, r = 0, 1, 2 \tag{9}$$

The SPEI-based classification is provided in Table 1. It is to be observed that when SPEI drops to less than -2, it is said to be extremely dry and if it exceeds 2, it is classified as extremely wet. Hence, based on severity, there are three types, i.e., moderate, severe and extreme drought.

3 Results and Discussion

Figures 3 and 4 show the Variation of rainfall and Potential Evapotranspiration estimated by the Hargreaves equation, respectively.

The SPEI results for each year considering the rainfall and PET are presented in Table 2. The normal wet or dry conditions, moderate wet, severe wet, moderate drought and severe drought are represented in black, purple, blue, orange and red colors, respectively. It can be noted that Hyderabad district has undergone considerable annual variation in rainfall. It is worth noticing that the district has been in dry conditions (including severe and moderate drought) 7 times in 50 years. The result shows that the years 1965, 1966, 1972, 1973, 1985 and 1993 have experienced
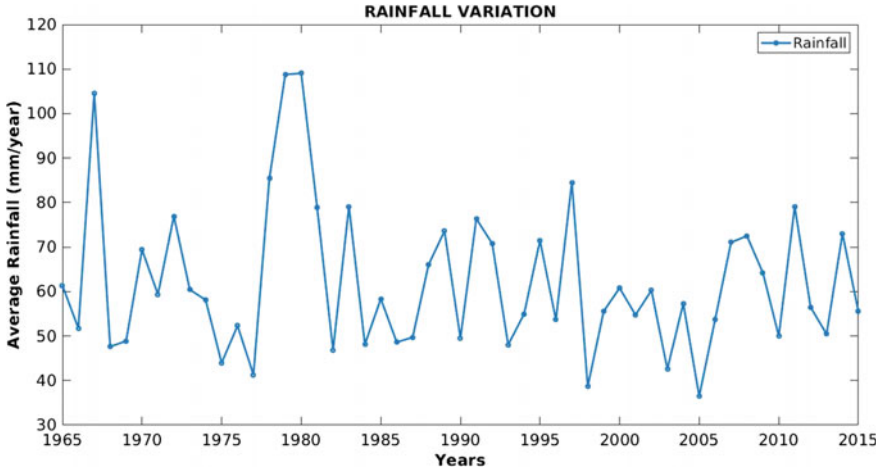
Fig. 3 Rainfall variation for the years 1965–2015
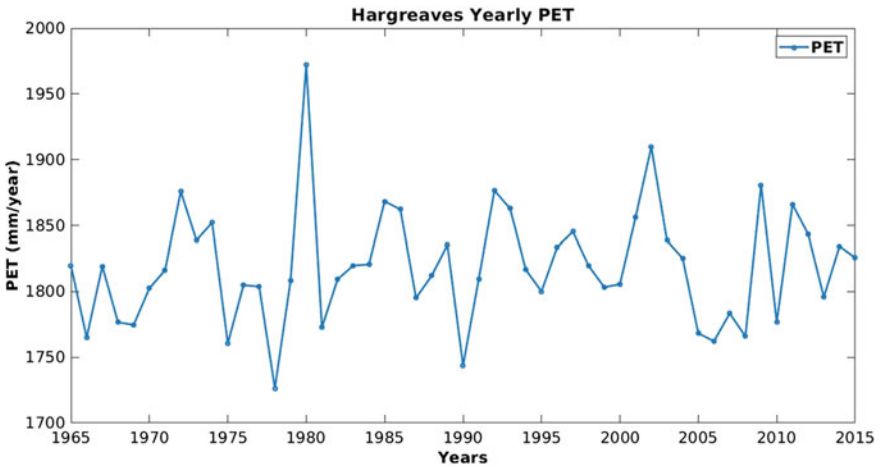
Fig. 4 Potential Evapotranspiration for the years 1965–2015

moderate drought with SPEI values −1.35, −1.06, −1.43, −1.31, −1.05 and −1.22, respectively. These years are also considered as drought years all over India based on earlier studies [9]. The years 1976, 1988, 1991, 1995, 1996, 2008 and 2014 were experienced as moderate wet years with SPEI values 1.21, 1.13, 1.08, 1.14, 1.21, 1.31 and 1.47, respectively. The year 2006 was characterized as severe wet with the SPEI value 1.65 and the year 2012 was found as severe dry with value −1.51 as per the standard ranges and classes of SPEI (Table 1). Figure 5 shows the variation of SPEI values for the years 1965–2015.

Table 2 Standardized Precipitation Evapotranspiration Index values over Hyderabad for 1965–2015

Year	SPEI	Year	SPEI
1965	−1.35	1991	1.08
1966	−1.06	1992	−0.62
1967	0.05	1993	−1.22
1968	−0.3	1994	−0.78
1969	−0.71	1995	1.14
1970	0.21	1996	1.21
1971	0.05	1997	0.62
1972	−1.43	1998	0.28
1973	−1.31	1999	0.26
1974	−0.87	2000	−0.023
1975	0.31	2001	0.008
1976	1.21	2002	−0.14
1977	−0.45	2003	−0.57
1978	−0.007	2004	0.30
1979	0.36	2005	0.61
1980	−0.53	2006	1.65
1981	−0.09	2007	0.75
1982	0.33	2008	1.31
1983	−0.19	2009	0.09
1984	0.28	2010	−0.34
1985	−1.05	2011	−0.56
1986	−0.74	2012	−1.51
1987	−0.22	2013	0.50
1988	1.13	2014	1.47
1989	0.35	2015	0.45
1990	0.62		

Normal wet or dry condition; Moderate wet; Severe wet; Moderate drought; Severe drought;
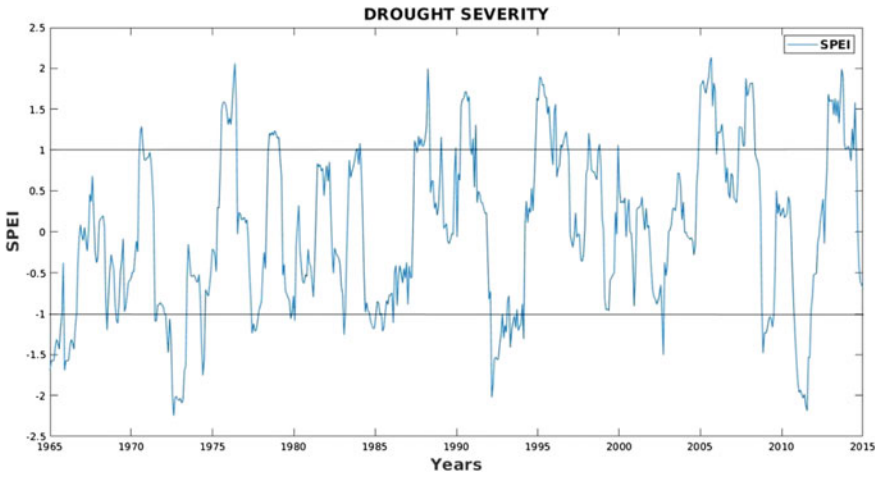
Fig. 5 Results of SPEI values for an urban semi-arid region, Hyderabad, for a 12-month time scale

Comparison of Rainfall and PET values in different severity classes of SPEI is presented in Table 3. Rainfall and Potential Evapotranspiration are the two major meteorological parameters to be used in the classification of wet and dry weather.

Table 3 Rainfall and PET values in different severity classes of Standardized Precipitation Evapotranspiration Index

Year	Rainfall (mm)	PET-Hargreaves (mm)	SPEI values			
			Moderate wet	Severe wet	Moderate dry	Severe dry
1965	61.37	1819.66	–	–	−1.35	–
1966	51.75	1765.03	–	–	−1.06	–
1972	76.94	1875.77	–	–	−1.43	–
1973	60.46	1838.71	–	–	−1.31	–
1976	52.31	1804.88	+1.21	–	–	–
1985	58.36	1868.26	–	–	−1.05	–
1988	66.03	1812.08	+1.13	–	–	–
1991	76.37	1809.58	+1.08	–	–	–
1993	48.04	1862.68	–	–	−1.22	–
1995	71.46	1800.14	+1.14	–	–	–
1996	53.64	1833.64	+1.21	–	–	–
2006	53.70	1762.27	–	+ 1.65	–	–
2008	72.50	1765.96	+1.31	–	–	–
2012	56.47	1843.40	–	–	–	−1.51
2015	55.54	1825.63	+1.47	–	–	–

Both the parameters are characterized by variability which differs from one particular climatic region to another, and it is heavily dependent on time scale. From the above comparison, it is found that rainfall and potential evapotranspiration proportionally increase or decrease in the domain area for moderate and severe wet or dry years. The year 2012 which is identified as severe dry with the SPEI value −1.51 received 56.47 mm of yearly average rainfall and 1843.40 mm of Potential Evapotranspiration, whereas the year 2006 which is characterized as severe wet year with the SPEI value 1.65 received 53.70 mm of rainfall and 1762.27 mm of Potential Evapotranspiration.

With this comparison, it is clear that SPEI is more sensitive to the changes in PET in the drought characterization compared to precipitation alone. More specifically, the difference between the rainfall and PET, which represent the atmospheric evaporative demand, is the defining factor in the drought characterization using SPEI. The characterization of dry and wet years as presented in this study will enhance the understanding of the climatic variability of precipitation and PET over dry and wet years. The wet and dry year characterization over an urban region based on SPEI has given a clear idea about the possible urban water resource planning and management.

4 Conclusion

The Standardized Precipitation Evapotranspiration Index (SPEI) is used to assess the meteorological droughts over Hyderabad, Telangana, India, using Rainfall data and Potential Evapotranspiration for the years 1965–2015. The results show that the Hyderabad region has undergone significant annual variation in monsoon rainfall. Seven droughts (including severe and moderate droughts) have appeared in the region over the period under consideration. This study concludes that estimation of dry and wet years by a suitable index, SPEI which includes potential Evapotranspiration along with precipitation, plays a vital role as it indicates early warning, monitoring and contingency planning, by computing severity levels and proclaiming the start and end of dry or wet seasons more accurately. The study limited the time scale of the drought index, SPEI, for a 12-month time accumulation period to study the annual drought variability. In this paper, however, it was shown that both the parameters including rainfall and PET influence the wet or dry season proportionally. Specifically, shorter time scale SPEI drought indices can provide the seasonal wet and dry variability of the region, which can provide a greater detail toward the water resources management. Further, the study used the Hargreaves equation to compute PET and the use of a more accurate PET model such as Penman-Monteith can provide accurate estimations of drought indices using SPEI.

References

1. Tsakiris G, Pangalou D, Vangelis H (2007) Regional drought assessment based on the Reconnaissance Drought Index (RDI). Water Resour Manage 21(5):821–833
2. World Meteorological Organization (WMO) (1975) Drought and agriculture. Technical note no 138, Report of the CAgM Working Group on Assessment of Drought, WMO, Geneva, Switzerland, p 127
3. Jain VK, Pandey RP, Jain MK, Byun HR (2015) Comparison of drought indices for appraisal of drought characteristics in the Ken River Basin. Weather Climate Extremes 8:1–11
4. Morid S, Smakhtin V, Moghaddasi M (2006) Comparison of seven meteorological indices for drought monitoring in Iran. Int J Climatol J R Meteorol Soc 26(7):971–985
5. Vicente-Serrano SM, Beguería S, López-Moreno JI (2010) A multiscalar drought index sensitive to global warming: the standardized precipitation evapotranspiration index. J Clim 23(7):1696–1718
6. Stagge JH, Tallaksen LM, Xu CY, Van Lanen HA (2014) Standardized precipitation-evapotranspiration index (SPEI): sensitivity to potential evapotranspiration model and parameters. In: Hydrology in a changing world, vol 363, pp 367–373
7. Vicente-Serrano SM, Van der Schrier G, Beguer_ıa S, Azorin-Molina C and Lopez-Moreno J I, (2015) Contribution of precipitation and reference evapotranspiration to drought indices under different climates. J Hydrol 526:42–54
8. Hargreaves GH (1975) Moisture availability and crop production. T ASAE 18(5):980–984
9. Monish NT, Rehana S (2020) Suitability of distributions for standard precipitation and evapotranspiration index over meteorologically homogeneous zones of India. J Earth Syst Sci 129(1):1–19
10. Sheng Y, Hashino M (2007) Probability distribution of annual, seasonal and monthly precipitation in Japan. Hydrol Sci J 52(5):863–877
11. McKee TB, Doesken NJ, Kleist J (1993) The relationship of drought frequency and duration to time scales. In: Proceedings of the 8th conference on applied climatology, vol 17, no 22, pp 179–183

Spatiotemporal Analysis of Drought Persistence of Peninsular India

V. Sreedevi and S. Adarsh

1 Introduction

Precipitation is one of the most important hydro-meteorological variables that affects the drought and flood events of a country. The accurate prediction of rainfall has been a topic of research for many years. The analysis of rainfall time series data over a long time period is one of the approaches used in rainfall prediction studies. The rainfall time series analysis helps to get a better idea about the drought climatology of a region [1]. The dependence of the present value of a hydrological time series for a longer time period is known as long-term dependence or persistence [2].

The Hurst exponent (H) proposed by Harold Edwin Hurst [3] is considered as a measure of persistence and the time series having the Hurst exponent value greater than 0.5 is predictable [4]. Different methods are available to compute the Hurst exponent values such as Rescaled range (R/S), Aggregated variances, Regression on periodogram, the Whittle estimator, Detrended Fluctuation Analysis (DFA) and Box counting method [5], [6]. Several studies have been performed to find the persistence in hydro-climatic variables like temperature [7], precipitation [6], [4], streamflow [5, 8], etc. Most of the studies followed the R/S method owing to its simplicity and robustness [4, 6, 9].

Drought is a natural phenomenon that originates from the deficiency of precipitation over an extended period of time. India is one of the most vulnerable drought-prone countries in the world. Several drought indices such as Palmer Drought Severity Index (PDSI), Standardized Precipitation Index (SPI), and Standardized Precipitation Evapotranspiration Index (SPEI) were developed in the past to estimate the drought severity [10]. In most of the studies, the drought characterization is made based on precipitation alone and SPI is the commonly used drought indicator [1, 11, 12]. The SPI can be computed for different aggregation time scales like 1 month,

V. Sreedevi (✉) · S. Adarsh
TKM College of Engineering, Kollam, India

APJ Abdul Kalam Technological University, Thiruvananthapuram, Kerala, India

3 months, 6 months, etc. to account for the meteorological, hydrological and agricultural droughts. The 3-month SPI represents short-term drought and can be used as a seasonal drought index, the 6-month SPI indicates the intermediate drought and the 12-month, 24-month and 48-month SPI represent the long-term drought. Soil moisture and the associated water stress and crop failures are better represented using 3-month SPI, while the 6-month SPI indicates the streamflow drought conditions and the 12-month and 24-month SPI values represent the groundwater drought conditions [13]. The temporal and spatial patterns of drought occurrence in India were studied by several researchers using SPI computed at different aggregation time scales [1, 11]. Non-parametric SPI can effectively capture the drought conditions in India [14]. Some of the recent studies used the DFA method to quantify the long-term correlations in the meteorological drought index [11, 12].

Global warming has affected the climate of all countries. Changes in precipitation and temperature have reduced glaciers/snow packs leading to the reduction in river flows. Drought events are upscaling in Asian countries due to delayed and changing precipitation distribution patterns [15]. Flood and drought events are frequently being witnessed in several Asian countries like India, Pakistan, Bangladesh, etc. The hydro-meteorological variables like precipitation, streamflow, temperature, etc. contributing to the disastrous events like floods and droughts are to be monitored and the underlying dependency in the time series values are to be studied. Understanding the persistence of drought may help in the improved prediction of drought conditions and understanding the likely behavior of drought in the future decades. This eventually may help in disaster preparedness and risk assessment of droughts. Tong et al. [16] determined eight extreme temperature indices and six precipitation indices of Inner Mongolia. They used DFA to find the persistence of extreme indices to get an understanding of likely trends in the future evolution of extremes. Chandrasekharan et al. [4] performed the persistence analysis on a set of synthetic database and commented on its link with the predictability of the series. Further, they applied it for monthly rainfall datasets of Cherrapunji. Pal et al. [9] examined the persistence of summer monsoon rainfall datasets of North East India and reported the process as anti-persistent in nature. However, no studies performed the in-depth persistence analysis of rainfall in other subdivisions and none compared its persistence with the corresponding drought index.

The present study focusses on the estimation of drought persistence in Peninsular India (PI) which comprises of six meteorological subdivisions. The objectives of the paper are (i) to study the persistence in the monthly, seasonal and annual rainfall of the homogeneous region and its subdivisions; (ii) to perform the Rescaled range (R/S) analysis on the SPI time series computed for different aggregation time scales and evaluate the drought persistence; (iii) to investigate the effect of the global climatic shift of 1976/1977 in the rainfall and drought persistence in Peninsular India.

2 Methods

A brief description of the SPI and Rescaled range (R/S) analysis is provided in the following section.

2.1 Standardized Precipitation Index (SPI)

The SPI evaluates the deficiency in observed precipitation and is widely used to monitor meteorological droughts. The SPI series can be computed for different aggregation time scales ranging from 1 to 48 months in general, for representing short-term, intermediate and long-term droughts. Either a non-parametric or gamma distribution-based approach can be followed to estimate the SPI [14]. The aggregated precipitation time series of various time scales (say 3 months, 6 months, etc.) is first used to fit the Gamma distribution function. The two-parameter Gamma distribution is not defined for zero values. Therefore, the Cumulative Distribution Function (CDF) is computed using a mixed formula in the form:

$$G_X(x) = p + (1 - p)C_X(x) \tag{1}$$

where p is the probability of zero values in the time series, $C_x(x)$ is the CDF of non-zero entries in the series and $G_x(x)$ is the CDF of the original data. Then an equiprobability transformation is performed to get the CDF of the standard normal distribution. This probability gives the SPI for a given accumulation time scale as

$$Z_n = \varphi^{-1}(G_X(x)) \tag{2}$$

in which $\varphi^{-1}(.)$ is the inverse of the CDF.

2.2 Rescaled Range Method (R/S)

Hurst [3] developed an approach to measure the correlation in a time series analysis. This is the most widely used method [4, 9]. The steps used in this method are as follows. The entire time series is divided into many shorter series in the first step.

1. The mean $\overline{x}$ is computed for the time series $x = x_1, x_2, x_3,...x_n$

$$\overline{x} = \frac{\sum_{i=1}^{n} x_i}{n} \tag{3}$$

2. A mean adjusted series is created.

$$y_s = x_s - \overline{x} \ for \ s = 1, 2, \ldots, n \tag{4}$$

3. The cumulative deviate series z is calculated.

$$z_s = \sum_{i=1}^{s} y_s \ for \ s = 1, 2, \ldots, n \tag{5}$$

4. Range series R is obtained.

$$R = \max(z_1, z_2, \ldots z_s) - \min(z_1, z_2, \ldots z_s) \tag{6}$$

5. A standard deviation series S is computed.

$$S = \sqrt{\frac{1}{s} \sum_{i=1}^{s} (x_i - \overline{x}(s))^2} \ for \ s = 1, 2, \ldots, n \tag{7}$$

where $\overline{x}(s)$ is the mean of the values in the time series.

6. Finally, the rescaled range series is calculated as

$$\left(\frac{R}{S} \right)_s = k s^H \tag{8}$$

where k is a constant and s is the length of each segment; $1 \leq s \leq n$, n is the entire length of the time series. R is the range of the time series and S is the standard deviation.

7. The slope of the line plotted between (R/S) and s on a log–log scale gives the Hurst exponent.

3 Study Area

India is divided into 36 meteorological subdivisions based on rainfall homogeneity by the Indian Institute of Tropical Meteorology (IITM) Pune. On the basis of monsoon characteristics, the meteorological subdivisions are again classified into five homogeneous monsoon regions: North East, Central North East, North West, West Central and Peninsular region. The present study focusses on the Peninsular region which consists of six meteorological subdivisions: Coastal Andhra Pradesh (CAP), Rayalaseema (RAY), Tamil Nadu and Pondicherry (TNP), Coastal Karnataka (CKT), South Interior Karnataka (SIK) and Kerala (KER) as shown in Fig. 1.

The monthly spatially averaged precipitation data of the meteorological subdivisions and homogeneous regions available at http://www.tropmet.res.in/ for the period
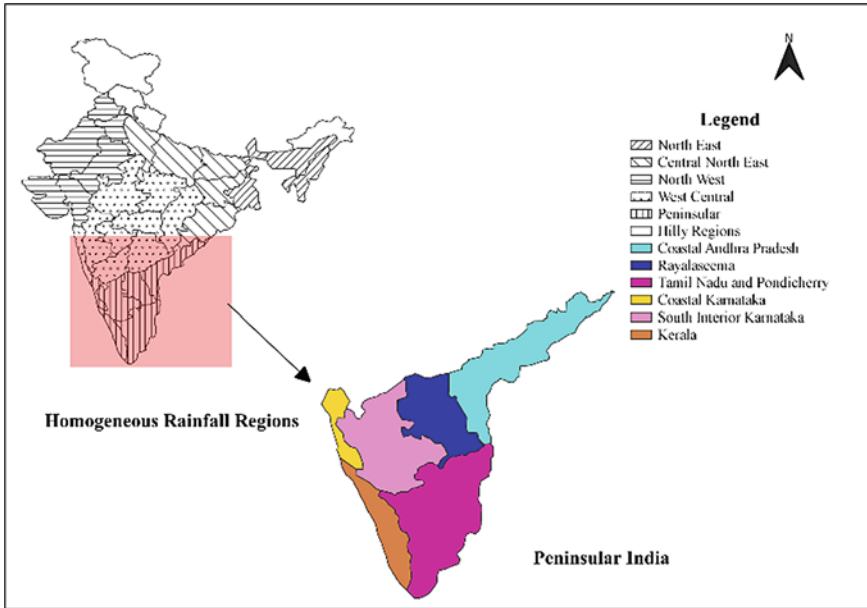
Fig. 1 Peninsular India

1871–2016 can be used for the estimation of SPI at different aggregation time scales. The data are homogenized using the procedure explained in Parthasarathy et al. [17]. The homogenized data corresponds to six subdivisions covering an area of 4,42,908 km².

In this study, the hydrologic persistence of meteorological drought index SPI of six subdivisions of Peninsular India for which the rainfall data available were estimated. First, the persistence of rainfall time series in the Peninsular region and its subdivisions was evaluated. The meteorological drought index SPI was computed at different aggregation time scales using the rainfall time series. The Global climate shift that occurred during the 1976/77 period is the most prominent and well-debated regime shifts and its influence in the Indian Summer Monsoon was well proven by the researchers [18, 19]. A more detailed analysis was done to identify the variation in persistence by dividing the total dataset into two: 1871–1976 and 1977–2016 owing to the effect of the global climate shift of 1976/1977 on the rainfall received in the Peninsular region. The Hurst exponent values were evaluated for the time series in two modes. The first mode comprised of the complete data and the second mode by partitioning the data into two subseries (from 1871 to 1976 and 1977 to 2016).

4 Results and Discussions

The results of the Hurst exponent computation and corresponding discussions are provided in this section.

4.1 Persistence of Rainfall

The Hurst exponent values were computed for monthly, seasonal and annual rainfall for Peninsular India (PI). Table 1 shows the values obtained for monthly, annual and seasonal rainfall for PI and the six subdivisions.

Monthly rainfall data of PI and its subdivisions displayed short-term persistence while the annual rainfall showed long-term persistence except in Tamil Nadu and Pondicherry and South Interior Karnataka. The Hurst exponent value below 0.5 can be interpreted as the result of a long-term shift between low and high amounts of rainfall. The monthly rainfall in the PI can be considered as volatile and rough [9].

The Southwest monsoon rainfall commonly known as the Indian Summer Monsoon Rainfall (ISMR) during June to September contributes the major portion of the annual precipitation in India. The Hurst exponent values computed for the seasonal rainfall of June to September exhibit Long-Term Persistence (LTP) for all the subdivisions except Kerala. A negative trend in the summer monsoon rainfall observed in the Kerala subdivision [20] can be linked with the reduced rainfall obtained during the El Nino years [21]. The persistence of monthly rainfall in the PI region also exhibits Short-Term Persistence (STP).

In order to investigate the observed STP in different subdivisions, the Hurst exponent values for all months were computed for the Peninsular region. Figure 2 shows the monthly variation of the Hurst exponent values for the six subdivisions and PI.

Table 1 Hurst exponent values of rainfall for Peninsular India

Subdivisions	Hurst exponent values						
	Monthly rainfall	Annual rainfall	Seasonal rainfall				
			JF	MAM	JJAS	OND
CAP	**0.40**	0.60	0.87	0.50	0.66	0.65
RAY	**0.41**	0.65	0.96	0.81	0.56	0.57
TNP	**0.34**	**0.38**	0.82	0.71	0.74	**0.49**
CKT	**0.32**	0.66	**0.46**	0.64	0.55	0.63
SIK	**0.35**	**0.45**	0.72	0.62	0.56	**0.44**
KER	**0.41**	0.73	0.72	0.69	**0.43**	0.85
PI	**0.32**	0.54	0.90	0.77	**0.46**	0.51

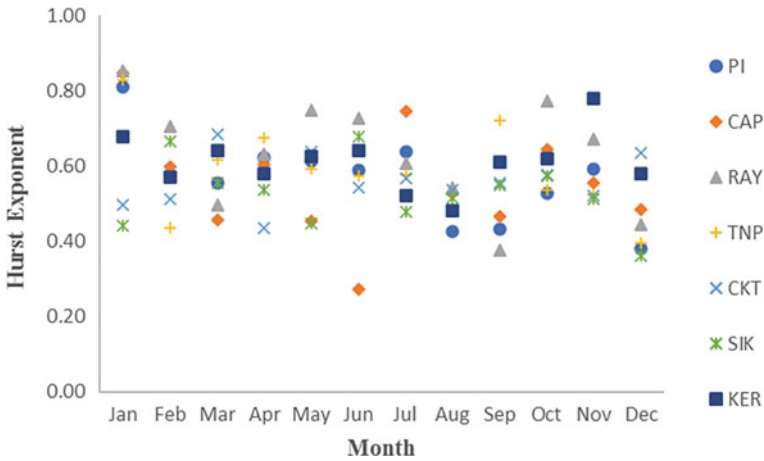*Note* The values in bold indicates short-term persistence

Fig. 2 Monthly variation of the Hurst exponent in Peninsular region

The rainfall time series data of August month of PI region and Kerala subdivision are found to be of short-term persistence. The persistence analysis performed for the annual series of individual months showed long-term persistence in the datasets of the post-monsoon season at the PI region and all of its subdivisions. STP was observed in all subdivisions except Kerala and Coastal Karnataka in the month of December.

4.2 Drought Persistence

The monthly SPI series is computed for different time scales: 1 month, 3 months, 6 months, 12 months, 24 and 48 months using monthly rainfall data for the Peninsular region and six of its meteorological subdivisions. The Hurst exponent values computed for the SPI time series are shown in Table 2.

SPI series derived from the monthly rainfall for all subdivisions shows long-term persistence. The persistence increases with the increase in the aggregation time scale. Since the Hurst exponent values are found higher than 0.5, the SPI time series (i.e., drought at different scales) are predictable [4].

4.3 Effect of Global Climatic Shift

In order to capture the temporal change in persistence, the analysis was performed by partitioning the rainfall and SPI time series with respect to the global climatic shift of 1976/1977. The rainfall data from 1871 to 1976 was considered as time series

Table 2 Hurst exponent values for SPI time series of PI

Subdivisions	Hurst exponent values					
	SPI-1	SPI-3	SPI-6	SPI-12	SPI-24	SPI-48
CAP	0.57	0.61	0.64	0.70	0.79	0.86
RAY	0.56	0.61	0.65	0.71	0.81	0.89
TNP	0.51	0.56	0.58	0.65	0.71	0.75
CKT	0.58	0.67	0.69	0.71	0.78	0.86
SIK	0.50	0.57	0.61	0.65	0.72	0.80
KER	0.67	0.71	0.72	0.76	0.82	0.91
PI	0.55	0.61	0.63	0.66	0.73	0.81

T1 and that from 1977 to 2016 as time series T2. Table 3 shows the Hurst exponent values for monthly and annual rainfall time series based on climatic shift.

The monthly rainfall series in PI and its subdivisions shows STP with respect to the global climate shift. The Hurst exponent values computed for the annual rainfall series before the shift (T1) were similar to that computed for the whole time series (T). The annual rainfall series of Tamil Nadu and Pondicherry exhibits LTP whereas that of Kerala and South Interior Karnataka shows STP after 1976.

The persistence analysis was performed on the rainfall values of different months and seasons using the T1 and T2 time series. Figure 3 shows the Hurst exponent values obtained for the rainfall and SPI time series based on climate shift.

LTP can be observed in the monsoon rainfall in PI and Kerala after the climatic shift. However, the seasonal rainfall series and the annual time series of different months displayed transitions in the nature of persistence with regional diversity. No transition was observed in the nature of persistence (short/long) of the drought index series.

Table 3 Hurst exponent values for monthly and annual rainfall time series based on climatic shift

Subdivisions	Hurst exponent values			
	Monthly rainfall		Annual rainfall	
	T1	T2	T1	T2
CAP	**0.38**	**0.37**	0.56	0.71
RAY	**0.38**	**0.37**	0.61	0.67
TNP	**0.39**	**0.42**	**0.46**	0.64
CKT	**0.33**	**0.23**	0.63	0.52
SIK	**0.41**	**0.36**	0.61	**0.36**
KER	**0.39**	**0.33**	0.76	**0.43**
PI	**0.33**	**0.33**	0.52	0.50

Note T1 = 1871–1976; T2 = 1977–2016. The values in bold indicate short-term persistence

(a) Rainfall of different months
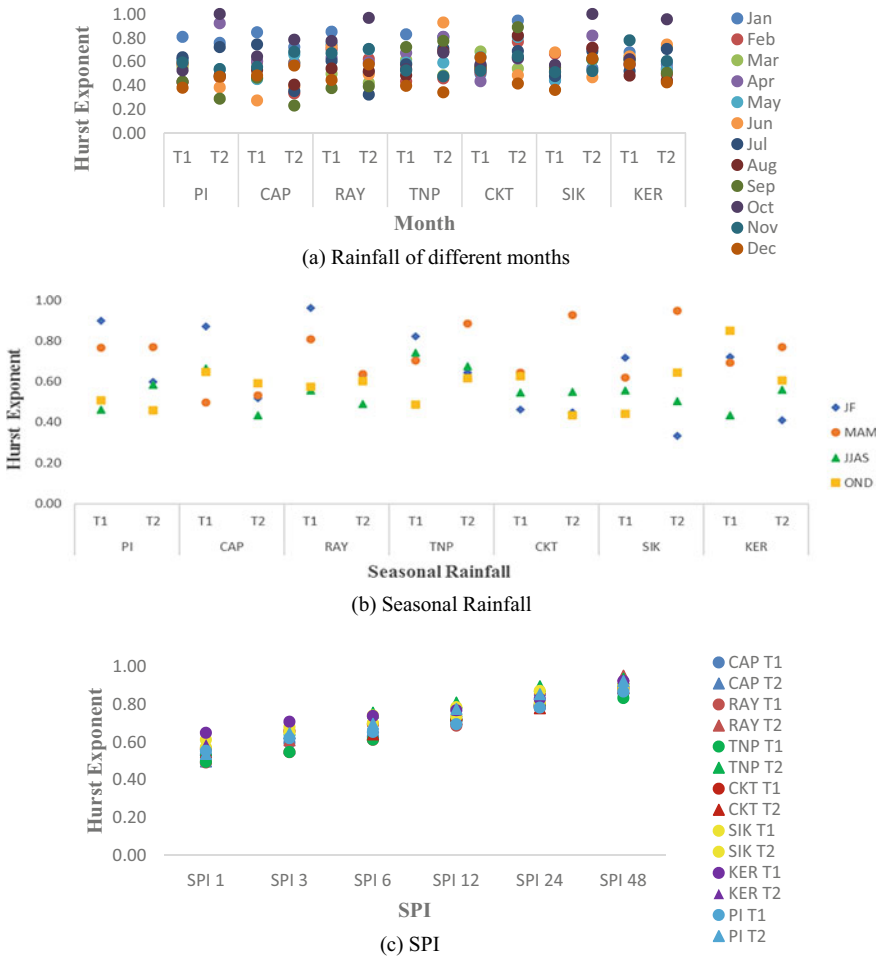

(b) Seasonal Rainfall

(c) SPI

Fig. 3 Hurst exponent values in PI based on climatic shift **a** Rainfall of different months. **b** Seasonal rainfall. **c** SPI

This study first performed a detailed persistence analysis of annual, seasonal and monthly rainfall of different meteorological subdivisions of PI. The Hurst exponent of rainfall at different temporal scales can be short term or long term for different analyses (H ranging from 0.23 to 0.76 for different cases). Similar observation can also be made from the studies by Chandrasekharan et al. [4] and Pal et al. [9] where the R/S method was applied for finding the persistence of rainfall in the North East region. More specifically, in our study, the monthly rainfall data of different subdivisions exhibited a short-term persistence. Adarsh et al. [11] computed the persistence of the SPI series of all the meteorological subdivisions using the multifractal DFA approach. They noticed LTP in the majority of the SPI series (computed at monthly scale) with an increase in persistence with aggregation scale. LTP was observed in

all the drought index series considered in this study for different aggregation scales ranging from 1 to 48 months. In this R/S-based method also, drought persistence increases with an increase in aggregation scale reinforcing it as a universal property. Even though the monthly rainfall exhibits STP, the drought indices derived from it may be long-term persistent indicating better predictability of drought over the rainfall.

The climatic changes may significantly influence the behavior of time series. For developing policies for efficient water resource management in the future, accurate modeling is necessary. The climate-induced non-stationarities may influence the accuracy of hydrological forecasting exercises, as the assumption of stationarity is inherent in conventional modeling processes. Therefore, the characterization of hydrological drought is essential to develop alternative and accurate modeling practices. The insight to long/short memory of time series quantified as its 'persistence' may help in the improved prediction of drought conditions. Also, it may help to get insights into the probable evolution of drought of a future time period. Many parts of the country including PI are agro dominated and the occurrences of drought may have a severe impact on our economy. So proper policy decisions for disaster preparedness and risk assessment of droughts for the future is essential, for which the drought characterization may help as a complementary scientific procedure.

5 Conclusions

The present study considered the monthly, annual and seasonal rainfall of Peninsular India and its six meteorological subdivisions for evaluating the persistence of drought quantified by the Hurst exponent. The specific conclusions of the study are as follows:

- The monthly rainfall time series of PI and its subdivisions showed short-term dependency.
- Annual rainfall time series of all subdivisions except Tamil Nadu and Pondicherry and South Interior Karnataka showed long-term persistence.
- The SPI estimates at different aggregation time scales all over the Peninsular region showed long-term dependency.
- The persistence of drought is found to be increasing with an increase in aggregation time scale.
- The persistence analysis performed for the seasonal rainfall revealed that the datasets of the post-monsoon season are long-term persistent at PI region and all of its subdivisions except Tamil Nadu and Pondicherry and South Interior Karnataka.
- No transition was observed in the nature of persistence (short to long or vice versa) of SPI time series and monthly rainfall series in PI and its subdivisions with respect to the global climatic shift of 1976/1977.

- The annual rainfall series of Kerala showed short-term persistence whereas that of Tamil Nadu and Pondicherry showed long-term persistence after the climate shift.
- The short-term persistence witnessed in the monsoon rainfall of Kerala and PI changed to long-term persistence after the climate shift.

The novel insights gained from the study can be used for improving the predictability efforts of meteorological drought in different subdivisions of India.

References

1. Kumar MN, Murthy CS, Sesha Sai MVR, Roy PS (2012) Spatiotemporal analysis of meteorological drought variability in the Indian region using standardized precipitation index. Met App 19:256–264
2. Koutsoyiannis D (2005) Hydrologic persistence and the hurst phenomenon. In: Lehr JH, Keeley J (eds) Water encyclopedia
3. Hurst HE (1951) Long-term storage capacity of reservoirs. Trans Am Soc Civil Eng 116:770–808
4. Chandrasekaran S, Poomalai S, Saminathan B, Suthanthiravel S, Sundaram K, Abdul Hakkim FF (2019) An investigation on the relationship between the Hurst exponent and the predictability of a rainfall time series. Met App 26:511–519
5. Szolgayova E, Laaha G, Blösch G, Bucher C (2014) Factors influencing long range dependence in streamflow of European rivers. Hydrol Process 28:1573–1586
6. López Lambraño A, Fuentes C, López-Ramos A, Mata J, López-Lambraño M (2018) Spatial and temporal Hurst exponent variability of rainfall series based on the climatological distribution in a semiarid region in Mexico. Atmósfera 31(3):199–219
7. Duhan D, Pandey A, Gahalaut K, Pandey R (2013) Spatial and temporal variability in maximum, minimum and mean air temperatures at Madhya Pradesh in central India. CR Geosci 345:3–21
8. Markonisa Y, Moustakis Y, Nasika C, Sychova P, Dimitriadis P, Hanel M., Máca P (2018) Global estimation of long-term persistence in annual river runoff. Adv Water Resour 113:1–12
9. Pal S, Dutta S, Nasrin T, Chattopadhyay S (2020) Hurst exponent approach through rescaled range analysis to study the time series of summer monsoon rainfall over northeast India. Theor Appl Climatol 142:581–587
10. Zargar A, Sadiq R, Naser B (2011) A review of drought indices. Environ Rev 19(1):333–349
11. Adarsh S, Deepthi B, Gayathri G, Aswathy SS, Bhagyasree S, Kumar DN (2019) Multifractal characterization of meteorological drought in India using detrended fluctuation analysis. Int J Climatol 1–22
12. Alves da Silva AS, Cunha Filho M, Simões Cezar Menezes R, Stosic T, Stosic B (2020) Trends and persistence of dry–wet conditions in Northeast Brazil. Atmosphere 11:1134
13. Thomas T, Nayak PC, Ghosh NC (2015) Spatiotemporal analysis of drought characteristics in the Bundelkhand region of Central India using the standardized precipitation index. J Hydrol Eng 20(11)
14. Mallenahalli NK (2020) Comparison of parametric and nonparametric standardized precipitation index for detecting meteorological drought over the Indian region. Theor Appl Climatol 142:219–236
15. Miyan M (2014) Droughts in Asian least developed countries: vulnerability and sustainability. Weather Clim Extrem 7. https://doi.org/10.1016/j.wace.2014.06.003
16. Tong S, Li X, Zhang J, Bao Y, Yongbin B, Na L, Si A (2019) Spatial and temporal variability in extreme temperature and precipitation events in Inner Mongolia (China) during 1960–2017. Sci Total Environ 649:75–89

17. Parthasarathy B, Kumar KR, Munot AA (1993) Homogeneous Indian monsoon rainfall: variability and prediction. Proc Indian Acad Sci-Earth Planet Sci 102(1):121–155
18. Miller AJ, Rayan DR, Barnett TP, Graham NE, Oberhuber JM (1994) The 1976–77 climate shift of the Pacific Ocean. Oceanography 7(1):21–26
19. Sahana AS, Ghosh S, Ganguly A, Murtugudde R (2015) Shift in Indian summer monsoon onset during 1976/1977. Environ Res Lett 10
20. Guhathakurta P, Rajeevan M (2008) Trends in the rainfall pattern over India. Int J Climatol 28:1453–1469
21. Rajeevan M, Pai D (2007) On the El Niño-Indian monsoon predictive relationships. Geophys Res Lett 34. https://doi.org/10.1029/2006GL028916

Water Security

The Role of Water Governance in Ensuring Water Security: A Case of Indian Cities

Siddh Doshi and Rutool Sharma

1 Introduction

Water is an unequally distributed, transient, highly variable yet renewable natural resource. While water is an inherent part of the natural environment, its use is essential to all economic and social activities [1]. Urban water has been both a catalyst of development, through the engineered approaches of pipe networks, and impetus for catastrophes [2]. Urban water has always gained social and political attention, primarily due to infrastructure financing, control, and governance mechanisms. Urban water resources are under serious threat due to the rapid rates of urbanization. Such threats lay further stress on developing and promoting adaptive and accommodative governance regimes to manage water resources. This gap has encouraged researchers and advocacy agencies to develop alternative conceptual tools and frameworks to address urban water nexus issues. These frameworks intend to study the issue of urban water from entry points like scarcity [1], equity [3], or decision-making, management, and use [4]. Apart from the recent discourses on developing improved frameworks, the contemporary commentary on urban water has evolved from a simple demand lead system design to a holistic approach considering microclimate and the overall ecosystem [5]. Similarly, the recent discussions over water security also aim to harness the productive prospects and reduce the destructive potentials of urban water systems [6].

While several attempts to develop an adaptive fit-to-purpose framework of urban water management have been made in the recent past, little progress has been measured on the ground. Each of these concepts of urban water management,

S. Doshi (✉)
Doctoral Candidate, Faculty of Planning, CEPT University, Ahmedabad, India
e-mail: siddh.doshi@cept.ac.in

R. Sharma
Assistant, Faculty of Planning, CEPT University, Ahmedabad, India
e-mail: rutool@cept.ac.in

like Green Infrastructure (GI), Integrated Water Resource Management (IWRM), Sustainable Urban Drainage Systems (SUDS), etc., have ventured towards the path of holistic development of urban water resources. Yet, most of these concepts have been limited to context-specific practices. Nevertheless, on close observation, one can find several overlaps amongst most urban water management concepts—one of the universal tools in almost all these concepts is water governance.

Interestingly, several theoretical literature and advocacy documents have equally empathized over the past few decades on water governance as a tool to address the contemporary issues of water crisis [1]. The term "water governance" has gained prominence in global literature quite quickly. The growing dominance of the term water governance can be seen in reviewing the term's use on various international platforms and research documents. For example, Google Scholar in the 1990s recorded 47 references (excluding citations) of "water governance" in comparison to 1270 for "environmental governance". While in 2020, there are 4110 references to "water governance" and 6580 for "environmental governance".

This article presents a brief overview of water governance's evolution and documents its perceived perspectives in literature. The research lists various definitions of the term water governance. The section concludes that while the perceived definition of water governance may be fuzzy and inconsistent, most recognized definitions have some common essential elements. The authors use these essential elements to develop a working definition of water governance for cities in developing countries. In the later section, the paper continues this discussion of water governance in developing countries' cities and explores the legal and regulatory framework existing in water governance, and suggests a way forward, taking India as a case study.

2 Evolution of Water Governance

Conference on Human Environment in 1972 brought a new paradigm to review issues related to the environment and natural resources on the international platform. This was the first time the world accepted that there is growing evidence of human-made harm leading to dangerous levels of pollution in water. The conference ended with an official declaration, commonly known as the Stockholm Declaration of 1972, which identified 26 principles concerning human impact on the environment. Principle 2 of the declaration mentions, "The natural resources of the earth, including the air, water, land, flora and fauna and especially representative samples of natural ecosystems, must be safeguarded for the benefit of present and future generations careful planning or management, as appropriate". Thus, water was put on the global agenda for the first time, not from the governance perspective but from pollution. Since then, the UN has convened several conferences that advocated the need to pay attention to natural resources and the environment. However, these conferences brought the term water governance into international policy documents in a much ad-hoc manner [7]. Notable ones in the next three decades include Mar del Plata Conference of 1977, Water and Sanitation Decade of the 1980s, UN Conference on Environment and

Secure **equitable access** to water for all people	Ensure that **water infrastructure** and services deliver to **poor people**	Promote **gender equity**	Appropriately **allocate water** among competing demands
Share benefits	Promote **participatory sharing** of benefits from large projects	**Improve water management**	Protect **water quality** and ecosystems
Manage risks to cope with variability and **climate change**	Encourage more **efficient service** provision	**Manage water** at the lowest appropriate level	**Combat corruption** effectively

Fig. 1 Initial Actions for Water Governance based on Bonn Conference 2001 (Adapted from UN World Water Development Report (526), by UNESCO [12])

Development of 1992, Dublin Conference on Water and the Environment of 1992, World Water Forum since 1997, and the Millennium Development Goals 2000; all elaborated on the issues around water resources [8].

Amongst all the above conferences, the 1992 Dublin Conference's targets can be directly related to water governance's current notion. The outcome of this conference "The Dublin Statement on Water and Sustainable Development" recognized the increasing scarcity of water due to the different conflicting uses and overuses of water and laid down recommendations for action at the local, national, and international level through four major guiding principles. Principle 2 discussed involving a participatory approach in water development and management, while principle 3 discussed women's central role in the provision, management, and safeguarding of water. Thus, these two principles laid down preliminary aspects related to water governance, though indirectly. Accordingly, it can be marked as the threshold platform that initiated the discussion on urban water governance [9]. The concept of governing water was formally discussed in the 2000 Hague World Water Forum, where water governance was identified, and the discussions then claimed "water crises as a governance issue"[10]. This statement advocated that water systems and supplies' failures are not necessarily the result of water scarcity or lack of technical possibilities but due to inefficient water governance. Policy advocacy quickly took up this concern. In 2001 at the International Conference on Freshwater (held at Bonn), it drew the attention of the international audience on the importance of water governance. The Boon conference ranked water governance as one of the three priority action areas (besides capacity building and knowledge sharing, and financial mobility of resources) [11]. However, the Bonn conference led to over 27 recommended actions without a set timeline to achieve its targets. These included 12 recommendations for water governance [12], which help trace water governance's initial intent as a concept.

It can be observed from the list above (Fig. 1) that, from its inception, the term "water governance" was addressing a diverse range of challenges. The nomenclature rose to the limelight almost spontaneously in several international organizations with the flourishing dialogue and international water movement. Soon the term operationalized in global policy documents and advocacy. The first definition was expressed in 2002 by such a leading international water organization Global Water Partnership (GWP)[1] and later modified and adopted by the UN. The definition states:

> The governance of water, in particular, can be said to be made up of the range of political, social, economic and administrative systems that are in place, which diretly or indirectly affect the use, development, and management of water resources and the delivery of water services at different levels of society. Governance systems determine who gets what water, when, and how and decide who has the right to water and related services and benefits. [1, 11, 13]

Almost during the same time, there was another definition by UNDP about water governance that is noteworthy:

> The political, economic, and social processes and institutions by which governments, civil society, and the private sector make decisions about how best to use, develop, and manage water resources. [14]

While these initial attempts of defining water governance are associated with a larger notion of governance, it also considered the nuances of the sector-specific concepts like service delivery. The recognition of water governance by such prominent agencies leads to the recognition of water governance in academic circles. Attempts to define water governance could be observed in academic literature as well. Most of these attempts were driven by exploring the future trajectories of this naïve term. One such noticeable definition is as follows:

> The development and implementation of norms, principles, rules, incentives, informative tools, and infrastructure to promote a change in the behaviour of actors at the global level in the area of water governance. [8]

More recently, the Organization of Economic Corporation and Development (OECD), which is actively working on urban water systems, defines water governance as follows:

> The range of political, institutional and administrative rules, practices and processes (formal and informal) through which decisions are taken and implemented, stakeholders can articulate their interests and have their concerns considered, and decision-makers are held accountable for water management. [15]

Apart from these definitions, even the Sustainable Development Goals (SDGs), through their goals, 6.5.1 and 6.5.2, have laid substantial emphasis on concepts

---

[1] Established in 1996, by the World Bank, United Nations Development Programme (UNDP) and Swedish International Development Cooperation Agency (SIDA), the Global Water Partnership, encompasses international government agencies, donor organizations, and public and private institutes actively engaged in the water sector. Currently, GWP has about 3,000 Partner organizations in 179 countries.

that use water governance as a tool for implementation. Furthermore, it has been envisaged that appropriate water governance implementation shall place a crucial role in achieving the SGD goals [16].

Each definition and interpretation brings its own set of specific concepts and motives. Such commentary could lead to fragmentation of the term into newer ideas and would do little good to the larger picture. These complexities and multiple challenges have helped water governance attain the title of a wicked problem [17].

Despite the fuzziness, the evolution of the term "water governance" seems to have some standard essentials. The paradigm notion of water governance includes designing institutional frameworks and public policies that can mobilize resources to support their functions independently and are socially accepted. The Central argument of water governance discourses goes beyond water as a utility to water as a resource. While incorporating this, water governance also addresses the concerns of water policy and its formulation. Thus, holistically approaching this term, overlaps with economic and technical aspects are found along with indications on solving or exploring administrative and political elements [9]. Inferring from here, one can conclude the water governance is concerned with the relationship of social, political, and economic organizations and institutions that are important for the management and development of water resources.

This lack of uniformity in defining the term water governance calls for a need to develop a clearer and fit-to-purpose definition. This is crucial, particularly in developing countries, where there are limited information and clarity of these overlaps and interplays. This calls for a need to establish a consultative and participatory approach while forming water governance systems. Water resources are not confined to urban limits and boundaries. The consideration of hydro-geographical boundaries while developing the water governance framework is another challenge.

Furthermore, despite all the claims for holistic considerations, these definitions fail when applied differently. Thus, implying the importance of adaptivity in the water sector while defining water governance. The development of newer, often overlapping, water management concepts and their interpretation of water governance structures also require careful attention. The situation further blurs in developing counties like India, where several agencies in the urban water nexus overlay.

3 Water Governance in Developing Countries—A Case of India

Universally dialogues on access to water services, lack of institutional capacities, and infrastructural provisioning in developing countries have been discussed in academic literature [18]. The same has been advocated by development agencies who emphasize transforming the existing water resource infrastructure to achieve sustainable development and resilience targets in developing countries [19]. Such interventions help achieve the desired global goals and targets and enhance ownership amongst the

community members and strengthen their bargaining capacity with the government for water services [20]. It can also address issues such as the need for bottom-up water approaches for the global south countries. As most developing countries have an incomplete network of existing infrastructure services, integrated network approaches, propagated as a larger part of water governance, could be implemented with relative ease. It can cover, theoretically, a large aspect of water governance, India.

Yet, the challenge of connecting proclaimed theories and concepts to the practicalities of implementation remains uncontested. Also, it is to note that majority of these definitions of water governance are conceptualized in the global north, i.e., in the context of developed nations, making their replication in the global south (the developing countries) would demand a closer understanding and engagement alongside local idiosyncrasies. If such considerations are neglected, the envisaged benefits, as per the extended definition, may not be possible, leading to contradictory consequences and limited progress economically, socially, and environmentally in public health. Hence, while considering the implementation of water governance elements in cities of the global south, right collaborations between local and international experts, through the support of authorities and advocacy organizations, become quintessential.

The water governance inequalities in the global south have varied origins. Simultaneously, some scholars suggest it to be due to the historical legacies; others denote this with the usage of arbitrary water categories that privilege certain forms of water collection over the others. Hence water governance in the global south can be considered "many overlapping conflicts" that find roots in colonial policy segregation, discriminatory land policies, and associated complications for upgrading contemporary urban settlements [21]. Also, most of these situations require a context-specific consideration, and thus, no umbrella framework could be derived. For this study, we shall consider the contemporary water governance framework of India. This section would critically analyse the legal and regulatory framework existing in the Indian context and suggest a way forward.

India is a signatory to numerous international treaties and frameworks aimed at tackling issues on the water. The SDG 6 of UN's Sustainable Development Goals aspires to provide clean water and sanitation to all; the Sendai Framework on Disaster Risk Reduction aims at achieving disaster resilience of signatory nations, with clear targets to manage disaster risk effectively. The country has also signed water-sharing treaties with neighbouring countries. These, along with other factors, play an essential role in deciding its national and state water policies.

Water is a State subject, as per India's Constitution, implying that water governance is decentralized at the state level. Water management and governance within a state is the responsibility of the numerous municipal and district level bodies in urban areas and the different tiers of Panchayats in rural areas [22]. With 16% of the global population, the country must meet its water demands with merely 4% of the global freshwater resources [23]. With more than 75 million people unable to access clean drinking water, India fares worst in Asia in terms of the percentage population without access to safe, potable water [22].

The rapid pace of urbanization, poverty, the encroachment of watersheds, and unsustainable water resource use have increased Indian cities' vulnerability to water risks. The looming water crisis became apparent when various cities, including Bengaluru, Shimla, and Chennai, reached the brink of "day-zero"—exhausting their freshwater supply. Floods have become common in major Indian cities, with nearly all metropolitan and secondary cities reporting urban flooding instances during monsoons. The civic authorities struggle to address such issues, owing mainly to water governance challenges.

India's water governance issues include an intricate decision-making system, inter-state conflicts over water rights, insufficient technical and financial capacity, inadequate water-related expertise amongst decision-makers, especially at the local level [22]. Despite the launch of a gamut of initiatives, the country struggles to improve its water resource management. These issues can be attributed to the incomplete decentralization, inadequate monitoring of project implementation, and an obsolete approach to urban planning.

4 Conceptualizing Water Governance in India

The political and institutional complexities are one of the primary reasons for the failure of these integrated water resource models [24]. The implementation of water governance, as discussed above, heavily emphasize planning, developing, and managing at basin scale the resources. This can seldom be possible; for instance, the National Water Policy (NWP) 2012 of India has suggested practising basin plans, yet no such plans exist [25]. Thus, despite policy rhetoric advocating these concepts, governments worldwide focus on structural, regulatory, and efficiency mechanisms, and there has been limited impact on the systems [26]. This shows an apparent "policy failure". The need for understanding this disconnect between implementation and policy needs to be analysed. While there is elaborate literature on this phenomenon regarding environmental policy, little exploration to address a similar gap in urban water management is seen [27].

So, it is necessary to identify the critical elements of the term "water governance", based on its interpretation in several context-specific water management concepts, policy, and advocacy documents to undermine its multisectoral and multidisciplinary scope. This identification of essentials could then be considered a checklist for defining the term (Fig. 2). Such an exhaustive list could further be used to evaluate any future definition or interpretation of the term water governance.

While the elements listed (Fig. 2) are not represented in any hierarchical form, the grading and preferences will completely depend contextually. Moreover, the premise of fit-to-purpose definitions emphasize on the need for accommodative context-specific flexibility. Acknowledging the same, the authors of this paper advocate these five elements (Fig. 2) as the fundamental elements for the definition and implementation of water governance for any developing country. Based on the above-identified essential elements of the term water governance, this research advocates that:
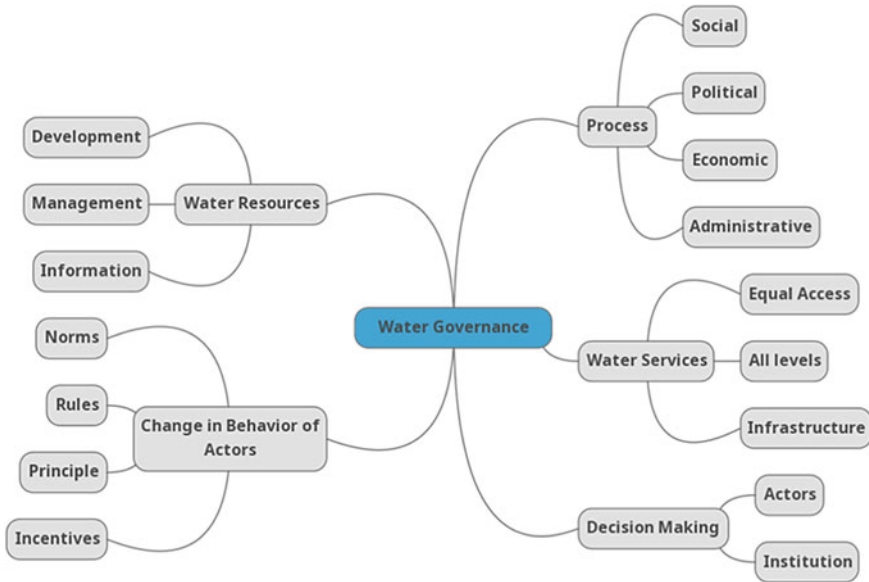
Fig. 2 List of critical elements in defining the term "water governance" derived from documented literature (*Source* Authors)

Water governance facilitates (for actors and institutions) the decision-making process (in terms of Social, Economical, Political and Administrative) for protection/conservation, development, management, and documentation of water resources with the desire to change the behaviour of actors and institutes (through norms, rules, principles, policies, and incentives) in lines with the contemporary discourses on sustainability and resilience.

5 Discussions and Way Forward

Water governance is a key to achieving the targeted SDGs, particularly SDG6, and would be necessary for sustainable use and management of urban water systems. While there is no one agreed-upon definition of water governance in literature, there are several interpretations of the term. The research presents a brief evolution of water governance and attempts to identify a generic definition for the Indian context. However, while defining the definition, the authors of this research have tried to keep the definition as adaptive as possible to make it a fit-to-purpose definition for developing countries at large. The study also discusses the dilemmas that developing countries, specifically India, possess in terms of policy and legislation while addressing the concept of water governance.

While defining the concept of water governance, the study subtly opens up several questions on developing a fit-to-purpose framework for water governance. The contemporary commentaries on water-sensitive cities also have identified water

governance as a promising concept towards achieving water sensitivity. Such studies could also be used as a foundation to develop an integrated water governance framework for water-sensitive cities. The study further nudges to investigate linkages amongst the various identified water governance parameters contextually to derive context-specific implications. Thus, the research authors also consider this research an entry point into the more extensive discussions of adaptive and participatory water management resources.

References

1. Woodhouse P, Muller M (2017) Water governance—an historical perspective on current debates. World Dev 225–241
2. Bell S (2014) Renegotiating urban water. Process in Planning
3. Zwarteveen M, Kemerink-Seyoum JS, Kooy M, Evers J, Guerrero TA, Batubara B, Wesselink A, et al (2017) Engaging with the politics of water goverance. WIREs Water 1–9
4. Wilson NJ, Harris LM, Nelson J, Shah SH (2019) Re-theorizing politics inwater governance. Water Gov Retheorizing Polit 1–13
5. Fletcher TD, Shuster W, Hunt WF, Ashley R, Butler D, Arthur S, Viklander M, et al (2015) SUDS, LID, BMPs, WSUD and more—the evolution and application of terminology surrounding urban drainage. Urban Water J 525–542
6. Grey D, Sadoff CW (2007) Sink or Swim? Water security for growth and development. Water Policy 545–571
7. Gupta J, Akhmouch A, Cosgrove W, Hurwitz Z, Maestu J, Ünver O (2013) Policymakers' reflections on water governance issues. Ecol Soc 35
8. Pahl-Wostl C, Gupta J, Petry D (2008) Governance and the global water system: a theoretical exploration. Global Gov Water Trends Processes Ideas Fut 419–435
9. Rogers P, Hall AW (2003) Effective water governance. Global Water Partnership Technical Committee (TEC), Sweden
10. GWP (2000) Towards water security: a framework for action. GWP, Stockholm
11. Sehring J (2009) The politics of water institutional reform in neopatrimonial states: a comparative analysis of Kyrgyzstan and Tajikistan. VS Verlag für Sozialwissenschaften, Wiesbaden
12. UNESCO (2003) Water for people, water for life. United Nations Educational, Scientific and Cultural Orgnaisation (UNESCO) and Berghahn Books, Barcelona
13. Lautze J, de Silva S, Giordano M, Sanford L (2011) Putting the cart before the horse:water governance and IWRM. Nat Res Forum 1–8
14. UNDP (2004) Water governance for poverty reduction. United Nations Development Programme, New York
15. OECD (2015) OECD principles on water governance. Adopted by the OECD Regional Development Policy Committee

16. FAO (2019) Land and water governance to achieve the SDGs in fragile systems. Food and Agriculture Organisation of the United Nations, Rome
17. Head B (2010) Wicked problems in water governance: paradigm changes to promote water sustainability and address planning uncertainty. The urban water security research alliance technical report no 38
18. Bichai F, Flamini AC (2018) The water-sensitive city: implications of an urban water management paradigm and its globalization. Wiley Interdisc Rev Water 1–9
19. Poustie MS, Deletic A (2014) Modeling integrated urban water systems in developing countries: case study of Port Vila, Vanuatu. AMBIO 1093–1111
20. Adams EA, Zulu L, Ouellette-Kray Q (2020) Community water governance for urban water security in the Global South: status, lessons, and prospects. WIREs Water
21. Lu F, Ocampo-Raeder C, Crow B (2014) Equitable water governance: future directions in the understanding and analysis of water inequities in the global South. Water Int 129–142
22. Ahmed M, Araral E (2019) Water governance in India: evidence on water law, policy, and administration from eight indian states. Water
23. NITI Aayog (2020) India voluntary national review 2020, Decade of action—taking SDGs from global to local. NITI Aayog, Government of India, New Delhi
24. Pandit C, Biswas AK (2019) India's national water policy: 'feel good' document, nothing more. Int J Water Resource Dev 1015–1028
25. Biswas AK, Rangachari R, Tortajada C (2009) Water resources of the Indian subcontinent (pp 400). Oxford University Press, New Delhi
26. Farrelly M, Brown R (2011) Rethinking urban water management: experimentation as a way forward? Global Environ Change 721–732
27. Nevill J (2007) Policy failure: Australian freshwater protected area networks. Aust J Environ Manage 35–47

Making Indian Cities Water-Sensitive: A Critical Review of Frameworks

Sameer Kumar, Siddh Doshi, Gargi Mishra, and Mona Iyer

1 Background

Asian cities have contributed over 65% of the global urban expansion in the twenty-first century, resulting in the century being deemed the 'Asian Urban Century' [1]. Of this, the largest urban transformation is occurring in Indian cities [2]. India's urban population of approximately 377 million people accounts for merely one-third of its total population. This may give the impression that India is predominantly rural. However, the rapid urbanization in the twenty-first century has led to the emergence of many secondary cities. Nearly half the country's population is projected to reside in cities by 2050, adding an extra 416 million urban dwellers [3]. A rapid increase in the urban population is often followed by rapid urban sprawl, uncontrolled development, growth of informal settlements, encroachment of low-lying areas and catchments of waterbodies, overexploitation of resources, and an inability of authorities to provide basic infrastructure, as has been observed in numerous Indian cities.

While the demand for water is constantly increasing, the availability of water resources remains limited. India accounts for 17% of the world's population whereas it has merely 4% of the world's freshwater sources [4]. 60% of this is in the Ganga-Brahmaputra-Meghna basin. This unequal distribution of natural water sources, coupled with the rapidly increasing population and haphazard development, results in immense stress on the country's water resources. An assessment by the World

S. Kumar (✉) · S. Doshi · G. Mishra · M. Iyer
CEPT University, Ahmedabad, India
e-mail: sameer.kumar@cept.ac.in

S. Doshi
e-mail: siddh.doshi@cept.ac.in

G. Mishra
e-mail: gargi.mishra@cept.ac.in

M. Iyer
e-mail: mona.iyer@cept.ac.in

Resources Institute revealed that most of India are under high-to-very-high water stress [5]. Climate change has further aggravated these challenges. Several cities around the world are facing a water crisis, some even approaching 'Day Zero', the day by which they would run out of water. Indian cities are also facing a severe water crisis; the NITI Aayog, in its 2018 report, identified 21 major cities on the verge of approaching zero groundwater levels by 2020 [6]. WaterAid has estimated that more than 12% of the country's population is already experiencing the Day Zero scenario [7, 8].

The increased vulnerability to disasters and the looming water crisis in several cities has resulted in the formulation of numerous international treaties and policies. India is a signatory to several such documents including the Paris Agreement, Sendai Framework for Disaster Risk Reduction, and the Sustainable Development Goals. One of the major highlights of these documents is the demand for immediate action with observable impacts by 2030. The international treaties and agreements have resulted in a gamut of policy interventions at the national and provincial levels. The water sector has also witnessed tremendous efforts towards becoming sustainable.

India has revised its urban and rural development strategies in the past few years. The policy focus has widened from a mere provision of water to citizens to a provision of safe water and sanitation. The Government of India has launched a gamut of initiatives in this regard. Further, new initiatives have been launched that strive to achieve sustainable development in the country. Despite making progress across various sectors, India is still struggling to make its cities more sustainable. The urban development policies need to widen their scope to make cities more 'water-sensitive'.

2 Methodology

The intensifying water and climate crises in Indian cities demand a swift and holistic solution. Amongst the existing urban water management paradigms, the water-sensitive city concept offers a promising solution. However, a fit-for-purpose framework needs to be developed; one that is localized to the Indian context.

This paper comprises a critical assessment of the numerous frameworks formulated to tackle water issues. For this, major water challenges faced by Indian cities were first identified through a literature review. Simultaneously, the literature on the urban water management paradigm to tackle water issues were studied. The concept of water-sensitive cities was found most suitable to resolve water-related issues of Indian cities. Therefore, this concept was used to formulate the parameters to assess the five identified frameworks. These frameworks were selected based on their application to cities and their scope. The selected frameworks aspire to address the prevailing urban water issues. Further, these have found applications in several cities in different countries. The contents of the selected toolkits were analysed based on the six parameters considered necessary to become water-sensitive. These include improved infrastructure, built environment, disaster resilience, community empowerment, strengthening institutions, and environmental considerations. The paper uses

the assessment to suggest a way forward for prospective frameworks devised to help Indian cities to become water-sensitive.

3 Literature Review

3.1 Evolution of Different Paradigms for Urban Water Management

Concerns over inefficient water supply and sanitation systems have resulted in the emergence of new terminologies and techniques. Some examples of these include low impact development (LID), sustainable urban drainage systems (SuDS), water-sensitive urban design (WSUD), best management practices (BMP), Stormwater quality improvement devices (SQIDs), and Integrated Urban Water Management (IUWM) [9]. While these terminologies are predominantly aimed at improving urban drainage systems, the concept of integrated urban water management has been in vogue since the 1990s. It envisages an integrated approach towards the management of all parts of the water cycle within a catchment, considering the roles and interactions amongst various institutions involved in water supply, groundwater, wastewater, and stormwater management [9]. Climate change and its consequential effects have played a pivotal role in defining and redefining these terminologies, with the inclusion of environmental considerations in the new water-sensitive frameworks. The evolution of the numerous paradigms on urban water management as traced by researchers [9, 10] has been illustrated in Fig. 1.
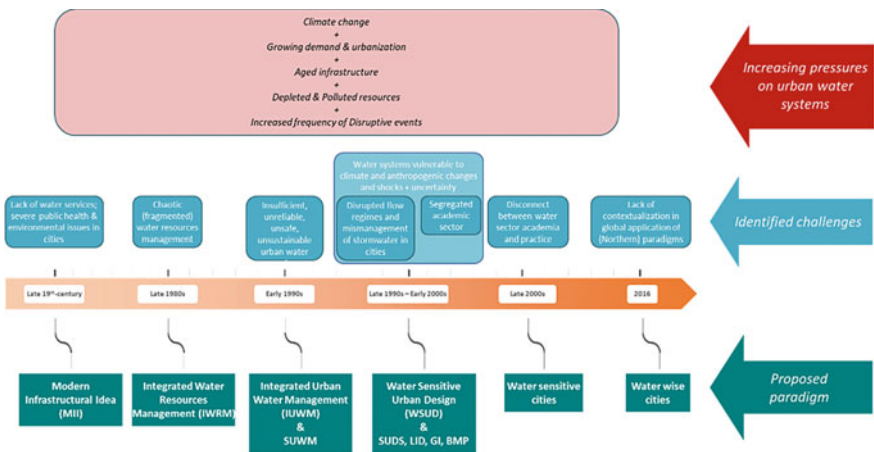

Fig. 1 Evolution of new urban drainage paradigms. Adapted from Fletcher et al. [9] and Bichai et al. [10]

The scope of the different terms and their underlying principles were found to have significant overlaps and two broad principles common across all concepts, viz., (i) mitigation of hydrological changes and evolution of a flow regime aligned to the natural levels, and (ii) improved water quality and reduced pollution [9]. Subtle differences exist in the way these principles are expressed within each concept. Further, the nomenclature of some terms is derived from the "descriptions of techniques and practices" [9]. Figure 2 illustrates the classification of the various terminologies based on their specificity and primary focus [9].

As evident in Fig. 2, the 'green infrastructure' paradigm is the most extensive, both in terms of its primary focus and specificity. 'Integrated urban water management' and 'water-sensitive cities' also have a diverse focus area, ranging from local stormwater management concepts to the larger urban water management cycle. Unlike several other paradigms, these do not focus on merely the technical solutions, rather employing broader principles and concepts to devise an effective solution. This paper analyses the selected frameworks with the lens of water-sensitive cities.
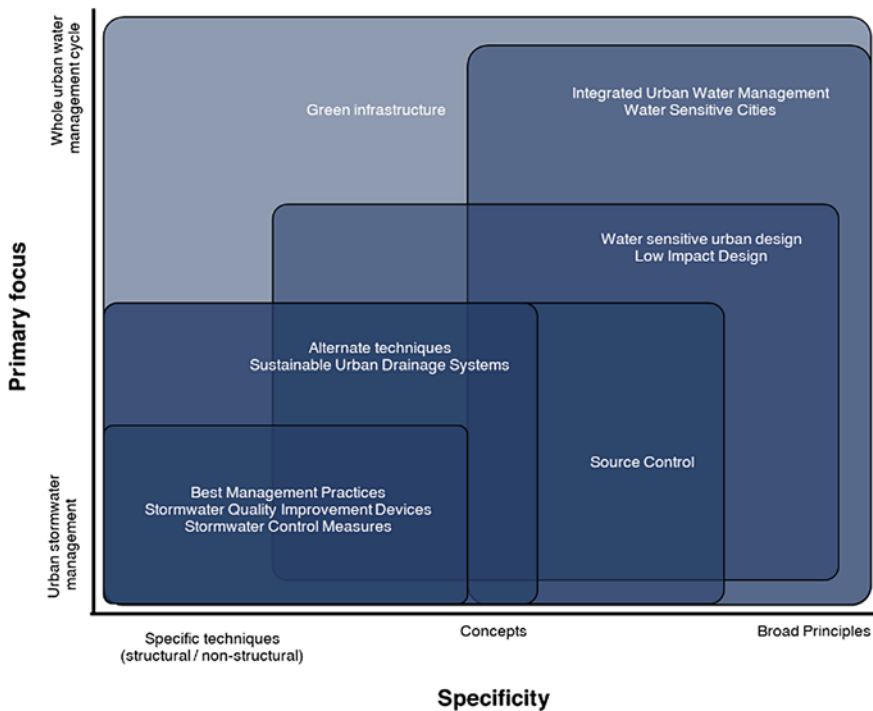

Fig. 2 Classification of urban drainage terminologies based on their specificity and primary focus. Adapted from Fletcher et al. [9]

3.2 Defining a Water-Sensitive City

The last decade has witnessed the emergence of a new concept called 'water-sensitive cities'. One of the first uses of this term was by the Cooperative Research Centre for Water-Sensitive Cities (CRCWSC) in the aftermath of a water crisis in Australian cities [11]. A gamut of literature on water-sensitive cities provides numerous definitions for such cities. Environmental protection, water security, improved technologies, enlightened citizens, and stronger institutions are the common aspects across these definitions [12–14]. As per CRCWSC, a water-sensitive city shall have four broad components—it must be (i) livable, (ii) resilient, (iii) sustainable, and (iv) productive. CRCWSC has identified different stages of water sensitivity based on the kind of issues tackled by its plans and policies (see Fig. 3). Three pillars of water-sensitive cities have been identified by researchers [14].

Variations have been observed in the applications of the different concepts, with the developed nations, i.e., global north, using them to overcome environmental challenges, whereas the developing nations (global south) apply them for basic infrastructural provisions [11]. These variations are due to the difference in the challenges faced by different countries. The cities of the global north have already achieved most of the milestones shown in Fig. 3, whereas those in the developing countries are yet to attain the status of a 'drained city'; the latter are more prone to social,
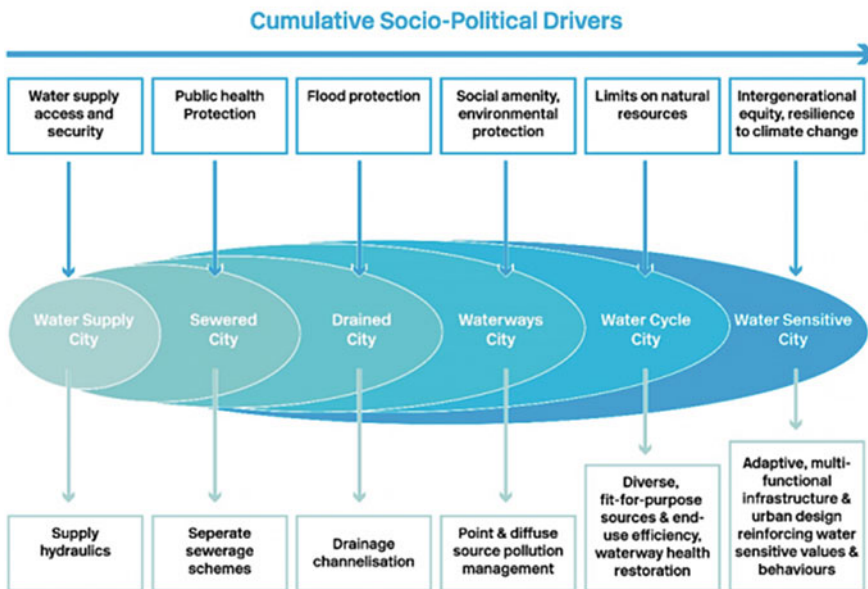

Fig. 3 Urban water transition framework—different stages of becoming a water-sensitive city. Reproduced from https://watersensitivecities.org.au/solutions/wsc-index/

institutional, technological, and economic challenges including poverty, poor institutional capacity, inefficient technologies, and resistance to change [11, 12]. The cities of the global south, therefore, need to leapfrog the steps to achieve the status of water-sensitive cities.

3.3 The Indian Context

India has been undergoing rapid urbanization since the beginning of the twenty-first century. The country's urban population has increased by 31.8% between 2001 and 2011. The number of million-plus cities during the same period increase from 35 to 53 [15]. The country's urban population of 377 million is expected to rise to 606 million by 2030 and 793 million by 2050 [4]. Unlike the dynamic nature of the population, the availability of resources is constant, rather showing a decreasing trend due to unsustainable use. The authorities' plans for urban development are inefficient in coping with the rapid urbanization, resulting in an increase in slum population, overexploitation and illegal extraction of water, encroachment in catchments of waterbodies and low-lying areas, and several other challenges. The municipal water supply in Indian cities shows stark disparities, varying between 37 and 298 lpcd with the duration of supply varying between once in six days to daily supply in different cities [16].

India, with 85% of its land vulnerable to climate-induced natural disasters, was ranked 5th in the Global Climate Risk Index 2020 [4]. A study by the Water Resources Institute found India to be amongst the critically water-stressed countries of the world [5]. Several cities, including Bengaluru, Shimla, and Chennai, have faced severe water crisis in recent years. The water demand is expected to increase in the subsequent years. With merely 4% of the world's freshwater resources available to its population, India faces a daunting challenge. The unequal distribution of water sources and the consequences of climate change further complicates the situation. The water demand is expected to be twice the available supply by 2030 [4].

Numerous strategies and frameworks have been formulated and applied to address the urban water issues in Indian cities. These have marginally improved the conditions, but the situation remains grim with most cities, especially the rapidly developing secondary cities, unable to address emerging challenges like urban flooding, droughts, and calamities due to climate change. The governments along with the planning agencies need to formulate more efficient and innovative strategies to tackle the looming water crisis across Indian cities.

3.4 Parameters for Assessment

The review of the numerous urban water management paradigms and the Indian context helped ascertain the most suitable paradigm that can be applied to tackle the water issues in Indian cities. A holistic solution to address the inadequate water
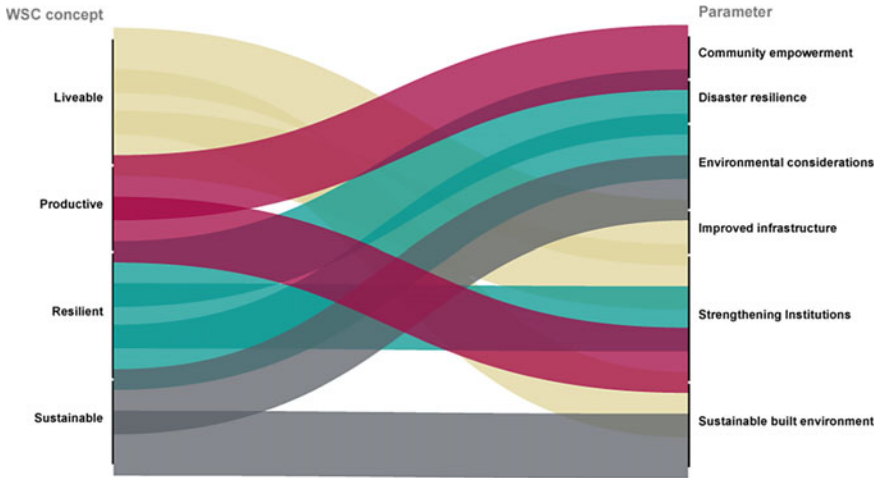
Fig. 4 Parameters for the assessment derived considering the fundamental aspects of WSC

supply infrastructure, environmental conservation, and high vulnerability to disasters is needed. The concept of water-sensitive cities provides an overarching solution to these issues.

Literature review of the concept revealed four fundamental aspects of water-sensitive cities, viz., livable, sustainable, resilient, and productive. The parameters for assessment of the frameworks were derived considering these aspects (Fig. 4).

Indian cities are yet to achieve 100% coverage of the water supply and sewerage network. The quantity and quality of water supplied are also inadequate in several cities. A framework to make Indian cities must include parameters aimed at infrastructural improvements. For this research, the parameter 'improved infrastructure' considers improving the provision of water and sanitation services, ensuring adequate quality and quantity of supply, while also considering the cost to the consumers, i.e., affordability of infrastructural provisions. 'Infrastructure' is also considered to include solid waste, wastewater, and sewage treatment services.

'Sustainable built environment' requires technologies and paradigms (e.g., WSUD) that help develop harmony between the built environment/built form and natural environment. These include water-sensitive urban design, land-use regulations like mixed-use communities, and adopting an integrated approach to urban planning [17].

The transition to water-sensitive cities requires conservation and restoration of the environment and natural resources [14]. The research, therefore, assesses the environmental considerations, including spatial reservations, preserving critical habitats and ecosystems, mapping and active monitoring of natural resources, reducing pollution, and promoting sustainable consumption.

The Intergovernmental Panel on Climate Change defines 'resilience' as the '*ability of a system and its component parts to anticipate, absorb, accommodate or recover from the effects of a hazardous event in a timely and efficient manner*' [18]. The disaster resilience of a city is, therefore, its ability to mitigate and recover from the effects of disasters. The large urban population, the looming water crisis, and the consequences of climate change have increased the vulnerability of cities to disasters. A water-sensitive city framework must, therefore, measure the disaster resilience of cities. The probable indicators include records of past events including spatial extent (map), capacity building of authorities, public awareness campaigns, regular monitoring, and setting up emergency response centres.

Major challenges faced by local institutions in Indian cities include inadequate technical and financial capacity, unavailability of collated data, overlapping jurisdictions, and indistinct responsibilities [19–21]. A lack of accountability and transparency in governance is another hindrance to efficient urban planning [22, 23]. These considerations have been incorporated under the parameter 'strengthening institutions' in this study.

Community participation is found to play a pivotal role in the success of plans and strategies [19]. A top-down approach to planning results in inefficient urban development. Active involvement of the local communities in the plan-making process is needed. The importance of community participation has also been identified by the Government of India in its Smart Cities Mission [20]. This research, therefore, includes 'community empowerment' through awareness, active participation, and training and capacity building in the assessment of the selected frameworks.

4 Assessment of Toolkits and Frameworks

Numerous frameworks have been formulated globally to tackle the numerous water challenges. These incorporate the applications of different techniques and strive to achieve different yet overlapping goals. The assessed frameworks include CRCWSC's Water-Sensitive City toolkit, City Water Resilience Approach formulated by Arup and SIWI, the USAID Toolkit for Climate Resilient Water Utility Operations, the IUWM Toolkit for Indian Cities developed by ICLEI, and the Urban Water Security Toolkit devised by the Centre for Water and Sanitation, CRDF. The Urban Water Security Toolkit and the IUWM Toolkit have been prepared and applied to the Indian context; the USAID's Toolkit has been used in several water districts of the Philippines; the CWRA has found applications in cities in the Global North—including those in United Kingdom, USA—as well as those of the Global South—in South Africa, Mexico, and Jordan; the Water-Sensitive City Toolkit formulated by CRCWSC has been used across numerous Australian cities, as well as in Fiji, Indonesia, Myanmar, and China (see Fig. 5).

The major challenges faced by Indian cities in the twenty-first century relate to water security, governance, environmental degradation, and vulnerability to disasters. There is an imminent need to ensure the availability of adequate quantity and
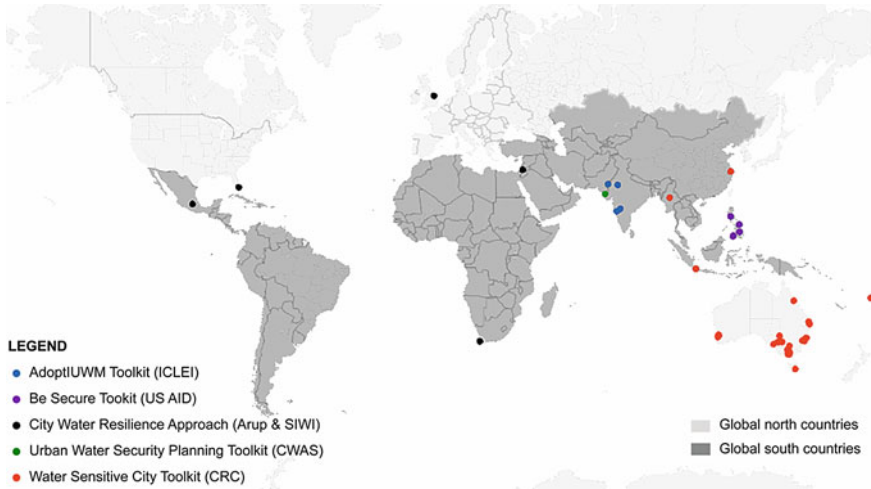
Fig. 5 Applications of selected toolkits shown with respect to the Global North-South divide

proper quality of water to all; improvements in water supply and sanitation infrastructure will help attain this goal. Such provisions are inefficient in the absence of strong institutions and without the support of local communities. Planning regulations also play a vital role in ensuring water security, thereby attaining sustainable development. The development strategies also need to incorporate provisions that strive to balance the built and natural environment. The increasing vulnerability of Indian cities to disasters also needs to be addressed through disaster resilience strategies. The paper, therefore, assesses the toolkits and frameworks using six broad criteria, viz., improved infrastructure, sustainable built environment, ecological considerations, strengthening institutions, community empowerment, and disaster resilience.

Stark variations were observed in the provisions of the assessed toolkits. The Indian toolkits are aimed at ensuring adequate infrastructural provisions, while also proposing considerations towards protecting the ecological resources; the provisions of the toolkits applied mostly in the global north are more evenly distributed amongst the chosen parameters, with a lower emphasis on the provision of infrastructure. This skewed result can be attributed to the prevailing condition of cities in different regions. The developing nations of the global south are still struggling to provide the basic infrastructure; they usually follow the conventional, compartmentalized approach to urban planning. The global north cities have already provided the basic amenities owing to their better capacities and availability of more resources; they follow a more cohesive approach to urban planning, emphasizing more on community empowerment and ecological considerations.

The Urban Water Security Toolkit formulated by CWAS-CRDF lays excellent emphasis on the provision of basic infrastructural services. It also includes provisions aimed at ecological conservation. The toolkit lacks provisions to improve disaster resilience and the empowerment of communities. It does not emphasize sufficiently

on improving the built environment which would result in massive improvements in water security. The IUWM toolkit devised by ICLEI also lays sufficient emphasis on improving basic infrastructural provisions; the inadequate emphasis on strengthening institutions, built environment, disaster resilience, and community empowerment are its drawbacks.

All toolkits laid emphasis on the improvement of water and sanitation infrastructure; there was a difference in the sub-categories. While all the toolkits strive to provide basic services, only a few explicitly mention water pricing and reduced consumption of water. The toolkits which include water pricing, availability at affordable rates, and reduced consumption have been formulated (and implemented) in the cities of the global south, which face issues like poverty and overutilization of resources.

While an integrated approach to urban planning finds mention in the toolkits devised for cities of the global north as well as those of the global south, the latter do not promote the application of innovative techniques for sustainable development. USAID's *Toolkit for Climate Resilient Water Utility Operations* was an outlier for disaster resilience with the maximum proportion of provisions (38%), while less than 10% of the indicators in other toolkits pertaining to this parameter.

The Water-Sensitive City toolkit of CRCWSC is amongst the most balanced toolkits under this study. It adequately emphasizes all the aspects considered necessary by the authors for developing water-sensitive cities, barring disaster relief, which finds insufficient mention in the document. The Arup and SIWI's City Water resilience Approach also contains a well-balanced set of provisions. It, however, does not address issues pertaining to developing a sustainable built environment. Disaster resilience and ecological considerations were also marginally inadequate. The USAID's toolkit was formulated to ensure disaster resilience in the water-scarce and disaster-prone cities of the Philippines. It does not address issues on environmental conservation and community empowerment.

None of the toolkits can be considered 'perfect' for direct application to develop water-sensitive cities in India; each document comprises some beneficial aspects, while also lacking in some others (see Fig. 6). These can, however, act as an inspiration to formulate a fit-for-purpose water-sensitive city framework for Indian cities.

5 Key Learnings and the Way Forward for Indian Cities

The large urban population and high population densities in Indian cities have resulted in an extreme amount of stress on their natural resources, especially water resources. Poverty and rapid migration to cities coupled with the compartmentalized approach towards urban planning further complicate the urban challenges including the vulnerability to disasters including floods, droughts, and cyclones. Authorities should take cognizance of the numerous urban challenges and learn from international experiences to address such issues. Indian cities are still striving to become drained cities
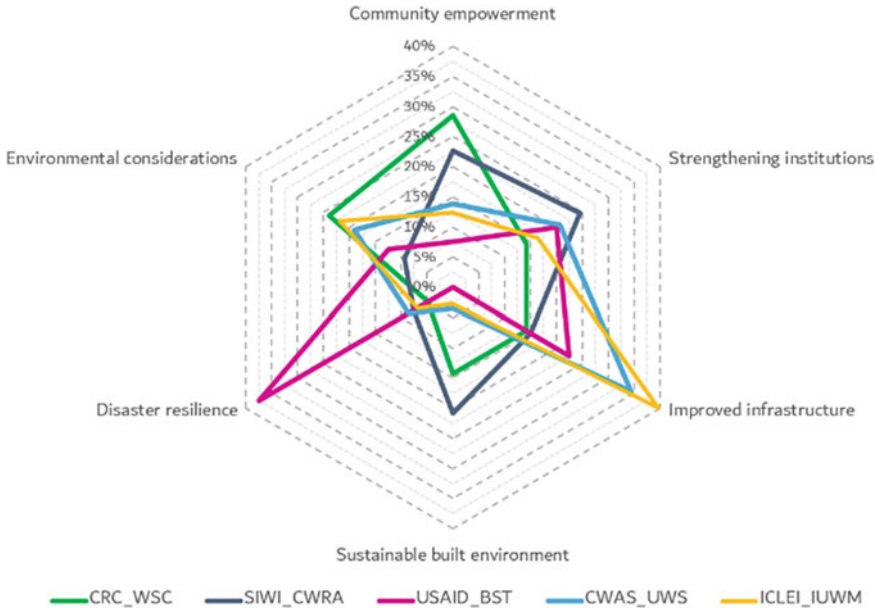
Fig. 6 The toolkits lay varying emphasis on different parameters towards becoming water-sensitive cities

(Fig. 3). The fast-approaching deadline to United Nation-Sustainable Development Goals' call-to-action demands a leapfrogging in these cities' evolution to water-sensitive cities. The frameworks assessed under this study can help them tackle the rapidly increasing urban water challenges; they can act as a foundation for the formulation of a fit-for-purpose framework for water-sensitive Indian cities.

The formulated framework must prioritize the issues with reference to the Indian context while also addressing the global needs. This includes strengthening the local institutions which struggle to cope with their financial and technical capacities; the inclusion of all stakeholders in the plan-making process is also necessary; empowered local communities forming the large urban population would play a significant role in the successful implementation of development strategies and policies. Indian cities' vulnerability to disasters and the looming water crisis must also be addressed by the frameworks. Incorporating these, amongst other aspects, will help the planning agencies, researchers, and other stakeholders in developing water-sensitive Indian cities, complementing the national as well as global efforts to achieve sustainable development.

The use of technology for data collection, analysis, and monitoring implementation will help the planning agencies devise more effective strategies. Indian cities have a large number of institutions bestowed with responsibilities, which often tend to overlap, resulting in governance issues; the roles and responsibilities of each institution must be defined clearly for effective governance and planning [4]. Indian cities are still struggling to provide adequate quality and quantity of infrastructural services

to their citizens. The use of the latest technology and innovations, often learnings from the traditional practices, can help eliminate the constraints faced by authorities in making relevant provisions. Further, the top-down approach followed in the conventional urban development model needs to be transformed; a bottom-up/cyclic approach must be adopted, wherein the local communities are included in the plan-making and implementation processes; such an approach will help plan and manage the limited resources more efficiently [24–26]. Empowered communities manage their limited resources more efficiently while reducing the burden on the authorities. Indian cities including Bengaluru and Bhuj have benefited from this approach. Therefore, a water-sensitive city framework for Indian cities must include provisions in this regard.

Sustainable development of cities requires integrated urban planning both in terms of different sectors and different scales. Urban densities can be regulated (through FSI and urban design norms) to increase the available public open spaces. Environmental considerations must be at the core of development strategies to avert the looming water crisis and tackle the increased vulnerability of cities to disasters. Multi-scalar planning and buffer zones will help protect the waterbodies and their catchments. Prohibiting development around sensitive areas through regulations is also necessary.

Indian cities need to improve their disaster resilience strategies significantly through interventions towards improving planning, record-keeping, and forecasting techniques. The statutory development or master plans should strive to address the increasing vulnerability of cities to disasters like urban floods and droughts. These should include provisions for preventing and coping with such emergencies. A disaster management plan must be formulated for each city with provisions for emergency response in case of calamities. Unstructured strategies like the capacity building of authorities and the education of citizens are also necessary.

These recommendations will help Indian cities become not just 'water-secure' but also 'water-sensitive and resilient'. A framework that includes the aforementioned suggestions will help agencies formulate more sustainable and resilient urban development strategies and ensure their effective implementation for the creation of water-sensitive and water-secure cities.

References

1. UN-HABITAT (2012) State of the World's Cites 2012/2013: United Nations Human Settlements Programme. In: United Nations Human Settlements Programme (UN-HABITAT), 152. https://www.unhabitat.org
2. Prasad S (2019) Why the world should be watching India's fast-growing cities | World Economic Forum. https://www.weforum.org/agenda/2019/01/india-urbanization-why-the-world-should-watch/. Accessed 4 Jan 2021
3. UNDESA (2018) World urbanization prospects. In: Demographic research, vol 12. https://www.population.un.org/wup/Publications/Files/WUP2018-Report.pdf
4. NITI Aayog (2020) Decade of action—taking SDGs from global to local India voluntary national review 2020
5. World Resources Institute (2020) Aqueduct water risk atlas. https://www.wri.org/applications/aqueduct/water-risk-atlas/#/?advanced=false&basemap=hydro&indicator=bws_cat&lat=23.162457214216634&lng=77.24349975585939&mapMode=view&month=1&opacity=0.8&ponderation=DEF&predefined=false&projection=absolute&scenario=optimi. Accessed 9 Aug 2020
6. NITI Aayog (2019) Composite water management index (Cwmi), pp 1–42. https://niti.gov.in/sites/default/files/2019-08/cwmi-2.0-latest.pdf
7. Hydrofinity (2019) Day zero is looming for 21 Indian cities. https://www.hydrofinity.com/blog/day-zero-is-looming-for-21-indian-cities. Accessed 26 Dec 2020
8. WaterAid (2019) Beneath the surface : the state of the world's water 2019
9. Fletcher TD, Shuster W, Hunt WF, Ashley R, Butler D, Arthur S, Viklander M, et al (2015) SUDS, LID, BMPs, WSUD and more—the evolution and application of terminology surrounding urban drainage. Urban Water J 12(7):525–542. https://doi.org/10.1080/1573062X.2014.916314
10. Bichai F, Cabrera Flamini A (2018) The water-sensitive city: implications of an urban water management paradigm and its globalization. Wiley interdisciplinary reviews: water 5(3):e1276. https://doi.org/10.1002/wat2.1276
11. Mishra G, Acharya G, Iyer M, Doshi S (2020) Deconstructing water sensitivity: experiences from global cities. IOP conference series: earth and environmental science 592:012012. https://doi.org/10.1088/1755-1315/592/1/012012
12. Barron NJ, Kuller M, Yasmin T, Castonguay AC, Copa V, Duncan-Horner E, Deletic A, et al (2017) Towards water sensitive cities in Asia: an interdisciplinary journey. Water Sci Technol 76(5):1150–1157. https://doi.org/10.2166/wst.2017.287
13. Rogers BC, Dunn G, Hammer K, Novalia W, de Haan FJ, Brown L, Chesterfield C (2020) Water sensitive cities index: a diagnostic tool to assess water sensitivity and guide management actions. Water Res 186:116411. https://doi.org/10.1016/j.watres.2020.116411
14. Wong THF, Brown RR (2009) The water sensitive city: principles for practice. Water Sci Technol 60(3):673–682. https://doi.org/10.2166/wst.2009.436
15. Ministry of Housing & Urban Affairs (2021) Urban growth : ministry of housing and urban affairs, Government of India. http://ww.mohua.gov.in/cms/urban-growth.php. Accessed 4 Jan 2021
16. Panwar M, Antil S (2015) Issues, challenges and prospects of water supply in urban India. IOSR J Hum Soc Sci Ver II 20(5):68–73. https://doi.org/10.9790/0837-20526873
17. Loftness V (2013) Sustainable built Environment sustainability/sustainable built environment, Introduction. In: Loftness V, Haase D (eds) Sustainable built environments, pp 620–633. https://doi.org/10.1007/978-1-4614-5828-9_925
18. AECOM International Development (2017) Toolkit for climate-resilient water utility operations. https://files.globalwaters.org/water-links-files/Toolkit
19. CEPT University (2016) Moving Bhuj towards water security
20. Doshi S, Roy P, Iyer M, Mishra G (2020) The need and rise of secondary smart cities: a case of Bhuj. In: IOP Conf Ser Earth Environ Sci 592:012010. https://doi.org/10.1088/1755-1315/592/1/012010

21. Jha R (2020) The unfinished business of decentralised urban governance in India. Observer Res Found (340). https://www.orfonline.org/research/the-unfinished-business-of-decentralised-urban-governance-in-india-61201/
22. Correa C (2014) India: accountability and governance. https://urbanage.lsecities.net/essays/india-accountability-and-governance. Accessed 12 Jan 2021
23. Oberoi R (2013) Institutionalizing transparency and accountability in indian governance: understanding the impact of right to information. IOSR J Hum Soc Sci 11(4):41–53. https://doi.org/10.9790/0837-1144153
24. Church SP, Payne LB, Peel S, Prokopy LS (2018) Beyondwater data: benefits to volunteers and to local water from a citizen science program. J Environ Planning Manage 62(2):306–326
25. Smith JL (2008) A critical appreciation of the "bottom-up" approach to sustainable water management: embracing complexity rather than desirability. Local Environ 13(4):353–366. https://doi.org/10.1080/13549830701803323
26. Neef A (2009) Transforming rural water governance: towards deliberative and polycentric models. Water alternatives, pp 53–60

Urbanization and its Impact on Groundwater Security

Assessing Groundwater Depletion in Southern India as a Function of Urbanization and Change in Hydrology: A Threat to Tank Irrigation in Madurai City

Aman Srivastava and **Pennan Chinnasamy**

1 Introduction

Groundwater is an important water resource that has contributed significantly to the agricultural sector of India. Of the total groundwater extraction, India extracts 67% for irrigation purposes and 87% for total consumptive uses [1, 2]. In the last 50 years, the total land under groundwater irrigation has increased to 27 million hectares in 2010 as compared to 21 million hectares under surface water irrigation [3]. On the contrary, the unlimited extraction of groundwater has resulted in drastic depletion of the quality and quantity of groundwater. As a consequence, groundwater security is endangered, especially in the arid and semi-arid climatic zones [4–7]. The groundwater extraction has increased by 500% in the last 50 years [8]. Consequently, India has become the highest groundwater extractor with an annual extraction of 245 km^3, which is approximately 25% of the world's groundwater resources [1]. The current groundwater situation is complex with the past literature revealing that the groundwater crisis of depletion of the aquifer is evident across diverse groundwater systems in India [6, 9–12].

Most arid and semiarid regions of the Southern Indian peninsula experience frequent drought and over-exploitation of groundwater resources due to extensive agricultural practices [13, 14]. To combat this, historically, many traditional water recharge structures have been constructed along with strategic locations with settlements, and agricultural fields. One such structure is an irrigation tank which is an

A. Srivastava · P. Chinnasamy (✉)
Center for Technology Alternatives for Rural Areas (CTARA), Indian Institute of Technology Bombay, Mumbai 400076, India
e-mail: p.chinnasamy@iitb.ac.in

P. Chinnasamy
Rural Data Research and Analysis (RuDRA) Lab, Indian Institute of Technology Bombay, Mumbai 400076, India

artificial reservoir used primarily for irrigation in India [15, 16]. These water infrastructures are considered one of the oldest water harvesting technology that was practiced primarily for irrigation purposes for more than 2000 years in Southern India 17, 18, 5]. Tank irrigation ensured a regular supply of water in the adjoining command areas and at the same time ensured potential groundwater recharge to increase the efficiency of well-irrigation [19].

Historically, the tank cascade systems have been a primary water source for the people of Madurai [20, 21]. One of the systems amongst them is the Vandiyur Tank Cascade System (VTCS), wherein Vandiyur tank is one of the largest tanks existing inside the city limits in VTCS and is rapidly being encroached due to urbanization [22], Srivastava and Chinnasamy [17]. Since the 1990s, Madurai has been experiencing rapid urbanization and increased groundwater extraction through tubewells and borewells, due to the increase in Madurai's population size and population density. The population of the city has increased from 0.4 million in 1951 to 1 million (more than 280% increment) in 2011 [23]. With a population density of 733 persons/km^2 in 1990, it increased to 823 persons/km^2 in 2011, and currently, has more than 1000 persons/km^2. Vaigai River, its elegant system of tanks, and agricultural land are the first prey for this urbanization juggernaut. With the increase of urbanization and migration to the city, agricultural activities have been impacted drastically. Due to reduced dependency on the ancient tank cascade system, the farmers have started ignoring the feeder channels and irrigation tanks. This has led to an increased siltation rate in the tank bed, thereby reduced storage potential in tanks and thus decreased groundwater recharge [5].

Therefore, detailed and holistic investigations on the surface—groundwater interactions are required in order to formulate sustainable groundwater development and security plans. Such plans will be useful for developing a comprehensive scheme for artificial and natural recharge of phreatic groundwater by considering the variations in the geomorphic setup and the complex hydrological and hydrogeological conditions. Given this context, the study's primary objective is to understand the influence of changing climatology and land-use patterns on groundwater availability, security, and sustainability in Madurai city. Secondary objectives include understanding the impacts of negative percentage departure of the rainfall, fluctuations in groundwater extraction levels, land use land cover transformations due to urbanization, and rapid change in the rate of surface runoff on the Vandiyur tank cascade system. The study further focused on suggesting appropriate rehabilitation strategies for attaining surface water—groundwater management and security in the changing climate, hydrogeological, and environmental context. The aforementioned objectives require good quality and quantity of observation data, however, obtaining such data is challenging. In such instances when observation data is limited, the use of Remote Sensing (RS) data and Geographical Information System (GIS) has been widely used to bridge data gaps [17, 5], and hence used in this study.
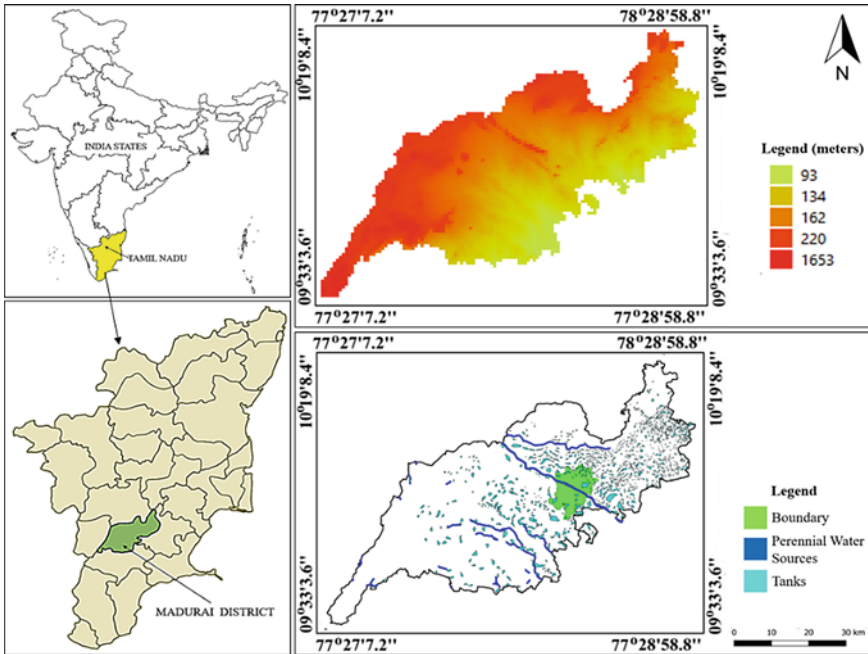
Fig. 1 Location of study site in Madurai district, Tamil Nadu, India (Inset showing the location of Madurai in India and the Digital Elevation Model of Madurai)

2 Methods

2.1 Study Site

The Madurai city represents the administrative headquarter of the Madurai district and is known to be more than 2500 years old [24]. Geographically, it is located between 9.93 °N and 78.12 °E in the Southeast of the Western Ghats[1] at an average elevation of 101 m above mean sea level in the Indian state of Tamil Nadu (Fig. 1) [25]. The city is situated on the bank of the Vaigai river having flat and fertile plains covering an area of 109 km^2. The Madurai district is surrounded by Dindigul district in the North, Theni district in the West, Sivagangai district in the East, and Virudhunagar district in the South. It is the second-largest in terms of area and third largest in terms of population in the state (population of 1,017,865) [26].

The average annual rainfall of Madurai city is about 858 mm [27] which is lesser than the Madurai district's annual average rainfall of 928 mm [28]. The highest rainfall occurs in October, with an average of 191 mm during the Northeast monsoon. Bureau of Indian Standards [29] classifies Madurai city as a warm and humid climate

---

[1] Western Ghats, also known as Sahyadri Range, is a mountain range located parallel to the Western coast of the Indian peninsula; representing one of the 10 biogeographic regions.

zone with temperatures varying between 20 °C and 40 °C during the summer season (between March to June) while 18 °C and 29 °C during the winter months (December to February) [30, 31]. Whereas the occurrence of groundwater has been observed both in shallow fractures, especially located in the phreatic conditions, and deep fractures across unconfined and confined aquifer conditions. The variations of depth to groundwater level during pre-monsoon and post-monsoon season fluctuate between 3.13 to 7.66 m and 1.86 to 5.74 m below ground level, respectively [32, 33]. The major soil type identified in the city are red loam (found at the periphery of the city), clay loam (predominant inside the city), black cotton, and alluvial soil. The region in and around the flat and fertile plains of the city is largely utilized for agriculture activities being irrigated through the canals of the Periyar and Sathaiyar dam. The major agricultural crop is paddy followed by pulses, millets, oilseeds, cotton, and sugarcane [27].

Vandiyur tank cascade system, having 21 tanks in three cascading networks, is the study site and located in Madurai city [22, 5]. This study focuses on one of the networks of VTCS having eight watersheds spread across urban (Vandiyur and Kosakulam-Parsurampatti-Kodikulam), peri-urban (Thiruppalai and Siruvour), and rural areas (Kulamangalam and Veerapandi), as shown in Fig. 2. Each watershed is having system tanks and all these tanks are part of VTCS. The name of the watershed and the tank located within each has been given the same nomenclature (for example, the Veerapandi watershed (*T2*) has been named after the Veerapandi tank located
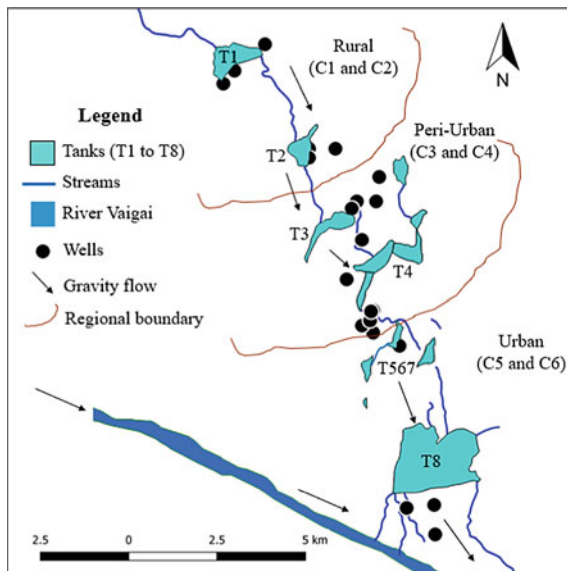

Fig. 2 Location of tanks, watersheds (*T1* to *T8*), and wells (*W1* to *W25*) in Vandiyur tank cascade system (VTCS) in Madurai city (*Rural Watershed have T1: Kulamangalam tank and T2: Veerapandi tank; Peri-urban Watershed have T3: Thiruppalai tank and T4: Siruvour tank; Urban Watershed have T567: Kosakulam-Parsurampatti-Kodikulam tank and T8 Vandiyur tank*)

in the Veerapandi village). These tanks are interconnected to each other through surplus streams, wherein tank *T1* and *T2* are located in the rural watershed, tank *T3* and *T4* in the peri-urban watershed, and tank *T567* and *T8* in the urban watershed. The observation wells (tube wells and borewells) considered for the present study have been selected from each watershed. The surplus water from the Vandiyur tank (last tank of VTCS) becomes a recharge stream for the Vaigai river, situated at its downstream.

2.2 Fieldwork, Data Collection, and Data Processing

The present study encompasses both field (primary data collection) and technical (secondary data analysis) aspects, including both quantitative (data-based) and qualitative (survey-based) research methods [17, 5]. The groundwater data were collected from the Central Ground Water Board (CGWB) archives [1, 8, 32]. Also, the data of the tubewells and borewells adjoining the VTCS has been obtained through field surveys. The wells located in the vicinity of the tanks (mostly downstream of the tank or behind the tank bund) have been taken for the present study rather than the wells located far away from the tank bund. The qualitative interviews were conducted for the 25 well points with the communities settled in the vicinity of the surface water storage structures (tanks). The objective was to guesstimate the depth of extracting groundwater for the past decade.

The Open Data Kit (ODK) Collect App was used to document quantitative information by conducting structured interviews with the local communities and NGOs. The same 25 wells were visited and its depth to water extraction level was measured using meter tape between 2018 and 2020. In order to get the historic analysis of the depth to extraction levels of the wells, the structured interview included questions on the status of the depth of extraction of groundwater below the surface in the past 15 and 10 years and recent years. The location of each well was recorded using Global Positioning System (GPS) Essential App. All the collected data were transferred in M.S. Excel and then imported into QGIS for spatial analysis of groundwater. The analysis of the rainfall was based on the last 50 years of India Meteorological Department (IMD) data [34]. This data was used for the calculation of the percentage departure of the rainfall for the study period.

2.3 Remote Sensing and Data Processing

The assessment of the urbanization trend in Madurai city was based on Remote Sensing (RS) data. The RS images were obtained using Google Earth Pro software for the years 2002 and 2018. The study period 2002–2018 was selected, as clear satellite imagery prior to the year 2002 was unavailable in the Google Earth Pro database. Each watershed map consisted of at least one tank whose surplus water

release became the recharge stream for the next downstream watershed. For developing thematic land-use classes from the watershed boundary, the manual supervised classification method [17, 35 5, 36] was used. Following this, manual photointerpretation was conducted that allowed better capturing of qualitative and quantitative evidence on major land use land cover (LULC) alterations. The LULC classifications included—agriculture, barren land, and forest (non-urbanized cover),tanks and surface recharge streams (surface water storage cover); and built-up regions (urbanized cover consisting of buildings, residential houses, playgrounds, and related concrete covers). Using this information of LULC and refering to Srivastava and Chinnasamy [17], the curve number was identified for various land covers using the Soil Conservation Service Curve Number (SCS-CN) approach [37]. The weighted curve numbers were calculated based on the area of each land use in the identified watershed. The comprehensive analysis was carried out with a baseline focus for the trends of the urbanization, the pattern of the rainfall, the fluctuation in the groundwater levels, and the resulting surface runoff from Madurai city between 2002 and 2018.

3   Results

3.1   Assessing Rainfall and LULC Pattern

The normal annual rainfall was estimated to be 930 mm (average 1950–2017). Results indicated that for 11 years of the study period, the annual percentage departure in rainfall was deficient (Fig. 3a). The current decade (since 2012) has been critical concerning the percentage departure of the rainfall. The rainfall showed an erratic pattern where the percentage departure of the rainfall was recorded to be 46% (maximum) in the past 6 years (Fig. 3b). Similar findings were obtained by Chinnasamy and Srivastava [5] and Srivastava and Chinnasamy [17].

Results from areal imagery analysis (Fig. 4) showed a rapid increase in the urban area, up to 300%, between 2002 and 2018 in peri-urban and urban regions of Madurai city. The cover of the urbanized area was recorded highest for Vandiyur watershed (*T8*) followed by Thiruppalai watershed (Fig. 4). The urbanized cover was found in less than 5% of the entire rural watersheds (*T1* and *T2*) as shown in Figs. 5 and 6. In general, the urbanized cover has increased in all the watersheds since 2002. Another classification of the land considered for the present study was agriculture, forest, and barren land (non-urbanized cover). Agriculture practices are dominant in rural watersheds (Fig. 6). Tanks serve as a primary source of irrigation apart from seasonal rainfall and canal water supply from the Periyar and Sathaiyar dam located upstream of Kulamangalam watershed (*T1*). Overall, the non-urbanized cover has been reduced in all the watersheds since 2002. Saravanabavan et al. [38] also identified the built-up cover (43% of entire Madurai city) to be the most dominating land use land cover classification with an area of 61 km^2, followed by fallow land (20%), cropland (14%),
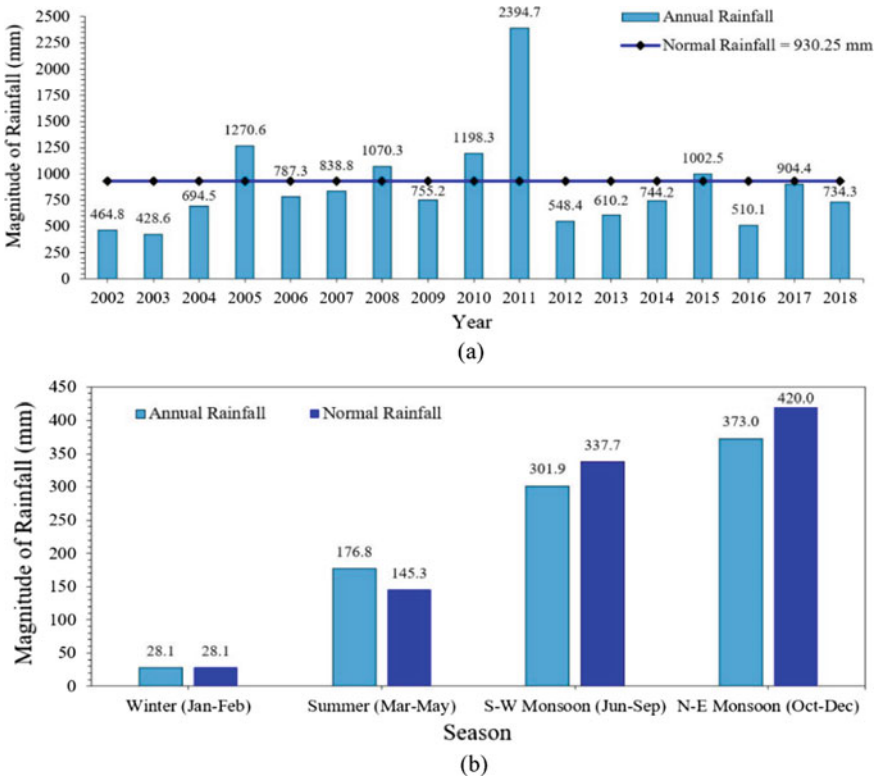
Fig. 3 Rainfall status in Madurai: **a** Average annual rainfall with reference to normal annual rainfall (1950–2017), India since 2002; **b** Season-wise rainfall distribution (*Source* India Meteorological Department (IMD))

and tank water spread area (13%). The study on LULC change by Kundu et al. [23] indicated the decline in the non-urbanized area (by 24%) whereas, the built-up area increased by more than 200% in the entire Madurai city between 2001 and 2018. Similar findings were observed in coherence with the aforementioned findings by Srivastava and Chinnasamy [17, 39].

The percentage change in the LULC across eight interconnected watersheds in Madurai city is summarized in Fig. 7. The highest percentage increment in urbanized cover was recorded to be more than 330% in Siruvour watershed (*T4*) followed by Thiruppalai watershed (*T3*) with an increment of more than 210%. Both *T3* and *T4* are located in the peri-urban region. The reason behind the rapid urbanization in the peri-urban region is attributed to its location and feasibility of expansion. The Vandiyur watershed is close to its saturation concerning land area availability. Therefore, the expansion of the city is happening through Thiruppalai and Siruvour which is located next (at the upstream) to the Vandiyur. Also, agricultural activities are becoming limited due to rainfed-based farming practices having unreliable
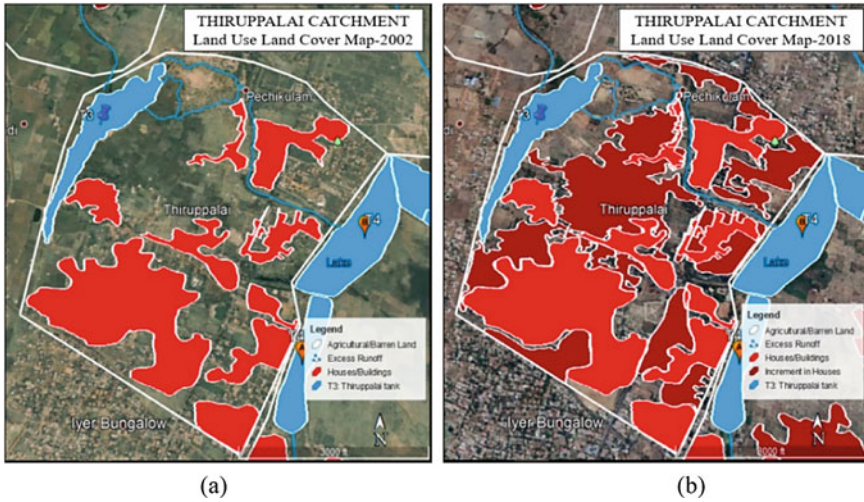
Fig. 4 Land use land cover (LULC) change in Thiruppalai watershed, Madurai India: **a** LULC in 2002 and **b** LULC in 2018 (*Source* Google Earth Pro)
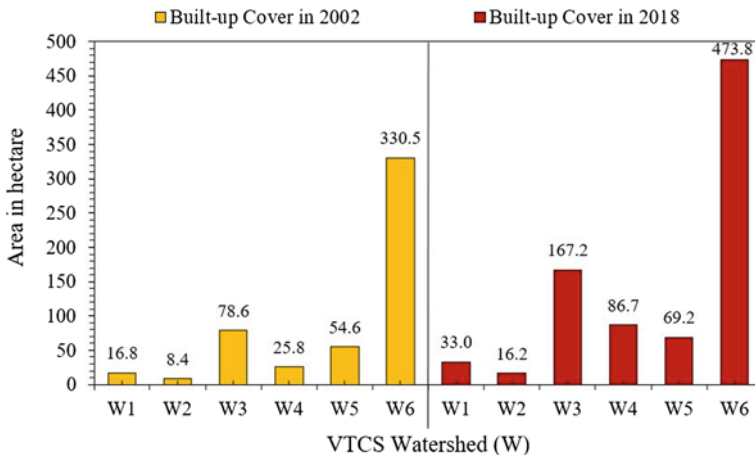
Fig. 5 Change in the built-up area across watersheds in Madurai, India (*Source* Field investigation)

irrigation water supply from the silted (unmanaged) tanks. This allowed the rapid conversion of the agricultural land (command area) into non-agricultural land. The highest decrement in the percentage cover of the non-urbanized region was recorded in the Siruvour watershed (49%). Whereas, Vandiyur watershed ranked second with a 27% decrement followed by Siruvour with a 23% decrement in the non-urbanized region. This newly available land is accommodating the expansion of the urbanizing cover of the city. Similar inferences were drawn by Chinnasamy and Srivastava [5].
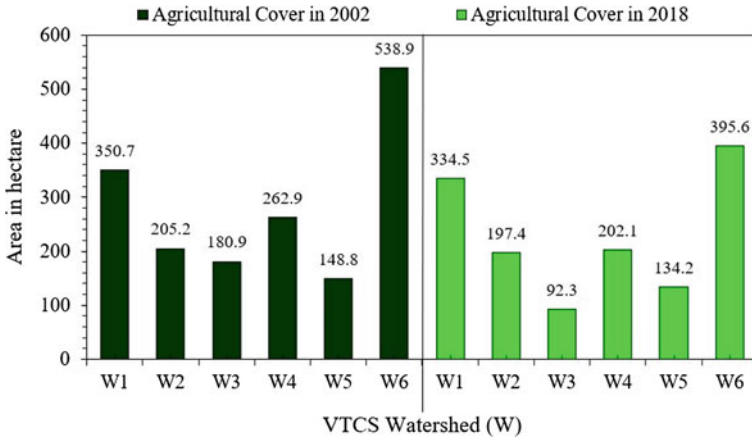
Fig. 6 Change in the non-urbanized area (agriculture, forest, and barren land) across watersheds in Madurai, India (*Source* Field investigation and using Subramanya [37] and Srivastava and Chinnasamy [17])
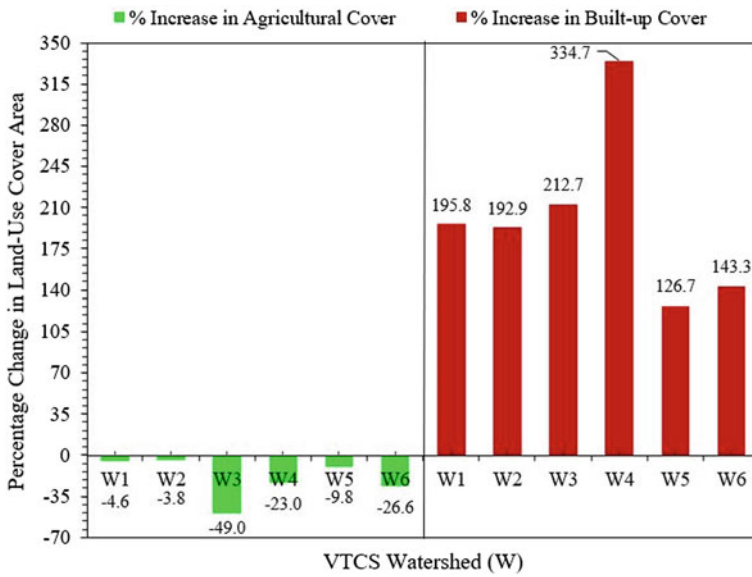
Fig. 7 Comparative analysis of percentage change in the urbanized and non-urbanized area across watersheds in Madurai, India (*Source* Field investigation)

   Results further indicate that the rural watersheds have been least affected due to urbanization primarily due to two reasons. First, the villagers are actively participating in tank-fed-based agricultural development in association with DHAN (Development of Humane Action) Foundation (a grassroot development organization in South India), wherein, the tanks are maintained through the participation of the village community [17, 40, 5]. Villages have formed their own water associations headed by *Sarpanch* (village head). Apart from this, villagers they also participate in the desiltation process (once a year during summer) of the tank by contributing financially or by voluntary donation through labor time. The second reason could be that the villages are located far from the urban region and hence are not much influenced by the impact of urbanization.

3.2 Surface Runoff Analysis

The temporal change in LULC resulted in an increment in the curve number, leading to an increment in the runoff in all the watersheds (Fig. 8). The highest runoff was recorded from Vandiyur watershed (*T8*) (>86%) in 2018 followed by Kosakulam-Parsurampatti-Kodikulam watershed (*T2*) having 85% of surface runoff. Both the watershed is located in the urban region of the Madurai city. The least surface runoff was recorded in rural areas (~70%), followed by a peri-urban region with a variation of 75 to 80%. Consequently, rural areas have more provision for groundwater recharge, whereas the increasing impervious cover is resulting in higher surface runoff from the watersheds (as evident from *T567* and *T8*). As a result of erratic rainfall patterns, rapid urbanization, and increased surface runoff, the discharge into the VTCS decreased, which led to a decrease in the natural recharge of groundwater in the areas adjoining
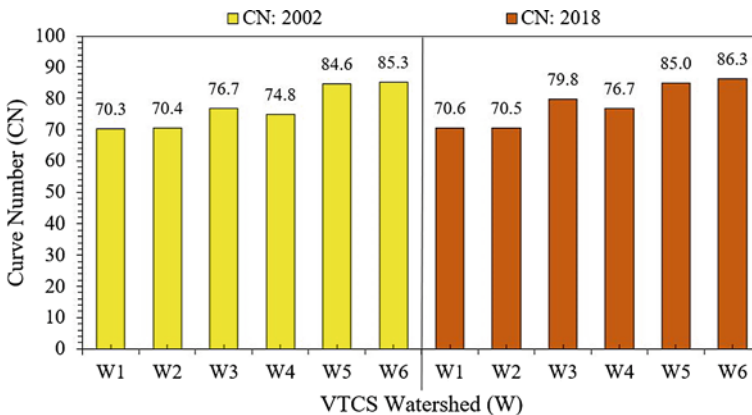
Fig. 8 Change in surface runoff across interconnected watersheds in Madurai, India (*Source* Field investigation and using Boughton [37] and Srivastava and Chinnasamy [17])

the tanks. Similar correlations can be seen in the studies conducted in rural-Madurai by Srivastava and Chinnasamy [17].

3.3 Groundwater Trend Analysis

Results showed an increase in the number of borewells and tubewells in the vicinity of the tanks by 250%, particularly in the urban areas resulting in the over-exploitation of the groundwater resources. Moreover, all the participants in the survey mentioned the increasing depth for extracting groundwater since the year 2003. Field survey and groundwater data also indicated that, from 2003, approximately 60% of the groundwater levels have gone from safe (annual natural recharge above the annual extraction rate) to critical status (annual extraction above annual natural recharge), leading to unsustainable groundwater levels. The depth of tubewell and borewell to extract these groundwater resources was found to increase at an alarming rate from eight meters on average in the year 1990 to 60 m in 2007 (650% increase) to a further 200 m in 2018 (2400% increase). This accounts for a drop in groundwater level of seven meters/year.

The spatial analysis revealed the higher groundwater declining rates concerning the depth of extraction in the urban regions (wells located close to the bank of the river Vaigai) followed by peri-urban (wells located at the central region of the VTCS) while the least rates were recorded in the rural areas (uppermost region of the entire VTCS) (Fig. 9). The declining groundwater extraction levels can be attributed to urbanization which has abruptly influenced the LULC and regional hydrology pattern, thereby resulting in less water for recharge. The average depth

Fig. 9 Spatial analysis of fluctuation in-depth to Groundwater extraction in Vandiyur tank cascade system, Madurai, India (*Source* Field investigation)

to extract groundwater was determined to be 200 m below ground level in urban regions whereas the same for the peri-urban was 75 m and for the rural regions was 10 m. These wells were located in the vicinity of the tanks.

4 Discussions

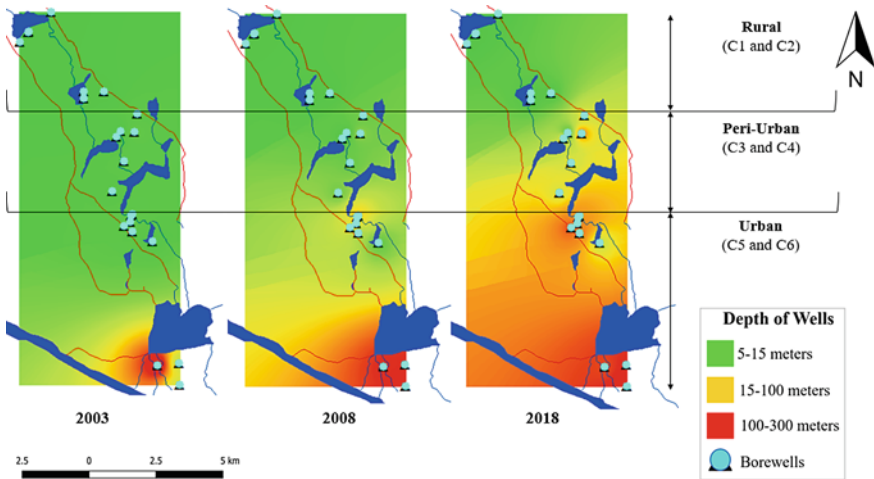The current study results show that there is high connectivity between groundwater and surface water resources in Madurai city. Field investigation revealed that the tanks located in the rural region are still functioning as irrigation tanks. The water from the sluices of these tanks is used for distributing water to command areas at its downstream. This analogy provides preliminary confirmation to the hypothesis that the wells in the rural areas are getting higher recharge from the tanks. On the contrary, the command area in the urban tanks is completely urbanized, and thus the tanks fundamentally act as a flood moderator instead of irrigation source. The depth of extracting groundwater below surface level in the urban areas is much higher than the rural areas which could be due to poor recharge from the tanks and due to higher rates of groundwater extraction. Therefore, the recharge process of groundwater, especially in regions of hard rock aquifer, is essential for the determination of groundwater reserves and their assessment. The results further indicated that the rainfall pattern has changed drastically which has a direct impact on flood generation and reduction in groundwater recharge. As a consequence, water security is under threat and demands attention from the decision-makers, policy-makers, and local communities (stakeholders) to collectively draft and implement stringent policies to protect the water infrastructures (tanks) [41]. Results on LULC revealed that the impervious area increased which resulted in the increase of depth to groundwater levels. Furthermore, urbanization also led to over-extraction and reduction in natural recharge avenues. This correlation implies that VTCS is experiencing the impact of urbanization. Improper management, anthropogenic stressors (in view of illegal settlements and blockage of canals and feeder channels), and unsustainable groundwater use rates have caused the groundwater levels and the net tank water holding capacity to decrease steadily [17, 5]. The depth of groundwater extraction in peri-urban and urban areas was recorded more than 200 m below ground level. These regions have become either overexploited due to unlimited groundwater extraction or turned critical due to its continued depleted levels for several years. Therefore, participatory groundwater management [6, 36, 42], rehabilitation and maintenance of percolation tanks [5, 17], and strengthening local institutional governance [7, 36, 42] towards ensuring water security are much-needed given the alarming unsustainable groundwater scenarios in the VTCS region.

Artificial recharge methods such as Managed Aquifer Recharge (MAR) techniques, as discussed by Dillon et al. [43], have to be taken up urgently in these over-exploited and critical regions. Augmentation of the recharge wells is necessary to make them suitable as a potential drinking water source by recharging the deep fractures [12]. The desilting of the tanks was found to be the most pressing

recommendation in the study area, which is in coherence with previous studies (for example, [3, 15, 17, 44]). There is thus a need to conduct evidence-based research for understanding the role of the modern tanks amidst extreme climatic events across South India [5, 17, 45, 46] in order to differentiate and redefine the tank's functionality in terms of whether structures facilitate percolation or provide irrigation water to the command areas. This approach, in turn, can foster assurance towards both domestic and agricultural water security, environmental water balance, and support to primarily livelihood activities for socially marginalized and poor local communities, as discussed by Srivastava et al. [6, 7]. In the current decade, Public Works Department (PWD), Madurai Corporation, and the local Water User Associations (WUAs) are taking many initiatives to restore the tanks in VTCS [5, 17, 40]. Some of the initiatives are bund strengthening, dead storage creation, Prosopis clearance, channel clearance, and walkers park establishment. But these activities are challenged due to limited resources and poor community-level participation. Groundwater levels of densely urbanized areas of Madurai city such as Gomathipuram, Tahsildar Nagar, Melamadai, Managari, Anna Nagar, and K. K. Nagar are dropped below 180 m. This has transformed the locality into an open market for portable water [17, 47, 48]. The revival, restoration, and rehabilitation of VTCS could provide scope towards holistic groundwater and surface water management for sustaining water resources in rapidly urbanizing regions of Madurai city.

5   Conclusions

The current study used a combination of observation data (government data and survey data) and remote sensing data (satellite imagery) to quantify the impact of urbanization on traditional water harvesting structures (such as tanks) and groundwater scenarios. Results from the current research found that even though the rainfall is changing rapidly in the region, the rapid urbanization of the region has led to an increase in surface runoff and groundwater depletion. This has also led to the falling storage levels in the traditional tanks and an increase in siltation rates. Loss of ownership towards cascading tanks consequently caused tanks to become disposal sites for solid waste. The current research showcased the need for delivering an integrated understanding of scope to combat the fluctuating groundwater levels and erratic rainfall patterns in the scenario of rapid urbanization across VTCS. Such scientifically validated results can ensure that the conservation works are planned and implemented meticulously with people's involvement. Additionally, such approaches can aid in the formulation of best management practices to enhance the tank ecosystem, overall environmental development, and the highest possible returns (in terms of tank's services) along with sustainability. Finally, the study observed that even though the cascading tanks and groundwater are interconnected, they are managed separately by different government agencies. Due to limited holistic understanding, one agency does not complement the other, resulting in challenging environments for collaboration. Therefore, to maximize the benefits of these traditional tanks, all associated

water management agencies should work in collaboration and take a holistic approach in reviving and maintaining traditional tanks.

References

1. Central Ground Water Board (CGWB) (2014) Dynamic groundwater resources. Government of India, Ministry of Water Resources. New Delhi, India
2. Patel MP, Gami B, Patel A, Patel P, Patel B (2020) Climatic and anthropogenic impact on groundwater quality of agriculture dominated areas of southern and central Gujarat India. Groundwater Sustain Dev 10. https://doi.org/10.1016/j.gsd.2019.100306
3. Palanisami K, Meinzen-Dick R, Giordano M (2010) Climate change and water supplies: Options for sustaining tank irrigation potential in India. Econ Polit Week 45(26/27):183−190. https://www.jstor.org/stable/40736699. Accessed 17 Jan 2021
4. Chinnasamy P, Hsu MJ, Agoramoorthy G (2019) Groundwater storage trends and their link to farmer suicides in Maharashtra State India. Front Public Health 7:246. https://doi.org/10.3389/fpubh.2019.00246
5. Chinnasamy P, Srivastava A (2021) Revival of Traditional Cascade Tanks for Achieving Climate Resilience in Drylands of South India. Frontiers in Water (3). https://doi.org/10.3389/frwa.2021.639637
6. Srivastava A, Khadke L, Chinnasamy P (2021) Web application tool for assessing groundwater sustainability—a case study in Rural-Maharashtra, India. In: Vaseashta A., Maftei C (eds) Water safety, security and sustainability. Advanced Sciences and Technologies for Security Applications. Springer, Cham. https://doi.org/10.1007/978-3-030-76008-3_28
7. Srivastava A, Khadke L, Chinnasamy P (2021) Developing a web application-based water budget calculator: attaining water security in Rural-Nashik, India. In: Kolathayar S et al (eds) Climate change and water security. Lecture Notes in Civil Engineering, vol 178. Springer Singapore. https://doi.org/10.1007/978-981-16-5501-2_37 (In Press)
8. Central Ground Water Board (CGWB) (2014) Ground water year book—2013–14. Government of India, Ministry of Water Resources. New Delhi, India
9. Chinnasamy P, Agoramoorthy G (2015) Groundwater storage and depletion trends in Tamil Nadu State India. Water Resourc Manage 29(7):2139–2152. https://doi.org/10.1007/s11269-015-0932-z
10. Chinnasamy P, Maheshwari B, Dillon P, Purohit R, Dashora Y, Soni P, Dashora R (2018) Estimation of specific yield using water table fluctuations and cropped area in a hardrock aquifer system of Rajasthan, India. Agric Water Manage 202:146–155. https://doi.org/10.1016/j.agwat.2018.02.016
11. Maheshwari B (2017) Improved village scale groundwater recharge and management for agriculture and livelihood development in India. Australian Centre for International Agricultural

Research (Report No.: FR2017/23), Canberra, Australia. http://www.aciar.gov.au/files/final_report-marvi_22-09-2017.pdf. Accessed 17 Jan 2021

12. Saha D, Marwaha S, Mukherjee A (2018) Groundwater resources and sustainable management issues in India. In: Saha D, Marwaha S, Mukherjee A (eds) Clean and sustainable groundwater in India. Springer hydrogeology, pp 1−11. Springer, Singapore

13. Palanisami K, Mohanasundari T (2019) Rainfall uncertainty and drought proofing strategies by farmers in Southern India. Int J Civil Environ Agric Eng 1(1):35–40. https://doi.org/10.34256/ijceae1915

14. Hazell PB, Ramasamy C (1991) The green revolution reconsidered: the impact of high-yielding rice varieties in South India. Johns Hopkins University Press, Baltimore, USA

15. Reddy VR, Reddy MS, Palanisami K (2018) Tank rehabilitation in India: review of experiences and strategies. Agric Water Manage 209:32–43. https://doi.org/10.1016/j.agwat.2018.07.013

16. Sakthivadivel R, Shah M (2019) Will Kudimaramathu make communities think tanks again? A study of tanks in transit, coping mechanism of communities and government action. Water Policy Research Highlight, International Water Management Institute (IWMI), Sri-Lanka

17. Srivastava A, Chinnasamy P (2021) Water management using traditional tank cascade systems: a case study of semi-arid region of Southern India. SN Appl Sci 3:281. https://doi.org/10.1007/s42452-021-04232-0

18. Shanmugham CR, Kanagavalli J (2013) Technology of tanks: the traditional water bodies of rural India. Reflection Publication Trust, Madurai, Tamil Nadu, India

19. Ratnavel SM, Gomathinayagam P (2018) In search of ancient wisdom: irrigation tanks. Reflection Publication Trust, Madurai, Tamil Nadu, India

20. Seenivasan R, Kanagavalli J (2014) Dying tanks in Urban areas: what can be done with them? Rev Dev Change 19(1):109–122. https://doi.org/10.1177/0972266120140106

21. Sivasankar V, Omine K, Msagati TA, Chandramohan A (2014) Evaluation of groundwater quality in Madurai City, South India for drinking, irrigation and construction purposes. Arab J Geosci 7(8):3093–3107. https://doi.org/10.1007/s12517-013-0994-2

22. Ali J, Appsamy S, Antony JT (2019) Hydrobiological studies of Vandiyur lake, Madurai, Tamil Nadu, India. Science Arena Publications—Specialty J Biol Sci 5(1):24−33. https://sciarena.com/storage/models/article/HwjYmg2thCKuA9YHDD4oSmAIPQsQjcuBqRMmJaPic2I1iMeuWrm4d5OTGxxY/hydrobiological-studies-of-vandiyur-lake-madurai-tamil-nadu-india.pdf. Accessed 17 Jan 2021

23. Kundu D, Pandey A, Sharma P, Bhusan S, Mondal B, Lahiri B, Sharma TC, Vijh S (2018) India: National urban policies and city profiles for Delhi and Madurai. Research Report, National Institute of Urban Affairs, GCRF Centre for Sustainable, Health and Learning Cities and Neighbourhoods (SHLC)

24. Kundu D, Lahiri B, Pandey A, Sharma P (2019) City profile: Madurai, India. Environ Urbanization ASIA 10(2):308–330. https://doi.org/10.1177/0975425319867487

25. Balaji G, Thirumaran K (2019) Evaluating the impact of urbanization on the physiochemical parameters of the Urban river system: a study on Vaigai river, Madurai. Environ Urbanization ASIA 10(1):116–131. https://doi.org/10.1177/0975425318822337

26. Census of India (2011) Census of India 2011: Provisional population totals. Office of the Registrar General and Census Commissioner, New Delhi, India

27. Bavani M, Ramachandran VS, Prasad R (2020) Mulaipari—a traditional cultural ritual associated with farming in Tamil Nadu. Int J Multidisc Res 6(3):1−9. http://admin.crrps.in/uploads/roots/previous/pdf/February%202020.pdf#page=13. Accessed 17 Jan 2021

28. Rajasekaran RH, Selvaraj MS, Ramanathan J (2018) A novel data-driven DSSE method to achieve water sustainability for farmers in Madurai district, India. In: 9th International conference on computing, communication and networking technologies, pp 1–7 (ICCCNT). IEEE

29. Bureau of Indian Standards (BIS) (2005) National building code of India-2005. Bureau of Indian Standards, New Delhi, India

30. Misra GC (2012) Revisiting the provisions concerning means of egress designing as per national building code of India 2005. Fire Eng 37(4):7–18. http://www.indianjournals.com/ijor.aspx?target=ijor:fe&volume=37&issue=4&article=002. Accessed 17 Jan 2021

31. Subhashini S, Thirumaran K (2018) A passive design solution to enhance thermal comfort in an educational building in the warm humid climatic zone of Madurai. J Build Eng 18:395–407. https://doi.org/10.1016/j.jobe.2018.04.014
32. Central Ground Water Board (CGWB) (2010) A report on Madurai district. Government of India, Ministry of Water Resources, New Delhi, India
33. Thivya C, Chidambaram S, Rao MS, Gopalakrishnan M, Thilagavathi R, Prasanna MV, Nepolian M (2016) Identification of recharge processes in groundwater in hard rock aquifers of Madurai District using stable isotopes. Environ Process 3(2):463–477. https://doi.org/10.1007/s40710-016-0137-3
34. India Meteorological Department (IMD) (2017) Rainfall statistics of India-2017. Hydromet Division, India Meteorological Department, Lodi Road, New Delhi. Report No. ESSO/IMD/HS/Rainfall Report/01(2018)/24
35. Taylor JR, Lovell ST (2012) Mapping public and private spaces of urban agriculture in Chicago through the analysis of high-resolution aerial images in Google Earth. Landsc Urban Plan 108(1):57–70. https://doi.org/10.1016/j.landurbplan.2012.08.001
36. Srivastava A, Chinnasamy P (2021) Developing village-level water management plans against extreme climatic events in Maharashtra (India)—a case study approach. In: Vaseashta A., Maftei C. (eds) Water safety, security and sustainability. Advanced Sciences and Technologies for Security Applications. Springer, Cham. https://doi.org/10.1007/978-3-030-76008-3_27
37. Boughton WC (1989) A review of the USDA SCS curve number method. Soil Res 27(3):511–523. https://doi.org/10.1071/SR9890511.
38. Saravanabavan V, Balaji D, Preethi S (2019) Identification of dengue risk zone: a geo-medical study on Madurai city. Geo J 84(4):1073–1087. https://doi.org/10.1007/s10708-018-9909-9
39. Srivastava A, Chinnasamy P (2021) Investigating impact of land-use and land cover changes on hydro-ecological balance using GIS: insights from IIT Bombay India. SN Appl Sci 3:343. https://doi.org/10.1007/s42452-021-04328-7
40. DHAN Foundation (2020) Centre for urban water resource, DHAN Vayalagam (Tank) Foundation. https://www.dhan.org/dhancure/. Accessed 17 Jan 2021
41. Shah M (2019) Crafting a paradigm shift in water. In: Singh A, Saha D, Tyagi A (eds) Water governance: challenges and prospects. Springer water, pp 341−368), Springer, Singapore
42. Thatte CD (2018) Water resources development in India. Int J Water Resour Dev 34(1):16–27. https://doi.org/10.1080/07900627.2017.1364987
43. Dillon PJ, Pavelic P, Page D, Beringen H, Ward J (2009) Managed aquifer recharge: An introduction. Waterlines Report Series by National Water Commission, Australian Government
44. Sakthivadivel R, Gomathinayagam P (2006) Rehabilitation and management of tanks in India. Asian Development Bank, Publication Stock, No. 122605, Philippines
45. Khadke L, Pattnaik S (2021) Impact of initial conditions and cloud parameterization on the heavy rainfall event of Kerala (2018). Model Earth Syst Environ. https://doi.org/10.1007/s40808-020-01073-5
46. Mishra V (2020) Long-term (1870–2018) drought reconstruction in context of surface water security in India. J Hydrol 580. https://doi.org/10.1016/j.jhydrol.2019.124228
47. Ramesh M (2018) India's water crisis: lessons from Madurai, a city that adopted tanks and suffered after abandoning them. https://www.firstpost.com/india/indias-water-crisis-lessons-from-madurai-a-city-that-adopted-tanks-and-suffered-after-abandoning-them-5011701.html. Accessed 17 Jan 2021
48. Sivasubramaniyan K, Rajendran S (2019) Mitigating drinking water crisis in Tamil Nadu. Int J Res Granthaalayah 7(8):301−317. https://doi.org/10.29121/granthaalayah.v7.i8.2019.673

Prediction on Water Security Level of Saskatchewan Using Regression-Based Models

Md Saiful Arif Khan, Armin Aalirezaei, and Golam Kabir

1 Introduction

Water security lies in freshwater's obtainability as per requirement and on economic and social issues as well [1–3]. United Nations (UN) conceded water security assurance as to the resilient approach toward achieving the sustainable development goal and prepared to strengthen the safety of water supplies. Hence planning to achieve a resilient water supply, identifying and estimating the critical factors for warranting water security is required [4]. Before forecasting water security levels, appropriate water security parameters are needed to be identified on the local or individual, national, or global aspects. While each aspect is crucial to some extent, several studies emphasize the importance of local-level criteria [5, 6].

Being a spacious and diverse county, Canada needs to consider the factors of a wide range of clusters and federal and provincial stages to get a reliable water security level. The local authorities are exclusively accountable for water management. The consumers of water may struggle for lack of water security due to rising demand, fluctuations in supplies, risks associated with land use for human-made activities; and a rapid-emerging corporate environment [7]. Therefore, a proper water management plan incorporated with uniformity, integrity, sincerity, cooperation, clarity is crucial for sustainable and developing eco-friendly class, financial efficacy, and communal well-being [8–10].

Md S. A. Khan (✉) · A. Aalirezaei · G. Kabir
Industrial Systems Engineering, Wascana Pkwy, University of Regina, Regina, SK S4S 02, Canada
e-mail: mkx007@uregina.ca

A. Aalirezaei
e-mail: arminaalirezaei@uregina.ca

G. Kabir
e-mail: golam.kabir@uregina.ca

In view of the above discussion for the necessity of water security and the importance of estimating local indicators, the primary goals of this research are as under:

- Distinguishing time-sequential parameters of water safety components for Saskatchewan.
- Generating linear and nonlinear regression-based forecast model to investigate and assess time sequence parameters of water security to support decision-makers for tactical planning to magnify.
- Applying the prediction model by using real data of the Saskatchewan Water Security Agency.

2 Literature Review

2.1 Water Security Perception

Almost eighty percent of the world population is in a vulnerable situation against water security due to Climate change and excessive consumption of water due to population growth [11]. At the 2nd World Water Forum (2000) held in the Ministerial Declaration on Water Security by the United Nations in the era of the twenty-first century, the water security notion has been articulated as a policy-level problem [12]. Because of the complicated features of water security, it is much more needed to estimate and compute than realizing the importance of water security [13].

2.2 Surface Water Management

River water is a plentiful supply of surface water. It is essential to select and enumerate the impressions of Integrated Water Resources Management (IWRM) at the water body level for suitable shallow water administration. Several studies were done on the application of novel technology that aims to ensure surface water security. A study revealed that the basin water sustainability could be upgraded by using the Bow River Integrated Model (BRIM). The model incorporates water requirement, circulation, and operate underneath varied climate conditions, the sum of consumers, financial conditions, and administration strategies [14]. Several studies were done on the use of different techniques that aims to ensure surface water security. Such as the technique to purify water by proposing a model to eradicate cyanobacterial contaminants [15], model to monitor microcystins to ensure water security [16].

2.3 Water Security Prediction Model

Developing a water security prediction model is a useful tool to accommodate the rising demand for water. By employing different measuring tools, a prediction model for water security can be developed. To improve the existing community water system, these prediction models can play a crucial role. The prediction model's performance relies on the precise historical data, and data preprocessing is an important step that enhances data reliability to predict water security accurately [17].

2.4 Factors of Water Security

To understand the various features of water security, multiple schemes have been designed and applied to determine and measure parameters to outline the measures of water insufficiency hazard, tension, water deficiency, and durability [18, 18]. Quantitative microbial risk assessment strategies can guide the decision-making process to increase water safety [20]. Polluted drinking often is the reason for outbreaks of different waterborne illnesses. Thus the impact of determining drinking water quality is very important for keeping sound public health. The drinking water quality standard can be measured by detecting the quality of potable water effects on the human body. The study's realization can guide developing suitable strategies and improving the standards of potable water quality [21]. Surface water is considered one of the most treasured wealth in the world. Thus, the source water protection (SWP) plan is a key component of the Integrated Water Resources Management (IWRM) and essential for ensuring durable water distribution arrangement [22].

From the above discussion on available literature on water security, the study reveals a study gap in the water security assessment sector in Canada. Hence, considering the impact of water security against sustainable development, the environment, economy, and society, a water security prediction model is obligatory. Using linear and nonlinear regression to evaluate and forecast anticipated pointers of the Saskatchewan water security agency of Canada is entirely new and the key outcome of this research. In the upcoming days, the prediction technique can comprehend the trend and anticipate the time sequence parameter value.

The results offer a credible output for decision-makers to calculate criteria for enhancing the degree of water quality, and the understanding will assist them with the efficient planning process on the way to attain resilient growth.

3   Methodology

In the beginning, the time series parameters of the Saskatchewan water security unit are identified. Then, the regression function is used to examine and forecast the time series parameters. Finally, the developed model is applied by putting the real data taken from Saskatchewan's Water Security Agency.

3.1   Identification of Water Security Parameters

The Water Security Agency of Saskatchewan published reports to present the annual performance. The parameters that are being used in the water security prediction model have been identified from the Water Security Agency's published annual report for the year 2015–16 and 2016–17. The Water Security Agency of Saskatchewan is accountable for handling Saskatchewan's water resources, maintaining the quality of potable water and managing wastewater, keeping the information about water, etc. [23, 24].

Eight years of data have been gathered from the competent authority of Saskatchewan's report. The authority's goal is to implement quality development strategies that will reduce the performance indicators that have a detrimental effect on water protection and increase the performance indicator values that will produce more benefits. Regarding this study, seven pointers under three key clusters, such as water usage, threat, and quality, were extracted and populated using official government data based on data availability. Table 1 offers a list of indicators.

A brief outline of these seven parameters is mentioned below.

Table 1   List of Parameters for Saskatchwan water secuirty unit [23, 24]

Cluster	SI. No	Parameters
Consumption	1	Communal water usage in wintertime
	2	Percentage of population in the province insured by a comprehensive source water protection plan
Threat	3	Hazard allied with dams of water security agency
	4	Number of substandard dams that needs repair
	5	Number of sewage effluent discharges that cause threat to freshwaters
Quality	6	Conformity to standards quality of potable water
	7	Potable water quality fulfillment

Parameter 1: Communal water usage in wintertime

Based on the provincial water management strategy, water consumption and usage differences are very common. Research has shown that regulations for water conservation are not stable across the nation. Due to the lack of municipal data, categorization, investigation, and projection of municipal water usage estimates are hindered [25]. Since precipitation does not impact the communal water usage in the winter (November to March), the actual requirement for winter municipal water use is considered to be met here. Usage of water includes water in domestic works, industries, and municipal utilities like firefighting, road construction, municipal swimming pools and rinks, and the water loss because of system fault. The usage of water is determined by yearly community water use annals and population data. Here, the measurement unit is a liter per person per day. Data on annual water usage and population data have been obtained from the Water Protection Agency and the Ministry of Health.

Parameter 2: Percentage of population in the province insured by a comprehensive source water protection plan

The indicator shows the proportion of the residents living in a region where a strategic planning phase for the Water Protection Agency has been accomplished. In contrast, the South Saskatchewan SWP Plan was primarily implemented in 2007 [26]; the western Prairie Provinces' water supplies were catastrophic in terms of quality and quantity through key informant interviews. It is notable that, according to population data from the 2011 Census of Canada, the Water Protection Agency originally planned to protect areas with a higher population density and where most of the population of the province (89 percent) lives.

Parameter 3: Hazard allied with dams of Water Security Agency

This measure shows the threat of the Water Security Agency's dams. In upgrading the dams to appropriate standards, it is a parameter of protecting the dams to advance. In order to ensure dam protection, current risk detection, and potential risk assessment are critical. Risk calculation is carried out using probabilistic means [27]. The probability is calculated as a fraction here, which is appraised as the likelihood of a failure compounded by a failure's consequences. The greater value designates a higher threat. Therefore, a lower risk ratio indicates a safer structure. For instance, the risk ratio was lowered to 0.275 in 2016/17 from 0.281 in 2015/16 due to reconstruction work was undertaken at Avonlea Dam and Zelma Dam.

Parameter 4: Number of substandard dams that needs repair

Typically, dams have been built with a design life of 50 years, and most dams of Saskatchewan are now reaching or exceeding their design life. Dams aging has significantly impacted the viability of dams and the protection measures of dams as well as community awareness are regularly improving over time. Hence, adequate maintenance upgrades are needed to ensure the resilience of the existing dams [28]. The Water Security Agency is accountable for the activity and management

in Saskatchewan, based upon the guidelines of the CDA. Therefore, this parameter lists the number of dams needed to be renovated by the Water Protection Agency to meet the norm in compliance with the Canadian Dam Association's Dam Safety Guidelines (2007). This parameter does not define the seriousness of the deficiencies diagnosed, unlike the risk ratio. This indicator is an effective instrument for calculating defective dams' production over time [23, 24].

Parameter 5: Number of sewage effluent discharges that cause threat to Freshwaters

Risk assessment is essential in estimating the possible risks of water contamination. Two main probable threats, like the risk related to the discharge of manufacturing and agrarian dirt waste into the freshwater [29]. This measure indicates the potential risks linked with the amount of discharges of effluent into the source waters due to under-standard handling of wastewater, over-occupied schemes, or under-infrastructure schemes. This parameter has a great impact on the prediction of water protection as it is the most important process of calculating the number of significant possible sources that pollute water.

Parameter 6: Conformity to standards quality of potable water

Acquiescence with the standard quality of potable water is determined by the mutual compliance with disinfection and bacteriological drinking water requirements. This measure involves both the effects of testing of bacteriological quality of water and the amount of sterilizer that exists in potable water. As microbial contamination in water sources can easily recognize significant diseases, the disinfection and bacteriological quality are distinctive. In the environment, an outbreak of waterborne disease has severe effects that impend and undermine consumer trust in the protection of municipal drinking water [30]. Therefore, this parameter is a valuable means for drinking water protection forecasting, and satisfactory decontamination is necessary to guarantee healthy potable water and avoid the aquatic epidemic.

Parameter 7: Potable water quality fulfillment

Potable water quality fulfillment demonstrates the assurance of the inhabitants in their supply of drinking water quality. Consumer input on potable water quality is a crucial measure for the efficient administration of potable water supplies, the setting of water quality requirements, and the monitoring of potable water quality [31]. It is measured based upon the input from a yearly survey carried out on the residents in Saskatchewan. This metric is the percentage of respondents who thought they were really or somewhat secure in their tap water consistency. This parameter tests the Water Security Agency's efficiency in the production of secure drinking water sources, including municipal supplies, pipelines, and large commercial water systems, throughout the province.

To forecast the values for future years, linear and nonlinear regression function have been described in the following section.

3.2   Regression Analysis Methods

Regression analysis is the statistical method for assessing the relationships between variables in statistics [32, 32]. To simulate data, we can use a model and then analyze the simulated data. This will assist you to design better experiments. Regression analysis is commonly used for prediction [34, 34].

Linear Regression

A fundamental type of multiple linear regression is simple linear regression (SLR). It analyzes the linear relationship between a dependent variable and an independent variable [36]:

$$Y = \lambda_0 + \lambda_1 X + \text{ç} \tag{1}$$

Step 1: Gather the response variables and measurable variables, defined as

$$Y = \begin{bmatrix} y_1, & y_2, & \ldots \ldots, & y_n \end{bmatrix} K \tag{2}$$

$$X = [x_1, \ x_2, \ \ldots \ldots, \ x_n] K \tag{3}$$

Step 2: We need to minimize the sum of errors ç for calculating $\lambda = [\lambda_0, \lambda_1]$:

$$
\begin{aligned}
P(\lambda_0, \lambda_1) \quad &= \min \text{ç}^K \text{ç} \\
&= \min (y_i - \lambda_0 - \lambda_1 x_i)^K (y_i - \lambda_0 - \lambda_1 x_i) \\
&\qquad \text{Hence, } P(\lambda_0, \lambda_1) = \min \sum (y_i - \lambda_0 - \lambda_1 x_i)^2 \\
i &= 1 \ldots \ldots n.
\end{aligned}
\tag{4}
$$

Formulate $x_1, x_2, \ldots, x_n$ into $n \times 2$ matrix termed the design matrix:

$$\ddot{X} = \begin{pmatrix} 1 & x_1 \\ 1 & x_2 \\ . & . \\ . & . \\ . & . \\ 1 & x_n \end{pmatrix} \tag{5}$$

As per the invertibility of $\ddot{X}^K \ddot{X}$. The λ can also be computed by

$$\lambda = \left(\ddot{X}^K \ddot{X} \right)^{-1} \ddot{X}^K Y \tag{6}$$

Step 3: Take the ç and λ to get the final model:

$$Y = \lambda \ddot{X} + ç \tag{7}$$

Nonlinear Regression

Nonlinear regression is a technique to fit some designated equation with data. Nonlinear regression methods, as with linear regression, evaluate parameter values which minimize the sum of the squares of the distances of the data points to the curve [36].

The typical nonlinear regression model is

$$Y = f(X, \lambda) + ç \tag{8}$$

$$\text{for } Y = \left[Y_1, \ Y_{2, ...,} Y_n\right]^K \tag{9}$$

$$X = \left[X_1, \ X_{2, ...,} X_n\right]^K \tag{10}$$

$$\lambda = \left[\lambda_1, \lambda_{2, ...,} \lambda_n\right]^K \tag{11}$$

$$ç = [ç1,...., çn] \tag{12}$$

Because of the parabolic regression model, for this analysis we need to use equation

$$Y = \lambda_0 + \lambda_1 X + \lambda_2 X^2 + ç. \tag{13}$$

Step 1: Gather the response variables and measurable variables, defined as

$$Y = \left[y_1, \ y_{2, ...,} y_n\right]^K \tag{14}$$

$$X = [x_1, \ x_2, \ ...., x_n] \ K \tag{15}$$

Step 2: We need to minimize the sum of errors ç for calculating $\lambda = [\lambda_0, \lambda_1, \lambda_2]$:

$$
\begin{aligned}
P(\lambda_0, \lambda_1, \lambda_2) \quad &= \min ç^K ç \\
&= \min (Y - X\lambda)^K (Y - X\lambda) \\
\text{Hence, } P(\lambda 0, \lambda 1, \lambda 2) &= \min \sum (Y - \lambda_0 - \lambda_1 X_i - \lambda_2 X_i^2)2 \\
i &= 1......n.
\end{aligned}
\tag{16}
$$

As per the invertibility of $B^K B$.

$$B = \begin{pmatrix} 1 & X_1 & X_1^2 \\ 1 & X_1 & X_2^2 \\ . & . & . \\ . & . & . \\ . & . & . \\ 1 & X_1 & X_n^2 \end{pmatrix} \tag{17}$$

The λ can also computed by

$$\lambda = \left(B^K B\right)^{-1} B^K Y \tag{18}$$

Step 3: Take the ç and λ to get the final model

$$Y = B^K \lambda + ç \tag{19}$$

4 Results and Discussions

The methods explained in the previous section were used to forecast the water safety indicator values for future periods. The linear and nonlinear regression-based functions were developed using Microsoft Excel 2019.

4.1 Data Collection

From the yearly reports of the Saskatchewan water resource management authority, i.e., Water Security Authority (WSA), all data for seven criteria from 2009 to 2016 has been obtained.

4.2 Data Analysis

The secondary data that has been collected from the reports of Water Security Agency is displayed in Table 2. The seven parameters, chosen from the available data, are Communal water usage in wintertime, Percentage of population in the province insured by a comprehensive source water protection plan, Hazard allied with dams of Water Security Agency, Number of substandard dams that needs repair, Number of sewage effluent discharges that cause threat to Freshwaters, Conformity to standards quality of potable water, Potable water quality fulfillment. The comparison between

Table 2 Numeral Figures of selected parameters of the year 2009 to 2016 for water management authority of Saskatchewan (Water Security Agency 2016)

Parameter No	Year—Actual values							
	2009	2010	2011	2012	2013	2014	2015	2016
1	360	343	334	384	353	355	340	337
2	73	75	82	85	88	88	89	89
3	0.218	0.211	0.23	0.243	0.285	0.274	0.246	0.281
4	21	21	23	25	26	24	29	30
5	114	112	105	128	120	111	109	86
6	98	98	96	95	95	95	95	96
7	90	89	86	90	88	88	89	84

linear and nonlinear regression functions is shown. Microsoft Excel 2019 was used to calculate and evaluate the coefficients of regression and related errors apropos to each parameter (Tables 3 and 4).

Table 3 Parameter's predicted value using linear regression

Parameter No	Year – Predicted values							
	2009	2010	2011	2012	2013	2014	2015	2016
1	360.1743	361.8886	363.6029	365.3172	367.0315	368.7458	370.4601	372.1744
2	77.5834	80.0001	82.4168	84.8335	87.2502	89.6669	92.0836	72.7500
3	0.2156	0.2250	0.2344	0.2438	0.2532	0.2626	0.2720	0.2814
4	20.4168	21.6906	22.9644	24.2382	25.5120	26.7858	28.0596	29.3334
5	118.9971	116.6042	114.2113	111.8184	109.4255	107.0326	104.6397	102.2468
6	97.3330	96.9520	96.5710	96.1900	95.8090	95.4280	95.0470	94.6660
7	89.5836	89.1312	88.6788	88.2264	87.7740	87.3216	86.8692	86.4168

Table 4 Parameter's predicted value using nonlinear regression

Parameter No	Year – Predicted values							
	2009	2010	2011	2012	2013	2014	2015	2016
1	348.8333	353.9046	356.7139	357.2612	355.5465	351.5698	345.3311	336.8304
2	71.8834	77.0502	81.3004	84.6340	87.0510	88.5514	89.1352	88.8024
3	0.2071	0.2237	0.2379	0.2497	0.2591	0.2661	0.2707	0.2729
4	20.8750	21.7560	22.7680	23.9110	25.1850	26.5900	28.1260	29.7930
5	107.8757	115.0188	118.9833	119.7692	117.3765	111.8052	103.0553	91.1268
6	98.4957	97.1148	96.0673	95.3532	94.9725	94.9252	95.2113	95.8308
7	88.9166	89.0358	88.9646	88.7030	88.2510	87.6086	86.7758	85.7526

Table 5 Model evaluation between linear and nonlinear (polynomial) regression model

Mean Absolute Percentage Error (MAPE)	
Linear function	Polynomial function
0.0582	0.0292
0.0476	0.0095
0.0450	0.0526
0.0353	0.0340
0.0815	0.0527
0.0079	0.0029
0.0150	0.0143

4.3 Comparison Between Linear and Nonlinear Regression Functions

To predict time series models one of the most prevalent methods is linear or nonlinear regression (Guidolin & Pedio, 2018). To evaluate the regression function the projected functions can be compared with each other. A comparison between linear and nonlinear regression functions is presented in Table 5. It is clearly visible from Table 5 that nonlinear regression model has lower ratio of error than linear regression method in each case except for parameter 3.

The linear and nonlinear regression tendencies for each parameter are depicted in Fig. 1.

4.4 Study Implication

Determining criteria of water protection makes administrators evaluate their decision-making plans and satisfaction of stakeholders and consider compliance with guidelines of administration. Water resources section supervisors can substitute these requirements on basis of the parameters of their association. Moreover, predicting of strategic-level results encourages executives to identify the water security's forthcoming movements and be encouraged keeping in higher urgency to the indicators with more demanding tendencies. If certain parameter does not indicate good results, acceptable annual strategies, long-term targets, regional tactical strategies, and organizational executive strategies may also be implemented.
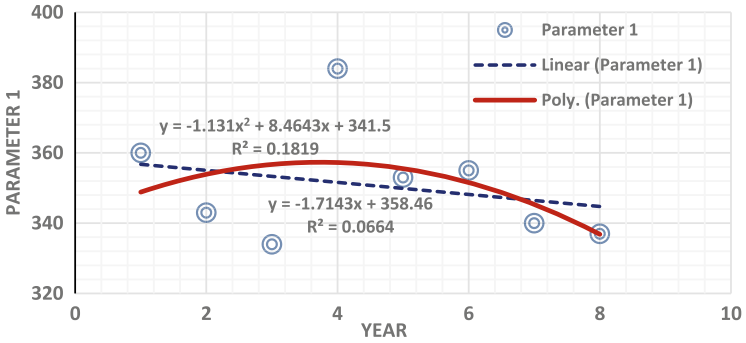
(a) Parameter 1
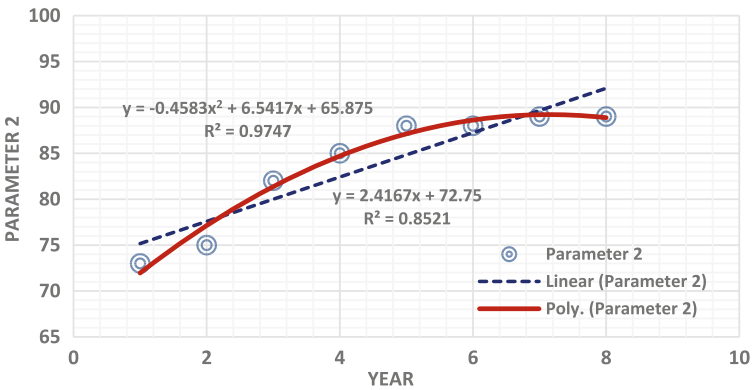
(b) Parameter 2
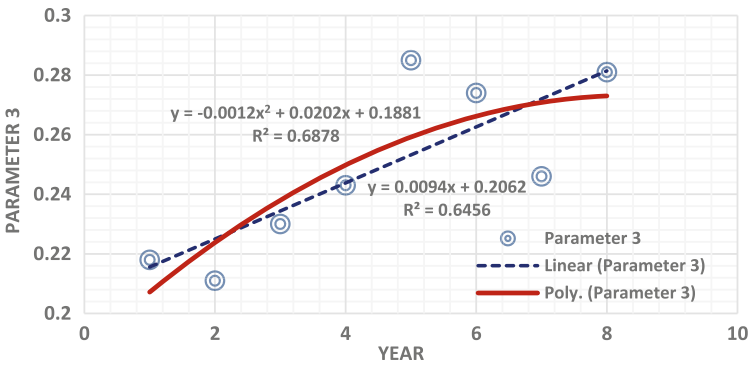
(c) Parameter 3

Fig. 1 Evaluation of linear and nonlinear regression functions for **a** Parameter 1, **b** Parameter 2, **c** Parameter 3, **d** Parameter 4, **e** Parameter 5, **f** Parameter 6, **g** Parameter 7

(d) Parameter 4

(e) Parameter 5

(f) Parameter 6

Fig. 1 (continued)

$y = -0.0952x^2 + 0.4048x + 88.607$
$R^2 = 0.3373$

$y = -0.4524x + 90.036$
$R^2 = 0.2865$

(g) Parameter 7
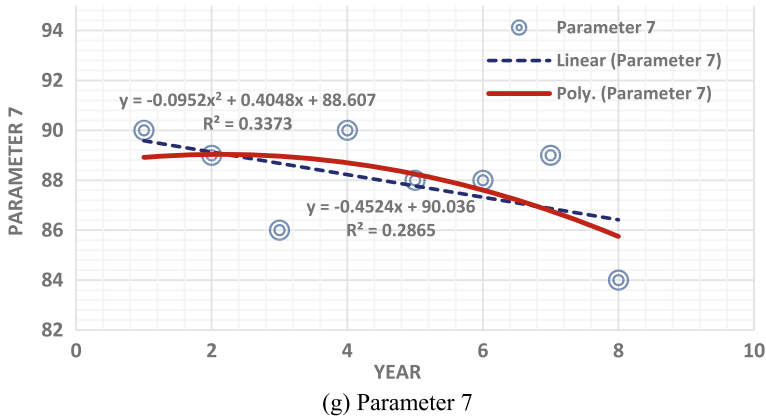
Fig. 1 (continued)

5   Conclusions

Decision-makers in contemporary water protection administration schemes pay attention to data analytics in a significant way. To achieve realistic results, the choice of input data is very critical. The results and discussion and Table 5 for model evaluation between linear and nonlinear (polynomial) regression models suggest that the nonlinear regression model performed better than linear regression.

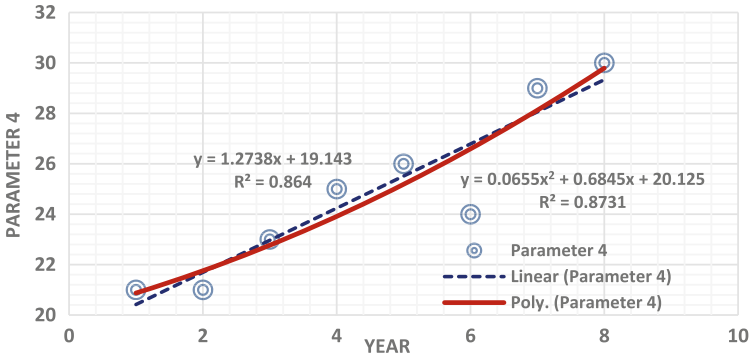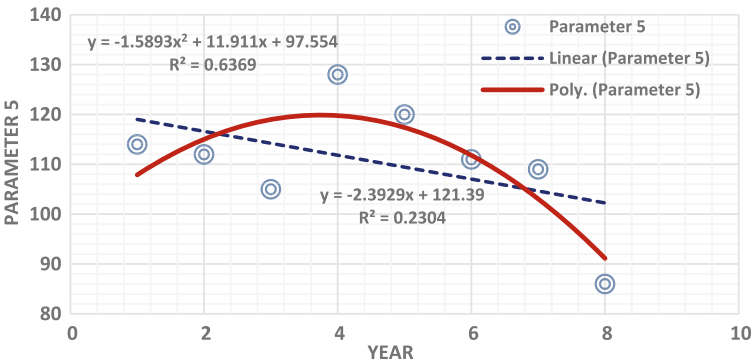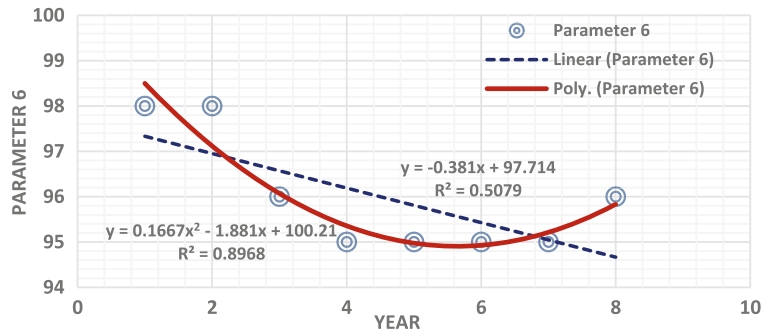For the province that has been studied here, it is observed from Fig. 1 that conformity to standards quality of potable water follows a concave pattern. Although the measures of wintertime communal water, number of sewage effluent discharges that cause threat to freshwaters & usage, potable water quality fulfillment display declining tendency, percentage of population in the province insured by a comprehensive source water protection plan, hazard allied with dams of Water Security Agency, number of substandard dams that needs repair, number of sewage effluent discharges that cause threat to freshwaters show increasing styles over time. Given these trends, revenue can be high or low based upon the blend of direct and indirect overhead. The authority should decide what the best yield rate for the water safety arena is. Given these patterns, turnover may be high or low based on the blend of direct and indirect expenses. For the water security field, the management should determine what the perfect turnover rate is.

Since performance prediction may be a challenge for each organization, other organizations with the same issues may similarly apply this research method to forecast similar nonlinear series in the sense of limited data in general. This research has some limitations. The complicated matter in this study was collecting provincial data. To resolve this shortcoming, the Security Agency's annual reports were used to obtain the criteria required for the model. It would be beneficial to note that when the raw data series changes noticeably or expands vigorously, various models'

estimated accuracy will quickly decrease; different prediction methods would be needed in those circumstances.

References

1. Gain AK, Giupponi C, Wada Y (2016) Measuring global water security towards sustainable development goals. Environ Res Lett 11(12):124015
2. Opperman JJ, Orr S, Baleta H, Garrick D, Goichot M, McCoy A, Vermeulen A (2020) Achieving water security's full goals through better integration of rivers' diverse and distinct values. Water Secur 10:100063
3. Gunda T, Hess D, Hornberger GM, Worland S (2019) Water security in practice: the quantity-quality-society nexus. Water Secur 6:100022
4. Garrick D, Iseman T, Gilson G, Brozovic N, O'Donnell E, Matthews N, Young W (2020) Scalable solutions to freshwater scarcity: advancing theories of change to incentivise sustainable water use. Water Secur 9:100055
5. Jensen O, Wu H (2018) Urban water security indicators: Development and pilot. Environ Sci Policy 83:33–45
6. Babel MS, Shinde VR, Sharma D, Dang NM (2020) Measuring water security: a vital step for climate change adaptation. Environ Res 109400
7. Krueger E, Rao PSC, Borchardt D (2019) Quantifying urban water supply security under global change. Glob Environ Chang 56:66–74
8. Hall JW, Borgomeo E, Bruce A, Di Mauro M, Mortazavi-Naeini M (2019) Resilience of water resource systems: lessons from England. Water Secur 8:100052
9. Su Y, Gao W, Guan D (2020) Achieving urban water security: a review of water management approach from technology perspective. Water Resour Manage 1–17
10. Zhu D, Chang YJ (2020) Urban water security assessment in the context of sustainability and urban water management transitions: an empirical study in Shanghai. J Cleaner Prod 275:122968
11. Allan C, Xia J, Pahl-Wostl C (2013) Climate change and water security: challenges for adaptive water management. Curr Opin Environ Sustain 5(6):625–632
12. World Water Assessment Programme (United Nations), & UN-Water (2009) Water in a changing world (vol 1), Earthscan
13. Cook C, Bakker K (2012) Water security: debating an emerging paradigm. Glob Environ Chang 22(1):94–102
14. Wang K, Davies EG, Liu J (2019) Integrated water resources management and modeling: a case study of Bow river basin, Canada. J Cleaner Prod 240:118242
15. Hitzfeld BC, Höger SJ, Dietrich DR (2000) Cyanobacterial toxins: removal during drinking water treatment, and human risk assessment. Environ Health Perspect 108(suppl 1):113–122
16. Otten TG, Xu H, Qin B, Zhu G, Paerl HW (2012) Spatiotemporal patterns and ecophysiology of toxigenic Microcystis blooms in Lake Taihu, China: implications for water quality management. Environ Sci Technol 46(6):3480–3488
17. Zubaidi SL, Ortega-Martorell S, Al-Bugharbee H, Olier I, Hashim KS, Gharghan SK, Al-Khaddar R (2020) Urban water demand prediction for a city that suffers from climate change and population growth: gauteng province case study. Water 12(7):1885
18. Damkjaer S, Taylor R (2017) The measurement of water scarcity: defining a meaningful indicator. Ambio 46(5):513–531

19. Howlett MP, Cuenca JS (2017) The use of indicators in environmental policy appraisal: lessons from the design and evolution of water security policy measures. J Environ Policy Plann 19(2):229–243
20. Bichai F, Smeets PW (2013) Using QMRA-based regulation as a water quality management tool in the water security challenge: experience from the Netherlands and Australia. Water Res 47(20):7315–7326
21. Li P, Wu J (2019) Drinking water quality and public health. Expo Health 11(2):73–79
22. Cyr-Gagnon J, Rodriguez MJ (2019) Optimizing data management for municipal source water protection. Land Use Polic
23. Water Security Agency 2015–16 Water Security Agency Annual Report. Retrieved from https:// www.wsask.ca/Global/About%20WSA/Annual%20Reports%20and%20Plans/Water%20S ecurity%20Agency%20Annual%20Reports/WSA-Annual-Report-2015-16.pdf. Accessed 29 Dec 2020
24. Water Security Agency 2016–17 Water Security Agency Annual Report. Retrieved from https:// www.wsask.ca/Global/About%20WSA/Annual%20Reports%20and%20Plans/Water% 20Security%20Agency%20Annual%20Reports/WSA-Annual-Report-2016-17-WEB.pdf. Accessed 29 Dec 2020
25. Ellingson N, Hargiss CL, Norland J (2019) Understanding municipal water use and data availability: a case study across North Dakota, USA. Water Resour Manage 33(14):4895–4907
26. Rawlyk FX, Patrick RJ (2013) Capacity needs for source water protection plan implementation: lessons from the South Saskatchewan River. Can J Urban Res 22(1):20–45
27. Hariri-Ardebili MA (2018) Risk, Reliability, Resilience (R3) and beyond in dam engineering: a state-of-the-art review. International journal of disaster risk reduction 31:806–831
28. Meghella M, Eusebio MA (2002) Risk assessment tool to effectively support decision makers to prioritize maintenance, repair and upgrading of dams. Dam Maintenance Rehabil 159–168
29. Li C, Sun L, Jia J, Cai Y, Wang X (2016) Risk assessment of water pollution sources based on an integrated k-means clustering and set pair analysis method in the region of Shiyan. China. Sci Total Environ 557:307–316
30. Rizak S, Hrudey SE (2008) Drinking-water safety–challenges for community-managed systems. J Water Health 6(S1):33–41
31. Ochoo B, Valcour J, Sarkar A (2017) Association between perceptions of public drinking water quality and actual drinking water quality: a community-based exploratory study in Newfoundland (Canada). Environ Res 159:435–443
32. Kleinbaum D, Kupper L, Nizam A, Rosenberg E (1988) Applied regression analysis and other multivariable methods, PWS-Kent, Boston, Mass
33. Draper H, Smith NR (1998) Applied regresssion analysis, 3rd edn. Wiley, New York
34. Bowerman BL, O'Connell RT, Koehler AB (2004) Forecasting, time series, and regression, thomson learning
35. Yin S, Huang Z (2014) Performance monitoring for vehicle suspension system via fuzzy positivistic c-means clustering based on accelerometer measurements. IEEE/ASME Trans Mechatron
36. Yang Y (2015) Development of the regional freight transportation demand prediction models based on the regression analysis methods. Neurocomputing 158:42–47

Studying the Water Scarcity in the Downstream Due to Factors in the Upstream—A Case Study

Tham Hong Duong

1 Overview

Mekong is an international river, flowing through many countries in South East Asia. Many studies indicated that dams on the mainstream of this river lead to numerous conflicts and problems that needed to be solved, both in social, economic, and environmental aspects. There are actually so many hydropower dams built from upstream to downstream, and the reason for conflicts is that this river played a very important role in the specific region, where there are at least six countries, i.e., China, Lao, Thailand, Myanmar, Cambodia Vietnam lived beneficially thanks to resource taken from this river. This river supplies electrical energy, food, echo diversity, and fishery products for these countries.

Mekong River Basin region is also the most crowded population community with more than 60 million people. But nearly 85% of the population in the rural areas earned their daily livings and lived along the river with fishery and agriculture [1]. The living condition of a great part of the region is under the standard level.

Many global organizations have had continuously set forward strategic plans for speeding up economic development for this region, so one of the most key factors is energy for the region. So HEP (an abbreviation of the hydro-electrical power) is the prior option because this solution is reasonable for mountainous topography like Lower Mekong River Basin (LMRB, where Laos is the most suitable for developing this energy), it is cheap, less polluted than fossil energy, and may contribute for irrigation when necessary. Reservoirs associated with dams can be used to regular the flow when necessary and for irrigation purposes [2].

However, this kind of energy faces so many negative impacts on the environment, affecting the economic and social aspects [3]. Disadvantages of hydropower dams are:

T. H. Duong (✉)
Ho Chi Minh City Open University, Ho Chi Minh City, Vietnam
e-mail: tham.dh@ou.edu.vn

Ecosystem damage;
Loss of land;
Siltation;
Flow shortage;
CO2 and CH4 emission from reservoirs;
Resettlement for people;
Other failure hazards (reservoir-induced seismicity [4]).

Unfortunately, HEP in the condition of global climate change, combined as a double-action has caused so much and increasingly negative impacts: alter the regime of water flow and runoff to regions and subregions in LMRB, Drought/Flood as severe weather from places to places, loss of biodiversity, Green House Gas (GHG) emission, etc.; besides, it leads to decline in fishery and agricultural productivity, reduction of sediment (for being trapped behind dams) to downstream regions, etc., and especially water quality and usage. More seriously, reservoir-induced seismicity due to the high pressure of reservoir water on substrata of geo-morphological structure [5] might be another threat.

As such, water resource in downstream was seriously affected by Mekong River Hydropower dams, together with seawater rising due to climate change has resulted in a lack of water both in quantity, quality (salinity intrusion and pollution), reduce land for infiltration and surface storage into ponds or lakes…a question is how can we point out water scarcity using data related to dams and to climate change?

This article will study quantitatively the effects of factors of the upstream such as dam-related environment, i.e., catchment, runoff, flow discharge…to predict the water scarcity in the downstream. The limitation of the study is on the time period when the data was collected.

2 Methodology

2.1 Conditions, Variables, and Parameters to be Considered

Climate change. Water scarcity is currently keen and urgent. Salinity intrusion together with extreme weather caused by El Nino make the situation worse than ever. So a lot of factors to be taken into account should be as follows:

- Natural conditions of downstream countries/regions;
- Socio-Political conditions of the countries located along the River.
- Conditions of Water usage of each country in the region.
- What are the factors contributing to water scarcity in downstream regions?

Conflicts. Some examples for the non-sustainable development is Lao's HEP might cause negative impacts for Cambodia, then, in turn, Cambodia takes natural resources prior to Vietnam. Nearly 40 big dams in the mainstream of the Mekong and its

tributary areas built by these countries affect seriously the most downstream Mekong Delta of Vietnam. There are visible conflicts and invisible ones.

Visible conflicts

- Literature reviews over the concepts of sustainable development indicated due to the construction of hydropower dams upstream of the Mekong river, each MRC country has a degradation in economic aspects (agricultural production, fishery, and forestry), environment (i.e., degradation and loss of biodiversity) and social aspect (poverty increases as population increases), especially riparian citizen [3,6,7]. In another situation, China releases water from the Jing Hong dam for drought protection in Vietnam, but Thailand warned the water raised so fast that the fishery and agriculture were negatively affected.
- PDR Lao for years wants to be an electricity export country in LMRB, has built at least 23 HEP dams along the mainstream of Mekong River and by 2020 at least more 90 dams will be constructed. Big Xayaburi (1285 MW) and rather a small Don Sahong (just 260 MW) are both approved by the government (the main contractor is Thailand and Malaysia, respectively) [8]. A question is that Lao is an MRC country, why Lao didn't counsel other downstream MRC countries unilaterally disobeyed any Mekong Agreement signed in 1995 by member countries.
- Phnom Penh Post [9] recently published on 6 April 2016 said that 11 proposed dams in the LMB will damage Cambodia's economy by nearly $450 million per year, (Vietnam will suffer a higher loss, about $760 million per year). But in turn, the country keeps on construct the Stung Treng dam (nearly 1000 MW) which can push more than 10,000 to resettle to other places. The Phnom Penh Post abovementioned also said: Don Sahong dam built in Lao's territory will cause "disastrous effects (quoted) for downstream countries", i.e., Cambodia and Vietnam. So, the question is that meanwhile, the MRC upstream countries knew clearly the negative impacts to downstream, why they don't give up hydropower dam projects in the mainstream of Mekong River?

Invisible conflicts

Invisible conflicts are those in a complicated system where this is cause but also being the effect of the other.

- Statistical data (Pornsook C, 2000 [10]) indicated that only thousands of hectares of rice pad of Korat Plateau (Thailand), requires nearly 6.32 billion cubic meters of water. Water for irrigation for North East Plateau of Thailand can be enough of 325,000 Ha paddy rice field, has taken 17% water in the dried season of Tien and Hau River. But whether Thailand may /may not give up the good ambition of being a top leading rice exporting country in the region or not, it seems there is uncertainty that the fishery and agriculture were negatively affected (Fig. 1).
- Another negative impact of dams is a reduction of sediment that is trapped behind dams. Reported data indicated that with data in 1983, it is 160 million metric tons of suspended sediment per year poured into East Sea (Milliman and Meade, 1983

Fig. 1 Dams in LMRB. Korat Plateau (KP in the figure) is a very vast and relatively dried area which has huge demand of water irrigation [10]
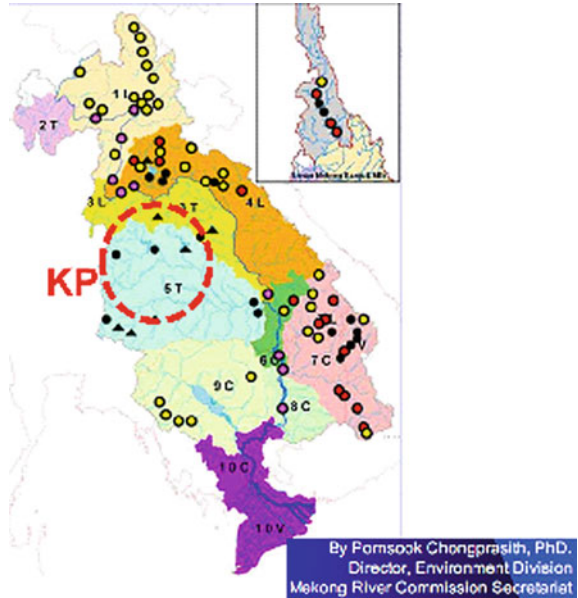
Fig. 2 Degradation in sediment from upstream to downstream countries [11]
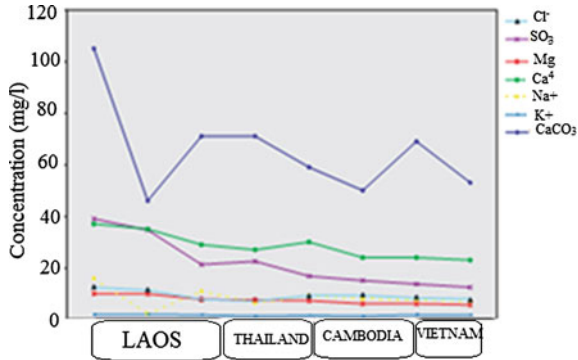
[11]). But until 2010 (after 27 years), it decreases nearly 90 times to 155 Mt per month[1] although discharge increases someway (Fig. 2).

2.2 Data Collection for Model

A causal loop model for understanding the reason for water scarcity has been established (Tham, D.H, 2011 [13]). The goal of this study is to find out the relationship

---

[1] Calculation with discharge 60,000 cubic meters/sec × 86,400 s × 30 days/month × 1.500 ppm (Zuo Xue, J. Paul Liu and Qian Ge, 2010) [12].

between HEP dams-related factors and Water Use, in the condition of climate change (Fig. 3).

Data from the period from 1995 to 2000 (post-dam period) are collected. These were independently recorded ones in stations of PDR Lao, Thailand, Cambodia, and Vietnam. For the practicable purpose, the mean values are obtained from the documentations reported by MRC in 2010 [14]. There are 8 variables including:

- **RSRVOIR**, "water surface" = Sum-up areas of water surface of reservoirs upstream in China before 2000 added to areas of reservoirs in specified country of LMB; for example, to find area of reservoirs in PDR Lao, we take area of reservoirs associated with dams in upstream China built before 1995 (i.e. Manwan) *plus* the area of reservoirs in PDR Lao's territory;
- **GHGEMIT** (with label "CO_2 CH_4 (ton)") = amount of greenhouse gases emitted into atmosphere per capita, in million tons CO_2 equivalent [15];
- **CATCHMNT** with label "area basin (km2) = Area of catchment in km^2;
- **RAINFALL** (with label "rainfall in mm") = Rainfall in mean value, in mm, [21];
- **FLOW** (with label "discharge ($milm^3$)") = Discharge measured in each country, million m^3 [16];
- **EVAPO** (with label "evaporation in mm") = Evaporation in mm [16];
- **RUNOFF** (with label "runoff in mm") = depth of runoff in mm;
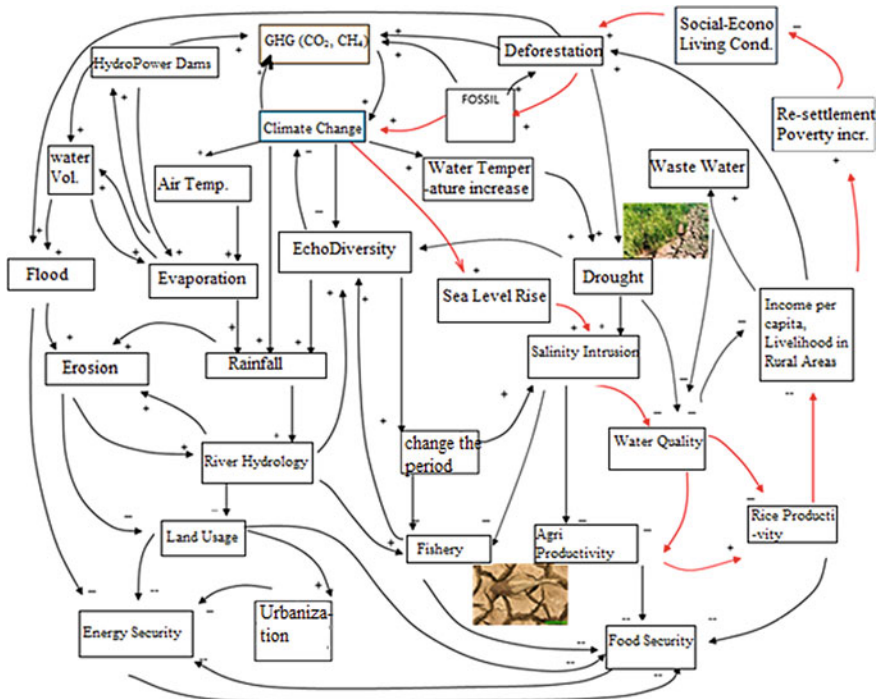
Fig. 3 Causal loop for a system dynamic between the effective factors

Table 1 Table captions should be placed above the tables

MRC Countries	RSRVOIR*	GHGEMIT	CATCH-MNT	RAINFALL**	FLOW***	EVAPO	RUN OFF	DEFOREST
	(Km^2)	(mTon/cap)	(10^3 km^2)	(mm)	(M.m^3)	(mm)	(mm)	(10^3 km^2)
Lao	451.93	17.40	202	69	5270	7	2000	129.4
Thai	1144	351.30	184	148	2560	40	700	515.3
Cambodia	415	22.70	155	181	2860	25	550	131.4
Vietnam	480	176.90	65	5	1160	15	350	137

Source *(WRI, 2009); **(IMC, 1988); ***IPCC, COP8, MRC

- **DEFOREST** (with label "area of deforest") = Area of deforestation, 10^3 km^2

  These variables as independent variables are tabulated in Table 1.

3   Results

3.1   Correlation Between Factors of the Environment in the Existing Condition

Vietnam is the most downstream country in the region. By conducting a multi-variable linear regression, an equation for the correlation between different factors of the upstream natural factors and the water condition in the downstream regions, as in Fig. 4.

3.2   Equation of Water Balance

The equation of Water Balance is as follows [17]:

$$R = P + Q - E - I - \Delta S \tag{1}$$

where R is the runoff, P is the precipitation, Q is the discharge, I is the infiltration and ΔS is the storage downstream. The condition of water scarcity happens when the demand for water use excesses the runoff throughout the catchment. This situation will not take the be water spraying time of agricultural crops into account that may exacerbate the scarcity. By assigning the trend of increase or decrease of each individual factor in the Table of correlation, the storage has proved to be lowered, as in Fig. 5.

Correlations

		water surface	CO2 CH4 (ton)	Evapo in mm	Rainfall (mm)	Runoff (mm)	area of deforest	Discharge(mil m3)	AreaBasin(km2)
water surface	Pearson Correlation	1	.910*	.829	.326	-.180	.998**	-.246	.313
	Sig. (1-tailed)	.	.045	.086	.337	.410	.001	.377	.343
	N	4	4	4	4	4	4	4	4
CO2 CH4 (ton)	Pearson Correlation	.910*	1	.747	.025	-.442	.891	-.555	-.102
	Sig. (1-tailed)	.045	.	.126	.488	.279	.054	.223	.449
	N	4	4	4	4	4	4	4	4
Evapo in mm	Pearson Correlation	.829	.747	1	.662	-.543	.857	-.501	.171
	Sig. (1-tailed)	.086	.126	.	.169	.229	.071	.250	.415
	N	4	4	4	4	4	4	4	4
Rainfall (mm)	Pearson Correlation	.326	.025	.662	1	-.111	.388	.066	.587
	Sig. (1-tailed)	.337	.488	.169	.	.444	.306	.467	.206
	N	4	4	4	4	4	4	4	4
Runoff (mm)	Pearson Correlation	-.180	-.442	-.543	-.111	1	-.191	.975*	.700
	Sig. (1-tailed)	.410	.279	.229	.444	.	.404	.012	.150
	N	4	4	4	4	4	4	4	4
area of deforest	Pearson Correlation	.998**	.891	.857	.388	-.191	1	-.243	.340
	Sig. (1-tailed)	.001	.054	.071	.306	.404	.	.379	.330
	N	4	4	4	4	4	4	4	4
Discharge(mil m3)	Pearson Correlation	-.246	-.555	-.501	.066	.975*	-.243	1	.767
	Sig. (1-tailed)	.377	.223	.250	.467	.012	.379	.	.117
	N	4	4	4	4	4	4	4	4
AreaBasin(km2)	Pearson Correlation	.313	-.102	.171	.587	.700	.340	.767	1
	Sig. (1-tailed)	.343	.449	.415	.206	.150	.330	.117	.
	N	4	4	4	4	4	4	4	4

*. Correlation is significant at the 0.05 level (1-tailed).

**. Correlation is significant at the 0.01 level (1-tailed).

Fig. 4 Correlation between some factors of environment in period 1995–2000
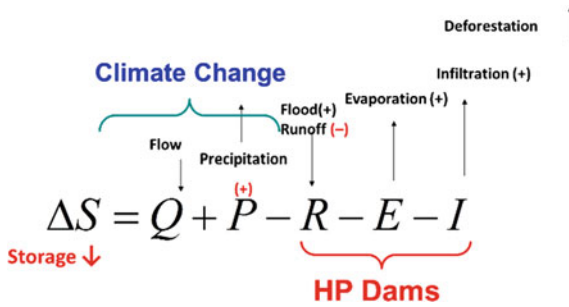
Fig. 5 Correlated factors result in a decrease of the storage to the most downstream country Vietnam

3.3 Discussion

This study is personally the author's viewpoint explaining scientifically the water scarcity downstream by using a correlation matrix and the equation of the water balance, that bases upon data mining in a specific period.

- There are unavoidable conflicts in the upstream, both in visible and invisible issues. The key controversy is the way of upstream countries in governing water use and the policy of sharing the natural resource implemented by upstream countries.

- This study only aims to entail some key factors in the upstream. The approach is to analyze the correlation matrix in Fig. 3. By comparing quantitatively the trend of increase or decrease of the specific factor associated with others in the water balance equation, there are factors of climate change and those of upstream dam projects. Factors of the upstream strongly depend on the construction activities and their consequence, including environmental, hydrological, and social aspects.
- The overuse of the water resource aiming to increase the productivity in agricultural activities results in the water scarcity of the downstream countries, but have not been listed in the correlation matrix. Besides, the sea level rising causes the water polluted.
- Solution for mitigating the water scarcity may come from the way of cooperation between MRC countries, construction of some water storing and a transformation from some agricultural activities to the fishery with a higher value obtained.
- This study only suggests an approach for estimating the water condition of water use downstream in relationship with factors upstream. The more efficient approach for studying the water scarcity the downstream according to factors of the upstream is the system dynamics [18].

4 Conclusions

The Mekong is an international river, but factors in the upstream caused water scarcity downstream. In the situation in which hydropower dams are constructed on the mainstream, the consequence has been proved clearly to impacts negatively to people community and its livelihood, environment, and economics of the downstream as well. Projects of the hydropower dams have continuously harmed and damaged the natural environment, have caused a change in the hydrological regime, and disturbed the water balance from regions to other regions. Causes and effects is a complex system with many different factors. A scheme of the causal loop is created that serves as a good material for studying the system dynamics.

By investigating the data of 8 variables about the water condition in the regions from the upstream to downstream, which their correlations are applied to the equation of the water balance, the results point out a water scarcity in the downstream regions. There are factors for water management downstream. They are still required further studies for explaining water scarcity in a more detailed way in the future.

References

1. Mekong River Commission (2005) Overview of the hydrology of the Mekong Basin, Vientiane MRC
2. Goh E (2010) China in the Mekong River Basin: the regional security Implications of resource development on the Lancang Jiang, working paper of Rajaratnam School of International studies, Nanyang Technological University

3. Atshshi L et al (2007) Estimating global climate change impacts on hydropower projects: application in India, Sri Lanka and Vietnam. http://www.thefreelibrary.com/
4. Joshi UR, Maskey RK, Kafle KR (2020) A review on the mechanism of reservoir-induced-seismicity for Nepalese context. Nepal J Sci Technol (NJST) 19(1):215–221. https://doi.org/10.3126/njst.v19il.29823
5. Pailoplee S (2014) Earthquake hazard of dams along the Mekong mainstream. J Nat Hazards 74:1813–1827. https://doi.org/10.1007/s11069-014-1287-0
6. Kristensen J (2001) Food security and development in the lower Mekong River Basin—a challenge for Mekong River commission, Asia and Pacific forum on poverty: reforming policies and institutions for poverty reduction, Manila
7. State of Basin Report (2003), ISSN 1728–3248, 316 pages, published by Mekong River Commission, Phnom Penh, Cambodia
8. Johnston R, Lacombe G, Hoanh CT, Noble A, Pavelic P, Smakhtin V, Suhardiman D, Kam SP, Choo PS (2010) Climate change, water and agriculture in the greater Mekong Subregion, IWMI research report 136, International Water Management Institute. ISBN: 978–92–9090–728–2
9. Phnompenhpost.com (2016) Mekong dams' annual impact put at $450 M. http://www.phnompenhppost.com/national, Igor Koussov, publication date on April 6th 2016
10. Pornsook Chongprasith: Mekong climate change and Adaptation initiative. Presentation at the International Conference, MRC for sustainable development, 34 slides.
11. Kummu M, Varis O (2007) Sediment-related impacts due to upstream reservoir trapping, the lower Mekong River. J Geomorphol 85(2007):275–293
12. Ge Q, Chu F, Xue Z, Liu JP, Du Y, Fang Y (2010) Paleoenvironmental records from the northern South China Sea since the last glacial maximum. J Acta Oceanol Sinica 29:46–62
13. Tham HD (2010) A suggested approach for riverbank erosion prediction—a case study of the Dong Thap province in Mekong Delta, Vietnam. In: Proceedings of International Symposium, Exhibition, and short course on geotechnical and geosynthetics engineering: challenges and opportunities on climate change. Bangkok, Thailand
14. Evaporation from water surface - engineering toolbox, website http://www.engineeringtoolbox.com/evaporation-water-surface-d_690.html
15. Climate change baseline assessment working paper (2010) Volume I and II, MRC SEA hydropower on the Mekong mainstream
16. Fuchs HJ (2004) Data availability for studies on effects of land cover changes on water yield sediment and nutrient load at catchment of lower Mekong Basin, working paper in cooperation programme between MRC and GTZ, Götingenf
17. Kazama S, Sawamoto M, Nawarathna NB (2001) Simple analysis on future water resource in Mekong Basin. In: Proceedings of XXIX IAHR Congress, Beijing
18. Popovich CJ, Simonovich SP, McBean GA (2010) Use of an integrated system dynamics model for analyzing behaviour of the social-economic-climatic system in policy development. Water Resources Research Report, University of Western Ontario, ISSN: (print) 1913–3200; (online) 1913–3219;ISBN: (print) 978–0–7714–2838–8; (online) 978–0–7714–2839–5

Prediction Model for Evaluating the Raw Water Quality Parameters and Its Significance in Pipe Failures of Nuclear Power Plant

P. Suganya, G. Swaminathan, B. Anoop, S. P. Sathiya Prabhakaran, and M. Kavitha

1 Introduction

Majority of the plant auxiliaries in nuclear power plant depends on the water resource to remove the non-radioactive thermal loads. Such daily raw water requirements will vary from 5000 to 7000 m^3 per day. Water quality monitoring and management techniques are required for the prediction & evaluation of its effect on the component failures. Optimization and water quality modeling caters to only 5–10% of the total research on water quality (data from the Scopus database). Unplanned plant outages and economic losses are enormous in water chemistry failures [3, 10, 13, 18, 20, 22]. Almost 90% of pipe failures in nuclear power plants occur due to leaks, and the failure mechanism that continues to be a significant one is erosion-corrosion. This erosion-corrosion mechanism is a significant failure mechanism factor in small and large diameter pipelines [9]. The undesired phenomena due to low water quality can be prevented if proper chemical conditioning and preventive measures were taken at the appropriate time [20, 22].

The performance of the water supply systems with specific importance to water quality can be measured by various indicators like mean, variance & other statistical tools. The acceptance of a water sample is based on the mean and standard deviation, rather than the exceeding value [24]. This assessment process is seen as a statistical decision of a particular problem. However, a wide gap exists in these classical methods to predict the severity with respect to time [14]. Response surface methodology combines the mathematical and statistical tools to model and optimize

P. Suganya (✉) · M. Kavitha
BHAVINI, Kalpakkam, Tamilnadu 603127, India
e-mail: suganya_bhavini@igcar.gov.in

P. Suganya · G. Swaminathan · S. P. S. Prabhakaran
National Institute of Technology, Tiruchirapalli 603127, India

B. Anoop
Indira Gandhi Centre for Atomic Research, Kalpakkam, India

the system parameter after determining the correlation between the independent variable [19]. RSM is used extensively to design and optimize the parameters to minimize the number of experiments and to find the relation between each individual parameter [4, 8, 25].

Profuse quantity of research on contaminant transport, water quality with specific importance to pollutant & its degrading effect has been conducted [11, 12]. The performance of artificial neural network (ANN) and multilinear regression (MLR) models in predicting the BOD, COD was better. Most of the models were utilized to study the impact of industrial and human interference on the environment. Degradation of biological pollutants, DO variation in the natural water streams, and the fate of hazardous & organic contaminants from industrial effluent are among the most researched topic [5, 28, 29, 31].

The majority of the exceedance in the water chemistry levels pose severe damage to the component and warrant hefty economic losses [6, 7, 15, 17, 21, 27]. These water chemistry violations may slowly develop into a pipeline failure and prevent the system from performing its intended function and hinder nuclear power plant operations. The plant water auxiliary systems are highly required to maintain the safe state of the reactor to prevent any unforeseen exposures damages. Safety functions are grouped and ranked into safety classes based on the consequences of the failure of safety functions performed by the system & the occurrence probability of its failure. Plant water auxiliary systems are classified under safety class: 3 and seismic category: 1 [1]. The availability of the plant water auxiliary system even after the reactor shutdown ensures decay heat removal and maintains the reactor systems in the poised state. Hence, developing a prediction model for water chemistry violation in the source of raw water of the nuclear power plant will be highly beneficial to manage and act promptly to the situation.

The main objective of this research is to develop a prediction model with the existing water quality data to correlate the effect of other water quality parameters on the conductivity. Further studies are carried out with this data to manage and plan for the pipeline failures in auxiliary water systems of the nuclear power plant. Once a model has been developed, it can be adopted in the system, and necessary actions can be formulated to prevent major disasters.

2 Material and Methodology

The process flow diagram of the plant water auxiliary system with its end system load is depicted in Fig. 1. Plant water auxiliary system supplies raw water to the safety-related unit coolers (SRSW coolers), which removes the thermal loads from various safety-related systems like safety chillers, gas compressors, reactor auxiliary systems like concrete cooling systems, radiation shielding systems, spent subassembly coolers, etc. Mostly carbon steel is used as the material of construction for auxiliary water system pipelines.
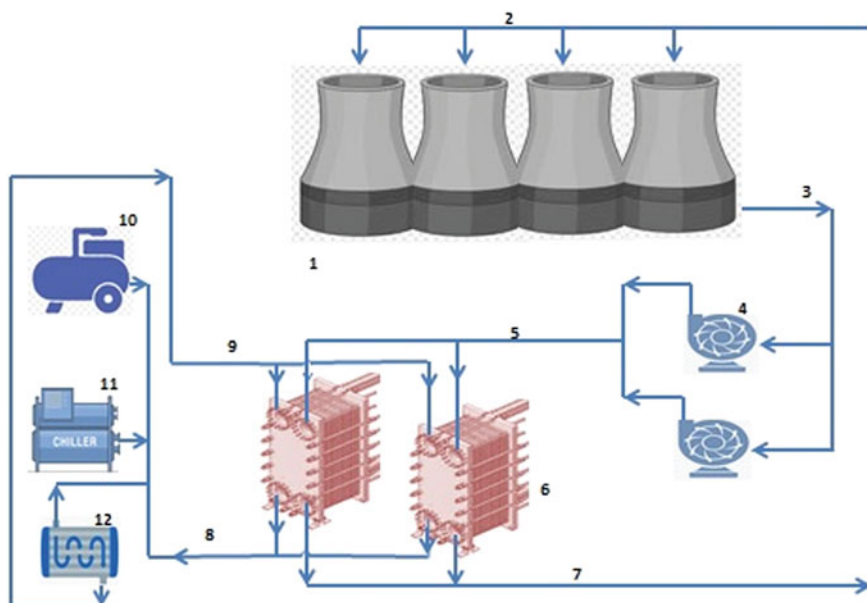
Legend:

1. Cooling Tower (CT)	2. Hot raw water to CT
3. Cold raw water from CT	4. Raw water pumps
5. Raw water to the unit cooler	6. Unit Coolers
7. Raw water from the cooler	8. DM water to system loads
9. DM water from system loads	10. Gas compressors
11. Safety chillers	12. Reactor Auxiliary loads

Fig. 1 Flow diagram of plant water auxiliary system

The water quality of this plant's water auxiliary system is collected for a period of 3 years (January 2018 to September 2020). Quantitative and qualitative analysis of water samples is carried out as per the standard method for examination of water [2].

This data is used for multivariate regression analysis by response surface methodology using Design-Expert software. Conductivity is chosen as the response parameter, and other water quality parameters like alkalinity, sodium, chloride, iron, silica, hardness are given as input variables. The performance of the multilinear regression model is evaluated by the correlation of coefficient and P-value of the model, as indicated in the ANOVA table. These two criteria indicate the goodness of fit for the model.

After this multivariate regression analysis, major chemistry violation which intensifies to pipeline failures is identified case by case. Statistical analysis of the data is performed using JASP Software. The results obtained from the prediction model

are compared with available pipe failure cases, and a suitable recommendation is proposed.

3 Results and Discussion

3.1 Experimental Run and Optimization of Water Quality Parameters

The multilinear regression equation obtained for the predicted model is given by the following equation.

$$
\begin{aligned}
\text{Conductivity, } Y =\ & 92.9 - 3.58\,X_1 + 1.29\,X_2 + 7.77\,X_3 - 1.85\,X_4 + 4.45\,X_5 \\
& + 185.22\,X_6 - 25.17\,X_7 + 0.12\,X_1X_2 + 0.1\,X_1X_3 \\
& + 0.019\,X_1X_4 - 0.023\,X_1X_5 - 9.8\,X_1X_6 - 0.31\,X_1X_7 - 0.5\,X_2X_3 \\
& + 0.027\,X_2X_4 - 0.016\,X_2X_5 + 24.85\,X_2X_6 - 0.22\,X_2X_7 - 0.006\,X_3X_4 \\
& - 0.0036\,X_3X_5 + 18.84\,X_3X_6 + 0.46\,X_3X_7 - 0.004\,X_4X_5 + 3.18\,X_4X_6 \\
& + 0.046\,X_4X_7 - 4.18\,X_5X_6 + 0.2\,X_5X_7 - 120\,X_6X_7 + 0.0009\,X_1{}^2 \\
& + 0.07\,X_2{}^2 + 0.15\,X_3{}^2 + 0.0026\,X_4{}^2 - 0.0016\,X_5{}^2 - 277.86\,X_6{}^2 \\
& + 0.8\,X_7{}^2
\end{aligned}
$$

Where X_1 is the M-alkalinity, X_2 is the total hardness, X_3 is the calcium hardness, X_4 is the sodium, X_5 is the chloride, X_6 is the iron, X_7 is the silica levels in the water. The results of the ANOVA are represented in Table 1. The evaluation criteria for the model is given by the R^2 value and P-value of the model. The goodness of fit of the predicted model is determined by the R^2 value of at least 0.8. The coefficient of correlation for the model is 0.98. The P-value of the model is <0.0001. This states that a model is significant and has a good fit.

Figure 2 shows the actual and predicted plot for the model. Only little variation is seen in the actual and predicted model. The residuals are evenly distributed along the straight line (Fig. 3). Hence, the model could be used for predicting the response variable. Figure 4 shows the response surface graphs for the response variable conductivity. There exists a heavy interaction between conductivity and sodium, chloride. Moderate interaction between the conductivity and iron is prevalent (Fig. 4a–f). The effect of sodium, chloride, iron, and silica is more significant than the hardness and alkalinity terms (Table 1). Iron and silica being present in smaller quantities when compared to sodium and chloride levels, the influence of these two parameters on the conductivity is more significant. The raw water quality analysis results indicate that the effect of hardness or alkalinity levels are less when compared to sodium and chloride levels. Hence, by taking preventive measures to control the levels of sodium and chloride, corrosion failure on pipelines can be minimized.

Table 1 ANOVA table

Source	Sum of squares	df	Mean square	F-Value	P-Value
Model	9.906E + 06	35	2.830E + 05	117.18	<0.0001
A-M- Alkalinity	539.23	1	539.23	0.2233	0.6380
B-Total Hardness	2179.20	1	2179.20	0.9023	0.3453
C-Ca Hardness	57.01	1	57.01	0.0236	0.8783
D-Sodium	12,191.90	1	12,191.90	5.05	0.0277
E-Chloride	2261.32	1	2261.32	0.9363	0.3364
F-Iron	7363.35	1	7363.35	3.05	0.0850
G-Silica	10,995.12	1	10,995.12	4.55	0.0362
AB	4255.61	1	4255.61	1.76	0.1885
AC	962.87	1	962.87	0.3987	0.5298
AD	3556.11	1	3556.11	1.47	0.2289
AE	3973.43	1	3973.43	1.65	0.2037
AF	3170.63	1	3170.63	1.31	0.2556
AG	1772.65	1	1772.65	0.7339	0.3944
BC	16,980.08	1	16,980.08	7.03	0.0098
BD	3467.41	1	3467.41	1.44	0.2347
BE	1088.33	1	1088.33	0.4506	0.5042
BF	18,787.57	1	18,787.57	7.78	0.0067
BG	765.71	1	765.71	0.3170	0.5751
CD	89.38	1	89.38	0.0370	0.8480
CE	21.07	1	21.07	0.0087	0.9258
CF	3587.50	1	3587.50	1.49	0.2269
CG	1258.75	1	1258.75	0.5212	0.4727
DE	2222.67	1	2222.67	0.9203	0.3406
DF	5399.15	1	5399.15	2.24	0.1392
DG	279.55	1	279.55	0.1157	0.7347
EF	10,889.05	1	10,889.05	4.51	0.0371
EG	10,938.82	1	10,938.82	4.53	0.0367
FG	15,530.93	1	15,530.93	6.43	0.0134
A^2	0.6704	1	0.6704	0.0003	0.9868
B^2	2043.63	1	2043.63	0.8461	0.3607
C^2	2346.44	1	2346.44	0.9715	0.3276
D^2	2775.89	1	2775.89	1.15	0.2872
E^2	1582.87	1	1582.87	0.6554	0.4208
F^2	2556.95	1	2556.95	1.06	0.3069
G^2	4516.06	1	4516.06	1.87	0.1757

Table 1 (continued)

Source	Sum of squares	df	Mean square	F-Value	P-Value
Residual	1.763E + 05	73	2415.29		
Lack of fit	1.763E + 05	69	2555.30		
Pure error	0.0000	4	0.0000		
Cor total	1.008E + 07	108			
$R^2 = 0.98$; $R^2_{adj} = 0.97$; CV (%) = 6.65					

Fig. 2 Actual and predicted plot
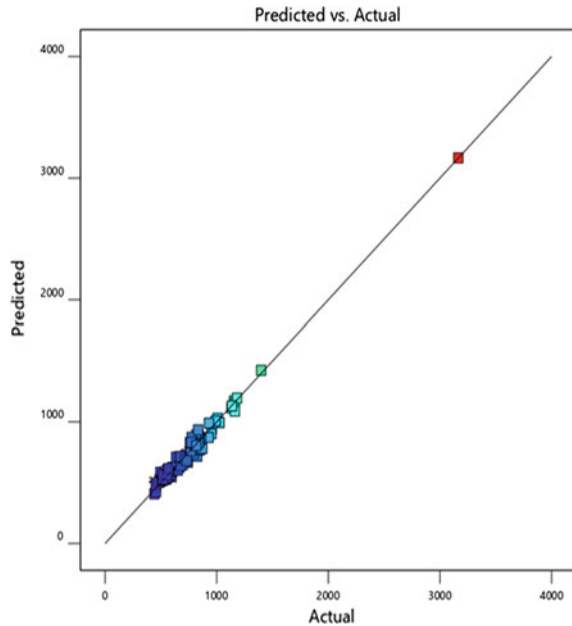
3.2 Effect of Water Chemistry on Pipe Failures

Table 2 gives the mean observed water quality parameters for 3 years and its comparison with the recommended levels. All the water quality parameters are observed to be within the recommended levels. But the chloride levels are slightly deviating. When the chloride levels are examined individually, it was deduced that marginally higher levels are received sporadically. The number of exceedance of chloride levels, when compared to the sample population, is found to be 0.3. This exceedance of chloride values above 200 ppm is not continuous, but occasionally the limits are exceeded.

Figure 5 indicates the density curve for the water quality parameter of a total sample population. The distribution curve for Total dissolved solids, M-alkalinity, Total hardness were definite and fell within the criteria. The chloride distribution levels were distributed over a wide range and are skewed.

Fig. 3 Normal probability
plot of the residuals
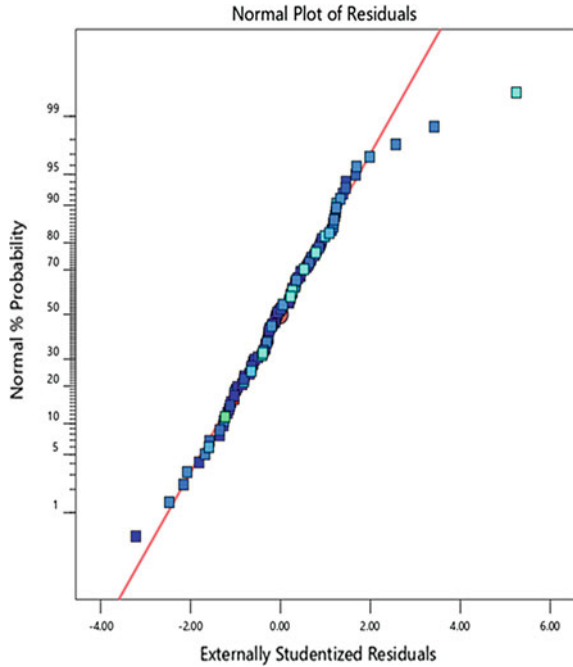
The prediction model was applied to study the conductivity and chloride levels by varying each parameter through a range of values obtained from the field. The conductivity values were predicted under two cases viz. when maximum exceedance value is reached for each parameter, and when values are always in the range (Table 3).

From Table 3, it is seen that there is a high possibility of chemistry failures in pipelines and other components if the water quality parameters go beyond the range (category: 1). Generalized corrosion, pitting corrosion plays a significant role in carbon steel pipeline failures due to exceeded chloride levels [23, 30, 31]. A severe corrosion process takes place in the internal surfaces of unlined carbon steel pipelines when exposed to violated water quality parameters [26]. High deposition of corrosion products inside the pipelines happens when this category 1 water is used in the system for 12 months. Over a while, these deposits further interfere, leak & block the system flow. This results in the frequent system, equipment outages. However, if the range of values (category: 2) obtained in these three years is continuing in the same manner, there is minimum or no cases of chemistry failures. Therefore, to avoid system failures, it is recommended to maintain the chemistry levels as per the category: 2 values.
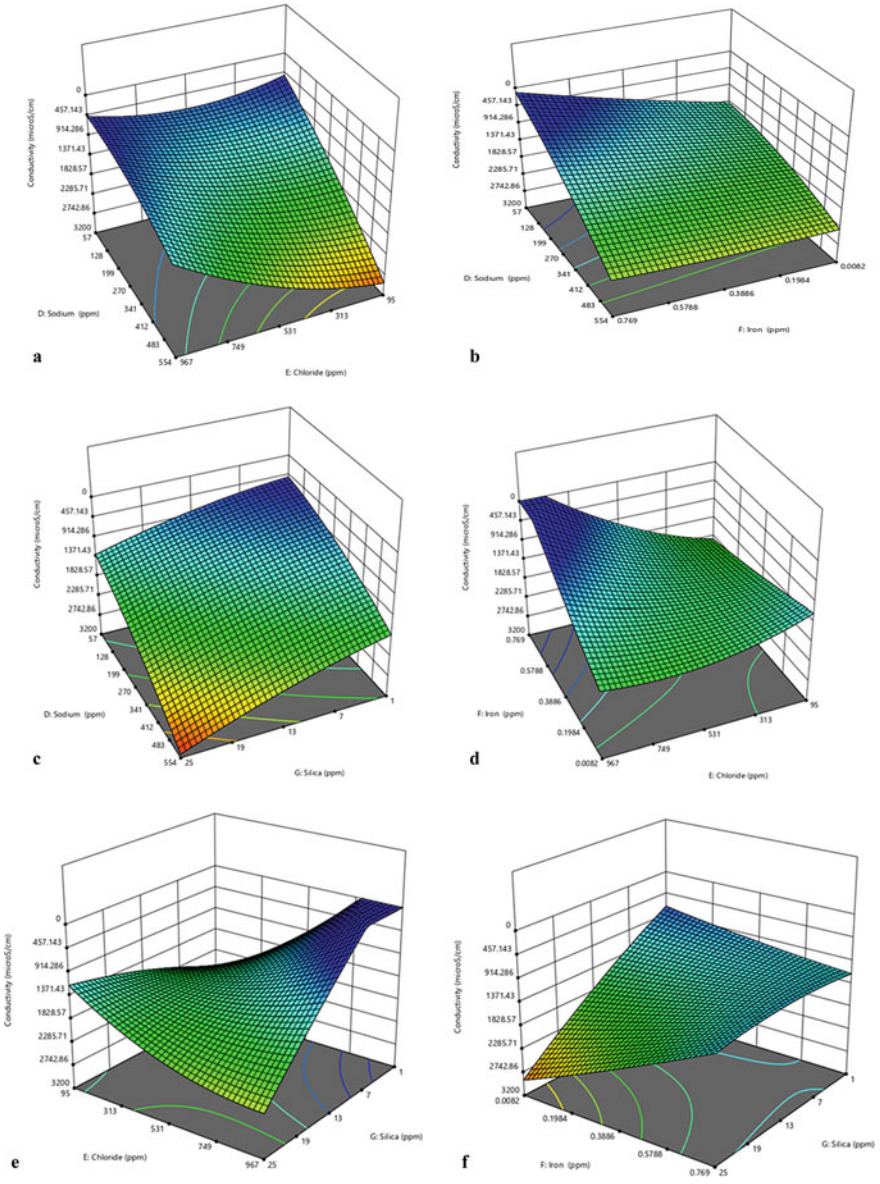
Fig. 4 a–f Response surface plots for conductivity

Table 2 Recommendation for preventing chemistry failures

Parameter	Recommended levels [16]	Mean observed levels	Remarks
pH	6–8	7.6	Acceptable as per standard
Turbidity	<NTU	3.4	Acceptable as per standard
TDS	<1350 ppm	409	Acceptable as per standard
M-Alkalinity	300 ppm	42	Acceptable as per standard
Total hardness	<300 ppm	44	Acceptable as per standard
Chloride	<200 ppm	206	Slightly above the standard
Iron	<0.3 ppm	0.1	Acceptable as per standard
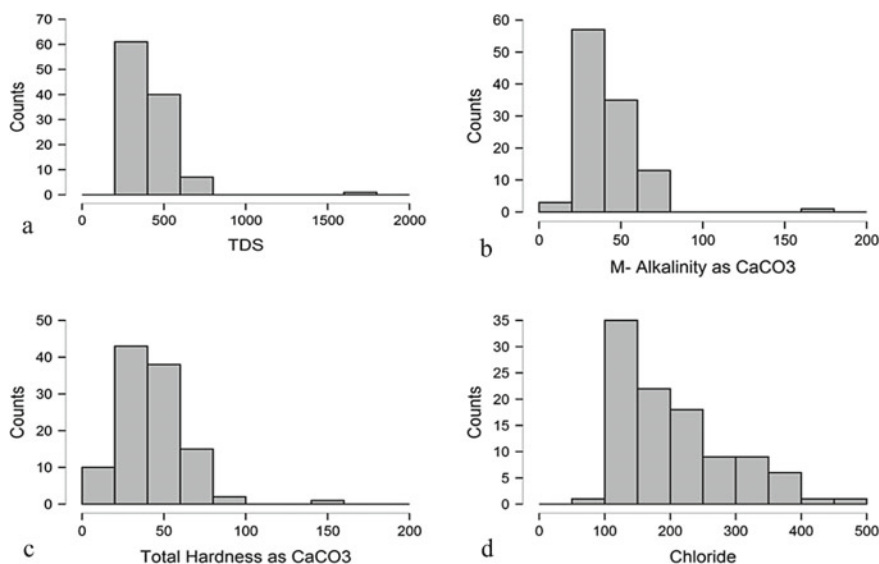
Fig. 5 **a–f** Histogram and Density plots for water quality parameters

Table 3 Predicting chemistry failures

Parameter (ppm)	Cat: 1 Max. exceedance value	Cat:2 Normal range
M-alkalinity	50–70	30–50
Total hardness	50–70	40–50
Calcium hardness	20–50	20–30
Sodium	100–500	100–250
Chloride	100–700	100–250
Iron	0.1	0.1
Silica	5–15	5–10
No of runs	30	30
No of violations	90% of the cases were exceeded	NIL in conductivity 01 in chloride

4 Conclusion

The advancement of statistical and data analysis technology was outsourced in this article for developing a prediction model for evaluating the colossal water qualitative data. The predicted model is significant and can be used to predict water quality levels. It was found that sodium, chloride, iron, and silica significantly affect conductivity levels. All the input parameters had a quadratic relationship with conductivity. Further, the exceedance levels of the water quality parameter are anticipated under two categories, and a suitable range of values for minimizing the chemistry failures is provided. These exceedance levels and the significance of corrosion failures were also enumerated. The obtained range of values, when maintained in the system, will reduce equipment outages and increase the operation cycle.

References

1. AERB (2003) Safety classification and seismic categorisation for structures, systems and components of Pressurised Heavy Water Reactors SG No. AERB/NPP-PHWR/SG/D-1. AERB
2. APHA (1998) Standard methods for examination of water and wastewater. 20th edn. AWWA, Washington DC
3. Jawwad AK, Mohamed IK (2020) The combined effects of surface texture, flow patterns and water chemistry on corrosion mechanisms of stainless steel condenser tubes. Eng Fail Anal 109. https://doi.org/10.1016/j.engfailanal.2020.104390
4. Adesina OA, Abdulkareem F, Yusuff AS, Lala M, Okewale A (2019) Response surface methodology approach to optimization of process parameter for coagulation process of surface water using Moringa oleifera seed. S Afr J Chem Eng 28, 46–51. https://doi.org/10.1016/j.sajce.2019.02.002
5. Ahmed U, Mumtaz R, Anwar H, Shah AA, Irfan R, García-Nieto J (2019) Efficient water quality prediction using supervised machine learning. Water 11:2210
6. Ajmal TS, Arya SB, Udupa KR (2019) Effect of hydrodynamics on the flow accelerated corrosion (FAC) and electrochemical impedance behavior of line pipe steel for petroleum industry. Int J Press Vessels Pip 174:42–53. https://doi.org/10.1016/j.ijpvp.2019.05.013
7. Asami K, Kikuchi M (2003) In-depth distribution of rusts on a plain carbon steel and weathering steels exposed to coastal–industrial atmosphere for 17 years. Corros Sci 45(11):2671–2688. https://doi.org/10.1016/S0010-938X(03)00070-2
8. Behera SK, Meena H, Chakraborty S, Meikap BC (2018) Application of response surface methodology (RSM) for optimization of leaching parameters for ash reduction from low-grade coal. Int J Min Sci Technol 28(4):621–629. https://doi.org/10.1016/j.ijmst.2018.04.014
9. Bush SH, Do MJ, Slavich AL, Chockie AD (1996) Piping failures in United States nuclear power plants 1961–1995. Ski Report 96:20
10. Chih Hung Lin (2014) Yuh Ming Ferng: Predictions of hydrodynamic characteristics and corrosion rates using CFD in the piping systems of pressurized-water reactor power plant. Ann Nucl Energy 65:214–222. https://doi.org/10.1016/j.anucene.2013.11.007
11. Cho KH, Pachepsky Y, Ligaray M, Kwon Y, Kim KH (2020) Data assimilation in surface water quality modeling: a review. Water Res 186:116307. https://doi.org/10.1016/j.watres.2020.116307
12. Dimri D, Daverey A, Kumar A, Sharma A (2021) Monitoring water quality of River Ganga using multivariate techniques and WQI (Water Quality Index) in Western Himalayan region of Uttarakhand, India. Environ Nanotechnol Monit Manage 15:100375. https://doi.org/10.1016/j.enmm.2020.100375

13. Ferng YM (2008) Predicting local distributions of erosion–corrosion wear sites for the piping in the nuclear power plant using CFD models. Ann Nucl Energy 35:304–313. https://doi.org/10.1016/j.anucene.2007.06.010
14. Hashimoto T, Stedinger JR, Loucks DP (1982) Reliability, resiliency, and vulnerability criteria for water resource system performance evaluation. Water Resour Res 18(1):14–20
15. Hoang TA, Ang HM, Rohl AL (2007) Effects of temperature on the scaling of calcium sulphate in pipes. Powder Technol 179(1):31–37. https://doi.org/10.1016/j.powtec.2006.11.013
16. International Atomic Energy Agency (2011) Good practices for water quality management in research reactors and spent fuel storage facilities Nuclear energy series No. NP-T-5.2. IAEA
17. Lin CH, Ferng YM (2014) Predictions of hydrodynamic characteristics and corrosion rates using CFD in the piping systems of pressurized-water reactor power plant. Ann Nucl Energy 65:214–222. https://doi.org/10.1016/j.anucene.2013.11.007
18. Li M, Wang Y, Liu Z, Sha Y, Korshin GV, Chen Y (2020) Metal-release potential from iron corrosion scales under stagnant and active flow, and varying water quality conditions. Water Res 175. https://doi.org/10.1016/j.watres.2020.115675
19. Montgomery DC (2013) Design and analysis of experiments, 8th edn. Wiley, Hoboken
20. Pourali O, Kadijani HG, Khangheshlaghi FM (2017) Chemical conditioning and monitoring to control and minimize chemistry related damages in Heller dry cooled combined cycle power plants. Anti-Corros Methods Mater 64(2):188–208. https://doi.org/10.1108/ACMM-02-2016-1648
21. Quddus A, Al-Hadhrami LM (2009) Hydrodynamically deposited CaCO3 and CaSO4 scales. Desalination 246(1):526–533. https://doi.org/10.1016/j.desal.2008.11.005
22. Rajakovic-Ognjanovic VN, Zivojinovic DZ, Grgur BN, Rajakovic LV (2011) Improvement of chemical control in the water-steam cycle of thermal power plants. Appl Therm Eng 31:119–128. https://doi.org/10.1016/j.applthermaleng.2010.08.028
23. Sarin P, Snoeyink VL, Bebee J, Jim KK, Beckett MA, Kriven WM, Clement JA (2004) Iron release from corroded iron pipes in drinking water distribution systems: effect of dissolved oxygen. Water Res 38(5):1259–1269. https://doi.org/10.1016/j.watres.2003.11.022
24. Smith EP, Hughes KYC, Shabman L (2001) Statistical assessment of violations of water quality standards under Section 303(d) of the clean water Act. Environ Sci Technol 35:606–612
25. Suganya P, Swaminathan G, Anoop B, Prasad GS, Nagarajan J (2020) Assessing the factors affecting the water chemistry parameters in the auxiliary water system of a nuclear power plant. SN Appl Sci 2:1889. https://doi.org/10.1007/s42452-020-03693-z
26. Tang Z, Hong S, Xiao W, Taylor J (2006) Characteristics of iron corrosion scales established under blending of ground, surface, and saline waters and their impacts on iron release in the pipe distribution system. Corros Sci 48:322–342. https://doi.org/10.1016/j.corsci.2005.02.005
27. Utanohara Y, Murase M (2019) Influence of flow velocity and temperature on flow accelerated corrosion rate at an elbow pipe. Nucl Eng Des 342:20–28. https://doi.org/10.1016/j.nucengdes.2018.11.022
28. Verma AK, Singh TN (2013) Prediction of water quality from simple field parameters. Environ Earth Sci 69(3):821–829. https://doi.org/10.1007/s12665-012-1967-6
29. Zare Abyaneh H (2014) Evaluation of multivariate linear regression and artificial neural networks in prediction of water quality parameters. J Environ Health Sci Eng 12(1):40. https://doi.org/10.1186/2052-336X-12-40
30. Zeng L, Chen G, Chen H (2020) Comparative study on flow-accelerated corrosion and erosion-corrosion at a 90° carbon steel bend. Materials (Basel) 13(7):1780. https://doi.org/10.3390/ma13071780
31. Zhang H, Zhao L, Liu D, Wang J, Zhang X, Chen C (2020) Early period corrosion and scaling characteristics of ductile iron pipe for ground water supply with sodium hypochlorite disinfection. Water Res 176:115742. https://doi.org/10.1016/j.watres.2020.115742

Drinking Water Quality Assessment of Public Tube-Wells and Their Spatial Distribution in the Rangpur City of Bangladesh

Fazle Rafi, Ashik Iqbal , **Md. Rabiul Islam, Sabrina Rashid Sheonty, and Ruaida Armin**

1 Introduction

Rangpur is one of the major cities in the northern part of Bangladesh and was declared as the 7th administrative division of Bangladesh on 25 January 2010 [1]. After becoming the new administrative division, a new window of economic opportunity is opened in this city. Many people from non-privileged villages facing Monga (Local Famine of northern Bangladesh) started migrating to the city area in search of better opportunity [2]. Thus, a rapid increase in urbanization was spotted in the last decade. Many large, medium, small-scale, micro, and cottage industries have been formed in discrete fields for manufacturing different products, mining, quarrying, electricity, gas, air conditioning supply, and construction work in Rangpur city [3]. With the industrial and economic development, urbanization expanded rapidly. In 2009 the build-up area was 10.73% and in 2019 is 28.26% of the total area of Rangpur city [4].

The rapid growth of urbanization and industrialization lead to regularly congregating a lot of working-class people. In this context, the demand for consumptive water use has prominently increased. There is no structured water supply system in Rangpur city and people use various kinds of sources for drinking water [5]. The

F. Rafi
Confidence Power Rangpur Limited, Pairaband, Bangladesh

A. Iqbal (✉)
Bangladesh University of Engineering and Technology, Dhaka, Bangladesh

Md. R. Islam
Khulna University of Engineering & Technology, Khulna, Bangladesh

S. R. Sheonty
Military Institute of Science and Technology, Dhaka, Bangladesh

R. Armin
Sher-E-Bangla Agriculture University, Dhaka, Bangladesh

supplied jar water, bottled water, deep-wells, and tube-wells are the most popular drinking water sources in Rangpur city. Most of the people use groundwater for drinking, cooking, and other consumptive purposes extracted with tube-well [6]. Though the residential and official users ensure their drinking water quality by using water-filter and treatment system, the low-income people don't have the solvency to do it. They are the most vulnerable water users in this city. The main source of drinking water for these slum-dwellers and working-class people are public tube-wells installed at the masjids, schools, colleges, universities, marketplaces, bus stands, and roadside. As these sources are open for all, the authority was not pestered about the water quality and there is no proper monitoring of water quality of this water. Most of the users are constantly drinking this water out of unawareness and ignorance about the quality. Thus, the health of such a huge population is vulnerable to the drinking water. Hence, the water quality of these public tube-wells has become a major concern now. Moreover, due to rapid urbanization the groundwater table is continuously declining and the hydrochemistry is changing, becoming more diverse and complex [7]. Though the groundwater table is decreasing in the northern part of Bangladesh, the water table remains 3.27 m below ground surface in the wet season and 7.5 m in the dry season in Rangpur area, making the groundwater easily accessible for tube-wells [8, 9]. Apart from that, the physio-chemical and heavy-metals present in groundwater may cause high toxicity and the consumption of contaminated water may lead to severe health problems including diarrheal diseases, jaundice, typhoid, damaged or reduced mental and central nervous function, hypertension, hyperkeratosis, restrictive lung and kidney disease, Wilson's disease and hemochromatosis and gangrene [10–13].

In spite of significant health impact, there are only a few studies on groundwater and its contaminations in Rangpur district that have been conducted [14–16]. But there isn't any specific study focusing the public tube-well water quality in Rangpur city. Thus, this study attempts to assess the water quality of the public tube-wells of Rangpur city and determine whether it is within the allowable limit for drinking according to the ECR1997 of Bangladesh and WHO guidelines. This water source is chosen for study because this is the main drinking water source of the most vulnerable low-income people residing in Rangpur city and contamination of this water source can impose significant health threat to that huge amount of people. For this purpose, some vital water quality parameters were analyzed from the collected water samples to compare the drinking water criterion. This study also aims to visualize the spatial distribution of the water quality parameters through GIS mapping. Using the GIS map of the Rangpur city area, the water quality parameters in the whole region can easily be distinguished.

2   Study Area

Rangpur City is located in the northern part of Bangladesh. The city lies between the latitude of 25°42' to 25°47' N and the longitude of 89°12' to 89°19' E. The total area of the city is 205.76 square kilometers and is in the floodplain of the Teesta River basin [15]. The average annual rainfall is 2192 mm in Rangpur [14]. Some crucial locations were strategically selected for sampling from where many people of different classes and professions collect their drinking water. The water samples were collected from the public tube-wells located at New Shen Para, Kamarpara Bus stand, Pouro Bazar, Dorsona More, Modern More, Jumma Para, Dhap, Central Bus Terminal, New Engineers Para, Tajhat, Lalbag, Rail Station, Parker More, Jahaj Company, and Salbon Mistry Para of Rangpur city which are labeled from WS1 to WS15, correspondingly. The study area is shown in (Fig. 1).
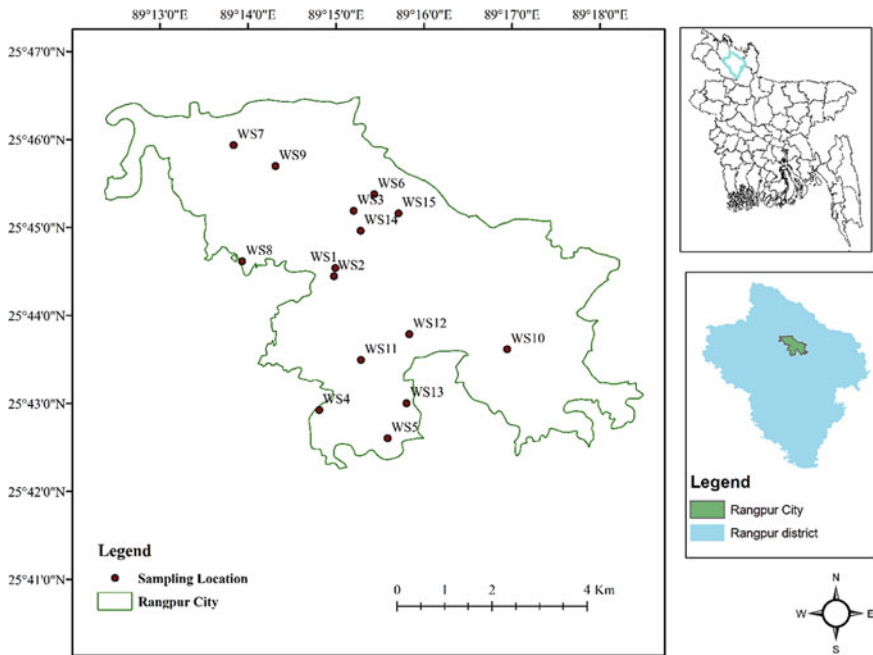

Fig. 1 Study area

3 Methodology

3.1 Sample Collection

Fifteen water samples from public tube-wells were collected from different strategically selected locations in the Rangpur city area in September 2020. Water samples were collected in one-liter polypropylene bottles. Before the sample collection, all the bottles were cleaned with diluted hydrochloric acid and deionized water, followed by a repeated wash with the water sample. Before collecting the water samples, the water was pumped out from tube-wells for about 15 min to avoid stagnancy and water sampling contamination. After the collection of water samples, all the bottle's mouths were sealed tightly. The sample bottles were labeled with the date and sampling location. After taking the samples, some important parameters, i.e., pH, Total Dissolved Solids (TDS), Conductivity, Dissolved Oxygen (DO), Alkalinity, Total Iron, Phosphate, Copper, and Chloride for each sample were tested.

3.2 Laboratory Testing

The physical parameters such as pH, TDS, Conductivity, DO were measured and recorded on the spot during sample collection. pH, TDS, conductivity, and DO were measured by HACH multimeter (Model: HACH HQ40d), and it was calibrated before the reading. The EDTA titrimetric method was used to measure Total Hardness, and Alkalinity was measured with the titrimetric method using 0.02 N Sulfuric acid. Chloride was measured by the Standard $AgNO_3$ method. Total Iron, Phosphate, and Copper were determined by Spectrophotometer (HACH DR6000). Chemical analyses of the samples were conducted using the standard method recommended by American Public Health Association [17].

3.3 Statistical Analysis

The test result was analyzed in both Microsoft Excel 2016 software and IBM SPSS statistics 25 software. The minimum, maximum, mean, median, and standard deviation for each parameter were computed in SPSS. After that, the box and whisker for each parameter were plotted using Microsoft Excel [18].

3.4 GIS Mapping

GIS map for the whole study area in Rangpur city has been developed to delineate the spatial distribution of water quality parameters. The ESRI ArcGIS 10.5 software was used to map the spatial distribution [19]. The administrative boundary map was collected from Humdata of MapAction. The excel sheet of test result data was added to ArcGIS by x,y data plotting and geo-referenced to WGS 1984 co-ordinate system. Then this data was exported as a layer and used for mapping. The geoprocessing tools were utilized to delineate each water quality parameter's spatial distribution in the Rangpur city area. The thematic map for each parameter in the Rangpur city area was generated by the Inverse Distance Weighted (IDW) interpolation technique of the 3D analyst tool of ArcGIS [20].

4 Results and Discussions

4.1 Laboratory Test Results

The tested sample's value represents the state of the physical and chemical parameters present in the water sample. The limit of these parameters in water is different for different uses. The Environment Conservation Rules (Bangladesh), World Health Organization, European Union, US EPA, India (BIS), and other environmental organizations have set a standard limit for different parameters for drinking water. The study results are compared with the ECR 1997 and WHO limit to assess the water quality of Rangpur city [21, 22]. The test result of different parameters of samples is shown in Table 1.

pH: pH refers to the hydrogen ion concentration present in water sample and pH value higher than 7 refers to the water is alkaline and less than 7 is acidic. The maximum and minimum pH value in the tested samples is 7.44 and 5.94, respectively. Mean, median, and standard deviation value from the statistical analysis is 6.75, 6.72, and 0.37, respectively. Except for one, all other sample's pH values are within the recommended standards of WHO and ECR1997. The pH value of one sample below the limit is 5.94 and this water is slightly acidic in taste but drinking this water would not be hazardous.

Total Dissolved Solids (TDS): Total Dissolved Solids (TDS) value of all the tested samples is within the limit of WHO and ECR1997 standards. The TDS value varies between 380 mg/l to 71.2 mg/l with a mean of 186.2 mg/l. The median and standard deviation are 146.4 mg/l and 111.12, respectively. The value of TDS shows the water of all the tube-wells is very aesthetic to drink.

Table 1 Test result of different parameters of Rangpur city and ECR and WHO standard value

Sample ID	pH	TDS (mg/L)	Conductivity (µS/cm)	DO (mg/L)	Total Hardness (mg/L)	Alkalinity ss (mg/L)	Total Iron (mg/L)	Copper (mg/L)	Phosphate (mg/L)	Chloride (mg/L)
WS1	6.72	371	779	7.36	232	170	0.09	0.45	0.27	81.39
WS2	6.56	344	717	2.7	162	184	0.76	0.01	0.27	73.45
WS3	6.82	89	193.9	5.25	50	82	0.08	0.01	0.27	7.94
WS4	7.26	71.2	167.6	3.51	56	46	0.5	0.02	0.24	17.86
WS5	6.94	243	530	3.94	271	138	0.12	0.01	0.27	49.63
WS6	7.44	134.5	282	5.15	90	124	0.02	0.03	0.37	5.95
WS7	6.69	271	642	4.28	158	116	1.93	0.08	0.23	33.74
WS8	6.45	380	887	3.3	258	196	0.09	0.15	0.14	69.45
WS9	6.59	96.2	219.2	5.47	70	72	0.07	0.01	0.46	9.92
WS10	7.2	86	153.8	4.75	54	74	0.53	0.01	0.46	6.94
WS11	6.82	91	156.4	5.12	56	80	0.85	0.01	0.35	7.94
WS12	6.82	83.3	178.8	3.96	46	44	5.99	0.16	1.06	17.86
WS13	6.65	170.5	358	4.61	56	74	2.09	0.02	0.36	29.77
WS14	5.94	146.4	316	3.25	96	120	5.52	0.02	0.43	9.92
WS15	6.43	215.9	449	2.5	110	90	0.07	0.01	0.07	51.61
ECR 1997	6.5–8.5	1000	–	6	200–500	–	0.3–1	1	6	150–600
WHO	6.5–8.5	1000	400	–	500	–	1–3	2	–	600

Conductivity: The maximum and minimum value of conductivity in the tested sample is 887 μS/cm and 153.8 μS/cm, respectively. A total of six samples exceeds the recommended standard of WHO for drinking this water. Two samples slightly exceed the limit, and the other four sample values are very high. Mean, median, and standard deviation for conductivity is 401.98 μS/cm, 316.00 μS/cm, and 250.70, respectively.

DO: The DO value of tested samples is found between 7.36 mg/l to 2.50 mg/l, with a mean of 4.34 mg/l. The median and standard deviation are 4.28 mg/l and 1.25, respectively. Only one sample has a DO value of more than 6 and others have relatively low DO. These tube-wells samples were extracted from groundwater and the variations in DO are because of the tube-well's depth.

Total Hardness: The maximum and minimum total hardness value is 271.00 mg/l and 46 mg/l, respectively. The mean, median, and standard deviation of total hardness is 117.67 mg/l, 90 mg/l, and 79.55. Six samples are soft; four samples are moderately hard; two samples are hard and the rest three are very hard, according to the WHO guideline. Though all the samples are within the limit, people might find taste issues with the hard water.

Alkalinity: The maximum value of Alkalinity is 196 mg/l, and the minimum value is 44 mg/l. Mean, median, and standard deviation are 107.33 mg/l, 90 mg/l, and 47.84, respectively. The water samples are within the standard limit and are very good for drinking.

Total Iron: Higher iron concentration may cause color, taste issues, and toxicity for human health. The maximum value of the total iron is 5.99 mg/l, and the minimum value is 0.02 mg/l. Mean, median, and standard deviation for iron are 1.24 mg/l, 0.5 mg/l, and 1.94, respectively. Four water samples exceed the permissible limit of ECR 1997, but two are more than 5 mg/l, which is not very suitable for drinking. The iron removal technique should be used for the water of these two tube-wells.

Copper: The maximum and minimum value of Copper is 0.45 mg/l and 0.01 mg/l. The mean, median, and standard deviation is 0.067 mg/l, 0.02 mg/l, and 0.117, respectively. Though one sample has a higher value of copper present in the water, all the samples meet Copper's guideline value. The samples are free from copper toxicity.

Phosphate: The maximum value of Phosphate is 1.06 mg/l, and the minimum is 0.07 mg/l in the tested samples. The mean, median, and standard deviation are 0.35 mg/l, 0.27 mg/l, and 0.225. According to the standard of ECR 1997, the Phosphate in drinking water lies in a good range and suitable for drinking.

Chloride: The higher amount of chloride present in water may cause salinity. The maximum chloride concentration is 81.39 mg/l, and the minimum is 5.95 mg/l in the study area. The mean, median, and standard deviation for chloride concentration is 31.56 mg/l, 17.86 mg/l, and 26.86. There are no samples in which chloride concentration exceeds the standard limit according to WHO and ECR.

The box and whisker plot from statistical analysis of different parameters is shown in (Fig. 2).
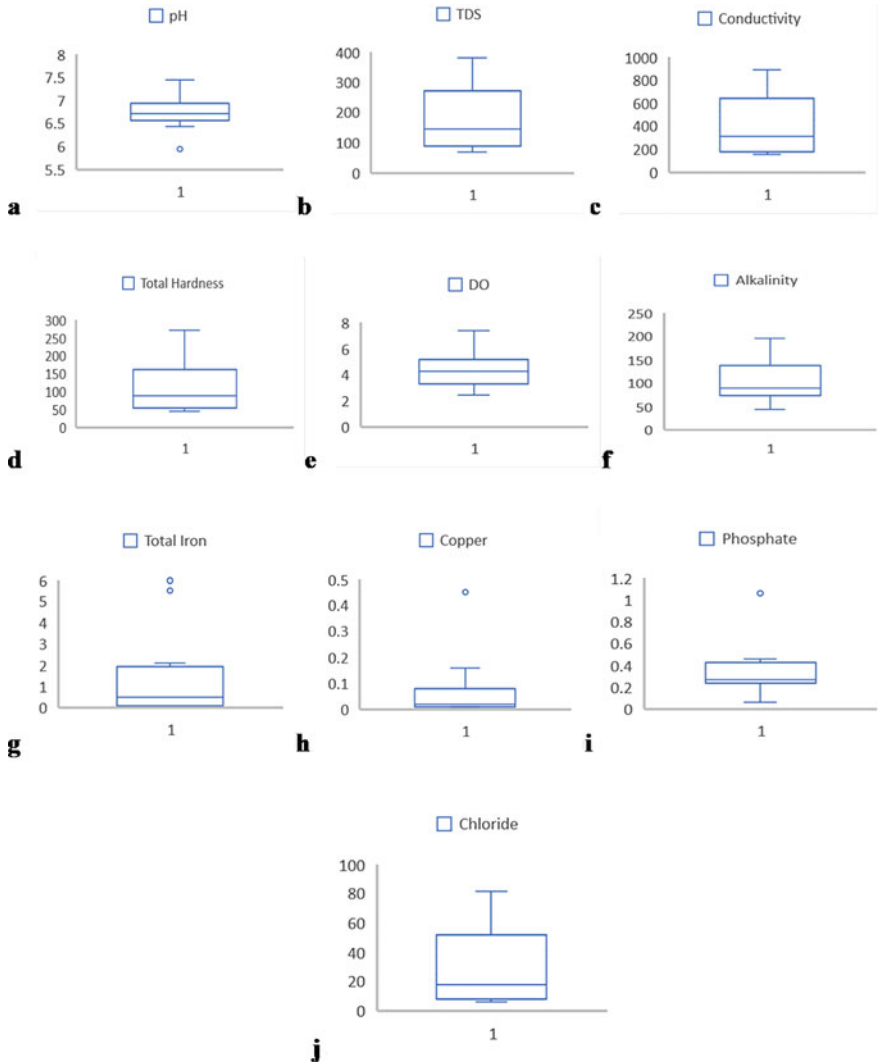
Fig. 2 Box and Whisker plot of **a** pH, **b** TDS, **c** Conductivity, **d** DO, **e** Total Hardness, **f** Total iron, **g** Alkalinity, **h** Phosphate, **i** Copper, and **j** Chloride

According to water quality standard, all the tested parameters of the sample from New Shen Para shows satisfactory result which indicates that this tube-well water is allowable for drinking. Similar kind of water quality is observed in the Kamarpara Bus Stand, Pouro Bazar, Dorsona More, Modern More, Jumma Para, Central Bus Terminal, New Engineers Para, Tajhat, Lalbag, and Salbon Mistry Para which concludes tube-well water of these areas is suitable for drinking. The DO and Conductivity value in some Rangpur city locations are not within the limit of ECR

1997 and WHO, but this does not create any significant risk for consumption. No necessary treatment is required for this region, and the water can be used for safe consumption.

The iron concentration is higher in Dhap and Parker More area according to ECR 1997 guideline, though other parameters are within the limit. Though drinking the water of these two tube-wells may not cause significant harm, still it is recommended to treat the iron before drinking. A very high concentration of iron is found in Rail Station and Jahaj Company. Whether the other water quality parameters are within the acceptable limit, the iron removal treatment must have to be conducted to drink the water of these two tube-wells. Otherwise, consumption of water from these two tube-wells can cause severe health issues such as skin and hair problems, nausea, stomach problems, etc.

4.2 Spatial Distribution Map

Inverse Distance Weighted (IDW) interpolation tool of GIS was used for mapping the Rangpur city area's water quality parameter value adjacent to the sampling locations. Spatial distribution maps for different water parameters for Rangpur City are shown in (Fig. 3). The value of the map is illustrated from the highest to lowest value with stretched color from deep to light.

The value of Electrical Conductivity, TDS, Total Hardness, and Alkalinity is found in quite similar spatial pattern throughout Rangpur city but a relatively higher concentration is observed in the west region than the other parts of the city. The pH value is lower in the central and north-western part and comparatively higher in the southern part of the city. In the central and mid-south region, the iron is found in very high concentration, while in other regions, the Iron concentration is deficient. Copper is found higher in the mid-west part of the city and lower in eastern and southern regions. A higher phosphate concentration is found in the mid-south part than the other parts. Some areas in the mid-west region have higher chloride concentration but the southern area has a lower concentration of chloride. The water quality of all the Rangpur city is quite good and people can use the tube-well water for drinking purposes without any health risk.
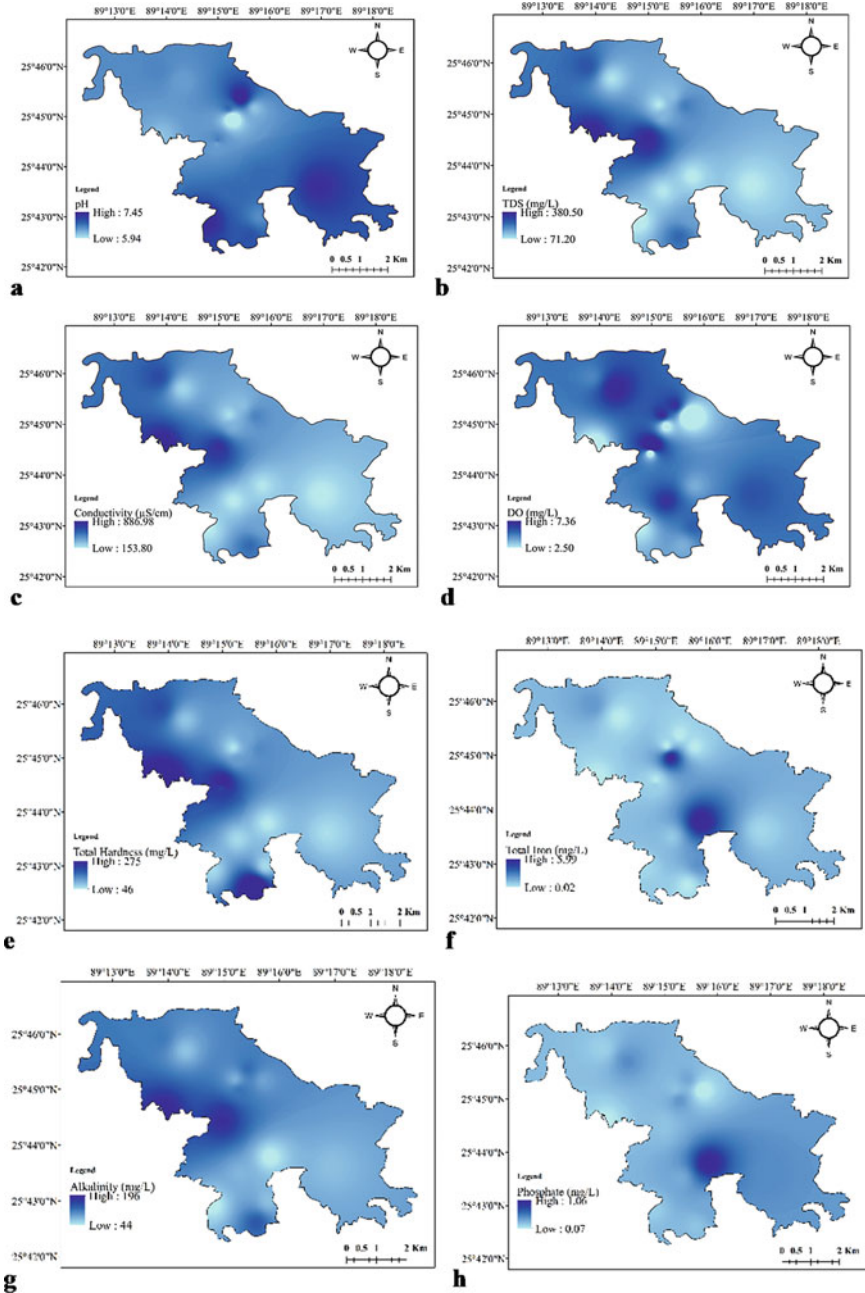
Fig. 3 Spatial distribution maps for **a** pH, **b** TDS, **c** Conductivity, **d** DO, **e** Total Hardness, **f** Total iron, **g** Alkalinity, **h** Phosphate, **i** Copper, and **j** Chloride for Rangpur City
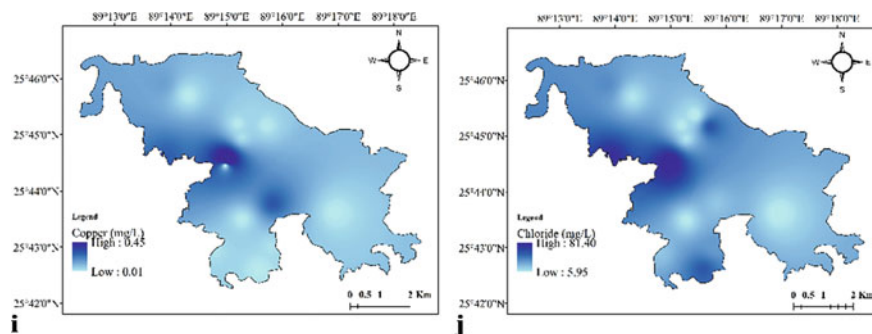
Fig. 3 (continued)

   Though the results indicate that now the water quality of the tube-wells is satisfactory for drinking, but it has to be remembered that the water quality differs in different seasons. The samples were collected in the month of September after the monsoon but during the rainy season, there can be fluctuations in some water quality parameters which need to be monitored. So, seasonal variation of drinking water quality is necessary and it can be explored as a further research topic.

5   Conclusion

With the rapid growth of population and unplanned urbanization, supply of safe drinking water to people of all classes has become a new challenge for Rangpur city. This paper attempts to assess the drinking water quality of the low-income people who are the most vulnerable people to have access of safe drinking water. The results show that tested parameters of the collected water samples are satisfactory in quality. This assessment of water quality ensures that still now slum-dwellers, working-class, and low-income people are having safe drinking water. This is a relief for the working-class people of Rangpur city as they have one fundamental necessity of life with good quality. But the drinking water quality can change time to time due to contamination. There could have some seasonal variation in the water parameters, which needs to be assessed as well. So, monitoring of temporal change of drinking water is necessary in order to ensure the access of safe drinking water to the dwellers of Rangpur city. Moreover, microbial and arsenic are two other critical parameters for drinking water that can be tested in further study. Finally, from the results, it can be reinforced that the water quality of the tube-wells in Rangpur city is quite satisfactory and suitable for drinking.

References

1. Rangpur Division (2020) http://rangpurdiv.gov.bd/site/page/7be6cff4-18fd-11e7-9461-286 ed488c766/%E0%A6%AC%E0%A6%BF%E0%A6%AD%E0%A6%BE%E0%A6%97% E0%A7%87%E0%A6%B0%20%E0%A6%AA%E0%A6%9F%E0%A6%AD%E0%A7% 81%E0%A6%AE%E0%A6%BF. Accessed 29 Dec 2020

2. Hassan MS, Mahmud-ul-islam S (2015) Urban area change analysis in the Rangpur Sadar Upazila, Bangladesh using landsat imageries. Int J Sci Res (IJSR) 4(1):469–474

3. BBS: Economic Census 2013 - District Report (2016) Rangpur. Reproduction, Documentation & Publication (RDP) Section Bangladesh Bureau of Statistics, Bangladesh

4. Rahman MN (2019) Urban expansion analysis and land use changes in Rangpur city corporation area, Bangladesh, using Remote Sensing (RS) and Geographic Information System (GIS) techniques. Int J Adv Study Res Work 2(10):22–30

5. JICA (2012) Data collection survey on water supply sector in local municipalities in Bangladesh. local government division, The Government of the People's Republic of Bangladesh

6. Ahmad SA, Khan MH, Haque M (2018) Arsenic contamination in groundwater in Bangladesh: implications and challenges for healthcare policy. Risk Manage Healthc Policy 2018(11):251–261

7. Zhang Q, Miao L, Wang H, Hou J, Li Y (2020) How rapid urbanization drives deteriorating groundwater quality in a provincial capital of China. Pol J Environ Stud 29(1):441–450

8. Mojid M, Parvez M, Mainuddin M, Hodgson G (2019) Water table trend—a sustainability status of groundwater development in north-west Bangladesh. Water 11(6)1182:1–15

9. Zzaman RU, Nowreen S, Newton IH (2019) Groundwater fluctuation in response to annual rainfall in north-west region of Bangladesh. In: Haque A, Chowdhury AIA Proceedings from the 7th International Conference on water and flood management 2019. Springer, Switzerland, pp 250–266

10. Momodu MA, Anyakora CA (2010) Heavy metal contamination of ground water: the surulere case study. Res J Environ Earth Sci 2(1):39–43

11. Bhuiyan MAH, Bodrud-Doza M, Islam ARMT, Rakib MA, Rahman MS, Ramanathan AL (2016) Assessment of groundwater quality of Lakshimpur district of Bangladesh using water quality indices, geostatistical methods, and multivariate analysis. Environ Earth Sci 75(12)(1020):1–23

12. Mohod CV, Dhote J (2013) Review of heavy metals in drinking water and their effect on human health. Int J Innovative Res Sci Eng Technol 2(7):2992–2996

13. Brewer G (2010) Risks of copper and iron toxicity during aging in humans. Chem Res Toxicol 23(2):319–326

14. Yesmeen R, Zakir H, Alam M, Mallick S (2018) Heavy metal and major ionic contamination level in effluents, surface and groundwater of an urban industrialised city: a case study of Rangpur city. Bangladesh. Asian J Chem Sci 5(1):1–16

15. Islam ARMT, Bodrud-Doza M, Rahman M, Amin S, Chu R, Al Mamun H (2019) Sources of trace elements identification in drinking water of Rangpur district, Bangladesh and their potential health risk following multivariate techniques and Monte-Carlo simulation. Groundwater Sustain Dev 9(4):100275

16. Islam ARMT, Shen S, Bodrud-Doza M, Rahman M, Das S (2017) Assessment of trace elements of groundwater and their spatial distribution in Rangpur district. Bangladesh. Arabian J Geosci 10(95):1–14

17. APHA: T (2102) Standard methods for the examination of water and wastewater. 22nd edn. American Public Health Association (APHA), American Water Works Association (AWWA) and Water Environment Federation (WEF), Washington DC, USA

18. Shardt YAW (2015) Using Excel® to do statistical analysis. In: Statistics for Chemical and Process Engineers, pp. 363–398. Springer, Cham

19. Goyal S, Chaudhary B, Singh O, Sethi G, Thakur P (2010) GIS based spatial distribution mapping and suitability evaluation of groundwater quality for domestic and agricultural purpose in Kaithal district, Haryana state. India. Environ Earth Sci 61(8):1587–1597
20. Srivastava P, Gupta M, Mukherjee S (2011) Mapping spatial distribution of pollutants in groundwater of a tropical area of India using remote sensing and GIS. Appl Geomatics 4(1):21–32
21. ECR: Environment Conservation Rules (1997) Department of environment, ministry of environment and forest, Government of the People's Republic of Bangladesh. Dhaka, Bangladesh
22. WHO: T (2011) Guidelines for drinking–water quality. 4th edn. World Health Organization Press. Geneva, Switzerland

Assessment of the Sustainability of Water, Sanitation and Hygiene on Educational Institution: A Case Study of Rajshahi City Corporation

Farhana Afroz, Shad Hossain, and Rafia Anjum Rimi

1 Introduction

Water, sanitation, and hygiene (WASH) access is important for the safe development and growth of children worldwide. Every kid has the right to adequate access to WASH, as stated in the Convention on the Rights of the Child (United Nations, 1989). Despite recent progress in the areas of water and sanitation throughout the world, more than 2.3 billion people still lack access to sanitation and others are unable to practice basic hygiene [11].

The challenges of WASH remain plague for the developing world. Despite decades of international emphasis on these concerns, significant rates of illness and mortality from avoidable water-related illnesses continue, particularly among young people. More than one billion people require better water supplies [5], and over 2.5 billion people need access to safe sanitation [6].

Secure and sufficient supply of water and sanitation at educational institutions are prerequisites for students' right to basic education [24]. The achievement of the Millennium Development Goals (MDGs) for universal primary education, gender equality, and child mortality, as well as the Sustainable Development Goals, and in particular Target 6 on clean water and sanitation by 2030, have all been linked to the availability of adequate water, sanitation, and hygiene facilities in educational institutions [33]. According to academic studies, having proper WASH facilities in schools can enhance children's education and wellbeing by lowering the number of school days lost due to menstrual periods or offering more possibilities for learning activities [8, 14, 19, 22].

Improvements in health associated with improved water quality are smaller than those obtained by increasing the quantity of water, which enables better hygiene practices in person and in the home [12, 18]. Population groups consuming more water

F. Afroz (✉) · S. Hossain · R. A. Rimi
Department of Urban and Regional Planning, Rajshahi University of Engineering and Technology, Rajshahi 6204, Bangladesh

generally have better health than those using less water. It has been shown consistently for different health effects, such as common diarrhoeal infections, diarrhoeal morbidity and child development [12, 17]. Upgrades to water and sanitation may not always result in improved health. To address concerns about basic issues such as hand washing, correct fecal waste disposal, and drinking water safety, hygiene education is required [35].

Millions of school-aged children lose or fail to complete their education as a result of disease caused by polluted drinking water and inadequate sanitation. In 2002, about 500 million school-aged children lived in households without improved water supplies. Unfortunately, the majority of schools lack adequate sanitary facilities [31]. Numerous studies have found that children who are afflicted with intestinal worms do poorly in school. When sanitation is accessible, 11% more females attend school, according to the World Health Organization (WHO) [34].

Because of diseases contracted in the school environment, many students in both developing and emerging countries miss school [21]. The school atmosphere is an important setting as the social patterns and attitudes of many children are taught at school. In educational and non-educational settings, School WASH strategies boost overall sanitation, hygiene and routine water intake [14].

In underdeveloped countries, girls are frequently responsible for collecting water, which can take several hours each day, leaving them with little time or energy to learn. Second, girls, especially those who are menstruating, may be reluctant to attend school [3]. And for that reason, menstrual hygiene in the WASH sector has become a largely overlooked problem.

In Zimbabwe, Moyo, Makoni, and Ndamba [25] discovered that menstrual patterns were same in both rural and urban schools, indicating that menstruation was not seen as a subject that required particular attention. There were not enough ablution facilities and sick rooms, and toilet ratios did not satisfy government regulations of one squat hole for every 15 girls and 20 boys. Because there were no incinerators or other adequate disposal facilities in urban schools, the girls flushed their sanitary pads down the toilet, causing sewage line clogs. In most situations, school toilets are not designed to meet the unique needs of boys and girls.

Environmental factors, such as polluted drinking water, poor hygiene and sanitation, are thought to be responsible for 94 percent of the causes of diarrhoeal disorders (Prüss Üstün & Corvalán 2006). For example, of the total documented 1.5 million diarrhea-related fatalities in 2012, an estimated 502,000 and 280,000 fatalities were attributed to a lack of water and sanitation, respectively [29]. As a result, school absenteeism is a strong predictor of both childhood illnesses and educational performance [9]. Clean drinking water in schools appears to have an impact on student health and increased absenteeism [27, 7].

Schools are one of a location for disease transmission among children but systemic and educational changes can reduce disease spread [1]. WASH treatments reduce morbidity and mortality resulting from diarrheal disease [10, 13, 16] and have been associated with reduced risk of trachoma [23], ascariasis [15] and acute respiratory infections [28].

Bangladesh is a developing country in the world and Rajshahi is one of the educational cities of Bangladesh having many school, college and universities. That's why Rajshahi is called the 'Educational City' of Bangladesh. This city is helping huge number of students to continue their study. But most of the educational institutes of Rajshahi are more or less concerned about the water hygiene and sanitation facilities for the students. Students spend long time of their day in schools, colleges or in varsities. So it is important for them to have pure source of drinking water, better sanitation and hygiene facilities in their institutions.

This study aims to upheld the present scenario of the WASH facility of different educational institutions in Rajshahi City. After considering the problems that have arisen as a result of the current state of these facilities, the study has also focused on providing some necessary directions to solve these problems.

2   Materials and Methods

We used a cross-sectional study as we attempted to explain the state of water and sanitation-related hygiene actions at one point in time by gathering data from various schools, colleges and varsities. All the students from various kinds of educational institutions in Rajshahi City were the targeted population.

2.1   Study Site and Population

As our study area was the Rajshahi City Corporation (RCC), we completed our survey within the bounded area. While surveying, we found most of the schools and colleges are located in the Shaheb Bazar area which is known as the city center of the Rajshahi city. But most of the varsities are located in the off-center of the city (Fig. 1).

There are a total of 33 educational institutions under Rajshahi City Corporation. Among them, 13 are high schools, 10 colleges, 3 schools and colleges together and 7 varsities. All the Kindergarten schools were excluded from the survey to ensure the accuracy of the research and survey. About 5,24,863 students are studying in these educational institutions.

2.2   Study Design and Institution Sampling

Though the total amount of students were huge, but using 90% confidence level we got 68 students as sample number. During the survey, we use the quota sampling survey as the survey method. According to this method, we survey 60% girls and 40% boys of the total sample. So by calculation, we get 40 girls and 26 boys for the
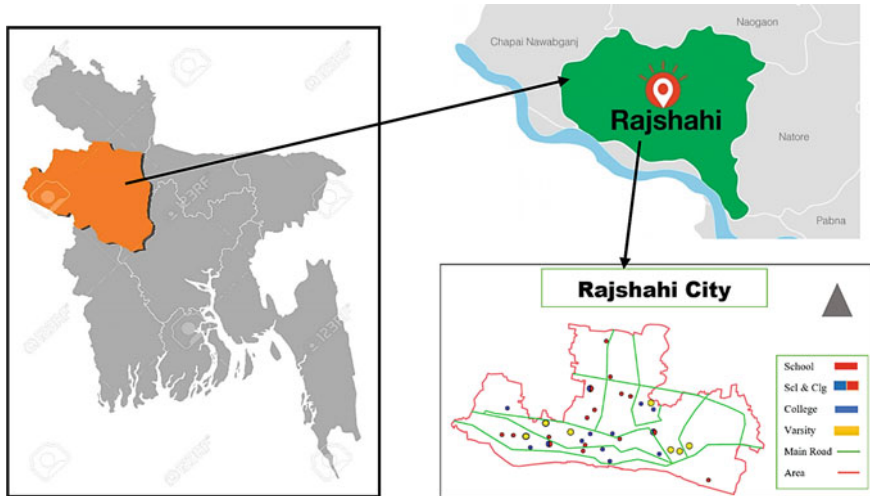
Fig. 1 Location of Rajshahi city

survey. We again divide these 68 students into school, college and varsity zones. At the school and college level, the number of samples was 25, while at the varsity level the number of samples was 18.

2.3 Data Collection Procedure

Data were collected via field survey from 33 qualifying institutions during unannounced visits. All the students surveyed received the best of their information on the availability of pure drinking water, soap and water for hand-washing, washroom cleaning materials, menstrual items for girls, disposal of menstrual products, supply of water in washroom, dustbin facility, ventilation condition and lighting condition in both of classroom and washroom, etc.

2.4 Data Collection Method

In this study, the primary data were collected from the questionnaire survey and Participatory Rapid Appraisal (PRA) tools.

The secondary data were collected from different journals, websites and educational institutions. Water, sanitation & hygiene (standard, facility and effects of their absence, etc.) related data were collected from World Health Organization (WHO).

After collecting all the data from different sources, data were organized in SPSS, and Excel and Arc GIS Pro was used for mapping data. Finally, considering all the

data and suggestions from the students, some standards were provided to improve the WASH facility in the educational institution. The research concluded with some effective recommendations about the necessity of having WASH facility in every educational institution.

3 Results and Discussion

3.1 Results

3.1.1 Drinking Water Availability

Students have to stay in school for a very long time during the day. After this time they need plenty of drinking water. Now if there is no drinking water in the school, or if the water is not healthy, it can be the cause of illness. The graph shows that drinking water is available in 82% of the total institutions (Fig. 2). However, about 33% of the available water in educational institutions is unhealthy to drink. Only 49% of school water is safe to drink. Through the survey, it was also found that out of the institutions where drinking water is available, 58% of schools and colleges use tap water, 24% use tube wells. Only 18% of institutions provide filtered water (Table 1).
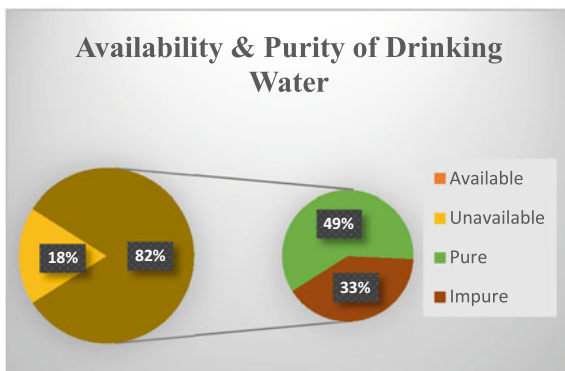
Fig. 2 Drinking water availability

Availability & Purity of Drinking Water

Table 1 Source of drinking water

Sources of drinking water	Percentage (%)
Tap	58
Filter	18
Tube Well	24

Table 2 Classroom and washroom condition

	Condition Facility	Bad	Medium	Good
Washroom	Lighting	35%	18%	42%
	Ventilation	41%	23%	36%
	Water Condition	24%	34%	42%
Classroom	Lighting	39%	16%	45%
	Ventilation	29%	13%	58%

3.1.2   Classroom and Washroom Condition

It is very important for a school to have good ventilation and lighting conditions in both classrooms and washrooms. If the lighting in the classroom is not good, it can disrupt the students' studies and all the work. And if the ventilation condition is not good then there will be problems in ventilation, which can lead to saffocation among the students, which in turn can lead to their hygienic problems. Same for washroom. If the lighting facility, ventilation facility and water condition in the washroom are not good then the students may face hygienic problems (Table 2).

According to the survey, about 35%, 41% and 24% of the institutions have poor lighting, ventilation and water condition in washroom. And about 39% and 29% of the institutions have poor lighting and ventilation conditions in classroom. It is also found that overall 50% of the institutions have good washroom and classroom facilities.

3.1.3   Dustbin Facility

About 65% of the institutions do not have any kind of dustbin in the classroom. Only 35% of institutions have dustbins in the classroom (Fig. 3). Dustbins in the washroom are also a necessity. But only 47% of the institutions have a dustbin in the washroom.
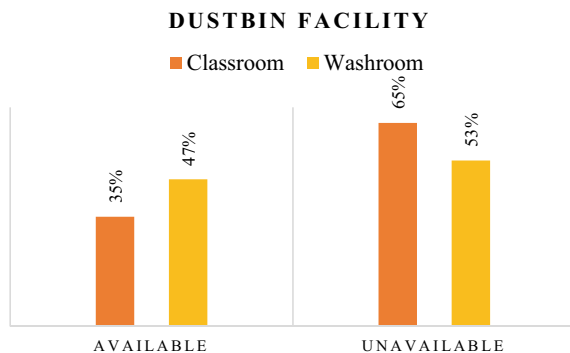
Fig. 3 Dustbin facility

DUSTBIN FACILITY
■ Classroom ■ Washroom

35%   47%   65%   53%

AVAILABLE   UNAVAILABLE

Fig. 4 Separate washroom

Separate Washroom Faciity for Boys & Girls

- Yes
- No

Table 3 Washroom per floor

Washroom amount	Percentage (%)
<2	12
2–5	76
>5	12

Fig. 5 Hand wash facility

Handwash Facility

71% 29% 17% 12%

- Yes - No - Handwash - Soap
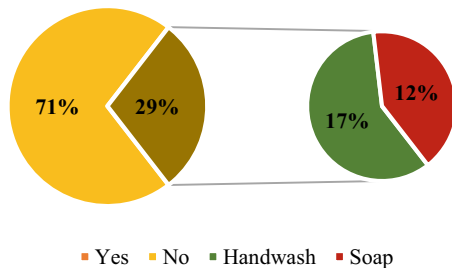
3.1.4 Washroom Facilities

Adequate number of washrooms in the school is very necessary for the students (Fig. 4). Surveying all the educational institutions in RCC, about 76% of the institutions have 2–5 washrooms on each floor. And 12% institutions have only 2 washrooms on each floor. Many of these institutions do not have separate washroom facilities for boys and girls. According to the survey, only 44% of institutes have separate washroom facilities for boys and girls. And 56% of the institutions do not have this separate washroom facility (Table 3).
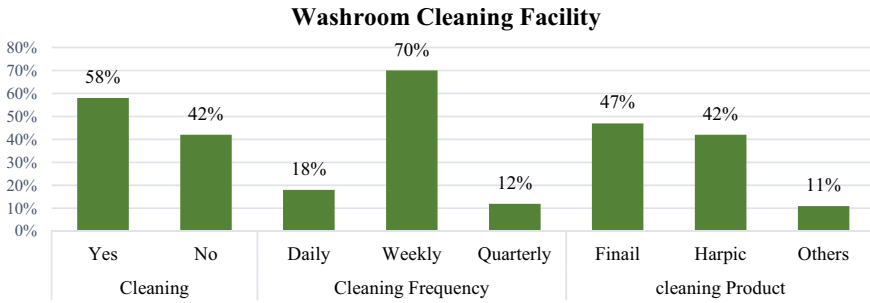
Washroom Cleaning Facility

Fig. 6 Washroom cleaning facility

3.1.5 Hand Wash Facility

The first rule of hygiene is to use hand wash after using the washroom (Fig. 5). But if the school does not have that facility then it becomes difficult for the students to maintain hygiene. 71% of the surveyed institutions do not have any hand wash facility. Only 29% of institutions have this facility. However, only 17% of these 29% institutions use hand wash. The remaining 12% use soap for handwashing.

3.1.6 Washroom Cleaning Facility

Regular and timely cleaning of school washrooms is essential (Fig. 6). This is because the unwashed washroom can have a serious impact on the health of the students. When students in the survey were asked to talk about the washroom cleaning facility of their institution, 58% of the students reported that their institution was frequently cleaned and 42% said that washrooms are not frequently cleaned at their institutions, so they get a lot of bad smells from their washrooms. For that reason, they do not use the school washrooms. It is also found that 18% do daily washing, 70% do weekly washing and 12% institutions quarterly clean the washroom. About 47% of these institutions use phenyl as a cleaning product, which creates very bad smell and harpic is used in 42% of the institutions.

3.1.7 Facility for Girls

When students were asked if there were separate facilities for girls' periodical time in educational institutions, 92% said no. Only 8% of the students report having this facility at their institution. It is also learned that there is no bin facility for sanitary pads in 88% of the institutions (Table 4).

3.1.8 Satisfaction Level

When students were asked at the last minute of the survey whether they are satisfied with the WASH facility of their institution or not (Fig. 7). Then 47% say they are not satisfied. 42% of the students said that they are satisfied with the WASH facility of their institution. But 11% of students did not comment. Also, when they are asked for a recommendation about the WASH facility, 80% of the students want to have a sanitary pad and pad bin facility in their institution. 68% of students expressed their desire to have separate washroom facilities for boys and girls at their institution. 76% of students wish to improve the water condition of their washroom. And 83% of students wish to have filters at the institution.

3.2 Discussion

According to the data surveyed in this study, 82% of the institutions are supplied with drinking water, of which 33% are impure. There is a tendency to supply unclean water in schools. In comparison, filtered water is used in colleges and varsities. The lighting and ventilation conditions in the washrooms and classrooms of most of the institutions are very bad which can hinder the health development of the students. Also about 60% of the institutions on average have no dustbin anywhere in both these washrooms and classrooms. Due to which they have to take classes in the dirty classroom. It is very harmful to their health. Most of the schools do not have separate washrooms for boys and girls. However, in college and varsity this picture is different. Separate washroom facilities can be seen in most of the colleges and varsities. Observing all the educational institutions of RCC, it is seen

Table 4 Facility for girls

Facility for girls	Yes (%)	No (%)
Facility for menstrual period	8	92
Bin for sanitary pad	12	88

Fig. 7 Satisfaction level

Satisfaction Level

- Satisfied
- Unsatisfied
- Neutral
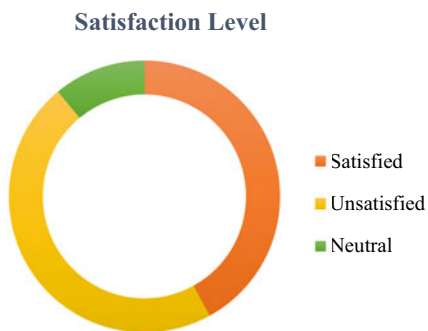
that most of the institutions are unaware of the healthy environment, which is very bad for the students studying in those institutions. The survey found that 71% of the institutions do not have hand wash facilities. Most of the institutions that offer these facilities are the private institutions. Many institutions are also indifferent about washroom cleaning. And the products used for washroom cleaning are also known to be unhealthy for students by surveying. It is the responsibility of an institution to provide all the facilities to the girls at school during menstrual periodic time. But about 92% of the institutions do not provide any facility for menstrual period in girls. Also, no bin is provided for dropping pads at 88% Institution. These results show how difficult it is for a girl to go to school and continue study during menstrual time. Considering all these, it is seen that 47% students are dissatisfied with about the WASH facilities of their institution. From this study, it is clear that most of the RCC institutions are unhygienic in terms of WASH facilities, which is very detrimental to the health of the students of those institutions. All these institutions should take steps in this regard. And in every institution, it is very important to provide all kinds of facilities for girls during menstrual period.

4 Conclusion

This research examined the impact of water, sanitation and hygiene facilities on health of students in educational institutions. The research aimed at cataloging and characterizing the current state of these facilities and providing some recommendations. Although WASH facilities were available at some of the institutions, the study found that they were insufficient in terms of facility-user ratios, accessibility, and proper operation and maintenance.

The overall rationale behind WASH facility is logical. The evidence summed up in this paper supports the institution's environment having a huge impact on its student's health. To achieve equal access to education as a right for all students, the fundamental causes of providing water and sanitation in the school environment and their effects on health and educational outcomes need to be tackled through more thorough study, political action and successful intervention.

References

1. Adams J, Bartram J, Sims J, Chartier Y (2009) Water, sanitation and hygiene standards for schools in low-cost settings. Geneva, Switzerland, World Health Organization
2. Alexander KT, Oduor C, Nyothach E, Laserson KF, Amek N, Eleveld A, Mason L, Rheingans R, Beynon C, Mohammed A, Ombok M (2014) Water, sanitation and hygiene conditions in Kenyan rural schools: are schools meeting the needs of menstruating Girls? Water 1453–1466
3. Anon (2004) Water and sanitation programme. The case of water and sanitation. S.l.: s.n

4. Antwi-Agyei P, Mwakitalima A (2017) Water, sanitation and hygiene (WASH) in schools: results from a process evaluation of the national sanitation campaign in Tanzania. J Water Sanitation Hyg Dev

5. Asian Development Bank (2007) Smarter sanitation—new business, Unusual Tool. S.l.: Asian Development Bank

6. Asian Development Bank (1999) Handbook for the economic analysis of water supply projects. S.l.: Asian Development Bank

7. Blanton E et al (2010) Evaluation of the role of school children in the promotion of point-of-use water treatment and handwashing in schools and households—Nyanza Province, western Kenya, 2007. Am J Trop Med Hyg 82:664–671

8. Bowen A, Ma H, Ou J, Billhimer W, Long T, Mintz E, Hoekstra RM, Luby S (2007) A cluster-randomized controlled trial evaluating the effect of a hand washing promotion program in Chinese primary schools. Am J Trop Med Hyg 76:1166–1173

9. Bundy D, Guyatt H (1996) Schools for health: focus on health, education and the school-age child. Parasitol Today 12:1–14

10. Cairncross S et al (2010) Water, sanitation and hygiene for the prevention of Diarrhora. Int J Epidemiol 39:193–205

11. Cairncross SBUKP (1996) The public and domestic domains in the transmission of disease. Trop Med Int Health 1:27–34

12. Esrey SA, Potash JB, Roberts L, Shiff C (1991) Effects of improved water supply and sanitation on ascariasis, diarrhoea, dracunculiasis, hookworm infection, schistosomiasis, and trachoma. Bull World Health Organ 69:609–621

13. Fewtrell L et al (2007) Water, sanitation and hygiene: quantifying the health impact at national and local levels in countries with incomplete water supply and sanitation coverage; WHO environmental burden of disease. World Health Organization: Geneva, Switzerland, vol 15

14. Freeman MC, Greene LE, Dreibelbis R, Saboori S, Muga R, Brumback B, Rheingans R (2012) Assessing the impact of a school-based water treatment, hygiene and sanitation programme on pupil absence in Nyanza Province, Kenya: a cluster-randomized trial. Tropical Med Int Health 17:380–391

15. Fung I, Cairncross S (2009) Ascariasis and handwashing. Trans R Soc Trop Med Hyg 103:215–222

16. Garrett V et al (2008) Diarrhoea prevention in a high-risk rural Kenyan population through point-of-use chlorination, safe water storage, sanitation, and rainwater harvesting. Epidemiol Infect 1463–1471:136

17. Gasana J, Morin J, Ndikuyeze A, Kamoso P (2002) Impact of water supply and sanitation on diarrheal morbidity among young children in the socioeconomic and cultural context of Rwanda (Africa). Environ Res 90:76–88

18. Huttly SR, Morris SS, Pisani V (1997) Prevention of diarrhoea in young children in developing countries. Bull World Health Organ 75:163–174

19. Jasper C, Le TT, Bartram J (2012) Water and sanitation in schools: a systematic review of the health and educational outcomes. Int J Environ Res Public Health 9:2772–2787

20. Jasper C, Le TT (2012) Water and sanitation in schools: a systematic review of the health and educational outcomes. Int J Environ Res Public Health 2772–2787

21. Koopman JAJE (1978) Diarrhea and school toilet hygiene in Cali. Colombia 107:412–420

22. Lopez-Quintero C, Freeman P, Neumark Y (2009) Hand washing among school children in Bogota. Colombia. Am J Public Health 99:94

23. Montgomery M, Desai M, Elimelech M (2010) Assessment of latrine use and quality and association with risk of trachoma in rural Tanzania. Trans R Soc Trop Med Hyg 104:283–289

24. Mooijman A (2012) Water, Sanitation and Hygiene (WASH) in schools: a companion to the child friendly schools manual. S.l.: UNICEF

25. Moyo S, Makoni FS, Ndamba J (2004) An evaluation of national sanitation policy with an emphasis on sexual maturation needs of girls vis-a-vis menstruation. Life skills, sexual maturation and sanitation: What's (not) happening in our school?. Weaver Press

26. Mulogo EM, Matte M (2018) Water, sanitation, and hygiene service availability at rural health care facilities in Southwestern Uganda. Hindawi
27. O'Reilly C et al (2008) The impact of a school-based safe water and hygiene programme on knowledge and practices of students and their parents: Nyanza Province, western kenya, 2006. Epidemiol Infect 136:80–91
28. Patel M et al (2012) Impact of a hygiene curriculum and the installation of simple handwashing and drinking water stations in rural Kenyan primary schools on student health and hygiene practices. Am J Trop Med Hyg 87:594–601
29. Prüss-Ustün A, Bartram J, Clasen T, Colford Jr JM, Cumming O, Curtis V, Bonjour S, Dangour AD, De France J, Fewtrell L, Freeman MC (2014) Burden of disease from inadequate water, sanitation and hygiene in low-and middle-income settings: a retrospective analysis of data from 145 countries. Tropical Med Int Health 19:894–905
30. Prüss-Üstün ACC (2012) Preventing Disease Through Healthy Environments. World Health Organization, Geneva
31. UNICEF, WHO (2004) Meeting the MDG drinking water and sanitation target: a midterm assessment of progress. New York, USA: UNICEF
32. United Nations (2016) Convention on the rights of the child. Geneva: United Nations. http://www.ohchr.org/en/professionalinterest/pages/crc.aspx. Accessed 26 Sep 2016
33. United Nations (2015) United Nations General Assembly 2015 Transforming our world: the 2030 agenda for sustainable development. United Nations, New York. https://sustainabledevelopment.un.org/post2015/transformingourworld. Accessed 2 Feb 2017
34. World Health Organization (WHO) (2012) The World health report 2002, reducing risks, promoting healthy life. http://www.who.int/whr/2002/en/whr02_en.pdf. Accessed 15 Jun 2012
35. Yacoob M, Whiteford L (1994) Behaviour in water supply and sanitation. Hum Organ 53:330–335

Analyzing the Impact of Lockdown on Rejuvenation of Rivers in Uttar Pradesh, India

Pranjal Pandey, Akanksha, Madhuri Kumari, and Sonal Bindal

1 Introduction

During the COVID-19 lockdown phase, miraculous improvement in the river quality attracted the attention of scientists and researchers worldwide. They are now emphasizing on the promising effects of nature-based solutions such as the natural restoration process of the river due to the sudden halt in industrial activities, thus reviving the natural ecosystem of the river [17]. The current COVID-19 pandemic has highlighted the importance of Nature-Based Solutions (NBS) and their relative influence on diverse components of the environment. Lockdown had a negative impact on the worldwide economy, however it gave the environment time to rejuvenate itself. As most anthropogenic activities ceased significant qualitative and quantitative changes in the environment were noticed and further analyzed from a very local to global scale [20]. In India, nationwide lockdown was declared on 25th March 2020, and and it was extended four times till 18th May 2020. Different types of restrictions were imposed in different areas/regions throughout each phase of lockdown.

In India too, huge changes were observed in the air and water quality which remained sub-standard due to industrial activities [27]. One of the environmental advantages witnessed during the lockdown phase was the returning of dolphins in the Ganga River in the Vikramshila Gangetic Dolphin Sanctuary (VGDS) in Bihar, as nature was able to take a break from human intrusion [21]. According to the definition of the NBS given by the European Commission [10], "Natural-based solutions are environmental solutions that are inspired and supported by nature, with the goal of benefiting the environment, society, and economy while also contributing to the balance of human well-being and environmental protection." Such solutions are cost-effective and implemented using the latest technological and engineering innovations

P. Pandey (✉) · Akanksha · M. Kumari
Department of Civil Engineering, Amity University Uttar Pradesh, Noida, India

S. Bindal
National Institute of Disaster Management, Ministry of Home Affairs, New Delhi, India

[18]. Indeed, this new paradigm shift in improving surface water quality naturally without human intervention or the use of advanced technology has given hope to the ongoing problems of water security in the country [4].

Water is the most basic necessity of life [15]. For human growth, assured accessibility to consumable water is crucial. India is home to 18 percent of the human population and 15 percent of the animal population worldwide [14]. It has only 2 percent of the landmass and 4 percent of global freshwater reserves [9]. The definition of water security given by UN-Water serves as a starting point for the dialogue in the UN forums. As per the definition, water security is defined as the ability of a community to safeguard sustainable access to adequate quantities of and justifiable quality water for the conservation of livelihoods, human well-being and socio-economic development, to ensure safety against water contamination and water-related disasters and for preliminary protection against water-borne pollution and disasters and for conserving ecosystems in an ethos of peace and political stability [30]. It is essential to limit risk of water hazard which can be achieved via a complete and fair valuation of the available resources and by ensuring sustainability within the ecosystem at all parts of the hydrological cycle [29]. The problems revolving around water is linked mainly with environmental and food security, further out of which water security is linked with fresh and safe water supply for drinking, food and sanitation [1]. Freshwater resources are gradually becoming inaccessible due to discharge of tremendous amounts of untreated, chemical and hazardous waste in surface water because of industrial and domestic activity [25]. Most of the small rivers and streams have turned into wastewater drains in the name of urbanisation and economic advancements. Further, these smaller streams confluence with big rivers such as Ganga & Yamuna for which nowadays the treatment has become difficult [2]. It not only affects the current water security scenario but also threatens the future of water as well.

The basin of Ganga is huge, densely populated and the largest source of surface water [24]. Almost 43% of population depends on Ganga River and its tributaries [11]. The basin is spread across Uttrakhand, Himachal Pradesh, Delhi, Uttar Pradesh, Bihar, Jharkhand, Rajasthan, Madhya Pradesh and West Bengal [8]. The Ganga River was declared as a national river in 2008. The quality of Ganga and Yamuna River and their tributaries such as East Kali and Hindon River has been moderately to severely affected due to the anthropogenic factors such as barrages, dams, industrial (tanneries, paper & sugar mills) and domestic (household sewers) waste water drains [3, 26]. Stringent lockdown steps have had a major impact on rivers and other lotic habitats in India.

Within a few weeks after lockdown, the water quality achieved by Ganga, India's longest and holiest river, was more pronounced than what government policies/regulatory agencies have achieved in decades.

This study made a first attempt to quantify the levels of multi river water quality pollution during pre-lockdown, lockdown and post-lockdown in the era of COVID-19 pandemic. The objective of the study is to assess and analyze the status of water quality in major rivers of Uttar Pradesh such as Ganga and Yamuna and its important tributaries East Kali and Hindon. Additionally, an observation was made regarding the effectiveness of the nature-based solution in order to understand the impact of

the natural rejuvenation process for surface water bodies during three phases of COVID-19.

2 Materials and Methods

2.1 Study Area

Uttar Pradesh is India's most populous and fourth-largest state. It lies in the country's north-central region. It is the most populated state in India and the most populous country subdivision in the world with around 200 million inhabitants. The state's two main rivers, the Ganges and Yamuna, join Triveni Sangam in Allahabad and flow further east as the Ganges. In terms of pollution levels, Uttar Pradesh has six most polluted rivers, such as Hindon, Kishni, Kali East, Kali West, Dhamola and Yamuna. The situation of these six rivers was named "deadly alarming" by a study conducted by the World Water Monitoring Day Organization (WWMDO) [13].

The first case of COVID-19 reported in the state of UP is in the district of Ghaziabad on 5 March 2020 and the state underwent lockdown on 25 March 2020 along with the other states of India after the emergency was declared by the Prime Minister on the night of 24 March 2020. However, the usual riverside businesses such as tourism were affected even before 21 March because of the emergence many COVID positive cases which were reported in different parts of the state. Since the industry and tourism activities closed completely after 25 March 2020, the emissions from these sources have almost stopped, which provided an opportunity to analyze the lockdown effect on rivers [19]. The present study focuses on four stretches of Uttar Pradesh rivers, including two main rivers, Ganga and Yamuna, and two of its tributaries, Kali East and Hindon, respectively (ref. Fig. 1).

River Ganga- The river starts from Moradabad district and ends at Gazipur district in UP. Wide number of industrial cities such as Kannauj, Farrukhabad, Kanpur, Prayagraj and Varanasi are situated on its banks. 16 out of 56 drains outfalls are from Kanpur itself and discharge of 2213 MLD of sewage (107 tonnes per day BOD load) [5]. In the existing catchment area of the Ganga River, there are 591 water-polluting industries. The sectors belonging to Sugar, Pulp & Paper, Distillery, Cloth, Tannery & Slaughter House and so on are grossly polluting in nature. In Jajmau, Banthar and Site-2 Unnao, three tannery clusters exist. The total sewage discharged into the Ganga River from 85 untapped drains is approximately 434.88 MLD, as described above. There are mainly 06 districts, i.e., Kanpur Nagar, Unnao, Raebareli, Prayagraj, Mirzapur & Varanasi that are located in the catchment area of the Ganga river, namely (Fig. 1). The sewage and other effluent produced from these cities contribute to increasing the river's organic load [28].

River Yamuna The river begins in the GB Nagar district and ends in the district of Prayagraj at the confluence with Ganga. The 300 industries in the catchment generate 856,101 MLD waste over 35 drainage systems. Total waste disposed of in
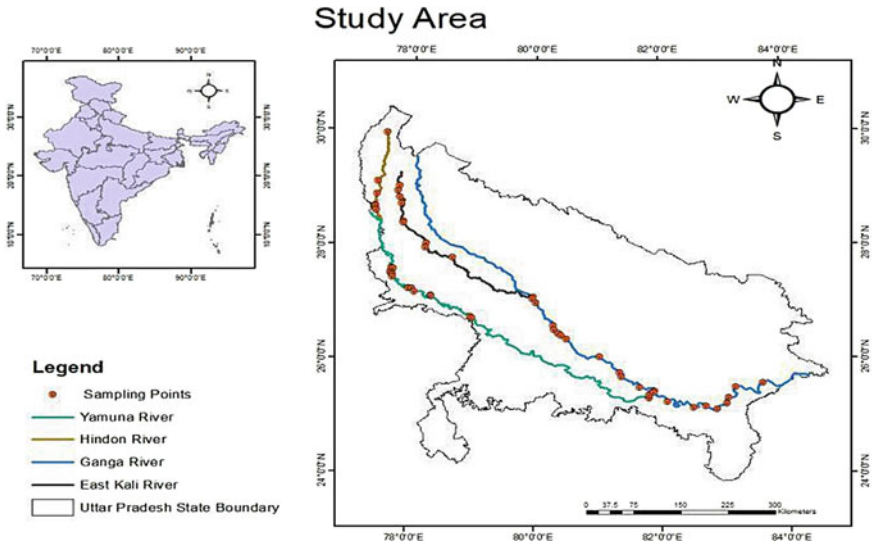
Fig. 1 Study Areas spread across the river Ganga, Yamuna, Kali and Hindon covering 44 number of monitoring locations

the Yamuna river through 35 major drains is around 807.53 MLD, as stated above. Gautam Budh Nagar, Vrindavan, Mathura, Agra, Firozabad, Etawah, Kalpi Hamirpur and Prayagraj are the major polluting cities that are located in the catchment area. The industries have treatment plants for effluent and they discharge their processed effluent through 18 drains, where the treated industrial effluent is mixed with the sewage. The sectors belonging to Sugar, Pulp & Paper, Distillery, Cloth, Slaughter House, etc., are grossly polluting in nature [28].

Hindon The river originates in the Saharanpur district from the lower Shivalik range and flows through Meerut, Gaziabad and ends at the confluence of the Yamuna river in the GB Nagar district. Via 31 drains, a cumulative discharge of 674,033 MLD is reported. Total 78.39 MLD direct discharge of waste is done from 453 industries located in the catchment after treatment. In the catchment area of the specified stretch of the River Hindon from Saharanpur to Ghaziabad, there are 06 districts: Saharanpur, Muzaffarnagar, Shamli, Meerut, Baghpat and Ghaziabad. The sewage and other waste created from these towns add to the river's organic load. The industries are grossly polluting in nature, primarily belonging to Sugar, Pulp & Paper, Distillery, Textile, Slaughter House, etc. [28].

East kali river It originates from Muzaffarnagar district and flows through Meerut, Hapur, Bulandasheher, Aligarh, Kasganj and finally confluence with Ganga river in Kannauj. Total 589.113 MLD waste is discharged from 94 industries through 17 drains in 120 km long stretch out of 550 Kms. The polluted stretch of the Kali River East starts from the Muzaffarnagar district of Antwara (in Khatauli Region) and flows south, south east via Meerut Town, Hapur, Gulaothi Town (Bulandshahar). The industrial sectors belonging to Sugar, Pulp & Paper, Distillery, Cloth, Slaughter

House, etc., are grossly polluting in nature. In the Hapur-Pilkhuwa Development Authority industrial area of UPSIDC, there is a textile industrial cluster of around 13 units. In the catchment area of the Polluted Stretch of River Kali, there are 5 cities and towns (East). On the basis of the 2011 Census, the approximate sewer generation is 275.25 MLD. In the catchment area of the river, there are 05 city areas, namely Meerut, Hapur, Khatauli, Modi Nagar and Gulaothi. The sewage and other waste generated from these cities contribute to the river's organic load [28].

3 Methodology

A multi-water quality parameter comparative analysis is performed for the selected Rivers using data obtained from UPPCB such as Dissolved Oxygen (mg/l), Biological Oxygen Demand (mg/l), Total Coliform (MPN/100 ml) and Fecal Coliform (MPN/100 ml). The qualitative and quantitative analysis is carried out by using prescribed standards as referred by CPCB. The lower DO and higher BOD concentration ensures organic pollution whereas the TC and FC concentration ensure sewage contamination. In all the major districts, as per the given population density, a 10 km buffer area (ref. Fig. 2) is chosen around the sampling locations. The key source of water pollution is due to the industrial load and sewage load from the surrounding
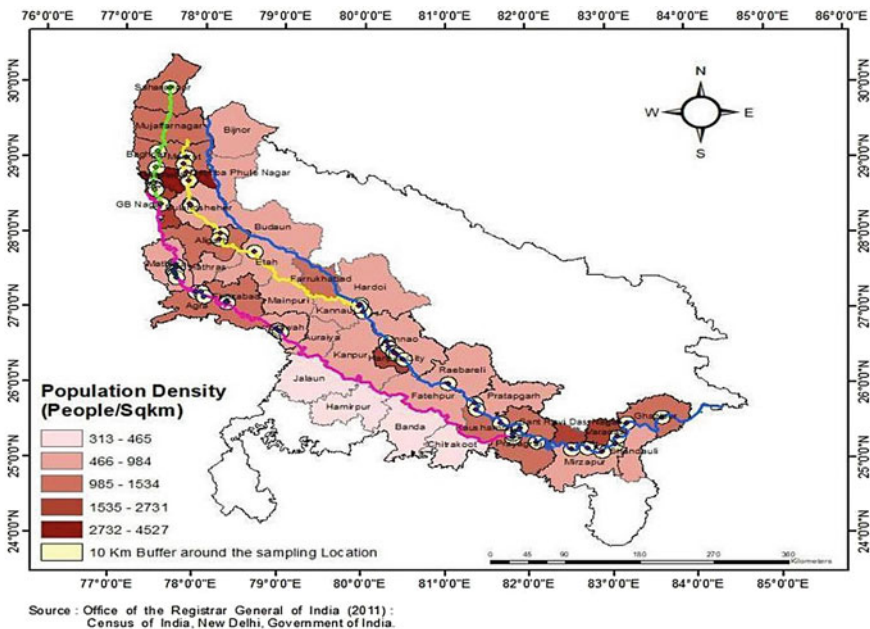

Fig. 2 Population density around major rivers of study area representing the industrial and domestic water demand areas

factories and residential settlements (population), i.e., roughly within the 10 km river reach. The buffer region maps were created using geospatial tools such as ArcGIS 10.7 software.

An extensive statistical analysis has been performed for understanding the river water quality parameter data for all the four rivers obtained from Uttar Pradesh Pollution Control Board data bank. Four parameters—Dissolved Oxygen (DO) in mg/l, Biochemical Oxygen Demand (BOD) in mg/l, Total Coliform (TC) in MPN/100 ml and Fecal Coliform (FC) in MPN/100 ml are considered and compared simultaneously. For depicting the temporal variation in accordance with the different lockdown phases the time period of 10 months, i.e., from January 2020 to October 2020 the timeline of the study is chronologically categorized into 3 phases. The pre-lockdown phase comprises of river water quality data of three months, i.e., January 2020, February 2020 and March 2020, during lockdown phase includes data from April 2020 to June 2020 and for post-lockdown phase, July 2020–Oct 2020 months are considered.

4 Results and Discussion

Figure 3a-d shows the average concentrations of DO, BOD, FC and TF in the pre-, during and post-lockdown period. There was variation observed in all the parameters in the Ganga river monitored through 22 sampling stations. DO during pre-lockdown period was observed to be lowest as 7.10 mg/l and highest as 11.20 mg/l, whereas during lockdown period the lowest range varied as 6.67 mg/l and highest 9.25 mg/l and in post-lockdown period, a sudden increase in the lowest range value was observed as 6.10 mg/l and highest as 8.20 mg/l as shown in Fig. 3a. The BOD lowest value varied as 1.75 mg/l and highest as 4.33 mg/l in pre-lockdown period, during lockdown period lowest value was observed as 2.00 mg/l and highest as 3.90 mg/l and during post-lockdown period lowest value was observed as 2.33 and highest as 4.23 mg/l as shown in Fig. 3b. FC during pre-lockdown period was observed to be lowest as 967 MPN/100 ml and highest 24,667 MPN/100 ml, whereas during lockdown period the lowest range varied as 567MPN/100 ml and highest as 12,467 MPN/100 ml and in post- lockdown period the lowest value varied as 1250 and highest as 19,100 MPN as shown in Fig. 3c. This suggests that there has been a decrease during lockdown period, and a sudden increase in the lowest FC prevalence. TC during pre-lockdown period was observed to be lowest as 2000 and highest as 49,000 MPN/100 ml, whereas during lockdown period was varied as lowest as 1700MPN/100 ml and highest as 41,667 MPN/100 ml and in post-lockdown significant increased in lowest values as 2450 MPN/100mland highest as 49,750 MPN/100 ml.

The average DO, BOD, FC and TF concentrations in the pre-, during and post-lockdown period can be observed in Fig. 4a–d. There was a substantial variation observed in all the variables in the Yamuna River monitored through 20 sampling stations along the river stretch in Uttar Pradesh state. FC during pre-lockdown period
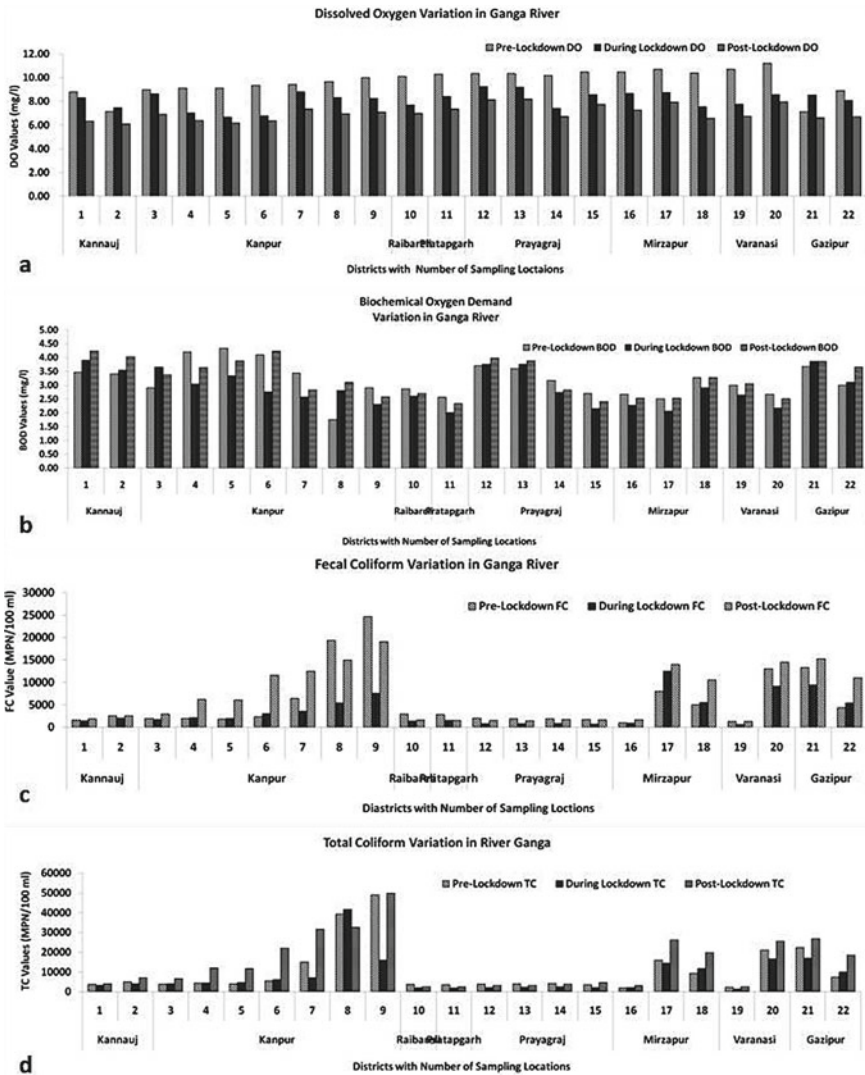
Fig. 3 Variation in the concentration of **a** DO, **b** BOD, **c** FC and **d** TC in river Ganga at all the sampling locations during pre-, during and post-lockdown periods

was observed to lowest as 997 and highest as 90,333 MPN/100 ml, whereas during lockdown period the lowest range varied as 417 MPN/100 ml and highest as 60,500 MPN/100 ml and in post-lockdown period a sudden increase in the lowest range value was observed as 520 MPN/100 ml and highest as 53,250 MPN/100 ml. The lowest values of TC varied as 2042 MPN/100 ml and highest as 120,000 MPN/100 ml in pre-lockdown period, during lockdown period lowest range was observed as 1533
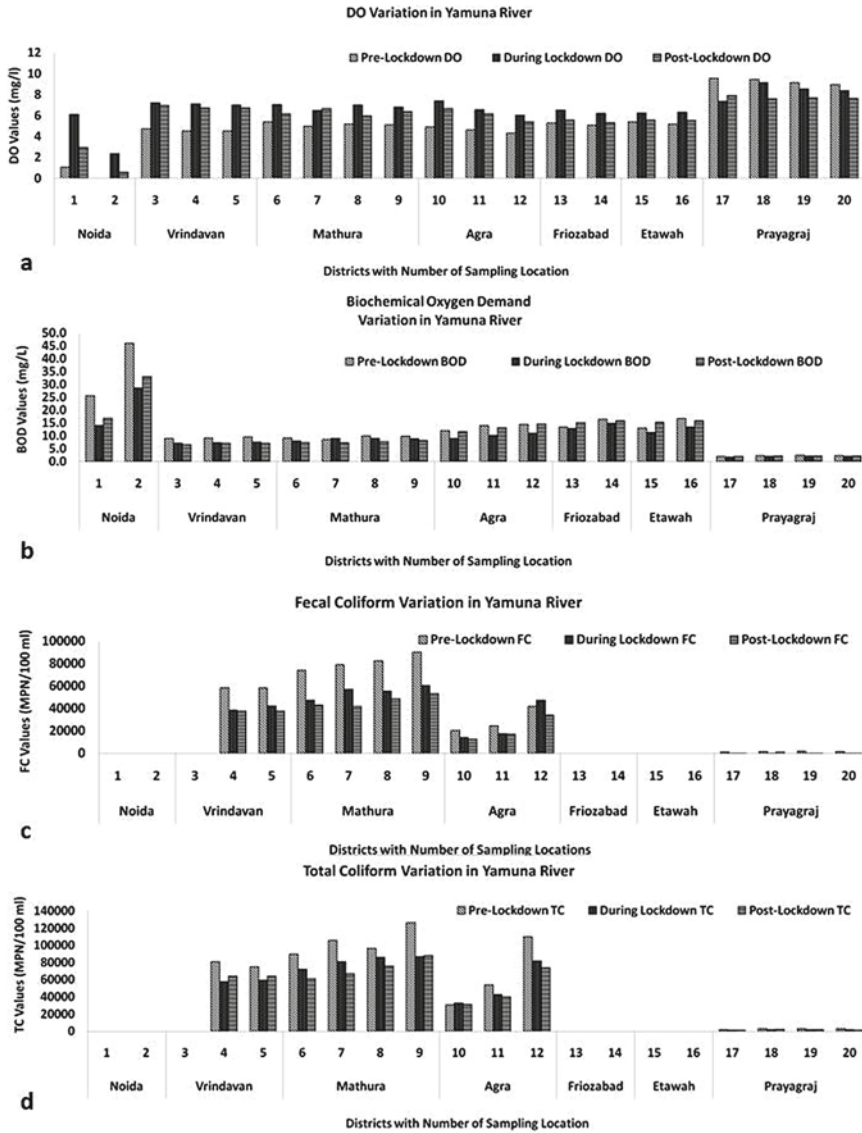
Fig. 4 Variation in the concentration of **a** DO, **b** BOD, **c** FC and **d** TC, respectively in river Yamuna at all the sampling locations during pre-, during and post-lockdown periods

MPN/100 ml and highest as 87,000 MPN/100 ml and a significant increase in the range values during post-lockdown period, i.e., lowest as 1375 MPN/100 ml and highest as 88,250 MPN/100 ml (ref. Fig. 4c and d). The range of DO during pre-lockdown period was observed to be lowest as 0 mg/l and highest as 9.55 mg/l, whereas during lockdown period the lowest range varied as 2.1 and highest as 9.1 mg/l

and in post-lockdown period a sudden increase in the lowest range value was observed as 0.6 mg/l and highest as 7.9 mg/l. The values of BOD lowest value varied as 2.1 mg/l and highest as 46.0 mg/l in pre-lockdown period, the range during lockdown period was observed to be lowest as 1.7 mg/l and highest as 28.5 mg/l and a significant increase in the lowest range values during post-lockdown period as 2.0 mg/l and highest as 33 mg/l (ref. Fig. 4a and b).

In case of River Hindon, the variation observed in the range values of selected water quality parameters throughout 7 sampling stations along the river stretch in Uttar Pradesh state were as follows: the range of TC during pre-lockdown period was observed to be lowest as 83,000 MPN/100 ml and highest as 180,000 MPN/100 ml, whereas during lockdown period the range varied lowest as 7767 and highest as 400,000 MPN/100 ml and in post-lockdown period a sudden increase in the range value was observed to be lowest as 79250and 1,110,000 MPN/100 ml. The values of FC varied in lowest as 11,667 MPN/100 ml and highest as 275,000 MPN/100 ml in pre-lockdown period, the range during lockdown period was observed to be lowest as 104,333 and highest as 460,000 MPN/100 ml and a significant increased in the range values during post-lockdown period, i.e., lowest as 113,333 and highest as 2,317,500 MPN/100 ml (ref. Fig. 5c and d). The range of DO during pre-lockdown period was observed to be lowest as 1.27 mg/l and highest as 2.13 mg/l, whereas during lockdown period the lowest range varied as 0.63 mg/l and highest as 1.93 mg/l and in post-lockdown period a sudden increase in the range value was observed, i.e., lowest as 0.83 mg/l and highest as 1.82 mg/l. The values of BOD varied in the lowest range as 16 mg/l and highest as 77 mg/l in pre-lockdown period, the range during lockdown period was observed to be lowest as 11 mg/l and highest as 59 mg/l and a significant increase in the range values during post-lockdown period, i.e., lowest as 20 mg/l and highest as 51 mg/l (ref. Fig. 5a and b).

Similarly, for East Kali River, the variation observed in the range values of selected water quality parameters throughout 10 sampling stations along the river stretch in Uttar Pradesh state were as follows: the range of TC during pre-lockdown period was observed to be lowest as 5450 MPN/100 ml and highest as 1,600,000 MPN/100 ml, whereas during lockdown period the lowest range varied by 3850MPN/100 ml and highest as 2,533,333 MPN/100 m/l and in post-lockdown period a sudden increase in the lowest range value was observed as 3650 MPN/100 ml and highest as 5,600,000 MPN/100 ml. The values of TC varied in lowest range as 26,333 MPN/100 ml and highest as 2,150,000 MPN/100 ml in pre-lockdown period, the range during lockdown period was lowest value observed as 9467 and highest as 2,500,000 MPN/100 ml and a significant increased in the range values during post-lockdown period lowest as 10,000 MPN/100 ml and highest as 7,400,000 MPN/100 ml (ref. Fig. 6c and d).

The range of DO during pre-lockdown period was observed to be lowest as 4.4 mg/l and highest as 7.1 mg/l, whereas during lockdown period the lowest range varied by 3.1 mg/l and highest as 7.7 mg/l and in post-lockdown period a sudden increase in the range value was observed, i.e., lowest as 4.6 mg/l and highest as 6.0 mg/l. The values of BOD varied in lowest range as 6 mg/l and highest as 66 mg/l in pre-lockdown period, the range during lockdown period was observed to be lowest as
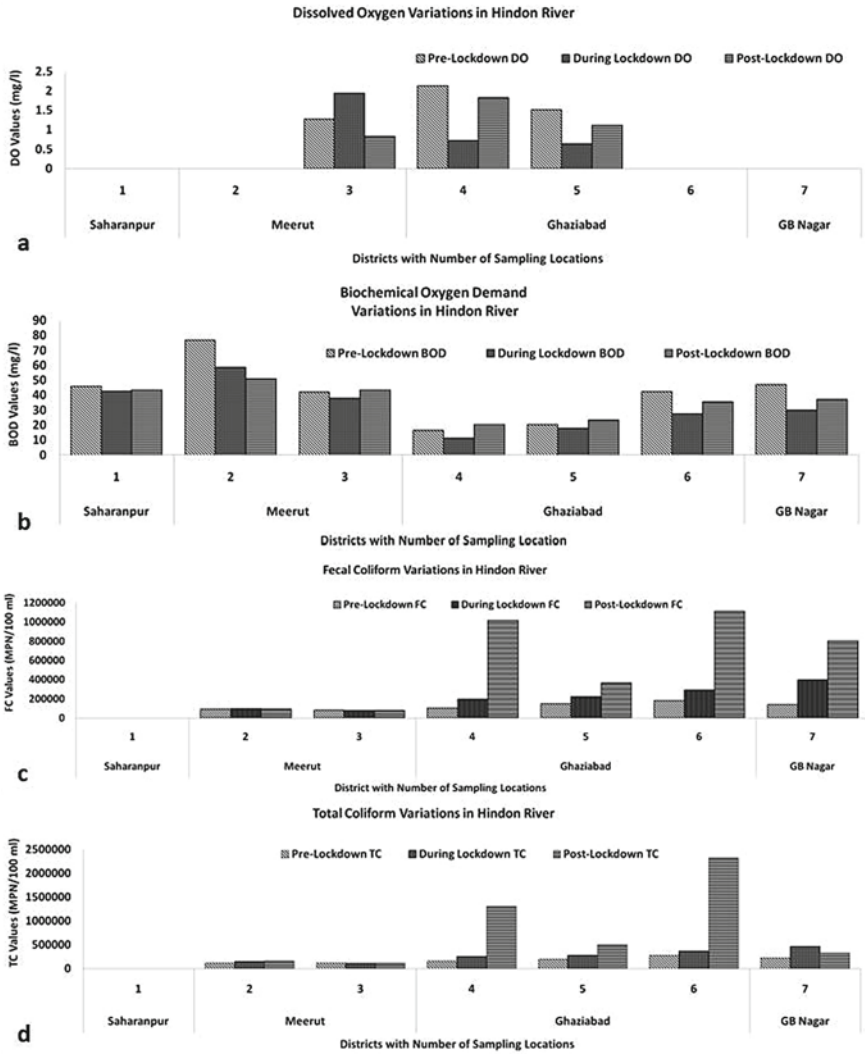
Fig. 5 Variation in the concentration of **a** DO, **b** BOD, **c** FC and **d** TC, respectively in river Hindon at all the sampling locations during pre-, during and post-lockdown periods

3 mg/l and highest as 58 mg/l and a significant increase in the range values during post-lockdown period, i.e., lowest as 5 mg/l and highest as 61 mg/l (ref. Fig. 6a and b).
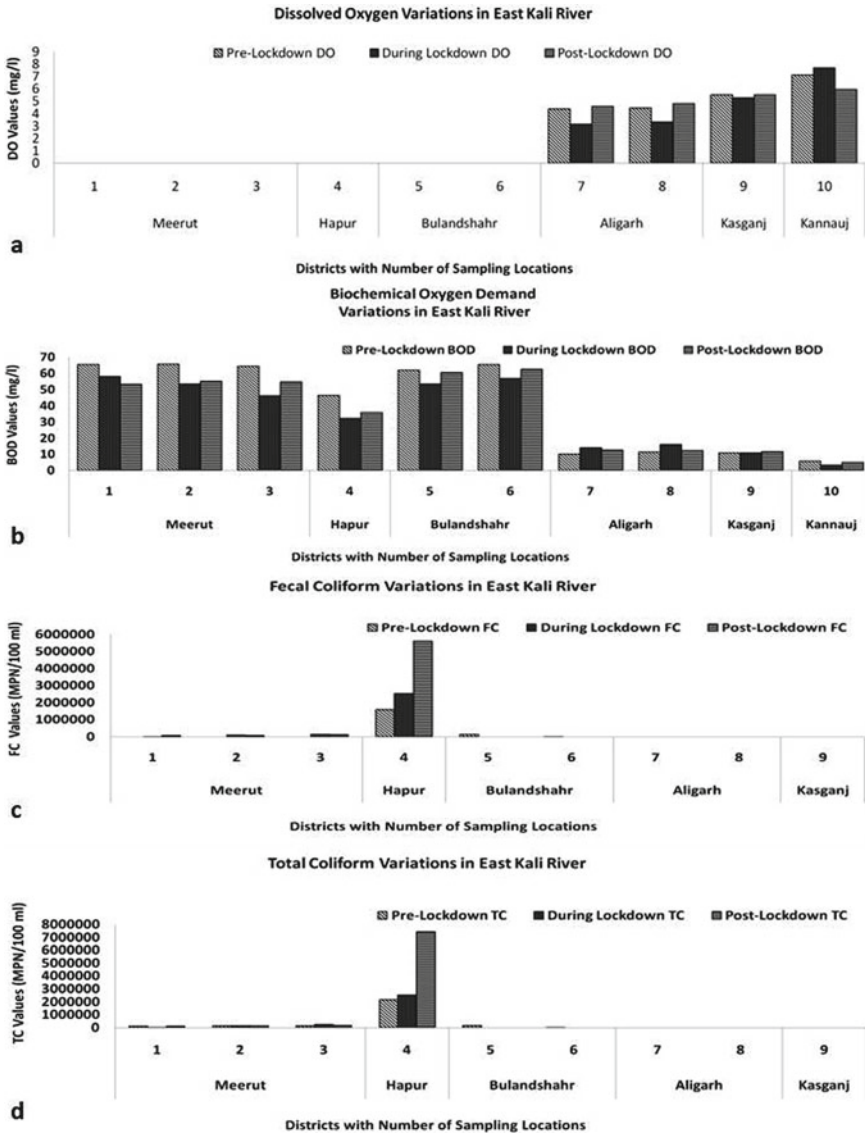
Fig. 6 Variation in the concentration of **a** DO, **b** BOD, **c** FC and **d** TC, respectively in river East Kali at all the sampling locations during pre-, during and post-lockdown periods

4.1 Discussion

Overall it can be observed from the above graphs that how the maximum values of fecal Coliform, Total Coliform (ref Fig. 7a and b), Biochemical Oxygen Demand and DO (ref Fig. 8a and b), have varied in three all phases. It can be clearly incurred
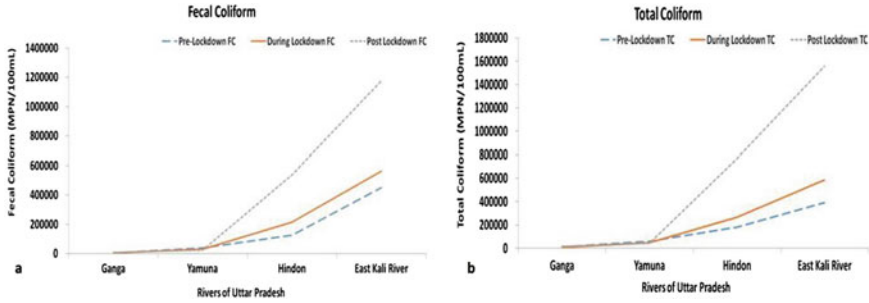
Fig. 7 Variation in the concentration of **a** FC and **b** TC, respectively in all four rivers during pre-, during and post-lockdown periods
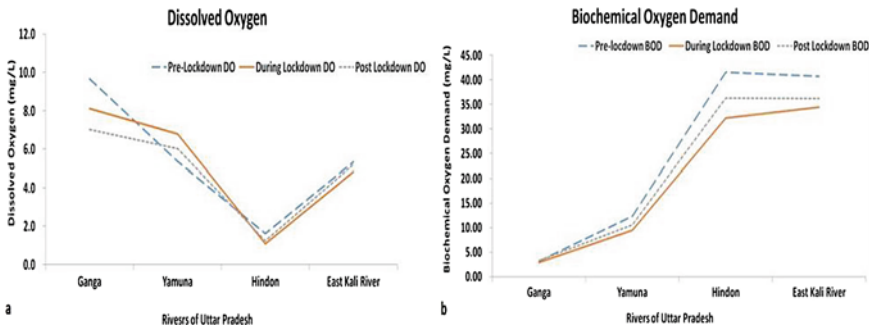

Fig. 8 Variation in the concentration of **a** DO and **b** BOD, respectively in all four rivers during pre-, during and post-lockdown periods

from the combined comparative graphs of all selected rivers that there has been a significant increase in the concentration of water quality parameters from pre- to during lockdown and during to post-lockdown. In the River Ganga, the Fecal Coliform has slightly decreased by 36% during lockdown period, and then increased by approximately 80% in post-lockdown period with respect to during lockdown phase whereas the Total Coliform decreased by 24% during lockdown period and drastically increased by 81%, In case of DO, the amount of DO was slightly decreased by 16.1% during lockdown phase and 13.4% during post-lockdown phase when compared with during lockdown phase whereas BOD was decreased by 8% during lockdown period and increased by 2% in post-lockdown phase in comparison to lockdown period.

In the case of river Yamuna, the fecal Coliform has slightly decreased by 29% during lockdown period, and then further decreased by 12% in post-lockdown period with respect to during lockdown phase whereas the Total Coliform decreased by 21% during lockdown period and further decreased by 6%, In case of DO, the amount of DO was increased by 26% during lockdown phase and decreased by 11.5% during post-lockdown phase when compared with during lockdown phase whereas BOD was

increased by 22% during lockdown period and decreased by 4% in post-lockdown phase in comparison to lockdown period.

In case of River Hindon, the Total Coliform has dramatically increased by 47% during lockdown period, and then further exacerbated by approximately 98% in post-lockdown period with respect to during lockdown phase whereas the fecal Coliform immensely increased by 72% during lockdown period and drastically increased by approximately 85%, when compared with during lockdown period. In case of DO, the amount of DO was decreased by 33% during lockdown phase and significantly increased by 14% during post-lockdown phase when compared with during lockdown phase whereas BOD was decreased by 22% during lockdown period and increased by 12.5% in post-lockdown phase in comparison to lockdown period.

In case of river Kali (East), the Total Coliform has dramatically increased by 49% during lockdown period, and then further exacerbated by approximately 95% in post-lockdown period with respect to during lockdown phase whereas the fecal Coliform increased by 25% during lockdown period and drastically increased by approximately 81%, when compared with during lockdown period In case of DO, the amount of DO was decreased by 9.5% during lockdown phase and significantly increased by 7.8% during post-lockdown phase when compared with during lockdown phase whereas BOD was decreased by 15.3% during lockdown period and increased by 5.18% in post-lockdown phase in comparison to lockdown period.

The above observations suggest that in all four selected rivers there has been a decrease in pollution load during lockdown period. This is supported by the fact that during lockdown loads of wastewater discharge was reduced as the Industrial load was eliminated in the rivers. Other activities such as tourism, fairs, bathing and cloth washing near the ghats were curtailed. However, a sudden increase in the Coliforms values were observed in River Hindon and East Kali during the lockdown which may have been caused as the domestic sewage would have increased owing to increased demand for water to maintain hand-washing hygiene. These observations indicated that both domestic and industrial effluent contribute to river contamination, and that the sewerage discharge was not the main cause of concern. To ensure water security in terms of surface water quality and quantity, appropriate surface water treatment for both industrial and domestic wastewater is required.

5   Conclusion and Recommendations

The worldwide imposition of lockdown has caused both positive and negative impacts on water quality of rivers flowing through India. The pollution severity of river water at the monitoring stations is directly correlated to the industrial activities in the surrounding areas. Alongside the closure of industries, the anthropogenic activities were restricted to control the viral transmission during the COVID-19 pandemic scenario. This had great impact on the water quality which has been reported through several news articles and scientific papers.

The present study is a first attempt to compare and evaluate the spatio-temporal variability of water quality parameters in river water such as DO, BOD, Fecal Coli and turbidity in all three lockdown phases, i.e., pre-, during and post-lockdown. Several research papers have reported the impact on surface water quality during the two phases, i.e., pre-lockdown and lockdown. However, this research sought to provide insight into the post-lockdown water quality scenario of four important rivers in Uttar Pradesh, namely, Ganga, Yamuna, Hindon and Kali. Also, the authors have attempted to understand nature's response on restoration of river by limiting the anthropogenic activities. It was observed that River Ganges and River Yamuna recorded considerable improvement in water quality due to partial closure of industries discharging effluents, restricted tourism activities and closure of other commercial establishments. However, River Hindon in western U.P showed slight improvement in the water quality indicating that the untreated wastewater from small drains is the main source of water pollution as against industrial effluents. There was no improvement in water quality of River Kali, thus signifying the level of overexploitation that has resulted in the destruction of its natural ecosystem. It was clearly observed from the comparative analysis of the water quality parameters for all four rivers on average during all three phases. Moreover, considerable changes in the values of DO, BOD, Turbidity and Fecal Coli were observed during post-lockdown period as compared to lockdown period. This can be due to sudden increase in the sewage influx during lockdown period along with the increased discharge of industrial effluent during post-lockdown period.

The trend analysis observed during this study gives an insight on the natural restoration phenomenon of river bodies. The river scientists have placed emphasis on the concept of nature-based solutions as an alternative for reducing the flood risk and improving the ecological quality. These solutions practically aim at restoring the natural in-stream processes in order to enhance the ecosystem functions as well as the delivered services. The sudden restrictions in the industrial activities led to a drastic decrease in the amount of anthropogenic pollution and gave nature an ample amount of time to breath and rejuvenate on its own without requiring any expensive water treatment method.

There is an urgent need to re-investigate the main source of pollution and reorient all river cleaning policies. Industries need to comply strictly with discharge standards accompanied by strong enforcement of laws and regulations vis-a-vis a strong framework of monitoring and vigilance. There is an urgent need to expand the monitoring network across the rivers of India to understand the mechanism of its pollution. Also, to keep the river water clean for a longer run, an optimal discharge will have to be maintained. A new paradigm for river restoration in a natural way must be explored as a long-term and cost-effective futuristic solution for mitigating pollution as well as flood risk.

References

1. Asthana,V, Shukla AC (2014) Water security in India: hope, despair, and the challenges of human development. Bloomsbury Publishing USA
2. Bhadula S, Joshi BD (2012) An assessment of the impact of sewer drains on the main canal of River Ganga, within Haridwar city. Uttarakhand, India
3. Bhutiani R, Khanna DR, Kulkarni DB, Ruhela M (2016) Assessment of Ganga river ecosystem at Haridwar, Uttarakhand, India with reference to water quality indices. Appl Water Sci 6(2):107–113
4. Cooper R (2020) Water security beyond Covid-19
5. CPCB (Central Pollution Control Board) (2020) Impact of lockdown on water quality of river Ganga. CPCB, Ministry of Environment, Forest and Climate Change, Govt. of India, New Delhi. Accessed 20 Nov 2020
6. Cronin AA, Prakash A, Priya S, Coates S (2014) Water in India: situation and prospects. Water Policy 16(3):425–441
7. Deka BJ, Bohra V, Alam W, Sanasam S, Guo J, Borana L, An AK (2020) Environment impact assessment of COVID-19. In: Integrated risk of pandemic: Covid-19 impacts, resilience and recommendations. Springer, Singapore, pp 169–195
8. Dutta V, Dubey D, Kumar S (2020) Cleaning the River Ganga: impact of lockdown on water quality and future implications on river rejuvenation strategies. Sci Total Environ 743:140756
9. Ercin AE, Hoekstra AY (2014) Water footprint scenarios for 2050: a global analysis. Environ Int 64:71–82. https://doi.org/10.1016/j.envint.2013.11.019
10. Faivre N, Fritz M, Freitas T, de Boissezon B, Vandewoestijne S (2017) Nature-based solutions in the EU: innovating with nature to address social, economic and environmental challenges. Environ research 159:509–518
11. FAO (2019) FAO Aquastat. http://www.fao.org/land-water/databasesand-software/aquastat/en/. Accessed 30 Nov 2020
12. Government of India (GoI) (1999) Integrated water resource development: a plan for action. Report of the National Commission on Integrated Water Resources Development (NCIWRD). vol 1. Ministry of Water Resources, Government of India
13. Headlines Vashishtha L (2010) Western Uttar Pradesh rivers are among the most polluted in India. India Today. Retrieved 12 January 2021
14. Howard G, Bartram J, Williams A, Overbo A, Geere JA, World Health Organization (2020) Domestic water quantity, service level and health. World Health Organization
15. Jayaswal K, Sahu V, Gurjar BR (2018) Water pollution, human health and remediation. In Water Remediation. Springer, Singapore, pp 11–27
16. Karl TR, Melillo JM, Peterson TC (eds) (2009) Global climate change impacts in the United States, Cambridge Univ. Press
17. Kumaravel SK, Subramani RK, Sivakumar TKJ, Elavarasan RM, Vetrichelvan AM, Annam A, Subramaniam U (2020) Investigation on the impacts of COVID-19 quarantine on society and environment: Preventive measures and supportive technologies. 3 Biotech, 10(9):1–24
18. Lafortezza R, Sanesi G (2019) Nature-based solutions: Settling the issue of sustainable urbanization. Environ Res 172:394–398
19. Lokhandwala S, Gautam P (2020) Indirect impact of COVID-19 on environment: A brief study in Indian context. Environ Res 188:109807
20. Mandal I, Pal S (2020) COVID-19 pandemic persuaded lockdown effects on environment over stone quarrying and crushing areas. Sci Total Environ 732:139281
21. Mandal S (2020) COVID-19 imposed lockdown might be a boom for aquatic ecosystem. Curr Sci 118(11):1641
22. Meybeck M (2003) Global analysis of river systems: from Earth system controls to Anthropocene syndromes. Phil Trans R Soc Lond B
23. Ourloglou O, Stefanidis K, Dimitriou E (2020) Assessing nature-based and classical engineering solutions for flood-risk reduction in urban streams. J Ecol Eng 21(2)

24. Pal S, Kundu S, Mahato S (2020) Groundwater potential zones for sustainable management plans in a river basin of India and Bangladesh. J Cleaner Prod 257:120311
25. Pink RM (2016) India: drought, climate change, and poverty. In: Water Rights in Southeast Asia and India. Palgrave Macmillan, New York. pp 63–91
26. Sinha R, Mohanta H, Jain V, Tandon SK (2017) Geomorphic diversity as a river management tool and its application to the Ganga River. India. River Res Appl 33(7):1156–1176
27. Somani M, Srivastava AN, Gummadivalli SK, Sharma A (2020) Indirect implications of COVID-19 towards sustainable environment: an investigation in Indian context. Bioresour Technol Rep 11:100491
28. UPPCB Action Plans reports for Ganga, Yamuna, Hindon and East Kali Rivers. http://www.uppcb.com/action-plan-june2019.htm. Accessed 20 Dec 2020
29. Vörösmarty CJ, McIntyre PB, Gessner MO, Dudgeon D, Prusevich A, Green P, Davies PM (2010) Global threats to human water security and river biodiversity. nature, 467(7315):555–561
30. Water UN (2013) Water security & the global water agenda. UN water analytical brief. UN University, Hamilton, Canada
31. World Water Assessment Programme (2009) Water in a changing world. The United Nations world water development report 3 (UNESCO)

Prevention of Saltwater Intrusion: A Laboratory-Scale Study on Electrokinetic Remediation

Abhishek A. Sutar and Veerabhadra M. Rotte

1 Introduction

1.1 Saltwater Intrusion and Conventional Ways of Its Prevention

Increased population along with improvement of living standard is forcing water demand to rise sharply in past few decades [1]. In coastal areas, for fulfilling the domestic, agricultural, industrial, and tourist water needs, groundwater is mostly overexploited [2]. Naturally fresh water flows from aquifers toward the sea and ground water flows from high level to low level, and this naturally occurring process prevents saltwater intrusion into fresh groundwater aquifers [3]. This phenomenon may get reversed due to long term climate change, sea level change, and tidal intensity fluctuations. Manmade activity like excessive pumping of fresh groundwater in coastal areas causes up-coning of transition zone as shown in Fig. 1, which has high impact on sea water intrusion. Saltwater intrusion can lower the potability of water and makes it difficult to use for other purposes like agricultural or industrial use [4]. Research has been going on to find out measures of controlling saltwater intrusion for protection of freshwater sources. The primary aim of these methods is to increase freshwater flow and reduce saltwater flow [5].

A. A. Sutar · V. M. Rotte (✉)
Civil Engineering Department, Institute of Infrastructure Technology Research And Management, Ahmedabad 380026, India
e-mail: vmrotte@iitram.ac.in

A. A. Sutar
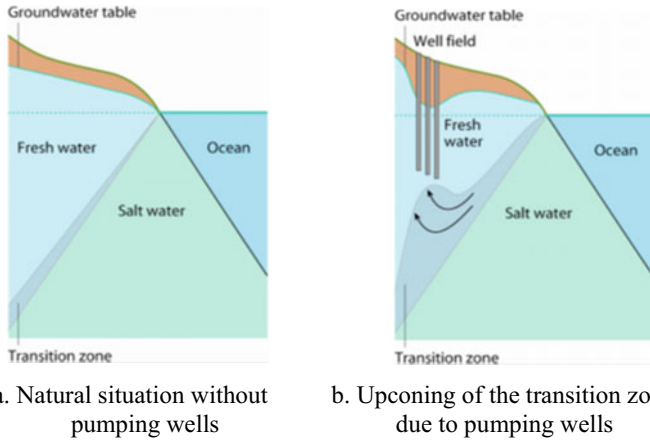e-mail: abhishek.sutar.18pc@iitram.ac.in

a. Natural situation without pumping wells

b. Upconing of the transition zone due to pumping wells

Fig. 1 Effect of excessive pumping in coastal areas (After Bereyso [18])

Hussain et al. [6] reviewed techniques for controlling saltwater intrusion and reported methods like reduction of pumping rate, relocation of pumping wells, permeable subsurface/surface barrier, hydraulic barrier, artificial recharge wells, abstraction barrier, and combination of any of these methods. It is very difficult to select the optimum control method due to limitations like performance efficiency, cost, etc. Due to high cost of installation, it is profitable to combine two or more methods to introduce efficient control technique [7].

1.2 Electrokinetic Remediation for Saltwater Intrusion

When direct current is applied to soil through electrodes, then pore water flows from positive to negative electrode. Electrokinetic treatment includes electro-osmosis, electrophoresis, electrolysis, and electro-migration, combining effect of all this phenomena causes movement of water. Malekzadeh et al. [8] reviewed electrokinetic dewatering of soil and reported that it is affected by soil type, zeta potential, pH, temperature, water content, soil salinity, electrical resistivity and conductivity, type of electrodes, etc. Electrokinetics plays an important role in different remediation applications. It has been used as an in-situ technique for contaminant mobilization and recovery. It is done by applying a low electrical potential between anode and cathode electrode array inserted in the soil [9]. This technology is applicable for containment of soils where conventional techniques are not applicable, and soils have very low permeability. Electrokinetic barrier or fencing is same type of application in which electrokinetics shuts the pollutants from moving into neighboring un-polluted ground. The hydraulically generated movement of ions is opposed by combined effect of electro-osmotic flow and electro-migration [10]. Electrokinetic barrier is an application of electrokinetic remediation technology. This technology

has been developed for its practical use by Lageman and Pool [11] since 1980s. The main focus is given on electro-migration in case of remediation studies which includes movement of ions causing desalination of soils during the process [12]. In case of saltwater intrusion seawater flows in freshwater aquifers and contaminate the fresh groundwater source. Under the effect of DC field sodium and chloride ions which are major components of seawater are transported toward barrier and get trapped and deposited near to opposite electrode while fresh water passes toward other side of barrier. The deposited ions can be removed from ground periodically [13]. Electrokinetic remediation method is cost effective, easy to install, and operate [14, 15]. This method does not disturb the original nature of soil [16]. Electrokinetic remediation can be considered as eco-friendly and sustainable technique due to very less use of chemicals, and it can be given power by renewable energy sources like solar energy or wind energy [17]. Bereyso et al. [18] applied electrokinetic barrier in a lab scale setup for prevention of salt migration and allowed transfer of desalinated water through the barrier. The decreased conductivity on downstream side of barrier as compared to upstream side is the principal finding, but the scope was limited to a constant 12 V potential difference. The viability of this technology in practical use on field needs to obtain more insights into electrokinetic applications in the remediation area [19]. The main aim of the present study is to evaluate optimum efficiency of experimental parameters like spacing of electrodes and electrode materials for prevention of saltwater intrusion and integrating feasibility of the technique for its practical use. Further, it can be elaborated that the study aims to capture chloride and sodium ions present in salt water near the electrodes to some extent that the treated water on downstream side of the electrokinetic barrier can be used for drinking or agricultural use as per standards.

2 Materials

2.1 Soil

The experiments were carried out on river sand having specific gravity of 2.6 and passing through 600 micron sieve. Grain size distribution of the sand shows that the sand is poorly graded. The initial electrical conductivity of the sand was measured as 220 µS/cm. It was found to be same for all samples and need not be required to wash sand by deionized water before each test.

2.2 Water

Experiments were conducted by 75% saturation of the sand with potable water having conductivity 210 µS/cm. T.D.S. of the water was noted to be 110–115 with 8.7–9.2

Fig. 2 Saltwater wells and freshwater pumping wells
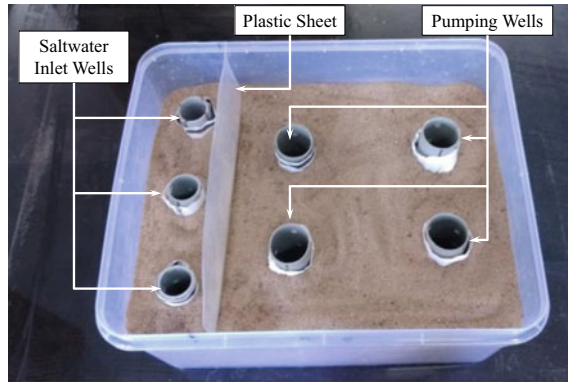
pH. Seawater contains 75% of sodium chloride as major salt thus AR grade sodium chloride meeting ACS standards was used having 99% purity. 70 mg of NaCl was weighed and mixed thoroughly into 1 L water by using stirrer, and it was added on saltwater side of the setup. The electrical conductivity of the saltwater was found to be 1.625 mS/cm with T.D.S. of 747 and 9.2 pH. Sand on the right side of the vertical plastic sheet has been saturated by normal potable water through four perforated pumping wells (Fig. 2). Simultaneously, on left side of the sheet, saltwater was added into the perforated saltwater inlet wells to create actual seaside condition.

2.3   Electrodes

Based on the study by Malekzadeh et al. [20] stainless steel and graphite solid rods with 11 mm diameter and 105 mm length were used for supplying direct current to the sand.

3   Experimental Test Setup, Procedure, and Program

Experiments were carried out in a transparent plastic container box with dimensions 360 mm × 290 mm × 180 mm with reference of Tumalla et al. [21]. To prevent surface water losses, it was covered with lid from top. Two holes of 6 mm diameter were drilled on side edge to house electrical supply wires. The box was divided into two parts by a temporary plastic sheet having very less thickness making the saltwater side of area 70 mm × 295 mm and fresh water side of area 290 mm × 295 mm as shown in Fig. 2. The sheet was held vertically in between saltwater side and freshwater side of the box while filling the sand into box.

The sand was poured simultaneously on both sides and tamping was done to achieve uniform density of 1.365 gm/cm^3 having relative density of 80%. Flow

characteristics of water depend upon the density of sand significantly. If the density of sand in the setup is different for each test then the flow characteristics of water will varie and affect the results of the experiments. In view of this, uniform density has been attained in all the tests. Total 16 kg of sand was filled in the box up-to 100 mm height. For measuring electrical conductivity and pH of water, two pumping wells were installed on the either side of electrokinetic barrier by using PVC hollow pipes with 37 mm internal diameter, 120 mm height, and 12 mm thickness. For allowing water inflow into these pipes 5 mm diameter holes with 30 mm center to center spacing were drilled on periphery of the pipes in staggered pattern. Similarly, for pouring salt water along the salt side of the setup three PVC pipes of internal diameter 30 mm and 120 mm height with 12 mm thickness were used. For prevention of soil particles into these perforated hollow pipes, cotton cloth around and from bottom side of these pipes was wrapped as shown in Fig. 3. The PVC pipes for pumping wells and salt wells were inserted by simply pushing without much disturbing the density of sand. Electrodes were installed in series with 40 mm center to center spacing between same polarity electrodes and required center to center spacing between opposite polarity electrodes as shown in Fig. 4. Potable water was poured in freshwater side through

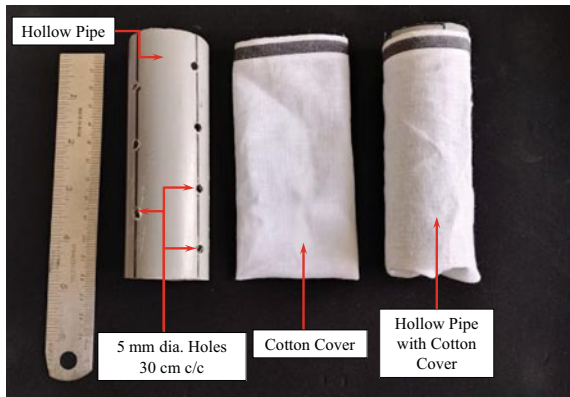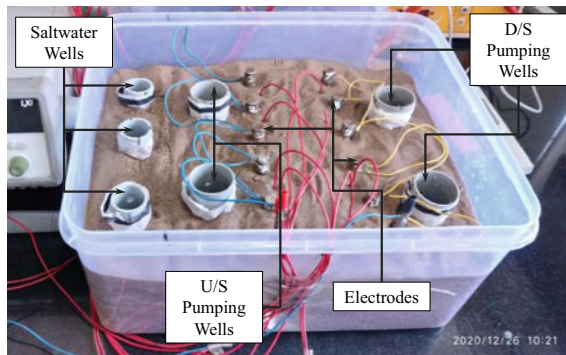**Fig. 3** Details of perforated pipe and cotton cover

Fig. 4 Details of electrodes, U/S wells, and D/S wells

pumping wells and simultaneously salt water was poured in saltwater side of the box through saltwater wells. The sand in whole setup was saturated for 75% such that there should not be any freely flowing surface water to cause ill results by mixing of saltwater and freshwater. The vertical plastic sheet was removed slowly, and DC supply was started.

pH of water from wells was monitored manually by measuring it with WELL-TRONIX's AUTO pH System PM300 (Fig. 5). pH electrode was inserted in each well every hour and reading was noted to the accuracy up to 0.01 pH. Similarly, conductivity of the water was measured by using EQUIPTRONICS' Conductivity meter EQ667 (Fig. 6). For measuring T.D.S., handy T.D.S. meter was used. The details of complete setup are shown in Fig. 7. With these arrangements of electrodes, water was observed to flow from anode to cathode. Due to electrokinetic barrier only water and not the salts will flow from anode to cathode. Electrical conductivity, T.D.S., pH were measured manually at every hour for 24 h.

The experiments were performed to study the effect of Electrode Spacing and Electrode material on the electrical conductivity, total dissolved solids, and pH. All
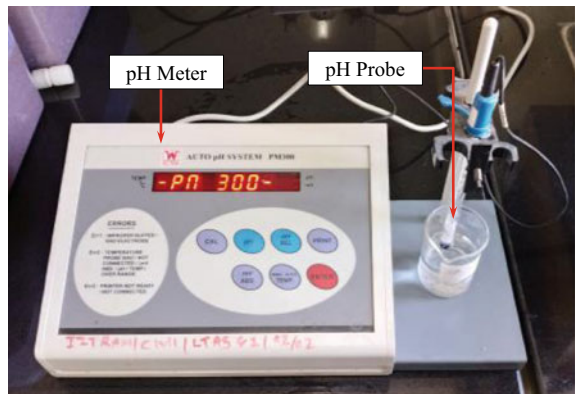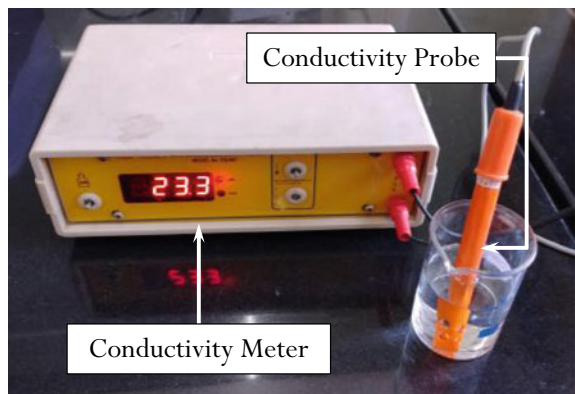

Fig. 5 pH meter
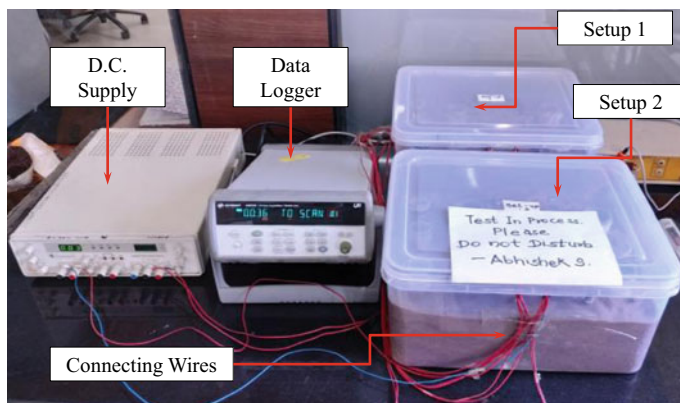

Fig. 6 Conductivity meter

Fig. 7 Details of complete setup with D.C. supply and data logger

Table 1 Test program of the present study

Test name	Electrode spacing	Electrode material	Voltage
Control test	NA (cm)	NA	NA (V)
EKR-1	5	Graphite	10
EKR-2	10	Stainless steel	10
EKR-3	10	Graphite	10

the tests were continued up to 24 h. The test program with all details is shown in Table 1. Control test was also carried out in which no electrode was used and no potential difference has applied. The main purpose of control test is to compare the effect due to electrokinetic with control test and to find out efficiency of the electrokinetic barrier under different working conditions.

4 Results and Discussions

4.1 Influence of Spacing on Electrical Conductivity and Total Dissolved Solids

The electrical conductivity of soil water is measured to derive soil salinity. Electrokinetic remediation experiments were carried out by varying the center to center spacing between cathodes and anodes as 5 cm (EKR-1) and 10 cm (EKR-3). All cathodes were placed in a single row, and all anodes were placed in single row to form electrode array having c/c spacing as required. A potential difference of 10 V was maintained for all the experiments except control test in this series. Figure 8 shows
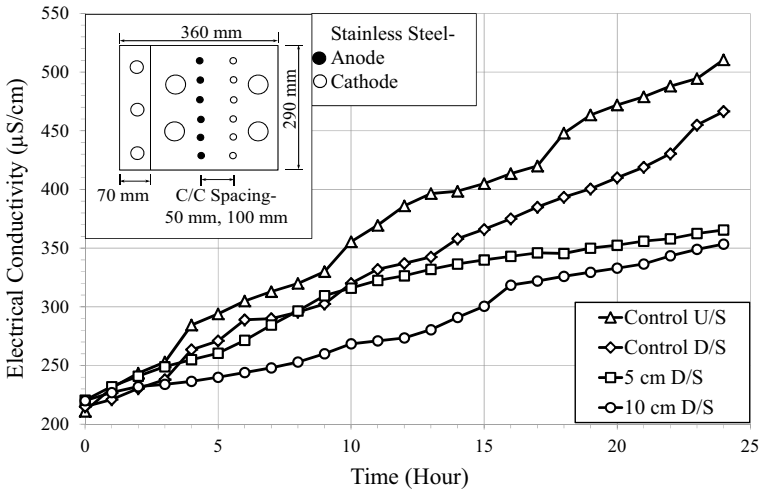
Fig. 8 Effect of spacing on electrical conductivity

variation of electrical conductivity of water with time for upstream and downstream wells of control test and only downstream wells of electrokinetic tests.

The rate of increase in electrical conductivity was observed to be more for control test as compared to electrokinetic tests. It was noticed for EKR tests, with an increase in center to center spacing between cathodes and anodes, rate of increase in electrical conductivity decreases with time. This is because of increase in spacing, an area under the influence of electric field increases causing efficient ions exchange with more absorbed ions on the large area of soil surface producing low electrical conductivity. Figure 9 shows variation of total dissolved solids with time for control test and electrokinetic tests. As time passes T.D.S. values were observed to increase. The T.D.S. values of upstream wells were noticed on the higher side as compared to downstream wells for control test. The figure indicates that with increase in spacing of electrodes, T.D.S. values decreases significantly. Chloride and sodium ions get prevented from flow at larger area under influence of applied potential for large spacing between the anodes and cathodes. Thus, only water is allowed to flow indicating less dissolved solids in downstream wells for more spacing in EKR tests.

4.2 Influence of Electrode Material on Electrical Conductivity and Total Dissolved Solids

Experiments were carried out to find out effect of electrode material on different parameters. Stainless steel (EKR-2) and graphite (EKR-3) electrodes have been used in current experiments. Electrode configuration was kept unchanged with 10 cm center to center spacing. A potential difference of 10 V was maintained for all
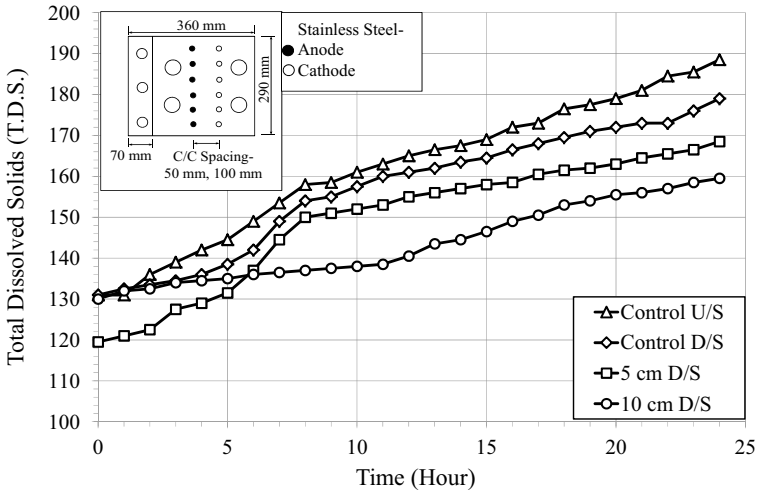
Fig. 9 Effect of spacing on total dissolved solids

experiments except control test in this series. Figure 10 shows variation of electrical conductivity of water with time. It is clear from figure that electrical conductivity for all tests increases with time. It was also noticed that stainless steel electrodes show lower values of electrical conductivity as compared to graphite electrodes. Variation of total dissolved solids with time has shown in Fig. 11. The graph for T.D.S. values for control test is much similar to electrical conductivity graph. The T.D.S. values are lower for stainless steel electrodes as compared to graphite electrodes. The stainless
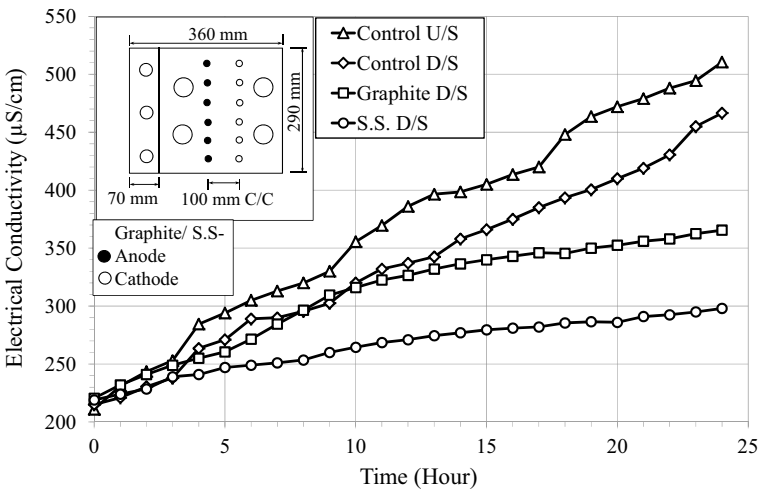
Fig. 10 Effect of electrode material on electrical conductivity
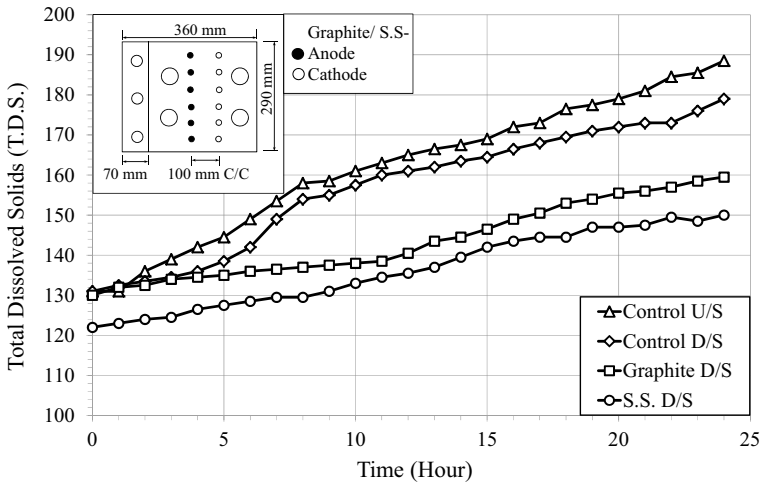
Fig. 11 Effect of electrode material on total dissolved solids

steel gives much better electro-osmotic effect over graphite electrodes. Graphite is carbon electrode which results in large voltage drop in later stages of experiments causing inefficient results as compared to stainless steel electrodes.

4.3 Effect of Different Parameters on pH

The manual tracking of pH was also done to find out effect of spacing and electrode material on pH. The change in pH directly relates to electrolysis occurring in soil. In all experiments the initial pH values from downstream pumping wells are in range of 9.2–10.2 which was not observed to change in a particular manner. The final values were also in the same range and did not follow any relation with time giving random variation. Rather the experiment duration was just 24 h which may need to be increased up to 72 h in order to obtain acidic and basic fronts due to oxidation reduction reaction to find out the effect of different parameters on pH of water in upstream and downstream wells.

5 Conclusions

Total two set of experiments were carried out for analyzing effect of spacing and electrode material on different parameters of the tests. Based on the results obtained from experiments, the following conclusions can be obtained.

1. Control tests show higher values of electrical conductivity and T.D.S. of water in downstream pumping wells as compared to EKR tests with increase in time. In case of EKR tests due to applied voltage the chloride and sodium ions of saltwater from upstream side got prevented from flow near electrodes which was not observed in the case of control test thus the values of electrical conductivity and T.D.S. are high in control tests.

2. For constant applied potential and electrode material as spacing between electrodes increases the electrical conductivity and T.D.S. values of water in downstream pumping wells decreases. It occurs due to an increase in spacing of electrodes, area under influence of an electric field increases. This causes efficient ion exchange over large surface area of soil giving decreased electrical conductivity and T.D.S. values.

3. Stainless steel showed lower values of electrical conductivity and T.D.S. as compared to graphite electrodes in downstream pumping wells for constant voltage and spacing between electrodes. Graphite is a carbon electrode which gives large voltage drop in later stages of electrolysis. This large voltage drop in case of graphite causes inefficient electro-osmosis and less control on ion flow giving high values of electrical conductivity and T.D.S. as compared to stainless steel.

4. It is confirmed from the figures of electrical conductivity that EKR-2 gives 68.53% reduction in the values of electrical conductivity as compared to control test. Similarly, EKR-3 gives 47.02% reduction and EKR-1 gives 42.25% reduction in electrical conductivity values. This can be directly related to the salinity of water, and we can say that EKR-2 with 10 cm center to center spacing of stainless steel electrodes the saltwater intrusion can be minimized up to 68.53% as that of control test which is optimum finding of the experiment.

Further research needs to be focused in order to analyze effect of voltage, salt concentration of source saltwater wells, grain size of soil, and other material of electrodes like copper, aluminum, etc. Experiments may be planned to lasts for more than 24 h duration for obtaining better results of electrolysis reaction in order to find out effect of varying parameters on pH of water in downstream wells.

References

1. Neumann B, Vafeidis AT, Zimmermann J, Nicholls RJ (2015) Future coastal population growth and exposure to sea-level rise and coastal flooding - a global assessment. PLoS One 10(3):e0118571

2. Hamed Y, Hadji R, Redhaounia B, Zighmi K, Baali F, El Gayar A (2018) Climate impact on surface and groundwater in North Africa: a global synthesis of findings and recommendations. Euro-Mediterranean J Environ Integr 3:25

3. De Breuck W (1991) "Hydrogeology of salt-water intrusion: methods and instruments", Verlag Heinz Heise GmbH & Co KG, vol 223. Hannover, Germany

4. Gopinath S, Srinivasamoorthy K (2015) Application of geophysical and hydrogeochemical tracers to investigate salinisation sources in Nagapatinam and Karaikal Coastal Aquifers, South India. Aquat Procedia 4:65–71

5. Goswami RR, Clement TP (2007) Laboratory-scale investigation of saltwater intrusion dynamics. Water Resour Res 4(43)

6. Hussain MS, Abd-Elhamid HF, Javadi AA, Sherif MM (2019) Management of seawater intrusion in coastal aquifers: a review. MDPI J Water 11(12):2467

7. Pla JM, Ghiglieri G, Uras G (2014) Seawater intrusion and coastal groundwater resources management. Examples from two Mediterranean regions: Catalonia and Sardinia. Contrib Sci 171–184

8. Malekzadeh M, Lovisa J, Sivakugan N (2016) An overview of electrokinetic consolidation. of soils. Geotech Geol Eng 34(3):759–776

9. Acar YB, Alshawabkeh AN (1993) Principles of electrokinetic remediation. Environ Sci Technol 27(13):2638

10. Mitchell JK, Yeung TC (1990) Electro-kinetic flow barriers in compacted clay. Transp Res Rec 1288

11. Lageman R, Clarke RL, Pool W (2005) Electro-Reclamation, a versatile soil remediation solution. Eng Geol Spec Issue Electrokinet Remediat 77:191–201

12. Acar YB, Alshawabkeh AN (1993) Principles of electrokinetic remediation. Environ Sci Technol 27(13)

13. Lageman R, Pool W (2009) Experiences with field applications of electrokinetic remediation. In Electrochemical remediation technologies for polluted soils, sediments and groundwater, vol 33. Wiley, pp 697–717

14. Khalid S, Shahid M, Niazi NK, Murtaza B, Bibi I, Dumat C (2017) A comparison of technologies for remediation of heavy metal contaminated soils. J Geochem Explor 182:247–268

15. Virkutyte J, Sillanpää M, Latostenmaa P (2002) Electrokinetic soil remediation — critical overview. Sci Total Environ 289(1–3):97–121

16. Page MM, Page CL (2008) Electroremediation of contaminated soils. J Environ Eng 128(3):208–219

17. Baek K, Mao X, Ciblak A, Alshwabkeh A (2012) Green remediation of soil and groundwater by electrochemical methods. GeoCongress

18. Bereyso E, Tummala CM, Tewari S (2019) Going underground for source water protection: evaluating lab-scale electrokinetic barriers against saltwater intrusion. In: World environmental and water resources congress, vol 133

19. Shadi HH, Molelekwa GF, Bruggen BVD (2014) Electrokinetic remediation technique: an integrated approach to finding new strategies for restoration of saline soil and to control seawater intrusion. ChemElectroChem 1(7):1104–1117

20. Malekzadeh M, Sivakugan N (2017) Double drain electrokinetic stabilization of dredged mud using stainless steel electrodes and application of surcharge. KSCE J Civ Eng 21(7):2615–2621

21. Tummala CM, Tewari S (2018) Effects of variability of electrode materials and configurations on performance of electro-kinetic barriers against sea-water intrusion. In: World environmental & water resources congress, Minneapolis, MN, June 3-7

On-Site Grey Water Treatment Integrated with Constructed Wetland for Household Appliance

Vinayak K. Patki, P. V. Vijay Babu, and Adinath Palase

1 Introduction

Extreme utilization of regular water assets because of fast urbanization has required quest for elective wellsprings of water for non-consumable purposes. The potential sources which can be investigated incorporate gathered water, recycled water, and ocean water. Recycled water from each family is a fitting decision as it gives extension to water protection, contamination counteraction and decentralized treatment. Black water and dim water are two significant contributory floods of homegrown wastewater. Dim water has incredible potential for reuse because of its accessibility and low toxin strength, when contrasted with sewage. In non-industrial nations like India, recovery of dim water for non-consumable use is fundamental because of non-presence of sewerage framework in the vast majority of the towns/urban areas and groundwater contamination because of removal of untreated sewage. Akratos and Tsihrintzis [1] considered impact of temperature, HRT, vegetation and permeable media on expulsion effectiveness of pilot-scale level subsurface stream developed wetlands. Evacuation execution of the built wetland units was excellent; since it came to on a normal, BOD, TKN, and ortho-phosphate (P-PO$_4{}^{3-}$) were all reduced by 89, 65, and 60%, respectively. Temperature has an effect on all pollutant removal efficiency. For temperatures above, it seems that an 8-day HRT was sufficient for appropriate elimination of organic debris, TKN, and P-PO$_4{}^{3-}$. 15 °C. Bouchaib et al. [2] zeroed in on dim water treatment, reusing for latrine flushing with the correlation of low and cutting edge treatment draws near. The minimal expense unit comprised

---

V. K. Patki (✉) · A. Palase
Department of Civil Engineering, N.K. Orchid College of Engineering and Technology, Solapur, Maharashtra, India
e-mail: vinayakpatki@orchidengg.ac.in

P. V. Vijay Babu
Chemical Engineering Department, Dr. Babasaheb Ambedkar Technological University, Lonere, Maharashtra, India

of a rock even stream developed wetland planted with Phragmites followed by an upward stream multi-facet sand channel. For the examination, two innovative units to be specific; MBR and a sequencing cluster reactor (SBR) and an inherent UV light were utilized. The good presentation of the minimal expense unit was accounted for. Then again, it was tracked down that the presentation of MBR and SBR units was brilliant with profluent quality adjusting to reusing norms for latrine flushing. Lee et al. [3] examined nitrogen expulsion in built wetland frameworks. The survey is of the present status of nitrogen evacuation innovation, zeroing in on existing sorts of wetlands, the systems of nitrogen expulsion, major natural components comparative with nitrogen evacuation, and the activity and the board of the wetlands. Langer-graber et al. [4] concentrated high-rate nitrogen evacuation in a two-stage subsurface vertical stream built wetland. In their examination two-stage framework was worked with a natural heap of 40 g COD/m^2 d for the whole system, that is, with a specific surface area requirement of 2 m^2 per person equivalent. Average nitrogen removal efficiencies of 53% and average nitrogen elimination rates of 2.7 gN/m^2 d and 986 g N/m^2 yr, respectively, could be accomplished without distribution, in this manner permitting development with sans energy stacking frameworks. Yalcuk and Ugurlu [5] thought about level and vertical built wetland frameworks for land-fill leachate treatment are compared. Leachate was treated with natural pollution, alkali, and heavy metals using constructed wetland frameworks, and the influence of taking care of method was measured. The effect of several sheet materials (rock and zeolite surface) was also investigated. A pilot-scale investigation was conducted on subsurface stream-built wetland frameworks that functioned in both vertical and flat modes. The bedding material of two vertical frames differed from one another. Individually, the frameworks were planted with cattail (Typha latifolia) and operated indistinguishably at a stream rate of 10 l/day and water-driven maintenance seasons of 11.8 and 12.5 days in vertical 1, vertical 2, and flat frameworks. Fixation based normal evacuation efficiencies for VF1, VF2 and HF were NH_4–N, 62.3%, 48.9% and 38.3%; COD, 27.3%, 30.6% and 35.7%; PO_4–P, 52.6%, 51.9% and 46.7%; and Fe (III), 21%, 40% and 17%, respectively. Better NH_4– N evacuation execution was seen in the upward framework with zeolite layer than that of the upward 2 and even framework. Conversely, level framework was more successful in COD expulsion (Konnerup et al. [6]). Treatment of homemade wastewater was considered in tropical, underground stream-built wetlands planted with Canna and Heliconia. The evacuation rate constants for COD as fitted by the main request model were determined to be 0.283 and 0.271 m/d, respectively, for Canna and Heliconia beds. Nitrogen (N) and phosphorus (P) evacuations were low in comparison to stacking rates, although full N expulsion was greater in Canna-planted beds than in Heliconia-planted beds owing to Canna's faster growth rate. Vymazal [7] examined utilization of built wetland for wastewater treatment. The examination revel that to accomplish better treatment execution, to be specific for nitrogen, different kinds of built wetlands could be joined into half and half frameworks. Avila et al. [8] considered an exploratory HCW framework comprising of 3 phases of various wetland arrangements (for example, two vertical stream beds followed by a level underground stream and a free water surface wetland in order), as well as the character of its final outburst. The overall

evacuation rate was 97 percent TSS, 78 percent COD, and 91 percent BOD5. Vertical stream beds achieved a significant natural matter reduction (77 percent BOD5) and an exceptional nitrification limit (74 percent NH4-N expulsion). Denitrification and water sterilisation were minimal in level and free water surface wetlands. In general, the three-stage cross-breed designed wetland framework has proved the ability to construct an appropriate eco-innovation for wastewater treatment and reuse in small networks of warm climate areas. Avila et al. [9] focused on a full-scale HCW system made up of three stages of diverse wetland layouts for domestic wastewater treatment and reuse in small networks. It was made up of three wetlands: a 317 m2 VF, a 229 m2 HF, and a 240 m2 FWS (Free water surface). The VF and HF wetlands were planted with basic reed (Phragmites australis), whereas the FWS had a mix of plant and animal species. TSS, BOD5, and NH4–N ejection proficiency was obtained at 98–99 percent. Nitrification and denitrification occurred as a result of the interaction of high-impact and anoxic sites within the marsh bed. Similarly, cross breed framework has been shown to have a high sterilisation limit. Saumya et al. [10] investigated the design and evaluation of a model subsurface stream wetland seeded with Heliconia angusta for the treatment of produced dark water. The experiment findings revealed a significant reduction in BOD (48.62 percent), COD (27.63 percent), turbidity (92 percent), and TSS (81.75 percent). NEERI [11] presented the challenges, which included dim water treatment alternatives, demonstrations of current frameworks, and a cost–benefit analysis of dim water. NEERI and UNICEF (Bhopal) have developed, implemented, and evaluated dim water reuse systems for small buildings (schools) in provincial areas. The therapeutic options used include physico-natural therapy. The actual treatment, which consisted of a rock sand canal and a wetland, was organic. Sonavane et al. [12] examined achievability of Constructed Wetland Treatment framework for septic tank gushing. The examination uncovered that rate expulsion of 65–80% BOD, 55–90% suspended strong 22–66% TKN and 12–26% phosphorous evacuation for 4-multi day maintenance time. Bindu et al. [13] examined poison expulsion from homegrown wastewater with Taro (Colocasia esculenta) planted in a subsurface stream framework. The consequences of their investigation uncovered that the subsurface stream frameworks planted with C. esculenta could diminish the nitrate and phosphate substance of the wastewater, other than natural matter. The nature of treated water from the raceways with plants was superior to those without plants. Additionally C. esculenta was found to oppose COD focus as high as 1650 mg/L. Patil and Munavalli [14] examined the exhibition assessment of an Integrated available Greywater Treatment System in a tropical locale with essential settling/filtration, auxiliary developed wetlands and tertiary adsorption treatment for an inn building. They tracked down a predictable execution in the Upflow-Downflow channel. In their investigation the COD was decreased by 70% and turbidity by 70%. The TKN and microorganism expulsion was 70% and 85% separately in the general framework. Graaff et al. [15] conveyed the achievability of applying a UASB reactor for the treatment of concentrated dark (latrine) water at 25 °C. The reactor exhibited a stable operation and removed more than 78% of the incoming COD.

In this investigation it was chosen to

- Evaluate the ebb and flow physical and natural frameworks of dim water treatment announced in writing concerning their pertinence to Indian conditions.
- Design and foster pilot scale dim water treatment framework fusing fundamental treatment, different blends of physical and natural cycles.
- Carry out Performance assessment investigations of dim water treatment blends for evacuation of pollutants.

2 Materials and Methods

2.1 Foundation of Greywater

To treat the greywater for the school in working in grounds, the mixture type nearby greywater treatment plant was utilized. It can likewise be alluded as on location Integrated Greywater Treatment plant. In Preliminary treatment, Filtration System was utilized and for Secondary treatment the Constructed Wetland was utilized. The On-Site plant is as demonstrated in Fig. 1. The Greywater treatment plant constructed for the hostel building had integrated system consisting of primary filtration and secondary wetland system. The combine system was called as Integrated On-site Greywater Treatment Plant. The arrangements of primary and secondary treatment technology are shown in Fig. 2.

2.2 On-Site Integrated Greywater Treatment Plant Process

A number of physical, chemical, and biological processes are used in the greywater treatment process. Therapy is often divided into two phases, known as primary and

Fig. 1 On-site treatment plant

Fig. 2 Line sketch of treatment technology

secondary treatment. Filtration is used in the main treatment, and the wetland system is used in the subsequent treatment. Primary treatment is used to separate and remove inorganic elements and suspended particles that would clog or damage the pipes owing to inorganic matter in the water. The basic treatment was carried out in three phases using three distinct materials. The initial step included varied sizes of sand. Brick powder and a brick bat were used in the second step. Charcoal powder and charcoal chunks were used in the third step. The primary treatment includes treatment using sand, brick bats and charcoal powder. In the first stage the grey water was allowed to move under gravity through sand layers of different thickness and sand particles of different effective diameter. In the second stage the grey water was allowed to move under gravity through brick layers of different thickness and brickbat particles of different effective diameter. In the third stage the grey water was allowed to move under gravity through charcoal layers of different thickness and charcoal particles of different effective diameter.

2.2.1 Surface Overflow Rate (Hydraulic Loading)

To maintain the hydraulic flow, rate several trails were taken to get the optimum flow, so as to increase the efficiency of primary treatment. The trails conducted to get the optimum flow are as stated below.

2.2.2 Trial No. 1 First Stage: (Sand Filter)

In the first trial the sand passing through a sieve size of 2.36 mm was used. It was cleaned from dust. The lower 15 cm layer was filled with gravel of size passing through 12.5 mm and retaining on 20 mm sieve. The top layer was then completely filled with fine sand. This fine sand layer was used in regarding to block the colloidal impurities and to reduce the Total Suspended Solids.

Second Stage (Brickbats Filter): In the first trail the brick was crushed in fine powder and the powder was then sieved through the sieve of 2.36 mm sieve and then filled in the second tank. The lower layer in the second tank of 15 cm was filled with coarse gravel as that used in first tank. The crushed brick powder was used as it gives larger area for surface adhesion to water molecules, which might reduce the acidity, Total Dissolved Solids, etc.

Third stage (Charcoal Filter): The third tank was filled with coal powder used in brick manufacturing plants. This was sieved through a size of 2.36 mm and then filled in the tank. The lower layer was also used of gravel. The charcoal powder was used to give more contact surface for helping in reduction of alkalinity, pH, conductivity, etc. The flow obtained was very slow which resulted in the failure of the plant and overflow from each of the tank due to very less voids present in the sand, brick powder and the coal powder. The top layer was fully clogged in a very short duration of time. Due to this a revision was carried and conducted as in trial no 2.

2.2.3 Trail No. 2

First stage (Sand Filter): In the first stage the coarse particle of gravel was used which was of size passing through 12.5 mm and retaining on 10 mm for the complete tank except for the last 15 cm was filled with gravel retaining on 20 mm. The number of air voids in this case increased but the retention time as reduced. The larger air voids were kept in order to help the greywater get mixed with oxygen and thus reducing the BOD and COD. The colloidal impurities were to be blocked at the top surface, but this was not seen as the voids were very large.

Second stage (Brickbats Filter): In second trail the brick was broken into chips of size 20 mm and filled in the tank. The last layer was filled with gravel as that in the tank 1 for the lower 15 cm. The size of bricks was large due to which no removal was seen in acidity and TDS. The water passed very swiftly so reduction in any chemical parameter of water was seen.

Third stage (Charcoal Filter): In this tank coarser particles of wooden coal were used as it contains large voids and also the carbon content is high. The lower level was same as that of tank 1 and tank 2 filled with gravel for bottom 15 cm layer. The coal was used was of cylindrical shape wooden coal, having diameter 1 to 4 cm and length 10 to 15 cm. This coal layer was not compacted as it would result in crushing of coal thus blocking the path of water. This increased the air voids in the charcoal. The hydraulic flow rate obtained in this trail was very fast and the retention time was very less, due to which no filtration and treatment was seen in the system. The water was retained for a very small time in the primary stage due to which it was not that effective. Another trail with mixed material size was conducted.

2.2.4 Trail No. 3

This trail was finalized after taking care of the hydraulic loading and the rate of the flow. This trail was basically an average of trail 1 and trail 2.

First stage (Sand Filter): The third trail was conducted by using the combination of trail 1 and trail 2. The lower layer consisted of coarser gravel of 12.5 mm and the top 15 cm layer consisted of gravel retaining on 4.75 mm sieve. Due to this combination the top layer blocked the soap particles and any other coarser impurity, thus reducing the TSS and turbidity, whereas the voids in lower section helped mixing of oxygen to mix with water and hence reduce the BOD, COD effectively. The cross section is as shown in Fig. 3. The layer at top needed to be scrapped and replaced every 3 to 4 weeks. The time when the scrapping was to be done, and the tank needed maintenance, a strong odour was expelled from the tank making it difficult for breathing. This was a major disadvantage of the primary treatment.

Second Stage (Brickbat Filter): In this trail the lower layer consisted of gravel to avoid blockage in the pipe for the layer of 12 cm. The middle layer of 32 cm consisted of the brick bats of size passing through 20 mm and retaining on 12.5 mm. The top layer of 25 cm consisted of brick particles of size passing through 4.75 mm and retaining on 2.36 mm. This layer consisted of bricks which has a large amount
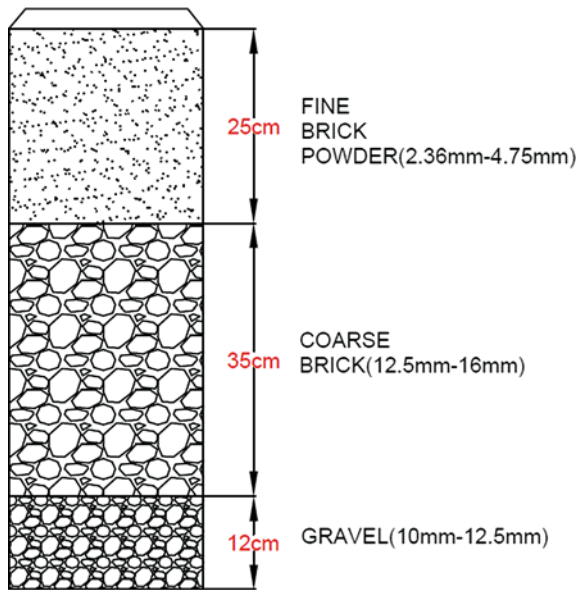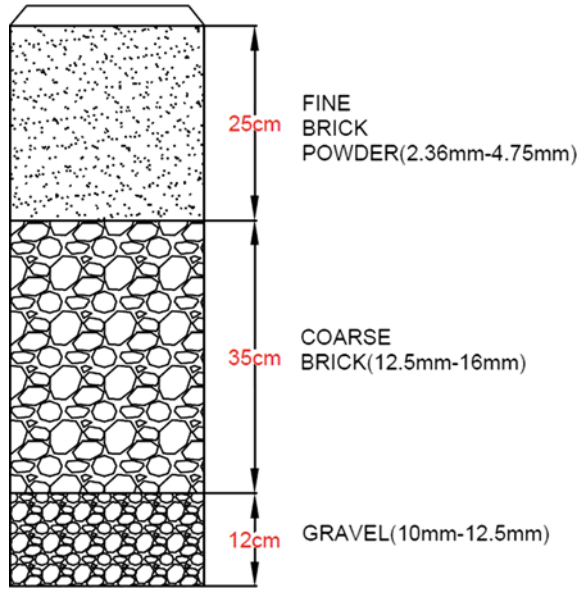

Fig. 3 Cross section of stage 1—sand filter.

of lime and thus helps in reducing the acidity and also due to porosity the TDS was also reduced. The cross segment is as shown in Fig. 4.

Third Stage (Charcoal Filter): The bottom most layer consisted of gravel for avoiding blockages in the pipe connections. The middle layer had charcoal of size retaining on 12.5 mm and passing through 20 mm. The cross section of the charcoal tank was as shown in Fig. 5.

The top layer had crushed charcoal particles. This charcoal consists of high carbon content. The charcoal was used to remove the alkalinity, dissolved and suspended solids, conductivity, etc. In this trail the flow rate was maintained and no overflow of the tanks was observed. Thus, this combination was finalized.

2.3 Constructed Wetlands (CWs)

The wetlands are constructed in order to reduce the nitrogen and phosphorus. The area was decided according to UN-HABITATS Journal of Greywater treatment.

2.3.1 Surface Area of Constructed Wetlands

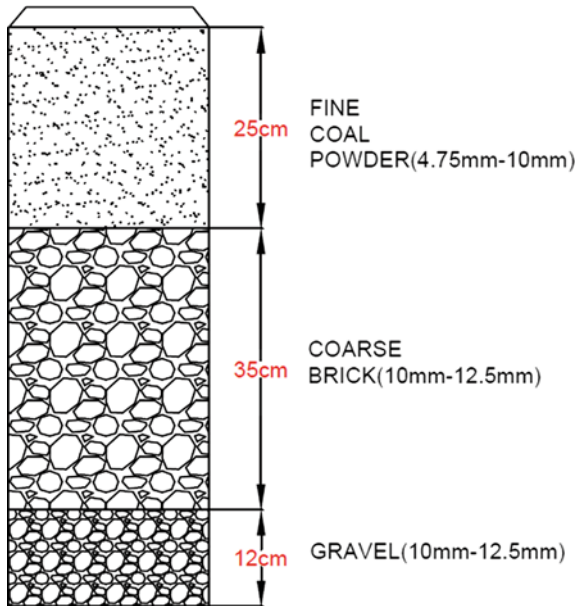The area was calculated as per the UN-HABITATS given by the empirical equation stated below.

Fig. 5 Cross segment of stage 3—charcoal filter

A = Qd (lnCi–lnCe)/KBOD.

Where

Ci = Influent BOD5 mg/day.

Ce = Effluent BOD5 mg/day BOD rate constant KBOD = 0.23 mg/day.

Flow rate (Q) per day by 8 persons = 100*8/1000 = 0.8 m3/day.

Therefore, surface area of constructed wetland.

A = 0.8*(ln 50 –ln 20)/ 0.23.

n = 3.187 m2.

Thus, an area of 3.2 m2 was provided. The surface area of the constructed wetland was as shown in Fig. 6
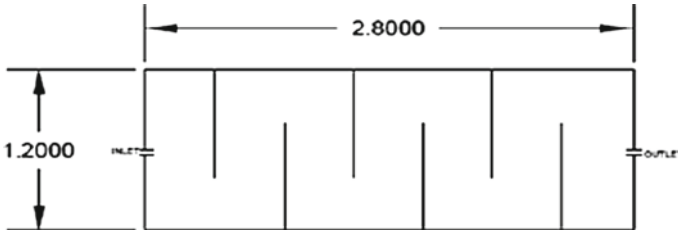
Fig. 6 Line sketch of secondary treatment

3 Results and Discussion

3.1 Grey Water Characterization

To assess the practicality of the Integrated in the vicinity Gray Water Treatment System, an examination was done. The progressions in the dim water quality boundaries after each phase of treatment were considered. The dark water tests at each stage are as demonstrated in Fig. 7.

The normal dark water quality trademark subtleties after each stage are as referenced in Table 1. The outcomes showed that BOD5/COD proportion is in the scope of 0.46–0.733 demonstrating managability of dark water for organic treatment. It can likewise be seen that the nature of crude dark water was uniform all through the investigation period. Be that as it may, the central point of contention to be noted with respect to biodegradation of natural matter is the supplement unevenness. The

Fig. 7 Water sample collected at each stage

Table 1 Characteristics of raw and treated grey-water

Sr. no	Parameters	Stage 1	Stage 2	Stage 3	Stage 4	Stage 5
1	pH	7.31 ± 0.34	7.45 ± 0.6	7.36 ± 0.5	7.27 ± 0.3	7.20 ± 0.22
2	Acidity (mg/L)	23.27 ± 1	19.33 ± 1	15.66 ± 1	12.11 ± 1	9.5 ± 1
3	Alkalinity (mg/L)	124.78 ± 8	110.89 ± 4	102.89 ± 4	93.33 ± 4	84.55 ± 5
4	Chloride (mg/L)	83.66 ± 1.07	76.2 ± 1.9	68.98 ± 4	62.03 ± 2.9	56.52 ± 2.22
5	BOD_5 (mg/L)	53.91 ± 2.5	44.61 ± 0.3	34.22 ± 2	27.52 ± 0.2	22.75 ± 1
6	COD (mg/L)	98.81 ± 2.1	85.65 ± 1.5	76.52 ± 2.8	67.77 ± 1	62.34 ± 1.4
7	TKN	19.8 ± 1.4	18.2 ± 1	16.2 ± 0.1	14.8 ± 0.8	5.3 ± 0.6
8	Turbidity (NTU)	66.51 ± 4.5	51.65 ± 6.5	36.71 ± 6.2	22.42 ± 3.7	12.05 ± 0.12
9	Phosphorus (mg/L)	2.6286 ± 0.2	2.3 ± 0.1	1.87 ± 0.1	1.5 ± 0.1	0.6 ± 0.1

outcome demonstrates that there is slight lopsidedness between carbonaceous matter and supplements. The other trademark showed that the dim water is almost nonpartisan, low in ionic strength, and turbidity. The line of treatment for this quality ought to incorporate expulsion of suspended solids, natural matter and supplements. The normal worth of dim water quality boundaries after each phase of essential treatment and the auxiliary treatment are as referenced in Table 1.

The significant boundaries of the investigation were COD, BOD, nitrogen and phosphorus. The evacuation proficiency of dark water quality boundaries in the essential stage, optional stage and absolute effectiveness of incorporated plant is referenced in Table 2. The pressure driven stacking was extremely high in the first part of the day hours because of the understudies finishing their everyday tasks, for

Table 2 Percentage removal of parameters in treatment process

Parameter	Primary treatment (%)	Secondary treatment (%)	Over-all efficiency of removal (%)
BOD_5	50.00	18.00	58.00
COD	32.00	8.10	37.00
Phosphorus	43.07	60.00	77.17
Nitrogen	25.00	65.00	73.00
Acidity	47.95	21.55	59.18
Alkalinity	25.20	9.40	32.23
Turbidity	66.29	44.15	81.87
Chloride	25.82	8.89	32.41

example, brushing and washing towards the beginning of the day hours which will add to the dim water. It tends to be obviously seen from Table 2 that the evacuation of BOD, COD and Turbidity was exceptionally high in the essential treatment though the expulsion of nitrogen, phosphorus and turbidity was in the auxiliary treatment.

3.1.1 Primary Treatment

The main parameters that were removed in the primary treatment are COD, BOD, turbidity, acidity, alkalinity and Total Dissolved Solids. The results and the removal efficiency of each parameter are as mentioned below.

3.1.2 Biochemical Oxygen Demand (BOD$_5$)

In the essential treatment because of most extreme air voids present in the changes layers of sand, bludgeons, charcoal the oxygen get blended in the dark water hence lessening the BOD. The phases of BOD evacuation of BOD are as demonstrated in Fig. 8. It tends to be seen from Fig. 8 that the BOD rate is not uniform in the two phases. In the primary stage it is more whereas in secondary stage the removal rate decreases. In primary treatment the removal of BOD$_5$ is half and in optional treatment the expulsion of BOD$_5$ is 18%. The BOD/COD proportion in the influent went from 0.36 to 0.54 demonstrating that the crude sewage is genuinely biodegradable and can be viably treated. Figure 8 demonstrates the progressions in influent and gushing grouping of BOD$_5$.The BOD has been adequately diminished on account of the microbial layer around the rock, bludgeons and charcoal as they burn-through the natural matter from the dark water by using the oxygen from the voids. BOD5 is a


Fig. 8 Stage-wise BOD removal
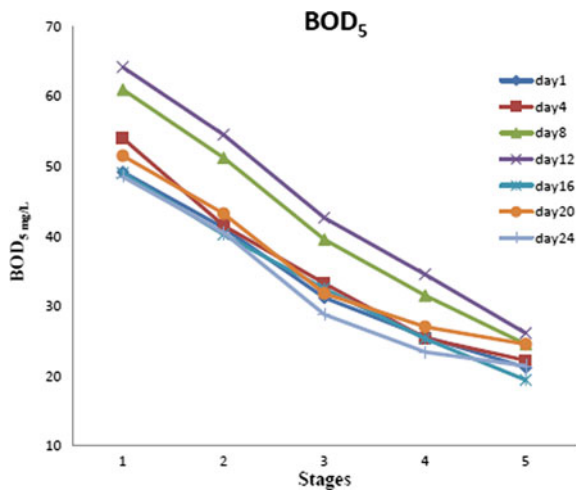
percentage of the amount of oxygen required by high-impact animals to break down natural materials in water. Expulsion of the solvent BOD5 occurs in constructed wetlands as a result of microbial growth attached to plant roots, stems, and leaf litter that have fallen into the water. Because green growth is absent with entire plant inclusion, water surface re-air circulation provides considerable oxygen sources for these reactions, notwithstanding plant transport of oxygen from the leaves to the rhizosphere (thin district of soil straightforwardly affected by roots). Attached and suspended microbial is responsible for the evacuation of dissolvable natural mixes that are contaminated organically both violently and anaerobically. Poisons are removed from the wetlands via a number of complicated physical, synthetic, and organic processes.

3.1.3 Chemical Oxygen Demand (COD)

The COD is generally referred to total organic and inorganic matter present in the water. The inorganic matter present in grey water was higher than the organic matter due to non-mixing of organic waste such as sewage, vegetables, and food as the grey water was collected from the hostel building. The removal of COD was higher in the primary stage compared to that in secondary stage. The removal of COD in each stage is as shown in Fig. 9.

The heavier inorganic matter of large size was trapped in the upper layer of each stage due to the less air voids in the upper layer. The small inorganic matter gets reduced in the sand, brick, charcoal layer due to absorption of water in each layer and while expulsion of water out of the brickbats the water was removed but the dissolved inorganic impurities gets trapped in each layer. In primary treatment maximum air voids are present because this oxygen get mixed into the grey-water and COD value get reduces. The values of COD of untreated and treated samples are shown in Table 1. The high substance of absolute disintegrated solids and complete suspended solids were answerable for higher synthetic oxygen interest (COD). It

Fig. 9 Stage-wise COD removal
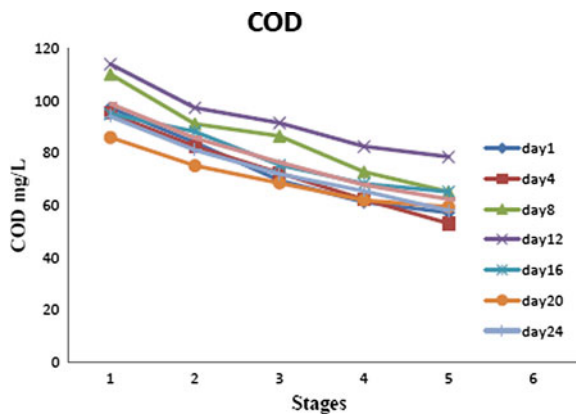
can be seen from Fig. 9 that the COD worth continues lessening consistently in both essential and auxiliary stage, yet the decrease is more in the essential treatment as the decrease of COD in essential treatment is 32% and in optional treatment is 8.1%.The COD evacuation in essential stage is more a result of sand, bludgeon and charcoal containing greatest voids and along these lines helping the blending of oxygen to diminish the natural matter and more modest air voids in the upper layer prompts decrease the inorganic matter.

Turbidity

Table 1 describes the stage-by-stage elimination of turbidity. The turbidity of a sample is determined by the number of contaminants present. The higher the concentration of garbage, the higher the turbidity. After the first week of therapy, the turbidity had decreased. However, when handled with sand, brickbats, and a charcoal filter, the turbidity was decreased from 80.2 NTU to 6 NTU. According to BIS standards for treated grey water, turbidity of treated grey water treatment, turbidity of treated samples should be less than 10 NTU (Environment Agency, 2011), and the findings demonstrated a considerable increase in greywater quality. Figure 10 shows that the turbidity reduction efficiency in primary treatment is 66.49 percent and 44.15 percent in subsequent treatment. Because of the tiny size of the air gaps in the top layers of sand, bricks, and charcoal layer, turbidity is eliminated. Turbidity was decreased in subsequent treatment due to hydraulic retention time and subsurface flow. In primary and secondary treatment, all dissolved and suspended particles are eliminated, reducing turbidity. The tiny layers at each level of primary treatment retained all colloidal particles, significantly lowering turbidity in the primary stage.
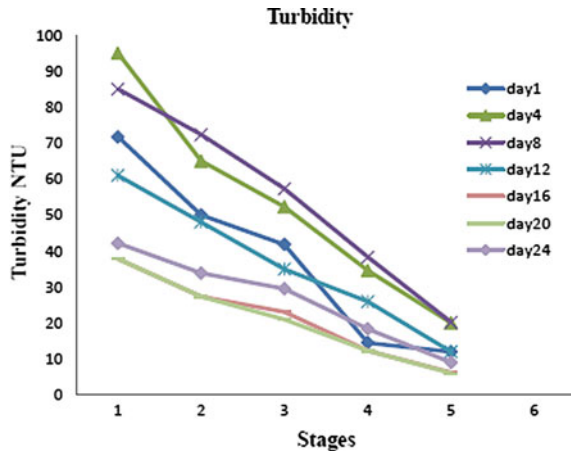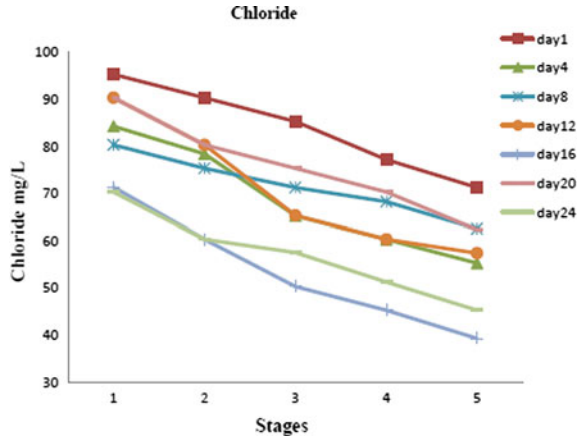

Fig. 10 Stage-wise turbidity removal

Fig. 11 Stage-wise chloride removal

3.1.4 Chloride

Because urine and waste water mingle, the chloride concentration of grey water rises. While microorganisms devour the treated sample in the rhizosphere, the chloride content is lowered to 2.1 mg/L following treatment. According to BIS guidelines, the quantity of chloride in treated grey water should be less than 2 mg/L, but it should be less than 0.5 mg/L for garden reuse. Figure 11 shows that the elimination of chloride is 25.82 percent in the main treatment and 8.89 percent in the subsequent treatment. The elimination of chloride was not as effective as planned.

3.1.5 Alkalinity

Alkalinity is an essential characteristic, and a rise in alkalinity may be caused by the presence of several ions in the soil, such as carbonate, bicarbonate, and hydroxide. In our investigation, the average alkalinity of the untreated samples was 137 mg/L, whereas the treated samples had a value of 60 mg/L. The alkalinity of grey water is caused by the soap in the water, which is naturally alkaline. The alkalinity of the water steadily decreases at each step as soap particles get caught in each layer, lowering the alkalinity of the water. Figure 12 depicts the progressions of alkalinity convergence in influent and gushing. The alkalinity evacuation productivity in necessary treatment was 25.20 percent, whereas it was 9.40 percent in optional treatment. Because there was no microbial layer organisation, there were no changes in alkalinity in the first fourteen days. Following fourteen days, when the microbial layer forms and is coated by coal particles, it becomes acidic in nature and so effectively aids in the lowering of alkalinity. The nitrogen and phosphorus from the water are also removed in the auxiliary treatment, which is a part of the cleaner, lowering the alkalinity in the optional treatment as well.

Fig. 12 Stage-wise
alkalinity removal
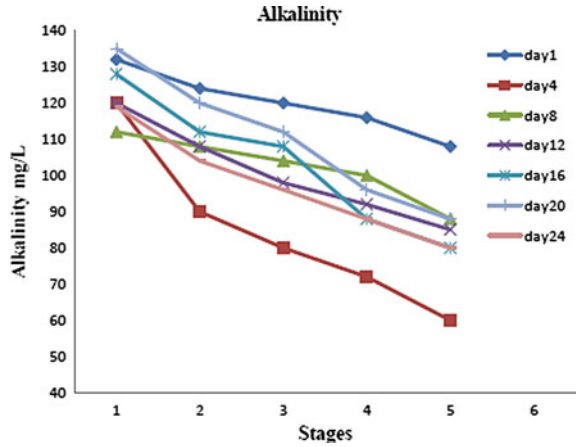
3.1.6 Acidity

The acidity in the grey water was very little due to the alkaline nature of grey water.
The removal of the acidity at each stage is as shown in Fig. 13. In general, when
basic substances added to an acidic substance the base reacts with the acid to reduce
the acidity and neutralize the sample. In the same way due to high alkalinity in the
grey water the acidity of the raw grey water was nearly about 25 mg/L. The treatment
was seen in the primary treatment due to the presence of the brickbats. The bricks
are made from the lime material which is alkaline in nature and thus reacts with the
acidity and helps in reducing it. The acidity also reduces in the secondary stage due
to the alkaline nature of the black cotton soil used in the constructed wetlands.

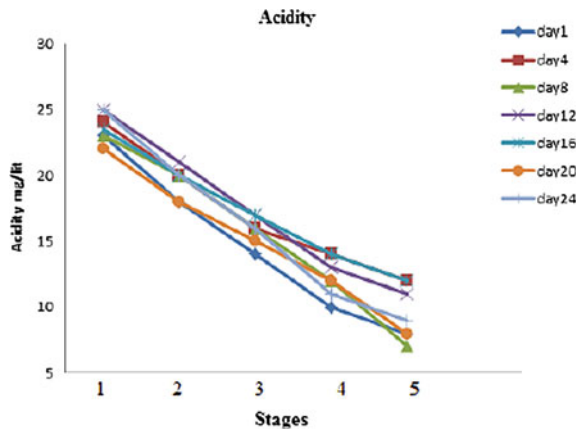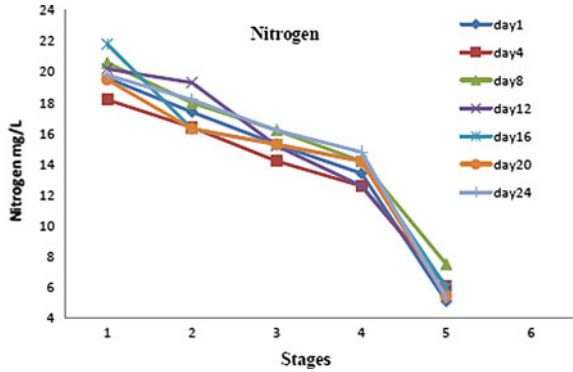**Fig. 13** Stage-wise acidity
removal

Fig. 14 Stage-wise nitrogen removal

3.2 Secondary Treatment

The important parameters that were studied in the secondary stage are the removal of nitrogen and phosphorus. Although the BOD was also considerably reduced in the secondary treatment, it has been explained in Sect. 3.2.1.

3.2.1 Nitrogen

In essential treatment in general expulsion of nitrogen is under 25% and in optional treatment the evacuation of nitrogen is 65%. The variety of influent and profluent Nitrogen in Constructed Wetland framework was concentrated all through the period. Dim water filtration components in built wetland are accomplished by miniature organic entities around the root zone. From Fig. 14, it is seen that the normal evacuation of nitrogen is 73% in wetland. Canna-indica plants retain nitrogen for their development and accordingly help in evacuation of nitrogen. The horizontal stream design was utilized in the built wetland stream to permit water to remain in the wetlands for a more drawn out timeframe and accordingly helping in nitrogen expulsion. The evacuation components for nitrogen in developed wetlands are complex and incorporate volatilization, ammonification, nitrification/de-nitrification, and plant take-up and grid adsorption (Fig. 15). The significant evacuation system in the vast majority of the built wetlands is microbial nitrification/de-nitrification. Alkali is oxidized to nitrate by nitrifying microbes in oxygen consuming zones. Nitrates are changed over to di-nitrogen gas by denitrifying microscopic organisms in anoxic and anaerobic zones.

3.2.2 Phosphorus

The general effectiveness of phosphorus in essential stage is 43% and in optional stages it is 60%. The variety of influent and profluent phosphorus in Constructed

Fig. 15 Nitrogen transformations in constructed wetlands
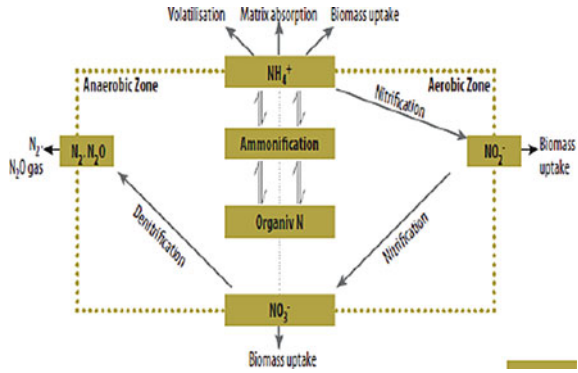
Wetland framework was concentrated all through the period. The treatment of phosphorus in each stage is as demonstrated in Fig. 16. The canna indica plants assume a huge part in the evacuation of phosphorus.

The major process responsible for phosphorus removal in constructed wetland is the sub-surface flow stage. Phosphorus is an essential requirement for biological growth. An excess of phosphorus can have secondary effects by triggering eutrophication within a wetland, leading to algal blooms and other water quality problems. Phosphorus removal in wetlands is based on the phosphorous cycle and can involve a number of processes. Primary phosphorus removal mechanisms include adsorption, filtration and sedimentation. Other processes include complexation/precipitation and assimilation. Particulate phosphorus is removed by sedimentation, along with suspended solids. The configuration of constructed wetlands provides extensive uptake by Biofilm and plant growth, as well as by sedimentation and filtration of suspended materials. Phosphorus is stored in the sediments, biota, (plants, Biofilm and fauna), detritus and in the water. The rapid growth of the canna indica plants shows the effective removal of nitrogen and phosphorus from grey water. The plants need the nitrogen and phosphorus for their growth. The growth of the plants was

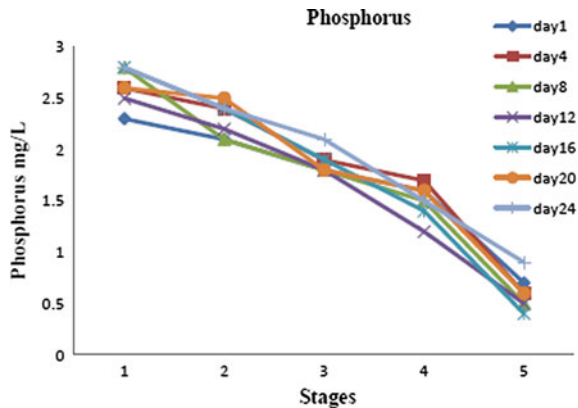**Fig. 16** Stage-wise phosphorus removal

Fig. 17 The rapid growth of Canna Indica plants

very fast, and the plants were well suited to the environment within duration of 2 to 3 weeks. The growth of canna indica plants at every week of the study is as shown in Fig. 17.

As the study was made for 8 students, thus in this way it can be seen that the removal of all parameters in the complete treatment is very impressive and can be used for household application. The treated water also can be used for the purposes like flushing and gardening in the houses.

3.3 Advantages and Disadvantages of Primary Treatment

3.3.1 Advantages of Primary Treatment

A primary grey water treatment system needs less acreage and provides for more control over the grey water treatment process. CWs that discharge to surface water, for example, need 4–10 times the land size of a basic grey water treatment plant. As a result, the efficiency is less responsive to environmental factors. This initial filtering process might result in more consistent effluent quality.

3.3.2 Disadvantages of Primary Treatment

The fundamental downside of basic grey treatments is their expensive construction and maintenance costs. Construction costs are typically one-tenth to one-half of those of comprehensive treatment systems. Every month, the top layers must be scrapped because particles get blocked in the upper voids. As a result, the expense of maintenance is substantial.

3.4 Limitations of Constructed Wetland

There are different restrictions of the built wetlands of which the most significant are noted beneath.

3.4.1 Evaporation

The evaporation of water is a major problem in the constructed wetlands in Solapur, India. The temperature in Solapur in summers varies from 40 ± 60 °C. The evaporation losses are very high during this period and may be of about 22 to 30%. This results in lower discharge at the end of the constructed wetlands.

3.4.2 Precipitation

During the monsoon season due to the precipitation the flow in the wetlands will increase which in turn increases the flow rate and mixing of rainwater and grey water. This problem may not be generally encountered in Solapur region due to a very less rainfall but may generally affect the high precipitation zones.

4 Conclusions

In this study Integrated On-site Grey Water Treatment System (IOGTS) consisting of gravity down flow filtration system as primary treatment whereas constructed wetlands as secondary treatment was used. The primary filtration consisted of three stage filtration processes, consisting of sand, brickbats and charcoal in each stage respectively. Each of these stages consisted of particles of various effective sizes of varying thickness of layer. The conclusions that can be drawn are as follows:

1. There was effective removal of various parameters such BOD (50%), COD (32%), turbidity (66.29%), alkalinity (25.20%), acidity (47.95%) and chloride (25.82%) in the primary treatment.

2. The upper layer in each primary stage was very useful for the removal of turbidity. Due to small size the colloidal particles get trapped in the upper layer.
3. The BOD and COD in the grey water reduces in each stage due to the microbial growth attached on the surface of the filter media, which in presence of the oxygen reduced the organic matter from the water.

The secondary treatment was done by using the canna indica plants. The vegetation played an important role in the grey water treatment. The various conclusions that can be drawn from the obtained results are as follows:

1. The removal of efficiency for nitrogen is 65% and that for phosphorus is 60%.
2. The root zone played important role in the removal of these parameters from the grey water.
3. The BOD also reduced in this layer due aerobic layer in the root zone of the plants.

Overall removal efficiency of various parameters by integrated wetland system are as follows:

1. The BOD removal efficiency by integrated wetland system is 58%.
2. The COD removal efficiency by integrated wetland system is 37%.
3. The phosphorus removal efficiency by integrated wetland system is 77.17%.
4. The nitrogen removal efficiency by integrated wetland system is 73%.
5. The turbidity removal efficiency by integrated wetland system is 81.87%.
6. The acidity removal efficiency by integrated wetland system is 59.18%.

IOGTS dependent on eco-accommodating innovation was discovered to be vigorous, savvy, proficient, effectively operable (viable) and least automated alternative for dim water treatment. Activity of IOGTS for longer length showed that it is a supportable framework.

The advantages of dim water reusing include the following: Reduced utilization of new water, less strain on septic tanks or treatment plants, more successful cleansing, achievability for locales inadmissible for a septic tank, diminished utilization of energy and synthetics, ground water re-energize, plant development, recovery of supplements, expanded mindfulness and affectability to nonpartisan cycles each day. In the forthcoming days because of water shortage this kind of treatment frameworks may end up being useful.

References

1. Akratos CS, Tsihrintzis VA (2007) Effect of temperature, HRT, vegetation and porous media on removal efficiency of pilot-scale horizontal subsurface flow constructed wetlands. Ecol Eng 29(2):173–191
2. Bouchaib H, Bey I, Douch A, Ghazi N (2008) Greywater treatment and recycling for toilet flushing: comparison of low and high tech treatment approaches. Water Pract Technol 3(2)
3. Lee C, Fletcher T, Sun G (2009) Nitrogen removal in constructed wetland systems. Eng Life Sci 9(1)

4. Langergraber G, Leroch K, Pressl A, Rohrhofer R, Haberl R (2009) A two-stage subsurface vertical flow constructed wetland for high-rate nitrogen removal. Water Sci Technol

5. Yalcuk A, Ugurlu A (2009) Comparison of horizontal and vertical constructed wetland systems for landfill leachate treatment, bioresource technology 100(9)

6. Konnerup D, Koottatep T, Brix H (2009) Treatment of domestic wastewater in tropical, subsurface flow constructed wetlands planted with Canna and Heliconia. Ecol Eng 35(2):248–257

7. Vymazal J (2010) Constructed wetlands for wastewater treatment. Water 2(3)

8. Avila C, Salas JJ, Martin I, Aragon CA (2013) Integrated treatment of combined sewer wastewater and stormwater in a hybrid constructed wetland system in southern Spain and its further reuse. Ecol Eng 50

9. Avila C, Garfi A, Garcia J (2014) Three-stage hybrid constructed wetland system for wastewater treatment and reuse in warm climate regions. Ecol Eng 61

10. Saumya S, Akansha S, Rinaldo J, Suthindhiran K (2015) Construction and evaluation of prototype subsurface flow wetland planted with Heliconia angusta for the treatment of synthetic greywater. Environ Sci J Clean Prod. https://doi.org/10.1016/J.JCLEPRO.2014.12.019,CorpusID: 155021469

11. National Environmental Engineering Research Institute (NEERI) (2007) Greywater Reusein Rural Schools − Guidance Manual

12. Sonavane PG, Munavalli GR, Ranade SV (2007–08) Feasibility of constructed wetland treatment system for septic tank effluent. J IPHE India 3:32–36

13. Bindu T, Sylas VP, Mahesh M, Rakesh PS, Ramasamy EV (2008) Pollutant removal from domestic wastewater with Taro (Colocasia esculenta) planted in a sub surface flow system. Ecol Eng 33(1):68–82

14. Patil YM, Munavalli GR (2016). Performance evaluation of integrated on-site grey water treatment system in a tropical region. Ecol. Eng. 95:492–500

15. Graaff M, Temmink H, Zeeman G, Buisman C (2010) Anaerobic treatment of concentrated black water in a UASB reactor at a short HRT. ResearchGate. https://doi.org/10.3390/w20 10101

Application of Nano Technology in Waste Water Treatment

Komal P. Mehta [ID]

1 Water Treatment and Nanotechnology

Availability of good quality water is going to be a great challenge in coming century. All water supply practices are facing challenges. More than 700 million are lacking for availability of drinking water as per minimum daily requirement. The regularization in standard of quality of water has given new vision to the existing water treatment and distribution systems. Increase in population and change in climate are adding pressure on water sources. The water and waste water technologies currently in practice have limitation for providing good quality of water with least disturbance in environment. It is expected that use of nano technology will provide highly efficient techno economical solution for waste water treatments.

A nanometer is 10^{-9} at which scale, size dependent properties of materials can be different from their large counterparts. Size can be beneficial property for application in waste water treatment. The process of photosynthesis in which plants convert carbon dioxide into energy is best example which can be related to chloroplasts, tiny structures made up of many nano scale thylakoid disks containing chlorophyll. Enzymes that catalyze chemical reactions are also examples of nano technology available in nature. Some user specific characteristics like surface area, reactivity, sorption, etc. are providing advantage of its usage. Other beneficial characteristics are quantum confinement, super paramagnetism, surface Plasmon resonance which are discontinuous properties, e.g., nano magnetite for removal of heavy metals—large surface area to volume ration, for advanced oxidation and reduction processes hypercatalysts—enhanced catalytic property, disinfection—antimicrobial, self-cleaning and repairing—multi functionality, surface structure to decrease adhesion—self-assembly, and nano electrode—high conductivity [1].

K. P. Mehta (✉)
Professor (Dr.) Civil Engineering Department, Drs. Kiran and Pallavi Patel Global University, KPGU, Vadodara, Gujarat, India

1.1 Nano-Adsorbents

Adsorption can be used for removal of all types of contaminants for water and waste water treatment. Adsorbents has limitation of surface area or active sites; sorption kinetics and less possibility of selection are available. Nano-adsorbents give more efficiency as it can give more surface area, less distance of inter particle diffusion, by high specific surface area and sorption sites, short intra-particle diffusion distance, and pore size.

1.1.1 Organic Removal

On adsorption of organic chemicals, carbon nano adsorbents are better than activated carbon is proved (Pan and Xing 2008). Due to more surface area and diversified interactions, increase in efficiency is achieved. The outer surfaces can be considered as area of adsorption by CNTs [2]. Adsorption is more for polar organic compounds due to diversified pollutants by CNTs. It has a tendency to aggregate in aqueous solution and leave molecules of water, post exposure prophylaxes interactions, bonding of hydrogen atoms, and also electrostatic interactions [2]. Adsorption of positively charged elements like antibiotics can be more as it can be attracted by the electrostatic interactions [3].

1.1.2 Removal of Heavy Metal

With metal ions, CNTs show high adsorption and fast kinetics. It happens mainly due to surface functional groups through electrostatics attraction and chemical bonding [4] due to which CNT adsorption capacity is increased due to surface oxidation. Research data confirms that CNTs are good adsorbents compared to activated carbon for heavy metals like Cu2þ, Pb2þ, etc.

1.1.3 Regeneration and Reuse

Cost of adsorption is dependent on regeneration. Reverse of CNT adsorption is possible by reducing the solution pH which can recover 90–100% metals [5]. In majority case studies, the adsorption capacity of it is maintained efficiently after several cycles of regeneration and reuse while few cases showed reduction also in adsorption after regeneration.

1.1.4 Metal Based Nano-Adsorbents

Sorption is dependent on dissolved metals and oxygen in metal oxides [6]. Once, adsorption of metal ions on outer surface followed by, intra particle diffusion with micro pore walls. They show good adsorption, rapid kinetics, less intraparticle diffusion distance, and larger number of surface reaction sites.

1.1.5 Polymeric Nano-Adsorbents

Dendrimers are invention of polymeric materials. They are capable of removing both organics and heavy metals as they are tailored adsorbents. They are having many branches and single dispersion macromolecules. There materials have high impact on properties (physical and chemical) due to their structure. For sorption they have hydrophobic interior shells. For adsorption of heavy metals they have tailored exterior branches.

2 Potential Application in Water Treatment

Due to advancement in the quantum world, new treatment processes adapted in practice are adsorption, catalytic degradation, and nano filtration. Because of increase in population, drought, and pollution of existing sources of water, application of nano technology in water treatment is increasing. More than 1 billion people do not have good quality water for usage, and more than 2 billion people do not have water for daily use, WHO (2004). In last 50 years new methods are found for water treatment for making it available for people with improved quality. There are mainly three membrane processes which include Reverse Osmosis, Ultra filtration, Microfiltration. In last 100 years membranes of nano filtration are developed as filter material between ultra filtration and reverse osmosis. Their applications are increasing for treatment of water, waste water, surface water, sea water, groundwater, etc.

3 Membranes and Membrane Processes

Water treatment is required for removal of pollutants from it. As per size of pollutants, membranes provide a layer which works as obstruction. They can provide automation, less land and chemicals utilization, flexible design due to modular configuration which makes its use possible as a key component [7]. Requirement of energy consumption is high, and it is a barrier for its wide application in membrane processes. As per provision of material of membrane, its performance can be decided. Addition of nano materials in manufacturing of membranes increases permeability,

Table 1 Membrane separation processes

Type of membrane	Pore size (nm)	Pressure (Bar)	Product water
Reverse osmosis	<0.6	30–70	Pure water
Nano filtration	0.6–5	10–40	Pure water and low molecular solutes
Ultra filtration	5–50	0.5–10	All above and macro molecules
Mocro filtration	50–500	0.5–2	All above and colloids

fouling resistance, and mechanical and thermal stability, and it can also contribute for decrease in contaminants and self-cleaning if filter (Table 1).

3.1 Nano Fiber Membranes

With complex pore structures nano fibers can prepare nano mats due to high surface area and porosity of nanofibers. Characteristics of electrospun nano fibers can be altered like diameter, morphology, composition, secondary structure, and spatial alignment. Without significant fouling, nanofiber membranes can remove smallest particle with great efficiency. Nano fibers are used for making multi-functional media/membrane due to its properties which includes use of materials like TiO2.

3.1.1 Nano Composite Membranes

Researchers have tried addition of nano materials into membranes for creating multi-functional effect on nano technology in membranes. By increasing hydrophilicity of the membrane, fouling can be reduced which is main purpose of addition of hydrophilic metal oxide. Membrane surface hydrophilicity, fouling resistance, and water permeability can be increased due to addition of metal oxide nano particles like alumina, silica [8], zeolite [9], and TiO2. Addition of inorganic nano particles increases mechanical and thermal stability of polymeric membranes, and negative effect on compaction and heat on membrane permeability is reduced [9]. Efforts are made to develop photo catalytic inorganic membranes consisting of nano photo catalysts (normally nano-TiO2 or modified nano-TiO2).

3.1.2 Thin Film Nano Composite (TFN)

Development of TFN emphasizes on addition of nano materials into the active layer of thin film composite (TFC) membranes through casting solutions or surface modification. Factors like permeability, negatively charged ion, etc. can be increased due to addition of nano zeolites [10]. Compared to available RO membranes, these membranes shows efficiency of doping at 0.2 % wt. With 250 nm nano zeolites with higher permeability and better salt rejection (>99.4%) than RO membranes are available in market [11]. This technology is awaiting for commercialization. Addition of nano-TiO2 (up to 5 wt%) in to the TFC active layer has increased the rejection of membrane with maintenance of the permeability. Rise in cost is because of water flux, defect formation in nano-TiO2.

3.1.3 Biologically Inspired Membranes

These are permeable and very selective. Aquaporins are the protein channels for regulating the flux of water across membranes. It is used in polymeric membranes due to its characteristics of high selectivity and water permeability which can improve efficiency of membrane. For production of more water permeability E-coli has been incorporated into polymer vesicles.

3.1.4 Forward Osmosis

To get water from low to high osmotic pressure, FO uses osmotic gradient, after which the diluted solution is treated by Reverse Osmosis to receive pure quality of water. It gives benefits compared to RO that membrane is less prone to fouling, and it can work even at low pressure. Forward Osmosis has drawn solute which is easily separable from water. References show that to recover draw solute through flocculation magnetic nanoparticles were used [12].

4 Photo Catalysis

For removing residual pollutants and microbial pathogens, advanced oxidation process such as Photocatalytic oxidation is in process. Photocataytic oxidation enhances biodegradability as it can remove hazardous and non-biodegradable pollutants. It can be used as a first step for removal of organic compound. Main problem is kinetics because of limited light fluency and photocatalytic activity.

4.1   Nano-Photocatalyst

TiO2 optimization is very widely used as due to less toxicity, less cost, and chemical stability in treatment of water and waste water. It produces an electron/hole (e/hþ) pair as it absorbs a UV photon. Nano TiO2 increases photo activity with optimization of particle size, shape by noble metal doping, maximizing reactive facets, treatment of surface to increase contaminant adsorption. TiO2 photocatalysis is the end result of process of fast recombination of e, and hþ is cause of its kinetic reaction.

4.1.1   Potential Applications in Water Treatment

The factors to decide efficiency of treatment of water are configuration and operation parameters of the photo-reactor. Most commonly used TiO2 reactors are Slurry reactors. Catalyst immobilization accelerates its efficiency. Effects of TiO2 loading, pH, temperature, DO, contaminant type, light wavelength, and intensity are under observation. Nano-TiO2 facilitated solar disinfection (SODIS) is tested greatly, and it seems as it is safe option to give pure quality water in remote areas.

4.1.2   Disinfection and Microbial Control

The confusion between effective disinfection and formation of toxic disinfection by-products (DBPs) holds a great challenge for water industry. Research findings support the formation of toxic DBPs with use of various disinfectants, such as chlorine and ozone (e.g., halogenated disinfection byproducts, carcinogenic nitrosamines, bromate, etc.). The known option is due to its capacity of producing minimal DBPs with challenge of requirement of high dosage for some viruses (e.g., adenoviruses). These challenges urge the development of alternative methods that can enhance robustness of disinfection by avoiding DBP formation. Review on antimicrobial nano materials has highlighted the potential of nano technology in disinfection and also microbial control.

4.1.3   Antimicrobial Mechanisms

Most famous antimicrobial nano material is Nano-Ag in current era. It possess strong anti-microbial activity, wide antimicrobial spectrum, lower toxicity which makes its use easy, and it can prove a promising choice for disinfection of water and microbial control. It is proved at lab scale research that antimicrobial activity of nano silver largely stems by released silver ions [13]. It can be bended to thiol groups resulting in damage of enzymes [14]. Because of capacity of DNA replication, silver ions can incorporate cell changes structurally [15]. Due to which release rate and bio availability for toxicity of silver nano ions (Ag) is critical. It has important role

in antimicrobial activity due to its physio chemical properties. Its properties like size, shape, coating, and crystallographic facet relates it to kinetics of silver ions. Its presence reduces toxicity, and its lower concentration increases E coli growth [13]. With use of disturbance of cell membrane, oxidative stress, disruption of oxidizing cellular structure in direct contact of bacterial stress leads to killing of bacteria by Carbon Nano Tubes [16, 17].

5 Monitoring

Till date most difficult task in the treatment of water and waste water is lack of ability to detect fast growing pathogens, lower concentration of some pollutants, toxicity, and complexity of pollutants in water/waste water. With characteristics of sensitivity and selectivity innovative sensors can be designed to get fast response which may be utilized for fat treatment.

5.1 Pathogen Detection

Lab scale experiments like coli form bacteria is quite time consuming, and it cannot detect some viruses (hepatitis A and E, coxsackieviruses, echoviruses, adenoviruses, and Norwalk viruses), bacteria (Legionella and Helicobacter), and protozoan (Cryptosporidium and Giardia) [18]. They are involved with drinking water, so they should be dealt with up most priority. Disinfection can be effectively carried out only if microorganisms are detected properly. For identification of nano materials and agents research is in progress and at lab scale sensor development is also taken care by many research institutes [17].

5.1.1 Trace Contaminant Detection

Because of high absorption capacity and fast kinetics carbon nano tubes can identify trace metal and organic pollutant. In newly developing areas or plants of water treatment it is possible to include technology of Nano materials for the same.

6 Concluding Remarks

Due to unique characteristics of nano materials and possibility of its combination with existing treatment in the field of water and waste water treatment, its acceptance is increased world wide. The discussed materials are proved or in research stage at lab scale and commercial applications still to be worked out. Based on

current proofs of application of nano materials, its actual applications will be as nonabsorbent, nano technology enabled membranes, and nano photo catalysts, in construction, paint, coating, components of water and waste water treatment plant. Even though few products are available in market, its large scale usability is not at wide acceptance level. In POU systems also nano materials can be applied. The limitations to implement at large scale are temporary which includes its cost, risk to env., etc. It is expected that for solving such limitations research institutes, industries, government, etc. will hold hand together.

References

18 Mehta KP (2016) Nano technology in water treatment. Int J Eng Res Manag (IJERM) 03(7). ISSN:2349-2058

 1 Yang LX, Chen BB, Luo SL, Li JX, Liu RH, Cai QY (2010) Adsorption of organic compounds by carbon nanomaterials in aqueous phase: Polanyi theory and its application. Chem Rev 110(10):5989e6008

 2 Fujishima A, Zhang XT, Tryk DA Ion exclusion by sub-2-nm carbon nanotube pores

 3 Ge QC, Su JC, Chung TS, Amy G (2011) Engineered graphite oxide materials for application in water purification. ACS Appl Mater Interfaces 3(6):1821e1826

 4 Kelly KL, Coronado E, Zhao LL, Schatz GC (2003) Supported lipid bilayer membranes for water purification by reverse osmosis. Langmuir 26(10):7388e7395

 5 Koeppenkastrop D, Decarlo EH (1993) Preparation of nitrogen-substituted TiO(2) thin film photocatalysts by the radio frequency magnetron sputtering deposition method and their photocatalytic reactivity under visible light irradiation. J Phys Chem B 110(50):25266e25272

 6 Vecitis CD, Schnoor MH, Rahaman MS, Schiffman JD, Elimelech M (2011) Modeling Cd and Zn sorption to hydrous metal oxides. Environ Sci Technol 34(11):2215e2223

 7 Peter-Varbanets M, Zurbrugg C, Swartz C, Pronk W (2009) Using nanocomposite materials technology to understand and control reverse osmosis membrane compaction. Desalination 261(3):255e263

 8 Pendergast MTM, Nygaard JM, Ghosh AK, Hoek EMV (2010) A review of water treatment membrane nanotechnologies. Energy Environ Sci 4(6):1946e1971

 9 Lind ML, Jeong BH, Subramani A, Huang XF, Hoek EMV (2009) Influence of zeolite crystal size on zeolitepolyamide thin film nanocomposite membranes. Langmuir 25(17):10139e10145

10 Lind ML, Suk DE, Nguyen TV, Hoek EMV (2010) Effect of mobilecation on zeo- lite-polyamide thin film nanocomposite membranes. J Mater Res 24(5):1624e1631

11 SB, Zeng TH, Hofmann M, Burcombe E, Wei J, Jiang RR, Kong J, Chen Y (2011) Enhanced visual detection of pesticides using gold nanoparticles. J Environ Sci Health Part B-Pestic Food Contam Agric Wastes 44(7):697e705

12 Xiu ZM, Zhang QB, Puppala HL, Colvin VL, Alvarez JJP (2011) Differential effect of common ligands and molecular oxygen on antimicrobial activity of silver nanoparticles versus silver ions. Environ Sci Technol 45(20):9003–9008

13 Liau SY, Read DC, Pugh WJ, Furr JR, Russell AD (1997) Competitive adsorption of Pb2þ, Cu2þ and Cd2þ ions from aqueous solutions by multiwalled carbon nanotubes. Carbon 41(14):2787e2792

14 Kim J, Lee CW, Choi W (2010) The optical properties of metal nanoparticles: the influence of size, shape, and dielectric environment. J Phys Chem B 107(3):668e677

15 ZY, Bai HW, Lee J, Sun DD (2011) Anatase TiO(2) with dominant high-energy {001} facets: synthesis, properties, and applications. Chem Mater 23(18):4085e4093

16 Vikesland PJ, Wigginton KR (2010) Electronic-structure-dependent bacterial cytotoxicity of single-walled carbon nanotubes. Acs Nano 4(9):5471e5479

17 Cloete TJ, de Kwaadsteniet TE (2010) A hybrid sorbent utilizing nano particles of hydrous iron oxide for arsenic removal from drinking water. Environ Eng Sci 24(1):104e112

19 MM Pendergast, EMV Hoek (2011) Adsorption mechanisms of organic chemicals on carbon nanotubes. Environ Sci Technol 42(24):9005e9013

20 Lin YH, Tseng WL (2010) Adsorption of phenolic compounds by carbon nanotubes: role of aromaticity and substitution of hydroxyl groups. Environ Sci Technol 42(19):7254e7259; 3944 Water Res 47:3931,e3946 (2013)

21 Kang S, Mauter MS, Elimelech M (2008) Antibacterial effects of carbon nanotubes: size does matter. Langmuir 24(13)

22 Maximous N, Nakhla G, Wong K, Wan W (2010) Antifouling ultrafiltration membranes via post-fabrication grafting of biocidal nanomaterials. Acs Appl Mater Interfaces 3(8):2861e2868

23 Westerhoff P, Moon H, Minakata D, Crittenden J (2009) Arsenic adsorptive media technology selection strategies. Water Qual Res J Can 41(2):171e184

24 Lei JP, Ju HX (2012) C(60) aminofullerene immobilized on silica as a visiblelight- activated photocatalyst. Environ Sci Technol 44(24):9488e9495

25 Cai YQ, Jiang GB, JF, Zhou QX (2003) Comparative photoactivity and antibacterial properties of C-60 fullerenes and titanium dioxide nanoparticles. Environ Sci Technol 43(12):4355e4360

26 Diallo MS, Christie S, Swaminathan P, Johnson JH, Goddard WA Continuous highyield production of vertically aligned carbon nanotubes on 2D and 3D substrates. ACS Nano 5(6):4850e4857

27 Tiede K, Boxall ABA, Tear SP, Lewis J, David H, Hassellov M (2008) Current molecular and emerging nanobiotechnology approaches for the detection of microbial pathogens. Critical Rev Microbiol 36(4):318e339

28 Petryayeva E, Krull UJ (2011) Decentralized systems for potable water and the potential of membrane technology. Water Res 43(2):245e265

29 Dendrimer enhanced ultrafiltration. Environ Sci Technol 39(5):1366e1377

30 Tiraferri A, Vecitis CD, Elimelech M (2011) Detection and characterization of engineered nanoparticles in food and the environment. Food Addit Contam 25(7):795e821

31 Yin HS, Zhou YL, Ai SY, Chen QP, Zhu XB, XG, Zhu LS (2010) Effect of magnetite particle size on adsorption and desorption of arsenite and arsenate. J Mater Res 20(12):3255e3264

32 Benotti MJ, Stanford BD, Wert EC, Snyder SA (2009) Effect of TiO2 nanoparticles on fouling mitigation of ultrafiltration membranes for activated sludge filtration. J Membr Sci 249(1e2):1e8

33 Ramakrishna S, Fujihara K, Teo WE, Yong T, Ma ZW, Ramaseshan R (2006) Electrochemical carbon-nanotube filter performance toward virus removal and inactivation in the presence of natural organic matter. Environ Sci Technol 46(3):1556e1564

34 Vecitis CD, Zodrow KR, Kang S, Elimelech M (2010) Electrochemical multiwalled carbon nanotube filter for viral and bacterial removal and inactivation. Environ Sci Technol 45(8):3672e3679

35 Rao GP, Lu C, Su F (2007) Electrospun nanofibers: solving global issues. Mater Today 9(3):40e50

36 Mauter MS, Elimelech M, Osuji CO (2010) Environmental applications of carbon- based nanomaterials. Environ Sci Technol 42(16):5843e5859

37 Cloete TE, Kwaadsteniet Md, Botes M, Lopez-Romero JM Fabrication and characterization of multi-walled carbon nanotubes/polymer blend membranes. J Membr Sci 284(1e2):406e415

38 Lin DH, Xing BS (2008) Interaction of silver nitrate with readily identifiable groups: relationship to the antibacterial action of silver ions. Lett Appl Microbiol 25(4):279e283

39 Ji LL, Chen W, Duan L, Zhu DQ (2009) Interfacial polymerization of thin film nanocomposites: a new concept for reverse osmosis membranes. J Membr Sci 294(1e2):1e7

40 Qu XL, Brame J, Li Q, Alvarez JJP (2013) Localized surface plasmon resonance: nanostructures, bioassays and biosensing e a review. Anal Chim Acta 706(1):8e24

41 Rahaman MS, Vecitis CD, Elimelech M (2012) Nanotechnology for a safe and sustainable water supply: enabling integrated water treatment and reuse. Acc Chem Res 46(3):834e843

42 Kaufman Y, Berman A, Freger V (2010) Physicochemical determinants of multiwalled carbon nanotube bacterial cytotoxicity. Environ Sci Technol 42(19):7528e7534

43 Kitano M, Funatsu K, Matsuoka M, Ueshima M, Anpo M (2006) Platinized WO(3) as an environmental photocatalyst that generates OH radicals under visible light. Environ Sci Technol 44 (17), 6849e6854, 2006.

44 Lee J, Mackeyev Y, Cho M, Wilson LJ, Kim JH, Alvarez PJJ (2010) Polyamide thin-film nanofiltration membranes containing TiO2 nanoparticles. Desalination 219(1e3):48e56

45 Orge CA, Orfao JJM, Pereira MFR, de Farias AMD, Neto RCR, Fraga MA (2011) Probing single molecules and single nanoparticles by surface-enhanced Raman scattering. Science 275(5303):1102e1106

46 Hristovski KD, Westerhoff PK, Moller T, Sylvester P (2009) Removal of arsenate and 17-ethinyl estradiol (EE2) by iron (hydr)oxide modified activated carbon fibers. J Environ Sci Health Part A-Toxic/Hazard Subst Environ Eng 44(4):354e361

47 Mauter MS, Elimelech M (2008) Selforganized TiO2 nanotube layers as highly efficient photocatalysts. Small 3(2):300e304

48 Yang WR, Ratinac KR, Ringer SP, Thordarson P, Gooding JJ, Braet F (2010) Sensitive detection of polycyclic aromatic hydrocarbons using CdTe quantum dot- modified TiO(2) nanotube array through fluorescence resonance energy transfer. Environ Sci Technol 44(20):7884e7889

49 Sharma YC, Srivastava V, Singh VK, Kaul SN, Weng CH (2009) Sorption of divalent metal ions from aqueous solution by carbon nanotubes: a review. Sep Purif Technol 58(1):224e231

50 Brunet L, Lyon DY, Hotze EM, Alvarez PJJ, Wiesner MR (2009) SWNT-MWNT hybrid filter attains high viral removal and bacterial inactivation. Langmuir 26(24):19153e19158

51 Feng QL, Wu J, Chen GQ, Cui FZ, Kim TN, Kim JO (2000) The future of seawater desalination: energy, technology, and the environment. Science 333(6043):712e717

52 Gao W, Majumder M, Alemany LB, Narayanan TN, Ibarra MA, Pradhan BK, Ajayan PM (2011) TiO(2) photocatalysis and related surface phenomena. Surf Sci Rep 63(12):515e582

53 Lind ML, Ghosh AK, Jawor A, Huang XF, Hou W, Yang Y, Hoek EMV (2009) Ultrasensitive sensing of Hg(2þ) and CH(3)Hg(þ) based on the fluorescence quenching of lysozyme type VI-stabilized gold nanoclusters. Anal Chem 82(22):9194e9200

54 Kominami H, Yabutani K, Yamamoto T, Kara Y, Ohtani B (2001) Uptake of rare- earth elements from solution by metal-oxides. Environ Sci Technol 27(9):1796e1802

Groundwater Conservation Measures and Modeling Techniques

Geochemical Modeling of Groundwater in Tirupur Region, Tamil Nadu, India

K. Arumugam, K. Elangovan, T. Karthika, R. K. Sangeetha, and S. Vikashini

1 Introduction

The inverse modeling applies to situations where the enough data are available to define the flow path and changes in groundwater composition beside the path. Geochemical modeling frequently recognized as inverse modeling. Hydrochemistry studies and its examination are generally adopted to rebuild geochemical sequence of subsurface water from a spot of an aquifer to next setting in the converse course beside the water flow conduit [1]. This model calculates the segment mole transfers for accounting the differences in initial.

With the ending water composition all next to the flow conduit in groundwater process, the reliability of the results depends on suitability of the groundwater interaction method, accurateness of input data into the model, validity of the essential hydro-geochemical concepts in the region [2]. The element interactions between the soil components, bed rock in addition to groundwater, give a range of constituents. The modeling is a vital tool to predict the environmental formation. In hydrogeology, it is significant for investigating the performance of regional aquifer [3]. Geochemical modeling is a useful tool for forecasting the mobility and solubility of speciation

K. Arumugam (✉) · T. Karthika · R. K. Sangeetha
Department of Civil Engineering, Kongu Engineering College, Perundurai 638 060, India
e-mail: sixface@kongu.ac.in

T. Karthika
e-mail: rtkarthika.civil@kongu.ac.in

R. K. Sangeetha
e-mail: sangeetha.rk@kongu.ac.in

K. Elangovan
Department of Civil Engineering, PSG College of Technology, Coimbatore 641 004, India

S. Vikashini
Department of Pharmacy Practice, Nandha College of Pharmacy, Erode 638 052, India

of radionuclides in the aquatic environment [4]. The NETPATH model was used to provide details to the mass-balance of geochemical reactions of initial and final water point [5]. Numerical as well as mathematical methods were used to solve the contrary issues of heat transport and water flow [6]. Constraints of many modern inverse models are based on theoretical representation which directs to underestimation of uncertainty and statistical [7].

2 Study Area

The locality is in between the geographical area coverage: 11° 11'N to 11° 22'N longitudes and 77° 23'E to 77° 50'E latitudes and located at 55 km south east to Manchester city—Coimbatore (see Fig. 1). The study region is covered within 450 km^2. The average precipitation of study zone is 610 mm. The range of temperature varies from 21 °C to 45 °C and receives light rains as it is situated on the east (leeward) side of the Western Ghats. The study zone is characterized by an undulate topography with the elevated range from 290 to 322 m over the MSL and slopes steadily towards east direction. The Noyyal river diagonally separates the study zone into two identical sector. Nallar river along with the Noyyal river have been coupled with water quality problems by discharging unprocessed effluents into the rivers. Geomorphic units present in the study zone are shallow buried pediments, duri crust, etc. Based on petrography, the total area is with different grades gneissic rock types [8]. Soils in the area are red and brownish types.
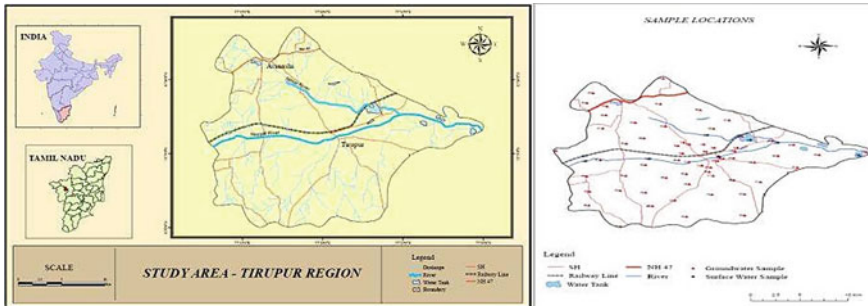

Fig. 1 Study area and sample locations

3 Materials and Methods

3.1 Materials

Within the identified boundary for study purpose, sixty two subsurface water samples were collected. About one third of samples were within the urban boundary of the Tirupur municipality as it was more contamination problem expected. For physico-chemical parameter analytical studies, the necessary instruments were appropriately checked as per the calibration principles in advance for the measurements according to the guide lines (9). The analyzed parameters along with the methods are given Table 1.

Saturation Index: Groundwater saturation with dissolved constituents is prone to deposit some constituents during the abstraction causing incrustation or utilization causing incrustation, blockage or scales in vessels. The various methods available to represent the level of water with regard to a mineral have been used. Water composition must be balanced with respect to minerals. Dissolution is continuing if the water is under saturated to any kind of mineral, whereas saturated water could indicate an enduring precipitation course [10]. For hydro chemical study, Saturation Index (SI) is generally used to describe the saturation status of minerals in groundwater. The equilibrium condition of the water with respect to a mineral phase can be determined by SI calculation using analytical data [11]. The saturation index is defined as follows:

Table 1 Parameters and the methods used for the analysis

Parameters	Methods
Electrical conductivity (EC)(μS/cm)	EC indicator
Total dissolved solids (TDS)(mg/l)	Conversion factor (0.55 to 0.75) x SEC
Calcium (Ca^{2+}) (mg/l)	Titration
Magnesium (Mg^{2+}) (mg/l)	Calculation (total hardness—calcium)
Sodium (Na^+) (mg/l)	Flame photo-meter
Potassium (K^+) (mg/l)	Flame photo-meter
Carbonatē (CO_3) (mg/l)	Titration with hydrochloric acid
2− Bicarbonate (HCO_3) (mg/l)	Titration with hydrochloric acid
Chloride (Cl^-) (mg/l)	Titration with Ag NO_3
2− Sulphate (SO_4) (mg/l)	Spectrophoto-meter
Nitratē (NO_3) (mg/l)	Colorimeter

$$\text{Saturation indexlog} = \frac{IAP}{K_s p} \tag{1}$$

The percentage of saturation is obtained as follows:

$$\text{Saturation index percentage} = IAP/K_s p \times 100\%, \tag{2}$$

where IAP is the ionic movement of the ions and $K_s p$ represents the solubility creation of the minerals. Saturation index should be taken carefully as it is based on the hypothesis of thermodynamic equilibrium for uncontaminated calcite.

It can be used as an important estimation of widespread carbonate constraints, particularly if combined with major physiochemical facial appearance of the aqueous environment [12]. The SI, regarding a certain solid phase, is a geochemical parameter to describe the tendency of solution to precipitation or dissolve in the phase. Saturation index < 0 shows under-saturation with reference to the particular mineral. Saturation index > 0 specifies as super saturation level with reference to the specific mineral. This index value identity reflects the discharging of groundwater from an aquifer containing sufficient mineral quantity with adequate inhabitant moment in time to reach the balance level [13, 14].

Mass Balance Simulation: In a combination at equilibrium, the activities of the chemical species available are associated by a set of equations of mass-action equilibrium [15]. The calculations of mass balance are made to account for the change in solution composition attributable to the precipitation or dissolution of the reactive phases. Mass balance equation of solution for a fastidious set of reactive phases producing a reaction of the form. The reaction accounts for the changes in composition of water by the quantity (moles/kilogram of water) of reactants that must dissolve into the water and products that ought to precipitate from solution as the water flows from an up gradient well to a down gradient region.

The principles of hydro-chemical mass-balance chemical reactions can be stated as the computation of the early aqueous components and the reactants generation to the total of the closing stage aqueous components. Overall mass-balance simulations are conceded against the basic elements. In aqueous solutions, if 'n' elements are measured, the quantity of suspension/deposition of the elements can be dogged by the mass-balance replication.

$$\sum_{i=1}^{n} a_{ij} x_j = b_i \tag{3}$$

where a_{ij} is i-th element of stoichiometric number with reference to j-th mineral, a dimensionless value to i-th element of the molar number generated by the absolute dissolution of 1 mol of the j-th mineral elements, x_j represents molar number which is the j-th mineral elements dissolves and b_i is describes increment of the i-th element in the aqueous quality. The probable mineral segment recognized in their reactions

is an indefinite phases which refers to the chosen chemical substances due to the resultant and reactants in the hydro-geological structure [16].

Various prospective conceptual models of different suites of reactive phases could account for the pragmatic changes in solution concentration all along the flow path, and it is confront of the modeler for eliminating unrealistic models. As the inverse method is based on mass balance computation only and as it does not essentially consider thermodynamic constraints on the system.

WATEQ4F Model. Modeling of speciation of groundwater composition is almost the chemical equilibrium computation of water–rock system [17]. They have been basically derived from the classical works which are confined to the speciation of major ions in pullover. A FORTRAN IV computer program of WATEQ4F models the thermodynamic species of mineral components in solution for a given water analysis. This WATEQ4F model contains an undated thermodynamic data, certain advanced means of handling the carbonate equilibrium, and a change which allows for a back substitution method for an early convergence of anion mass balance.

4   Results and Discussion

Hydro-chemical facies. The most important parameters of cations as well as anions are used to classify different types. Mainly the graphical procedures are followed for representing total dissolved solids concentration and their relative quantity extent of the dominant ionic species. Piper diagram [18] is extensively used to identify the dilemma concerning the evolution of groundwater. The geochemistry progression of groundwater samples can be implicit by plotting the parameter concentrations of cations and anions in Piper diagram. The types are typically with calcium (Ca)—sodium (Na), bicarbonate (HCO3), chloride (Cl) and sodium (Na), bicarbonate (HCO$_3$), chloride (Cl) types. The nine different water categories are identified (see Fig. 2).

WATEQ4F Model. The program consists five sub routine steps. In the first step, converting the limits of the concentration to molality and calculates all the temperature reliant data of the groundwater samples. In the second step, it initializes the values of individual species for the interactive mass. In the third, they calculate the activity coefficients and solve mass action and mass balance equations for the species measured. In the fourth step, it prints the outcome calculated from the aqueous model. Finally, it calculates and prints thermodynamic saturation status to water with respect to the various mineral contents measured by the program. The circulation of aqueous species is solved by a succeeding approximation routine concerning the concurrent solution particular mass balance equations that represent the aqueous model. Individual ion activity coefficients of the species were computed from the extended Debye–Huckel equation.

When the chemical representation is completed, it is useful to calculate modal concentration ratios and ion activity ratio for preparing the composition of water
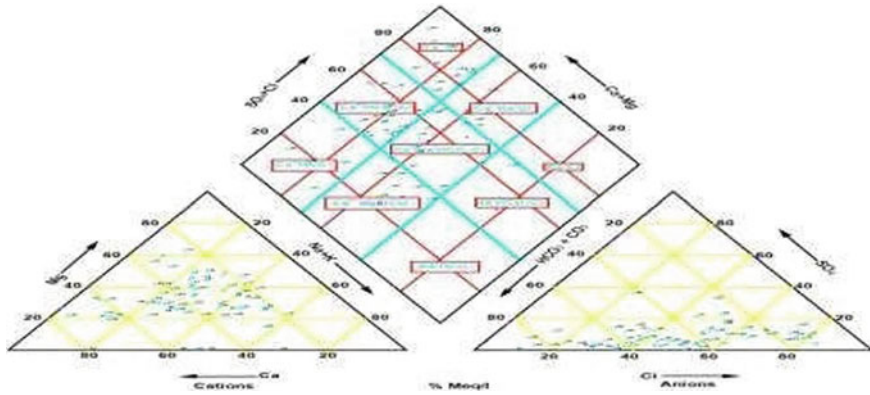
Fig. 2 Classification of water (after Piper [9])

and mineral permanence diagrams respectively. Comparison of these ratios with the related water can suggest possible origin of dissolved constituents and possible control by mineral reaction. A number of these ratios are considered in WQTEQ4F. The enthalpy of reaction at 25 °C has been intended for most of the conditions of equilibrium in WATEQ4F. The effect of pressure cannot be considered by the program. Even though gas partial pressures are rarely measured in natural waters, in several solutions, they can be calculated from the gas solubility constants and the water study. The partial pressure of CO_2 is measured as

$$LogPCO_2 = logaHCO_3 + logdaH - logaH_2O \tag{4}$$

The hydrochemical data from the field measurements and laboratory analysis were used to model the chemical equilibrium conditions of the aqueous environments.

The saturation indices intended for various minerals using WATEQ4F have been stipulated in Table 2. The numbers of samples performance saturation indices of less than 1.0, 0.1, 0.1 to 1.0 and greater than 1.0 for dolomites, calcite, aragonite, goethite and magnesite for the various minerals have been calculated using WATEQ4F.

Saturation of mineral species. The WATEQ4F speciation-solubility model [19] has been used for calculating the equilibrium sharing for the inorganic aqueous species which are found in the groundwater of Tirupur region. The investigation for the saturation index with reference to calcite, dolomite, goethite, aragonite and magnesite are made for the groundwater of the study area.

Calcite and Dolomite

Calcium carbonate equilibrium in contact with groundwater is the most significant geochemical reactions articulated in almost all the area of Precambrian terrain where retrograde metamorphism has formed more calcites. Calcium carbonate deposits can be dissolved by water and carbon dioxide of particular importance in calcium

Table 2 Saturation indices of minerals

Sample station	LOG IAP/KP			
	Calcite	Dolomite	Goethite	Aragonite
01	0.181	0.173	3.374	0.017
02	0.174	0.110	3.201	0.010
03	0.280	0.244	–	0.117
04	0.088	−0.313	3.645	−0.075
05	0.135	−0.048	–	−0.029
06	0.232	0.102	2.877	0.069
07	0.289	0.273	4.023	0.126
08	−0.027	−0.027	–	−0.190
09	−0.150	−0.754	–	−0.313
10	0.790	1.117	4.787	0.627
11	0.610	0.886	4.899	0.449
12	0.317	0.216	3.032	0.150
13	0.573	0.865	3.954	0.409
14	0.667	0.961	3.558	0.504
15	0.225	0.204	–	0.062
16	0.852	1.290	–	0.688
17	−0.461	−1.368	–	−0.624
18	0.242	0.201	3.135	0.079
19	0.433	0.501	3.894	0.270
20	0.464	0.820	4.013	0.300
21	0.288	0.154	4.294	0.125
22	0.755	0.685	–	0.592
23	0.548	0.713	–	0.384
24	0.451	0.550	–	0.288
25	0.195	0.084	2.835	0.031
26	0.536	0.668	3.760	0.372
27	0.148	−0.101	–	−0.016
28	−0.406	−1.351	3.473	−0.570
29	0.168	−0.011	2.474	0.004
30	0.771	0.570	3.732	0.607
31	−0.057	−0.874	–	−0.220
32	0.335	0.238	–	0.172
33	−0.067	−0.491	2.177	−0.230
34	0.514	0.684	4.186	0.351
35	−0.383	−1.321	2.802	−0.547

(continued)

Table 2 (continued)

Sample station	LOG IAP/KP			
	Calcite	Dolomite	Goethite	Aragonite
36	0.020	−0.558	–	−0.144
37	0.639	0.885	–	0.476
38	0.041	−0.299	–	−0.123
39	−0.294	−1.422	–	−0.458
40	0.453	0.512	3.831	0.290
41	0.774	1.111	3.290	0.610
42	0.727	0.718	4.035	0.563
43	0.344	0.365	3.980	0.181
44	−0.034	−0.355	–	−0.198
45	−0.016	−0.484	–	−0.179
46	0.527	0.589	3.842	0.364
47	0.138	−0.053	2.698	−0.025
48	0.379	0.557	4.304	0.216
49	0.164	−0.252	–	0.001
50	−0.026	−0.512	3.133	−0.189
51	0.215	0.228	–	0.051
52	0.302	0.293	–	0.139
53	0.174	0.028	4.700	0.010
54	0.477	0.686	4.081	0.314
55	0.807	1.288	5.355	0.644
56	0.623	0.857	4.379	0.459
57	0.254	0.239	3.765	0.091
58	0.136	−0.294	–	−0.027
59	−0.045	−0.537	3.389	−0.209
60	−0.169	−0.866	2.906	−0.333
61	−0.654	−1.620	–	−0.818
62	−0.447	−1.386	–	−0.610

carbonate cycle. Water in contact with air will readily attract CO_2 whereas under the right conditions it converts to weak carbonic acid

$$CO_2 + H_2O \rightarrow H_2CO_3 \tag{5}$$

This weak carbonic acid can be able to dissolve certain mineral species such as calcium carbonate to form bicarbonate,

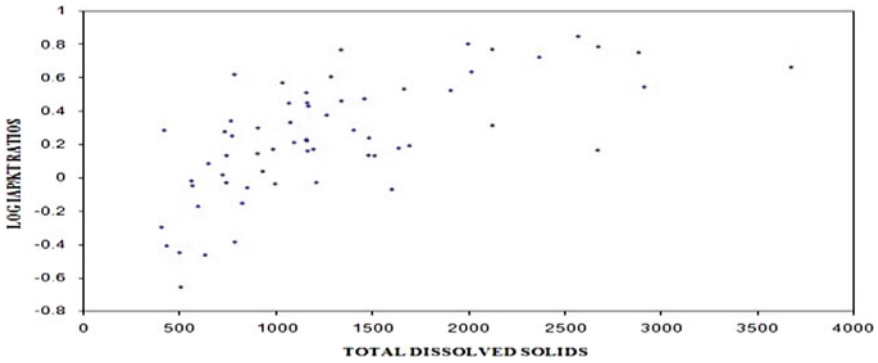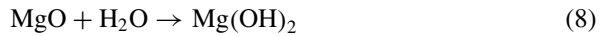$$CaCo_3 + H_2CO_3 \rightarrow Ca + 2HCO_3 \tag{6}$$

Fig. 3 Disequilibrium index using the program WATEQ4F for calcite

The disequilibrium indices for the mineral of calcite are calculated using WATEQ4F and their performance are shown (see Fig. 3).

Dolomite is characteristically associated with serpentinites and talc containing rocks and occurs in metamorphic source. At high ranking of metamorphism, the dolomite can break down into two stages [20] as follows:

$$CaMg(CO_3)_2 \rightarrow CaCo_3 + MgO + CO_2 \tag{7}$$

$$MgO + H_2O \rightarrow Mg(OH)_2 \tag{8}$$

The chemical constitutions of groundwater in the aquifers of carbonate is controlled by the reaction among the dissolved gases, groundwater and the minerals forming the aquifer rocks namely calcite and dolomite. The disequilibrium index for dolomite mineral is calculated using WATEQ4F and the recital are depicted (see Fig. 4).
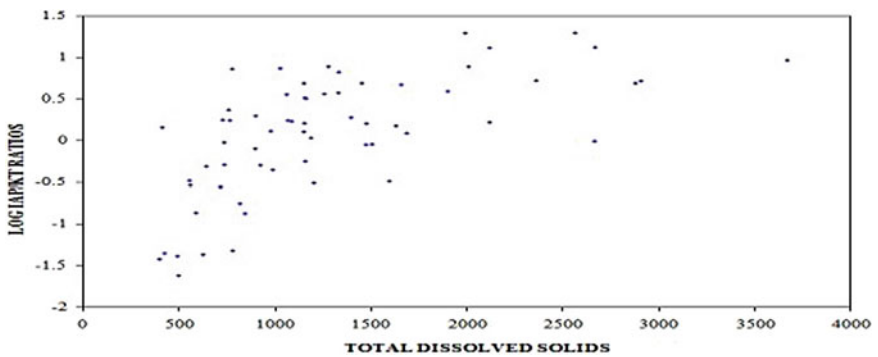
Fig. 4 Disequilibrium index using the program WATEQ4F for dolomite

Goethite and Aragonite

Weathering product of geothite is derived from various iron-bearing minerals in oxygenated environments. It a primary precipitate in hydrothermal, aquatic and marsh environments leading to oxidation of reduced iron comportment waters. The disequilibrium indices for goethite is intended using WATEQ4F. Aragonite is a less stable mineral than calcite. At typical temperature and pressure, aragonite is metastable and fairly inverts to calcite. Crystallization of aragonite may be induced in the presence of Sr, Mg, Pb, or $CaSO_4$. Aragonite is formed along with calcite at the temperature of 30 °C [21]. On the same temperature and pressure, aragonite is more soluble compare to calcite [22]. The disequilibrium indices for the aragonite are calculated using WATEQ4F, and their results are given (see Fig. 5). The results indicate that a number of the groundwater samples are saturated with the mineral constituents of aragonite.

Magnesite

Common occurrence of magnesite is an alteration of different magnesium containing igneous and metamorphic rocks. A carbonate mineral of magnesite ($MgCO_3$) is used as catalysts and in the preparation of fertilizers and magnesium chemicals. In this study, the majority of the groundwater samples are saturated (see Fig. 6).
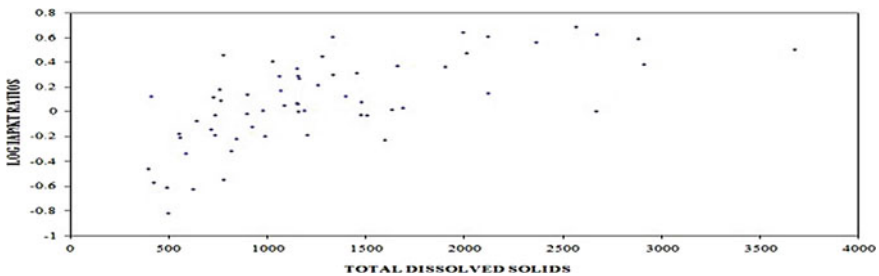

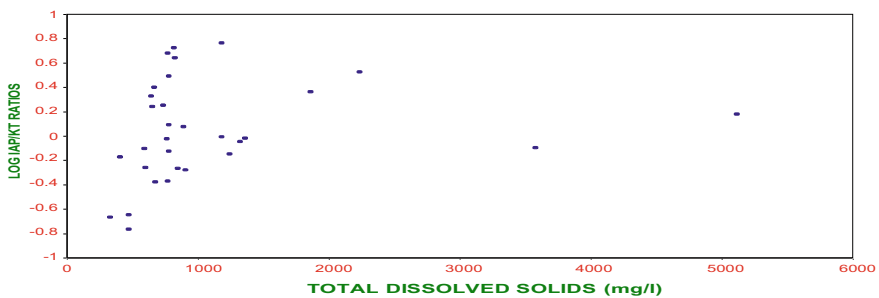**Fig. 5** Disequilibrium index using the program WATEQ4F for aragonite

Fig. 6 Disequilibrium index using the program WATEQ4F for magnesite

5 Conclusion

Based on dominant cations and anions, the hydro-chemical types are mostly the Ca-Na-HCO3-Cl and Na-HCO$_3$-Cl types. However, the water types are calcium-sodium-bicarbonate-chloride, sodium-bicarbonate-chloride, calcium-bicarbonate, calcium-sodium-chloride, sodium-chloride, calcium-sodium-bicarbonate, calcium-bicarbonate-chloride, sodium-bicarbonate and calcium-chloride categories. The investigation about the saturation of minerals proves that minerals species of calcite, dolomite, goethite and aragonite are saturated in majority of the study region.

References

1. Wang PM, Anderko A, Springer RD, Kosinski JJ, Lencka MM (2010) Modeling chemical and phase equilibria in geochemical systems using a speciation-based model. J Geochem Explor 106(1–3):219–225
2. Sharif ME, Davis RK, Steele KF, Kim B, Kresse TM, Fazio JA (2008) Inverse geochemical modeling of groundwater evolution with emphasis on arsenic in the Mississippi River Valley alluvial aquifer, Arkansas (USA). J Hydrol 350:41–55
3. Suma CS, Srinivasamoorthy K, Saravanan K, Faizalkhan A, Prakash R, Gopinath S (2015) Geochemical modeling of groundwater in Chinnar river basin: a source identification perspective. Aquat Procedia 4:986–992
4. Kumar A, Rout S, Narayanan U, Manish K, Mishra R, Tripathi M, Singh J, Kumar S, Kushwaha HS (2011) Geochemical modelling of uranium speciation in the subsurface aquatic environment of Punjab state in India. J Geol Min Res 3(5):137–146
5. Mohamed KF (2017) Applications of hydrogeochemical modeling to assessment geochemical evolution of the pliocene aquifer system in Wadi El Natrun Area, Western desert. Egypt Hydrol 5(1):7–14
6. Dai Z, Samper J, Ritzi R (2006) Identifying geochemical processes by inverse modeling of multicomponent reactive transport in the Aquia aquifer. Geosphere 2(4):210–219
7. Neuman SP (2003) Maximum likelihood Bayesian averaging of uncertain model predictions. Stoch Environ Res Risk Assess 17:291–305
8. Arumugam K, RajeshKumar A, Elangovan K (2015) Evolution of hydro-chemical parameters and quality assessment of groundwater in Tirupur region, Tamil Nadu. India Int J Environ Res 9(3):1023–1036
9. American Publish Health Association (APHA) (1995) Standard methods for the examination of water and wastewater, 17th edn. Washington, DC
10. Xiao J, Jin W, Jin. ZD, Fei Z (2014) Major ion chemistry, weathering process and water quality of natural waters in the Bosten lake catchment in an extreme arid region, NW China. Environ Earth Sci. https://doi.org/10.1007/s12665-014-3657-z
11. Aghazadeh N, Chitsazan NM, Golestan Y (2016) Hydrochemistry and quality assessment of groundwater in the Ardabil area, Iran. Appl Water Sci. https://doi.org/10.1007/s13201-016-0498-9
12. Vaiente T, Fatela F, Moreno F, Guise L, Patinba C (2009) A comparative study of the influence of geochemical parameters on the distribution of foraminiferal assemblages in two distinctive tidal marhses, J Coastal Res Spl 56:1439–1443
13. Appelo CAJ, Postma D (1996) Geochemistry groundwater and pollution. Balkema, Rotterdam 536
14. Langmuir D (1997) Aqueous environmental geochemistry. Prentice Hall, Upper Saddle River, p 600

15. Garrels RM, Thompson ME (1965) A chemical model for sea waters at 25 ^{0}C and one atmosphere total pressures. Am J Sci 260:57–66
16. Li P, Qian H, Wu J, Ding J (2010) Geochemical modeling of groundwater in southern plain area of Pengyang County, Ningxia, China. Water Sci Eng 3(3):282–291
17. Guangcai W (1990) Calculation of water-mineral reactions. Hydrogeol Eng Geol (in Chinese), 1(41)
18. Piper AM (1944) A graphic procedure in the geochemical interpretation of water-analysis. Trans Am Geophy Union 25:914–923
19. Prestemon LN (1992) Program WATEQ4F, A Fortran IV version of WATEQ, U.S. geological survey
20. Deer WA, Howie RA, Zussman J (1966) An introduction to the rock forming minerals, vol 528. ELBS publication, New York
21. Kitano Y (1962) The behavior of various inorganic ions in the separation of calcium carbonate from a bicarbonate solution. Bull Chem Soc Jpn 35:1973–1980
22. Seidell A, Princeton NJ (1958) Solutbilities of inorganic and metal organic compounds, 4th edn. Van Nostrand Co

Design of Storm Water Management System for the Water Stressed Areas in Palakkad District

Karthika Aravind, Megha Krishnan, Melvin Devassy, Noel Tharakan Renjith, and T. R. Rajalakshmi

1 Introduction

Seasonal drought like conditions is experienced in Kerala every year during the summer months, summer water scarcity problems exist in most of the regions, even in the months of normal rainfall. It can be seen from the Indian Meteorological Department (IMD) Reports that 14 districts of Kerala experienced severe rainfall shortage. This deficit has particularly affected the districts such as Wayanad, Palakkad and Thrissur. After the basic anaylsis we chose Palakkad as our study area. Our objective includes (1) Study and Identification of water stressed areas in Palakkad District using overlay analysis in ArcGIS by generating required thematic layers. (2) To find a solution and Design of the remedial measure. (3) To estimate the cost of the project. (4) Submittal of proposal to the relevant authorities.

The system used to reduce runoff of rainwater into streets, lawns and the improvement of water quality is Stormwater management system. Moreover, ground gets saturated by water after a heavy rainfall creates excess moisture that runs across the surface and into storm sewers and road ditches. Debris other pollutants gets carried into streams, rivers, lakes, or wetlands so it is always better to utilize this stormwater for ground water replenishment. For achieving this, we adopt the design of stormtech chambers for the water stressed areas under our study. The system of stormtech chambers is considered to be one of the most economic water harvesting systems along with super flexibility and enhanced performance.

For the identification of water stressed areas in Palakkad, we have decided to do the GIS mapping using the software ArcGIS v 10.3. Initially the data was collected which

K. Aravind · M. Krishnan · M. Devassy · N. Tharakan Renjith (✉)
Federal Institute of Science and Technology (FISAT), Hormis Nagar, Mookkannoor, Angamaly, Kerala 683577, India

T. R. Rajalakshmi
Federal Institute of Science and Technology (FISAT), Hormis Nagar, Mookkannoor, Angamaly, Kerala 683577, India

includes the slope map and attribute data for those factors that we have considered for the identification of water stressed areas. The factors considered includes mainly ground water level, rainfall data, slope, land-use and soil. The data required (in the form of slope map and attribute data) for our study area was collected from Indian Meteorological Department (IMD), Kerala State Disaster Management Authority (KSDMA) and also from the Soil survey Department, Palakkad. With these, the maps were created for Slope, Rainfall, Land use, Groundwater Level and Soil type using ArcGIS. After which overlay analysis was conducted and water stressed areas of Palakkad district was identified. Total nine such sites (villages) were identified. Again these nine villages were shortlisted into two based on their satellite view where we checked the presence of river and also considered the residential area where ground wa ter replenishment tends to be more useful. The identified sites are (1) MNKMHS School Ground, Melarkode Panchayat (GWL-25m), (2) Bungalow kunnu stadium, Kongad(GWL-10M). These sites were inspected and collected the basic details for the design of Stormtech chambers.

2   Methodology

2.1   Site Selection

2.1.1   Study Area

Palakkad, Kerala, India, with the GPS coordinates of 10° 47' 4.9308" N and 76° 39' 11.3220" E, in the southeastern part of the former Malabar district, out of the 14 districts of the South Indian state of Kerala. Population is around 132,728. 4,480 km^2 which is the total area of the district. Palakkad has a tropical wet and dry climate. Moderate temperature is prevalent round the year, with the exception in March and April being very hot and humid. Palakkad receives a very high amount of precipitation mainly due to the South-West monsoon. The wettest month is July, and the total annual rainfall is around 83 inches (210 cm). Palakkad has the maximum number of dams in the State, but the district faces severe drought conditions and acute water shortage. Average temperatures of up to 42 °C is recorded in Palakkad during summer. Palakkad is more prone to droughts when compared to other Districts of Kerala and hence it is prerequisite to study the intensity of drought in detail.
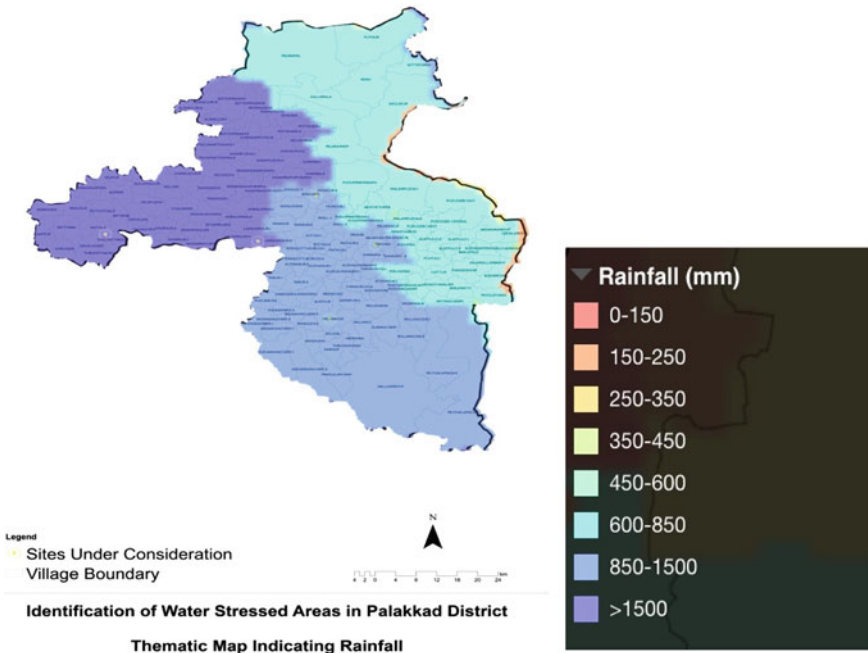
Fig. 1 Rainfall map for the year 2019 of Palakkad district

2.2 Preparation of Thematic Maps

2.2.1 Rainfall Intensity Map

The excel data of rainfall for Palakkad district was collected from Indian Meteorological Department (IMD), for four different rain gauge stations in Palakkad district for the year 2019. The data was inputted to the software as attribute table, and different ranges were selected and provided in millimeters. Then the resulting spatial rainfall map was considered as one of the thematic layers. The following is the map obtained for the year 2019 (Fig. 1).

2.2.2 Ground Water Level

Creating water level maps is one of the common mapping tasks in groundwater projects. The ArcHydro Groundwater (AHGW) is used to automate the process of creating water level maps in ArcGIS. Water levels taken from wells were summarized over a given time period. The data was collected from Department of Water Resources, RD and GD. The following shows the thematic map generated using the software (Fig. 2).
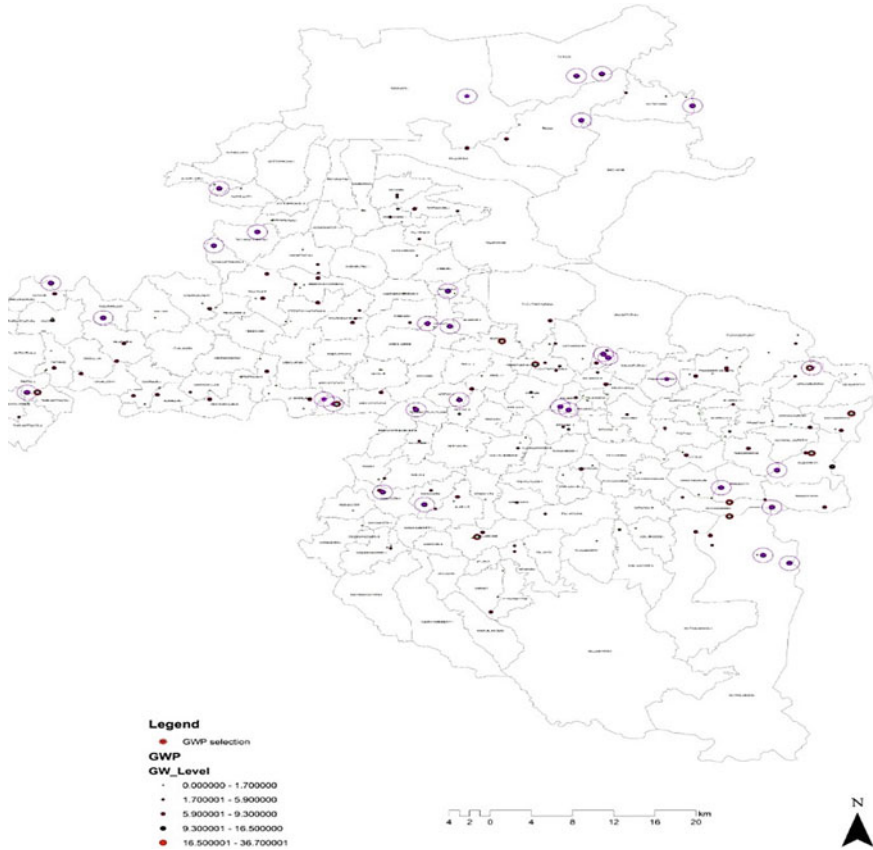
Fig. 2 Ground water level

2.2.3 Slope

Slope is an important factor. The slope map was derived from Aster DEM data, which can be downloaded from the Earth data, NASA, with 30m resolution, and slope is derived using spatial analyst tool in ArcGIS 10.3. Slope is generated using data collected from the Advanced Spaceborne Thermal Emission and Reflection Radiometer (ASTER), a spaceborne earth observing optical instrument. The only DEM that covers the entire land surface of the Earth is the ASTER GDEM (Fig. 3).

2.2.4 Land Use/Land Cover Map

Land use indicates how people are using the land, whereas land cover indicates the physical land type. As population increases, land use also increases. The rapid land use/land cover transformations increase the chances for the shortage of water.
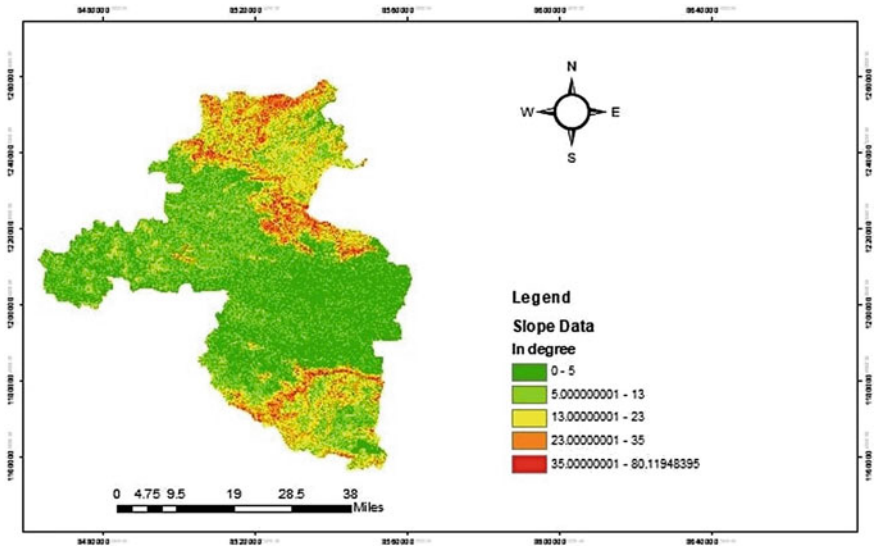
Fig. 3 Slope map

Thematic map of land use/land cover was obtained from Kerala State Remote Sensing and Environmental Centre (KSREC), Trivandrum (Fig. 4).

2.2.5 Soil Map

Soil characteristics invariably control penetration of surface water into an aquifer system, and they are directly related to rate of infiltration, percolation and permeability. The study area is predominantly controlled by black cotton soil, forest soil, hill soil, laterite soil, and mainly covered by laterite soil. Thematic map of soil was obtained from KSREC, Trivandrum (Fig. 5).

2.3 Preparation of Map for Finding Water Stressed Areas in Palakkad District

2.3.1 Overlay Analysis

Overlay analysis integrates spatial data with attribute data. Overlay analysis is done by combining information from one GIS layer with another GIS layer to derive an attribute for one of the layers. The overall objective must be identified. All of the remaining steps of the overlay process should contribute to this overall objective. The identified locations should be visited. Since the data for the model was created,
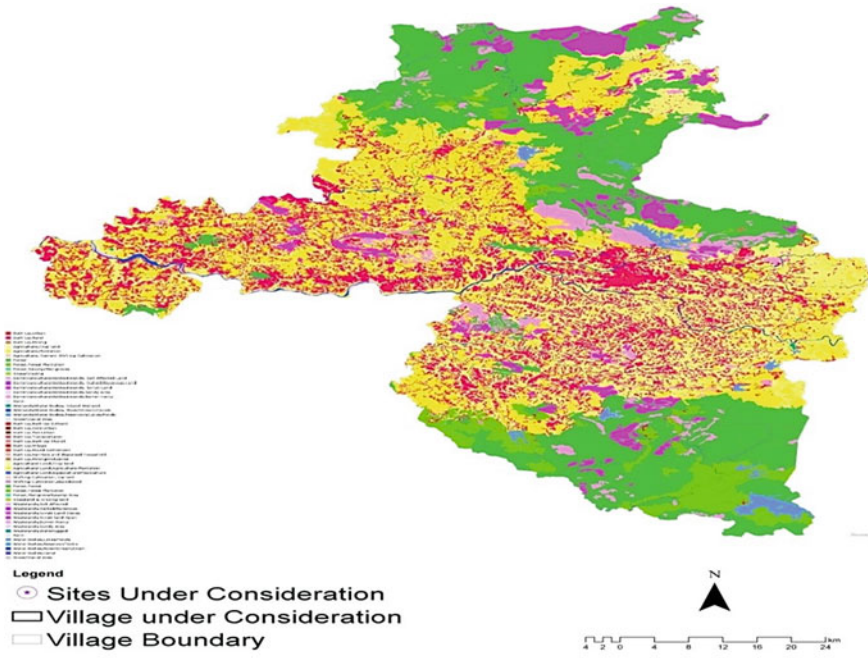
Identification of Water Stressed Areas in Palakkad District

Map Indicating Existing Landuse/Land Cover

Fig. 4 Land use

things could have changed. Thus, higher the value on the resulting output raster, the more desirable the location will be.

After the analysis of the different thematic layers, seven villages where taken into consideration from the district which was facing water shortage, low water table, high population etc. The seven villages are follows: Trittala, Thirumittakod_1, Lakkidiperur, Malapuzha, Kongad, Palakkad, Eruthempathy, Pattancherry, Melarkod (Fig. 6).

2.4 Site Selected

After conducting overlay of the maps, Melarkode village of Alathur Taluk was selected as one of the water-stressed areas. The ground water level of the area is about 25m on an average. Stormtech chambers was selected as a remedy to increase the ground water level of the area. The playground of the MNKMHS school Chitta-lancheri has been selected as a suitable site to install the Stormtech chambers as it
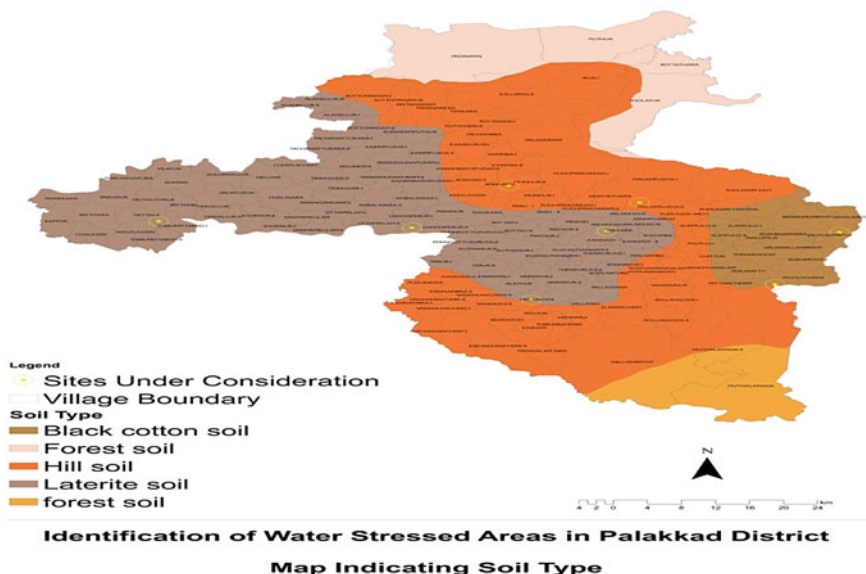
Fig. 5 Soil type

ensures the use ability of land. The selected area is densely populated, so the requirement of water is also high Ground water in the range of approximately 20–25 sq.km can be recharged; since the entire area of Melarkode village is about 25.42 sq.km, it will meet the requirement (Figs. 7 and 8).

2.4.1 Soil Type (from Soil Report)

Vettikad series: The soils of Vetikkad series are moderately deep, well drained, moderately fine textured, very dark grayish brown and acidic. They are formed from granite gneiss. They occur on moderately steep to steeply sloping hills with slope of 15–25 percent. The general elevation is 20–100 m above MSL.

Taxonomic class: Fine-loamy mixed isohyperthermic family of Typic Haplustepts. Typifying pedon Vettikad—Gravelly sandy clay loam—cultivated

Kinasseri series: The soils of Kinasseri series are deep, well drained and moderately permeable, fine textured, reddish brown and acidic. They are formed from gneiss.

They occur on mid land side and foot slopes with slope of 3–15 percent. The general elevation is 20–100 m above mean sea level.

Taxonomic class: fine—loamy, mixed, isohyperthermic, OxicHaplustepts. Typifying pedon Kinassery—gravelly sandy clay—cultivated.
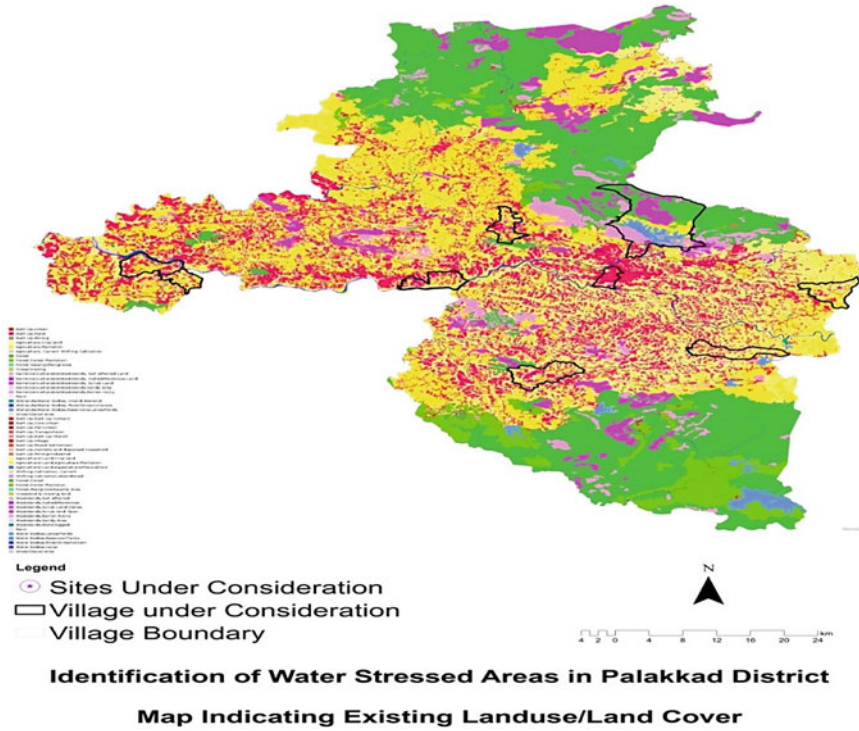
Identification of Water Stressed Areas in Palakkad District

Map Indicating Existing Landuse/Land Cover

Fig. 6 Overlay map with 9 identified villages

3 Materials

3.1 Chamber

Chambers should be manufactured from virgin, impact modified polypropylene or polyethylene copolymers and arch-shaped. Rows of the chamber should provide continuous, obstruction free internal space with no support panels in order to provide ease of access for inspection and maintenance requirements. As per project plans inspection ports shall be installed and constructed. The chambers shall be open-bottomed.

3.2 End Caps

End caps shall be injection moulded or rotor moulded from polyethylene or polypropylene resin and allow pipe connections with polyethylene pipe. All chamber

Fig. 7 Contour map of Melarkode Village

Fig. 8 School ground MNKMHS

rows shall be terminated with an end cap. End caps may incorporate cutting guides to allow easy field cutting for various diameters of pipe (Fig. 9).

Fig. 9 Chamber and end cap

Fig. 10 Manifold piping

3.3 Manifold Piping

Manifold piping shall be designed to ensure that peak flows are distributed (without scour of foundation stone) to the rows of chambers. To use equations of hydraulics as basis of manifold piping, it shall be of dual wall HDPE piping (Fig. 10).

3.4 Stone

In accordance with the chamber manufacturer's installation instructions, the foundation, embedment and cover stone should be selected.

3.5 Fabric

Between the chamber bottom and the stone foundation, a fabric is located along the entire length of the Isolator Row and the first 10.5 ft or 14.5 ft of all inlet rows. Fabric between the top of the Isolator Row chambers and the embedment stone and surrounding the entire chamber system shall be AASHTO M288 Class 2 non-woven for filtration.

4   Design and Installations

4.1   Design

The primary step of design of stormtech chambers is calculating the area required for the installation. The area of the village is around 25 sqkm in area, designing for this area, and we need to know the total rainfall for this area which we have collected from IMD (Indian Meteorological Department). Assuming the total runoff in that area to be 70 to 80% of total rainfall and by testing the infiltration rate of the soil by using infiltrometer. We could easily get the area required which is equal to Total runoff/Infiltration rate, and we get the area in sqm and an addition of 20% to this area for the safe design. The plot can be designed either in rectangular or square shape. The components that include in the design of stormtech chambers are (1) Aggregates, (2) Soil—Backfill-4 layers of 30 cm(compacted), (3) Manhole—Concrete M-30 Mix, (4) Chambers-PVC Prefabricated (Size—From Installation Guide), (5) Pipe—Upvc Material (Upvc-Unplasticized polyvinyl chloride), (6) Epoxy paint—Inside the chambers, (7) Water Proofing— Outside chambers.

The next step of the design is to calculate the number of aggregates required for the project. Aggregate size ranges from 20 to 50 mm, and the volume of aggregate is equal to the product of total area of installation and total height of installation and then deducting the inner volume of chambers. This can be done only after fixing the number of rows of chambers needed for plot size and also the chamber's inside diameter. Aggregate usually fills up 15–30 cm bottom layer, side filling up-to a height of chamber which is usually 1.5 m and the top layer of 30–40 cm.

4.2   Installation

4.2.1   General Requirements

Chamber products must be designed and installed in accordance with the manufacturer's minimum requirements. Structures shall be accurately located and properly oriented.

4.2.2   Site Preparation

Excavation must be free of standing water. The chamber bed's subgrade soil should be prepared as outlined in the engineer's drawings. The subgrade soil bearing capacity should be equal to or exceed the chamber manufacturer's required allowable subgrade soil bearing capacity.

4.2.3 Chamber Installation and Backfilling

Install chamber system flat or at constant slope between points an elevation indicated. The chamber bed is constructed by joining the chambers lengthwise in rows. Stone placement between chamber rows and around perimeter.

4.2.4 Protection

Pipe plugs in the inlet manhole pipes or Flex Storm Catch. All inlet and outlet structures should be protected against construction sediments.

4.2.5 Inspection and Maintenance

Chambers may incorporate an optional inspection port to allow for inspection of the stormwater system during normal operations. Inspection can also be accomplished through the inlet manhole connected to the Isolator Row requires confined space entry certification of the inspector. Maintenance of the Isolator Row shall utilize a Jet Vac process to remove sediments that have accumulated in the Isolator Row over time.

5 Conclusion

The primary purpose of this paper is to express how land and water should be managed to maximize the chances of providing cities and their inhabitants with water. Investigations of the relationships between various characteristics like rainfall, water scarcity, slope and groundwater level were undertaken. Following which the understanding was extended to different land areas, based on the assumption that all these factors play a major role in the management of stormwater resources.

The methodology was developed based on weightage analysis. Development and application of innovative designs using structural plastic materials provides substantial opportunity to minimize cost and maximize the service life of underground stormwater collection structures. Successful structural performance of these structures relies on application of engineering principles that are specific to the behaviour of structural plastic materials. Because of which, stakeholders in the stormwater industry must push for the development of efficient standards that guide designers, installers, and municipalities to systems that are proven to perform, environment friendly and lasting.

References

1. Mailhot DJ, Gandhi N, and McGrath TJ (2014) Corrugated stormwater chamber having sub-corrugations. U.S. Patent No. 8,672,583. 18 Mar. 2014
2. Pitt R, Voorhees J. (2018) ADS isolator row and stormtech infiltration Chambers in WinSLAMM–performance observations and unit process descriptions
3. Vitarelli RR (2009) Sediment monitor for a stormwater receiving system. U.S. Patent No. 7,596,999. 6 Oct. 2009
4. Berlin VT (2015) Stormwater master plan
5. Engineer, Site Design, et al. Standra details. CITY 71: 15
6. Strohman BP, Sharff PA (2013) Strategies for successful performance
7. Wanielista MP, Yousef YA (1992) Stormwater management. Wiley
8. Barbosa AE, Fernandes JN, David LM (2012) Key issues for sustainable urban stormwater management. Water Res 46(20):6787–6798
9. Adams BJ (2000) Urban stormwater management planning with analytical probabilistic models
10. Marsalek J, Chocat B (2002) International report: stormwater management. Water Sci Technol 46(6–7):1–17

Design of Storm-Water Drainage Network for Educational Institute

Nikunj K. Mangukiya, Kalpesh B. Baladaniya, B. Gopika, Nishant Sourabh, and P. V. Timbadiya

1 Introduction

Stormwater is the water from rain and melting snow. It can infiltrate into the soil, be held on the surface and evaporate, or runoff and end up in a nearby stream, river, or another water body [1]. In a natural area like a forest, the soil absorbs considerable amounts of stormwater, and plants can hold stormwater from the closest place where it falls so that runoff will be minimum [2]. But due to changes in land, the amount of stormwater that infiltrates or evaporates is also decreased [3]. Stormwater is the main cause of water pollution. It runs off solid surfaces and collects several pollutants. This contaminated runoff leads to the death of aquatic life and makes waterways an unhealthy place to live [4]. Untreated stormwater entering streams may lead to contamination of our drinking water supplies, problems with aquatic plants and animals, risks to public health, as well as increased flooding [5].

The stormwater drainage system generally consists of curbs, gutters, catch basins or inlets, manholes, etc. Proper design of storm drainage systems will lead to the solution of several stormwater drainage problems [6]. A storm drain is a portion of a storm drainage system that collects runoff from inlets and conveys it to somewhere and discharged into a channel, piped system, or water body. A storm drain may be an open conduit, a closed conduit, or a combination of both. Storm drain design consists of system planning, including data collection, pavement drainage, pavement details, and inlet spacing, size, and location of mains and manholes [7]. An adequate stormwater drainage system for any settlement is required to prevent the flooding of low-lying areas and discharging the stormwater safely to the nearby water body. Also, the development of the area will increase the runoff due to variation in hydrology [3].

N. K. Mangukiya (✉) · K. B. Baladaniya · B. Gopika · N. Sourabh · P. V. Timbadiya
Department of Civil Engineering, Sardar Vallabhbhai National Institute of Technology, Surat, Gujarat 395007, India

P. V. Timbadiya
e-mail: pvtimbadiya@ced.svnit.ac.in

In order to avoid the problem of flooding while considering the altered hydrology, an effective and planned stormwater drainage system is required. Furthermore, if such urban development is a coastal area, it may increase the complexity of the design of the stormwater drainage network due to the influence of the tidal cycle [8]. A stormwater drainage network is a trade-off between three main parameters, i.e., the slope of the drain, the velocity of the flow in the drain, and the cover to be provided above the crown of the drain. The change in one of these parameters results in a change in the design.

In India, the design of stormwater drainage network was carried out as per the Central Public Health and Environmental Engineering Organization (CPHEEO) manual [9] guidelines till the year 2019. The guidelines have specified several criteria for the design as per the allowable flooding duration based on the importance of the area. The frequency specified in the aforementioned manual is 1 in 0.5, 1 in 1, and 1 in 2 (Partial Duration Series (PDS)) for area peripheral residential areas, central and high-priced areas, and commercial and high-priced areas respectively. The design criteria of a city having the same topographical and meteorological condition in Asia are on the far conservative side than in India. They consider the design frequency from 1 in 2 to 1 in 25 years (PDS) depending upon the importance.

In the present study, the design of a stormwater drainage system for the Sardar Vallabhbhai National Institute of Technology (SVNIT) campus has been carried out as per the criteria of CPHEEO manual 2012. SVNIT is a residential institute which is situated in Surat city. On average, the city is being undergone flooding every two and a half years from 1869 to 1884. In 2006, 75% of the city was affected by floods. Due to flooding, the library basement of the campus was also destroyed. Every year, due to heavy rainfall, the water is accumulated on campus, and the breeding of mosquitoes and other insects will take place in waterlogged areas, leading to a harmful and dangerous environment for students and faculty. The poor stormwater drainage system will also lead to many problems, such as road transport problems and poor traffic conditions. The study presented in the paper aims to provide an efficient and useful separate stormwater drainage network for the SVNIT campus, which can be used in future developments. The methodology presented in the paper can be useful to other educational institutes in India.

2   Study Area and Data Collection

2.1   Study Area

The Sardar Vallabhbhai National Institute of Technology, Surat, commonly known as National Institute of Technology (NIT), Surat, or SVNIT, was established in 1961 by the Parliament of India as an engineering institute of higher education. The SVNIT campus is situated near the Ichchhanath area of Surat city of Gujarat, India, having latitudes of 21.16 °N and longitudes of 72.78 °E with approximately 100-hectare
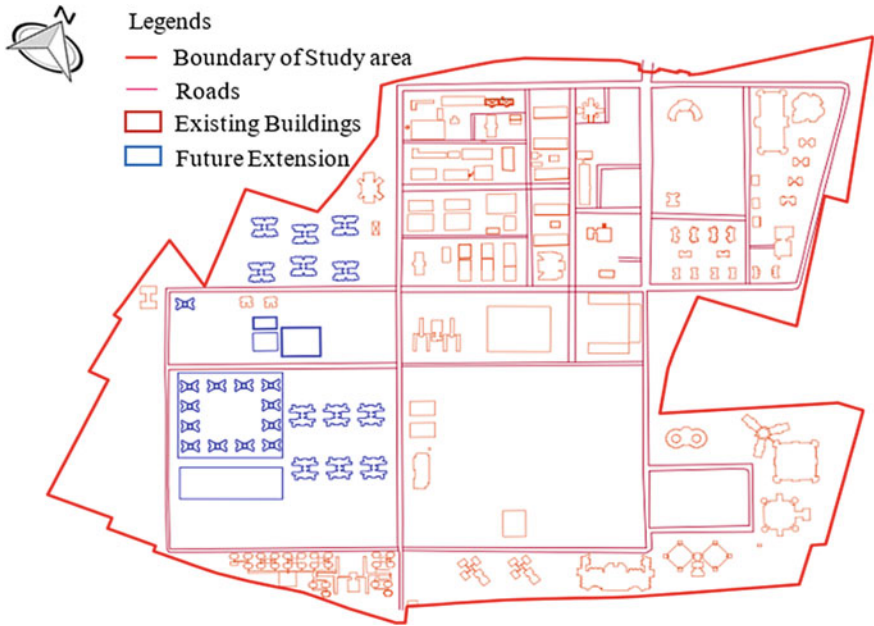
Fig. 1 SVNIT—Surat map showing the buildings and other features from the Masterplan

area. Figure 1 shows the map of the SVNIT campus. The institute campus has ten academic departments, laboratories, and central research facilities. The academic facilities of the institute are located in the north-western part of the campus, including departmental buildings, lecture halls, laboratories, the central library and the central computer center. In addition to it, the institute campus has a dispensary, a post-office, three guest houses, and one nationalized bank within the campus. The campus has one cafeteria, electrical substation, a water pumping station, and telephone exchange. The campus also has ten hostels with approximately 3500 students living on it. The campus has 5000 residents, including 210 faculty members. A campus is also a favorite spot for walkers and joggers who come regularly to the campus in the morning and evening time.

2.2 Data Collection

The physical attributes of the study area like the existing topography of the area, the land use pattern, and the master plan of the area were collected from the Estate section, SVNIT. This was further edited using the data obtained from the survey. Rainfall data are required to develop an Intensity–Duration–Frequency (IDF) curve for the study area from which the intensity of the corresponding storm duration can be obtained for different storm frequencies, which is then directly used to determine

the peak discharge generated. The hourly rainfall data from the year 1972 to the year 2013 is procured from the IMD rain-gauge station located at Rander, Surat, and has been utilized to develop IDF curves for the return periods of 2, 5, and 10 years. The outfall locations of the existing SVNIT stormwater drain system were identified, and R.L. of the outfall points were found out by survey.

3 Methodology and Design Basis

The methodology involves the preparation of existing topography, land-use land-cover map, and IDF curve for calculation of different design parameters. Figure 2 shows the flowchart of the methodology.

3.1 Preparation of Existing Topography

The existing topography map of the study area was prepared from the contour survey data of the year 2011 for the SVNIT campus collected from the Estate section, SVNIT, Surat. The obtained contour surveyed points were digitized first in ArcGIS Desktop v10.5 with the spatial reference coordinate of 'WGS 1984 UTM Zone 43 N'. The digitized contour points are then interpolated in the raster form by using the 'Topo to Raster' tool of Arc Toolbox featured in ArcGIS. Finally, the Georeferenced digital elevation model (DEM) of the campus is obtained. From the DEM, it has been
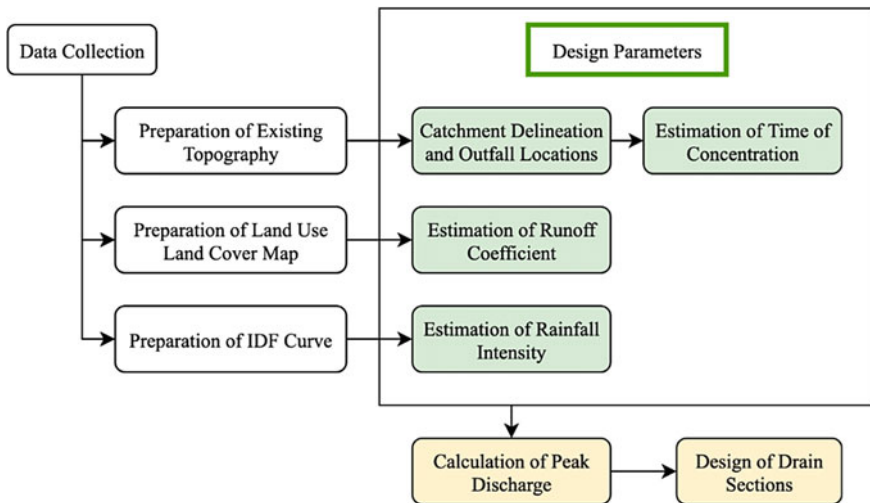

Fig. 2 Methodology flowchart

identified that the study area has a minimum elevation of 5.91 m and a maximum elevation of 9.45 m. The elevation value for the entire study area differs with a standard deviation of 0.37 m with a mean of 7.36 m.

Catchment delineation and outfall locations. The entire SVNIT campus area of 1 km^2 has been divided into four major catchments using the 'spatial analyst toolbox—Hydrology' in ArcGIS v10.5. Considering the topography of the area, a total of three outfalls are proposed. The main purpose to divide the area into three outfalls is to uniformly divide the discharge among them so that a particular catchment will not be overloaded. Delineated catchments and their properties are represented in Fig. 3 and Table 1.

Estimation of time of concentration. The time of concentration is the required for a drop of water to reach the outlet from the farthest point of the catchment. There are many empirical equations available for calculating the time of concentration. Kirpich equation is the commonly used formula which relates the time of concentration with
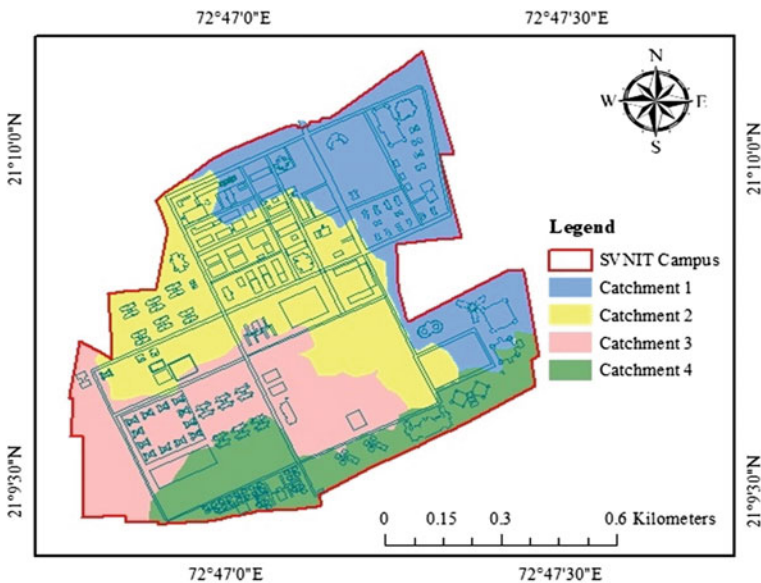

Fig. 3 Catchments considered for the present study

Table 1 Catchment properties

Catchment	Area (m^2)	Maximum travel length (m)	Slope of the catchment
Catchment 1	279,112.197	1038.6	1.367×10^{-3}
Catchment 2	317,665.414	1374.5	4.510×10^{-4}
Catchment 3	204,720.292	897.6	1.114×10^{-3}
Catchment 4	139,098.464	1367.6	6.873×10^{-4}

the slope of the catchment and length of travel [10]. As per the Kirpich (1940), the time of concentration is calculated by Eq. 1.

$$t_c = 0.01947 \, L^{0.77} \, S^{-0.385} \tag{1}$$

where t_c is the time of concentration (min), L is the length of travel of water (m), and S is the slope of the catchment.

3.2 Preparation of Land-Use Land-Cover Map

The land-use land-cover (LULC) map for the determination of runoff coefficient is prepared from the existing master plan of the SVNIT campus by using ArcGIS v10.5. The entire area of the SVNIT campus has been divided into three land-use patterns, i.e., buildings, roads, and vegetation areas. The LULC map is shown in Fig. 4. From the LULC map and the catchment map, the percentage area of different land use has been calculated which is shown in Table 2.

Estimation of runoff coefficient. The runoff coefficient represents the combined effect of catchment losses. It depends on rainfall intensity and characteristics of the
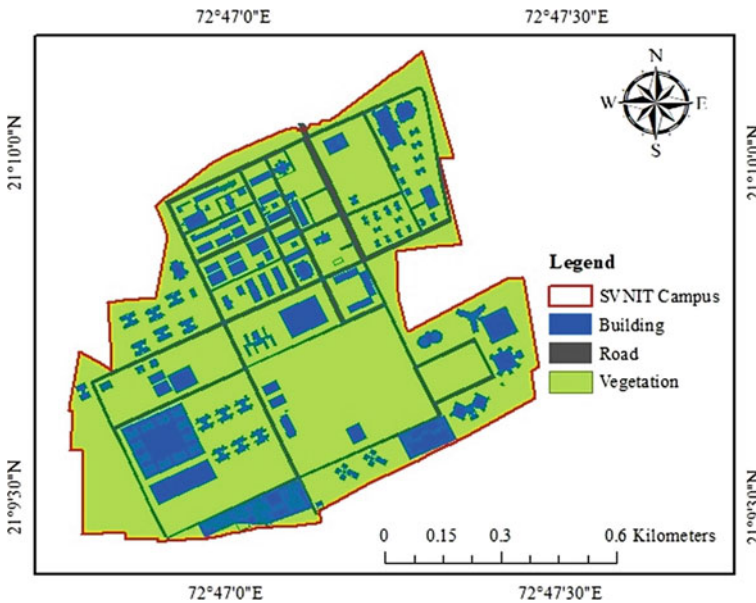

Fig. 4 Land use land cover map for SVNIT campus

Table 2 Percentage area of different land use for catchments

Catchment	Total Area (m^2)	Buildings (%)	Roads (%)	Vegetation (%)
Catchment 1	279,112.197	12.64	10.64	76.72
Catchment 2	317,665.414	16.11	9.80	74.09
Catchment 3	204,720.292	21.75	6.85	71.40
Catchment 4	139,098.464	27.80	4.38	67.82

surface [11]. For a non-homogeneous catchment, the weighted equivalent runoff coefficient has to be calculated as Eq. 2 [12].

$$C_e = \frac{\sum_1^N C_i A_i}{A}$$

(2)

where A_i is the sub-area i which is having a runoff coefficient C_i, A is the total area of the catchment, and N is the total number of sub-areas. The runoff coefficient C_i is considered as per the guidelines in the CPHEEO manual on sewerage and sewage treatment [9].

3.3 Preparation of IDF Curve

An Intensity–Duration–Frequency (IDF) curve indicates the mathematical correlation between the intensity of rainfall and its duration and frequency of occurrence. For the preparation of the IDF curve, rainfall series for different durations (i.e., 1-h, 2-h, 6-h, 12-h, and 24-h) are prepared first from the available rainfall data. The annual maximum depth of rainfall is calculated for each selected duration. Then each selected duration data series is fitted to Gumbel's extreme value probability distribution [13]. There are three asymptotic modes of extreme value distribution, i.e., Type I, Type II, and Type III. The most popular model for storm rainfall is the Extreme Value Type I (EVI) distribution [14, 15]. The function for EVI probability distribution is shown in Eq. 3. The parameters α and u are estimated by Eqs. 4 and 5 respectively. A reduced variate y can be defined as Eq. 6. The return period T can be calculated using Eq. 7.

$$F(x) = \exp\left[-\exp\left(-\frac{x - u}{\alpha}\right)\right]; \quad -\infty \leq x \leq \infty$$

(3)

$$\alpha = \frac{\sqrt{6}\, s}{\pi}$$

(4)

$$u = \bar{x} - 0.5772\alpha$$

(5)

$$y = \frac{x - u}{\alpha} \tag{6}$$

$$\frac{1}{T} = P(x \geq x_T) = 1 - P(x < x_T) = 1 - F(x_T) \tag{7}$$

where u is the mode of the distribution, s is the standard deviation, and $\bar{x}$ is the mean of the data.

3.4 Estimation of Peak Discharge and Design of Drain Sections

Considering all the above-mentioned parameters/terms, the peak discharge is calculated using the rational formula as given in Eq. 8 [16].

$$Q = 10 \, C \, i \, A \tag{8}$$

where Q is the peak discharge in $m^3 \, hr^{-1}$, C is the coefficient of runoff, i is the intensity of rainfall in $mm \, hr^{-1}$, and A is the area of the catchments in hectares. The commercial software adopted for modeling uses Manning's formula as shown in Eqs. 9 and 10 for the design of drain sections.

$$Q = A \times V \tag{9}$$

$$V = \frac{1}{n} \, R^{\frac{2}{3}} \, S^{\frac{1}{2}} \tag{10}$$

where V is the flow velocity, A is the cross-sectional area of the drain, n is the manning's roughness coefficient, R is the hydraulic radius, and S is the slope of the drain.

In addition to the above-mentioned design parameters, other design criteria were also considered as per the CPHEEO manual. The flow velocity is constrained within the range of 0.6–$2.7 \, m \, s^{-1}$. The minimum cover over the drain is considered as 0.6 m. The slope of the drains is constrained within the range of 1 in 500 to 1 in 5000. At every junction, the head loss is to be calculated based on the standard head loss formula. The crown elevation of the downstream pipe at any junction is assured to be less than all upstream pipes crowns. At every junction, one of the upstream pipes, which is hydraulically critical, will have the same invert as the downstream pipe, and there will be no fall in this line of flow. The other upstream pipe invert should also normally be matched with this level and falls eliminated by increasing the slope and thereby reducing the required flow area.

4 Design Parameters and Results

The CPHEEO manual on sewerage and sewage treatment suggest the return period of once in two years for the residential, commercial, and high-priced area. However, in the present study, return periods of 2-year, 5-year, and 10-year are taken into consideration for the design of the stormwater drainage network. The rational method to be used in the design of the stormwater drainage system assumes the intensity of rainfall to be uniform over the catchment. This intensity corresponds to the duration of rainfall equal to the time of concentration. The intensity–duration–frequency (IDF) relationship is derived from hourly rainfall data using Gumbel's method which is shown in Fig. 5.

The Indian standard specifies that for the developed area a 1 in 1-year rainfall frequency or a 1 in 2-year rainfall frequency is to be used. In the hydrologic practices, two methods for deciding the return period of rainfall are available. The more commonly used method is to prepare an Annual Maximum Series (AMS) and subject to frequency analysis by fitting a theoretical distribution. The other method is the analysis of a Partial Duration Series (PDS) which is constructed by counting all independent events above the threshold value. In this process, depending upon the threshold assumes, for a particular year there may not be any event and for another year there could be numerous events. Thus, while the AMS information would have one event per year, the PDS information would have a variable number of events per year, and the total number of events may be either less or more than the number of years. The method indicated in the CPHEEO manual is based on the PDS. However, the independence of the events in preparing the PDS data causes difficult problems. The return period as decided from AMS data and the PDS data are different but are theoretically related as shown in Eq. 11.

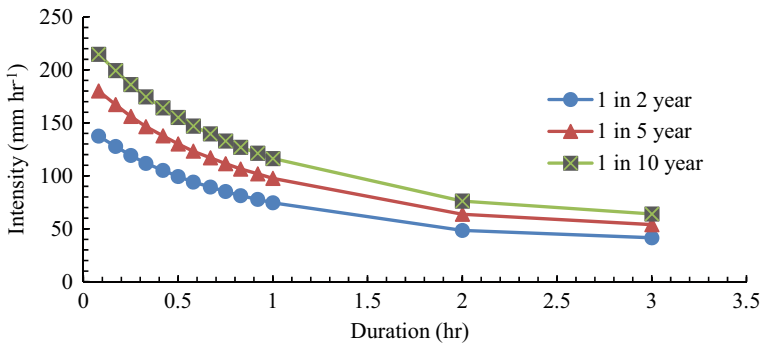$$T_p = -\frac{1}{\ln\left(1 - \frac{1}{T_a}\right)} \tag{11}$$

Fig. 5 IDF curve adopted for the stormwater design and analysis

Table 3 Coefficient of runoff for different land use pattern and return period

Land use pattern	C (2.56-year)	C (5.54-year)	C (11-year)
Buildings	0.75	0.80	0.83
Road	0.73	0.77	0.81
Vegetation/Recreational	0.30	0.33	0.36

where T_p is the average return period for level (threshold value) in PDS and T_a is the return period for AMS. Thus, the equivalent values for the return period 2-year, 5-year, and 10-year are taken as 2.56-year, 5.54-year, and 11-year respectively. The runoff coefficient is considered as per the guidelines in the CPHEEO manual and the final values that are used for the design purpose are shown in Table 3.

Bentley StormCAD v10.01 CONNECT Edition is used for the modeling and design of the stormwater drainage network of the SVNIT campus taking into consideration all the above-mentioned design criteria. The obtained results of the drain design for all four catchments are summarized in Tables 4 and 5. The layout of the

Table 4 Designed Storm-water drainage network for SVNIT campus

Parameters	Catchment 1	Catchment 2	Catchment 3	Catchment 4
Total length of network (m)	2900.6	2830.4	1661.9	1115.6
Maximum velocity (m/s)	1.52	1.67	1.59	1.95
Number of manholes	95	77	28	24
Invert level of the pipe draining to the trunk drain (m)	4.75	4.05	4.50	3.76
R.L. at outfall (m)	6.57	7.14	6.73	6.81
Discharge at outfall (m³/s)	1.12	2.47	1.25	2.61

Table 5 Details of the stormwater drainage network conduit for SVNIT campus

Diameter of drain (mm)	Length of the drain in catchment (m)			
	Catchment 1	Catchment 2	Catchment 3	Catchment 4
1200	57.7	390	194.3	235.1
1100	986.6	42.6	–	–
1000	–	43.8	–	240.2
900	–	143.9	384.9	–
800	1413.3	693.5	823.5	152.6
700	–	634.8	–	143.4
600	133.1	833.4	–	138.6
500	237.4	48.4	259.2	205.7
450	72.5	–	–	–
Total Length	2900.5	2830.4	1661.9	1115.6

Fig. 6 Layout of Pipe network for stormwater drainage

designed drain network is shown in Fig. 6. The cost estimate of the SVNIT campus stormwater drainage network is considered to be the future scope of the present work.

5 Conclusions

An efficient and separate stormwater drainage network has been designed for the SVNIT campus using STORMCAD v10.01. The total area of the SVNIT campus has been divided into four major catchments, and three outfall locations have been proposed. The outfalls of the drainage system have been taken care of at the same R.L. of SMC outlet provided in the institute to prevent backwater flow and waterlogging. The total runoff generated from the 100-ha area of the institute is 7.45 m^3 s^{-1} and has a stormwater network of about 8.51 km with the highest conduit diameter of 1200 mm. The model indicates that the designed network can take care of the runoff generated from buildings, roads, parking plots, gardens, and all other infrastructure and recreational areas and can give a solution for major problems of the present stormwater drainage system of SVNIT campus. It was ensured that the new development and facilities are free of flood hazards from major and smaller storm runoff

events. The methodology presented in the study can be useful to other educational institutes in India.

References

1. Wanielista MP, Yousef YA (1992) Stormwater management. Wiley, New York
2. Berland A, Shiflett SA, Shuster WD, Garmestani AS, Goddard HC, Herrmann DL, Hopton ME (2017) The role of trees in urban stormwater management. Landsc Urban Plan 162:167–177. https://doi.org/10.1016/j.landurbplan.2017.02.017
3. Locatelli L, Mark O, Mikkelsen PS, Arnbjerg-Nielsen K, Deletic A, Roldin M, Binning PJ (2017) Hydrologic impact of urbanization with extensive stormwater infiltration. J Hydrol 544:524–537. https://doi.org/10.1016/j.jhydrol.2016.11.030
4. Phillips R, Jeswani HK, Azapagic A (2018) Apul D (2018) Are stormwater pollution impacts significant in life cycle assessment? A new methodology for quantifying embedded urban stormwater impacts. Sci Total Environ 636:115–123. https://doi.org/10.1016/j.scitotenv.2018.04.200
5. Prudencio L, Null SE (2018) Stormwater management and ecosystem services: a review. Environ Res Lett 13(3):033002. https://doi.org/10.1088/1748-9326/aaa81a
6. Martin C, Ruperd Y, Legret M (2007) Urban stormwater drainage management: the development of a multicriteria decision aid approach for best management practices. Eur J Oper Res 181(1):338–349. https://doi.org/10.1016/j.ejor.2006.06.019
7. Overton DE, Meadows ME (1976) Stormwater modeling. Elsevier. https://doi.org/10.1016/C2013-0-11266-4
8. Saleh F, Ramaswamy V, Georgas N, Blumberg AF, Pullen J, Chen S, Holt T, Schmidt J (2019) An integrated weather–hydrologic–coastal–stormwater framework to model urban-coastal interactions: City of Hoboken application. J Flood Risk Manag 12(4):e12477. https://doi.org/10.1111/jfr3.12477
9. Manual on Sewerage and Sewage Treatment Systems. Central Public Health and Environmental Engineering Organization, Ministry of Urban Development, New Delhi (2012)
10. Kirpich ZP (1940) Time of concentration of small agricultural watersheds. Civ Eng 10(6):362
11. Mutreja KN (1990) Applied hydrology. Tata McGraw-Hill, New Delhi
12. Subramanya K (1991) Engineering hydrology. Tata McGraw-Hill, New Delhi
13. Natural Environment Research Council (1975) Flood Studies Report. HMSO, London
14. Chow VT, Maidment DR, Mays LW (1988) Applied hydrology. Tata McGraw-Hill, New York
15. Tomlinson AI: The frequency of high intensity rainfalls in New Zealand. Wellington, New Zealand (1980)
16. Kuichling E (1989) The relation between the rainfall and the discharge of sewers in populous districts. Trans Am Soc Civ Eng 20(1):1–56

Developing a Web Application-Based Water Budget Calculator: Attaining Water Security in Rural-Nashik, India

Aman Srivastava 🔾**, Leena Khadke** 🔾**, and Pennan Chinnasamy** 🔾

1 Introduction

Water is a limited freshwater resource and is essentially used for domestic, agricultural, industrial, and other development purposes [1, 2]. Over-exploitation of available water resources to meet individual requirements in the present context of climate change has put immense stress on global water security [3], thereby posing extraordinary challenges to the current water managers [4]. The total water resource available on the earth is constant; however, humans have been interfering directly or virtually with the hydrological cycle through land use land cover change, groundwater extraction, construction of dams, artificial rain, etc. [5–7]. The interference to the hydrological cycle at one stage can lead to serious consequences at some other stage due to the strong interdependency between the stages of the cycle [8]. India, having predominantly the rural and agricultural society, is no more exempted from the issue of water scarcity, security, and spatial non-uniformity in the water distribution [9–11]. The villages located in the arid and semi-arid climate zones of India experience erratic rainfall patterns with highly variable surface water storage [12]. The production through agriculture is primarily dependent on rainfall, as more than 60% of India's population relies on agriculture [13]. Studies also show the increase in integrated precipitable water in India by 4.69% against a 1 °C increment in regional

A. Srivastava (✉) · P. Chinnasamy
Centre for Technology Alternatives for Rural Areas (CTARA), Indian Institute of Technology Bombay, Mumbai 400076, India

P. Chinnasamy
e-mail: p.chinnasamy@iitb.ac.in

L. Khadke
Department of Civil Engineering, Indian Institute of Technology Bombay, Mumbai 400076, India

P. Chinnasamy
Rural Data Research and Analysis (RuDRA) Lab, Indian Institute of Technology Bombay, Mumbai 400076, India

warming [14]. More than the scarceness of the water is the mismanagement in the usage of this limited resource at a village level [15–17]. The increase in the demand for water-intensive activities and the effects of climate change has underlined the urgency and significance of sustainable management of water resources to attain water security [17–19]. Thus, there is a substantial need to understand the crucial components in the hydrological water balance so as to estimate water budgets.

Water is in a continuous recirculating hydrologic cycle involving *transportation components*, such as precipitation (or rainfall), evaporation, transpiration, infiltration, and runoff, and *storage components,* such as groundwater storage, soil moisture storage, and surface storage in the forms of ponds, lakes, reservoirs, etc. [20]. The first qualitative representation of the hydrologic cycle was introduced by Horton called Horton's representation of the hydrological cycle [21] which linked its significance with the major sectors, including agriculture, forestry, geography, economics, sociology, and politics. The interdependencies between the transportation and storage components of the hydrological cycle are quantified using the principle of continuity called the water budget equation [22]. Water budgeting of a particular catchment or a watershed helps the planner to design better water management policies and security provisions for the careful distribution of water [23].

In this regard, several attempts to develop a water assessment-based calculator have been undertaken in India. Puri et al. [24] used a water quality index calculator developed by the National Sanitation Foundation Information System to select the sampling points for measurement of the water quality index at various locations in the district of Nagpur in the Maharashtra state of India. Singh et al. [25] used a one-dimensional water balance model—Water Impact Calculator (WIC) developed by the International Crop Research Institute for the Semi-Arid Tropics, Hyderabad, India, to estimate the consumptive use. WIC required data on soil depth, evapotranspiration, precipitation, crop growth, topography, and crop management details as input. Surendran et al. [26] used Drought Indices Calculator (DrinC) software that calculates the drought indices such as Standard Precipitation Index, Reconnaissance Drought Index, and Streamflow Drought Index by providing an interface for the district of Madurai located in the semi-arid climatic zone of India. Awasthi et al. [27] developed a calculator to prepare a water budget of any discrete land unit such as agriculture and livestock using C language. The calculator estimated the water deficiency or surpluses of the land use.

The spatial information about water sources links statistical and socio-economic information to a location, bringing much-improved understanding and policy analysis both at the local (village) and state level (Central and State) [16, 17, 28]. In a general, estimation of the water availability, the study of the influence of hydrological and climatological parameters on water occurrence, circulation, and distribution on the earth and earth's atmosphere, and assessment of extreme events like flood and droughts [29] and strategies to combat them are of paramount importance [22], especially while proposing the sustainable water management and security plans [14, 17]. The designs and the operation of the projects are critical while developing a water supply irrigation and drainage network, flood control, coastal works, and recreational

uses of water. The precise estimation of the hydrological parameters such as precipitation, evaporation, and groundwater flow provides fundamentals to study the science of hydrology of a catchment or a watershed in a systematic manner. The major concern is identifying methods to optimize the usage of water obtained as precipitation through advanced computing and seamless modeling systems. However, this approach of water analysis and system design is expensive [30]. This is attributed to expensive modeling software and costly secondary data, even though the bulk of empirical formulae had been suggested by researchers for the estimation of the hydrologic parameters [14, 18, 21, 22, 31]. The task of data loading manually into the empirical relations while designing is time-consuming, tedious, and demands experience. Obtaining the data from the field and analyzing the same in the digital laboratory/computer systems increases the efforts, and expense, and further delays the work. To address this, an attempt has been taken in this study to use computer-based web applications for the estimation of the water budget by analyzing the abstractions of the precipitation from the given village-level watershed.

The primary objective of this study is to develop a water budget calculator (WBC) for estimation of the hydrological parameters using a server-side scripting language called PHP (Hypertext Pre-Processor that earlier stood for Personal Home Page). The secondary objectives include *(1)* the measurement of precipitation, calculation of the adequacy of the rain gauge station, estimation of the occurrence of extreme events, such as flood, assessment of the associated hydrological risk, calculation of the rate of evaporation, evapotranspiration, and infiltration, change in the depression storage, and estimation of surface runoff at micro-watershed level, with grounded case study from the rural-Nashik, India, and *(2)* developing water security plans and water governance strategies through local community participation under rural-settings. The objectives mentioned above require excellent quality and quantity of observation data; however, obtaining such data is challenging. In such instances, when observation data is limited, the use of Remote Sensing (RS) data, especially satellite imagery, has been widely used to address data gaps. This paper presents an integrated study using PHP, primary data, secondary data, RS, and field observations with a case study approach.

2 Methods

2.1 Study Area

The Shivaji Nagar is a remote village located in the Trimbakeshwar taluka (block) of Nashik district in the Maharashtra state of India (Fig. 1). The village is surrounded by the villages, viz., Holdar Nagar in the East, Somnath Nagar in the West, Vele at the South-West, Devergaon at South, and Peth taluka in the North. The village is geographically located at latitude 20.103883°N and longitude 73.55648°E, having a distance of 27 kilometers (km) from its administrative Trimbakeshwar taluka and
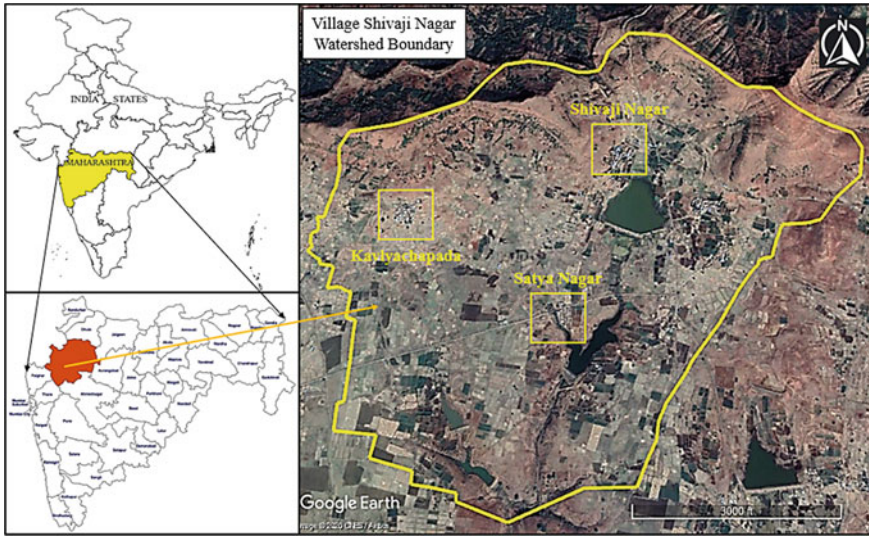
Fig. 1 Location of the study site—Shivaji Nagar village in the Nashik district showing three hamlets viz., Kavlyachapada, Shivaji Nagar, and Satya Nagar hamlets (insets showing the location in Maharashtra state and India)

42 km from Nashik district. The location of the study site lies in the Sahyadri range of Maharashtra, having a typical hilly climate with heavy rainfall. The average annual precipitation of the village is 207.2 centimeters (cm), and the average temperature of the place remains below 40 °C throughout the year. There are, in total, three hamlets under the boundary of Shivaji Nagar Gram Panchayat (GP) (village-level government in India) viz., Kavlyachapada, Shivaji Nagar, and Satya Nagar hamlets. The predominant occupation of the village is agriculture, and more than 90% of farmers practice rainfed farming. The source of water to the village is the South-West monsoon (June to September); however, during the non-monsoon period, other sources, such as check dams and small storage reservoirs, become the primary source for drinking water and irrigation. Although private wells are primarily employed for irrigation, the GP wells are typically used for supplying water for drinking water demand.

2.2 Development of Water Budget Calculator (WBC)

The WBC is developed using a server-side scripting language called PHP, with which a web application has been created, where all the hydrological parameters, targeted to be calculated, are available in a menu. The development of the WBC consists of nine operations, as depicted in Fig. 2 viz., *(1)* measurement of precipitation, *(2)* calculation of the adequacy of rain gauge stations, *(3)* probability of occurrence
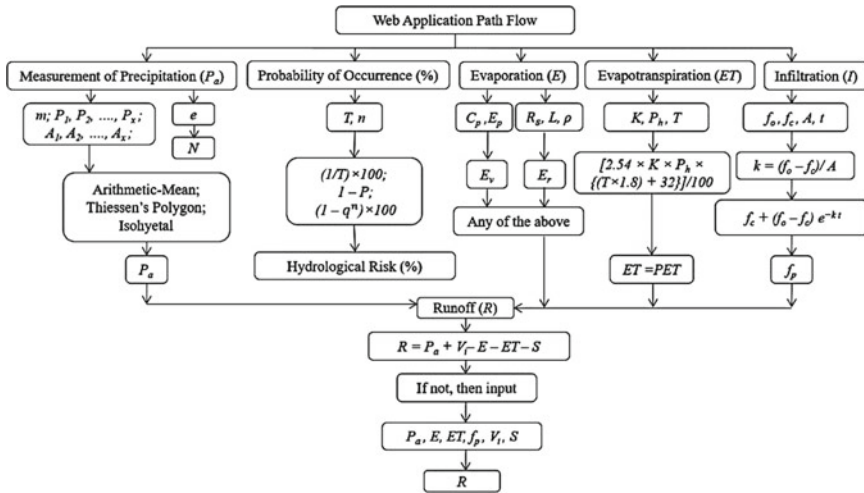
Fig. 2 Path flow for web application development of Water Budget Calculator (WBC) for Shivaji Nagar village in Nashik district of India

of extreme precipitation events, *(4)* assessment of hydrological risk, *(5)* volume of evaporation, *(6)* volume of evapotranspiration, *(7)* volume of infiltration, *(8)* volume of depression (surface) storage, and *(9)* volume of surface runoff. The calculator operates in the same sequence as listed from 1 to 9.

2.3 Measurement of Precipitation

In the present study, three methods on measurement of precipitation, namely, *(1)* Arithmetic-Mean method, *(2)* Thiessen-Mean method, and *(3)* Isohyetal method, have been used to convert the point sampling information of the magnitude of the rain gauge into precipitation over an area, such as at micro-watershed level. The WBC provides options for the user to select any of the methods to display the average precipitation (P_a). In this regard, the data on the number of rain gauges *(m)*, catchment area *(A)*, the magnitude of the precipitation measured from each station (P_x), where x is 1, 2, 3,…up to m, and the catchment area of each rain gauge (A_x) is required as input to WBC.

2.4 Adequacy of Rain Gauge Station

The WBC calculates the adequacy of the rain gauge station along with the measurement of precipitation with the same inputs. The optimal number of rain gauge stations

(N) required in the given catchment area has been obtained through statistical analysis using the values of the allowable degree of error in the measurement of the precipitation, expressed in percentage *(e)*, and the coefficient of the variation of the precipitation values *(C_v)*, as shown in Eq. 1. While the estimation of the value of C_v is based on the standard deviation *(SD)* of the precipitation values P_x from P_a, calculated using Eq. 2. Apart from the values of *m*, P_x, and A_x, the value of *e* is yet another necessary input needed to calculate the adequacy of the rain gauge station *(N)* in WBC.

$$N = \left(\frac{C_v}{e}\right)^2 \tag{1}$$

$$C_v = \frac{SD \times 100}{P_a} \tag{2}$$

2.5 Probability of Occurrence of Precipitation and Hydrological Risk

To record extreme events, such as floods, the probability of the occurrence *(P)* of extreme precipitation, such as precipitation, is expressed in terms of the return period *(T)*, as shown in Eq. 3. Whereas, in the case of the probability of the event not occurring in a year *(q)*, it is expressed as Eq. 4. While the binomial distribution has been used to calculate the hydrological risk [22, 32], which is fundamentally defined as the probability of the event occurring at least once in *n* successive years (frequency) and calculated in percentage, as shown in Eq. 5. The WBC calculates both the probability of occurrence (P) of precipitation and hydrological risk (h) with the input of the data on the return period *(T)* and frequency *(n)*.

$$P\% = \frac{1}{T} \times 100 \tag{3}$$

$$q\% = 1 - P\% = \left(1 - \frac{1}{T}\right) \times 100 \tag{4}$$

$$h\% = \left(1 - q^n\right) \times 100 \tag{5}$$

2.6 Estimation of Evaporation, Evapotranspiration, and Infiltration

The rate of evaporation (E_v) from the lake, or as such any surface water storage structures, has been calculated as a function of pan evaporation (E_p) by taking into account the pan coefficient (C_p) for two types of pan viz., *(1)* US Class A Evaporation Pan having an average value of C_p as 0.7, and *(2)* ISI Standard Pan, also called as Modified Class A Pan, having the value of C_p as 0.8 and is substituted, as shown in Eq. 6. In case, if the evaporimeters are not used in the estimation of evaporation depth, then the rate of the evaporation (E_r) is calculated based on the solar radiation (R_s) received per unit area, the mass density of the water (ρ), and the latent heat of vaporization *(L)*, as shown in Eq. 7. The data as input to WBC for the estimation of the depth of evaporation includes C_p, whereas the estimation of the rate of evaporation includes R_s and L, as the value of ρ is known.

$$E_v = C_v \times E_p \tag{6}$$

$$E_r = \frac{R_s}{L \times \rho} \tag{7}$$

The WBC estimates evapotranspiration using the Blaney-Criddle formula [8]. This empirical formula is based on data from the arid climatic conditions of the United States and takes into account the sunshine hours and temperature. The data as input to WBC for the estimation of the depth of evapotranspiration includes an empirical coefficient *(K)* that depends upon the type of the crop and the stage of the growth, monthly percent of annual day time hours (P_h), and average monthly temperature *(T)* in degree celcius (°C). For the given crop season, the depth of potential evapotranspiration *(PET)* is calculated, using Eq.

$$PET = ET = \frac{2.54 \times K \times P_h \times [(T \times 1.8) + 32]}{100} \tag{8}$$

.31
The WBC estimates the rate of infiltration using Horton's equation that primarily depends on three parameters viz., the initial rate of infiltration capacity (f_0), final constant rate of infiltration at saturation (f_c), and an empirical constant *(k)* depending primarily upon soil and vegetation and calculated, as shown in Eqs. 9a and 9b [12]. In this equation, the time from the beginning of the precipitation is represented by t, whereas the area under Horton's equation is represented by F_c. The data as input to WBC includes $f_0, f_c, t,$ *and* F_c. The WBC has been designed to calculate the value of k based on the already input data on f_0, and f_c.

$$f_p = f_c + (f_0 - f_c)e^{-kt} \tag{9a}$$

$$k = \frac{f_0 - f_c}{F_c} \tag{9b}$$

2.7   Estimation of Depression Storage and Surface Runoff

The WBC takes into account the change in the depression storage *(S)* based on the nature of depression, the type of the soil, slope of the watershed, the measure of the soil moisture, etc. The *S* is calculated as the difference between the initial water storage depth *(S$_1$)* to the final water storage depth *(S$_2$)*. The observed value of *S* obtained during the field survey is the direct input data for WBC. The volume of the water entering *(V$_i$)* into the watershed under consideration from the adjacent or another watershed has been taken into account in the water budget calculations. The estimation of the surface runoff *(R)* is based on the water budget equation and is expressed as shown in Eq. 10. The two options have been provided to the user for entering data into the WBC viz., *(1)* in the case if the user wanted to use the values of the other parameters (right-hand side of Eq. 10) for the estimation of *R*, then the WBC will automatically import those values directly into the equation, and *(2)* If the user wanted to input the fresh values of the other parameters, then WBC will provide separate entries for the input of the data for other parameters.

$$R = P_a + V_i - E_v - ET - f_p - S \tag{10}$$

2.8   Data Collection and Data Processing

The WBC is designed to estimate or calculate the aforementioned hydrological parameters using PHP. The data on the estimation of *E*, *ET*, *S*, and *R* has been obtained through recorded observations from the field. However, not all the data were obtained from the field for which the WBC is designed for. The unavailable data from the field includes *m*, *N*, *P$_x$*, *e*, *T*, *n*, *R$_s$*, *L*, *f$_0$*, *f$_c$*, *t*, and *F$_c$*. The study constructively assumed certian data, based on the experiences from the field investigation, for the village so as to validate the functionalities of WBC. The field surveys and the qualitative interviews were further conducted with the residents of the Shivaji Nagar village between May and July 2019 (at the interface of summer and monsoon). The purpose was to study and collect the information regarding the background of the field conditions concerning the functionalities of the surface water storage structures, availability of water across seasons, the type of the crops grown, and the significant changes in the land use land cover that happened in the past. The study comprehensively focused

on the data collection for the various hydrological parameters such as P, E, ET, G, S, and R.

Precipitation Data. The first hydrological parameter—P_a is obtained based on the analysis of the last 20 years of India Meteorological Department (IMD) rainfall data for the Trimbakeshwar taluka. The average annual rainfall in the area was calculated as 207.2 cm. Similar results were obtained by Sanjay et al. [33] Srivastava and Chinnasamy [17] and Gavit et al. [34]. However, to validate the accuracy of WBC in estimating N, m is assumed as seven, and the annual rainfall recorded for each rain gauge station in cm is considered as 130.0, 142.1, 118.2, 108.5, 165.2, 102.1, and 146.9. The values of P_a are obtained using the Arithmetic-Mean method. The value of e is assumed as 5%, whereas T for the extreme precipitation event is assumed 20 years, occurring at least once in 10 successive years *(n)*.

Evaporation Data. The ISI standard pan evaporimeter, specified by IS: 5973–1970, and also called as the Modified Class-A Pan, was used for the measurement of E. The monthly average depth of the water evaporated in May, June, and July was recorded at 1.40 cm/day (cm/d), 1.25 cm/d, and 0.60 cm/d, respectively. However, to validate the accuracy of WBC in estimating E with the other method, the R_s has been assumed as 200 watts/square meters (W/m^2) at a temperature of 25.0 °C, L of water as $2{,}441 \times 10^6$ joule/kilograms (J/kg), and ρ as 1,000 kg/cubic meters (kg/m^3), kept as default value in WBC. The parameters such as ground heat flux and sensible heat have been ignored for simplifying the calculations. Such an approach has been repeatedly used in past studies [35, 36].

Evapotranspiration and Infiltration Data. A large number of empirical formulae are available for the estimation of potential evapotranspiration (PET) based on climatological data [22, 32]. The current study uses the Blaney-Criddle formula, as it assumes that the PET is related to sunshine hours $[P_h]$ and temperature *[T]* [31]. The P_h in the study site for May, June, and July was measured as 7.8, 7.2, and 6.9 h, respectively. The values for T in the village (averaging maximum and minimum) for the same months were measured as 29.5, 27.5, and 25.0 °C, respectively. Apart from field data, the Central Water Commission (CWC) and the Food and Agricultural Organization (FAO) recommendations have also been considered for the estimation of evapotranspiration rates for the rest of the year [22, 32]. Depending upon the type of the crop and the stage of the growth, the K for the village is estimated as 0.6, 0.7, and 0.8 for May, June, and July, respectively. On the other hand, based on the soil survey and USGS method [37], the depth of infiltration was calculated. The value of f_0 was estimated as 6.5 millimeters/hour (mm/h), f_c was assumed as 1.5 mm/h, and k was 0.151/h.

Depression Storage Data. The surface storage capacity of the check dams was measured using remote sensing and field surveys. The depth of the check dams was obtained directly from the field, whereas the surface area was obtained using satellite images archived in Google Earth Pro. To identifying and classifying different land-use and depression storage in the study area, a manual supervised classification technique was employed using the polygon tool in Google Earth Pro [14, 15, 17]. In total, there were three check dams with an average depth of 4.5 m, 3 m (two of them are located in Shivaji Nagar hamlet), and 5.6 m (one is located in Satya Nagar
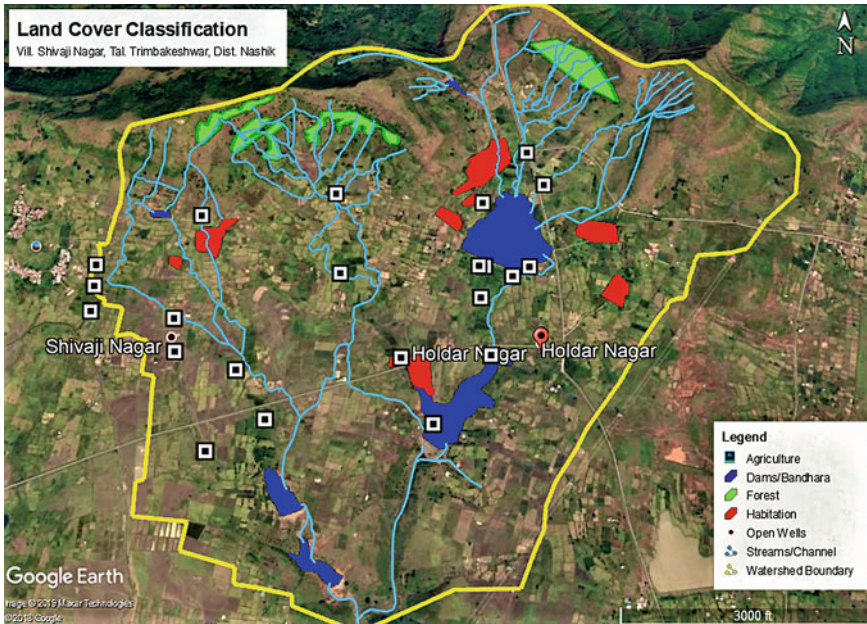
Fig. 3 Land use land cover classification of Shivaji Nagar village located in Trimbakeshwar Taluka (Tal. or Block) of Nashik district (Source: Google Earth Pro)

hamlet), respectively (Fig. 3) showing Shivaji Nagar watershed boundary having an area (~4.2 square kilometers) greater than its official geographical boundary. There were, in total, 11 open dug wells identified in the vicinity of the village whose volumes were calculated based on the measurement of (1) the total depth of the wells from the ground level to the base of the well and (2) the diameter of the well; both parameters were measured using meter tape for each well. The data on the runoff was measured based on the land use and land cover change (area), where the entire village was classified into four land-use classifications viz., forest, agriculture, habitation, and surface storage.

3 Results and Discussions

The efficiency of the WBC tool was analyzed by processing the data in two ways viz., *(1)* the data was analyzed by solving the problems manually, and *(2)* the data was input to the WBC, and the output was compared against *(1)*. The comparative analysis of the results obtained manually versus the results obtained using WBC was used for understanding the accuracy of the WBC tool. The present section focuses on the former (manual calculations) while the latter is covered in discussions (analysis with WBC calculations).

3.1 Precipitation Analysis

The manual estimation of the mean precipitation using the Arithmetic-Mean method *(P_{a,Arith})*, calculated using Eq. 11, was 130.43 cm, with a standard deviation *(SD)* of 22.54 (Eq. 12). Using *SD*, C_v was calculated as 17.28. Given *e* as 5%, the adequacy of the number of rain gauge stations *(N)* is estimated as 12, which represents the optimum number of rain gauges required in the given catchment (Eq. 13). Therefore, the number of additional rain gauges needed for the given catchment or watershed is the difference between the already existing rain gauge *(m)* and N, which eventually comes out as 5 (Eq. 14). Given *T* as 20 years, the probability of occurrence of the extreme precipitation is calculated as 5% (Eq. 15), while the probability of the not occurring of the same event eventually becomes 95% or 0.95 (Eq. 16). Substituting this value in Eq. 5 along with the frequency of the occurrence $(n = 10)$, the hydrological risk estimate was 40.13% (Eq. 17).

$$P_{a,\text{Arith}} = \frac{130.0 + 142.1 + 118.2 + 108.5 + 165.2 + 102.1 + 146.9}{7}$$
$$= 130.43 \text{ mm} \tag{11}$$

$$C_v = \frac{SD \times 100}{P_a} = \frac{22.545 \times 100}{130.43} = 17.28 \tag{12}$$

$$N = \left(\frac{C_v}{e}\right)^2 = \left(\frac{17.28}{5}\right)^2 = 11.95 \sim 12 \tag{13}$$

$$Additional\,Rain\,Gauge = N - m = 12 - 7 = 5 \tag{14}$$

$$P\% = \frac{1}{T} \times 100 = \frac{1}{20} \times 100 = 5\% \tag{15}$$

$$q\% = 1 - P\% \Rightarrow q = 1 - P \Rightarrow q = 1 - 0.05 = 0.95 \tag{16}$$

$$h\% = \left(1 - q^n\right) \times 100 = \left(1 - 0.95^{10}\right) \times 100 = 40.13\% \tag{17}$$

3.2 Evaporation Analysis

The pan evaporation approach considered Modified Class-A Pan for the measurement of the evaporation for which the value of C_p is 0.8 [22]. The monthly average depth of the water evaporated in May, June, and July for the village was recorded 1.4 cm/d, 1.25 cm/d, and 0.6 cm/d, respectively, whose average value *(E_p)* is calculated as

1.08 cm/d (Eq. 18). The rate of evaporation observed from a pan is corrected by the use of the pan coefficient to get the evaporation (E_v) from the surface water storage structures under similar climatic and exposure conditions. This provided the value of the rate of evaporation as 0.87 cm/d (Eq. 19). The other approach of estimating the rate of evaporation (E_r) is dependent on the solar radiation of 200 W/m² at a temperature of 25.0 °C, latent heat of vaporization of water of 2,441 × 10³ J/kg, and mass density of water having a default value of 1,000 kg/m³ [20]. Substituting these values in Eq. 7, E_r comes out as 0.71 cm/d (Eq. 20).

$$E_p = \frac{1.4 + 1.25 + 0.60}{3} = 1.08\frac{cm}{day} \tag{18}$$

$$E_v = C_p \times E_p = 0.8 \times 1.08 = 0.87\frac{cm}{day} \tag{19}$$

$$E_r = \frac{R}{L \times \rho} = \frac{200}{2441 \times 10^3 \times 1000} = 8.19 \times 10^{-8}\frac{m}{s} = 0.71\frac{cm}{day} \tag{20}$$

3.3 Evapotranspiration and Infiltration Analysis

The estimation of the potential evapotranspiration using the Blaney-Criddle formula was dependent on the average sunshine hours, which was identified as 7.8, 7.2, and 6.9 h for May, June, and July, respectively. The average temperature during the same months (averaging maximum and minimum) was measured as 29.5 °C, 27.5 °C, and 25.0 °C, respectively. Substituting these values in Eq. 8 along with the values of crop coefficient identified as 0.6, 0.7, and 0.8 for each aforementioned month [20], ET was estimated as 0.33 cm/d for May (Eq. 21), 0.35 cm/d for June (Eq. 22), and 0.35 cm/d for July (Eq. 23). Whereas, using Horton's equation and substituting f_0 as 6.5 mm/h, f_c as 1.5 mm/h, k as 0.15 l/h, and t as 10 h in Eq. 9, the infiltration capacity after 10 h was calculated as 0.26 cm (Eq. 24).

$$ET_{May} = \frac{2.54 \times 0.6 \times 7.8 \times [(29.5 \times 1.8) + 32]}{100} = 10.11\frac{cm}{month} = 0.33\frac{cm}{day} \tag{21}$$

$$ET_{Jun} = \frac{2.54 \times 0.7 \times 7.2 \times [(27.5 \times 1.8) + 32]}{100} = 10.43\frac{cm}{month} = 0.35\frac{cm}{day} \tag{22}$$

$$ET_{Jul} \frac{2.54 \times 0.8 \times 6.9 \times [(25.0 \times 1.8) + 32]}{100} = 10.80\frac{cm}{month} = 0.35\frac{cm}{day} \tag{23}$$

$$f_p = f_c + (f_0 - f_c)e^{-kt} = 1.5 + (6.5 - 1.5)e^{-0.15 \times 10} = 2.62mm = 0.26cm \tag{24}$$

3.4 Depression Storage Analysis

The satellite imagery was analyzed to estimate the total depression storage in the village watershed boundary. There were three check dams namely C_1, C_2, and C_3 with an average depth (d_1, d_2, d_3) of 4.5 m, 3 m, and 5.6 m, respectively, and having a surface area (a_1, a_2, a_3) of 2,807 m², 64,684 m², and 36,772 m², respectively. Apart from check dams, the village consists of 11 dug wells having diameter varying in the range of 6 m to 7.5 m (average diameter $(2r) = 6.64$) m) and the depth varying between 5 m and 16.5 m (average depth $(h) = 9.9$ m). Therefore, the total volume of the depression storage due to check dams (S_c) having a volume of 412,607 m³ (Eqs. 25a and 25b) and dug wells (S_d) having a volume of 3,771 m³ (Eq. 26) in the given village watershed area of 4,220,013 m² was estimated as 416,378 m³ (Eq. 31).

$$S_c = C_1 + C_2 + C_3 = (a_1 \times d_1) + (a_2 \times d_2) + (a_3 \times d_3) \tag{25a}$$

$$S_c = (2, 807 \times 4.5) + (64, 684 \times 3) + (36, 772 \times 5.6) = 412, 607 m^3 \tag{25b}$$

$$S_d = 11 \times (\pi \times r^2 \times h) = 11 \times \left(\pi \times \left(\frac{6.64}{2} \right)^2 \times 9.9 \right) = 3, 771 m^3 \tag{26}$$

3.5 Surface Runoff Analysis

The surface runoff was estimated using a water budget equation for the entire village watershed having an area of 4,220,013 m² across three months (between May and July having 92 days). Precipitation analysis showed that 91% of rainfall occurs during the monsoon. Assuming the total rainfall received in the village catchment as 80% (between May and July), the P_a volume was estimated as 6.9 M m³ (Eq. 27). The volume of water evaporated from the surface water storage structures was about 3.4 M m³ (Eq. 28), whereas the volume of evapotranspiration was estimated close to 1.4 M m³ (Eq. 29). Infiltration and additional volume inflow were assumed as 10% of the total precipitation that occurred within the watershed boundary, which comes out as 0.7 M m³(Eq. 30). The surface depression storage due to check dams and dug wells was estimated as more than 0.4 M m³ (Eq. 31). In terms of the rainfall-runoff relationship, the water budget equation can be represented as the difference between

precipitation (P_a) and losses (L). L signifies the volume of water from the watershed, which was not available for surface runoff due to evaporation, evapotranspiration, infiltration, and surface depression storage (Eq. 32). L contributes to the increment of soil moisture and groundwater storage. Using the water budget equation, the surface runoff was estimated as more than 1.8 M m^3. (Eqs. 32a and 32b).

$$P_a = 0.80 \times \left(\frac{207.2}{100} \right) \times 4,220,013 = 6,995,094\,\text{m}^3 \tag{27}$$

$$E_v = \left(\frac{0.87}{100} \right) \times 92 \times 4,220,013 = 3,377,698\,\text{m}^3 \tag{28}$$

$$ET = \left[\left(\frac{0.33}{100} \times 31 \right) + \left(\frac{0.35}{100} \times 30 \right) + \left(\frac{0.35}{100} \times 31 \right) \right] \times 4,220,013\,\text{m}^3$$
$$= 1,332,680 \tag{29}$$

$$f_p = V_i = \left(\frac{10}{100} \right) \times 6,995,094 = 699,509\,\text{m}^3 \tag{30}$$

$$S = S_c + S_d = 412,607 + 3,771 = 416,378\,\text{m}^3 \tag{31}$$

$$R = P_a + V_i - L = P_a + V_i - (E_v + ET + f_p + S) \tag{32}$$

$$R = 6,995,095 + 699,509 - (3,377,698 + 1,332,680 + 699,509 + 416,378) \tag{32a}$$

$$R = 1,868,351 m^3 \tag{32b}$$

3.6 Comparative Analysis

The validation of the WBC tool was checked by a comparative analysis between outputs obtained from WBC and manually obtained outputs. For this, the data for measurement of precipitation (m, P_x, and A_x), adequacy of the rain gauge station (e), assessment of hydrological risk (T and n), rate of evaporation (C_p and E_p), rate of evapotranspiration (K, P_h, and T), depth of infiltration (f_0, f_c, t, and F_c), and volume of runoff (P_a, V_i, E_v, ET, f_p, and S) were input to the WBC (such as the one shown in Fig. 4) to get WBC-based estimation. The output obtained from WBC for the adequacy of the rain gauge station and measurement of precipitation is shown in Fig. 5. The WBC calculated the number of rain gauge required in the catchment as 12 and the average precipitation as 130.3 cm. The output from WBC is identical
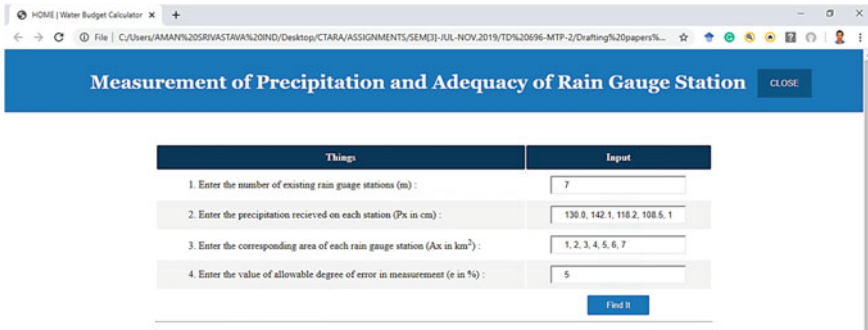
Fig. 4 Web application for Water Budget Calculator (WBC) showing input data for estimating the adequacy of rain gauge station and measurement of precipitation
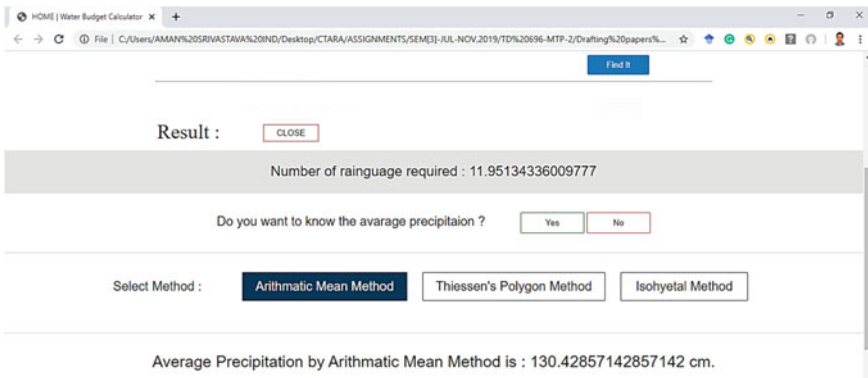

Fig. 5 Water Budget Calculator (WBC) showing outputs for the adequacy of rain gauge stations and measurement of precipitation

and consistent with the outputs obtained manually. The comparative analysis for the rest of the parameters indicates that the outputs from WBC operation and manual calculations are identical and consistent (listed in Table 1).

3.7 Opportunities for Water Management and Security Using WBC

The results obtained after WBC operations were scrutinized to understand the hydrological phenomena at the study site. Results indicated that the most dominant hydrological parameter in the village watershed between May and July 2019 is evaporation which was estimated as 48% of the total precipitation (received during the same duration) followed by surface runoff that was estimated as 26%. The evapotranspiration

Table 1 Comparative analysis of the outputs between the results obtained manually and the results obtained using the water budget calculator

Parameters	Manually calculated	WBC calculated
Measurement of Precipitation[*] (cm)	130.43	130.44
Adequacy of rain gauge stations	11.95	11.95
Probability of occurrence of extreme precipitation (in %)	5.00	5.00
Hydrological risk (in %)	40.12	40.12
Evaporation		
Pan Evaporation Method (cm/d)	0.87	0.87
Evaporation Method (cm/d)		
Rate of Evaporation Method (cm/d)	0.71	0.71
Depth of Evapotranspiration (cm) in		
May	0.34	0.33
June	0.35	0.35
July	0.36	0.37
Depth of Infiltration (cm)	0.26	0.26
Surface Runoff (m^3)	1,868,351	1,868,345

[*]*Precipitation has been estimated using the Arithmetic Mean Method*

was 20% of the total precipitation; however, the percentage volume of water identified as depression storage within the village watershed boundary was mere 6%. A few attributes to this huge water loss (in the form of evaporation, evapotranspiration, and the surface runoff which together becomes 94% of the precipitation received) from the watershed was due to the limited surface water storage capacity, poor maintenance of the existing check dams and reservoirs leading to their siltation, and the poor groundwater recharge potential. Similar inferences were observed by Srivastava and Chinnasamy [17] and Srivastava et al. [18]. Besides the findings from WBC, the study from the qualitative interview also validated the high rates of surface runoff from the village during monsoon due to its location over the steeper slopes of the Sahyadri hills. At the same time, the observation regarding depth to the water level in bore wells and dug wells showed the poor potential of the groundwater resources in that region. This could be attributed to the fact that the wells and the surface storage structures usually start getting up dry post-mid-winter. Thus, the water sources in the village were observed productive mostly from the mid-monsoon to post-monsoon season.

From the consideration of vulnerability to surface–groundwater storage and security at a village scale, there is a clear need to develop a robust mechanism on participatory forms of surface and ground water management and governance coupled with digitizing data collection using open-source web tools such as WBC (summarized in Fig. 6). The following series of steps could form the building block for village-level governance strategies with a considerable orientation towards WBC based web tools:

Fig. 6 Village-level facets for water management, governance, and security plan using Water Budget Calculator (WBC) (Wherein *P*: Precipitation; *R*: Surface Runoff; *E*; Evaporation; *ET*: Evapotranspiration; *I*: Infiltration; *S*: Depression Storage) (Source: Field investigation)
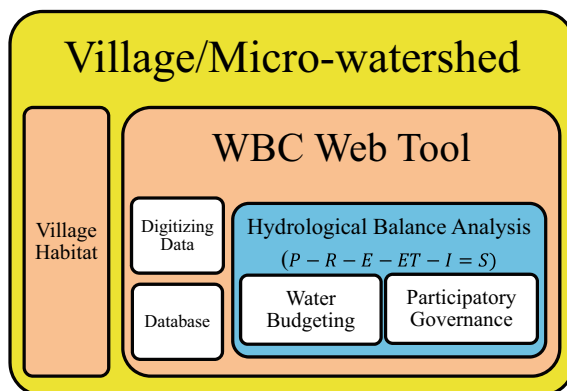
- It is recommended that the user should first develop a conceptual model for the given micro-watershed by specifically identifying the patterns of access to surface water sources (for example, check dams) and groundwater sources (for example, wells) and the associated social process that regulates its usage including agrarian and domestic practices.
- Status of available water resources can be obtained through conducting participatory rural appraisals (PRA) such as developing resource maps, social maps, Venn diagram, and by organizing focused group discussions, problem ranking exercise, qualitative interviews, transect walk, and other relevant community-based interactions involving villagers, farming and non-farming communities, representatives from educational institutions, and village-level administrative bodies [38].
- Once acquired the primary information on the prevailing trends of water usage and water security issues, scientific investigation through the surface–groundwater mapping approach can be adopted. It should demarcate location-specific surface–groundwater typologies to develop disaggregated hydrological and hydrogeological regimes by defining watersheds boundaries and mapping micro-level aquifers, respectively [39].
- To achieving participatory water governance, a pilot program on community mobilization on digital methods of collecting hydrologic and hydrogeologic data and hands-on training on mapping techniques can be organized at this stage.
- Then the WBC tool can be introduced and employed to quantify and analyze the surface–groundwater parameters and, at the same time, develop a comprehensive database for the water flow systems. This, in turn, provides scopes to prioritize location-specific water applications, such as for domestic, livestock, irrigation, and other primary livelihood purposes.
- Further, the key findings from the location-specific water attributes could be directed for effective decentralized management of surface–groundwater resources through water budgeting facets via community-level engagement. Such practices have been succeeded in dry parts of India such as Hiware Bazar and Ralegan Siddhi villages in Western Maharashtra (India) [20].

4 Conclusions

The primary objective of this study was to develop a Water Budget Calculator (WBC) using a server-side scripting language called PHP that resulted in a web application. This web application was designed to estimate the hydrological parameters at the micro-watershed or the village level th at included calculations on average precipitation, adequacy of the rain gauge station, estimation of the occurrence of extreme events such as flood or extreme rainfall, assessment of the associated hydrological risk, rate of evaporation and evapotranspiration, depth of infiltration, change in the surface depression storage, and estimation of surface runoff. The outputs obtained for these hydrological parameters using WBC were validated with the grounded field observations at the Shivaji Nagar village located remotely in the Sahyadri range in the Nashik district of the Maharashtra state in India. Field surveys along with qualitative and quantitative interviews with the villagers and Government officials provided primary data on the rate of evaporation and evapotr anspiration, and the depth of surface depression storage in the village. However, the data on the land use land cover and surface water storage area were obtained using remote sensing methods, while data on precipitation was obtained from secondary sources, and lack of certain data was assumed. The comparative analysis of the WBC-based outputs with manually solved outputs indicated high accuracy of WBC.

The development of user-friendly web applications, such as developed in this study, plays a role in monitoring performance in preparation for the water budget at the village-level. Acquisition and analysis of hydrological data of any catchment using WBC provide an opportunity to better understand the hydrological balance in terms of water security. This, in turn, provides a check over the sectoral specific water deficiency or surpluses thereby keeping the scope for careful water utilization. Community-level training programs over the conceptions of water budget along with the usage of web applications will increase overall sensitivity towards water-related applications. Such attempts are much more needed in these contexts and allow for the development of decentralized water management and security plans and designs.

References

1. Anbazhagan S, Jothibasu A (2016) Geoinformatics in groundwater potential mapping and sustainable development: A case study from southern India. Hydrol Sci J 61(6):1109–1123. https://doi.org/10.1080/02626667.2014.990966

2. Bajaj K, Thomas R, Yadav A, Datye A, Chakraborty S (2019) Hydrological linkages between different water resources from two contrasting ecosystems of western peninsular India: a stable isotope perspective. Isot Environ Health Stud 55(6):532–549. https://doi.org/10.1080/10256016.2019.1666121

3. Banerjee RR (2015) Farmers' perception of climate change, impact and adaptation strategies: a case study of four villages in the semi-arid regions of India. Nat Hazards 75(3):2829–2845. https://doi.org/10.1007/s11069-014-1466-z

4. England MI (2018) India's water policy response to climate change. Water Int 43(4):512–530. https://doi.org/10.1080/02508060.2018.1450569

5. Hutchings P, Franceys R, Mekala S, Smits S, James AJ (2017) Revisiting the history, concepts and typologies of community management for rural drinking water supply in India. Int J Water Resour Dev 33(1):152–169. https://doi.org/10.1080/07900627.2016.1145576

6. Kaushik N (2018) Impact of climate change on water resources in arid and semi arid region of Rajasthan. J Water Land Manag ISSN 16(2):0973–9300

7. Liu J, Yang H, Gosling SN, Kummu M, Flörke M, Pfister S, Hanasaki N, Wada Y, Zhang X, Zheng C, Alcamo J (2017) Water scarcity assessments in the past, present, and future. Earth's Future 5(6):545–559. https://doi.org/10.1002/2016EF000518

8. Mishra AK (2020) Variability of integrated precipitable water over India in a warming climate. Meteorol Appl 27(1):1–4. https://doi.org/10.1002/met.1869

9. Mouratiadou I, Biewald A, Pehl M, Bonsch M, Baumstark L, Klein D, Popp A, Luderer G, Kriegler E (2016) The impact of climate change mitigation on water demand for energy and food: an integrated analysis based on the shared socioeconomic pathways. Environ Sci Policy 64:48–58. https://doi.org/10.1016/j.envsci.2016.06.007

10. Nazemi A, Wheater HS (2015) On inclusion of water resource management in Earth system models–Part 1: Problem definition and representation of water demand. Hydrol Earth Syst Sci 19(1):33–61. https://doi.org/10.5194/hess-19-33-2015

11. Reddy VR (2018) Techno-institutional models for managing water quality in rural areas: Case studies from Andhra Pradesh, India. Int J Water Resour Dev 34(1):97–115. https://doi.org/10.1080/07900627.2016.1218755

12. Sajjad H, Nasreen I (2016) Assessing farm-level agricultural sustainability using site-specific indicators and sustainable livelihood security index: Evidence from Vaishali district. India Community Dev 47(5):602–619. https://doi.org/10.1080/15575330.2016.1221437

13. Singh R, Garg KK, Wani SP, Tewari RK, Dhyani SK (2014) Impact of water management interventions on hydrology and ecosystem services in Garhkundar-Dabar watershed of Bundelkhand region, Central India. J Hydrol 509:132–149. https://doi.org/10.1016/j.jhydrol.2013.11.030

14. Srivastava A, Chinnasamy P (2021a) Water management using traditional tank cascade systems: a case study of semi-arid region of Southern India. SN Appl Sci 3:281. https://doi.org/10.1007/s42452-021-04232-0

15. Srivastava A, Chinnasamy P (2021b) Investigating impact of land-use and land cover changes on hydro-ecological balance using GIS: insights from IIT Bombay India. SN Appl Sci 3:343. https://doi.org/10.1007/s42452-021-04328-7

16. Chinnasamy P, Srivastava A (2021) Revival of traditional cascade tanks for achieving climate resilience in drylands of South India. Frontiers in Water (3). https://doi.org/10.3389/frwa.2021.639637

17. Srivastava A, Chinnasamy P (2021) Developing village-level water management plans against extreme climatic events in Maharashtra (India)—a case study approach. In: Vaseashta A, Maftei C (eds) Water safety, security and sustainability. Advanced sciences and technologies for security applications. Springer, Cham. https://doi.org/10.1007/978-3-030-76008-3_27

18. Srivastava A, Khadke L, Chinnasamy P (2021) Web application tool for assessing groundwater sustainability—a case study in rural-Maharashtra, India. In: Vaseashta A, Maftei C (eds) Water safety, security and sustainability. Advanced sciences and technologies for security applications. Springer, Cham. https://doi.org/10.1007/978-3-030-76008-3_28

19. Srivastava A, Chinnasamy P (2021) Assessing groundwater depletion in Southern India as a function of urbanization and change in hydrology: a threat to tank irrigation in Madurai city. In:

S. Kolathayar et al. (eds), Climate change and water security. Lecture notes in civil engineering 178. Springer Singapore. https://doi.org/10.1007/978-981-16-5501-2_24 (In Press)

20. Todmal RS (2020) Understanding the hydrometeorological characteristics and relationships in the semiarid region of Maharashtra (Western India): Implications for water management. Acta Geophys 68:189–206. https://doi.org/10.3389/frwa.2021.639637

21. Horton RE (1933) The role of infiltration in the hydrologic cycle. Eos, Trans Am Geophys Union 14(1):446–460. https://doi.org/10.1029/TR014i001p00446

22. Subramanya K (2013) Engineering hydrology, 4th edn. Tata McGraw Hill Education Limited, New Delhi

23. Pandit C, Biswas AK (2019) India's national water policy: 'feel good' document, nothing more. Int J Water Resour Dev 35(6):1015–1028. https://doi.org/10.1080/07900627.2019.1576509

24. Puri PJ, Yenkie MKN, Sangal SP, Gandhare NV, Sarote GB, Dhanorkar DB (2011) Surface water (lakes) quality assessment in Nagpur city (India) based on water quality index (WQI). Rasayan J Chem 4(1):43–48

25. Singh AP, Bhakar P (2019) Development of groundwater sustainability index: a case study of western arid region of Rajasthan, India. In: Environment, development and sustainability, pp 1–25. https://doi.org/10.1007/s10668-020-00654-9

26. Surendran U, Kumar V, Ramasubramoniam S, Raja P (2017) Development of drought indices for semi-arid region using drought indices calculator (DrinC)–A case study from Madurai District, a semi-arid region in India. Water Resour Manage 31(11):3593–3605. https://doi.org/10.1007/s11269-017-1687-5

27. Awasthi MK, Awasthi A, Nema S (2019) WaBcal-A calculator for preparing water budget of discrete land unit. Int J Agri Environ Biotechnol 12(2):157–161. https://doi.org/10.30954/0974-1712.06.2019.12

28. Kumar MD, Pandit CM (2018) India's water management debate: Is the 'civil society' making it everlasting? Int J Water Resour Dev 34(1):28–41. https://doi.org/10.1080/07900627.2016.1204536

29. Khadke L, Pattnaik S (2021) Impact of initial conditions and cloud parameterization on theheavy rainfall event of Kerala (2018). In: Modeling earth systems and environment, pp.1–14. https://doi.org/10.1007/s40808-020-01073-5

30. Hazart A, Mori K, Tada K, Tosaka H (2014) Using surrogate modelling for fast estimation of water budget component in a regional watershed. In: 7th international congress on environmental modelling and software. San Diego, California, USA, pp 1583–1590

31. Blaney HF, Criddle WD (1950) Determining water needs from climatological data. USDA Soil Conservation Service. SOS–TP, USA, pp 8–9

32. Singh VP (2016) Chow's handbook of applied hydrology, 2nd edn. Tata McGraw Hill Education Limited, New Delhi

33. Sanjay C, Bhasker P, Damodare SL, Abhale AP (2018) Statistical analysis of seasonal rainfall variability in Nasik district by using GIS interpolation. J Pharmacognosy Phytochem 7(4):2072–2077

34. Gavit BK, Bonsod RD, Barai VN, Nimbalkar CA (2019) Analysis of rainfall received at Nashik district (Maharashtra state). BIOINFOLET 16(3):183–187

35. Bandyopadhyay A, Bhadra A, Raghuwanshi NS, Singh R (2009) Temporal trends in estimates of reference evapotranspiration over India. J Hydrol Eng 14(5):508–515. https://doi.org/10.1061/ASCEHE.1943-5584.0000006

36. Padmakumari B, Jaswal AK, Goswami BN (2013) Decrease in evaporation over the Indian monsoon region: implication on regional hydrological cycle. Clim Change 121(4):787–799. https://doi.org/10.1007/s10584-013-0957-3

37. Arnold RW (2016) Soil survey and soil classification. In: Environmental soil-landscape modeling. CRC Press, pp 50–72

38. Chambers R (1994) The origins and practice of participatory rural appraisal. World Dev 22(7):953–969. https://doi.org/10.1016/0305-750X(94)90141-4

39. Kulkarni H, Shah M, Shankar PV (2015) Shaping the contours of groundwater governance in India. J Hydrol: Regional Stud 4:172–192. https://doi.org/10.1016/j.ejrh.2014.11.004

Natural Hazards

A Review of Energy Dissipater as a Mitigation for Dam Risk Management

Aisyahira Melan, Agusril Syamsir, and M. H. Zawawi

1 Introduction

A dam is basically a man-made hydraulic structure built across a valley to provide sufficient water to users. However, there is a risk of dam overtopping during the extreme flood where the inflow of water increases and raise the reservoir level due to major rainfall situation. The problem of dam safety is one of the most important research topics of water conservancy projects, and many researchers pay much attention to study the risk of earth dam overtopping. To dispose surplus of water from the upstream to downstream effectively, a spillway system can be designed to pass safely floodwaters above, below, within, or around the dam [1]. These spillways are an important functional part of a hydroelectric facility.

Because of the conversion of whole potential energy into kinetic energy, water flowing over a spillway has a very high kinetic energy. Thus, a serious scour of the channel bed as illustrated in Fig. 1 may occur due to the high velocity of water that is discharged through the spillway or pipe outlet [2].

Along these lines, a hydraulic energy dissipator can be introduced as a device to protect the downstream area by scaling down the velocity of the flow to an acceptable limit. There are several types of energy dissipation devices that have been tried so far;

(i) Energy dissipation of block ramp (ii) Hydraulic jump type stilling basin, (iii) Stepped spillway, and (iv) Deflector—Flip bucket and ski-jump bucket [3]. Furthermore, the devices may be used as a barrier or obstruction to reduce the velocity of the flow resulting in better energy dissipation [4].

A. Melan (✉) · M. H. Zawawi
Department of Civil Engineering, Universiti Tenaga Nasional, Kajang, Malaysia

A. Syamsir
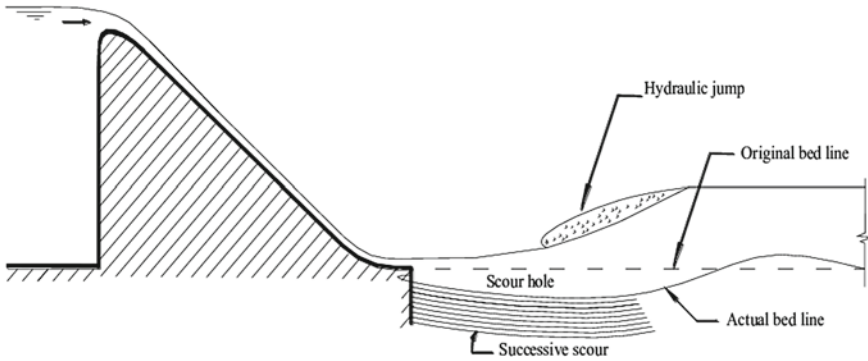Institute of Energy Infrastructure (IEI), College of Engineering, Universiti Tenaga Nasional, Kajang, Malaysia

**Fig. 1** Scour process downstream of a spillway [2]

2 Type of Energy Dissipator

2.1 Energy Dissipation of Block Ramps

Block ramps are naturalistic stream structures that are often used to satisfy a correct balance between hydraulic functioning and environmental impact. Chanson [1] Fig. 2 shows the illustration of the block ramp on the spillway. According to Pagliara, block ramps give a minor environmental impact compared to traditional hydraulic structures such as sills and check dams that usually became a barrier for fish migration, present problems of landscape insertion, and sometimes reduce solid transport. Pagliara et al. [5] Due to the large roughness, block ramps have been classified as an effective dissipation for the energy at the downstream of hydraulic structures such as spillways, over-flow dams, and trench weirs. A morphological and structural classification of block ramps is illustrated in Fig. 3 [6].

Various studies have been conducted to study the numerous aspects of block ramps. Pagliara and Chiavaccini [7] conducted an experiment to study the energy dissipation caused by the presence of a block ramp. With different bed materials, ranging from very coarse sand to small cobbles, the experiment is conducted on ramps, considering the different slopes of the bed ranging from 1 V:4H to 1 V:12H. Essentially, the amount of energy dissipation is a function of the slope, the relative

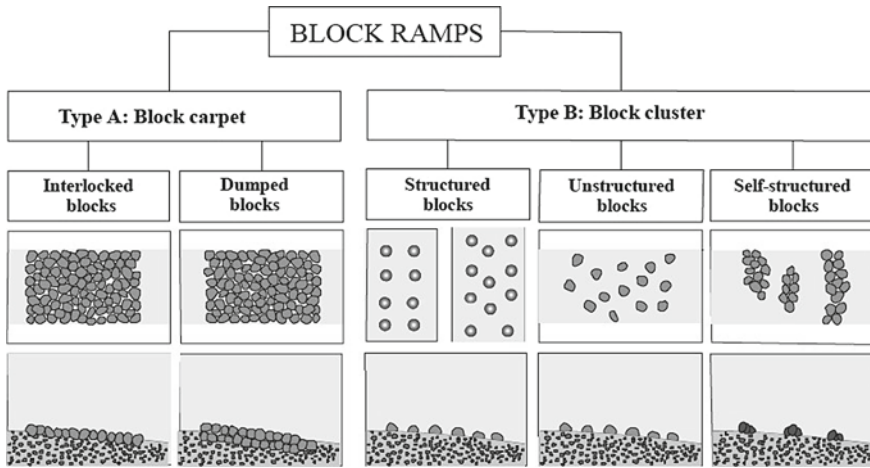**Fig. 2** Scour process downstream of a spillway [9]
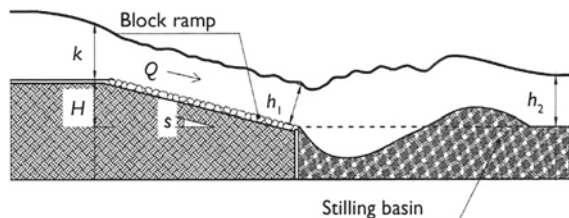
Fig. 3 Morphological and structural classification of block ramps [6]

submergence, and the ratio between the length of the slope and the critical water depth. Through this study, it can be concluded that the energy dissipation decreases with the slope of the ramp and from small-scale roughness to large-scale roughness [5].

Zulfequar et al. [8] studied the effect of energy dissipation at the block ramp with the existence of boulders on the bed. The experiment is conducted on a ramp where the boulders are hemispherical in shape, arranged in a staggered layout with base material on its bed. The author experienced that staggered arrangement contributes to the higher dissipation of energy in correlation to the boulder with random arrangements. Relative energy dissipation not only depends on discharge flow, but also depends on the concentration and the size of boulders. Furthermore, in comparison to the smooth base material, the author noticed that the dissipation of energy was considerably improved in conjunction with the flow resistance by the staggered arrangement of the boulders placed over the ramp. It shows that the relative dissipation of energy increases with the decreasing of the boulder's spacing [8].

2.2 Stepped Spillway and Cascade

A system of the spillway is an opening intended to spill securely the floodwater. The spillway is also required to dissipate the turbulent kinetic energy of the flow before it rejoins the natural river channel. Figure 4 shows a schematic diagram for a stepped spillway.

The construction of a step on the spillway contributes to the dissipation of the energy, subsequently diminishing the measure of downstream stilling structure. Novak et al. [3] Many studies, as well as engineering practices, show that the aeration
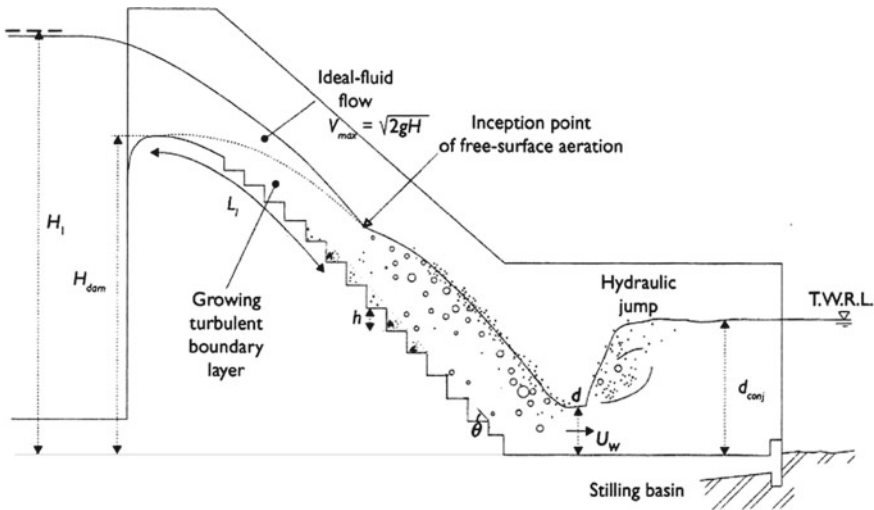
Fig. 4 Stepped spillway schematic diagram [1]

of flow and the vortex on the steps may dissipate the energy of the flow. Wu et al. [11] According to Roushangar et al. [12], the acceleration and final velocity of the flow may be reduced as the steps in the spillway act as roughness elements. The author believed that a stepped spillway has a stepped ogee-profile spillway instead of the traditional smooth ogee-profile spillway, where a series of drops are made in the invert from the area of the crest to the toe Roushangar et al. [12].

Gamal et al. [13] investigated the over-flow, through flow, and under-flow breakers in the stepped spillway. In the investigation, the author constructed a physical model of four steps to evaluate their effect in dissipating the energy. Breakers are installed over the steps of the spillway, providing three types of breakers as shown in Fig. 5. The experiment resulted in a significant improvement in dissipating the energy through the stepped spillway with the addition of appurtenance such as breaker. On the other hand, comparing the energy dissipation in three different types of breakers, it can be concluded that the three-hole breaker gave the maximum result in dissipating the energy [13].

Felder and Chanson [14] conducted an experiment to compare the effect of energy dissipation between uniform step heights and non-uniform step heights. A physical study was conducted with 5-stepped structure in a steady slope-stepped chute (1 V:2H). The rates of energy dissipation for all configurations were calculated in both skimming and transition flow regimes. From the physical study, the author noted that the rate of energy dissipation decreases with an increment of discharge. Nevertheless, there is inequality for all configurations in terms especially of the dissipation of energy as well as the pattern flow. A little difference in the rate of energy dissipation indicates that the design of a stepped spillway with non-uniform step height results in no improvement in terms of dissipation of energy at the end of the chute [14].

Fig. 5 Configuration of breakers [13]

Breaker without holes.

Breaker with small holes.

Breaker with large holes.
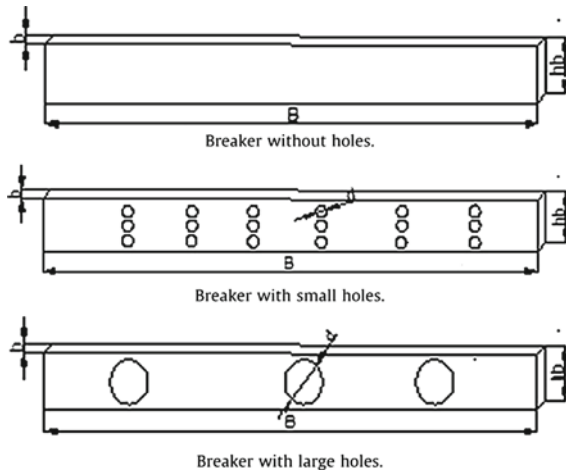
Chen [15] studied the factors influencing the energy dissipation ratio of the stepped spillway. In this study, some main factors that influence the energy dissipation ratio are noted as units discharge, dam slope, and height of the step. Due to the increment of turbulence kinetic energy that occurs during higher unit discharge, the dissipation of energy is shown to be decreased. The author believes that some additive structures should be designed to increase the energy dissipation rate. On the other hand, the smaller dam slope resulted in the increment of the energy dissipation ratio. The height of the step influences the energy dissipation ratio differently depending on the unit discharge. The influence of height becomes less with a large amount of discharge and vice versa. The energy dissipation ratio showed a slight increment with the addition in the step height. Thus, the author concludes that the suitable step height should be chosen depending on the unit discharge in the design [15].

## 2.3 Hydraulic Jump Type Stilling Basin

Due to their efficiency and simplicity, hydraulic jump type energy dissipators are popular and widely accepted while designing hydraulic structures such as weirs, dams, and barrages [16]. In an open channel, the hydraulic jump can be illustrated as a sudden and rapid transition from a supercritical to a subcritical flow. It is often used to dissipate the kinetic energy that produces from the high velocity of water flows in a hydraulic structure [3]. In order to reduce the energy contained in the flow, stilling basin is necessary to be built as an energy dissipater [17]. To stabilize the jump as well as improving the energy dissipation, additional devices may be introduced to the stilling basin.

According to Alikhani et al. [18], in designing a stilling basin, chute block, baffle block, and end sill are the device that are always being used with different configurations. Figure 6 shows the location of these appurtenances in the stilling basin. Each of these elements provides a different role to make sure the energy can be optimally dissipated. The first one is chute blocks normally placed into the inclined sections of the spillway. It is a group of concrete blocks that are commonly placed at the head of the stilling basin to generate turbulence prior to the hydraulic jump. The second element is baffle blocks. It is a freestanding concrete block placed in the main basin. Due to the high force that they have been subjected to and the potential for cavitation, these blocks are only used for flows below 20 m/s. Finally, the last element is end sills. It is a built-up lip at the tail of the basin, with or without blocks. The height of the end sills has the most significant impact on energy dissipation. Moreover, taller sills are reused in reducing the overall length of the stilling basin [18].

Yadav [16] et al. studied the design of a hydraulic jump type stilling basin for the over-flow weir of the canal at Warana dam. By applying Froude's model law, a physical model study is carried out in order to study the percentage of energy dissipator and the location of the jump depending on the amount discharge flow, the subcritical depth of flow, and the initial Froude number. The experiment is conducted in the laboratory considering variable discharge ranging from design charge to around 20% of design discharge. The experiment resulted in stabilizing the condition downstream for the overall flow scenario in the stilling basin. The author concluded that the arrangement of energy dissipation ensures that the length of the stilling basin is within an acceptable limit. Literally, the stilling basin length is possible to be minimum length to satisfy the location of the jump for varying discharge [16].

Ashraf [19] conducted an experiment to study the optimum shape of the baffle pier which gave the maximum dissipation of energy. In the experiment, 14 different models of baffle piers were introduced in the flume to have approximately the same pass of water flow, and the position of piers is set to be in a fixed position in a row. In this study, it is found that the model with a concave surface is able to increase the change of flow direction with low turbulence intensity in recirculation zone downstream baffle piers. Besides, the energy dissipation is higher than the other shape of the model. The author concluded that the vertical semi-circular section is
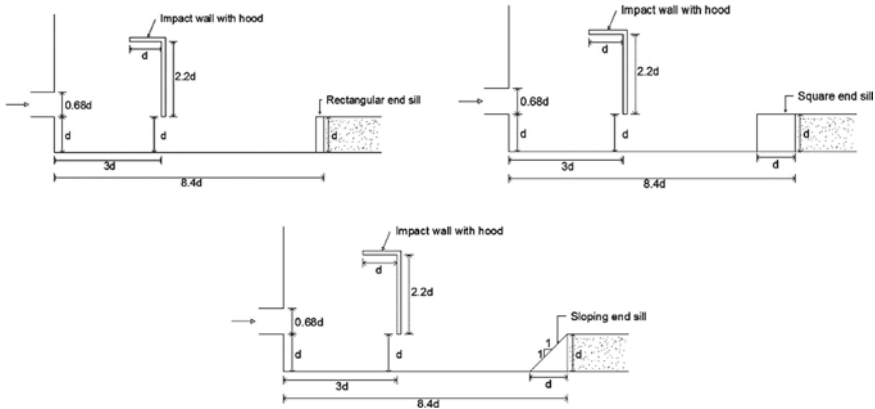
Fig. 6 Stilling Basin [1]
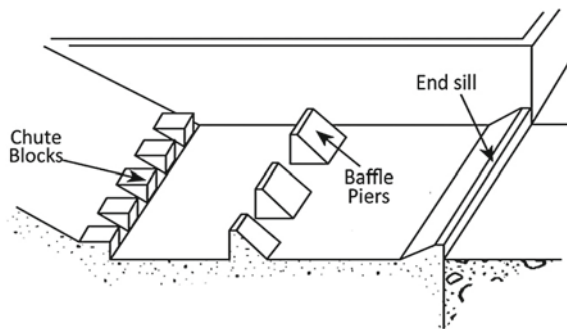
Fig. 7 Variation shape of end sill [20]

dissipating the energy higher than the other model. The author also believes that the right choice of baffle piers is important to have a stable hydraulic condition and a shorter stilling basin [19].

Tiwari et al. [20] inspected the energy dissipation by varying the shape of the end sill for the rectangular pipe outlet basin. The author mentioned that the sill plays an imperative role in reducing the length of the stilling basin and helps to enhance the flow pattern downstream of the channel. In the experiment, the 3 shapes of end sill were tested with three Froude numbers values as 1.85, 2.85, and 3.85. Figure 7 shows the shape of the variation of the end sill tested in this experiment. It is shown that the shape of the end sill affects the maximum depth of scour and hence the scour index. During this study, it was found that the sloping end sill (1 V:1H) with vertical face upstream improved the dissipation of energy compared to the other end sill [20].

2.4 Deflector—Flip Bucket and Ski-Jump Bucket

Nevertheless, in certain cases, it is suitable to direct the discharge water from the spillway into the river without pass across the stilling basin. In order to achieve effective energy dissipation, there are several types of deflectors used at the end of the release works of the hydropower project [21]. By constructing a deflector bucket at the toe of the spillway, the water strikes a riverbed which can provide a secure distance between the dam and spillway. Figure 8 shows the type of deflector that is commonly used as a spillway element. The flip bucket (also known as roller bucket) is deflecting the discharge water upwards to generate disintegration in the air whereas the jet of a ski-jump spillway spills horizontally [22].

Jian-Hua et al. [21] studied the effect of the slotted-flip bucket by varying the width and the angle of the slot. The author conducted the study theoretically and
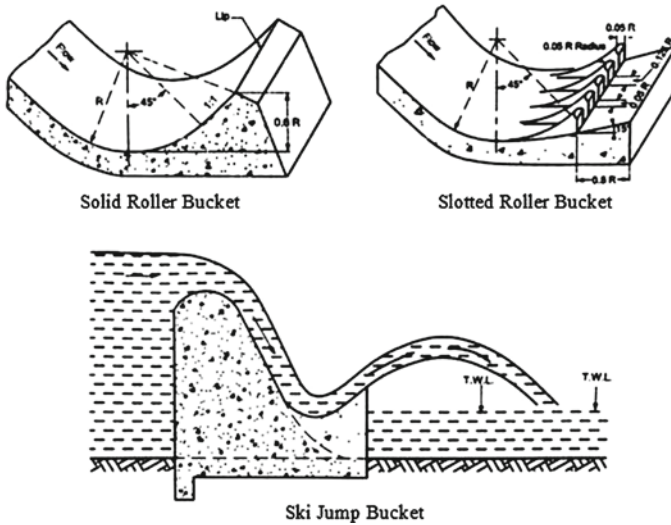
Fig. 8 Variation type of deflector [22]

experimentally to estimate the dissipation of energy. Throughout the experiment, it can be noticed that the slot helps the division of water flow, which develops three branches in the right, middle, and left. The effect of separation becomes greater as the slot angle increase resulting in higher energy dissipation [21].

In another study, Shantuo et al. [23] investigated the hydraulic characteristic of ski- jump-step energy dissipator by conducting an experiment. The study includes the fundamentals and performance of energy dissipation, flow regime, pressure distribution, and the characteristic of the air entrainment. For the stepped chute that having an immense discharge value, the author had introduced a method along with a new approach in dissipating the amount of energy. Figure 9 shows the sketch of the ski-jump-step energy dissipator developed in this experiment. It can be shown in the experiment that the dissipation of energy on the ski-jump-step energy dissipator is said to be greater than the other steps. The author also believes that the design of the aeration basin helps in dissipating the energy with a result of absorption of aeration in ski-jump jet during the development of water cushion. This is due to vortex formation and the impact of the jet flow. Moreover, the aeration basin provokes the preaereted flow and thus improves the performance of flow as well as the dissipation of energy in the stepped chute downstream. The author concluded that the defalcation of energy dissipation in the common stepped chute that has a higher discharge can be improved [23].

Heller et al. [24] studied the hydraulic of trajectory spillway which focuses on the countenance of the main flow for a 2-D jet where the jet is deflected into the atmosphere with the existence of a circular-shaped bucket. An experiment of a total of 91 tests was conducted which considering three different radii for the bucket (R = 0.10, 0.25, and 0.4 m). The deflection angles of the bucket were varied to 10, 15, 20,
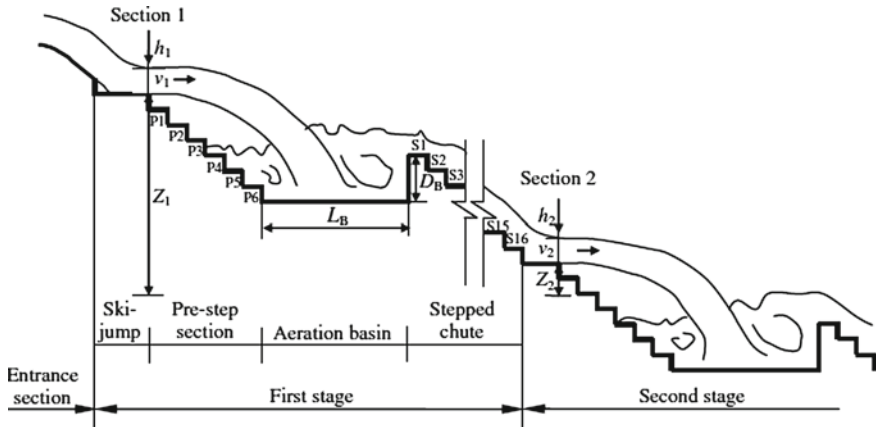
Fig. 9 The sketch of ski-jump-step energy dissipator [23]

25, 30, and 40°. The result demonstrates the increase in the rate of energy dissipation when the elevation difference between the tailwater channel and the takeoff point increase. In another hand, the dissipation of energy across a ski jump was also observed to improve with the deflection angle and smaller relative bucket curvature [24].

3 Basic Consideration

According to South Dakota Drainage Manual, there are some considerations which need to be fulfilled in selecting the type of energy dissipator; (i) debris control—debris control should be considering the limitation of clean-out access and dissipator should be able to pass the debris, (ii) flood frequency—the frequency of flood used in designing energy dissipator should be the same as flood frequency used for the culvert design, (iii) ice buildup—the size of dissipator structure should not obstruct the winter low flow and external dissipator may be used if ice buildup is a factor, (iv) tailwater relationship—depth of tailwater and maximum velocity for a range of discharge need to be determined by evaluating the hydraulic condition at the downstream, (v) cost—considering construction cost, replacement cost, maintenance cost, traffic delay cost, and the difficulty of construction, (vi) maximum culvert exit velocity—the velocity at the culvert exit should be consistent with the maximum velocity in the natural channel or should be mitigated using energy dissipator or channel stabilization [25].

4 Conclusion

To provide a long-term water reserve and protection of floods to our society, dams and reservoirs are the most effective alternative. The main component for the safety of the dam is the spillways system designed to safely pass the floodwater. At the high velocity of discharge, it is important to protect the downstream area by introducing and selecting the most suitable energy dissipator depending on location, the velocity of flow, and the initial Froude Number. During the literature review, it was noted that plenty of work has been carried out by past researchers related to the energy dissipator. Although there are many energy dissipation devices that have been designed in conjunction with spillways, outlet works, and canal structures, it is important to make model studies of individual structures to be certain that these will operate as anticipated due to the uncertainty that exists in the repetitive experiment and test regarding the overall performance characteristics of energy dissipators.

References

1. Chanson H (2015) Energy dissipation in hydraulic structure. CRC Press/Balkema, London, UK
2. Panwar A, Tiwari HL (2014) Hydraulic energy dissipators-a review. Int J Sci Eng Technol 3(4):400–402
3. Novak P, Moffat AIB, Nalluri C, Narayanan R (2007) Hydraulic structures. Taylor & Francis, New York, NY
4. Abourohiem MA, Abourohiem MA, Abourohiem MA (2018) Dissipation of mechanical energy over spillway through counter flow. J Croation Assoc Civil Eng 70(5):377–391
5. Pagliara S, Das R, Palermo M (2008) Energy dissipation on submerged block ramps. J Irrigation Drainage Eng 134(4):527–532
6. Ahmad Z, Srisvastava D (2014) Energy dissipation on block ramps with large scale roughness. J Hydraulics Eng 1–8
7. Pagliara S, Chiavaccini P (2006) Energy Dissipation on Block Ramps. J Hydraulics Eng 132:41–48
8. Ahmad Z, Petappa NM, Westrich B (2009) Energy dissipation on block ramps with staggered boulders. J Hydraulics Eng 135(6):522–526
9. Pagliara S, Palermo M (2008) Scour downstream of a block ramp in asymmetric stilling basins. Fourth Int Conf Scour Erosion A-23:240–245
10. Tuna M (2012) Effect of offtake channel base angle of stepped spillway on scour hole. Iranian J Sci Technol Trans Civil Eng 36(C2):239–251
11. Wu JH, Zhang B, Ma F (2013) Inception point of air entrainment over stepped spillways. J Hydrodyn 25(1):91–96
12. Roushangar K, Akhgar S, Salmasi F, Shiri J (2014) Modeling energy dissipation over stepped spillways using machine learning approaches. J Hydrol 508:254–265
13. Abdel Aal GM, Sobeah M, Helal E, El-Fooly M (2018) Improving energy dissipation on stepped spillways using breakers. Ain Shams Eng J 9(4):1887–1896
14. Felder S, Chanson H (2011) Energy dissipation down a stepped spillway with nonuniform step heights. J Hydraulics Eng 137(11):1543–1548
15. Chen Q (2005) Influencing factors for the energy dissipation ratio of stepped spillways. J Hydrodyn 17(1):50–57

16. Yadav BA, Sonaje NP, Sathe NJ (2015) Design of hydraulic jump type stilling basin at Warana canal. Elixir Int J 79:30286–30288
17. Abdurrosyid J, Wibowo GD, Setiyaningsih I, Adipura PJ (2018) Influence of baffle block and weir downstream slope at stilling basin of solid roller bucket type on hydraulic jump and energy dissipation. AIP Conf Proc 1977(040031):1–10
18. Alikhani A, Behrozi-Rad R, Fathi-Moghadam M (2010) Hydraulic jump in stilling basin with vertical end sill. Int J Phys Sci 5(1):025–029
19. Bestawy A, Hazar H, Ozturk U, Roy T (2013) New shapes of baffle piers used in stilling basins as energy dissipators. Asian Trans Eng 3(1):1–7
20. Tiwari HL, Goel A (2011) Experimental study of effect of end sill on stilling basin performance. Int J Eng Sci Technol (IJEST) 3(4):3134–3140
21. Hua Wu J, Fang Li S, Ma F (2018) Energy dissipation of slot-type flip buckets. J Hydrodyn 30(2):365–368
22. Thomas H (1976) The engineering of large dams. Wiley, New York
23. Qian S, Wu J, Ma F (2016) Hydraulic performance of ski-jump-step energy dissipater. J Hydraulics Eng 142(10):05016004
24. Steiner R, Heller V, Hager WH, Minor H-E (2008) Deflector ski jump hydraulics. J Hydraulic Eng 134(5):562–571
25. South Dakota Drainage Manual, Chapter 11, South Dakota Department of Transportation (2011)

Overview of Water Resources in Kerala and Feasibility of Coastal Reservoirs to Ensure Water Security

U. S. Amala Krishnan and Sreevalsa Kolathayar

1 Introduction

Kerala, the Gods own country, is rich in all the amenities they need for their existence. It is famous for its beauty of nature, greenery, backwaters, rivers, etc. The network of brackish water lakes and river estuaries distributed along the length is the greatest asset of the state. Kerala has 44 rivers. The drainage area and the total flow of some rivers are given in Table 1. Bharathapuzha, Periyar, Chaliyar, Pamba, Kallada, etc. are the major coastal rivers, and Vembanadu and Ashtamudi are the main among the 15 major lakes of Kerala.

2 Major Water Sources in Kerala

2.1 Rainwater

The average rainfall in the state is 3055 mm, which is double the national average. Kerala receives 69% of the annual rainfall during the Southwest monsoon and 16% during the Northeast monsoon and the remaining during summer (Fig. 1) (Customized Rainfall Information System (CRIS)). The water received as precipitation drains quickly into the sea due to the physiographical pattern and topography of the region. Kerala has been declared as drought-affected as there is a deficiency in rains. The farming activities get affected adversely due to the reduction in the number

U. S. Amala Krishnan
Sarathy Geotech Engineering Services Pvt. Ltd., Bangalore, India

S. Kolathayar (✉)
National Institute of Technology Karnataka, Surathkal, India
e-mail: sreevalsa@nitk.edu.in

Table 1 Hydrological parameters of major river basins in Kerala

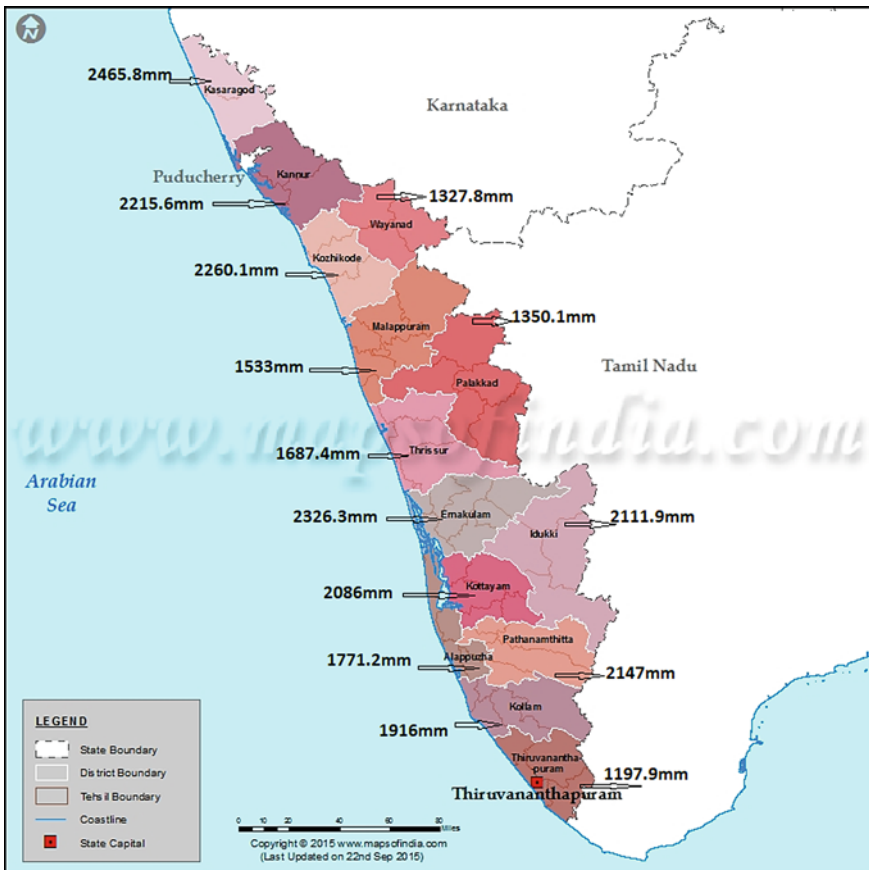| River	Drainage area (km^2)	Total flow (Mm^3)
Periyar	5284	5180
Bharathapuzha	6,186	4000
Meenachil	1272	1190
Manimala	847	1217
Pamba	2235	3961
Achenkovil	1484	2017
Muvattupuzha	1554	4780
Chalakudy	1404	1167
Karuvannur	1054	1413
Keecheri-Puzhakkal	635	975

Fig. 1 Map showing annual rainfall of Kerala districts (2016). *source* www.mapsofindia.com modified

of rainy days and erratic rainfall pattern, which in turn affects the food security of the state.

2.2 Groundwater

Groundwater is also a major water source in the state. The people of the state extract groundwater through open wells or bore wells. Population growth and rapid urbanization have led to increased use of groundwater resources in Kerala during the past several years. The net groundwater availability of the whole state is reported as 6.07 billion cubic meters (BCM) (http://www.kerenvis.nic.in/Database/WATER_820.aspx). Groundwater sources have been used for 80% of rural and 50% of urban population for domestic purposes and 50% for irrigation activities. The ease and simplicity of its extraction made this source accessible to all. But this mainstay has been declining because of the problems of declination of the water table, pollution of groundwater, seawater invasion, etc.

2.3 Other Resources

Along with rivers and wells sources like tanks, ponds, springs etc., surangas are also playing their roles in supplying water for both drinking and irrigation purposes. A suranga is a narrow horizontal tunnel, dug into laterite hills until a water spring is found. The porous laterite can store water. The clay in the laterite mud holds the water, which is the key in the process of surangas. There are about 510 surangas in Kasargod district of Kerala. There are around 1000 tanks and ponds in the state having more than 15,000 Mm^3 of water storage in summer. Around 240 natural springs are there in the highland regions of Kerala state which are used for drinking water supply and for small-scale irrigation in remote areas.

2.4 Water Supply Schemes

The major challenge in the water supply sector is the supply of drinking water of high quality to all the population. Kerala Water Authority (KWA) covers around 1.75 crore population (52.30% of the population) through their water supply schemes. KWA and KRWSA (Jalanidhi) are the two main agencies distributing drinking water in Kerala. KWA is involved in implementing major schemes and mainly concentrating on Urban Water Supply. Jalanidhi is involved in small Rural Water Supply Schemes.

2.5 Dams

Kerala is a region with plenty of dams. As there are plenty of rainfall and rivers, Keralites depend more on hydroelectric projects for electricity. There are around 33 dams and reservoirs locating in Kerala state. They also serve purposes like irrigation, drinking water supply, etc. Dams cause a disturbance to the flow of a river by converting it into a series of pools divided by dry stretches. Some of the major dams of Kerala are Idukki dam, Peringalkuthu, Sholayar, Peechi, Vazhani, Chimmony, Mattupetty, Kundala, Neyyar, Bhoothathankettu, Idukki, Malampuzha, Siruvani, Pothundi, Thumpoormuzhi, Kakki, Thenmala, Mangalam, Walayar, Idamalayar, Mullapperiyar, Kakkayam, Peruvannamuzhi, and Banasura Sagar. Dams stop the natural flow of the river and create a vast bed of water. It also destructs the evergreen forests, a lot of lands, etc. It causes sustained environmental impacts because of the variation of a river's flow and sediment transport. A dam also desists sediments that would naturally destroy downstream ecosystems. The flow rate of the river at the downstream end of the dam will depend on the amount of compensation flow. It also affects the water volume in rivers during dry seasons.

3 Current Status

Water is inseparably connected to the development of all societies and cultures. At the same time, these developmental activities increased immense pressure on water resources. The region is categorized under "water stress" since there was a reduction reported in the per-capita utilizable water availability from both surface flow and renewable ground flow [7]. Kerala has a coastal belt of 570 km (15% of the total area of the state). The rivers are facing serious threats due to human activities and climate change. Deforestation, sand mining, and plantation crops created an imbalance in the water cycle. Contamination is another major issue. E. Coli and coliform are the main bacteriological pathogens. As per studies, around 748 million people today lack an improved drinking water source in this monsoon-rich state. Our planet's freshwater resources have remained the same, but its demand has exceeded over the supply. There should be a balance between water supply and demand, otherwise, the world will face the serious issue of global water deficit. The sustainable development of a nation can only be achieved by proper water resource management. Drinking water shortage is the principal drought condition in Kerala. Bharathapuzha is the second-longest river in Kerala. One hundred seventy-five villages in the Palakkad, Thrissur, and Malappuram districts depend on this river basin alone for drinking water. This river stands as the main water source for various minor irrigation schemes also. The 41 among the 44 rivers flow towards the west and the rest to the east direction in Kerala. The basin area of the majority of rivers is located within the Western Ghats and the remaining originate from laterite hills [6]. The rivers debouch into the Arabian Sea. The river gets filled up during the monsoon but goes dry again after rain (Fig. 2). This

Fig. 2 Condition of Kerala's second-largest River, Bharathapuzha **a** during monsoon **b** during summer

is because the annual average water discharge through the river is simply flushing into the Arabian Sea. The discharge recorded by the Central Water Commission (CWC) at Kumbidi, 4000 million cubic meters of water from the Bharathapuzha, is simply allowed to flow into the Arabian Sea annually. Only less than 10 per cent (only 400 million cubic meters.) of this quantity of water can be stored in all the seven reservoirs of the basin. About 96–97 per cent of this huge quantity passes to the sea during the monsoon months. Not only Bharathapuzha but majority of rivers of Kerala are facing the same problem, and this is the prime reason for this water scarcity and drought conditions of the state. Industrialization and urbanization increased the serious issue of water scarcity. It consists of evaporation, condensation, sublimation, precipitation, transpiration, runoff, and infiltration. But due to unscientific developmental activities like filling of agricultural fields, cementing ground surfaces, and increased number of buildings decreased the process of infiltration.

4 Alternative Solutions

The average per-capita availability of piped water in the state of Kerala is 100.79 L per day. The estimated water demand and population are given in Table 2. The annual water demand of Kerala state is around 45.36. This section discusses alternative solutions for the efficient management of water resources in Kerala.

4.1 River Rejuvenation

River rejuvenation is an innovative and integrated method to harvest rainwater and recharge groundwater [1]. It reduces the rate of runoff, raises the water levels in the upstream watershed, and sustains the base flow and the runoff in the down-stream basin till the next rainy season. Relevant structures have to be designed based

on geomorphology, lithology, and geological structures. Rainwater harvesting is the most feasible solution in the monsoon-rich state of Kerala. Check dams, Nalah Bunds, Contour trenches, Percolation tanks, Soak pits, Subsurface dykes, Sand dams, Infiltration wells, Injection wells, Water pools, Subsurface dams or underground dams or sand dams, and Coastal reservoirs are the feasible structures for Kerala for rainwater harvesting. Boulder Checks reduce the speed of the water, prevent soil erosion, promote soil moisture, and in turn support natural vegetation. Recharge Wells allow water to percolate in the weathered zones, promote soil moisture, and in turn support natural vegetation. Recharge Bore Wells are constructed where water flow is more. It enables the rising of water levels in the bore and deep wells. It also raises the water table level in downstream areas. Water pools are water storage columns with a minimum spread area. It reduces evaporation and stands as a source of water for humans, cattle, and birds. The long-term permanent solution for the water problem is afforestation. It prevents soil erosion, accelerates water infiltration, and attracts more water to the gravity zone. It also enhances water retention through capillary action.

4.2   GroundWater Dams

Groundwater Dams or Sub Surface Dykes are a barrier across the stream below the ground surface that reduces the subsurface flow of the river system and stores water below ground. These dams check the flow of water out of the sub-basin and upsurge the storage within the aquifer. The subsurface dyke in the river course/stream can capture groundwaters flowing fairly near the surface. As the water is stored below the ground, there is no threat of land submergence. Evaporation loss and siltation can be prevented by employing subsurface dams. The potential disaster like the collapse of dams can be avoided.

4.3   Coastal Reservoir

The coastal reservoir is an emerging concept to store freshwater near the coast or in the sea itself by means of a dyke in the sea. This coastal reservoir has its own advantages in the case of land acquisition and forest clearance. Singapore is the smallest country that once experienced problems due to flood and drought at the same time as Kerala. They solved the issue by constructing a dyke across the mouth of the marina channel, Marina Reservoir, to store the rainwater and to prevent the saltwater intrusion into the river. This plan would be a clear source of freshwater during drought times. The construction follows a unique concept that can cater to the action of both saline and seawater.

4.4 Potential of Popular Lakes of Kerala

Thanneermukkam saltwater bund/ barrage across the largest lake of Kerala and the second-largest lagoon of India, the Vembanad Lake, is regarded as the largest mud regulator of the country (Fig. 3). The barrier was constructed in 1974 and it created a freshwater lake within brackish Vembanad lake fed by the rivers draining into the lake. The shutters of the barrier remain open during the monsoon and kept closed during the summer season to prevent saline water intrusion to the lake and agricultural lands. This has provided sufficient water for second crop cultivation for farmers. But because of unscientific operation and engineering practices, pollution increased and fish wealth reduced, as many fishes require saltwater to complete their life cycle. Proper revising and implementing scientific and innovative engineering techniques can improve the barrage's performance. The water stored by this barrage can meet all the domestic and irrigational water demands of the people of the beneficiary region.

Ashtamudi Lake is the second-largest lake in the state. The Kallada river formed by the conflux of three rivers, Kulathupuzha, Chenthurnipuzha, and Kalthuruthipuzhais, originates near Ponmudi in the Western Ghats. It emerges into the Ashtamudi wetland at Neendakara near Kollam town and enters the Arabian Sea after flowing a distance of about 121 km through the forests. A dike can be constructed at the outlet of the lake where it joins the sea. It will stop the mixing of saltwater with freshwater coming from the Kallada River. Even its small portion (one arm) is converted into a freshwater pond using a small dike, and it can meet the water demands of major districts of the state [9, 4, 5]. A recent study reported that people residing near Ashtamudi Lake are willing to pay for wetland restoration, mangrove conservation, and sustainable fisheries [8].
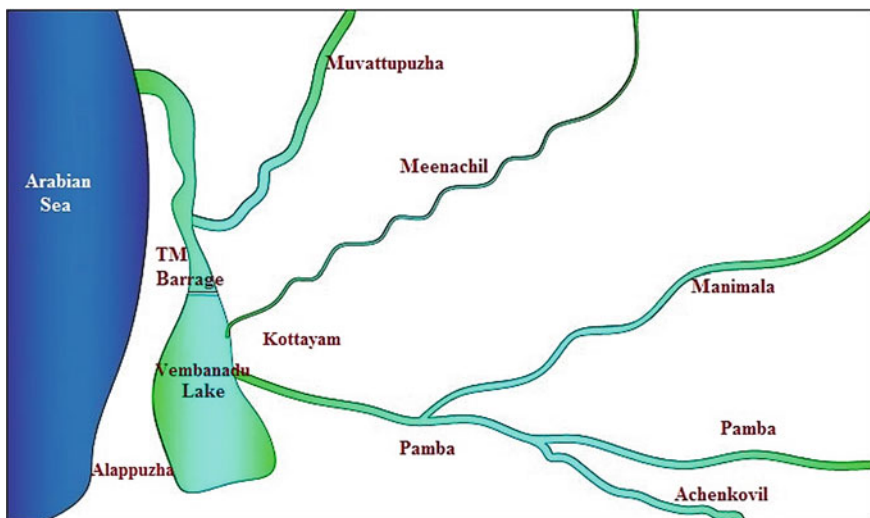

Fig. 3 Schematic representation of Thanneermukkam Barrage

5 Summary

This paper presented an overview of the water resource options in the state of Kerala, which faced frequent floods and droughts in recent years. Few recommendations to maintain existing water source options and alternative solutions are proposed in the paper. There is a need to conserve and maintain traditional water conservation structures. There is a need for community participation and awareness for water conservation at the regional level. The entire fresh floodwater, rather than simply allowing flowing into the sea and becoming saline, need to be stored appropriately. Kerala is blessed with many backwaters and lagoons. The rich freshwater resource of rivers merge with the sea and turns unfit for drinking as well as irrigation. Possible alternative solutions to ensure water security for the state of Kerala are river rejuvenation, groundwater dams, and coastal reservoirs. Implementing innovative engineering practices to check the flushing out of floodwater from the rivers and preventing the saltwater intrusion will make the drought effects immaterial for Keralites.

References

1. Chattopadhyay S, Harilal KN (2017) River restoration in Kerala: Developing a Co-Evolutionary Framework and River Restoration Action Plan for Thiruvananthapuram City.
2. Customized Rainfall Information System (CRIS), Hydromet Division, India Meteorological Department, Ministry of Earth Sciences
3. http://spb.kerala.gov.in/EconomicReview2016/web/chapter04_12.php Last accessed May 2018
4. Kolathayar S, Sitharam TG, Yang S (2019) Coastal reservoir strategy to enhance India's freshwater storage by impounding river flood waters: a detailed overview. Water Supply 19(3):703–717
5. Krishnan A, Kolathayar S (2020) Stability analysis of dike to impound freshwater in brackish water estuarine environment. Open Construction Build Technol J 14(1).
6. Latha A, Vasudevan M (2016) State of India's Rivers for India Rivers Week
7. Lathika M (2010).Water management for irrigation in Kerala. Economic and Political Weekly, pp 73–80
8. Sinclair M, Sagar MV, Knudsen C, Sabu J, Ghermandi A, Economic appraisal of ecosystem services and restoration scenarios in a tropical coastal Ramsar wetland in India. Ecosyst Serv 47:101236
9. Sitharam TG, Kolathayar S, Yang S, Krishnan A (2018) Concept of a geotechnical solution to address the issues of sea water intrusion in Ashtamudi Lake, Kerala. In: Civil infrastructures confronting severe weathers and climate changes conference. Springer, Cham, pp 238–246
10. Water–status of environmental related issues: Kerala ENVIS Centre, Sponsored by Ministry of Environment, Forests & Climate Change, Govt of India. http://www.kerenvis.nic.in/Database/WATER_820.aspx

Location-Specific Rainfall Threshold for Landslides in Select Micro-Watersheds in Coonoor Taluk, Tamil Nadu, India

Evangelin Ramani Sujatha ⓘ**, C. R. Suribabu** ⓘ**, and G. Kannan** ⓘ

1 Introduction

Nilgiris District in Tamil Nadu is a popular tourist destination in South India and has a dynamic population density. The hill region receives heavy rainfall and is frequently affected by landslides particularly during the monsoon season between October and December. Landslides often result in isolation of the hill station as it cut-offs the movement through roads and rails in the region. The annual recurrence of landslides in this region mandates the need for an Early Warning System (EWS) to help in the timely evacuation of the people and re-routing of traffic through road and rail. But, the interactions between the meteorological, geological and hydrological factors that trigger a landslide are complex, very specific to location and not clearly understood making the design and implementation of an EWS difficult [1]. The first step forward in the development of an efficient EWS is the determination of a reliable rainfall threshold that triggers the landslide in the region. It is also highly significant for the success of the mitigation strategies to be adopted in the event of a landslide hazard in the region. Rainfall threshold depends on a number of factors like the geology of the region, its climate and land-use patterns [1–3]. Numerous methods have been adopted by various researchers to determine the rainfall threshold based on the lithology, morphology, soil characteristics and hydrology of the region [1–9]. A threshold value for a landslide triggered by rainfall can be defined as the quantum of rainfall that is most likely to trigger a landslide [1]. The rainfall threshold to initiate a landslide can be, therefore, defined as the minimum rainfall intensity/duration/cumulative antecedent amount of rainfall that causes or reactivates the landslide [10, 11]. Some authors like Reichenbach et al. [12] and Guzzetti et al. [2] define the threshold as the rainfall, hydrological condition or soil moisture that triggers the landslide when exceeded. Wieczorek [5] defines a rainfall

E. R. Sujatha (✉) · C. R. Suribabu · G. Kannan
Centre for Advanced Research on Environment, School of Civil Engineering, SASTRA Deemed University, Thanjavur 613401, India

threshold to cause a landslide in terms of rainfall intensity that initiates slope instability for a specific geo-environment. Such thresholds can be broadly divided into physical and empirical thresholds [2, 3].

Physical thresholds are numerical models and depend on the rainfall necessary to cause a landslide and are established using physical slope models coupled with hydrological models [6, 13, 14]. These models are process based and require a large amount of spatial and temporal inputs on the physical parameters like the slope, soil characteristics (permeability, transmissivity, soil thickness, soil strength parameters its unit weight, pore water pressure and degree of saturation), land-use pattern and nature of vegetation in the region, spatial and temporal variation of rainfall and location and variation of the groundwater table [7, 13–15]. The major limitation with the process-based model is the requirement of specific geotechnical and hydrological data in large amounts thereby limiting its use at a regional scale.

Empirical thresholds are derived from the relationship between landslide occurrence and the rainfall event triggering the landslides. Empirical models study the rainfall events that result in landslides and usually are estimated as the lower bound lines that have resulted in a landslide in the region under study. They can be plotted in Cartesian, logarithmic or semi-logarithmic coordinates. Empirical thresholds can be broadly classified with respect to the rainfall measurements used—(i) thresholds that are based on precipitation measurement obtained for specific rainfall events which can either be single or multiple events; (ii) thresholds based on antecedent rainfall [4, 9, 11]; (iii) other thresholds like hydrological thresholds, etc. [6, 12, 16] and (iv) precipitation event and intensity thresholds [1, 2, 17]. These thresholds can also be grouped based on geographical extent like local, regional and global thresholds. Global thresholds attempt to define the minimum amount of rainfall below which landslides do not occur and are independent of the local lithology, morphology, land-use pattern and/or the rainfall pattern [18, 19]. Regional thresholds define the minimum rainfall that causes landslides for areas that extend from a few to several thousand square kilometres of the areal extent with similar climatic, physiographic and meteorological characteristics [20, 21]. Local thresholds are for specific areal extent defined by a local climate regime and geomorphology. They are applicable to a single landslide event or multiple landslides and extent from a few to several hundreds of kilometres [17, 22, 23]. But there is no clear distinction between regional and local rainfall thresholds based on their extent of applicability [11].

An attempt has been made in this study to identify the local rainfall threshold for a part of the Coonoor Taluk of Niligiri District in the Western Ghats region based on the multiple precipitation events associated with landslides in this region and antecedent rainfall. This rainfall threshold can be utilized for the development of an early warning system and can be extended to similar geo-environmental set-ups particularly in the Western Ghats. A scientific database of the details of landslides types, location and time of occurrence and a well-connected system of rain gauges that record minimum hourly data are essential to establish accurate and reliable rainfall threshold. But the Coonoor region has very limited information pertaining to rainfall and scientific records on the temporal landslide data. Also, the spatial variability in the factors causing landslides and anthropogenic interference further

complicates defining a rainfall threshold that can initiate a landslide. Hence, an antecedent rainfall threshold model that can utilize the available data to the best is selected and also an observation on the relation between landslide occurrence and rainfall shows that antecedent moisture conditions play a vital role in triggering landslides in this region.

2 Study Area

Three micro-watersheds (Fig. 1) were delineated around one of the most damaging landslides that occurred in November 2009 on a slope that housed a hospital in the heart of the Coonoor town to predict the threshold rainfall that can initiate a
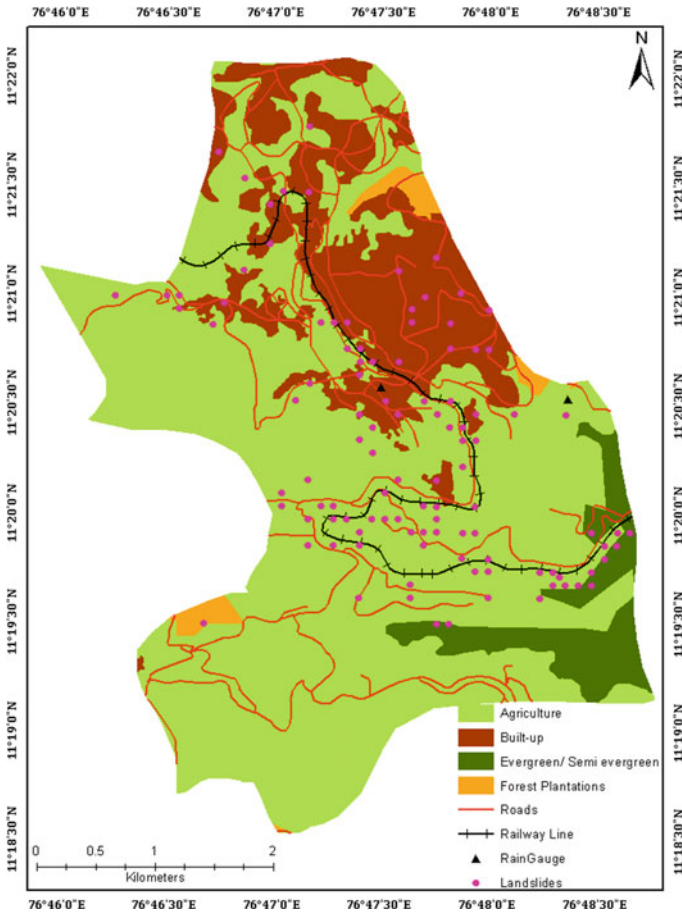

Fig. 1 Land-use Map of the Selected Micro-Watersheds

landslide in this region. The total area covered by the selected micro-watersheds was 31.46 square kilometres. This landslide is one of the very large volume landslides that occurred in this region. The selected area cuts across the most affected traffic corridor—the Coonoor–Mettupalayam traffic corridor—that houses both the highway connecting Mettupalayam and Ooty and also the Mountain Railway traffic. The climate, in general, is temperate in nature with an annual average temperature of 17 °C. The average variation in temperature over a 30-year period shows that the average minimum temperature dips to 8.6 °C in January and rises to 24.3 °C in May. Rainfall is spread throughout the year with an average annual rainfall of 1335 mm [24]. The altitude ranges between 1238 and 1969 m above the mean sea level. The slope in the region is predominantly gentle (i.e.) less than 15˚. The maximum slope in the area is 55˚. The bedrock is composed of principally charnockite. The vast expanse of the study area falls under agriculture, mostly tea plantations and the northern part comprise of high-density settlements. Patches of forest plantation and evergreen forest are present in the fringes of the micro-watersheds. The micro-watersheds are drained by a number of first-order streams.

The linear infrastructure congestion in this area has led to the destruction of the native forests to a large extent and has also given rise to unplanned urbanization. The anthropogenic interference has exceeded the self-sustaining capacity of the mountain ecosystem and this has led to a phenomenal increase in the occurrence of landslides in Coonoor. Maximum numbers of landslides are recorded in months between October and November when the rainfall recorded is highest. Also, the majority of the landslides are recorded after intense precipitation and are localized.

3   Rainfall Regime and Landslides

Records of daily rainfall were collected from Coonoor railway station, Glendale tea estate and Coonoor Municipality for the period 1992–2017. Daily rainfall data was used to calculate the antecedent rainfall relating to landslide occurrence. Historic records from 1935 till 2019 show that the annual rainfall exceeds 1000 mm [24]. Precipitation is maximum between October and December (monsoon season) and minimum in the post-monsoon period, January to March (Fig. 2).

The precipitation shows high inter-seasonal variation and inter-annual variation (Fig. 3). The variability is high in post-monsoon months of January and February and least in the pre-monsoon months between June and September. Heavy precipitation is concentrated in the months between October and December (North East Monsoon Season).

Multi-temporal landslide data was obtained from various sources like the field register of the railways department, national highways and state highways department, Geological Survey of India, newspapers, online resources and from published literature. The total number of landslides recorded in the period of study in the selected micro-watersheds was 106. The majority of the landslides occurred in the monsoon months between October and December. Landslides are shallow in nature
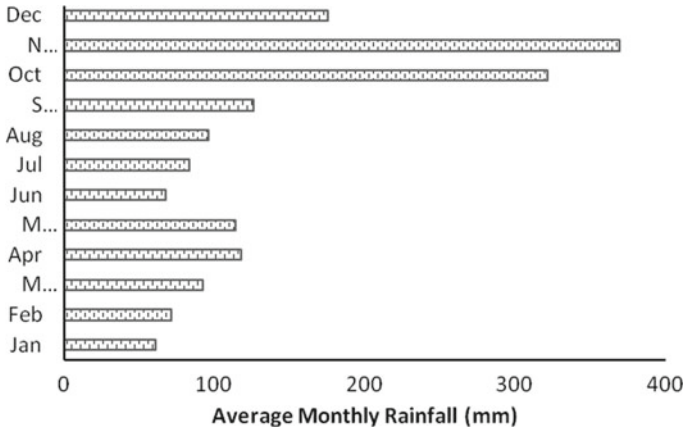
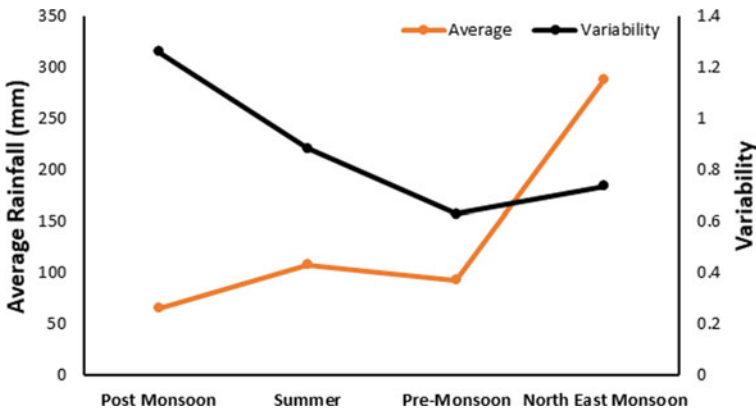**Fig. 2** Average monthly rainfall in the study area

Fig. 3 Variability in seasonal rainfall

and are of the types debris falls, earth slides, earth slumps and subsidence. Major traffic corridors are most affected by debris flows and cut-slope failures. Landslides are triggered by rainfall that causes an increase in pore pressure and subsequent slope failures. The landslide database consists of the coordinates of landslide location and date of occurrence. Landslides of all types are included in the study [25, 26]. Landslide database collected from various sources indicates that soil type, land-use pattern, proximity to linear infrastructures like roads and railway lines, slope gradient and proximity to streams influence the stability of the slopes but rainfall remains the single most important factor that triggers the landslide in the selected micro-watersheds.

4   Analysis of Rainfall Threshold

A description of the rainfall event and the associated landslide is required for the empirical threshold [3]. Intensity–duration relation and antecedent rainfall have been used to determine the rainfall threshold in this study as it is a trial-tested and commonly used threshold parameter relation to identify the rainfall threshold [1]. This parameter couple also provides the flexibility to define the intensity and duration based on data availability and the nature of the specific terrain [3]. The intensity (I)–duration (D) threshold connects the rainfall of specific duration (D) with mean rainfall intensity (I) in the corresponding duration. In general, the relationship is of the form $I = \alpha D^{-\beta} + c$. α, β and c are the empirical parameters and represents a straight-line pattern with 'c' equal to zero in typical cases [1]. The scaling factor (α) is the intercept of the log D–log I plot and β is its slope. The power law equation is used to fit the equation [1]. Power law equation is used to determine the rainfall threshold based on two basic assumptions—(i) there is a non-linear rise in the feasibility of landslide occurrence with the increase in rainfall intensity and (ii) with the increase in the duration of rainfall, the possibility of initiation of a landslide event decreases [11]. The empirical parameter 'β' describes the rate of decline of the critical intensity with the increase in duration. This equation indicates that both short duration–intense rainfall and long period–less intense rainfall can trigger a landslide [2]. Therefore, the occurrence of slope failure depends on the hydrogeological conditions of the slope in addition to the rainfall intensity and duration. Most rainfall thresholds fall between 1–100 h and 1–200 mm/hour intensity [1, 2]. The hourly intensity of rainfall or daily intensity can be used for determining the rainfall threshold equation depending on the availability of rainfall data [1, 9, 11].

Coonoor experiences rainfall all through the year. The temporal variability of rainfall in the selected micro-watersheds shows a seasonal variation (Figs. 2 and 3). The landslide occurrence pattern also follows the general trend of the rainfall pattern with the majority of landslides in the monsoon months between October and December. A total of 107 landslides are recorded in the period between 1992 and 2017 and all these landslides were triggered by rainfall. Landslides between 1992 and 2009 were used as test dataset to determine the rainfall threshold that triggers landslides in this region. The landslides that occurred between 2010 and 2017 were used to validate the threshold equation proposed from the test data. The daily intensity of the rainfall events associated with the landslide was calculated and plotted in the logarithmic scale against duration in days, also in the logarithmic scale [9]. Antecedent rainfall corresponding to one day, three days, five days, fifteen days and thirty days were plotted against the corresponding durations. The power equation of the best fit (i.e.) the threshold equation corresponding to 50% exceedance probability [3] for the selected micro-watersheds was obtained as
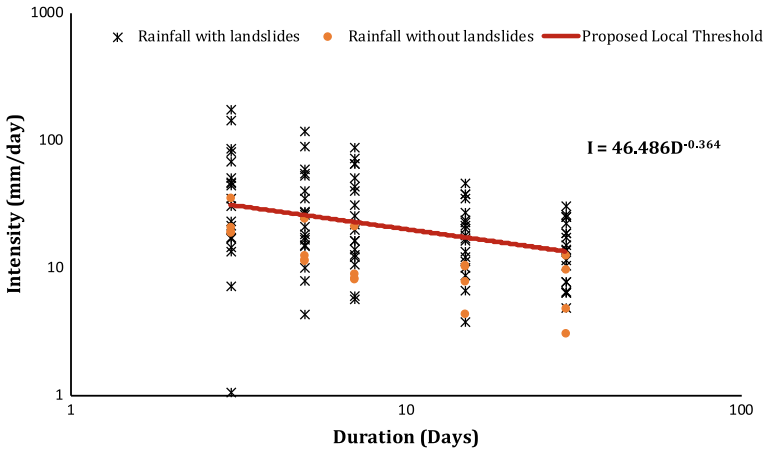
$$I = 46.486 * D^{-0.364}. \tag{1}$$

Fig. 4 Intensity–Duration Threshold for the Selected Micro-Watersheds

Intensity–duration study was adopted by authors Harilal et al. [1], Dikshit et al. [9] and Kanungo and Sharma [11] for Sikkim and Garhwal Himalayas and obtained comparable equations. This equation indicates that landslides would not occur in the selected area if the rainfall received is less than 46.486 mm/day.

Also, it demonstrates that a rainfall intensity of 13.48 mm/day for 30 days can also trigger a landslide indicating the influence of soil characteristics and moisture and also the importance of antecedent rainfall. Figure 4 indicates that almost all of the maximum rainfall without landslides (orange dots) were plotted below the threshold line indicating the better performance of the threshold equation in demarcating the rainfall causing landslides in the region.

5   Validation

The use of the threshold rainfall determined from the test data can be used for operational early warning system only after its validation. The landslides that occurred between the period 2010 and 2017 were used to validate the threshold equation. Fourteen landslides have occurred in this period and were associated with seven rainfall events. The threshold equation was fit to the selected antecedent rainfall periods (i.e.) 3, 5, 7, 15 and 30 days. It was found that application of threshold equation to 30 days antecedent rainfall period predicted five landslide events out of seven events positively. Also, Fig. 5 implied that all the maximum rainfall events without landslides in the test period between 1992 and 2009 were plotted well below the threshold line indicating that 30 days antecedent period is more effective in predicting the landslides in this region.

Table 1 Performance Appraisal of Proposed Local Threshold

Threshold	True Positive	True Negative	False Positive	False Negative	Sensitivity
Local	5	4	1	2	0.71
Specificity	Positive Prediction Power	Negative Prediction Power	Likelihood Ratio	Efficiency	True Skill Statistic
0.8	0.83	0.67	3.57	0.75	0.51

The threshold was validated using the threat score [9, 27, 28]. The Threat Score (TS) is calculated as the ratio between the True Positives (where landslides have occurred when the threshold was exceeded) and the sum of True Positives (TP), False Negative (where landslides have occurred when the threshold was not exceeded) and False Positive (where landslides have not occurred though threshold was exceeded). The threat score was calculated for the period from 2010 to 2014 for an Intensity–Duration threshold corresponding to 30 days antecedent rainfall and was found to be 0.625. Also, few other statistical measures are used to assess the performance of the proposed local threshold for the selected micro-watersheds (Table 1).

Table 1 shows that the predicted threshold has a good ability to predict classify the rainfall that triggers the landslides in the region and the overall efficiency of the predicted threshold model is fairly good.

6 Discussion

Rainfall thresholds are basic tools for assessing the stability of the slope and defining the minimum cut-off below which the probability of occurrence of landslide is very less and beyond this threshold, the probability of occurrence exponentially increased. There are still chances for false alarms which is often the major challenge. Uncertainties associated availability of rainfall data, its quality and information on the landslides particularly the date of occurrence have resulted in numerous attempts by various researchers to determine the rainfall threshold. Rainfall is often the triggering factor but the influence of other environmental, geotechnical and anthropogenic factors cannot be ruled out. Essentially, for the effective design and functioning of an early warning system parameters like pore pressure, soil moisture, slope movement, solar radiation and the vegetative pattern on the slopes should also be considered in addition to the rainfall threshold. The landslides in the selected micro-watersheds are often triggered by monsoonal rainfall which occurs over an extended period of time. The soil in the study area is fairly permeable and hence, prolonged rainfall (i.e.) antecedent moisture conditions play a major role in initiating the landslide event. Also, the unplanned urbanization and high built-up density have led to open drains that lead to saturation of the soil aggravation slope instability. The intensity–duration model and the antecedent rainfall models used to predict the rainfall threshold

indicate that a minimum 7-day antecedent rainfall is necessary to trigger landslides in the region in most cases. A prolonged period of nearly 30 days duration results in large volume landslides that cause major damage. Short intense rainfalls have also resulted in landslides but often such landslides are localized and happen in isolation.

7   Conclusions

This study attempted to establish the intensity–duration-based rainfall threshold that was built on antecedent rainfall. The rainfall threshold determined is location specific and serves as an input for the development of the early warning system for these specific micro-watersheds. The threshold determined to a large extent depends on the quality of the short-term rainfall data and has much scope to be improved. The study used a 25-year database from 1992–2017 with 107 landslides spread throughout the study area. The study points to the following conclusions; daily rainfall (short duration) events of intensity 46.486 mm/day can trigger landslides. Rainfall intensity of 13.48 mm/day exceeding 30 days duration can also induce landslides. Long-term antecedent rainfall plays a major role in triggering landslides in this region. The rainfall threshold can further be refined by expanding the database of landslides and their corresponding rainfall data.

Conflict of Interest   The authors declare no conflict of interest.

References

1. Harilal GT, Madhu D, Ramesh MV, Pullarkatt D (2019) Towards establishing rainfall thresholds for a real-time landslide early warning system in Sikkim. India. Landslides 16:2395–2408
2. Guzzetti F, Peruccacci S, Rossi M, Stark CP (2007) Rainfall thresholds for the initiation of landslides in central and southern Europe. Meteorol Atmos Phys 98:239–267
3. Segoni S, Piciullo L, Gariano SL (2018) A review of the recent literature on rainfall thresholds for landslide occurrence. Landslides 15:1483–1501
4. Aleotti P (2004) A warning system for rainfall-induced shallow failures. Eng Geol 73:247–265
5. Wieczorek GF, Morgan BA, Campbell RH (2000) Debris-flow hazards in the Blue Ridge of central Virginia. Environ Eng Geosci 6:3–23
6. Baum RL, Godt JW, Savage WZ (2010) Estimating the timing and location of shallow rainfall-induced landslides using a model for transient, unsaturated infiltration. J Geophys Res Earth Surf 115
7. Salciarini D, Tamagnini C (2015) Physically based rainfall thresholds for shallow landslide initiation at regional scales. In: Lollino G, Giordan D, Crosta GB, Corominas J, Azzam R,

Wasowski J, Sciarra N (eds) Engineering geology for society and territory, vol 2. Springer, Cham, pp 1041–1044

8. Salvatici T, Tofani V, Rossi G, D'Ambrosio M, Tacconi Stefanelli C, Benedetta Masi E, Rosi A, Pazzi V, Vannocci P, Petrolo M et al (2018) Application of a physically based model to forecast shallow landslides at a regional scale. Nat Hazards Earth Syst Sci 18:1919–1935

9. Dikshit A, Sarkar R, Pradhan B, Acharya S (2019) Kelzang Dorji Estimating rainfall thresholds for landslide occurrence in the Bhutan Himalayas. Water 11:1616

10. Varnes D (1978) Slope Movement types and processes. In: Transportation research board special report, pp11–33

11. Kanungo DP, Sharma S (2014) Rainfall thresholds for prediction of shallow landslides around Chamoli-Joshimath region, Garhwal Himalayas. India. Landslides 11:629–638

12. Reichenbach P, Cardinali M, De Vita P, Guzzetti F (1998) Regional hydrological thresholds for landslides and floods in the Tiber River Basin (central Italy). Environ Geol 35:146–159

13. Vanacker V, Vanderschaeghe M, Govers G, Willems E, Poesen J, Deckers J, De Bievre B (2003) Linking hydrological, infinite slope stability and land-use change models through GIS for assessing the impact of deforestation on slope stability in high Andean watersheds. Geomorphology 52:299–315

14. Bregoli F, Medina V, Chevalier G, Hürlimann M, Bateman A (2015) Debris-flow susceptibility assessment at regional scale: Validation on an alpine environment. Landslides 12:437–454

15. Reder A, Rianna G, Pagano L (2018) Physically based approaches incorporating evaporation for early warning predictions of rainfall-induced landslides. Nat Hazards Earth Syst Sci 18:613–631

16. Jakob M, Weatherly H (2003) A hydroclimatic threshold for landslide initiation on the North Shore Mountains of Vancouver. British Columbia. Geomorphology 54:137–156

17. Jaiswal P, van Westen CJ (2009) Estimating temporal probability for landslide initiation along transportation routes based on rainfall thresholds. Geomorphology 112:96–105

18. Caine N (1980) The rainfall intensity-duration control of shallow landslides and debris flows. Geogr Ann Ser A Phys Geogr 62:23–27

19. Cannon SH, Gartner JE (2005) Wildfire-related debris flow from a hazards perspective. In: Debris-flow hazards and related phenomena. Springer, Berlin, pp 363–385

20. Corominas J, van Westen C, Frattini P, Cascini L, Malet JP, Fotopoulou S, Catani F, Van Den Eeckhaut M, Mavrouli O, Agliardi F et al (2014) Recommendations for the quantitative analysis of landslide risk. Bull Eng Geol Environ 73:209–263

21. Jan C-D, Chen C-L (2005) Debris flows caused by Typhoon Herb in Taiwan. In: Jakob M, Hungr O (eds) Debris-flow Hazards and Related Phenomena. Springer, Berlin Heidelberg, pp 539–563

22. Marchi L, Arattano M, Deganutti AMT (2002) years of debris-flow monitoring in the Moscardo Torrent (Italian Alps). Geomorphology 46:1–17

23. Zêzere JL, Trigo RM, Trigo IF (2005) Shallow and deep landslides induced by rainfall in the Lisbon region (Portugal): assessment of relationships with the North Atlantic Oscillation. Nat Hazards Earth Syst Sci 5:331–344

24. Sujatha ER, Suribabu CR (2017) Rainfall Analyses of Coonoor Hill Station of Nilgiris District for Landslide Studies. IOP Conf. Ser. Earth Environ. Sci. 80:12066

25. Sengupta A, Gupta S, Anbarasu K (2010) Rainfall thresholds for the initiation of landslide at Lanta Khola in north Sikkim. India. Nat. Hazards 52:31–42

26. Nerella SP, Alajangi S, Dhakal D (2019) Landslide susceptibility mapping using GIS-Based likelihood frequency ratio model: A case study of Pakyong—Pacheykhani Area, Sikkim Himalaya. In: Proceedings of the proceedings of international conference on remote sensing for disaster management. Springer International Publishing, pp 569–586

27. Sarkar S, Kanungo DP, Patra AK (2006) Landslides in the Alaknanda valley of Garhwal Himalaya. India. Q. J. Eng. Geol. Hydrogeol. 39:79–82

28. Marques R, Zezere J, Trigo R, Gaspar J, Trigo I (2008) Rainfall patterns and critical values associated with landslides in Povoação County (São Miguel Island, Azores): relationships with the North Atlantic Oscillation. Hydrol Process 22:478–494